DISS. ETH NO. 25490

LIGHT FRAME TIMBER WALLS IN REGIONS OF LOW TO MODERATE SEISMICITY

A thesis submitted to attain the degree of
DOCTOR OF SCIENCES of ETH ZURICH
(Dr. sc. ETH Zurich)

presented by

LJUPKO PERIĆ

dipl. civil engineer, University Mostar
M.Sc. in earthquake engineering, University Ss. Cyril and Methodius, Skopje

born on 21.03.1961
citizen of
Baden (AG)

accepted on the recommendation of

Prof. Dr. Andrea Frangi	ETH Zürich
Prof. Dr. Božidar Stojadinović	ETH Zürich
Prof. Dr. Alessandro Palermo	University of Canterbury, NZ
Dr. René Steiger	Empa Dübendorf

2019

Acknowledgment

The development of this thesis took more than four years. Many people who deserve my gratitude, namely, my family, people at ETH and my office accompanied me on this way.
First of all I am very thankful for the support, love and understanding of my family, my wife Draženka, son Fran and daughter Dora for all the time they missed me.
I would also like to express my deep gratitude to my mentor Prof. Andrea Frangi, who gave me the opportunity to write this thesis in his group. Gratitude is also accorded to co-referents, Prof. Božidar Stojadinović, for his support and patience during our consultation meetings, Prof. Alessandro Palermo for all the discussions we had during his visits at ETHZ and Dr. René Steiger for his help and advices during the performance of the tests at Empa.

My thanks goes also to technicians Patrick Morf at the ETH laboratory, where fasteners exposed to cyclic loading were investigated, and for the support of Dr. Pedro Palma and his staff at Empa, where the Light Frame Timber Walls (LFTWs) sheathed with Gypsum Fiberboard (GFB) were tested. I am indebted to my friend and colleague, Dr. Gabriele Granello, who steadily helped me with optimization and improvement of Matlab and Opensees scripts, the core part of this study.

I would also like to thank all the fellows in the timber group, Thomas Ehrhart, Benjamin Kreis and Dr. Flavio Wanninger for their support during the development of my thesis.

I owe a great debt of gratitude to my office MWV Bauinegnieure AG, my partner Peter Hohn and to all employees, who had so much understanding for my efforts.

I would like to thank the Erne Holzbau AG company, represented by Patric Suter, Adrian Kirchhofer and Fabian Dinkel, for the financial and practical support through manufacturing and testing of the LFTW specimens sheathed with GFB.

My sincerest thanks to Dr. Catherine Whyte and Vesna Kitanovska, grad. philologist for helping me to correct and improve the style and grammar of the English language used to write this thesis.

Zürich, April 2019

Ljupko Perić

Abstract

A parameter study is carried out to investigate the applicability of Light Frame Timber Walls (LFTWs) in regions of low to moderate seicmicity. LFTWs sheathed with Gypsum Fibreboard (GFB) and Oriented Strand Board (OSB) are considered. The investigation is based on experimental results and numerical material and structural models. A parameter study is performed by means of performance-based seismic design, using nonlinear static pushover analyses and nonlinear time history analyses for seismic hazard zones characterized by design values of ground accelerations of 0.6, 1.0, 1.3 and 1.6 $[m/s^2]$. For this purpose, the response of a single fastener, either a nail or a staple, to cyclic loading is first estimated. The hystereses estimated for individual fasteners are then used to model a LFTW element within the MatLab-based computer program, MCASHEW developed by Folz and Filiatrault (2002) . The analysis is performed for different wall lengths of 2.4, 3.0, 3.6, 4.2 and 4.8 [m]. Stewart's 10-parameter hysteresis, obtained for each single wall length, is used to define the SAWS-material (Seismic Analysis of Woodframe Structures) incorporated in the Open Source Software OPENSEES. Then, multi-storey structures are modeled within OPENSEES and analyzed by pushover analysis and Nonlinear Time History Analysis (NLTHA).

For the NLTHA, 10 earthquakes from a Pacific Earthquake Engineering Research Center (PEER) database, referred to as the Next Generation Attenuation (NGA) database containing 3551 real ground motion records are selected and scaled to the required hazard levels. The results of the modal, pushover and NLTH analyses provide information about all degrees of freedom, the magnitude of the inter-storey drift ratios (IDR), roof displacements, vibration periods, mode shapes and hold-down (HD) forces. The parameters relevant for design are fixed in advance, as follows: the maximum inelastic vibration period is assumed to be $T^* \leq 1.7[s]$; the ductility demand is assumed to be $\mu \leq 3.0$. Based on the deformability of one-storey LFTWs sheathed with GFB and OSB, $IDR \leq 0.8$ and $IDR \leq 2.5$, are chosen, respectively. Based on analysis of the elastic behaviour, the maximum force in the HD devices is limited to $725[kN]$. The damage analysis leads to limits of damage index ratios (DI) of $DI \leq 0.8$ and $DI \leq 0.7$ for LFTWs sheathed with GFB and OSB, respectively. The outcomes of the analyses were admissible masses for the given number of storeys and the corresponding hazard zone, when one of the limiting criteria is reached. The serviceability criteria is checked by the condition that the wind load should not exceed $55\% = \frac{F_y}{1.8}$ of the yielding force of the LFTW element under consideration.

In the thesis, it is shown that, in European regions with low to moderate seismicity, the LFTWs can efficiently be used as components of multi-storey structures of up to 8 storeys. The earthquake excitation considered is represented by ground accelerations of 0.6, 1.0, 1.3 and 1.6 $[m/s^2]$, covering most of the European regions. The results of the pushover study are verified independently by NLTHA and Incremental Dynamic Analysis (IDA). Only the models which pass both analyses are adopted as decisive.

The procedure for estimation of the force-displacement relationship, and thus for estimation of the capacity curve based on the McCutcheon energy approach, suitable for hand calculations, is introduced. This enables a closer look at the problem as well as the estimation of the data, which were not the outcome of the more sophisticated methods used within this thesis.

Kurzfassung

Im Rahmen eines Forschungsprojekts werden, basierend auf verhaltensorientierten Bemessungsmethoden (Performance Based Design), die Grenzen der Anwendbarkeit von Holzrahmenwänden (HRW), beplankt mit OSB-Panels sowie Gipsfaserplatten als Aussteifung von mehrgeschossigen Holzbauten bei niedriger bis moderater Seismizität aufgezeigt. Die Analyse wird für vier Intensitäten der Erdbebeneinwirkung, charakterisiert durch die Bemessungswerte der horizontalen Bodenbeschleunigung von 0.6, 1.0, 1.3 und 1.6 $[m/s^2]$, durchgeführt.
Bei der Analyse der HRW wurde vom Verhalten eines einzelnen Verbindungsmittels (VM) (Nagel bzw. Klammer) ausgegangen. Die Antwort der VM einer Holzverbindung auf zyklische Beanspruchung wurde anhand von Versuchen ermittelt. Die dabei ermittelten Hysteresen der einzelnen VM wurden in das Computer-Programm MCASHEW- (ein MatLab-basiertes Programm), entwickelt durch Folt und Filiatrault (2002) eingegeben. Eine 10-parametrige Stewart-Hysterese für das jeweilige VM und für die jeweilige Wandkonfiguration wurden generiert.
Im nächsten Schritt wurden für jede untersuchte Wandlänge von 2.4, 3.0, 3.6, 4.2 und 4.8 [m] die auf den Stewart-Hysteresen basierten SAWS-Materialeigenschaften (Seismic Analysis of Woodframe Structures) in der Open Source Software OPENSEES modelliert und eine komplette modale, Pushover sowie Nonlinear Time History Analysis (NLTHA) durchgeführt.
Als Input für die NLTHA wurden 10 von 3551 realen Erdbebenaufzeichnungen vom Pacific Earthquake Research Center (PEER), genannt Next Generation Attenuation (NGA) Datenbank ausgesucht und nach bestimmten Kriterien auf die erforderlichen, den Gefährdungsstufen entsprechenden Antwortspektren-Niveaus skaliert. Die Ergebnisse der Pushover und der NLTHA-Analyse beinhalten sämtliche Bewegungsgrössen für alle Freiheitsgrade, gegenseitige Stockwerksverschiebungen (Interstory Drift Ratios (IDR)), verschiedene Niveaus des Duktilitätsbedarfs, Grundschwing- zeiten, Schwingungsformen sowie Verankerungskräfte in den Zugankern. Als ergebnisbestimmende Parameter wurden Grundschwingzeiten $T^* \leq 1.7[s]$, ein Duktilitätsbedarf $\mu \leq 3$, eine maximale gegenseitige Stockwerkverschiebung $IDR \leq 0.8\%$, für HRW beplankt mit Gipsfaserplatten sowie $IDR \leq 2.5\%$ für HRW beplankt mit OSB-Panels und eine Kraft in der Verankerung $F_{HD} \leq 725[kN]$ gewählt. Darüber hinaus wurden im Rahmen der Schadensanalyse die Schadensindexe $DI \leq 0.8$ für HRW beplankt mit Gipsfaserplatten bzw. $DI \leq 0.7$ für HRW beplankt mit OSB Panels als limitierende Grössen festgelegt. Das Ergebnis der Analyse sind zulässige Massen und eine zulässige Anzahl Geschosse von Holzbauten für die untersuchten Gefährdungsstufen, wobei für jede untersuchte Konfiguration eine der oben genannten Parametergrenzen erreicht wurde. Gleichzeitig wird die Gebrauchstauglichkeit unter Windeinwirkung kontrolliert. Für die Erfüllung des Kriteriums der Gebrauchstauglichkeit wurde der Ausnutzungsgrad des Tragwerks infolge Windeinwirkung auf $55\% = \frac{F_y}{1.8}$ der Fliesskraft F_y begrenzt.
Dieser Beitrag geht auf die Frage der Anwendbarkeitsgrenzen für aussteifende Standard- Holzrahmenwände (HRW) als Teil mehrgeschossiger Holzbauten in europäischen Regionen mit niedriger bis moderater Seismizität ein. Es wird gezeigt, dass die hier untersuchten HRW, dank deren

hervorragenden Eigenschaften, in bis zu 8-stöckigen Holzbauten als aussteifende Elemente ausreichenden Schutz gegen Erdbebeneinwirkung bieten und in mehrgeschossigen Holzbauten weiterhin erfolgreich eingesetzt werden können. Die Erdbebeneinwirkung wird für jede Stufe der Erdbebengefährdung, charakterisiert durch Bemessungswerte der horizontalen Bodenbeschleunigungen von 0.6, 1.0, 1.3 und 1.6 $[m/s^2]$, durch entsprechende Antwortspektren repräsentiert. Die Bandbreite der in dieser Arbeit berücksichtigten Bodenbeschleunigungen deckt gemäss [89] weite Teile Europas bezüglich der dort herrschenden Erdbebengefährdung ab. Die Ergebnisse der Pushover Analyse werden mittels einer Nonlinear Time History Analysis (NLTH) verifiziert. Die hier vorgestellte Parameterstudie stützt sich auf das im Rahmen des Programms des Consortium of Universities for Research in Earthquake Engineering (CUREE), 2002 von Folz und Filiatrault [32] und [30] entwickelte MatLab basierte Programm MCASHEW (Cyclic Analysis of Shear Walls). Es handelt sich dabei um ein Programm für die Analyse von HRW unter monotoner und zyklischer Beanspruchung von ein- und mehrstöckigen Strukturen. Im Rahmen dieser Arbeit wurde das Programm lediglich für die Evaluation des 10-parametrischen, mechanischen Modells eines einstöckigen HRW-Elementes verwendet.
Die Ergebnisse der auf dem mechanischen MCASHEW-Modell basierenden parametrischen Studie wurden zusätzlich mit einem unabhängigen Wekzeug nämlich der Incremental Dynamic Analysis (IDA) überprüft. Schliesslich wurden lediglich diejenigen Ergebnisse, die beide Analysen bestanden haben, als solche anerkannt.
Im Vorfeld wurde ein für die Handrechnung geeignetes, auf dem energetischen Ansatz von McCutcheon basierendes Verfahren für die Ermittlung der nichtlinearen Kraft-Verformungsbeziehung einer HRW vorgestellt. Das letztere Verfahren kann auf mehrgeschossige Bauten im Rahmen einer Erdbebenanalyse angewandt werden. Die Handrechnung dient der Ermittlung der nichtlinearen F-Δ-Beziehung, ermöglicht den Vergleich mit den Ergebnissen der Computergestützten Analyse sowie der Ermittlung weiterer, für die Analyse der HRW wichtigen Parameter, die durch die oben genannte Software nicht direkt ermittelt werden können.

Contents

Chapter 1

Introduction

The motivation for investigating the behaviour of light frame timber walls (LFTWs) under seismic loading will be addressed in this chapter. LFTWs, traditionally used as a part of the lateral load resisting system in timber structures, will be introduced. The configuration of a typical LFTW element with its constitutive elements will be presented and briefly described. The major assumptions and limitations related to the future parameter study will be outlined. An overview of the engineering and scientific methods used in this thesis will be described. The chapter will end with a sketch of the thesis organization.

1.1 Motivation

Until January 2015, fire protection provisions unfavourably affected the use of timber structures in Switzerland. According to these provisions, the timber structures were limited to a height of up to five storeys. Following the adoption of the new fire protection code in January 2015, the height of timber structures is governed mainly by their inherent mechanical and structural characteristics rather than by fire protection requirements. These new regulations enable the construction of middle- and high-rise timber structures, which will require appropriate lateral load resisting systems.

Lateral load resisting systems of timber structures used in Switzerland traditionally comprise of one- or two sided sheathed light frame timber walls (LFTWs). The sheathing material is either a Gypsum Fiberboard (GFB) or an Oriented Strand Board (OSB) panel. Staples or nails are used as connectors between the frame and the sheathing material.

To date the traditional LFTW lateral load resisting system has been applied to low- and mid-rise buildings in regions with low and moderate seismicity. The question which arose after the fire protection code changed is for which seismic hazard zones and up to how many storeys is the LFTW still suitable as a lateral load resisting system. The feasibility range for the use of a LFTW in terms of both seismicity hazard level and height of the structure should be estimated more precisely by means of Performance Based Seismic Design (PBD) and Nonlinear Time History Analysis (NLTHA).

To do so, a reliable prediction of wall element behaviour under monotonic and cyclic loading is of central importance. The highly nonlinear behaviour of each wall element must be described in terms of its characteristic bearing capacity using effective mechanical material properties.

1.2 Scope of the investigation

The main aims of this thesis are to reliably estimate the bearing capacity of traditionally used light frame timber walls for resisting ground accelerations. The focus is placed on seismic hazard zones and typical construction in Switzerland in terms of both the admissible mass subjected to the single wall element and the number of storeys in the structure. In this way, the efficiency and the potential of existing lateral load resisting systems will be evaluated. The results are design diagrams that will enable the engineer to easily read out which mass may be assigned to a single wall element for a certain seismic hazard level and a corresponding number of stories. It is recognized that an abundant number of parameters affect such an analysis. In order to establish a straightforward procedure, some limitations and simplifications were necessary. The following parameters have been considered:

- the type of sheathing material is either an oriented strand board (OSB) or a Gypsum Fiberboard (GFB) panel
- the thickness of the sheathing material is assumed to be 15$[mm]$
- the diameters of the fasteners used as connectors are $d = 2.87[mm]$ and $d = 1.53[mm]$, for nails and staples, respectively
- the distance between the panel-to-frame connectors is assumed to be 30$[mm]$ and 35$[mm]$ for OSB and GFB sheathing material, respectively
- the wall length is equal to $2.4, 3.0, 3.6, 4.2$ or $4.8[m]$
- the height of the structure is represented by the number of storeys, running from 1 to 8.
- the mass in tonnes $[t]$ acts on a single wall element at each storey level
- the design values of horizontal ground accelerations in the Swiss seismic zones Z1, Z2, Z3a and Z3b, correspond to a_{gd}=0.6 [m/s^2]; a_{gd}=1.0 [m/s^2]; a_{gd}=1.3 [m/s^2] and a_{gd}=1.6 [m/s^2], respectively

1.3 Assumptions and limitations related to LFTWs

This thesis does not aim to cover all potential design scenarios for a certain wall element, but instead intends to determine the best performance that a wall element can exhibit. The capacity of a wall element subjected to an earthquake excitation, is estimated using the following assumptions and simplifications:

- The force-displacement relationship of each single wall element is estimated based on a design using minimal distance between fasteners.
- Each wall element is sheathed on both sides with the same material.
- The spacing of the fasteners remains constant along the edges of the sheathing panel on both sides.
- A LFTW element represents one inelastic shear spring.
- The building is a simple sum of single, vertically stacked wall elements.
- The storey height remains constant over the height of the building.
- The storey masses are evenly distributed over the model height.
- Hold-Down devices are designed to remain elastic.
- Hold-Down devices do not affect the nonlinear response of the wall or the entire building.
- In order to obtain conservative results, no vertical loads are applied to the walls.

These simplifications lead to the following limitations:

- There is no variation in storey height.
- There is no variation in storey mass.
- The torsion effects are not considered in the model.
- The wall elements contain no openings.
- $P - \Delta$ effects are not considered.

1.4 Standard configuration of LFTWs

LFTWs are typically used in timber structures as the elements that carry the vertical gravity loads and provide the lateral stability of the building. A standard configuration of a LFTW consists of the following components, see Figure 1.1:

- Internal and external rails
- Top and bottom frame plates
- A sheathing panel on one or both sides
- Fasteners connecting the sheathing panels to the frame at a certain spacing
- Hold-down devices
- Shear keys, which could also be a part of robust hold down devices

All of these components combined constitute the composite structural element, which provides a considerable racking stiffness. The uplift and base shear forces are resisted by the

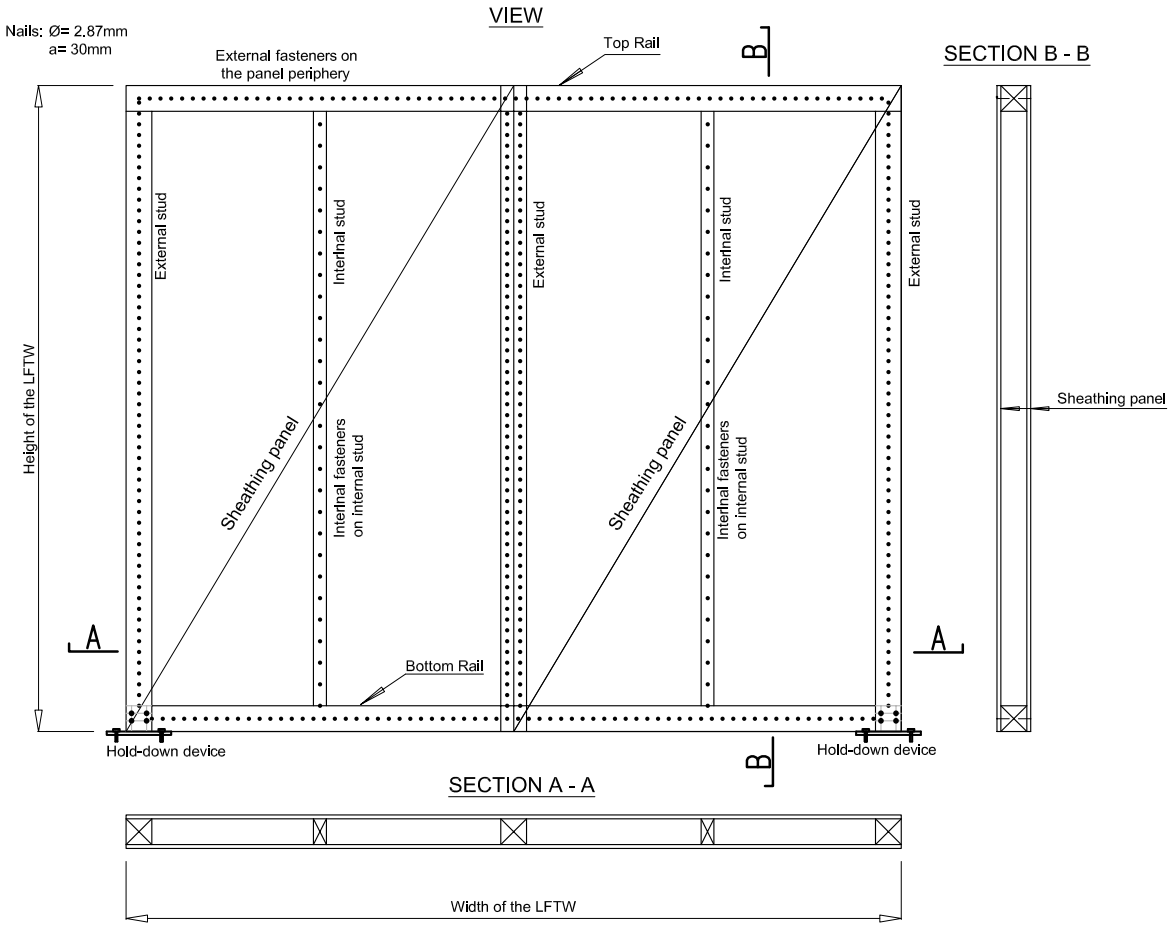

Fig. 1.1: Standard configuration of LFTW

hold-down devices, which are designed to be robust having one, two or three slotted-in steel plates. The sheathing panels (OSB or GFB) are produced in various standard sizes. Thus, the standard panel width determines the distances between the vertical edge and the internal studs. Fasteners are driven through the sheathing material into the timber frame using different spacings. The dimensions of the timber frame depends on the loading level. In this thesis the studs and rails with a strength class of GL24h are considered to have dimensions of $200 \cdot 200[mm]$, $240 \cdot 240[mm]$ or $300 \cdot 300[mm]$. The distances between the fasteners in the external studs for the walls analyzed within this thesis are chosen to be 30 or 35 [mm] for the OSB or GFB panels, respectively. The size of the panel, which defines the distances between the studs, is a multiple of the standardly used panel width, so that, for the wall lengths between 2.4 and 4.8 $[m]$, there is no unnecessary waste of panel material. For multi-storey buildings, the wall elements are vertically stacked, and they are connected using inter-storey steel connectors.

1.4.1 Utilization of LFTWs in the building assembly

Timber structures have been successfully used in Europe for centuries. Over time, various construction solutions have been established, aiming to become standards in the field of timber structures. Although certain similarity in design of timber buildings exists worldwide, some inherently different structural concepts have been developed in the last few decades in Switzerland (see e.g. Figures 1.6, 1.4 and 6.23). Those concepts are a result of increasing technical demands. In order to fulfill different physical requirements, standard timber ceilings with closed box cross sections became composite structures consisting of a timber and a concrete layer. The concrete layer can be added to the timber layer during prefabrication at the factory or it can be poured on-site. Relevant for this thesis is the fact that the slabs with a concrete layer can be considered as rigid bodies able to distribute the lateral loads evenly to the lateral load resisting system. The building presented in Figure 1.2 will be used as prototype building for different purposes. In this Chapter the prototype building is used to introduce all components a typical timber structure consists of. In Chapter 6 the prototype building will be used to enable the derivation of some basic dynamic parameters needed for the parameter study, whereby in Chapter 9 the prototype building will be used to compare force based seismic design (FBD) with the performance based engineering (PBE) approach, as proposed in this thesis.

The typical construction of a LFTW is shown in 2D view and 3D view in Figures 1.1 and 1.3, respectively. From Figure 1.2 it can be seen, that the slabs are conceived as rigid diaphragms. As in the case of traditional timber structures, composite slabs also carry gravity loads monodirectionally. The LFTWs themselves can be constructed as elements which carry both gravity and lateral loads or as elements which exclusively carry lateral loads, see also Figure 1.5. In order to clarify the connection details between the different building elements wall-wall, slab-wall, wall-external beam and anchorage of the wall and columns in the basement, the details are extracted from the structure and the design principles are shown in Figure 1.2 in a 3D view. A solution to how the composite slab could be connected to the load bearing as well as to the load non-bearing walls is presented in Figures 1.6, 1.4, 6.22 and 6.23 . Again, there are a number of possible

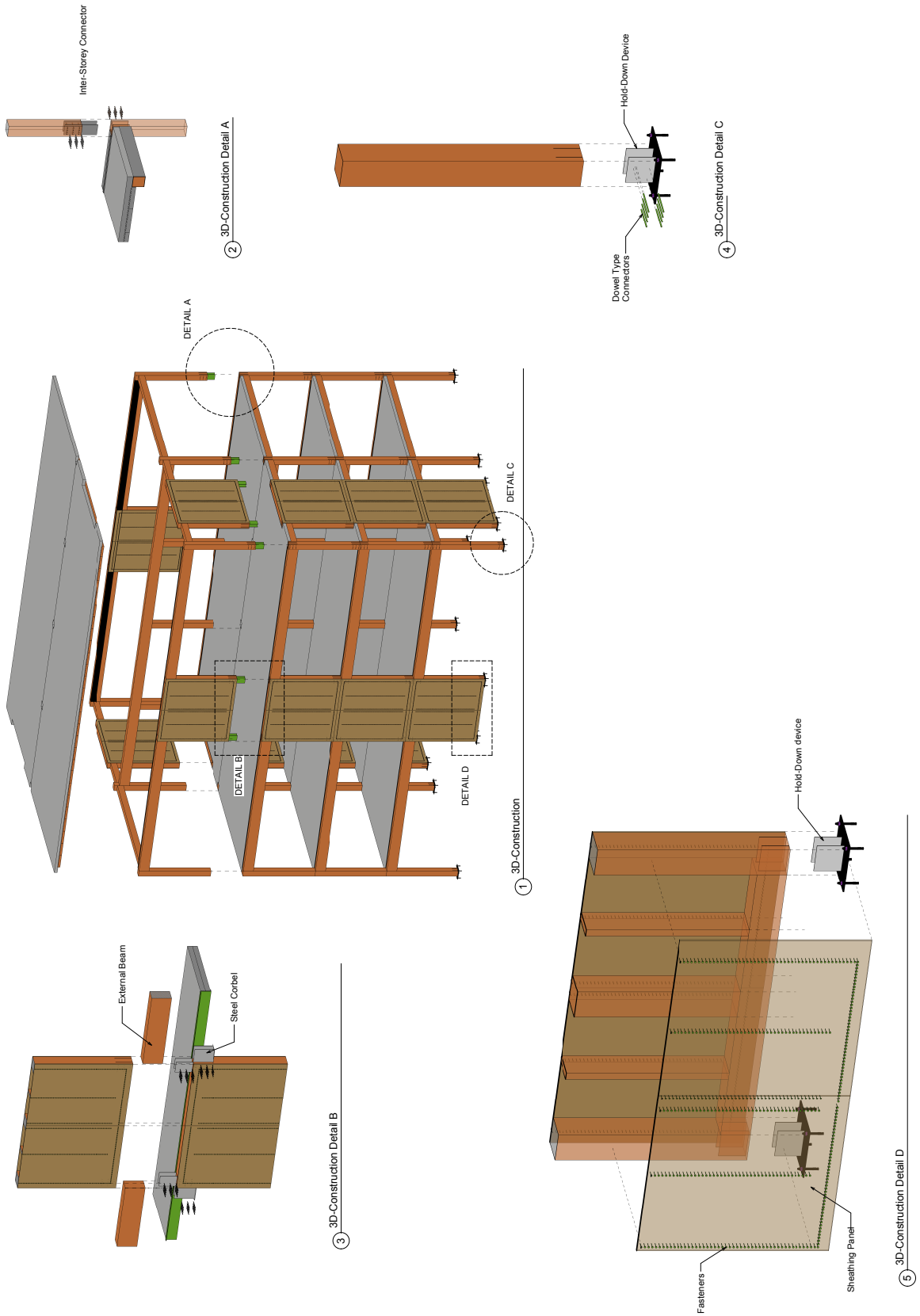

Fig. 1.2: The structure of a prototype building with its components

solutions for each of those details. Some of them are developed specifically for this certain case and some of them are generally accepted by practitioners. The alternative construction details related to the connection of the slabs to the walls as well as design possibilities of hold-down devices and inter-storey connectors are presented in Chapter 6 in more detail.

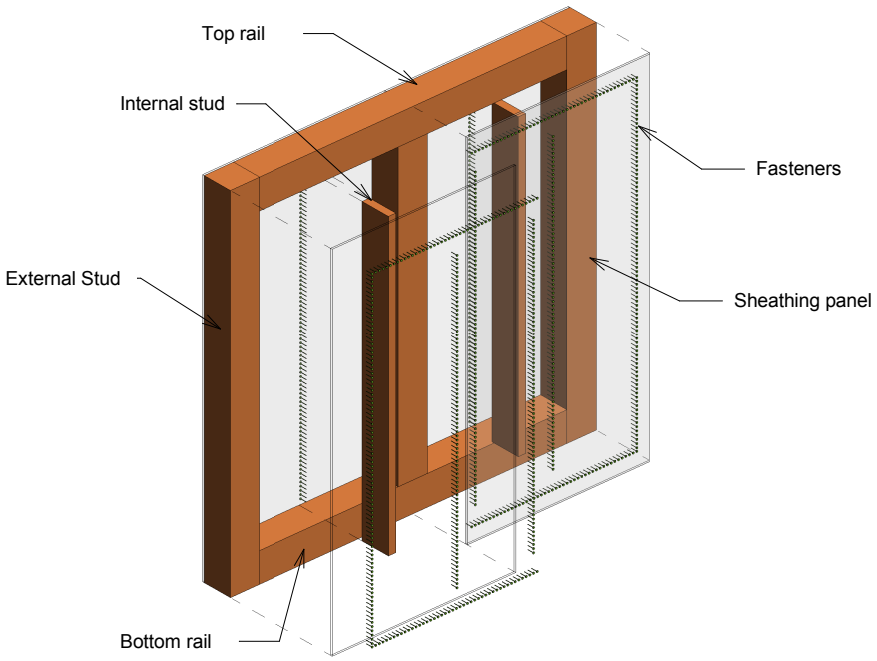

Fig. 1.3: Exploded view of a LFTW

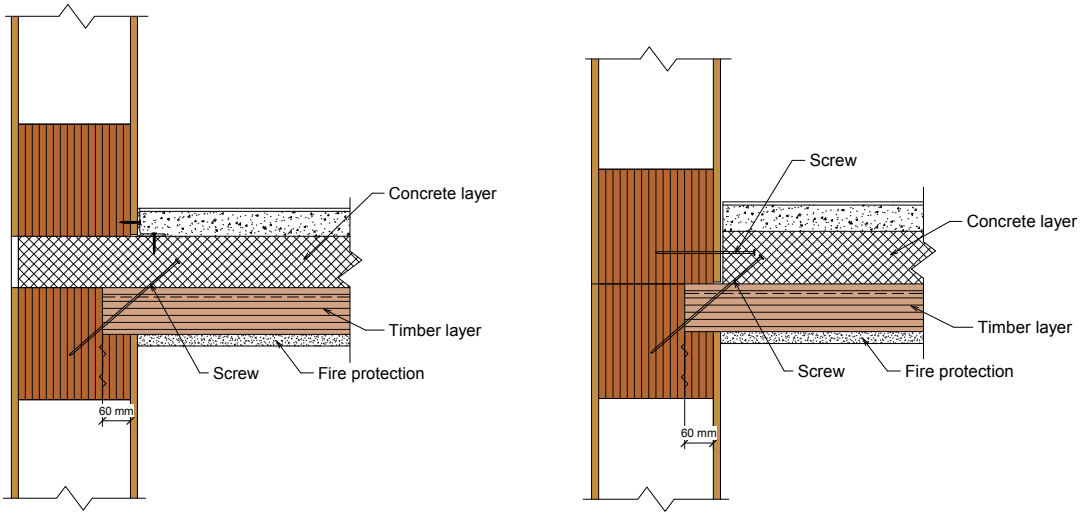

(a) (b)

Fig. 1.4: Common composite slab to bearing wall connections using a support surface comprised of a timber layer and a concrete layer 1.4(a): using a support surface comprised of only a timber layer 1.4(b)

A possible arrangement of the LFTWs are displayed in Figure 1.5.

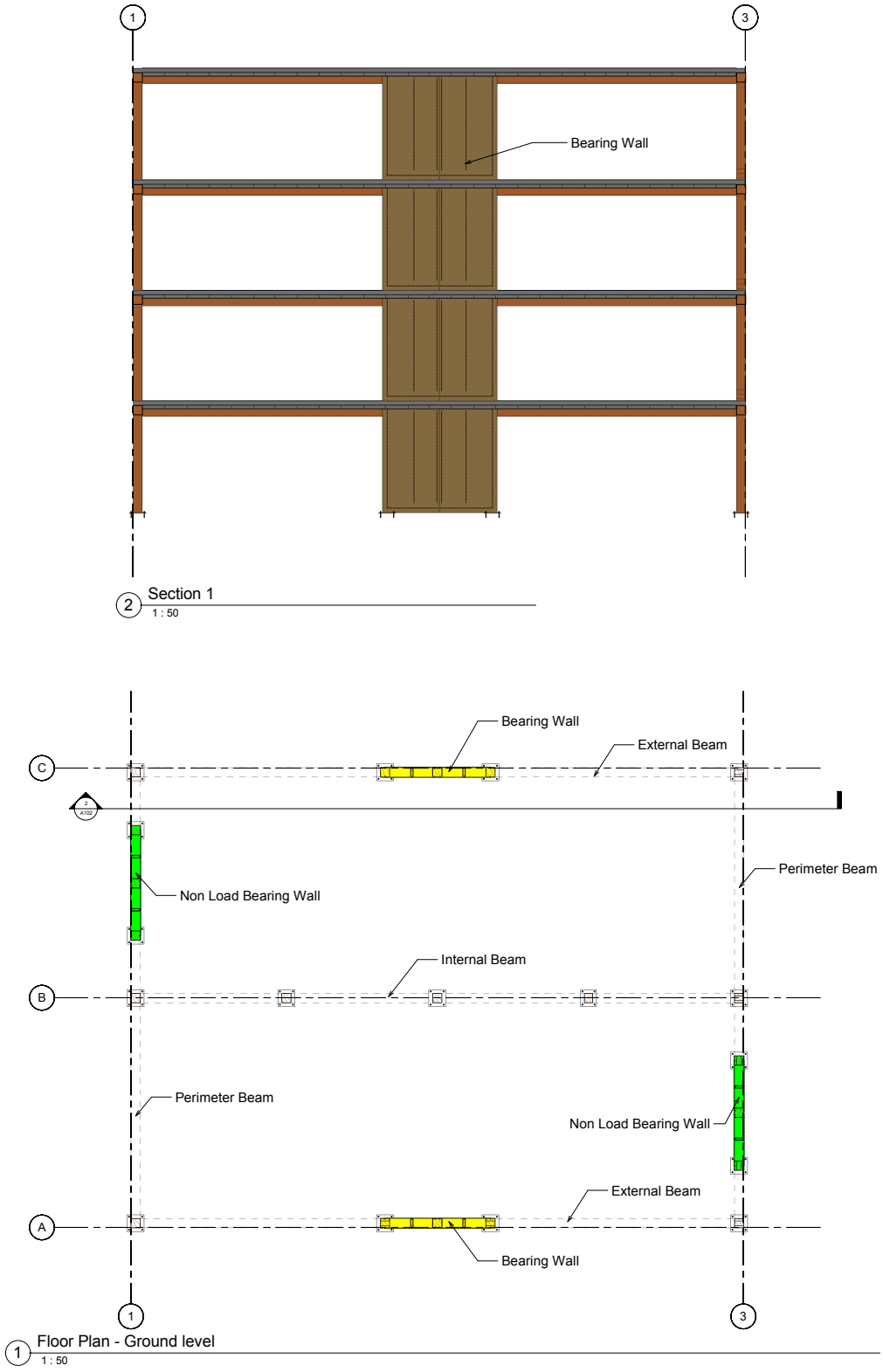

Fig. 1.5: LFTWs disposition in prototype building in plan view

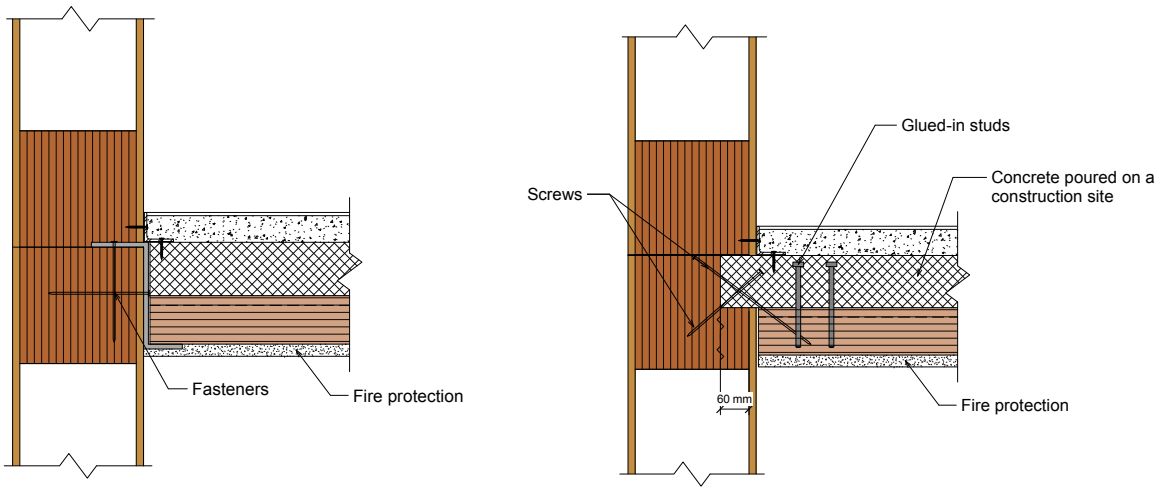

(a) (b)

Fig. 1.6: Composite slab to bearing wall connections using a steel corbel 1.6(a): using glued-in studs 1.6(b)

1.5 Scientific and engineering methodology used in the study

The reliable estimation of the applicability of LFTWs in regions of low to moderate seismicity requires a combination of a powerful mechanical model and an appropriate seismic design philosophy. The mechanical model of the LFTWs used herein is derived using MATLAB-based MCASHEW application developed by Folz and Filiatrault (2002) within the CUREE Project. The mechanical model of a shear wall element is based on the experimental response of a single fastener to cyclic loading. The tests are conducted on fasteners commonly used in standard OSB-timber connections. The established mechanical model, applied to LFTWs, accounts for the strength and stiffness degradation as well as for the pinching effects during the cyclic loading-reloading processes. Due to the difficulties with using a non-linear mechanical model within force based seismic design, the displacement based seismic design philosophy has been selected. Moreover, an extension of the performance based design toward performance based engineering (PBE) has been considered. The damage index (DI) is chosen to be the central performance indicator within PBE. This parameter is assessed using a non-linear time history analysis (NLTHA) within the parameter study performed herein. This approach has been divided into three steps:

- pre-processing to establish the hysteretic rules
- processing to performe the NLTHA, and
- post-processing to asses the fulfillment of the performance objectives.

The procedure used in this thesis is presented in Figures 1.7, 1.8 and 1.9. Finally, the results of the parameter study for the given performance objectives are checked and verified using an

independent, probability-based Incremental Dynamic Analysis approach, presented in Figure 1.10. More details related to the DI and IDA analyses are given in Chapter 4.

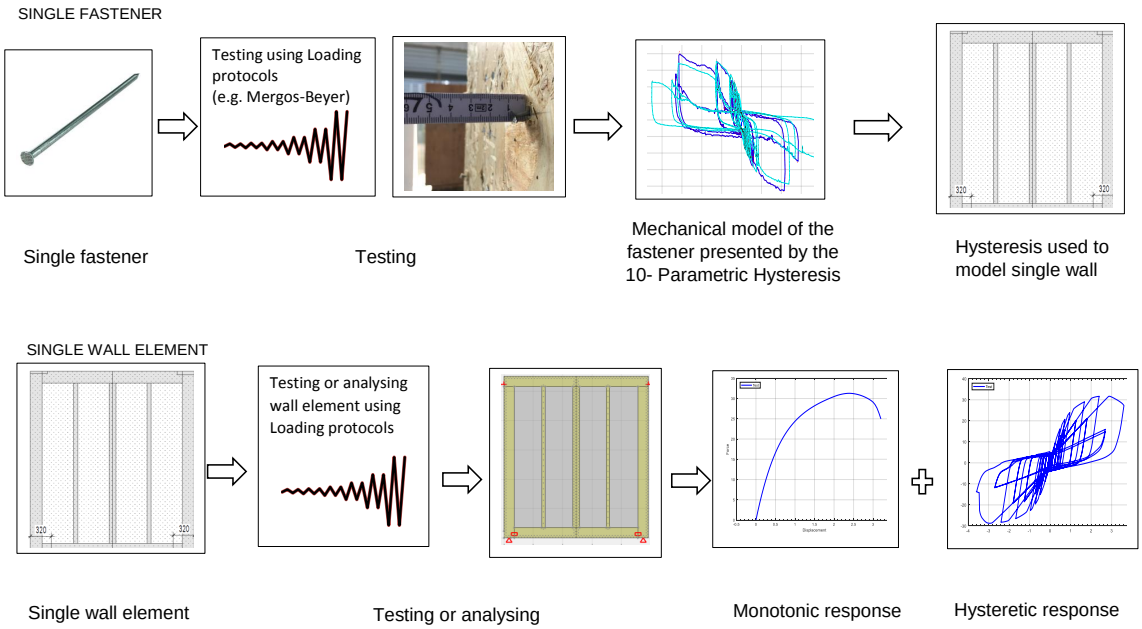

Fig. 1.7: Pre-processing analysis performed within this thesis to estimate cyclic material properties for NLTHA

1.6 Organization of the thesis

The thesis is organized in 10 Chapters.
Chapter 1 describes the motivation, the scope of the investigation as well as the main assumptions and simplifications made for the parameter study.

In Chapter 2, the historical review of the research related to the overall behaviour of the LFTWs under lateral loading is reported. It covers the testing of single fasteners as well as the testing of entire LFTW elements of different configurations under monotonic and reversed cyclic loading, the development of the analytical and numerical models as well as the influence of the type of the loading protocol on the results obtained from the testing of the shear wall elements. Moreover, the state of the art in design of LFTWs exposed to earthquake loading related to the current practice and regulations in the actual Eurocode 5 and Eurocode 8 has been surveyed. The limitations of the current procedures, adopted from Eurocode 8, referred to as force- and displacement-based design have been outlined. The need for improvement of these procedures has been pointed out and commented on. The features of performance based engineering as an alternative to the currently used design practice have been introduced.

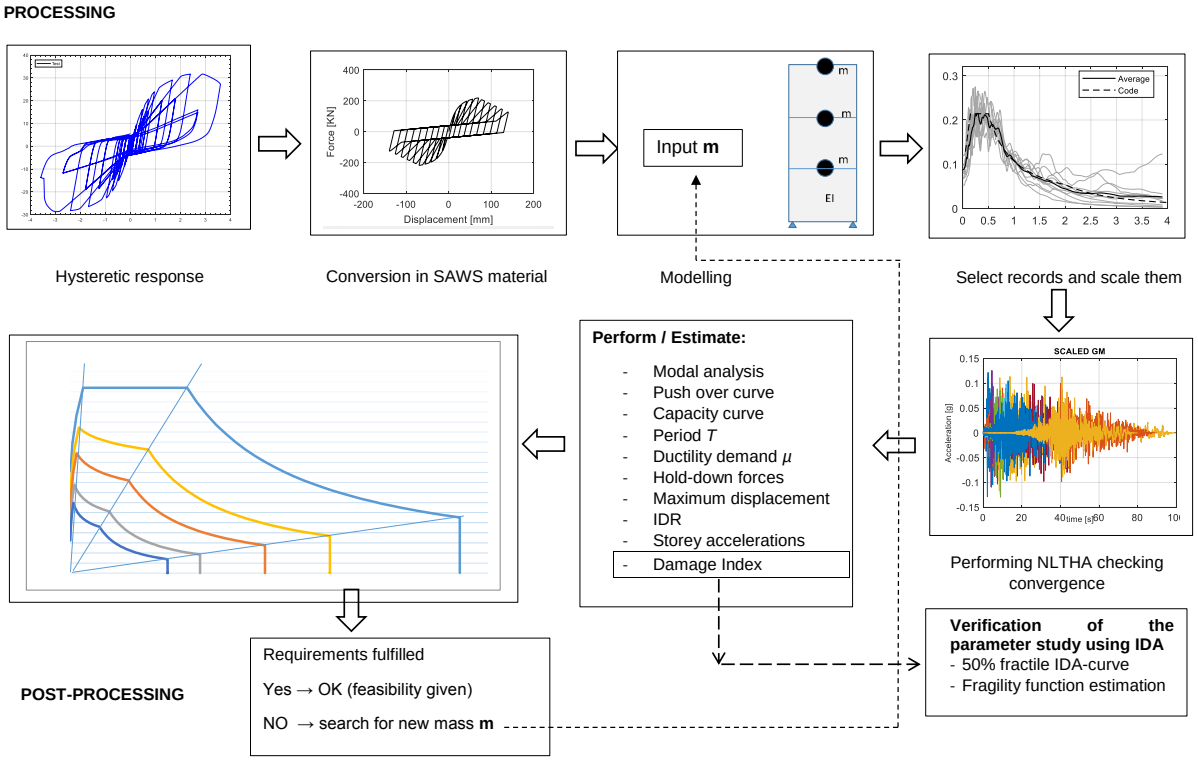

Fig. 1.8: Analysis and post-processing proposed in this thesis in order to check defined performance limit states

The development of the mechanical model of the LFTW element based on simple elastic shear field theory is part of Chapter 3, where the diversity in the functioning principals of the LFTWs is presented. After the functionality of all components of a LFTW has been described, the force-displacement relationship estimated by use of the energy based McCutcheon's approach is introduced. The application of the energy-based approach for estimation of the capacity curve of single and multi-storey structures is shown by means of a simple example calculated by hand. Furthermore, within Chapter 3, the experimental response of the single fasteners, nails and staples, to the cyclic loading is presented. The experimentally estimated, 10-parametric Stewart hysteresis has been fitted in the Matalb-based MCASHEW program and stored in the program library. Using the experimentally derived mechanical model of the single fastener defined by the Stewart hysteresis all LFTW elements have been modelled and analyzed under monotonic and cyclic loading. The numerically obtained response of the LFTW within MCASHEW again was a 10-parametric hysteresis, presented as a mechanical model of the shear wall element used for definition of the SAWS material within the pushover and NLTH analyses. The accuracy of the adopted mechanical model of the single fastener and thus of the entire wall element has been validated with tests on LFTWs sheathed with GFB, and by recalculating the tests carried out in the course of the NRP66 project studying the behaviour of LFTW sheathed with OSB. The mechanical models for nail and staple connectors as well as for LFTW elements with length of 2.4, 3.0, 3.6, 4.2 and 4.8 [m] have been derived and summarized in Chapter 3 for both OSB and

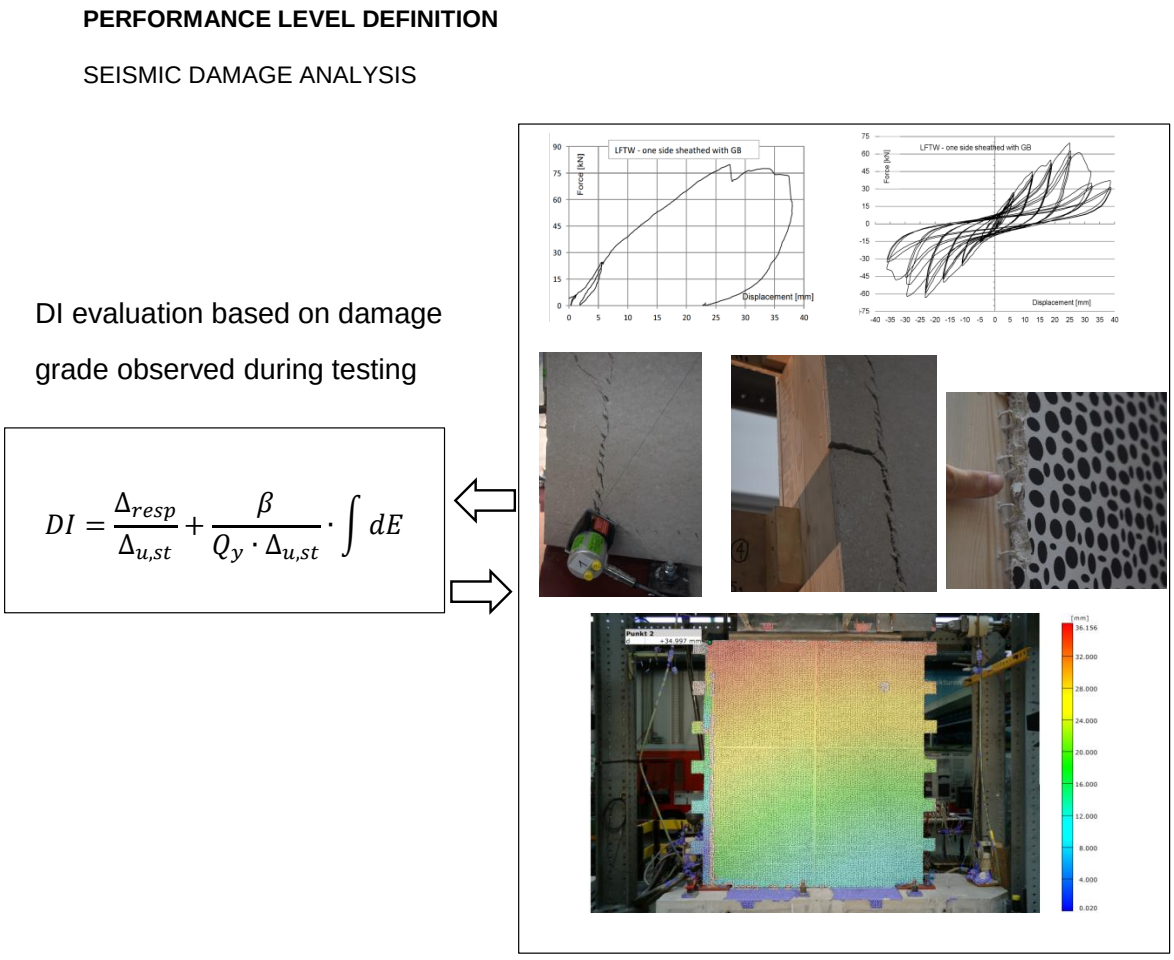

Fig. 1.9: Damage index estimation

GFB sheathing material. These have been used in the parameter study presented within this thesis.

An overview of the methods which are used in this thesis are discussed in Chapter 4. In particular, the link between the methods and the results they provide are specifically indicated. The techniques of selection and scaling of ground motion records, the modelling and the use of NLTHA are addressed.

Since the limit states are not clearly defined in Eurocode 8, a proposal for suitable performance limits for LFTWs sheathed with GFB and OSB panels is made, as presented in Chapter 4. The performance limits within performance based engineering are given in terms of the damage index (DI) analysis. Here, the life safety (LS) limit state damage indexes of $DI \leq 0.8$ and $DI \leq 0.7$ are proposed for LFTWs sheathed with GFB and OSB, respectively. The proposed immediate occupancy (IO), life safety (LS) and collapse prevention (CP) limit states have been verified by combining the results from the incremental dynamic analysis with the seismic demand given by the elastic Response Spectra (RS) for the corresponding hazard level in accordance with the probability of exceedance of 50%, 10% and 2% in 50 years and associated return periods of

VERIFICATION OF THE PARAMETER STUDY

FRAGILITY ANALYSIS

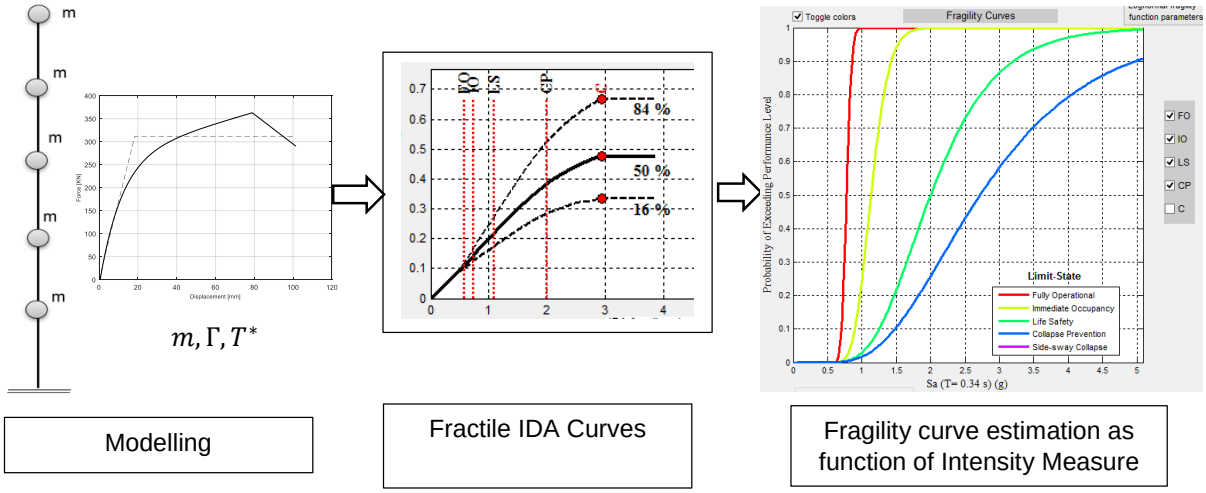

Fig. 1.10: Performance control using fragility analysis

72, 475 and 2475 years, respectively.

In Chapter 5, an overview of the seismic analysis of the multi-degree-of-freedom system used in this thesis is given. The modal and pushover analyses, the capacity spectra concept and the time history analysis are introduced. Finally, the key aspects of Incremental Dynamic Analysis (IDA) are demonstrated.

In Chapter 6, the fundamentals of the parameter study are given. The geometry of the LFTWs and the hold-down devices considered in the parameter study are presented. Furthermore, the handling of the $P - \Delta$ effects, gravity loads, mass distribution, damping, limiting periods of vibration and ductility are demonstrated and justified using the five-storey prototype building as an example.

In Chapter 7 and Chapter 8, the parameter study based on the mechanical model developed and presented in Chapter 3 is described for LFTWs sheathed with OSB and GFB panels, respectively. Within the parameter study, modal, pushover, NLTHA and Incremental Dynamic Analysis (IDA) have been performed. The results are summarized, presented and commented on in a tabular and graphical form.

The efficiency of the PBE used in the parameter study presented in this work is shown in Chapter 9. For this purpose, the wall elements designed with the force-based seismic design method have been re-analyzed applying the PBE- approach. The results are compared and

commented on in Chapter 9.

In Chapter 10, the main contributions of this work have been specified. For the performance of the parametric study, some mechanical models have been estimated by testing, while others have been derived from the work of other researchers. Some topics have not been treated within this thesis. Chapter 10 gives an overview of the topics which could be the subject of a future investigations.

The structure of the thesis is presented in Figure 1.11.

1.7 Summary

In this chapter, the motivation for the investigation related to the behaviour of LFTWs under seismic excitation has been presented. The light frame timber wall (LFTW) as the main subject of the future investigation has been described as a single element and as a part of a building structure. The scientific and engineering methods, intended to be used aside the well known and well established seismic design methods are briefly invoked. Additionally, the main assumptions and limitations of the further parameter study are listed. At the end the organization of the thesis has been shown.

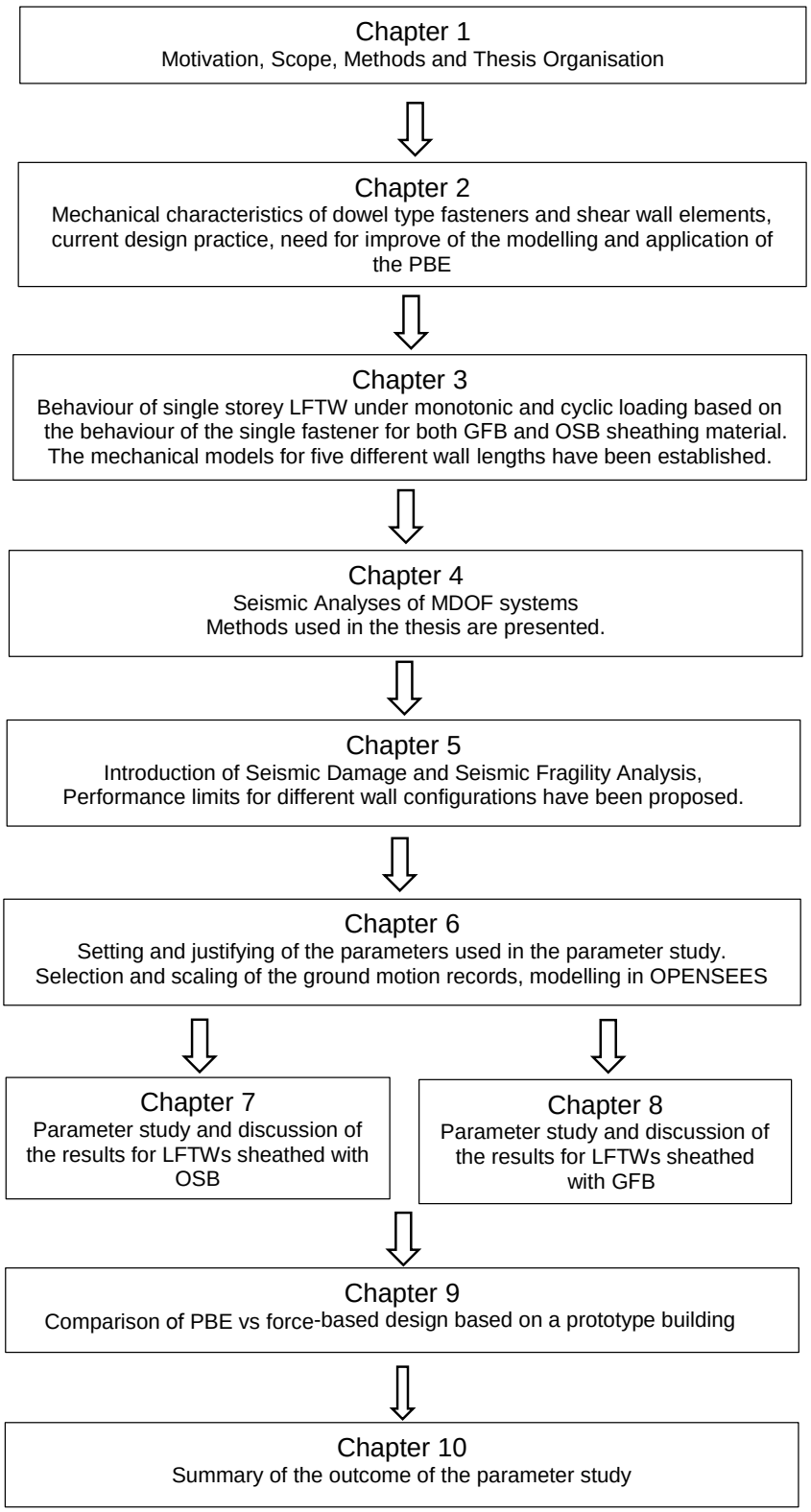

Fig. 1.11: Organization of the thesis

Chapter 2

State of the Art

The review of the state of the art presented herein focuses on the lateral load resting systems in timber structures in terms of their mechanical and dynamic characteristics, numerical modeling and the design practices in Europe.
In this chapter, the historical review related to the development of the analytical asymptotic function for single fasteners in timber connections as well as the efforts to analytically describe the behaviour of LFTWs subjected to lateral loading are presented. The importance of different types of loading protocols to assess the response of a shear wall is discussed. The current seismic design practices using force-based and displacement-based seismic design are reviewed. Finally, the drawbacks of the current design practice, as well as the need for reliable mechanical models combined with an appropriate seismic design philosophy for design of LFTWs are highlighted.

2.1 Mechanical Characteristics

Light frame timber walls (LFTWs), also known as timber shear walls, are the main structural elements in timber structures to resist lateral loads induced by wind and earthquakes. When discussing their mechanical characteristics, we generally address their overall performance under lateral loading. The global response of LFTWs to lateral loading depends on the behaviour of each individual component of the wall composite. The LFTW components commonly used in European construction are: timber frames, sheathing panels, dowel-type fasteners nails or staples and hold-down devices (see Figure 1.1 in section "Standard configuration of LFTWs"). It has been recognized early that timber framing, sheathing material and hold down devices behave predominantly in the elastic range when the structure is properly designed, even in the case of large wall deformations. See for instance, Gupta and Kuo (1985) in [38] and Filiatrault (1990) in [28]. The main contributions to the nonlinear force-displacement relationship of a shear wall element are the distortion deformations of the fasteners.

2.1.1 Mechanical characteristics of connections with dowel type fasteners

Dowel-type fasteners in shear walls are commonly loaded perpendicular to their axis. Their bearing capacity is governed by their mechanical characteristics and bending moment capacity, the embedding strength of the timber and the withdrawal resistance of the dowel. A basic mechanical model of the bearing capacity of a single fastener has been introduced by Johansen (1949) [46], and an extended model has been proposed by Meyer (1957) [68], incorporating different timber member thicknesses, and plastic instead of elastic bending capacity of the fastener. This modified Johansen's model has been implemented in Eurocode 5 [2].

Based on Johansen's model, only the peak strength of a dowel-type fastener in a timber connection can be estimated. No additional information, such as the force-deformation beahviour can be obtained. However Foschi [34], proposed a nonlinear asymptotic force-displacement curve (Equation 2.1), displayed graphically in Figure 2.1.

$$f_{fast} = f_0 + r_1 \cdot k_0 \cdot \delta \cdot [1 - e^{\frac{-k_0 \cdot \delta}{f_0}}], [N] \tag{2.1}$$

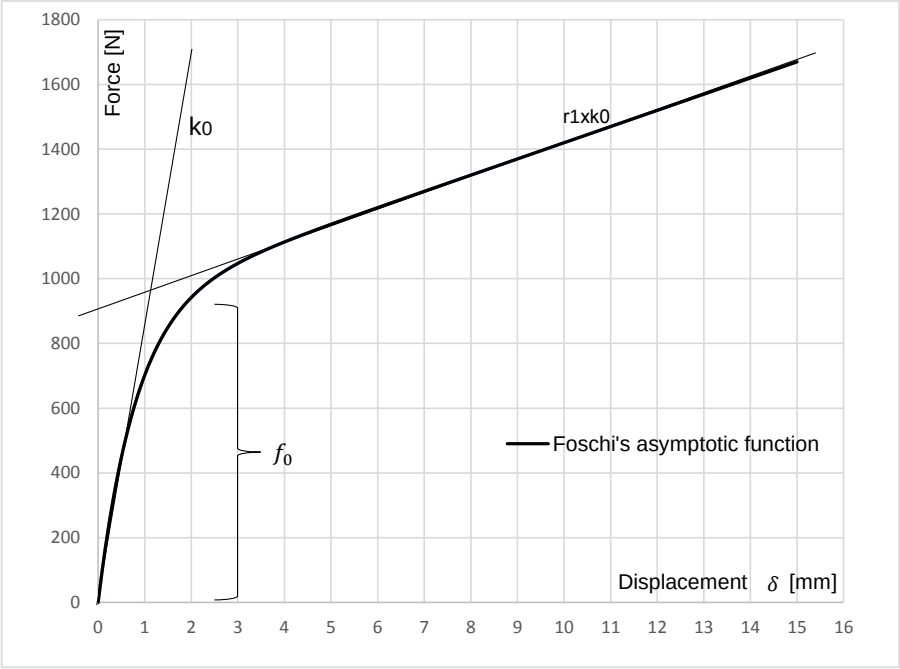

Fig. 2.1: Foschi's asymptotic function [34] to model force-displacement relationship of a dowel type fastener in timber connection

The asymptotic curve describes the force as a function of the fastener displacement. It depends on the initial and post-yielding stiffnesses, k_0 and k_1. As shown in Figure 2.1, Foschi's function has no limitation. Although Foschi's function is capable of describing a non linear fastener's response, it does not cover the entire response range of the fastener in a real connection. Dolan and Madsen (1994) have modified Foschi's function by introducing a maximum displacement $\delta_{max} = 9.0[mm]$, determined from experimental testing of dowel-type fasteners.

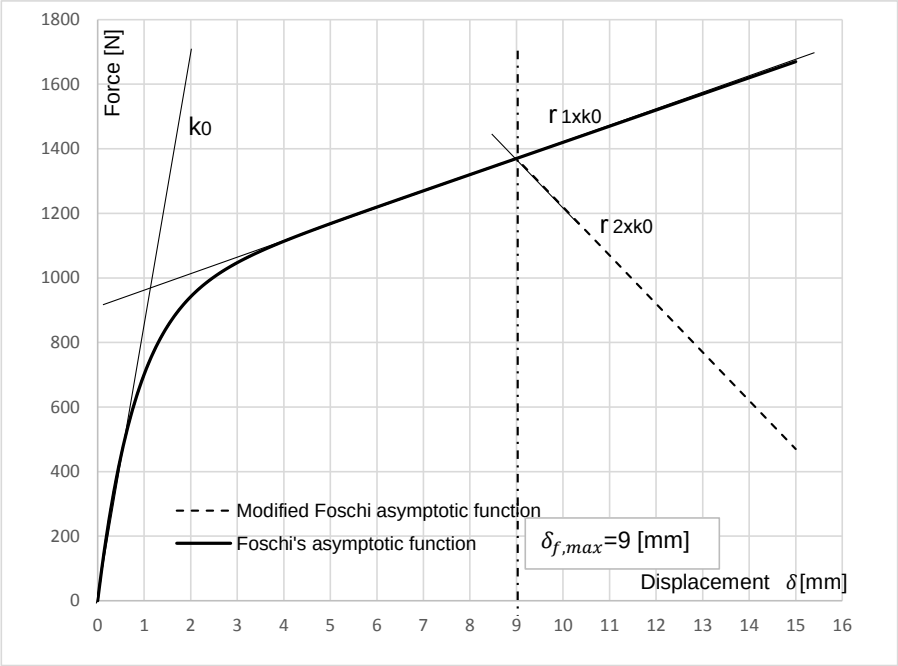

Fig. 2.2: Foschi's asymptotic function modified by Dolan-Madsen

Their complete force-displacement relationship, presented in Figure 2.2, can be written as follows (Equation 2.2):

$$f_{fast} = \begin{cases} f_0 + r_1 \cdot k_0 \cdot \delta \cdot [1 - e^{\frac{-k_0 \cdot \delta}{f_0}}] & for \quad \delta < \delta_{max} \\ r_2 \cdot k_0 \cdot \delta + (f_{max} - r_2 \cdot k_0 \cdot \delta_{max}) & for \quad \delta_{max} < \delta < \delta_{ult} \\ 0 & for \quad \delta > \delta_{ult} \end{cases} \tag{2.2}$$

Jorissen (1998), [47], has extended the bearing capacity model for single dowel connections to multiple fastener connections. He has proposed reduction factors for calculating the bearing capacity of multiple-fastener connections. However, this does not apply to structures subjected to lateral forces because no reduction in bearing capacity has been observed here. See Salenikovic (2000) [84] and Bernasconi (2016) [69].

The cyclic behaviour of dowel-type fasteners has been investigated by Stewart (1987) [92] and Dolan (1989) [22], not only on single dowel connections, but also on full-scale shear wall specimens, subjected to monotonic- and reverse-cyclic loading and shaking table excitations. It was reported that the failure mechanism of the connection was fastener withdrawal out of the timber frame under monotonic loading and fatigue failure under cyclic loading. The response of the dowel-type connection to cyclic loading was typically hysteretic, as presented in Figure 2.3.

2.1.2 Mechanical characteristics of the shear wall element

For shear wall analysis, an analytical or numerical model is required. Often, laboratory tests on shear walls subjected to lateral loads, have been carried out in order to calibrate different

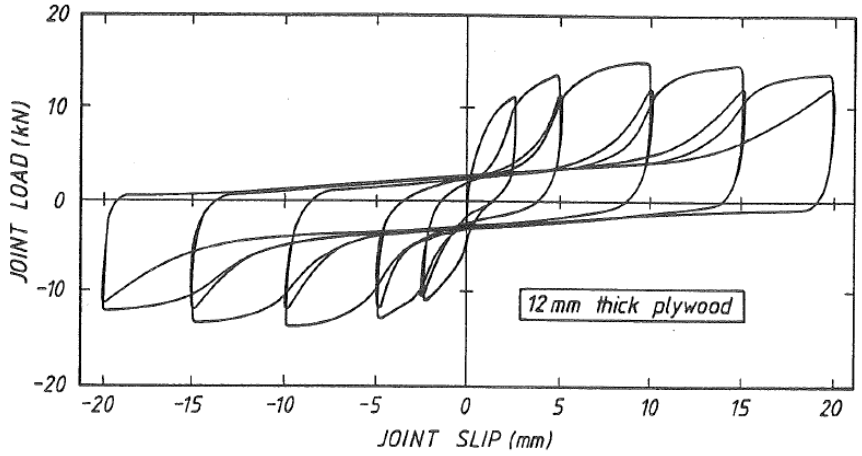

Fig. 2.3: Typical hysteretic dowel-type fastener response to cyclic loading, reported in [92]

analytical and numerical models. The response characteristics, such as stiffness, strength, displacement capacity, ductility factor, loss of stiffness, pinching effects and energy dissipation, are obtained as a result of monotonic and cyclic testing of single-storey wall specimens with varying size and configurations. However, during the last decade, multi-storey walls and even complete buildings have also been investigated under monotonic and artificially generated earthquake excitations. Moreover, comprehensive shake table tests have increasingly been performed.

Monotonic tests were mainly conducted in the 1960′s. Various researchers, including Neisel (1956) [73], Countryman (1952) [14] and Currier (1956) [15], have investigated the global behaviour of shear walls under monotonic loading. The general finding was that the wall stiffness and strength depended on the fasteners spacing and strength. The strength was found to be proportional to the wall length. It was also reported that the anchorage strength has significantly affected the wall strength.

The first cyclic testing was reported by Madearis (1966) [65]. A ductile failure mode was observed and the wall specimens exhibited horizontal displacements of up to 50 [mm], with an average of approximately 45 [mm].

By introducing 10 independent parameters, which describe the response of the shear wall element to cyclic loading, Stewart (1987) has created the basis for the development of a nonlinear spring element, capable of accounting for the initial stiffness, strength and stiffness degradation during cyclic loading, the pinching effects and the energy dissipation. His hysteretic rule was fitted to test results and implemented in a FE-program for nonlinear time history analysis, called RUAUMOKO (1994).

Dinehart and Shenton (1998), see [21], compared wall performance under monotonic and cyclic loading in 12 shear wall tests. They reported that the failure modes under static and cyclic loading were very different, and characterized by the pulling of the sheathing from the frame in the monotonic tests and fatigue failure of the fasteners in the cyclic loading tests. The

ductility observed in the cyclic tests was by 34-42% less then ductility observed in the monotonic tests.

Figure 2.4(a) shows a typical response due to monotonic (Wall 3) and cyclic loading (Wall 4 and Wall 5) obtained by testing. Nowadays, one can estimate the response of LFTWs using numerical analysis. The Figures 2.4(b) and 2.5 show exemplary the results of the numerical analyses of the Walls W3 and W4, tested in the course of the NRP 66 project.

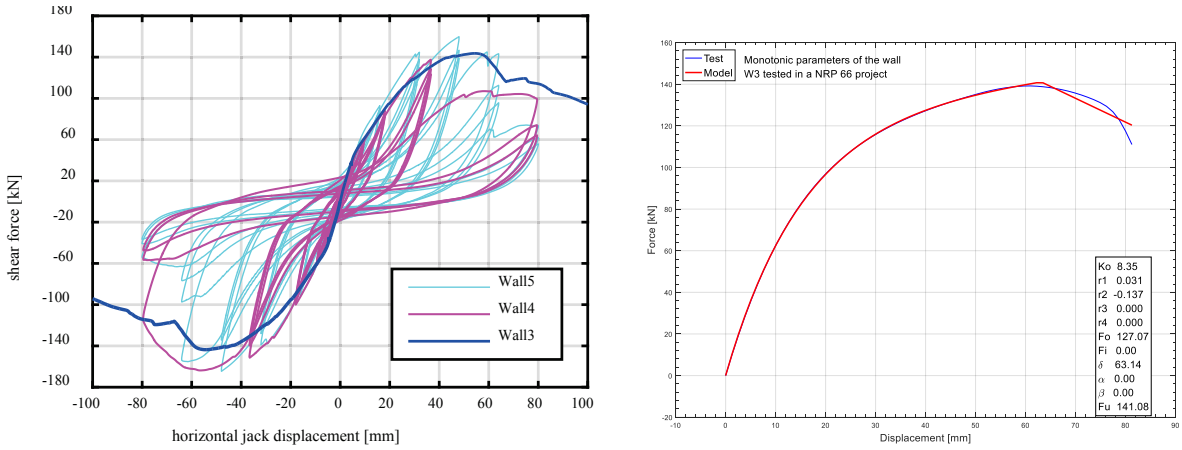

(a) (b)

Fig. 2.4: Response of the wall tested under monotonic and cyclic loading in the course of the NRP 66 project after [58], 2.4(a): Numerically obtained response of wall W3 to monotonic loading 2.4(b)

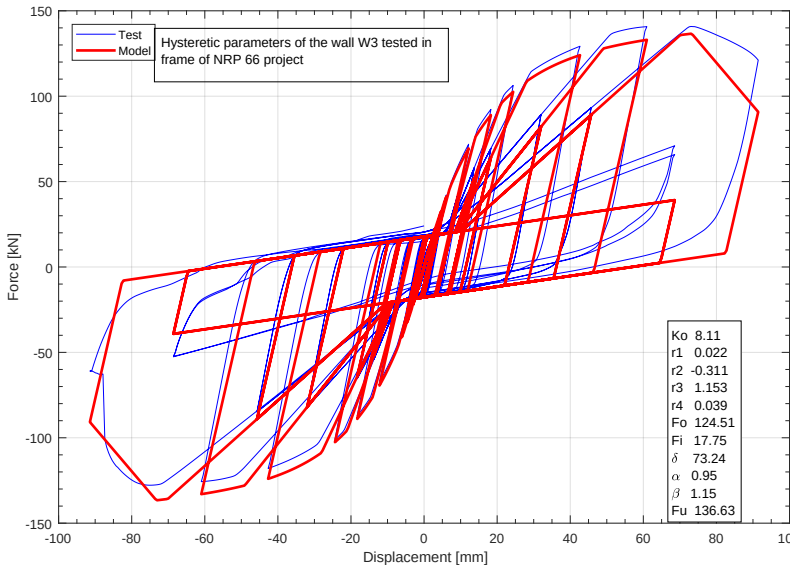

Fig. 2.5: Numerically obtained response of wall W3 to cyclic loading

The first cyclic tests conducted on timber shear walls led to the following conclusions:

- the wall stiffness depends on fastener size, fastener spacing and thickness and the type of sheathing material
- the strength depends on the fastener size, length and spacing
- the ductility depends on the ratio between the fastener diameter and the sheathing thickness
- the failure mechanism observed is ductile and related to the connection failure: pullout of the fastener under monotonic loading or fatigue failure of the fastener due to cyclic loading

As one can see from Figures 2.4(b) and 2.5, the mechanical characteristics of the timber shear wall can be described by six or ten parameters, for monotonic or cyclic loading, respectively (see also Table 2.1).

2.1.3 Analytical and numerical modeling

Each analytical or numerical model which describes the behaviour of a timber shear wall must be verified by tests. The testing is often cumbersome and expensive. For economical reasons, the complex and highly nonlinear behaviour of a timber wall element should be described by an appropriate analytical or numerical model.

In [94], Tuomi and McCutcheon proposed an analytical model considering the strength and spacing of the fasteners and the wall geometry. Gupta and Kuo proposed an analytical model which allowed for better consideration of the framing deformation within the wall composite [38]. In [61], McCutcheon proposed an energy-based method, which described the single-fastener forces in terms of the wall deflection. Patton-Mallory and McCutcheon in, [81], modified this method by developing an asymptotic equation for the fastener strength $f_{u,as}$ in terms of fastener distortion δ_n, according to the Equation 2.3.

$$f_{u,as} = \frac{A_0 \cdot \delta_n}{B_0 + \delta_n} \tag{2.3}$$

Although relatively simple, Equation 2.3 predicts the response of the shear wall subjected to lateral load reasonably well. A_0 and B_0 are constants that account for the load-deformation relationship of the fastener . $B_0 = 1$ produces a linear fastener response and $B_0 = 0$ produces a perfectly-plastic fastener response. Equation 2.3 is derived by equating the internal energy due to fastener distortion with the external energy. The external energy results from the external racking load and the displacement due to the fastener slip Δ_n. Subsequently, the racking external force F_{wall} can be expressed as a function of the fastener force, represented by A_0 and the geometric constant K_f, which depend on the location of each single fastener on the panel periphery.

$$F_{wall} = A_0 \cdot \sum \frac{K_f^2 \cdot \Delta_n}{B_0 + K_f \cdot \Delta_n} \tag{2.4}$$

As the fastener slip increases, the fastener force approaches the asymptotic ultimate strength $f_{u,as}$ and the corresponding racking force F_{wall}, approaches the ultimate value $F_{R,wall}$.

First, the constant B_0 was defined as the fastener slip at $50\% f_{u,as}$ and later it was replaced by Patton-Mallory and McCutcheon in [81] by $1.5\delta_{f,s}$, where $\delta_{f,s}$ is the fastener displacement at service level.

Dolan (1989) and Foschi (1974, 1991) started developing numerical FE-models by carrying out monotonic and cyclic tests. It was concluded that the cyclic hysteresis followed the monotonic envelope, and this fact was used by Folz-Filialtrault (2002) [32] to develop a hysteretic model, which can reproduce the fastener response under general cyclic loading.

The hysteretic model is essencially the previously mentioned modified Stewart hysteresis implemented in the FE-programs developed for shear wall analysis within the framework of the CUREE CalTech project (referred to as CASHEW [32]). Figures 2.4(b) and 2.5 present the results of the numerical monotonic and cyclic analyses of shear wall W3 tested in the framework of the NRP 66 project [37] using the CASHEW program. Judd proposed an oriented pair of coupled nonlinear spring elements [48] as an improvement to the orthogonally oriented nonlinear spring elements used in [32]. Numerical models have also been developed for 3D structures (see, e.g. [29]).
The physical meaning of the parameters used in [32], which define the numerical response of the shear wall under monotonic and cyclic loading, are summarized in Table 2.1.

Tab. 2.1: Physical meaning of the parameters which define monotonic and cyclic response of a shear wall in accordance with Figures: 2.4(b) and 2.5

Parameter	Description
K_0	initial stiffness
R_1	asymptotic stiffness expressed as percentage of the initial stiffness K_0
R_2	stiffness of decreasing branch of the monotonic force-displacement relationship as percentage of the initial stiffness K_0
R_3	unloading stiffness after each cycle as percentage of the initial stiffness K_0
R_4	reloading stiffness, as percentage of initial stiffness K_0, according to partial loss of the connection between the fastener and the surrounding wood
F_0	intersection point between asymptotic line and force axis
F_i	intersection with the force axis by passing through zero displacement during reloading process, reflecting the pinching effect
Δ_{max}	maximum displacement corresponding to maximum force
α	parameter which controls the degree of stiffness degradation
β	parameter which controls the degree of stiffness degradation related to the previous cycle

2.2 Loading Protocols

It is worth mentioning that, cyclic loading protocols were not standardized in the 1980s and a variety of loading protocols have been in use until the CUREE loading protocol was established in 2001 [54].

In [35], Gato and Uang (2003) investigated the effects of the monotonic, CUREE Caltech standard, the CUREE standard near-fault NF, the ISO 1998 and the sequential phased displacement SPD loading protocols. They found that the cyclic response of the woodframe shear walls strongly depended on the applied loading protocol. The CUREE loading protocol produced a wall peak strength that was comparable to that of the monotonic tests, though an average of 16% reduction in strength was observed under cyclic loading. Hence, a hysteretic rule is required for proper modelling of a structure, using data attained from cyclic tests. The ISO protocols have been found to be conservative despite their simplicity. The SPO loading protocols have been found to be inappropriate for LFTW testing. The CUREE protocol has been suggested to be the standard for future cyclic testing of timber shear walls. At the same time, the ISO 21581 monotonic and cyclic loading protocols have been used extensively in Europe. Since the loading protocols are intended to reflect the cumulative damage inflicted during an earthquake event, all of the loading protocols mentioned above, which represent the cumulative damage in regions of high seismicity, are not appropriate to represent the cumulative damage in regions of low and moderate seismicity. In [67], Mergos and Beyer (2014) have developed a procedure for constructing loading sequences for regions of low and moderate seicmicity. Among the different materials and types of structures for which the protocols have been proposed, there is also a proposal for timber shear walls. The Mergos-Beyer loading protocol is new and not widely used yet in Europe, but it has potential to be increasingly applied for research purposes, especially in Switzerland. Within the scope of this thesis, in addition to performing monotonic tests, the Mergos-Beyer loading protocol will be used for hysteretic parameter estimation for both a single fastener and an entire wall element. Additionally, for comparison purposes, hysteretic wall parameters will be estimated using results from tests with the CUREE cyclic loading protocol.

2.3 European Design Practice

The general rules for estimation of seismic actions as well as for design and detailing related to the lateral load resisting systems of buildings are covered by the Eurocode 8 (EC8) provisions. The intention of EC8 is to protect human lives and mitigate building damage for certain seismic hazard levels. Moreover, it is aimed at designing structures so that their behaviour under seismic excitation is more predictable and controlled. To achieve this goal, several design approaches have been prescribed in the EC8 provisions. Force based seismic design (FBD) is most often used in engineering practice. It appears either as an equivalent static lateral force approach or as an approach based on elastic and inelastic response spectra. The performance based seismic design (PBD) implemented in EC8 is based on the N2 method proposed by Fajfar at al. in [27]. The N2 method requires estimation of a pushover curve. When converted into a response

spectra format, the push over curve is also referred to as a capacity curve. Moreover, the N2 method requires estimation of inelastic response spectra, so that the pushover (capacity) curve and the spectral demand curves can be superimposed and graphed in the same diagram. In order to do so, both curves must be in the same Acceleration Displacement Response Spectra (ADRS) format. In EC8, the specific rules for timber structures are given briefly in section 8.

2.3.1 Force based seismic design

Force based seismic design has been extensively used in earthquake engineering for decades. In this short review, the focus is on the response spectrum approach that is most often used for the design of timber structures. The design process, implemented in EC8 [1], is sketched in Figure 2.6. This approach and its problems are addressed here. The force based design process begins with the development of a linear-elastic structural model, which represents the structure in its initial undamaged state. The initial stiffness of the real structure represented by this model must be known at onset of the design process. This is due to the fact, that initial stiffness is directly linked to the fundamental vibration period and, hence, with the imposed earthquake forces. However in a typical design approach, the proportioning of all structural members is a final step occurring at the end of the analysis process.
The initial stiffness assumption is then used in a modal analysis to determine the natural vibration periods and associated mode shapes of the structure. Because the initial stiffness/ fundamental period is not known in advance, it must be estimated by using rules of thumb or approximation tools. For example the Rayleigh method is capable of determining vibration periods with reasonably good accuracy, (see e.g. Chopra (2007) [9]) even for roughly assumed vibration shapes and approximately calculated displacements, arising from equivalent lateral static forces.
The next specific problem related to the FBD is the estimation of the structural ductility, μ which is necessary to determine a behaviour factor q. The behaviour factor q is a reduction factor mutually dependent on the ductility and vibration period. It accounts for amount of energy dissipated throughout the whole structure due to inelastic deformations.

In EC 8, Part 8, specific rules for timber structures and a range of behaviour factors are given based on the design concept and ductility class (low capacity to dissipate energy - dutility class DCL; medium capacity - DCM; high capacity - DCH) and on type of structure. The behaviour factors, listed in Table 8.1, range from $q = 1.5$ for ductility class DCL to $q = 5$ for nailed wall panels with ductility class DCH.

It is difficult to estimate the behaviour factor of timber shear walls, which exhibit deformations in the inelastic range even in case of small displacements. The difficulty to estimate the behaviour factor exists even in the case of walls with the same structural system and/or the same material. This has been analyzed in more detail by Prestley, Calvi and Kowalski (2007) in [83].

After assuming an initial stiffness, determining an initial vibration period and estimating the structural ductility and behaviour factor, the next step in the FBD employs a response

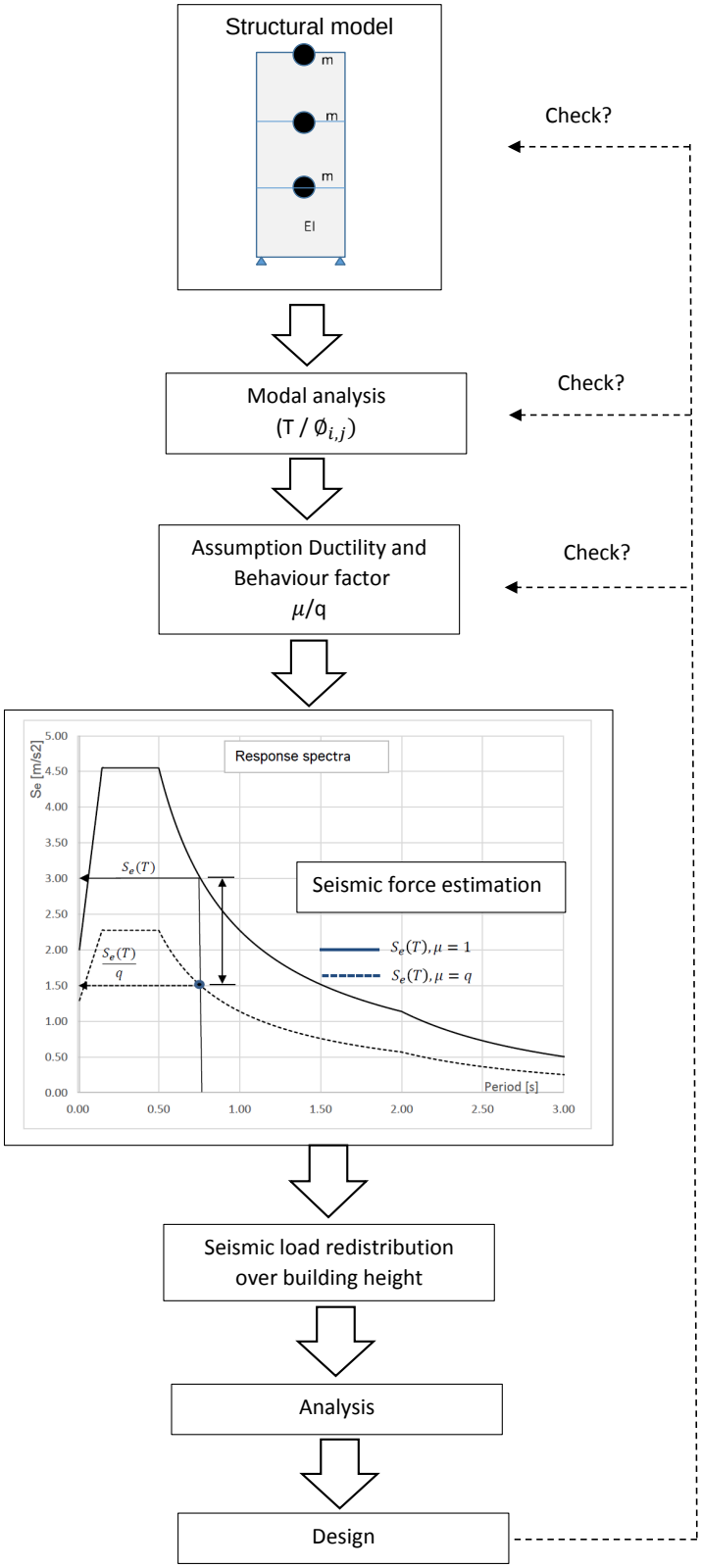

Fig. 2.6: Force based design procedure according to EC8 [1]

spectrum to determine the spectral acceleration and thus, the seismic forces. The structural model is then reanalyzed using these seismic forces and the structural elements are materialized and dimensioned based on the results. The new design must be compared with the initial stiffness estimation and when there is discrepancy, as will usually be the case, the entire process must be repeated. In summary, the drawbacks of FBD include:

- the stiffness and hence, the fundamental period of vibration must be assumed in advance
- the ductility is generalized for structural types and materials
- the behaviour factor, which is difficult to determine, accounts for both, energy dissipation and overstrength in one single value
- an iteration necessary to check the initial assumptions is usually neglected in the design practice

To make the drawbacks of the FBD more transparent, a timber shear wall element, designed in [6] by means of FBD, will be compared with the design results based on both non-linear time history analysis (NLTHA) and performance based seismic engineering (PBD) as well as incremental dynamic analysis IDA. This topic is discussed in more detail in Chapter 8.

2.3.2 Performance based design

In contrast to FBD, which is based on linear-elastic structural analysis, performance based seismic design requires nonlinear structural models. As mentioned before, performance based design has a great advantage by representing the system capacity and seismic demand in the same plot. This makes the approach more transparent, clear and attractive as presented in Figure 2.7. In performance based seismic design, usually a lateral monotonic load pattern, consistent with the first mode shape, is applied to a multi-story building. EC8 requires that the structure is then "pushed" to at least 150% of the displacement demand. This thesis follows the recommendations of Park (1989), [78], where the structure is pushed beyond its peak force capacity to the point where 80% of the peak force capacity remains. The resulting force-displacement plot generated is called a pushover curve. This pushover curve is than converted into capacity curve that represents an elastic-perfectly plastic force-displacement relationship of an equivalent single degree of freedom system (SDOF). It is characterized by the initial elastic stiffness, the yield strength and yield point. The displacement demand is defined by the intersection point between the initial stiffness of the equivalent SDOF system and the elastic response spectrum.

This method is not capable of taking into account the energy dissipation and cyclic loading effects. Since the pushover analysis is based on the assumption that a structure predominantly vibrates in its fundamental mode, the displacement shape is time independent. Moreover, the method cannot account for the higher mode shapes without additional efforts. This method uses the equal displacement rule to estimate the displacement demand for medium and long period structures. However this rule does not apply for structures with hysteretic loops, pronounced pinching and significant strength degradation effects, such as timber shear walls. Although,

different analytical models describe the nonlinear force-displacement relationship of a single storey shear wall (SDOF) with sufficient accuracy, even experienced analysts have difficulty estimating the nonlinear force displacement curve for multi-storey buildings (MDOF) through out the whole displacement range. Therefore, the models of multi-storey structures are often simplified and represented by an equivalent elastic system, which is unable to achieve accuracy required. A model of an equivalent elastic system is typical not only for hand calculations, but also for the majority of commercially used FE-programs. These programs do not involve uniaxial nonlinear spring elements needed for accounting for monotonic or orthogonally oriented coupled spring elements needed for accounting for cyclic loading. In order to explore this subject, a simple $2.4[m] \cdot 2.4[m]$ wall element, sheathed on both sides using nail fasteners spaced at $30[mm]$, has been modeled in SAP2000. Each nail was represented by a non-oriented pair of nonlinear spring elements, which were assigned to follow a hysteretic loop. Due to the large number of degrees-of-freedom arising from each single fastener considered in the model, a long time period was required to perform the calculation, even for such a simple model. If time history analysis had been performed, the results could not have been generated. Therefore, for this thesis, the OPENSEES platform has been used for the analyses, which allows for analyzing of nonlinear models exposed to earthquake loading.

Performance requirements and performance limit states according EC8-Part 1

According to Eurocode 8, each structure shall be constructed in such a way that two specific requirements can be met with an adequate degree of reliability:

- the no-collapse requirement and
- the damage limitation requirement.

The no-collapse requirement is associated with a design values of ground accelerations with a probability of exceedance of 10% in 50 years, corresponding to a return period of 475 years. According to the recommendation given in the code, the damage limitation requirement is associated with a probability of exceedance of 10% in 10 years, corresponding to a return period of 95 years.

In order to satisfy the fundamental requirements listed above, the following limit states should be checked:

- the ultimate limit states and
- the damage limitation states.

The ultimate limit states are associated with failure or collapse of a structure, whereas the damage limitation states are associated with exceeding certain serviceability requirements (see [1]).

The performance and compliance criteria given in EC8 do not specify in detail the displacement limits or expected amounts of damage associated with specific performance stages.

Specifying performance and compliance criteria is a matter of the engineer′s understanding and judgement. An indicator of displacement magnitude associated with performance limit states suggested for woodframe structures could be, for example, FEMA 356, where the prescribed drift limit for life safety limit state is 2% (PoE 10% in 50Y) and for immediate occupancy, it is 1% (PoE 50% in 50Y). Within this thesis, the performance limit states will be estimated for both OSB and GFB sheathing material, based on damage analysis considering nonlinear shear wall behaviour under monotonic and cyclic loading, and verified using incremental dynamic analysis (IDA).

Remarks on Eurocode 8-Part 3: Assessment and retrofitting of buildings

The Eurocode 8 - Part 1, dealing with general rules, and Part 3, dealing with assessment and retrofitting of existing buildings, have been approved in 2004 and 2005, respectively. The adoption of Part 3 led to some confusion because the section "Fundamental requirements", introduced the following three limit states for the first time, namely: Near Collapse (NC), Significant Damage (SD) and Damage Limitation (DL). However the code also recommends that "...The National Authorities decide whether all three Limit States shall be checked, or two of them, or just one of them... " Additionally, EC8 - Part 3, states that the appropriate level of protection is achieved by selecting corresponding return periods for each of the limit states. The Damage Limitation limit state corresponds to a return period of 225 years, and a probability of exceedance of 20% in 50 years. However, for the same limit state EC8 - Part 1 has a probability of exceedance 10% in 10 years corresponding to a return period of 95 years. Within two parts of the code two different paradigms meet each other. The design concept applied to new structures aims at proving sufficient safety to the structure, while the evaluation procedure, applied to existing structures aims at exhausting the strength capacity of the structure. In order to avoid complications, which would arise if different nomenclature and code recommendations are used, the focus of this thesis will be on the design rules for new structures.

2.3.3 Nonlinear Time History Analysis (NLTHA)

Considering that every problem, which should be solved in terms of both earthquake engineering and shear timber walls is predominantly dynamic and highly nonlinear and that the ground motions are random with a certain amount of uncertainty, nonlinear time history analysis (NLTHA) is the most accurate analysis tool, especially when compared with other, more simplified analytical methods. For a time history analysis, artificial or real ground motion records can be used. Eurocode 8 requires that a minimum of three accelerograms are considered. Artificial accelerograms should be generated in such a way that they achieve the best match to a 5% damped elastic response spectra in the period range of $(0.2 - 2.0) \cdot T_0$. Real records should be scaled in the same way. No value in the specified period range should be less than 90% of the elastic response spectra. Additionally, when at least seven nonlinear time history analyses are performed, the average of the response quantities can be used for design purposes.

In this thesis, NLTHA will be performed using 10, real ground motion records, from which the average response quantity will be extracted. These ground motions will be scaled to the required hazard level. Furthermore, at least 7 out of 10 EQ-records used must satisfy the convergence criteria. Otherwise the specific non-convergent earthquake record will be removed from the suite and replaced by a convergent one. Additionally, no selected and scaled earthquake records overstep the peak value in acceleration sensitive region of an elastic, 5% damped spectra, by more than 40%.

2.4 Consequences for Further Investigation and Improvements

2.4.1 Existing analytical procedure in relation to the aim of the investigation

General

The objective of this thesis is to define the feasibility range for the traditionally used LFTW in Europe in terms of building height and seismic hazard levels. Two different sheathing materials, namely OSB plates and gypsum board (GFB) are considered. To achieve this goal, a reliable analysis technique is required. As described in the previous section, the design procedure proposed in Eurocode 8 has severe drawbacks related to FBD and an inadequate definition of the performance levels within PBD.

Aplicability of FBD

In addition to the inconsistencies and difficulties related to the use of the behaviour factor q, which is crucial for FBD, the FBD procedure is not directly applicable for nonlinear elastic systems, such as shear timber walls. Hence, in order to perform analysis, an equivalent elastic system must be considered. The problems related to the topic of representing an inelastic system by an equivalent elastic system are analyzed in more detail in [10]. However, the FBD method provides an uncertain and uncontrolled structural behaviour associated with an unknown protection grade. FBD is not capable of providing sufficiently realistic analytical results, related to the investigations that are subject of this thesis.

Aplicability of PBD

Eurocode 8, defines the performance objectives within the framework of PBD at a quite general level. Furthermore, it does not define the performance measures. PBD is seldomly used as design method, although it is more appropriate than FBD in seismic engineering.

Consequencies

Consequently, a modified approach is needed to perform an analysis capable of confirming the compliance of the predefined performance limit states with a sufficient degree of reliability. To do so, the following procedure has been used:

- Hysteretic rule estimation for a single fastener
- Hysteretic rule estimation for wall elements
- Performance level definition for LFTW sheathed with GFB panels
- Performance level definition for LFTW sheathed with OSB panels
- NLTHA using a defined hysteretic rule
- Check as to whether the performance criteria are satisfied

For these purposes, NLTHA has been recognized to be the best available analytical tool. Moreover, within this thesis, the predefined drift limits which are different for OSB and GFB sheathing material, and contain not only displacements but also damage and corresponding energy dissipation quantities, are understood as being part of the improved PBD.

2.4.2 Mechanical characterization and modeling

In order to perform NLTHA, a hysteretic model of the shear wall element is required. Such models differ for different wall configurations, depending on the aspect ratio, material properties, fastener spacing, hold down devices, etc. Furthermore, the fasteners themselves are nonlinear elements that, among all of the components, contribute the most to the overall nonlinear behaviour of any shear wall element. Thus, for each fastener, a hysteretic model is established in order to model the shear wall properly, as presented in Figure 1.7. In this thesis, the hysteretic fastener behaviour in timber connections is obtained experimentally for the OSB sheathing material using nails and staples. The hysteretic response of the shear wall element is then evaluated using the MCASHEW program developed by Folz and Filiatrault (2001) in the CUREE CalTech project [31]. To validate the numerical model, the results obtained numerically and through tests are compared. The numerical results, based on the experimentally-obtained hysteretic model of a single fastener, show good agreement with the results from the tests carried out on wall elements sheathed with OSB plates in the NRP 66 project [37], as well as with the results from the experiments on walls sheathed with GFB, tested as a part of this thesis. Furthermore, in order to explore the feasibility range in regions of low and moderate seismicity, Mergos-Beyer loading protocols, [67] are used for both experimental testing of individual fasteners and numerical analysis of LFTWs. Typical results of the analysis are hysteretic models for each specific wall element, defined by 10 parameters, as presented in Figure 2.5.
Once the hysteretic models had been estimated numerically, they were validated by experimental testing or through comparison to the results of tests carried out by other researchers. A

hysteretic model for shear wall elements with different lengths ($2.4, 3.0, 3.6, 4.2$ or $4.8[m]$) is established. It is applied as a constitutive model representing a nonlinear shear spring element, also called SAWS material, used in NLTHA (Figure 1.8).

2.4.3 Performance level redefinition

As previously discussed, the performance levels are not clearly defined in EC8. Based on the general requirements, defined as no-collapse and damage limitation, the following two limit states for each wall configuration are defined within this thesis (see Chapter 5 for more details).

- Serviceability limit state (SLS) corresponding to the damage limitation requirement for shear walls with OSB and GFB sheathing material
- Ultimate limit state (ULS) corresponding to the no-collapse requirement for shear walls with OSB and GFB sheathing material.

Since timber shear walls are characterized by a highly nonlinear behaviour with a pronounced capability of energy dissipation, displacement alone is not the best indication of their seismic performance. In order to establish desirable performance criteria, the appropriate limit states should be defined first. The damage grade investigation conducted on existing buildings after severe events has shown that LFTW sheathed with GFB are sensitive to deformation increase (see e.g. [99]). Keeping in mind that LFTW with GFB sheathing material are traditionally used for low and mid-rise buildings in European regions of low and moderate seismicity, the damage based performance criterion seems to be appropriate for limit states definition. A clear drift limit definition is based on a damage index analysis (DIA) using the Park-Ang damage model, see [80]. This model considers deformation capacity under monotonic loading, maximum deformation imposed by a specific earthquake record and absorbed hysteretic energy during an earthquake. The same procedure for performance based estimation will be applied for LFTW sheathed with OSB panels, as presented in Figure 1.9 in previous chapter. The fragility analysis should confirm that the damage index analysis led to the appropriate performance level definition. Within the fragility analysis probability of collapse for certain intensity measure given damage measure will be estimated, as presented in Figure 1.10 in previous chapter.

In addition to the drift limits, the following performance limits are assumed:

- Vibration period $T_0 \leq 1.7[s]$,
- Ductility $\mu \leq 3.0$
- Hold-Down forces, remain in the elastic range.

The performance limits listed above are based on the engineer′s judgment, experience and preference in controlling the structural response under a specific earthquake excitation. The vibration period limitation is aimed at avoiding structures that are too flexible with long vibration periods and large deformations. The period limitation should reduce the vulnerability arising from inter-storey drifts in higher vibration modes, observed in NLTHA, as well as reduce the

vulnerability to service wind loads.
The ductility limitation should take into account the uncertainty in ductility estimation, but should also prevent excessive reduction of earthquake forces and an overestimation of the deformation capacity of the LFTW. Note that the ductility factors in the range $q > 3$ are accompanied with severe damages and difficult to achieve. As in this thesis will be shown, other performance limiting criteria will be achieved first, and therefore the inherent ductility capacity of LFTWs will not be fully exhausted. Therefore, for LFTWs sheathed with OSB the ductility demand $\mu \leq 3.0$ is set as limiting criteria within here presented work.

The derivation of the parameters used herein is the topic of chapters 5 and 6.

2.4.4 Summary

Since fire protection requirements have recently been modified in Switzerland, there is no longer height limitation for timber structures. Some European countries are developing new design guidelines for timber buildings without height limitations. Due to the limitations having existed in the past and the inadequate analysis and design techniques currently in use, there is a lack of reliable prediction of bearing capacity of lateral load resisting systems traditionally used for timber structures in Europe and particularly in Switzerland. To estimate the feasibility range for conventionally used timber structures in regions of low and moderate seismicity, NTHA and PBD will be simultaneously combined. In order to use NLTHA, constitutive nonlinear material models, which take into account strength and stiffness degradation and pinching effects during cyclic excitation will be developed for five different wall configurations and applied in NLTHA for two different sheathing materials. The numerical models are derived from and verified by means of testing. The method proposed in this thesis is unorthodox to some extent. Namely, the design process is usually straightforward, typically ending in the design of the element under consideration. Here, the approach is inverse. For a wall element with a known bearing capacity and cyclic behaviour, the maximum applicable mass as a function of the number of storeys and the seismic hazard will be searched. All predefined performance criteria must be satisfied. Additionally, performance limit states suitable for LFTW structures are established based on damage analysis. The proposed procedure has some distinct advantages. One works with material properties at the characteristic (real) strength level. No ductility and reduction factors or overstrength ratios must be assumed in advance. The advanced NLTH-analysis uses real material models. Performance criteria are simultaneously checked, providing a reliable estimation of feasibility range.

In order to provide designers with an additional, simple analytical tool for seismic design of multi-storey structures, which could be used for hand calculations, a capacity curve estimation based on simple elastic shear field theory is presented in addition.

2.5 Conclusions

In this chapter, the mechanical characteristics of dowel type fasteners in timber connections as well as the behaviour of the LFTW element subjected to lateral loading have been reviewed. The current, Patton-Mallory energy-based analytical approach, usually used for hand calculations, has been re-introduced. The drawbacks of the code-based seismic design procedures have been specified and discussed with respect to the applicability for the design of LFTWs. The need to establish a reliable mechanical model, which satisfactorily describes the behaviour of the LFTW subjected to lateral loading, is pointed out.

Performance-Based Design (PBD) is primarily used by engineers to identify strength and displacement capacity in comparison to the seismic demand. The methodology operates on the capcity curve, which is a representation of the first mode structural response. It is not capable of accounting for energy dissipation and cyclic loading effects. Furthermore, the PBD uses the equal displacement rule extensively, which does not apply to structures with pronounced pinching and significant strength and stiffness degradation effects. In comparison to PBD, Performance-Based Engineering is a superior methodology, since it is based on the best available analysis tool referred to as Non-Linear Time History Analysis (NLTHA), which uses non-linear hysteretic mechanical models of LFTWs, providing reliable analysis results. Moreover, after establishing the clear performance objectives such as HD-forces, ductility demand μ, inelastic period of vibration $T*$, Inter-storey Drift Ratio (IDR) and Damage Index (DI), one can design structures which behave in a desired manner, performing predictable within defined performance range. Additionally, based on the results of the analyses of the structure under design earthquake, the repair costs can be assessed. In the frame of PBD, the definition of the performance objectives on the life safety performance level is usually the topic discussed and developed in collaboration with the building developer. In the presented work the values of the different performance parameters have been evaluated, validated and proposed to the best of the author's knowledge and belief.

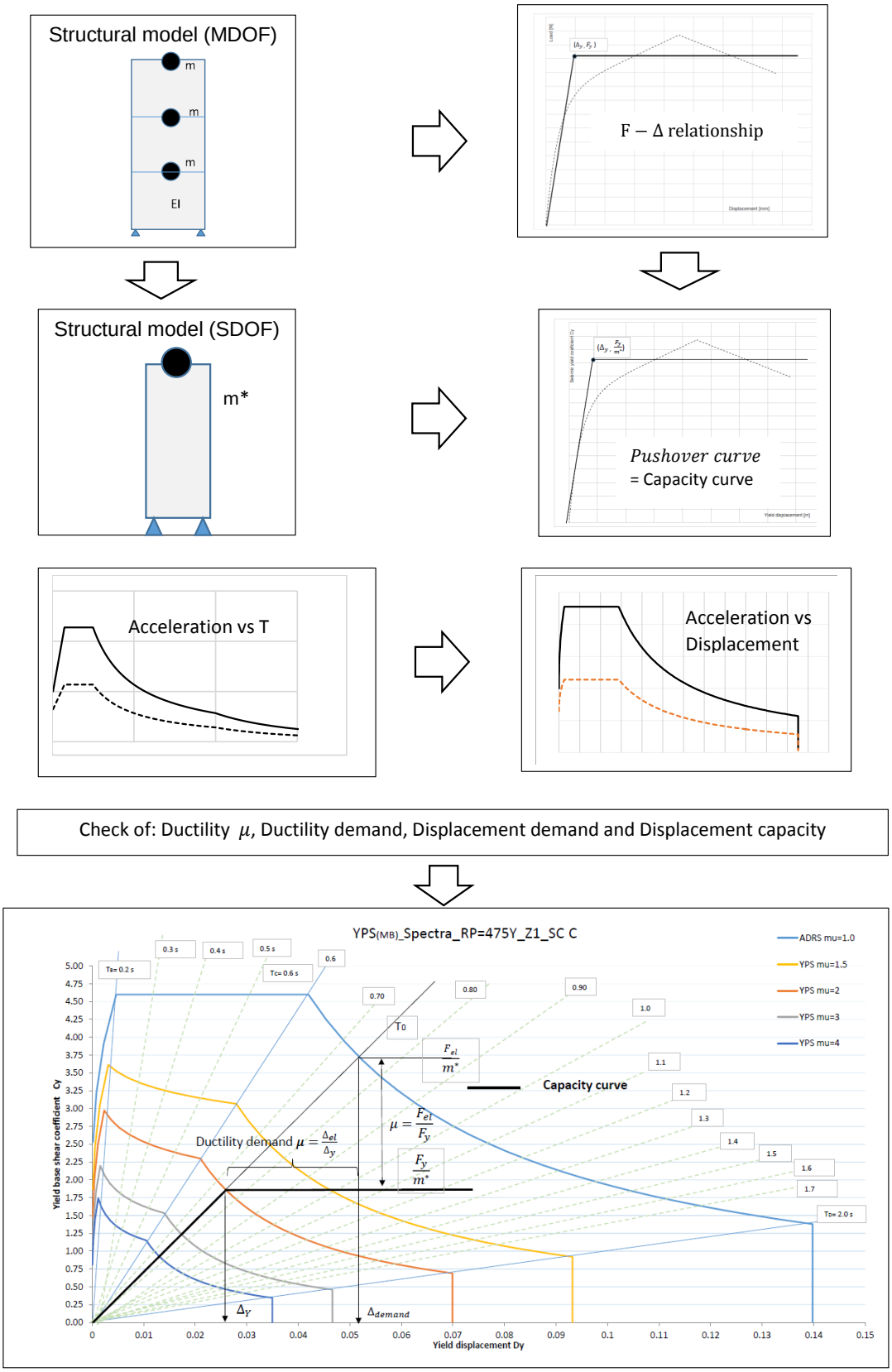

Fig. 2.7: Perormance based design procedure according to EC8 [1]

Chapter 3

Light Frame Timber Walls

In this chapter, the simple elastic shear field theory is briefly introduced. For the proper application of the shear field theory, more realistic then code-based estimations of bearing capacities of single fasteners are made by means of appropriate regression functions. The application of the simple shear field theory is demonstrated for an example that allows for hand calculation of the pushover curve of the single LFTW. The cyclic loading tests of the single fasteners, the test results and the estimation of the mechanical models are presented. Then, the behaviour of LFTWs sheathed with OSB and GFB, exposed to monotonic and cyclic loading, are presented and discussed. Finally, the mechanical models for different wall configurations, estimated numerically and verified by means of experimental testing, are proposed as the basis for the parameter study.

3.1 General Characteristics

Timber construction is regularly used for housing structures up to three storeys tall also in seismic prone regions as in the USA, Canada, New Zealand and Japan. Timber structures are widely-used in seismic prone regions all over the world because they exhibit good performance under earthquake excitations. These types of structures are inherently flexible, have small masses and they exhibit a considerable amount of lateral stiffness, due to the use of light frame timber walls (LFTWs) as the lateral load resisting system. LTFWs behave well when subjected to strong ground motions, providing appropriate safety along with low to moderate damage and low economical losses. Although timber structures are generally characterized by good performance, different wall configurations behave quite differently. Walls sheathed with OSB panels exhibit much greater deformation capacities when compared with walls sheathed with gypsum fibre board panels (GFB). Therefore, the applicability of these two types of walls will be assessed separately.

3.2 Behaviour of OSB Sheathed LFTWs under Monotonic Loading according to the Simple Elastic Shear Field Theory

3.2.1 Introduction

The first attempt to analytically describe the complex behaviour of LFTWs subjected to lateral loads was made by Patton-Mallory [81], Tuomi and McCutcheon [61] and Itani [44]. They used an energy based approach in order to derive a closed mathematical solution for the nonlinear relationship between lateral load and horizontal deflection due to applied nail slip. The derived solution presented in [61] is a simple exponential equation which relates the lateral load acting on the LFTW to its corresponding horizontal displacement. The elastic portions of the total displacements (flexural frame deformation δ_1, shear deformation of the sheathing panels δ_2 and rigid body rotation due to compression and elongation of the edge studs δ_3) were considered later on. Some improvements to the simple shear field theory, based on a numerical approach, are extensively discussed in [34], [92] and [22]. However, due to the simplicity and good accuracy of the simple shear field theory, it is widely used for the estimation of the racking stiffness and horizontal displacement of LFTWs. In this thesis, the simple elastic shear field theory is presented merely as a reference point for more sophisticated calculations based on nonlinear FE Analysis. The parametric study presented herein is based on the MCASHEW program (Cyclic Analysis of Shear Walls) and SAWS (Seismic Analysis for Woodframe Structures), developed by Folz and Filiatrault in 2002 in the CUREE-Caltech Woodframe Project [33] and [30].

3.2.2 Displacement analysis of LFTWs

The simple elastic shear field theory is based on the assumption that the contributions to flexural displacement of timber frame in the elastic range consists of: δ_1, shear deformation of sheathing panels δ_2 and rigid body rotation due to HD deformation and connection slip δ_3. The displacement contribution caused by the fastener slip δ_4 is inelastic even for small deformations. Thus, to estimate the total displacement response of the LFTW element, it is necessary to sum the displacement contributions of all the components for the corresponding lateral load.

Displacement due to the frame bending

Assuming that the LFTW is an equivalent cantilever beam subjected to a lateral load at the top, the flexural frame displacement can be easily estimated using the following well-known equation, based on the principle of virtual work (see also Figure 3.1).

$$\delta_1 = \int \frac{M \cdot M'}{EI} \cdot dx = \frac{1}{EI} \cdot \frac{2}{3} \cdot H \cdot \frac{F \cdot H^2}{2} = \frac{F \cdot H^3}{3EI} \tag{3.1}$$

The second moment of inertia I will be estimated using the contribution of the edge studs' cross-sections with surface area A_{st}.

$$I = 2A_{st} \cdot \frac{B^2}{2^2} \tag{3.2}$$

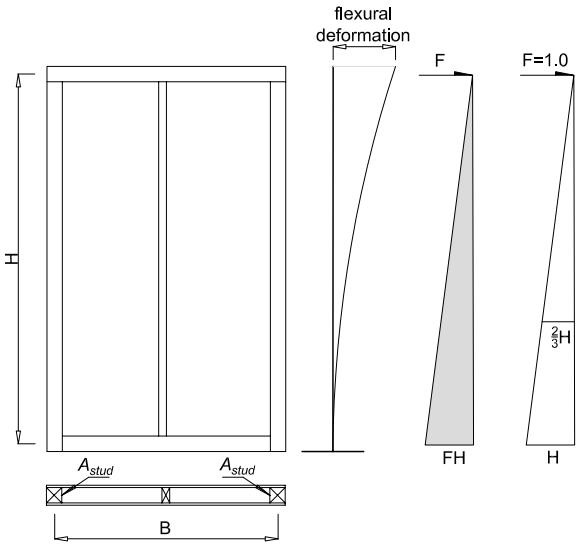

Fig. 3.1: Flexural displacement of the timber frame

Finally, the displacement due to bending of the equivalent frame is:

$$\delta_1 = \frac{F \cdot H^3}{3EI} = \frac{4F \cdot H^3}{3A_{st} \cdot 2E_{||} \cdot B^2} = \frac{2F \cdot H^3}{3A_{st} \cdot E_{||} \cdot B^2} \tag{3.3}$$

Displacement due to shear deformation of the sheathing panel

The displacement due to the shear deformation of the sheathing panel can be estimated in the same way (see also Figure 3.2).

$$\delta_2 = \int \frac{Q \cdot Q^{'}}{GA^*} \cdot dx = \frac{F \cdot H \cdot 1}{GA^*} = \frac{k_g \cdot F \cdot H}{G \cdot B \cdot 2 \cdot t_{sp}} \tag{3.4}$$

where coefficient $k_g = 6/5$ for rectangular cross-sections.

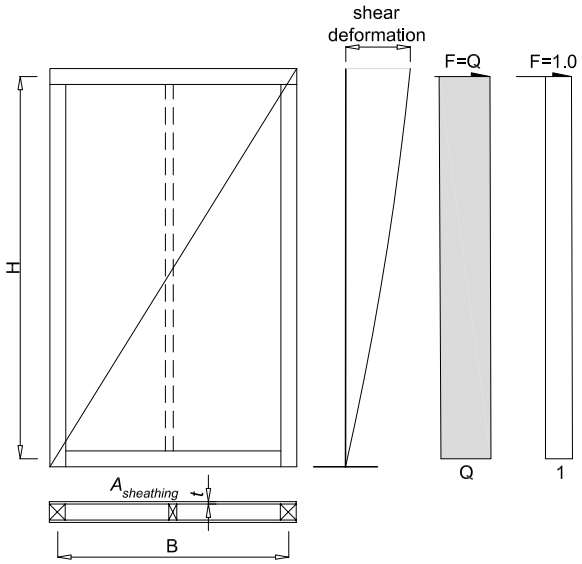

Fig. 3.2: Shear displacement of the sheathing panel

Displacement due to rigid body rotation

Rigid body rotation is caused by deformations arising within the hold-down devices and connection slip on the basement level.

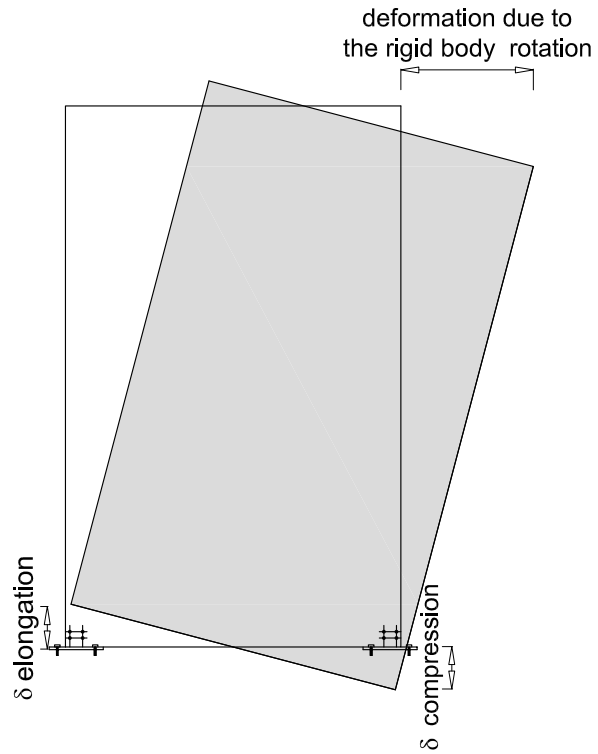

Fig. 3.3: Deformation due to rigid body rotation

Hold-down deformations

Hold-down (HD) devices are made of steel. The function of a HD device is to transfer compression, tension or shear forces into the ground. This provides uplift and shear resistance at the anchorage location. Typically used hold-down devices are industrially produced standard steel angle brackets with limited bearing capacity. Since the aim of this thesis is to estimate the best performance of LFTWs, the HD devices used in this study must be robust to prevent them from exhibiting plastic deformations or being the weakest element in the chain. In Figure 3.3, the displacements arising within the HD elements are denoted as $\delta_{HD,ten}$ and $\delta_{st,comp}$ for the tension and compression deformations of the stud, respectively.

Since the deformation of the stud under compression is constrained due to the direct contact between the stud and the foundation surface, the only deformation of the hold-down device under compression is due to the connection slip. This is assumed to be 1.0 [mm]. The displacement of the HD device in tension $\delta_{HD,ten}$ depends on what the HD device is designed for. It can be estimated as follows.

$$\delta_{HD,ten} = \frac{F_{stud}}{K_{HD,ser}} = \frac{F \cdot H}{B \cdot K_{HD,ser}} \tag{3.5}$$

where $K_{HD,ser}$ is the stiffness of the hold-down device in the elastic range. $K_{HD,ser}$ can be estimated by using [17] and [91]. $K_{HD,ser} = \rho^{1.5} \cdot \frac{d}{23}$ in [17] and $K_{HD,ser} = 3 \cdot \rho^{0.5} \cdot d^{1.7}$ in [91] are defined as values depending only on the timber density and the diameter of the dowel used. This formulas are based on [47]. If a connection is designed as a timber-steel connection with slotted-in steel plates, both design codes EC5 and SIA265 suggest multiplication of $K_{HD,ser}$ by 2, according to Equation 3.7.

The ultimate strength per shear plane and dowel can be estimated using the model proposed by Johansen, also called the European Yielding Model (EYM), which is implemented in [17] (Equation 3.6):

$$F_{v,R} = min \begin{cases} f_{h,1,k} \cdot t_1 \cdot d \\ f_{h,1,k} \cdot t_1 \cdot d \cdot [\sqrt{2 + \frac{4 \cdot M_{y,R}}{f_{h,1,k} \cdot t_1^2 \cdot d}} - 1] \\ 2.3 \cdot \sqrt{f_{h,1,k} \cdot M_{y,R} \cdot d} \end{cases} \tag{3.6}$$

all units in $[N]$ and $[mm]$

$$K_{HD,ser} = 2.0 \cdot \rho^{1.5} \cdot \frac{d}{23} \tag{3.7}$$

The required bearing capacity of HD devices can be taken from Figure 3.4, 3.5 and 3.6 for one, two and three slotted-in steel plates, respectively. The stiffness per shear plane and dowel is given in Table 3.1. Here, the timber studs are of the strength class GL24h with $\rho_k = 385[\frac{kg}{m^3}]$. The timber studs have dimensions $200 \cdot 200$ and $240 \cdot 240[mm]^2$ for small and moderate HD device forces and $300 \cdot 300[mm]^2$ for high HD device forces. The connections with one slotted

in steel plate consists of 6, 9 or 12 dowels. The connections with 2 or 3 slotted in steel plates, 8, 12 or 16 dowels of diameter d=8, 10, 12, 14 or 16 $[mm]$, and a steel strength $f_{uk} = 510[\frac{N}{mm^2}]$.

Tab. 3.1: HD stiffness per shear plane and fastener

Equation	8 mm kN/mm	10 mm kN/mm	12 mm kN/mm	14 mm kN/mm	16 mm kN/mm
$K_{HD,ser} = 2 \cdot \rho^{1.5} \cdot \frac{d}{23}$	5.78	7.22	8.66	10.1	11.55

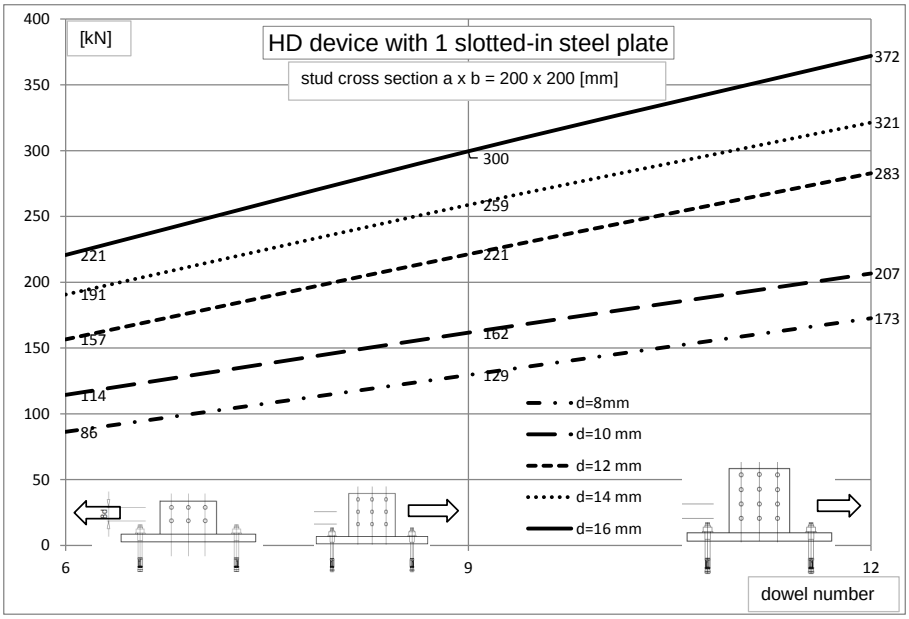

Fig. 3.4: Bearing capacity of hold-down devices with one slotted-in steel plate

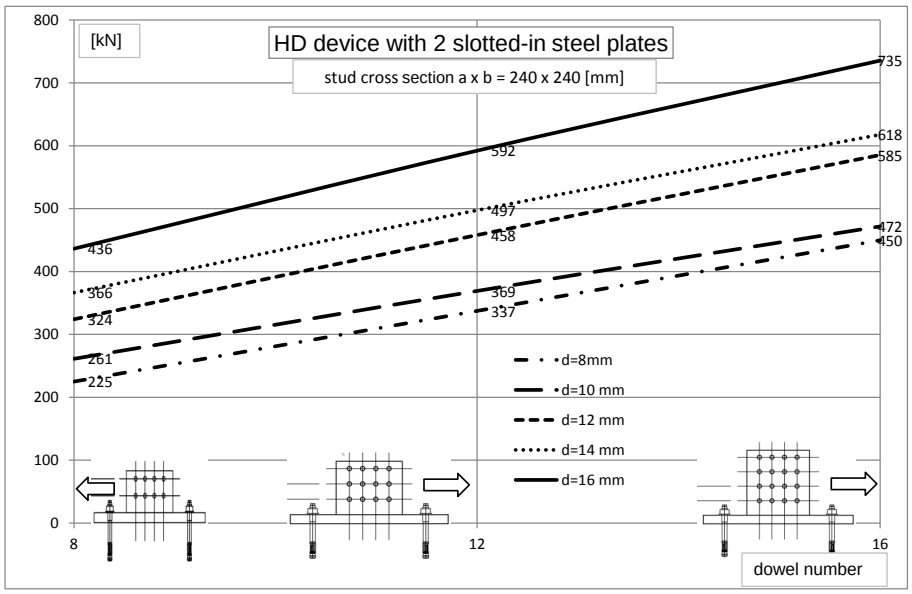

Fig. 3.5: Bearing capacity of hold-down devices with two slotted-in steel plates

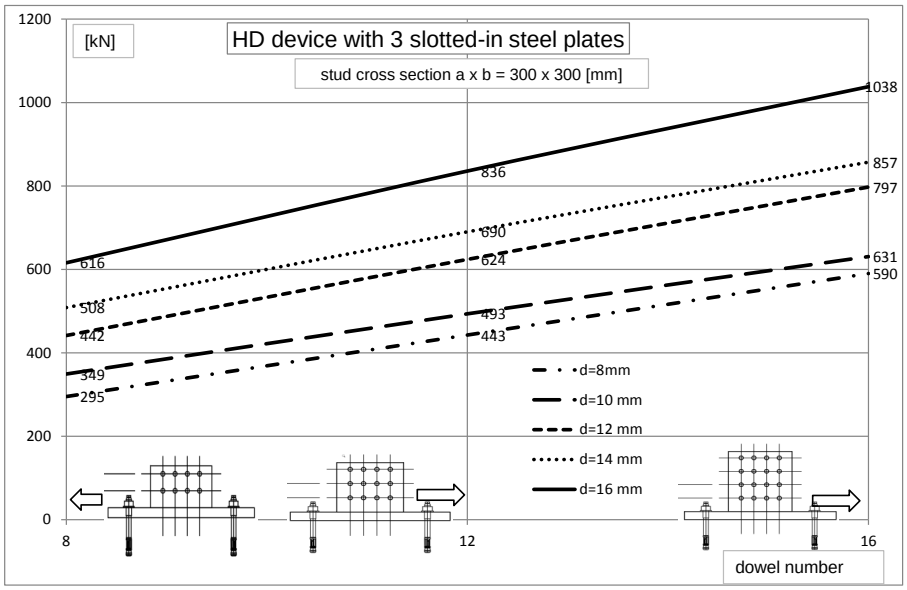

Fig. 3.6: Bearing capacity of hold-down devices with three slotted-in steel plates

The HD device containing two slotted-in steel plates and 12 dowels with d=8 mm used for wall testing in this thesis is shown in Figure 3.7.

Fig. 3.7: Hold-down device consisting of two slotted-in steel plates and 12 dowels with $d = 8mm$ (left) and an edge stud during testing (right)

The total elastic deformations due to the lateral loads acting on the top of the wall can be calculated by simple summing the previously listed individual contributions.

Displacement due to fastener slip

The nail slip is nonlinear from the very beginning. The deformation of a wall under lateral loading depends mainly on the displacements of a single fastener, which, together with the sheathing material, provide the wall element with racking stiffness. Thus, the relationship between the global lateral displacement induced by a global lateral force acting on the wall and the corresponding deformation of a single fastener should be established. Several exponential equations, which establish a relationship between the fastener distortion δ_n in terms of the global displacement due to the fastener slip Δ_n, and the fastener force f, as nonlinear function of δ_n, have been proposed by McCutcheon in [61] and in [81] and discussed, modified and extended in [43]. The asymptotic Equation 3.8 is widely used.

$$f = \frac{A_0 \cdot \delta_n}{B_0 + \delta_n} \tag{3.8}$$

where constant A_0 approaches the ultimate value of the fastener strength $f_{u,as}$ with increasing distortion δ_n. Constant B_0 takes into account the load-deformation relationship of a fastener; for a linear fastener response, $B_0 = 1$, and for a perfectly plastic response, $B_0 = 0$. Equation 3.8 is derived by equating the internal energy due to fastener distortion and the external energy due to external racking load and racking displacement due to fastener slip Δ_n. Subsequently, the racking external force F_{wall} can be expressed as a function of the fastener force represented by A_0 and the geometric constant K_f, which depends on the location of each individual fastener on the panel periphery.

$$F_{wall} = A_0 \cdot \sum \frac{K_f^2 \cdot \Delta_n}{B_0 + K_f \cdot \Delta_n} \tag{3.9}$$

As the fastener slip increases, the fastener force asymptotically approaches the ultimate strength $f_{u,as}$ and the corresponding racking force F_{wall} approaches the ultimate value $F_{R,wall}$.

Constant B_0 was initially defined as the fastener slip at $50\% f_{u,as}$ and replaced later on by Patton-Mallory and McCutcheon in [81] by $1.5\delta_{f,s}$, where $\delta_{f,s}$ is the fastener distortion at the service level. Finally, as reported in [18], Equation 3.10, was found to describe the wall racking almost exactly.

$$F_{wall} = \frac{a_0 \cdot f_{u,as} \cdot \frac{B}{s} \cdot \Delta_n}{b_0 \cdot 2 \cdot \delta_{f,s} \cdot (1 + \frac{H_p}{B_p}) + \Delta_n} = \frac{1.1 \cdot f_{u,as} \cdot \frac{B}{s} \cdot \Delta_n}{1.3 \cdot 2 \cdot \delta_{f,s} \cdot (1 + \frac{H_p}{B_p}) + \Delta_n} \tag{3.10}$$

In equation 3.10, B_p and H_p are the width and height of the sheathing panel, and s is the fastener spacing. Additionally, over the whole range of the panel aspect ratios, $0.5 < \frac{H_p}{B_p} < 2$ (see also [18]), the parameters $a_0 = 1.1$ and $b_0 = 1.3$ were found to remain almost constant. Furthermore, the best fit with the test results was achieved for $\delta_{f,s} = 0.6mm$. The racking displacement of the wall due to the nail slip Δ_n can be estimated by using the proposal made by Stewart, [92] and Deam, [18] according to Equation 3.11:

$$\Delta_n = 2 \cdot \delta_n \cdot (1 + \frac{H_p}{B_p}) \tag{3.11}$$

In order to establish a nonlinear relationship between the fastener distortion, the corresponding fastener force, the global racking displacement and the corresponding global force acting on the wall element, the ultimate asymptotic fastener strength $f_{u,as}$ must be considered with Equation 3.10. This will be the topic of the subsequent paragraph.

The starting point for derivation of the fastener strength $f_{v,R}$ is Equation 3.12, which is based on Johansen's model, implemented in [17]. The fastener strength in a connection depends on the mechanical characteristics of the timber and of the fastener's steel material as well as on the geometrical properties, including the thickness of the sheathing panel and the timber members and the diameter of the fastener.

$$f_{v,R} = min \begin{cases} f_{h,1,k} \cdot t_1 \cdot d \\ f_{h,2,k} \cdot t_2 \cdot d \\ \frac{f_{h,1,k} \cdot t_1 \cdot d}{1+\beta_0} \cdot [\sqrt{\beta_0 + 2 \cdot \beta_0^2 \cdot [1 + \frac{t_2}{t_1} + (\frac{t_2}{t_1})^2] + \beta_0^3 \cdot (\frac{t_2}{t_1})^2} - \beta_0 \cdot (1 + \frac{t_2}{t_1})] + \frac{f_{ax,Rk}}{4} \\ 1.05 \cdot \frac{f_{h,1,k} \cdot t_1 \cdot d}{2+\beta_0} \cdot [\sqrt{2 \cdot \beta_0 \cdot (1 + \beta_0) + \frac{4 \cdot \beta_0 \cdot (2+\beta_0) \cdot M_{y,Rk}}{f_{h,1,k} \cdot t_1^2 \cdot d}} - \beta_0] + \frac{f_{ax,Rk}}{4} \\ 1.05 \cdot \frac{f_{h,1,k} \cdot t_2 \cdot d}{1+2 \cdot \beta_0} \cdot [\sqrt{2 \cdot \beta_0^2 \cdot (1 + \beta_0) + \frac{4 \cdot \beta_0 \cdot (1+2 \cdot \beta_0) \cdot M_{y,Rk}}{f_{h,1,k} \cdot t_2^2 \cdot d}} - \beta_0] + \frac{f_{ax,Rk}}{4} \\ 1.15 \cdot \sqrt{\frac{2 \cdot \beta_0}{1+\beta_0}} \cdot \sqrt{2 \cdot M_{y,Rk} \cdot f_{h,1,k} \cdot d} + \frac{f_a x,Rk}{4} \end{cases} \tag{3.12}$$

with $\beta_0 = \frac{f_{h,2,k}}{f_{h,1,k}}$; all units in $[N]$ and $[mm]$

The global behavior of the shear wall strongly depends on the behavior of the fastener. Therefore in performance based earthquake engineering, knowledge of the load-displacement relationship is necessary. During the tests carried out by various researchers in the past, it was observed that the strength estimated when using Equation 3.12 did not correspond with the values obtained experimentally. Dolan, [22] and Dolan Madsen, [23] reported results from monotonic and cyclic nail connection tests. Figure 3.8, left, shows a typical load-displacement relationship of a nail fastener within a timber connection, while in Figure 3.8, right, the overall average load-displacement curve of the connection, with a maximum displacement of 9 mm, is presented. From Figure 3.8, it can be seen that, different sheathing materials connected with nails exhibit almost the same behavior at the maximum displacement of 9.0 mm. The ascending branch of the load-displacement curve is fitted to Foschi's exponential equation [34]. The maximum displacement value $\delta_{n,max}$ and the descending stiffness after the peak load was introduced by Dolan and Madsen, which completes the response definition of a nailed connection.

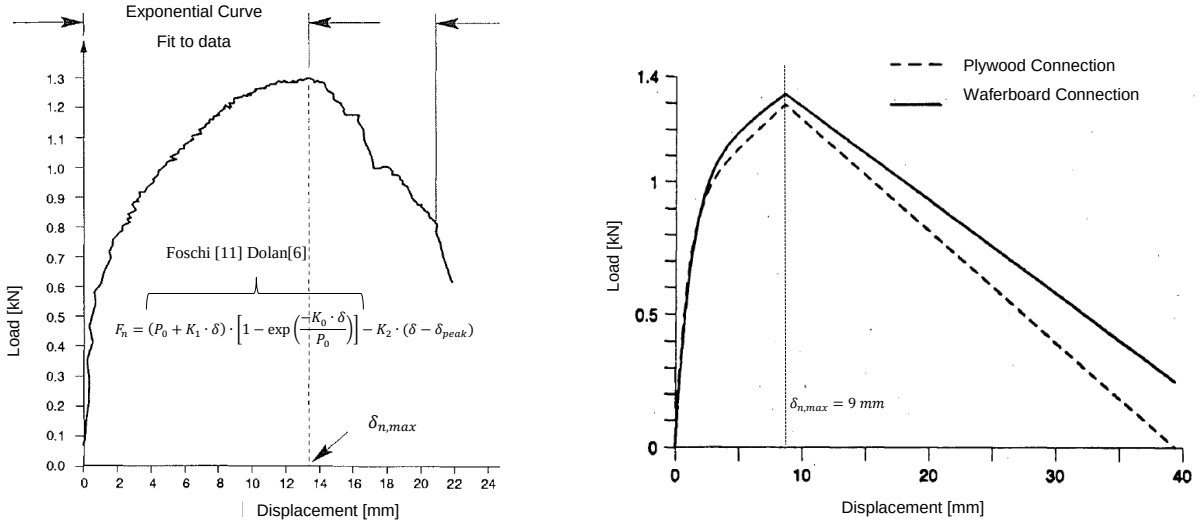

Fig. 3.8: Typical load - displacement curve obtained from the monotonic connection test according [23]

In [57], Loo et all. suggested using the parameters obtained by testing in [23] as a benchmark, so that the ultimate strength of any nail connection can be easily fitted to the Dolan-Madsen curve. In order to do so, W.Y.Loo, P. Quenneville and N. Chow (see [57]), compared the ultimate strength obtained by tests with those obtained by using the European Yielding Model (EYM). In this way, the theoretical and experimental values were connected, and the trend was described by a regression function, which allowed estimation of the ultimate nail strength in any timber connection. In this thesis, the values considered in [57] are extended by available experimental results of Mohamad, Bernasconi and Frangi [69], Peric (2016), and Vogt [101], as shown in Figure 3.9. The nail strength can be described by regression according to the Equation 3.13 (see also Figure 3.10).

$$f_n = 986.08 \cdot \ln\left(F_{EYM}\right) - 5484 \tag{3.13}$$

in $[N]$

Comparison between calculated and measured bearing capacity
fu,k ≥ 700 N/mm2

Reference	Loading Protocol	Sheating Type; Thickness	Density	Framing Type	Density	Nail_Typ	Nail_ Length	Nail_ Diameter	Calculated Bearing Capacity EC5	Bearing Capacity Test	Fitted to Dolan Nail 3.33 [mm]; Fmax =1370 [N]
		t_2 [-]; [mm]	$\rho_{1,k}$ [kg/m3]	t_1 [-]; [mm]	$\rho_{2,k}$ [kg/m3]	[-]	l [mm]	d [mm]	$R_{ch,calc}$ [N]	$R_{ult,mesured}$ [N]	
Dolan&Madson (1992)	monotonic	OSB;9	640	Spruce-Pin-Fir	420	8d	64	3.3	900.6	1325	**1212**
	monotonic	Canadian Softwood Ply; 9	450	Spruce-Pin-Fir	420	8d	64	3.3	900.6	1370	**1212**
Coyne (2007)	monotonic	OSB;11.1	640	Hem fir	460	6d	51	2.9	813.4	1239	**1111**
	monotonic	OSB;11.1	640	Hem fir	460	8d	64	3.3	983.7	1435	**1300**
	monotonic	OSB;11.1	640	Hem fir	460	10d	76	3.8	1213.2	1581	**1509**
	monotonic	OSB;15.9	640	Hem fir	460	10d	76	3.8	1322.9	1587	**1595**
	monotonic	OSB;19.1	640	Hem fir	460	10d	76	3.8	1422.4	1755	**1668**
Eikert Hong (2006)	cyclic	OSB;11.1	640	Hem fir	460	8d	64	3.3	983.7	1441	**1300**
Fonseca and Rabe (2009)	syclic	OSB;11.1	640	Douglas-Fir-Larch	490	8d	60	2.9	866.5	1226	**1174**
Fonseca et all (2006)	syclic	CSP; 11.9	450	Douglas-Fir-Larch	490	8d	60	2.9	886.2	1014	**1196**
		CSP; 11.9	450	Douglas-Fir-Larch	490	8d	64	3.3	1035.5	1076	**1351**
Vogt (2015)	cyclic	OSB;10	583 (550)	C24	390 (350)		65	2.8	726.9	1094	**999**
	cyclic	OSB;18	581 (550)	C24	390 (350)		65	2.8	955.2	1112	**1271**
	cyclic	OSB;18	581 (550)	C24	390 (350)		65	3.1	1043.8	1471	**1359**
	cyclic	OSB;18	581 (550)	C24	390 (350)		65	2.5	803.7	890	**1099**
Peric (2016)	cyclic	OSB; 12	550	C24	350		60	2.45	640.6	1005	**873**
	cyclic	OSB; 18	550	C24	350		60	2.45	732.7	1126	**1007**
	cyclic	OSB; 12	550	C24	350		60	2.87	748.5	1038	**1028**
	cyclic	OSB; 18	550	C24	350		60	2.87	931.2	1134	**1246**
Mohamad & Bernasconi (2015)	monotonic	OSB;18	550	GL24	380		60	2.45	761.6	904	**1045**
	monotonic	OSB;18	550	GL24	380		60	2.45	761.6	1057	**1045**
	monotonic	OSB;18	550	GL24	380		60	2.45	761.6	1036	**1045**
	monotonic	OSB;18	550	GL24	380		60	2.45	761.6	977	**1045**
	monotonic	OSB;18	550	GL24	380		60	2.45	761.6	1109	**1045**
	monotonic	OSB;18	550	GL24	380		60	2.45	761.6	1088	**1045**

Fig. 3.9: Overview of the considered measured and theoretical ultimate nail strength

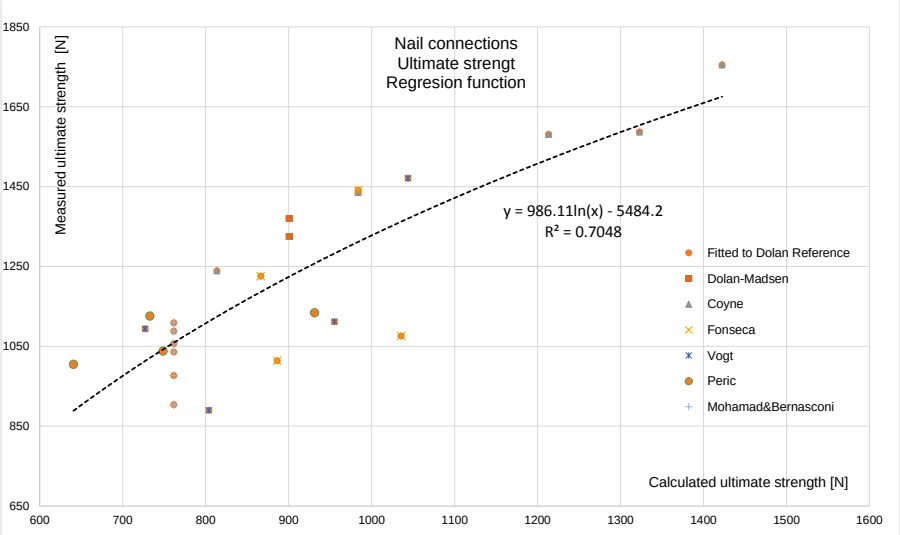

Fig. 3.10: Regression function of the measured and theoretical ultimate nail strength

Starting with Equation 3.12 and using the regression function shown in Figure 3.10, the more realistic fastener asymptotic strength can be estimated. Moreover, the parameters k_0, k_2, k_3 and $\delta_{n,max}$ (see also Figure 2.2), which define the Dolan-Madsen reference curve, can be used to estimate the nonlinear load-displacement relationship for different connection configurations. For example, for nails $d = 2.87[mm]$, $f_{u,k} = 700[\frac{N}{mm^2}]$; and OSB panels with thickness $t_1 = 12[mm]$, sheathed to the timber element with width $t_2 = 120[mm]$, characteristic density of OSB and timber element $\rho_{h1,k} = 550[\frac{kg}{m^3}]$ and $\rho_{h2,k} = 385[\frac{kg}{m^3}]$, respectively, the bearing capacity according to EC5 (2008) is $f_{v,d} = 791.0[N]$, and the estimated asymptotic strength using the regression function fitted to the Dolan-Madsen reference curve is $f_{as,u} = 1096.0[N]$, as presented in Figure 3.11.

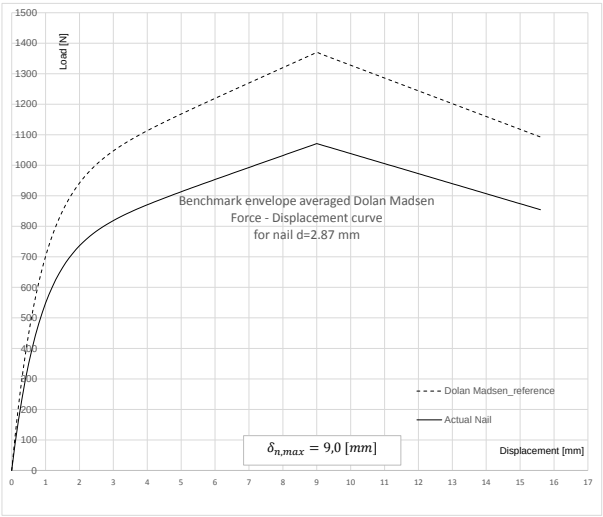

Fig. 3.11: Load-displacement curve for nail d=2.87 $[mm]$, OSB panel d=12$[mm]$, compared with the Dolan-Madsen reference curve

The experimentally obtained strength of the staples are summarized in Figure 3.12. For the purpose of completeness, the comparisons between the theoretically and experimentally obtained data as well as the estimation of the regression function is plotted in Figure 3.13. The comparison to the Dolan-Madsen reference curve for a staple with $d = 1.53[mm]$ is presented in Figure 3.14. The obtained regression function can be expresses as follows:

$$f_s = 567.51 \cdot \ln\left(F_{EYM}\right) - 2487.9 \tag{3.14}$$

in $[N]$

The procedure for creating the regression function and comparison with the reference curve for staples is similar to the approach applied for the nails, provided that the two staple shafts are properly substituted by an equivalent nail diameter:

$$W_{eq} = \frac{d_{eq}^3 \cdot \pi}{32} = \frac{2 \cdot d_{st}^3 \cdot \pi}{32} \tag{3.15}$$

in $[mm]$

$$d_{eq} = \sqrt[3]{2} \cdot d_{st} \tag{3.16}$$

in $[mm]$

Comparison between calculated and measured bearing capacity
fu,k ≥900 N/mm2

Reference	Loading Protocol	Sheating Type; Thickness t_2 [-]; [mm]	Density $\rho_{1,k}$ [kg/m3]	Framing Type t_1 [-]; [mm]	Density $\rho_{2,k}$ [kg/m3]	Staple_ Equivalent Diameter [-]	Nail_ Length l [mm]	Staple_ Diameter d [mm]	Calculated Bearing Capacity EC5 $R_{ch,calc}$ [N]	Bearing Capacity Test $R_{ult,mesured}$ [N]
Vogt	monotonic	OSB;18	581	Spruce-Pin-Fir	413	2.52	65	2	947.3	**1578.5**
	cyclic	OSB;18	581	Spruce-Pin-Fir	413	2.52	65	2	947.3	**1437.5**
	cyclic	OSB;18	581	Spruce-Pin-Fir	413	2.52	65	2	947.3	**1325**
	cyclic	OSB;18	581	Spruce-Pin-Fir	413	2.52	65	2	947.3	**1375**
	monotonic	OSB;18	581	Spruce-Pin-Fir	413	2.27	55	1.8	789.5	**1337.5**
	cyclic	OSB;18	581	Spruce-Pin-Fir	413	2.27	55	1.8	789.5	**1200**
	cyclic	OSB;18	581	Spruce-Pin-Fir	413	2.27	55	1.8	789.5	**1250**
	cyclic	OSB;18	581	Spruce-Pin-Fir	413	2.27	55	1.8	789.5	**1262.5**
	monotonic	OSB;18	581	Spruce-Pin-Fir	413	1.93	55	1.53	615.2	**1141.7**
	cyclic	OSB;18	581	Spruce-Pin-Fir	413	1.93	55	1.53	615.2	**991.7**
	cyclic	OSB;18	581	Spruce-Pin-Fir	413	1.93	55	1.53	615.2	**1141.7**
	cyclic	OSB;18	581	Spruce-Pin-Fir	413	1.93	55	1.53	615.2	**1050**
	monotonic	OSB;10	581	Spruce-Pin-Fir	413	1.93	55	1.53	526	**1000**
	cyclic	OSB;10	581	Spruce-Pin-Fir	413	1.93	55	1.53	526	**1000**
	cyclic	OSB;10	581	Spruce-Pin-Fir	413	1.93	55	1.53	526	**1091.7**
	cyclic	OSB;10	581	Spruce-Pin-Fir	413	1.93	55	1.53	526	**1141.7**
Mohamad &Bernasconi										
	monotonic	OSB-4; 18	572	GL24h ; 100	407	1.84	50	1.46	561.7	**1033**
	monotonic	OSB-4; 18	572	GL24h ; 100	407	1.84	50	1.46	561.7	**1038**
	monotonic	OSB-4; 18	572	GL24h ; 100	407	1.84	50	1.46	561.7	**1081**
	monotonic	OSB-4; 18	572	GL24h ; 100	407	1.84	50	1.46	561.7	**1030**
	monotonic	OSB-4; 18	572	GL24h ; 100	407	1.84	50	1.46	561.7	**1051**
	monotonic	OSB-4; 18	572	GL24h ; 100	407	1.84	50	1.46	561.7	**1181**
	monotonic	OSB-4; 18	572	GL24h ; 100	407	1.84	50	1.46	561.7	**1113**
	monotonic	OSB-4; 18	572	GL24h ; 100	407	1.84	50	1.46	561.7	**1149**
	monotonic	OSB-4; 18	572	GL24h ; 100	407	1.84	50	1.46	561.7	**1143**
	monotonic	OSB-3; 18	586	GL24h ; 100	407	1.84	50	1.46	561.7	**1059**
	monotonic	OSB-3; 18	586	GL24h ; 100	407	1.84	50	1.46	561.7	**1069**
Peric	cyclic MB	OSB; 12	580	C24 ; 100	350	1.93	50	1.53	561.23	**1176**
	cyclic CUREE	OSB; 12	580	C24 ; 100	350	1.93	50	1.53	561.23	**1258**
	cyclic MB	OSB; 18	580	C24 ; 100	350	1.93	50	1.53	588.4	**1362**
	cyclic CUREE	OSB; 18	580	C24 ; 100	350	1.93	50	1.53	588.4	**1256**

Fig. 3.12: Overview of considered measured and theoretical ultimate staple strength

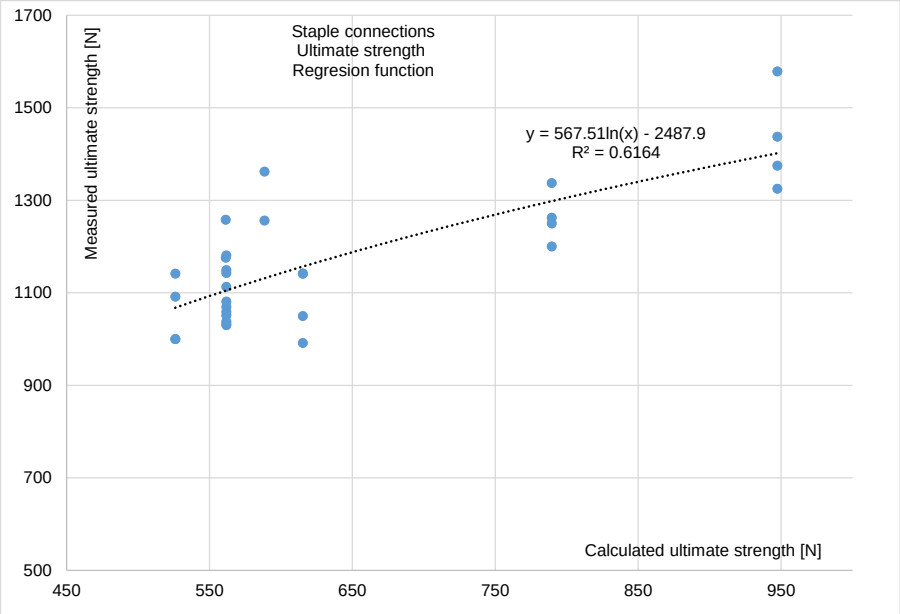

Fig. 3.13: Regression function of the measured and theoretical ultimate staple strength

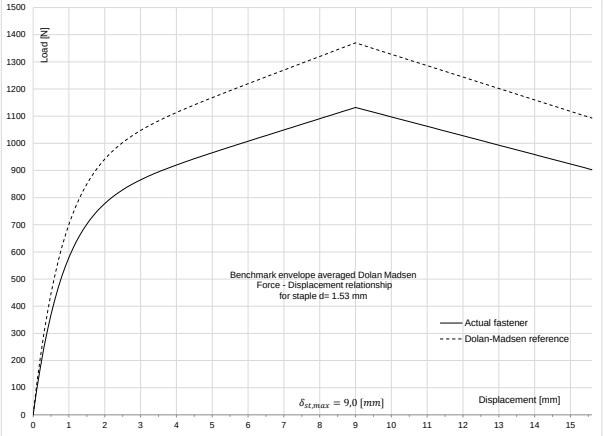

Fig. 3.14: Load-displacement curve for staple 1.53 mm, OSB panel d=12 mm, compared with the Dolan-Madsen reference curve

3.2.3 Summary of displacement analysis of LFTW

At the end of the Chapter 3, a displacement analysis based on the elastic shear field theory will be summarized and illustrated by means of an example. The individual elastic and inelastic displacement contributions are summarized in Table 3.2,

Tab. 3.2: Displacement contributions according to the elastic shear field theory

Frame bending	Panel shear	Rigid body rotation	Fastener slip
		HD displacement	
δ_1	δ_2	δ_3	δ_4
$\frac{2F \cdot H^3}{3A_{st} \cdot E_{\|\|} \cdot B^2}$	$\frac{k_g \cdot F \cdot H}{G \cdot B \cdot 2 \cdot t_p}$	$\frac{F \cdot H}{B \cdot K_{HD,ser}}$	$\frac{1.1 \cdot f_{u,as} \cdot \frac{B}{s} \cdot \Delta_n}{1.3 \cdot 1.2 \cdot (1+\frac{H_p}{B_p}) + \Delta_n}$

where $\Delta_n = 2 \cdot \delta_n \cdot (1 + \frac{H_p}{B_p})$

Example

The following example illustrates the approach described in Chapter 3: The LFTW with a width of $B = 3.6[m]$ and height of $H = 3.2[m]$ is sheathed on both sides with an OSB panel with a thickness of $t_p = 15[mm]$. The timber frame is of strength class GL24h with a characteristic value of density of $\rho_k = 385[\frac{kg}{m^3}]$ and a modulus of elasticity of $E_{||} = 11000[\frac{N}{mm^2}]$. The fasteners used are nails with $d = 2.87[mm]$; $f_{u,k} = 700[\frac{N}{mm^2}]$ and a spacing of $s = 30[mm]$. A timber frame and a hold-down device should be designed, and the wall displacements should be estimated at service limit state (SLS) for $\delta_{n,ser} = 0.6[mm]$ and at the ultimate limit state (ULS) for $\delta_{n,max} = 9.0[mm]$. The corresponding forces acting on the wall should also be estimated. For the selected SLS and ULS stages, the magnitude of the contribution of each single constituent part of the LFTW to the entire wall displacement should be estimated.

Design of frame and hold-down devices

Using EC5, nails with $d = 2.87[mm]$ and $f_{u,k} = 700[\frac{N}{mm^2}]$, OSB panels with $t_1 = 15[mm]$, width of the timber frame $t_2 > 120[mm]$, $\rho_{h1,k} = 550[\frac{kg}{m^3}]$, $\rho_{h2,k} = 385[\frac{kg}{m^3}]$, the bearing capacity according to EC5 (2008) is $f_{v,R} = 876.8[N]$ (failure mod d), and the estimated asymptotic strength using the regression function (approximation to the Dolan-Madsen reference curve) is $f_{as,u} = 1198[N]$.

For a maximum nail displacement of $\delta_{n,max} = 9.0[mm]$ and from $\Delta_n = 2 \cdot \delta_n \cdot (1 + \frac{H_p}{B_p}) = 2 \cdot 9(1 + \frac{3.2}{1.8}) = 50[mm]$, the corresponding force acting on the wall due to the nail slip of $9[mm]$ is: $F_{wall} = \frac{1.1 \cdot f_{u,as} \cdot \frac{B}{s} \cdot \Delta_n}{1.3 \cdot 1.2 \cdot (1+\frac{H_p}{B_p}) + \Delta_n} = 291[kN]$. The stud force can be estimated as: $F_{st} = \frac{F_{wall} \cdot H}{B} = \frac{291 \cdot 3.2}{3.6} = 259[kN]$ and for stud dimensions $200 \cdot 200[mm]^2$, the stress in the stud frame is $6.5[\frac{N}{mm^2}]$. From the bearing capacity of the hold-down device with one slotted-in steel plate with 12 dowels, a dowel diameter of $d = 16[mm]$ is needed to withstand the force of $258.7 \cdot 1.35 = 350[kN]$. Note that a hold-down device with 9 dowels would be sufficient, but in order to ensure elastic behavior, the demand should be multiplied by 1.35 (see also Chapter 5, Section 5.2). Once the frame and the hold-down device are designed, the hold-down device stiffness can be estimated using Table 3.1 as follows: $K_{HD,ser} = 11.6 \cdot 12 \cdot 2 = 277[\frac{kN}{mm}]$. As one can see from Table 3.2, all displacement portions δ_1; δ_2; and δ_4 can be calculated directly except for the displacement

portion δ_3, which consists of two different parts, HD displacement and connection slip. If the connection slip on each side is considered to be $1.0[mm]$, the displacement of the wall due to the rigid body rotation can be written as follows: $\delta_3 = (\delta_{HD,ten} + 1 + \delta_{st,com} + 1) \cdot \frac{H}{B}$; $\delta_3 = (0.933 + 1 + 0 + 1) \cdot \frac{3200}{3600} = 2.067[mm]$.[1]

Displacement magnitudes at SLS and ULS

The contribution of each individual component (frame bending, panel shear, rigid body rotation and fastener slip) to the entire wall displacement is summarized for the service limit state (SLS) and the ultimate limit state (ULS), in Table 3.3.

Tab. 3.3: Displacement contributions according to the elastic shear field theory

Frame bending δ_1	Panel shear δ_2	Rigid body rotation δ_3	Fastener slip δ_4	Wall displ. Δ_{wall}
$[mm]$	$[mm]$	$[mm]$	$[mm]$	$[mm]$
Displacement Contributions for $\delta_{n,ser} = 0.6[mm] \Rightarrow$ SLS				
0.53	4.53	1.23	3.33	9.62
5.5%	47.0%	12.8%	34.6%	100%
Displacement Contributions for $\delta_{n,max} = 9.0[mm] \Rightarrow$ ULS				
1.11	9.58	2.61	50.0	63.30
1.8%	15.1%	4.1%	79.0%	100%

At the SLS stage, the elastic displacement contributions from the frame bending, panel shear and the rigid body rotation are $6.287[mm]$, or 65.4% of the total displacement. The inelastic displacement induced by the fastener slip is $3.3[mm]$ or 34.6%. The force corresponding to the SLS stage is $137.5[kN]$ or 47.3% of $F_{wall,max} = 291[kN]$.

At the USL stage the elastic displacement contributions are $13.30[mm]$ or 21.0% of the entire wall displacement. The inelastic displacement is $50.0[mm]$ or 79.0%.

Nonlinear wall displacement applied on one, three and six storey wall

In order to complete the analysis of LFTWs sheathed with OSB panels based on the $F - \Delta$ energy approach proposed by McCutcheon $F - \Delta$ and integrated in simple shear field theory, the relationships for one, three and six storey buildings are estimated and presented in Figure 3.15(a) and 3.15(b). The lateral load is assumed to be equal to the shear wall resistance.

[1] The rigid body rotation at the actual force level can be estimated by using the rotation stiffness as follows: $\delta_3 = \tan(F \cdot \frac{H}{K_{rot}} \cdot \frac{\pi}{180}) \cdot H$, where F is force corresponding to the wall displacement, and K_{rot} is constant estimated from $\delta_{3,max}$ by using simple trigonometry $\alpha = \arctan(\frac{\delta_{3,max}}{H})$; $K_{rot} = \frac{F \cdot H}{\alpha(rad)} = \frac{F \cdot H \cdot \pi}{\alpha \cdot 180} = \frac{291 \cdot 3.2 \cdot \pi}{0.0467 \cdot 180} = 348.0[\frac{kNm}{rad}]$

In the case of three and six storey walls, the lateral load is distributed over the wall height according to a triangular seismic load distribution, accounting for the displacement of all the components at each storey. The $F - \Delta$ relationship provides the basis for the bi-linear capacity curve approximation, depicted in Figure 3.16. The bi-linear approximation used is based on the Equivalent Energy Elastic Plastic (EEEP) -approach, reported in [71], where the initial stiffness is defined using the displacement point corresponding to $0.4 \cdot F_{wall,max}$.

The approach shown in Section 3.3 is suitable for an analysis by hand for those engineers who do not work with models involving nonlinear FE-analysis. Using this approach, an engineer obtains a clear picture as to how the wall really performs at each displacement stage. On the other hand, the analysis that has been presented is not able to take into account the deterioration due to cyclic loading, which is characteristic of every earthquake excitation. More sophisticated approaches are the subject of the next section.

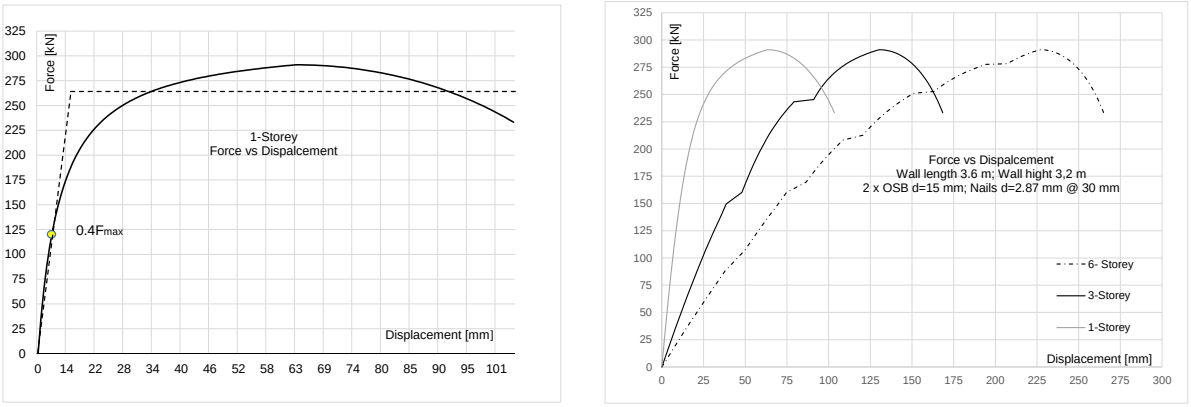

(a) (b)

Fig. 3.15: $F - \Delta$ relationship for a one storey wall B=3.6 [m], H=3.2 [m] 3.15(a): $F - \Delta$ relationship for one, three and six storey walls 3.15(b)

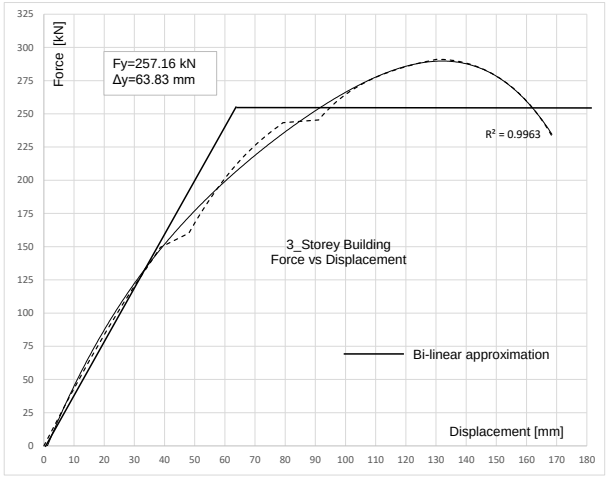

Fig. 3.16: Capacity curve of the three storey wall. Bi-linear approximation according to the EEEP-approach

3.3 Behaviour of OSB Sheathed LFTW under Cyclic Loading

3.3.1 Behaviour of a single fastener under cyclic loading

Dolan and Madsen have shown in[23] that the fasteners in timber shear walls respond non-linearly from the onset of monotonic loading. Under cyclic loading the fastener response is characterized by a pinched hysteretic behaviour accompanied by strength and stiffness degradation. In order to describe the real fastener force-displacement response the Foschi's exponential function (Equation 3.17) has been modified by Dolan and Madsen, introducing a maximum displacement value δ_{max} and a linear descending branch. Six parameters presented in Figure 3.17, $K_0, r_1, r_2, f_0, \delta_{max}$, and δ_{ult} are needed to describe the response of the individual fastener to monotonic loading. The cyclic behaviour can be defined by using the 10-parametric Stewart hysteretic model, which is described in [92]. In the CUREE- Caltech Woodframe Project, Folz and Filiatrault [33] and [30] have used the Stewart hysteresis to describe the response of a fastener subjected to cyclic loading in the MatLab-based computer program MCASHEW. The envelope for the cyclic response is given by Foschi's exponential monotonic curve, as presented in Figure 3.18.

$$f_{fast} = \begin{cases} f_0 + r_1 \cdot k_0 \cdot \delta \cdot [1 - e^{\frac{-k_0 \cdot \delta}{f_0}}] & for \quad \delta < \delta_{max} \\ r_2 \cdot k_0 \cdot \delta + (f_{max} - r_2 \cdot k_0 \cdot \delta_{max}) & for \quad \delta_{max} < \delta < \delta_{ult} \\ 0 & for \quad \delta > \delta_{ult} \end{cases} \tag{3.17}$$

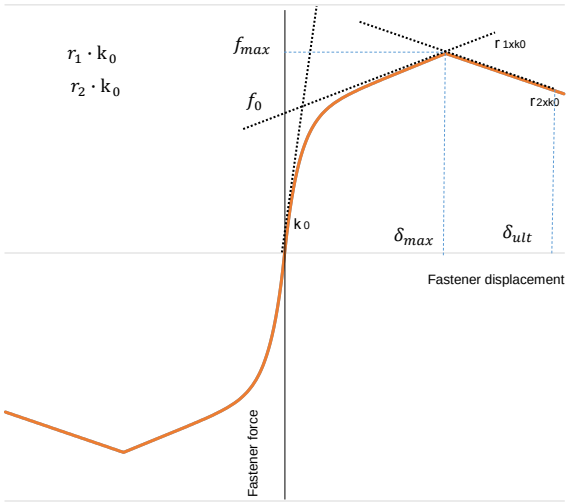

Fig. 3.17: $F - \Delta$ relationship of a sheathing to framing connector with curve defined by set of Equations 3.17

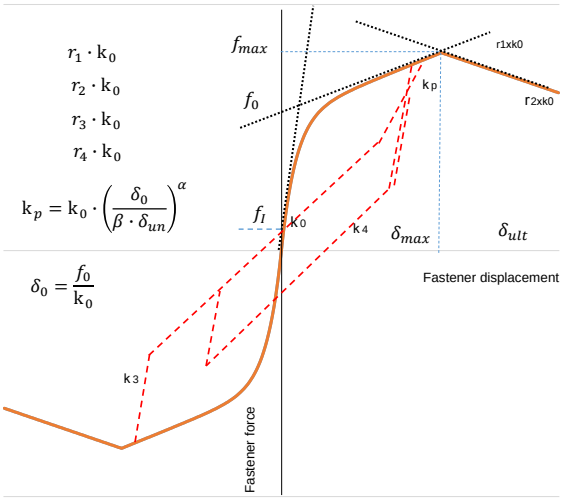

Fig. 3.18: $F - \Delta$ relationship of a sheathing to framing connector extended with parameters which define the fastener response under cyclic loading

Within the MCASHEW program, there is a possibility to read in monotonic or hysteretic test data and subsequently generate the required hysteretic parameters to define the monotonic or cyclic fastener response. However, there are only a few fasteners defined in the program library. Since all of them are based on US industrial products, materials and specific timber species, additional data using European materials are necessary to complete the MCASHEW program library. In this thesis, the cyclic loading response of nails and staples connecting with OSB panel sheathings to spruce timber members, has been investigated experimentally. In addition, the response of nails and staples to monotonic and cyclic loading has been the subject of investigation in [37]. A comprehensive investigation on nail and staple connections has been carried out in a NRP 66 project [37]. The results, presented in [69] and [37] for OSB plates with thickness $t_p = 15[mm]$, have also been incorporated to define the asymptotic and hysteresis parameter for nails and staples in CASHEW.

Experimental cyclic parameter estimation

A total of 30 connections (see Figure 3.23(a)) have been investigated using cyclic loading protocols. The number of fasteners in the connection, the fastener diameter, the OSB panel thickness and the cyclic protocol were varied. The fasteners used were nails with $d = 2.45$ and $2.87[mm]$ and staples with $d = 1.53[mm]$. The OSB panels had two different thicknesses, $t_p = 12$ or $18[mm]$, and the loading protocols used were CUREE [54] or Mergos-Beyer [67]. The later loading protocol has been developed for European regions of low to moderate seismicity. The tests performed on fasteners with different connection configurations are summarized in Table 3.4 and presented in Figure 3.19(a) and 3.19(b).

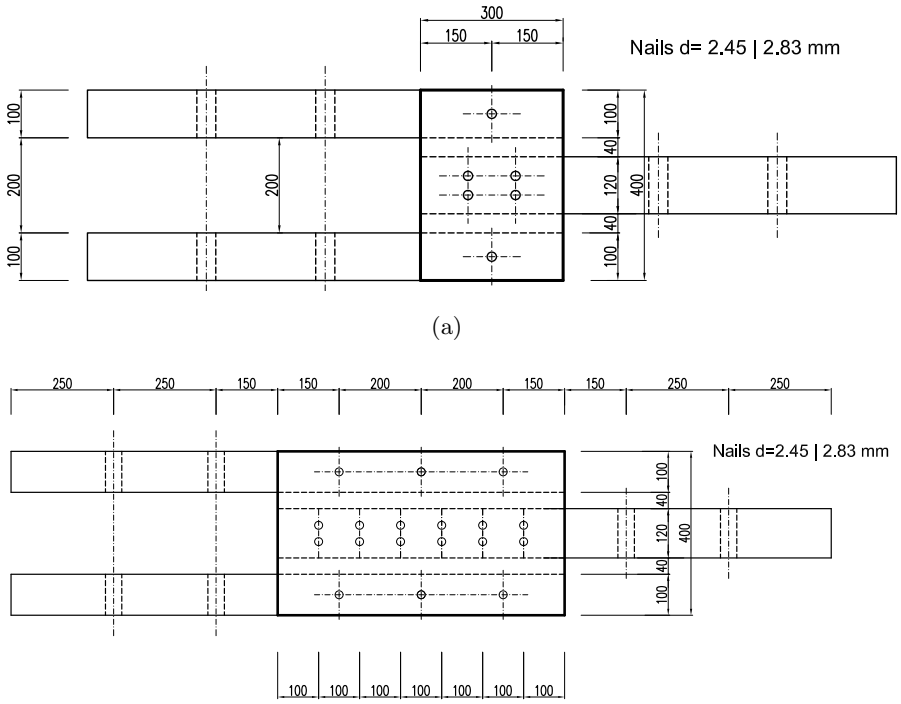

Fig. 3.19: Secimen with one-nail-connection 3.19(a): Specimen with three-nails-connection 3.19(b)

Tab. 3.4: Test program

Test ID	Fastener number	Specimen number
$na2.45 - osb12 - c$	$4 \cdot 1$	1
$na2.45 - osb12 - mb$	$4 \cdot 1$	1
$na2.45 - osb18 - c$	$4 \cdot 1$	1
$na2.45 - osb18 - mb$	$4 \cdot 1$	1
$na2.45 - osb12 - c$	$4 \cdot 3$	2
$na2.45 - osb12 - mb$	$4 \cdot 3$	2
$na2.45 - osb18 - c$	$4 \cdot 3$	2
$na2.45 - osb18 - mb$	$4 \cdot 3$	2
$na2.87 - osb12 - c$	$4 \cdot 1$	1
$na2.87 - osb12 - mb$	$4 \cdot 1$	1
$na2.87 - osb12 - c$	$4 \cdot 3$	2
$na2.87 - osb12 - mb$	$4 \cdot 3$	2
$st1.53 - osb12 - c$	$4 \cdot 1$	1
$st1.53 - osb12 - mb$	$4 \cdot 1$	1
$st1.53 - osb18 - c$	$4 \cdot 1$	1
$st1.53 - osb18 - mb$	$4 \cdot 1$	1
$st1.53 - osb12 - c$	$4 \cdot 3$	2
$st1.53 - osb12 - mb$	$4 \cdot 3$	2
$st1.53 - osb18 - c$	$4 \cdot 3$	2
$st1.53 - osb18 - mb$	$4 \cdot 3$	2
Total		30

Loading protocols

The loading protocols used for the tests were intended to represent the cumulative damage demand imposed by an earthquake. The majority of the loading protocols used worldwide have been developed to reproduce cumulative damage effects caused by strong ground motions. Gato

and Uang have investigated the differences in response of timber shear walls subjected to various loading histories. It is reported in [35] that different loading sequences significantly influence the performance of LFTWs. If the existing loading protocols, developed to capture the cumulative damage demands imposed by strong ground motions, are used for regions of low to moderate seismicity, the displacement or bearing capacity of the structures may be underestimated (see also [67]).

CUREE loading protocol

Due to the long variation in earthquake characteristics and also in the possible structural configurations, there is no "best" loading protocol. In the CUREE Caltech project (Krawinkler at all 2001 [54]), several loading protocols for testing LFTWs have been developed. The reference parameter chosen to represent the cumulative damage demand caused by strong ground motions is the maximum displacement Δ, usually set to the maximum displacement the LFTW can sustain, e.g. $\Delta = 2.5\%$ of the height . When the maximum displacement amplitude is reached, the specific performance of the investigated specimen is assessed. The loading protocol is presented in Figure 3.20. Although it is intended to be applied in regions of high seismicity, the CUREE loading protocol will be used in this thesis to enable comparison with the Mergos-Beyer loading protocol, which represents the cumulative damage demand in regions of low to moderate seismicity.

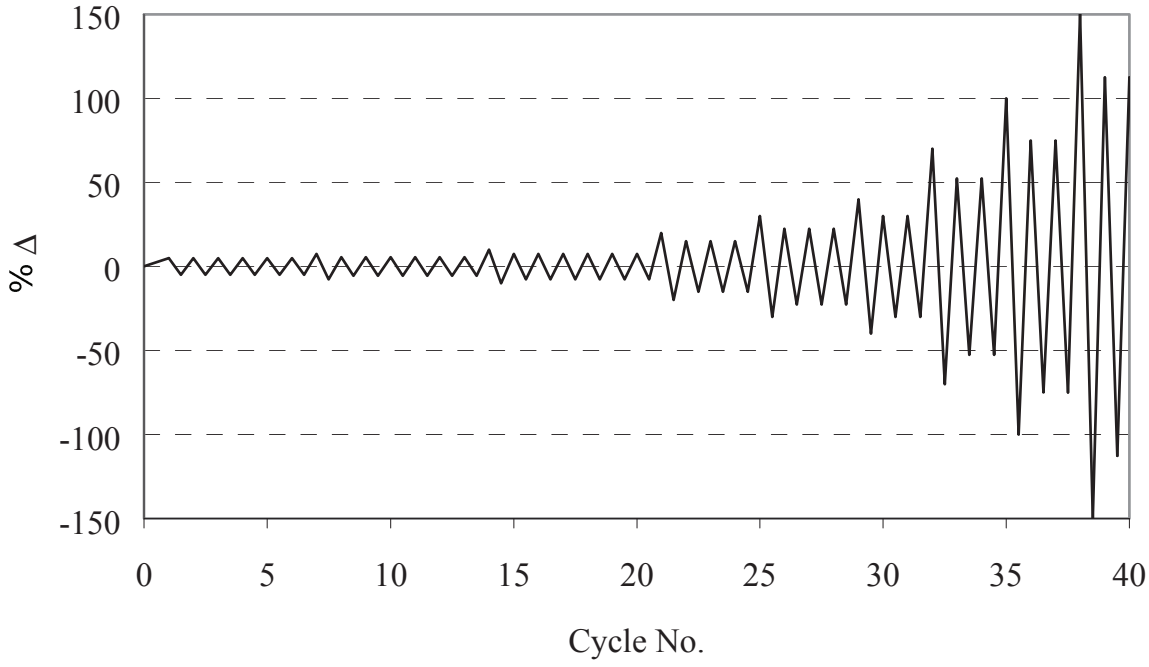

Fig. 3.20: CUREE loading protocol for testing of woodframe structures developed by Krawinkler et al. 2001 in frame of the CUREE Caltech project

Mergos-Beyer loading protocol

The development of the Mergos-Beyer loading protocol is presented in [67]. The methodology comprised four steps:

- Selection and scaling of ground motion records
- Selection of representative structural systems
- Calculation of cumulative seismic demands, and
- Establishment of loading protocols

The methodology has been developed for a wide range of structures and materials, such as reinforced concrete, steel, masonry and timber structures. Sixty earthquake records, which characterize the Swiss seismic conditions have been selected and scaled to the required hazard level. Cumulative damage effects depend on the type of structure considered. Timber structures are represented by a SDOF system whose response is based on Stewart's 10-parameter hysteretic model. The force amplitudes, which meet the calculated cumulative damage demands, are given in Equation 3.18. Two parameters, n_c and α_c, are needed to determine the normalized loading protocol sequence. The user can choose how many different amplitudes, n, and how many cycles per amplitude step, n_1, the loading protocol should contain.

$$f_{(x)} = -0.5 + 0.55 \cdot \ e^{(\frac{x}{n})^{\alpha}} \tag{3.18}$$

However, there are three possibilities to choose the appropriate loading protocol. For the most realistic stiffness of single-storey LFTW of $0.3[s]$, the amplitudes number in each subsequent cycle is 1, 2 or 3. If only one amplitude within a cycle would be chosen, the number of cycle sequences would be 13. Since the amplitudes continuously increase in each cycle, due to the number of repletion $n_1 = 1.0$, this specific Mergos-Beyer loading protocol would not provide information about strength and stiffness degradation within one specific cycle sequence. The loading protocol characterized by 13 different steadily increased amplitudes is not suitable for obtainining the information how the fastener behaves within one cycle with repeated amplitude.

In the case of the loading protocol with three equal amplitudes within a loading sequence the total number of loading sequences is reduced to merely three, which is not enough to represent the cumulative damage potential of the cyclic loading. In addition, the differences in the intensity of the amplitudes in two consecutive sequences are far too large, so that the behaviour of the structure in medium amplitude ranges would not be covered. So, the best results can be expected from the loading protocol containing two amplitudes within each cyclic sequence. As shown in Figure 3.21, in this work, an SDOF system with a natural period of vibration $t = 0.3[s]$, the number of different cycles sequences is $n = 6$ and the number of equal amplitudes within an cycle sequence has been chosen to be $n_1 = 2$ in order to construct the Mergos-Beyer loading protocol used for fastener testing. The structural performance is investigated at the life safety limit state. According to [17] this limit state correspondes to an Interstorey Drift Ratio (IDR) of 2% . The same loading protocol is also applied for the testing of LFTWs under cyclic loading.

Timber walls - Wayne Stewart (WS) hysteresis

	Vibration period T [s]	n_1 = 1	n_1 = **2**	n_1 = 3
n	0.1	26	12	7
α		3.94	3.97	9.81
n	0.2	15	7	4
α		2.96	2.93	2.85
n	**0.3**	13	**6**	3
α		3.16	**2.98**	2.71
n	0.5	11	5	2
α		3.16	3.07	2.48

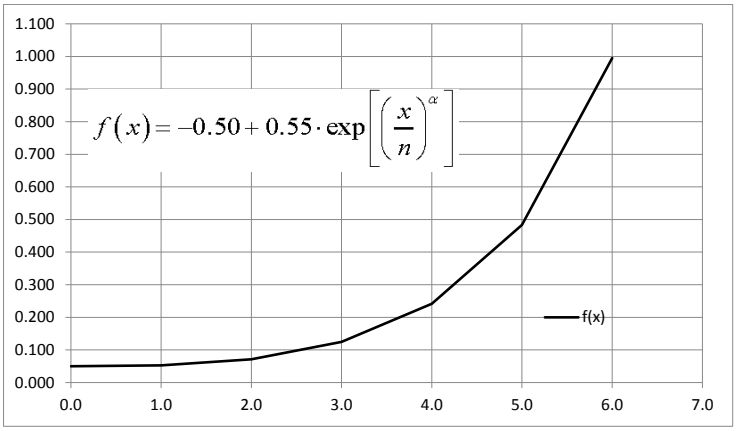

Fig. 3.21: Parameter chosen for the Mergos-Beyer loading protocol

The parameters chosen led to the loading protocol presented in Figure 3.22.

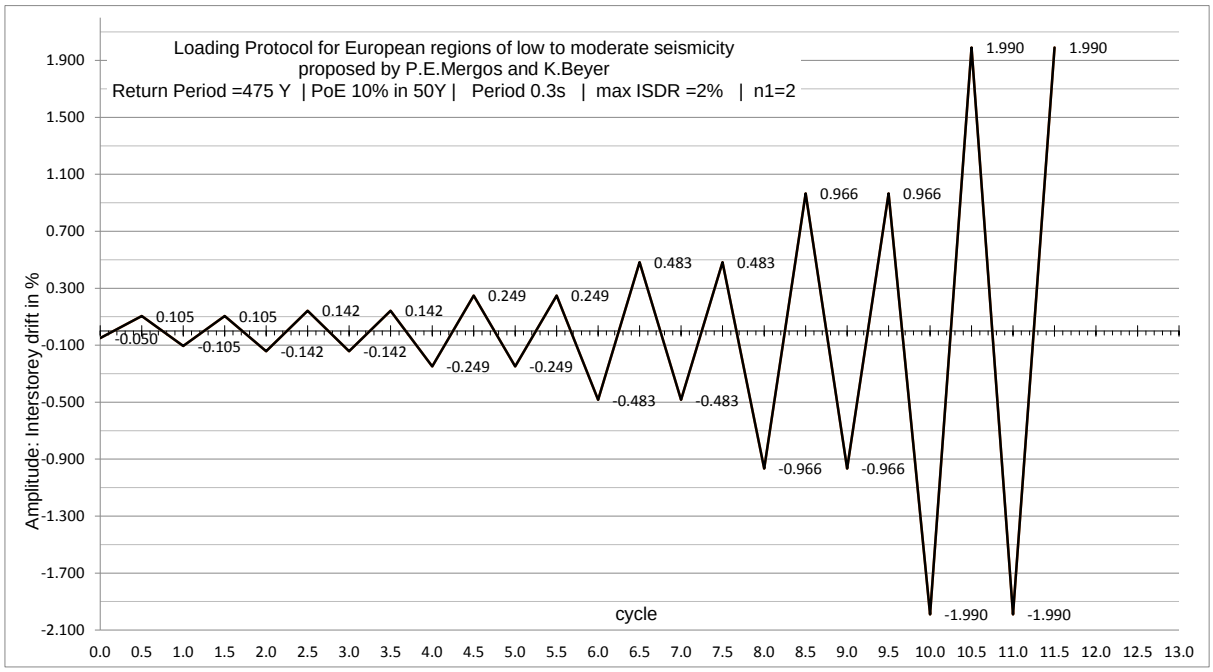

Fig. 3.22: Mergos-Beyer loading protocol corresponding to the parameters presented in figure 3.21

Test on nailed and stapled connections

Figure 3.23(b) shows a specimen with three nails on each stud member and each side before testing, and Figure 3.24(a) shows the specimen during testing. In Figure 3.24(b), a typical fastener pull-out behaviour under cyclic loading is presented. The specimens with one or three fasteners have been compared in order to investigate whether the number of fasteners affects the response. No differences have been observed, as can be seen in Figure 3.25. The response of a stapled connection containing four staples with $d = 1.53[mm]$ in a connection with OSB panels with $t_p = 12[mm]$ exposed to the Mergos-Beyer loading protocol is compared to the response

using staples with d=1.53 [mm] exposed to the CUREE loading protocol. The results are shown in Figure 3.26(a) and Figure 3.26(b), respectively.

(a) (b)

Fig. 3.23: A total of 30 specimens were tested in order to obtain the fastener response to cyclic loading 3.23(a): Connection specimen with three nails per timber member 3.23(b)

(a) (b)

Fig. 3.24: Specimen during the testing with "Kleine Schenk" with NDI and LVDT installation 3.24(a): Nail pull out during testing 3.24(b)

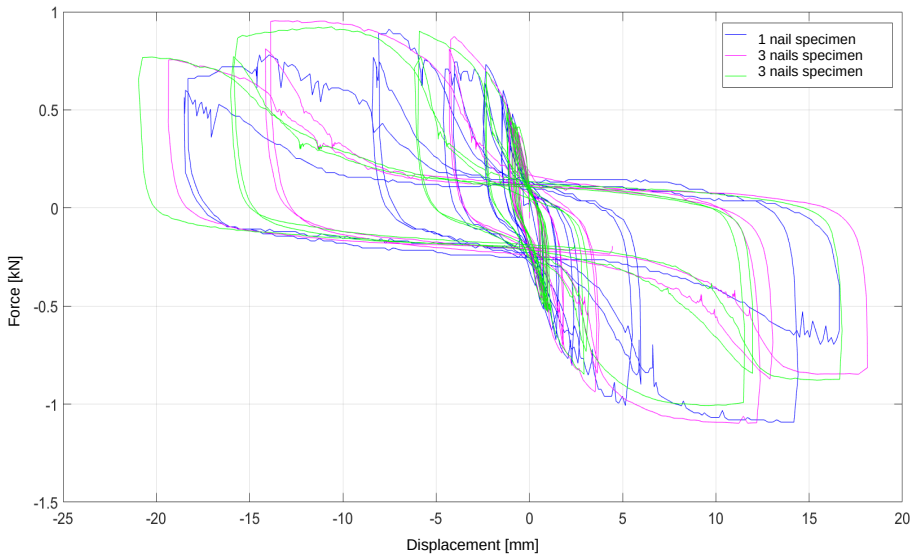

Fig. 3.25: Typical hysteresis obtained from cyclic loading for nail $d = 2.45[mm], t_p = 12[mm]$ under Mergos-Beyer loading protocol

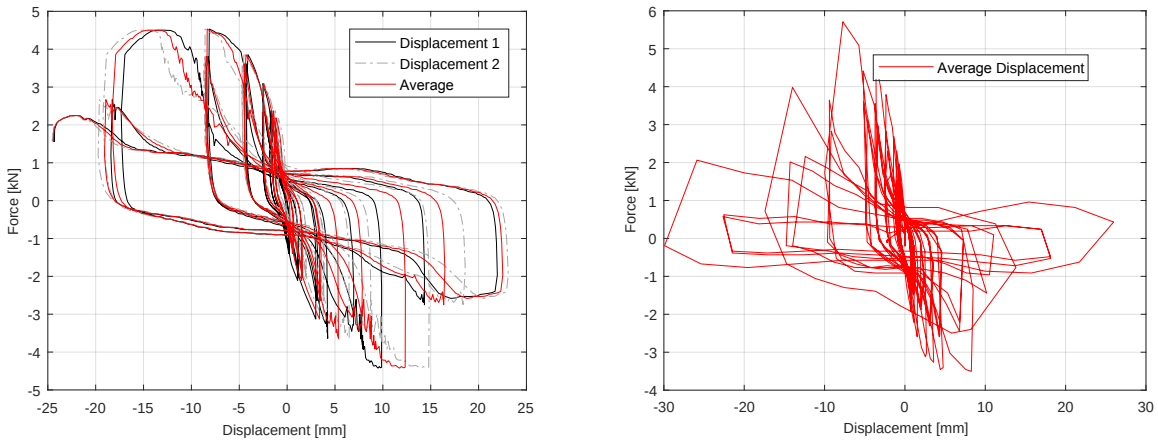

(a) (b)

Fig. 3.26: Response of the connection consisting of 4 staples with $d = 1.53[mm]$, OSB panel thickness $t_p = 12[mm]$ to Mergos-Beyer loading protocol 3.26(a): Response of the connection consisting of 4 staples with $d = 1.53[mm]$, OSB panel thickness $t_p = 12[mm]$ to CUREE loading protocol 3.26(b)

Raw data on the hysteretic fastener response have been imported into the MCASHEW program, and the tool MSTEWfit has been used to generate, the Stewart hysteresis parameters to achieve the best fit of the tested and the extracted curve. The success of the curve fitting is evaluated by comparing the cumulative energy dissipated during test and in the model. Figure 3.27 shows how the raw test data for nails with $d = 2.45[mm]$ and $t_p = 18[mm]$ have been read in the program. Figure 3.28 presents the Stewart hysteresis generated, displayed with the corresponding hysteresis parameters. The amounts of dissipated energy are approximately equal along the entire range, indicating sufficiently good agreement. In Figures 3.29, 3.30 and 3.31,

consolidated data from nails $d = 2.45, 2.87$ and $3.31[mm]$ are presented. The hysteretic data from different nail diameters and thicknesses of sheathing material are listed in Table 3.5, and data from staples with $d = 1.53[mm]$ are listed in Table 3.6. The hysteresis parameters for staples are not affected by different sheathing material thicknesses. The test results show, that the bearing capacity does not increase with increasing of the sheathing material thickness and can even decrease. This outcome can be understood by looking at the Johansen's equations and the role of the fastener length and the contribution of $f_{ax,Rk}$ to the bearing capacity (the fastener length was not adjusted during the testing to the thickness of the sheathing material). The estimated parameters of the Stewart hysteresis model for different staple diameters hold true for sheathing material thicknesses between $12 < t_p < 18[mm]$. Furthermore, the parameters for the staples with $d = 1.8$ and $2.0[mm]$, which were not tested, were fitted to the asymptotic equation proposed by Foschi [34] and were modified by Dolan [23]. The hysteretic parameters for the staples are given in Table 3.6.

Similar results were obtained in NRP 66 project, by Steiger, Bernasconi and Beyer, as reported in [37] and presented in Figure 3.32. Unexpectedly, for different sheathing thicknesses, the panel with $t_p = 12[mm]$ had the maximum bearing capacity, probably due to the rope effect.

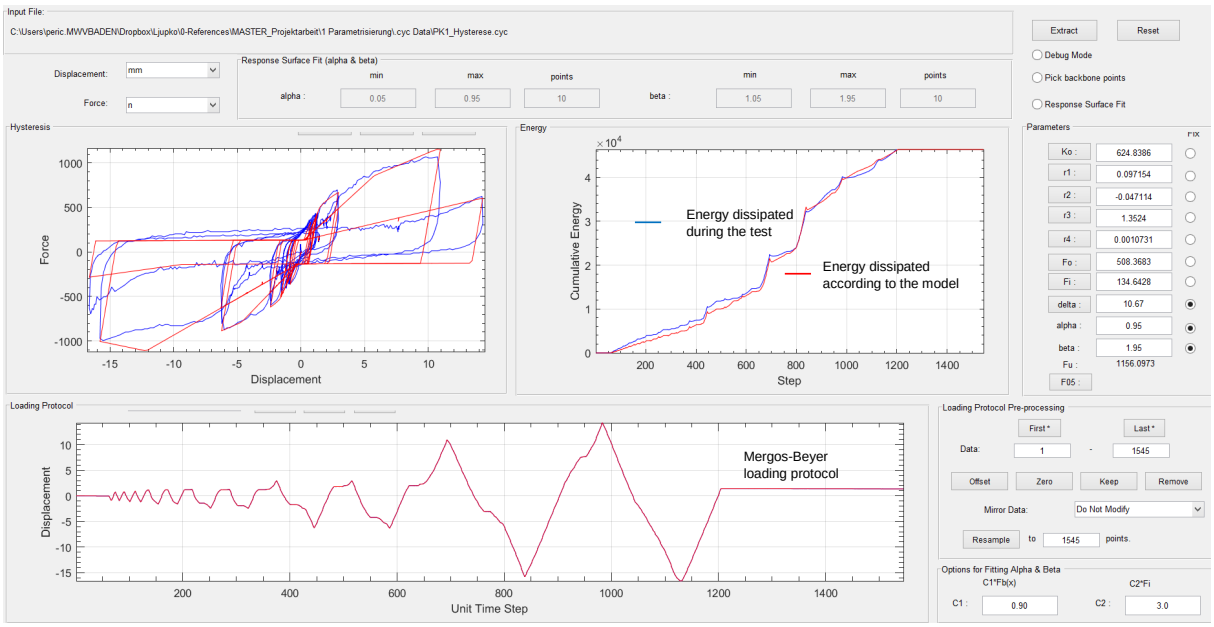

Fig. 3.27: User interface of the program MCASHEW program with generated Stewart hysteretic parameters

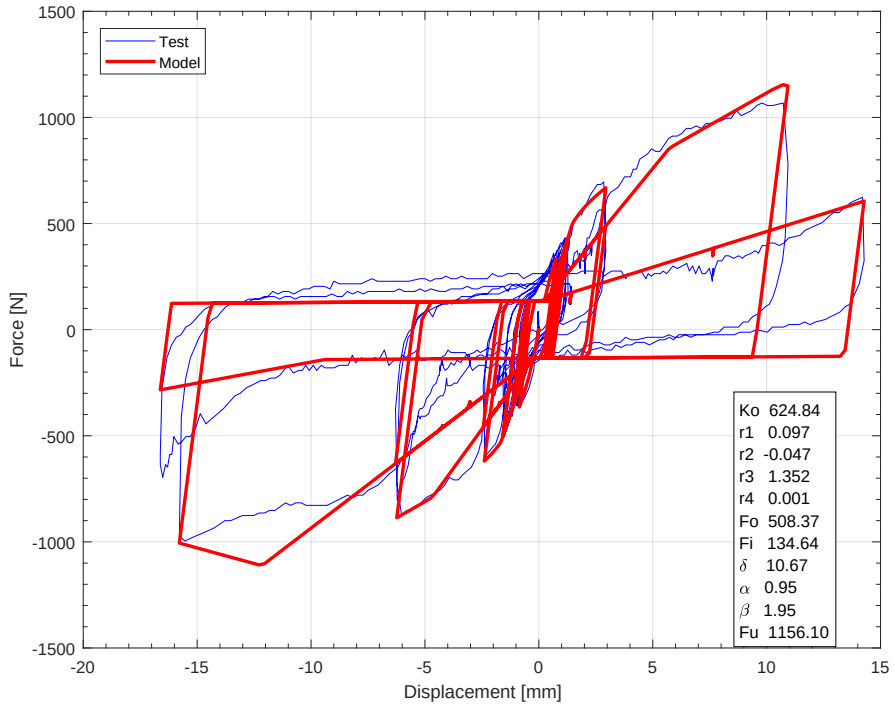

Fig. 3.28: Typical 10 parametric Stewart hysteresis obtained applying Mergos-Beyer loading protocol

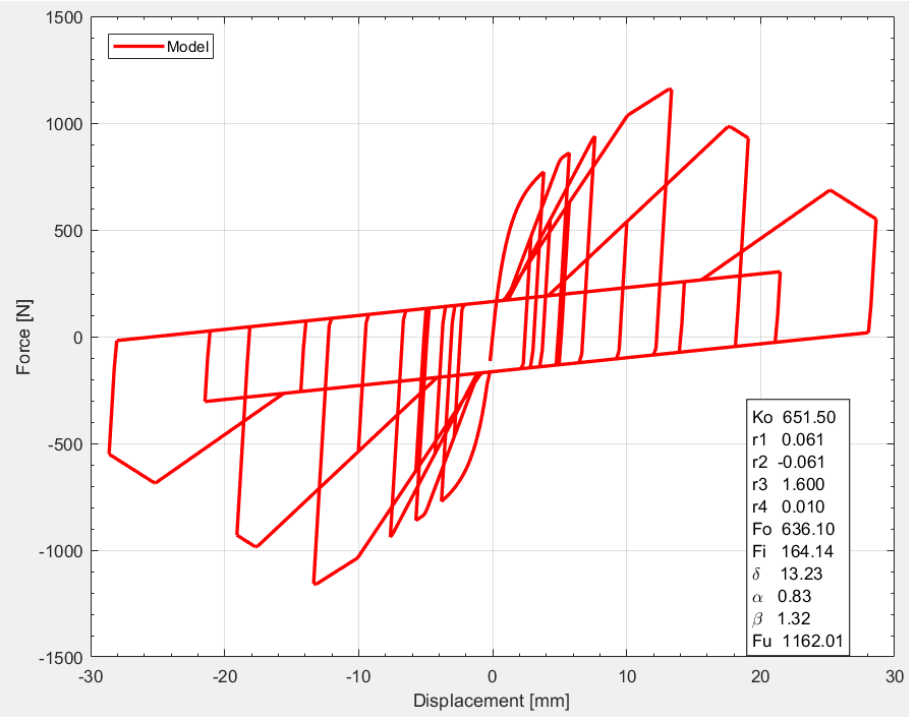

Fig. 3.29: Stewart hysteresis parameter for nail with $d = 2.45[mm]$ and $t_p = 15[mm]$

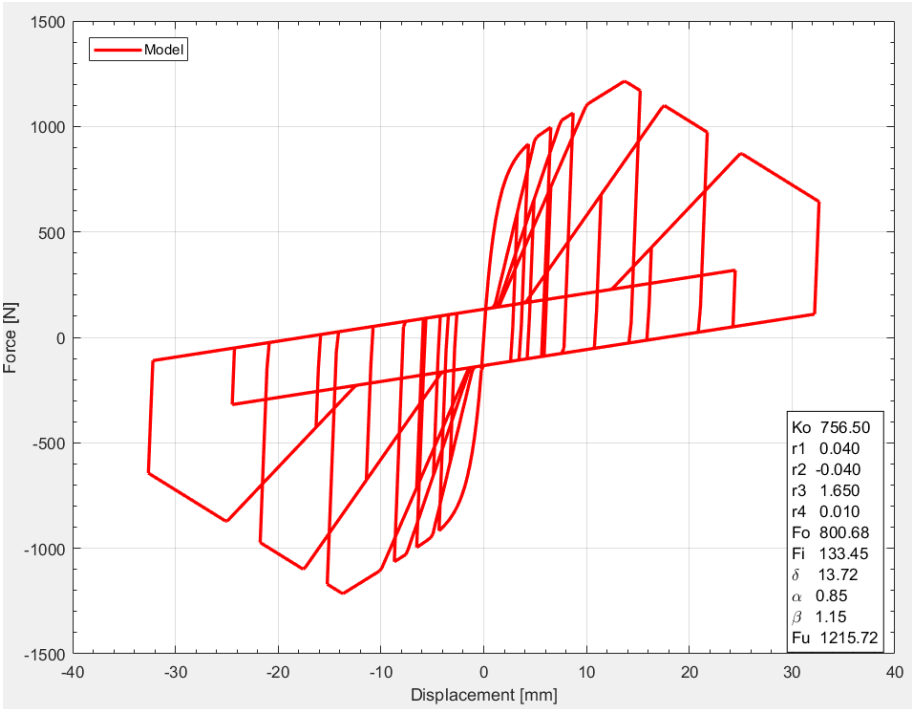

Fig. 3.30: Stewart hysteresis parameter for nail with $d = 2.87[mm]$ and $t_p = 15[mm]$

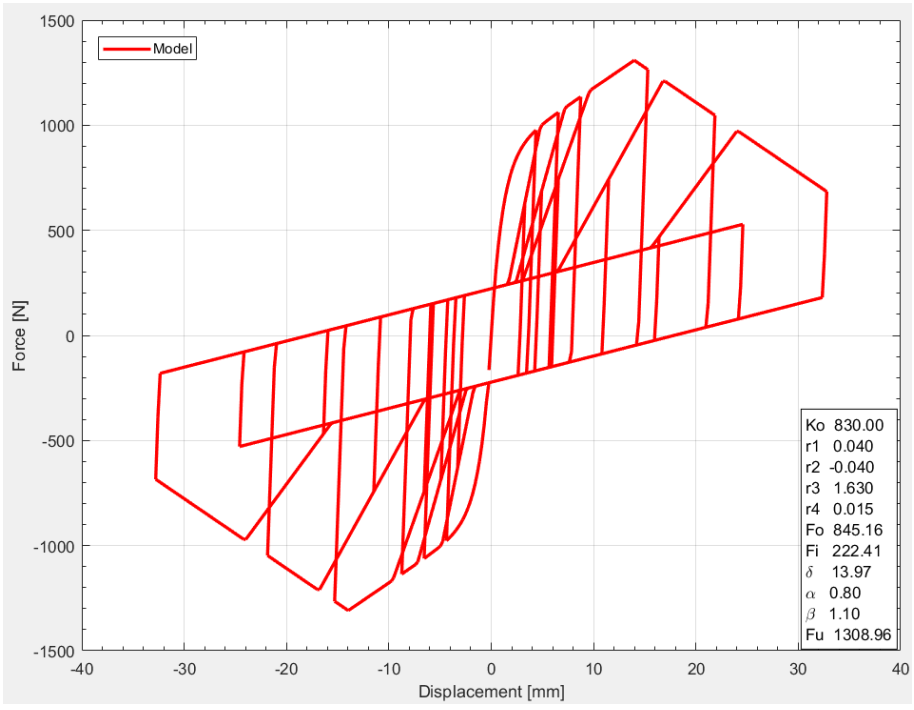

Fig. 3.31: Stewart hysteresis parameter for nail with $d = 3.31[mm]$ and $t_p = 15[mm]$

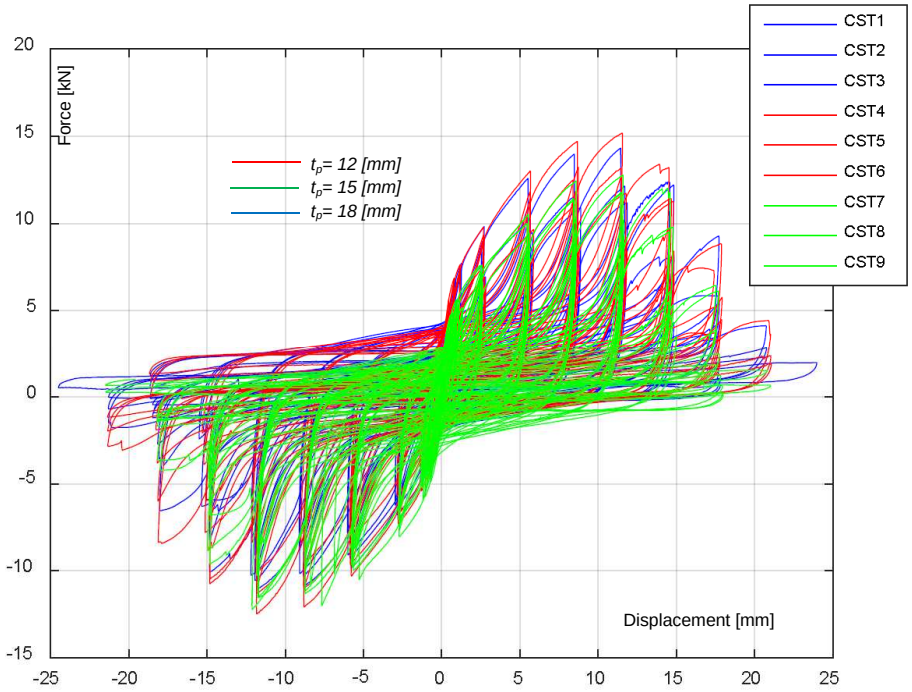

Fig. 3.32: Connection response to cyclic loading for different OSB panel thicknesses $t_p = 12, 15$ and $18[mm]$ according to [69]

Tab. 3.5: Parameters of the Stewart hysteresis for nails estimated by using the Mergos-Beyer loading protocol

d_{nail}	t_p	k_0	r_1	r_2	r_3	r_4	f_0	f_i	δ_{max}	α	β	f_{max}
[mm]	[mm]	[N/mm]	[-]	[-]	[-]	[-]	[N]	[N]	[mm]	[-]	[-]	[N]
2.45	12	636	0.085	-0.06	1.47	0.01	509	133	10.7	0.85	1.36	1066
	15	652	0.061	-0.061	1.60	0.01	636	164	13.2	0.83	1.32	1162
	18	676	0.055	-0.055	1.72	0.10	596	196	15.8	0.86	1.28	1183
2.87	12	689	0.45	-0.045	1.58	0.01	712	133	13.2	0.85	1.15	1121
	15	757	0.04	-0.04	1.65	0.01	800	147	13.7	0.85	1.15	1215
	18	789	0.04	-0.04	1.75	0.01	823	156	14.4	0.85	1.15	1276
3.31	12	757	0.05	-0.05	1.60	0.015	733	178	12.7	0.8	1.1	1226
	15	830	0.04	-0.04	1.63	0.015	845	222	14.0	0.80	1.1	1309
	18	895	0.035	-0.35	1.75	0.015	890	2.67	15.2	0.80	1.1	1369

Tab. 3.6: Parameters of the Stewart hysteresis for staples estimated by using the Mergos-Beyer loading protocol

d_{staple}	k_0	r_1	r_2	r_3	r_4	f_0	f_i	δ_{max}	α	β	f_{max}
[mm]	[N/mm]	[-]	[-]	[-]	[-]	[N]	[N]	[mm]	[-]	[-]	[N]
1.53	494	0.025	-0.094	1.74	0.011	978	149	12.0	1.0	1.21	1124
1.80	460	0.025	-0.01	1.73	0.011	1201	1593	12.0	1.0	1.21	1326
2.00	789	0.06	-0.05	2.13	0.005	1009	162	8.95	0.80	1.20	1432

3.3.2 Behaviour of the LFTW under cyclic loading

The behaviour of LFTWs under monotonic and cyclic loading was experimentally investigated by many researchers all around the world. All of the tests aimed to obtain force-displacement data on the response of LFTWs in order to calibrate or validate mathematical models. In this thesis the LFTW configuration tested at EMPA in NRP 66 project and reported in [37] was used the referent for validation of the numerical MCASHEW model. The hysteresis parameters obtained for a staple with $d = 1.53[mm]$ presented in Table 3.6.
The parameters which control both monotonic and cyclic analysis in MCASHEW are presented in detail in [31]. The fasteners are considered to be zero length non-linear spring elements. They are unidirectional for monotonic loading and orthogonally oriented bi-directional spring elements for cyclic loading. See figures 3.33(a) and 3.33(b).

In the NRP 66 project [37], [58], a typical LFTW configuration was investigated. The width was $B = 2.5[m]$, the height was $H = 2.8[m]$, the sheathing material was OSB/3, with $t_p = 15[mm]$ and staples with $d = 1.53[mm]$, and spacing of $50[mm]$, were used. The magnitudes of the vertical and lateral loading protocols were varied. The test set-up is shown in Figure 3.34. Tests with low vertical loads, monotonic quasi-static loading and the Mergos-Beyer cyclic loading protocol are suitable for comparison to numerical analyses performed within this thesis. According to [37] and [58], Walls 3 and 6 (for monotonic loading) and Wall 4 (for cyclic loading) were appropriate to be analyzed for comparison purposes. Figures 3.35(a) and 3.36(a) show the responses of Walls 3 and 4 subjected to monotonic and cyclic loading in physical tests, while Figures 3.35(b) and 3.36(b) show the response of the wall modeled in MCASHEW, subjected to monotonic and cyclic loading. The results obtained by tests under monotonic (Wall 3 and Wall 6) and cyclic loading (Wall 4) and the results from the analytical model based on the McCutcheon energetic approach (Wall 3) as well as the MCASHEW results for monotonic and cyclic loading (Wall 3) are summarized in Table 3.7 and compared. Unfortunately, the hysteretic parameters obtained by the tests are not listed in [37] and [58], so they cannot be compared. The few values available were the initial stiffness K_0 and shear resistance F_{max}. These are specified and compared in Table 3.7. The numerical MCASHEW model of Wall 3 with the staple diameter of $1.53[mm]$, Table 3.6, describes the real wall behaviour sufficiently accurately. The differences between numerically estimated and during the tests obtained wall strength and displacement capacity for the same Wall W3 under monotonic loading and the Mergos-Beyer loading protocol

is less than ±3.0%. The model based on the McCutceon energetic approach also describes the wall behaviour sufficiently well. Thus, modeling with MCASHEW was validated. Based on these findings, the approach presented previously was applied on walls with lengths of $2.4, 3.0, 3.6, 4.2$ or $4.8[m]$ in order to obtain a 10 parameter Stewart hysteretic model. Each wall length was represented by a non-linear shear spring element, defined by the 10 parameter Stewart hysteretic model. The fastener chosen for the parametric study was a nail with $d = 2.87[mm]$, a spacing of $30[mm]$, and an OSB sheathing plate with thickness of $t_p = 15[mm]$. The hysteretic parameters were estimated for both single and double sheathed LFTWs. These are summarized in Tables 3.8, 3.9, 3.10, 3.11 and 3.12.

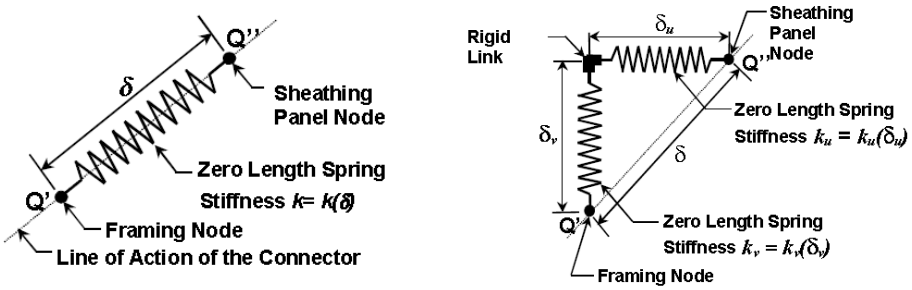

(a) (b)

Fig. 3.33: Unidirectional zero length non-linear spring element for monotonic loading 3.33(a): Bi-directional orthogonally oriented zero length non-linear spring element for cyclic loading 3.33(b) according to [31]

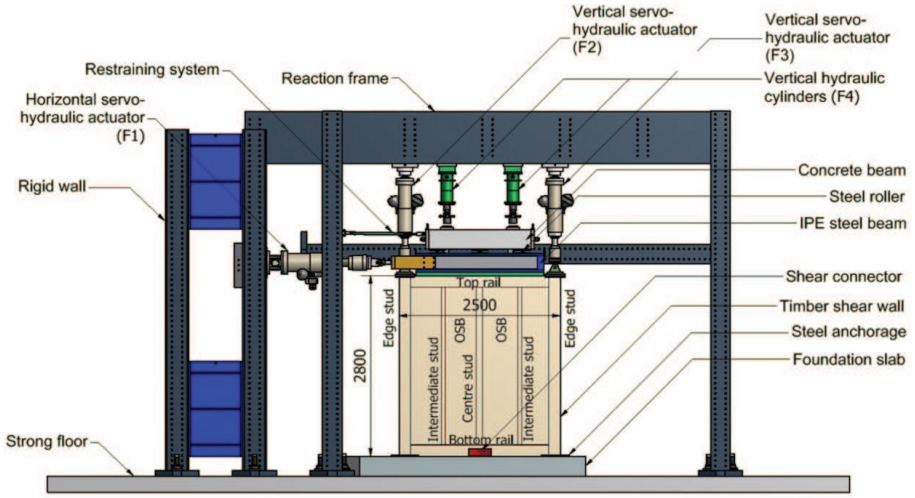

Fig. 3.34: Testing facility for testing of LFTWs at Empa within a Projet NRP 66 according to [37]

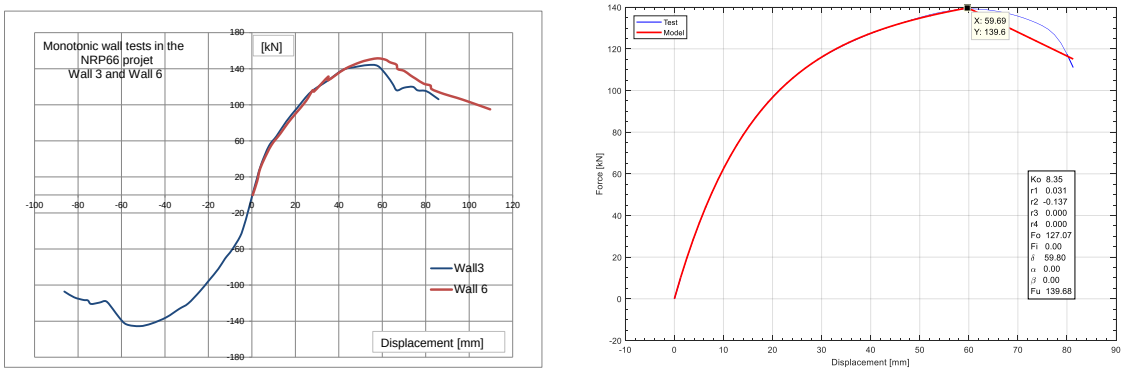

(a) (b)

Fig. 3.35: Response of Wall 3 and Wall 6 tested in the NRP 66 project [37], 3.35(a): Numerical response to monotonic loading of the wall modeled in MCASHEW using the staple parameters given in Table 3.6 3.35(b)

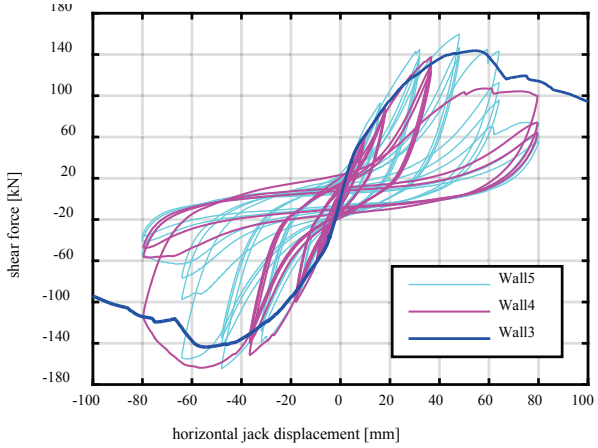

(a)

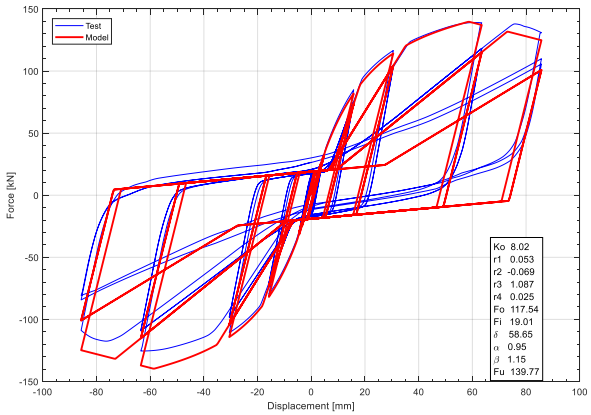

(b)

Fig. 3.36: Response to monotonic and cyclic loading of Wall 3 and Wall 4 tested in the NRP 66 project [37] 3.36(a):Numerical response of Wall 3, modeled in MCASHEW using the staple parameters given in Table 3.6, to the Mergos-Beyer loading protocol 3.36(b)

Tab. 3.7: Estimated parameter of Stewart hysteresis for the wall tested at Empa in the NRP 66 project [37]

Wall	protocol	K_0	R_1	R_2	R_3	R_4	F_0	F_i	Δ_{max}	α	β	F_{max}
		[kN/mm]	[-]	[-]	[-]	[-]	[kN]	[kN]	[mm]	[-]	[-]	[kN]
W3	Empa NRP project	9.9							57.9			144
	monotonic	100%							100%			100%
W6	Empa NRP project	8.7							58.5			152
	monotonic	88%							100%			106%
W4	Empa NRP project	8.9							58.5			152
	Mergos-Beyer LP	90%							100%			106%
W3	McCutcheon	6.4	0.027	-0.086			105.25		68.23			117
		81%							118%			81%
W3	CASHEW	8.35	0.031	-0.137			127.07		59.80			140
	monotonic	84%							103%			97%
W3	CASHEW	8.02	0.053	-0.069	1.09	0.025	117.5	19.0	58.65	0.95	1.15	1340
	Mergos-Beyer LP	81%							101%			97%
W3	CASHEW	8.11	0.022	-0.311	1.15	0.039	124.5	17.75	73.24	1.0	1.11	137
	CUREE LP	82%							126%			95%

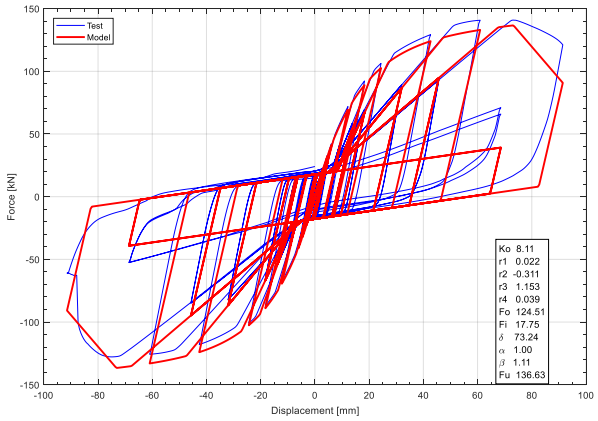

(a)

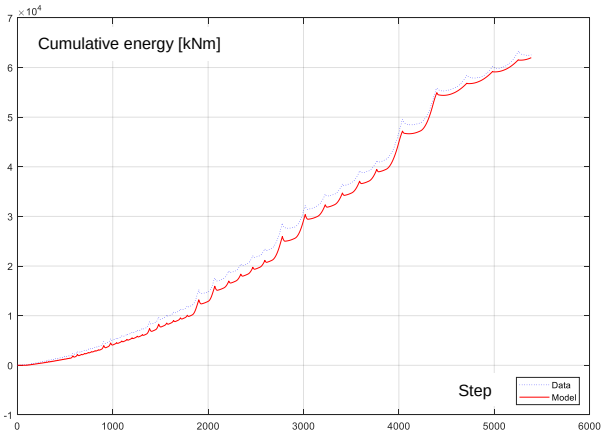

(b)

Fig. 3.37: Response of wall Wall 3 modeled in MCASHEW by using the staple parameters given in table 3.6 to the CUREE loading protocol 3.37(a): Cumulative energy dissipation of Wall 3 corresponding to the CUREE loading protocol 3.37(b)

Tab. 3.8: Estimated parameters of the Stewart hysteresis for a wall length of 2400[mm], wall height of 2800[mm], single and double sheathed wall with OSB3, $t_p = 15[mm]$, fastener: nail $d = 2.87[mm]$, spacing 30[mm], fastener hysteresis according to table 3.5

OSB	K_0	R_1	R_2	R_3	R_4	F_0	F_i	Δ_{max}	α	β	F_{max}
#	[kN/mm]	[-]	[-]	[-]	[-]	[kN]	[kN]	[mm]	[-]	[-]	[kN]
CASHEW monotonic loading											
1	9.5	0.037	-0.1	-	-	70.9	-	90.4	-	-	102.3
2	12.70	0.052	-0.20	-	-	138.0	-	94.2	-	-	200.0
CASHEW Mergos-Beyer loading protocol											
1	9.16	0.037	-0.11	1.18	0.015	69.4	14.6	90.3	0.85	1.15	99.7
2	12.86	0.052	-0.21	1.14	0.018	134.0	21.6	87.6	0.89	1.0	192.2
CASHEW CUREE loading protocol											
1	8.23	0.057	-0.047	1.04	0.018	69.5	12.6	76.8	0.95	1.05	105.7
2	13.12	0.054	-0.16	1.13	0.02	131.3	21.5	87.7	0.90	1.0	193.4
McCutcheon energy based approach											
1	6.39	0.027	-0.06	-	-	84.4	-	66.6	-	-	96.0
2	8.89	0.036	-0.088	-	-	168.8	-	73.1	-	-	192.1

Tab. 3.9: Estimated parameters of the Stewart hysteresis for a wall length of 3000[mm], wall height of 2800[mm], single and double sheathed wall with OSB3, $t_p = 15[mm]$, fastener: nail $d = 2.87[mm]$, spacing 30[mm], fastener hysteresis according to table 3.5

OSB	K_0	R_1	R_2	R_3	R_4	F_0	F_i	Δ_{max}	α	β	F_{max}
#	[kN/mm]	[-]	[-]	[-]	[-]	[kN]	[kN]	[mm]	[-]	[-]	[kN]
CASHEW monotonic loading											
1	14.03	0.043	-0.083	-	-	92.5	-	72.61	-	-	136.0
2	19.40	0.055	-0.11	-	-	181.0	-	80.95	-	-	268.0
CASHEW Mergos-Beyer loading protocol											
1	14.67	0.047	-0.025	1.19	0.018	87.6	15.5	62.63	0.85	1.15	130.7
2	19.84	0.061	-0.10	1.072	0.020	171.7	28.8	72.85	0.85	1.05	260.1
CASHEW CUREE loading protocol											
1	13.66	0.045	-0.15	1.2	0.007	87.6	13.3	66.8	0.85	1.14	128.8
2	20.14	0.055	-0.144	1.08	0.02	173.7	27.8	67.3	0.85	1.05	248.8
McCutcheon energy based approach											
1	8.45	0.026	-0.066	-	-	107.2	-	58.5	-	-	120.0
2	11.36	0.035	-0.10	-	-	214.4	-	65.5	-	-	240.0

Tab. 3.10: Estimated parameters of the Stewart hysteresis for a wall length of 3600[mm], wall height of 2800[mm], single and double sheathed wall with OSB3, $t_p = 15[mm]$, fastener: nail $d = 2.87[mm]$, spacing 30[mm], fastener hysteresis according to table 3.5

OSB	K_0	R_1	R_2	R_3	R_4	F_0	F_i	Δ_{max}	α	β	F_{max}
#	[kN/mm]	[-]	[-]	[-]	[-]	[kN]	[kN]	[mm]	[-]	[-]	[kN]
CASHEW monotonic loading											
1	14.94	0.043	-0.083	-	-	111.5	-	80.23	-	-	163.2
2	19.07	0.0485	-0.136	-	-	232.9	-	87.63	-	-	313.8
CASHEW Mergos-Beyer loading protocol											
1	15.13	0.05	-0.082	1.15	0.017	104.9	18.1	74.68	0.87	1.04	162.3
2	19.51	0.078	-0.173	1.12	0.021	196.8	36.2	74.85	0.85	1.15	310.7
CASHEW CUREE loading protocol											
1	14.8	0.065	-0.095	1.029	0.016	100.9	22.8	72.3	0.8	1.05	170.3
2	19.54	0.05	-0.085	1.075	0.023	218.0	35.0	72.0	0.85	1.05	289.0
McCutcheon energy based approach											
1	10.43	0.029	-0.073	-	-	128.0	-	53.32	-	-	144.0
2	13.63	0.039	-0.113	-	-	256.0	-	60.63	-	-	288.0

Tab. 3.11: Estimated parameters of the Stewart hysteresis for a wall length of 4200[mm], wall height of 2800[mm], single and double sheathed wall with OSB3, $t_p = 15[mm]$, fastener: nail $d = 2.87[mm]$, spacing 30[mm], fastener hysteresis according to table 3.5

OSB	K_0	R_1	R_2	R_3	R_4	F_0	F_i	Δ_{max}	α	β	F_{max}
#	[kN/mm]	[-]	[-]	[-]	[-]	[kN]	[kN]	[mm]	[-]	[-]	[kN]
CASHEW monotonic loading											
1	15.62	0.048	-0.075	-	-	142.6	-	77.11	-	-	201.1
2	23.44	0.0485	-0.142	-	-	296.4	-	83.38	-	-	389.7
CASHEW Mergos-Beyer loading protocol											
1	15.13	0.075	-0.059	1.10	0.0166	122.0	24.0	66.93	0.85	1.1	198.4
2	24.88	0.049	-0.13	1.1	0.031	267.5	46.8	78.31	0.85	1.05	362.5
CASHEW CUREE loading protocol											
1	15.97	0.068	-0.07	1.1	0.017	121.5	23.1	55.35	0.85	1.1	181.8
2	24.91	0.055	-0.085	1.1	0.022	261.6	44.5	65.77	0.85	1.05	350.8
McCutcheon energy based approach											
1	10.94	0.027	-0.068	-	-	150.0	-	61.7	-	-	168.1
2	14.56	0.036	-0.105	-	-	300.0	-	69.5	-	-	336.1

Tab. 3.12: Estimated parameters of the Stewart hysteresis for a wall length of 4800[mm], wall height of 2800[mm], single and double sheathed wall with OSB3, $t_p = 15[mm]$, fastener: nail $d = 2.87[mm]$, spacing 30[mm], fastener hysteresis according to table 3.5

OSB	K_0	R_1	R_2	R_3	R_4	F_0	F_i	Δ_{max}	α	β	F_{max}
#	[kN/mm]	[-]	[-]	[-]	[-]	[kN]	[kN]	[mm]	[-]	[-]	[kN]
CASHEW monotonic loading											
1	16.62	0.048	-0.125	-	-	149.1	-	69.93	-	-	204.4
2	25.25	0.0485	-0.12	-	-	329.0	-	91.82	-	-	439.9
CASHEW Mergos-Beyer loading protocol											
1	17.95	0.057	-0.15	1.16	0.017	131.1	24.4	76.63	0.86	1.05	209.5
2	25.95	0.072	-0.142	1.16	0.019	283.5	49.4	76.81	0.85	1.05	428.1
CASHEW CUREE loading protocol											
1	17.06	0.053	-0.092	1.08	0.022	140.4	45.9	76.24	0.85	1.05	210.3
2	27.48	0.067	-0.128	1.017	0.022	274.1	47.4	75.21	0.85	1.15	412.9
McCutcheon energy based approach											
1	12.68	0.029	-0.074	-	-	170.7	-	57.7	-	-	192.1
2	16.48	0.039	-0.116	-	-	341.3	-	65.8	-	-	384.1

3.4 Behaviour of LFTWs Sheathed with GFB under Monotonic Loading

3.4.1 Introduction

Gypsum fiberboard (GFB) as sheathing material has traditionally been used for low and mid-rise buildings in Switzerland and other European countries. It has also been used in New Zealand, USA and Canada for low and mid-rise buildings. It provides safety against fire, and is therefore preferably used in timber structures. If the material needed to meet fire protection requirements were also used as part of the lateral load resisting system, it would be beneficial in terms of both simplification in building construction and savings from an economical point of view. On the other hand, the GFB material is highly sensitive to the influences of water and moisture. In seismic engineering, timber walls sheathed with GFB are said to be non-ductile, possess little capability of dissipating energy, and exhibit an uncontrolled behaviour. Therefore the behaviour of LFTWs shethed with GFB has not been investigated in [70], and a recommendation not to use gypsum board as part of lateral load resisting systems has been given. Despite the general attitude toward the GFB sheathing material, the companies which have dealt with timber structures and have used GFB as sheathing material for decades are strongly interested whether a feasibility range for this type of structure exists. Moreover, if a single fastener connecting the GFB panel responds in non-ductile manner, it will limit global ductility of the structure.

The displacement analysis of LFTWs sheathed with GFB is similar to the analysis of LFTWs

sheathed with OSB panels. The elastic part of the wall displacement, presented in Chapter 3.3.2 can be estimated in the same way, using the corresponding elastic material properties. The only difference from the procedure based on simple shear field theory presented is, that GFB is used instead of OSB as the sheathing material. The GFB material considered in this study is known as trademark "Rigidur H-Gipsfaserplatten". Its elastic material properties are specified in the European technical approval ETA 08/0147. GFB panels are generally produced with thicknesses between 10 and 18$[mm]$. Following mechanical parameters are specified in the product approval. The density is $\rho = 1237[\frac{kg}{m^3}]$. The average modulus of elasticity is $E = 3500$ and $4500[\frac{N}{mm}^2]$ for bending parallel and perpendicular to the grain, respectively. The shear modulus is $G = 650$ and $1300[\frac{N}{mm}^2]$ parallel and perpendicular to the grain, respectively. GFB is widely used sheathing material in Switzerland for single or double sheathed LFTWs of low-rise residential buildings.

3.4.2 Behaviour of a single fastener subjected to monotonic and cyclic loading

Single fastener under monotonic loading

In general, there is limited data from monotonic and especially cyclic fastener tests in connections with GFB. This is because the GFB is said to be brittle, so that failure occurs due to the crushing of the sheathing material before the onset of fastener inelastic deformation. Nevertheless, in NRP 66 project within Module 1 (connections), testing of nails and staples connecting GFB panels to timber frame members under monotonic and cyclic loading was scheduled.

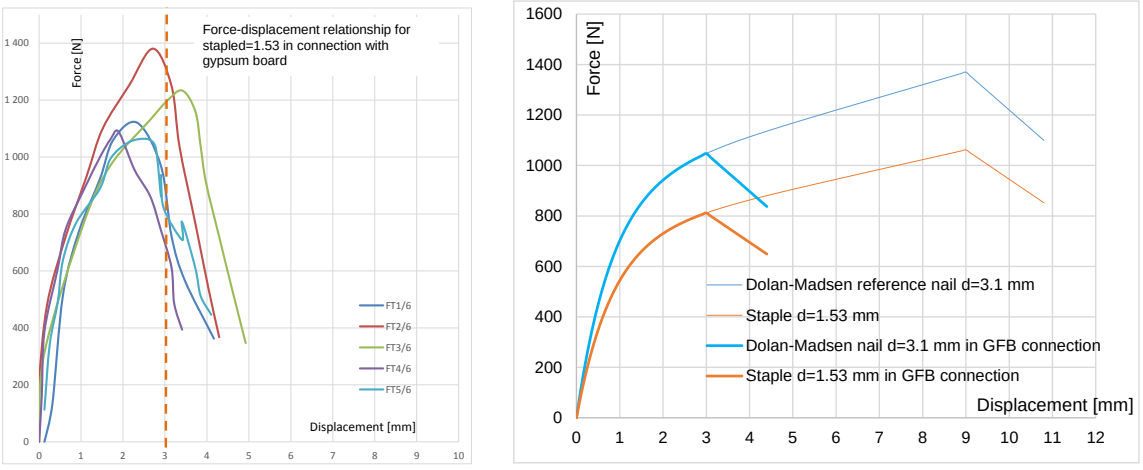

(a) (b)

Fig. 3.38: Force-displacement relationship of a staple with $d = 1.53[mm]$ in a GFB connection obtained by testing, 3.38(a): Proposed Foschi's exponential equation for the staple in the GFB connection derived from the Dolan-Madsen reference 3.38(b) with an descending branch imposed at maximum displacement of 3$[mm]$

Fig. 3.39: Failure of GFB in tension and in shear during the testing campaign, as reported in [70]

Following their investigation on connections with GFB, the research team involved in the NRP 66 project recommended canceling further tests on GFB connections [70]. Furthermore, due to the lack of connection ductility, the researchers recommended not using gypsum board in combination with lateral load resisting systems such as LFTWs. However, tension and shear tests on connections of GFB panels to the timber frame members created with staples and nails have been carried out as previously scheduled. The force-displacement relationship of staples with $d = 1.53[mm]$ in a connection with GFB board is shown in Figure 3.38(a), while the failure mechanism of the connection during testing is displayed in Figure 3.39.

As it can be seen from 3.38(a), the response appears to be elastic, onset of failure is unannounced for very small displacements in the range between approximately $2.0 - 3.5[mm]$. For such small displacements, it is reasonable to assume that the loading path is lying on the same Foschi's asymptotic curve, which has been also used by Dolan and Madsen for nail connections. Here, the maximum displacement is set to be 3 instead of $9[mm]$. The curve which obeys the Foschi's asymptotic function with an imposed limitation of $3.0[mm]$ is presented in Figure 3.38(b).

Similar recommendations can be found in S.J. Thurston in [93]. Thurston suggests using the following CASHEW parameters: a maximal displacement in the range of $2[mm]$ for screw fasteners, $3[mm]$ for nails and $4[mm]$ for nails with washer in connections with gypsum plasterboard. In this thesis, first the monotonic response of the fastener (see Figure 3.38(b)), and then the hysteretic model (see Figure 3.44) have been adopted. The first one has been derived from the regression function based on the Dolan-Madsen reference and a maximum imposed displacement of $3.0[mm]$. The second one has been fitted to Foschi$'s$ monotonic curve, where the hysteretic parameters have been partly modified to match the suggestion of Thurston in [93]. For the hysteretic model, the maximum fastener displacement has also been chosen to be $3.0[mm]$.

The parameters describing the hysteretic behaviour of a single staple in a GFB connection are given in Table 3.13.

Tab. 3.13: Proposed parameters of the Stewart hysteresis for staples $d = 1.53[mm]$ in connection with GFB, see also figure 3.44

d_{staple}	K_0	r_1	r_2	r_3	r_4	f_0	f_i	δ_{max}	α	β	f_{max}
[mm]	[N/mm]	[-]	[-]	[-]	[-]	[N]	[N]	[mm]	[-]	[-]	[N]
1.53	1220.0	0.065	-0.05	1.5	0.002	500.0	80.0	3.0	0.8	1.1	739.4

Wall element under monotonic loading

As reported previously in this chapter, if the bearing capacity of a single fastener can be estimated, the bearing capacity of the wall can also be estimated by means of the McCutcheon power function. For walls sheathed with OSB panels, the asymptotic force-displacement relationship can be described using Equation 3.10. The same type of equation can be used for walls sheathed with GFB. By comparing the experimental investigation on walls sheathed with GFB, reported in [101] and [7], with the analytical solution using the asymptotic function, the applicability of Equation 3.10 has been confirmed. The parameters a_0 and b_0 in Equation 3.19 have to be adjusted in order to reproduce the best fit to the test results in terms of both the displacement capacity and maximal strength.

$$F_{wall} = \frac{a_0 \cdot f_{u,as} \cdot \frac{B}{s} \cdot \Delta_n}{b_0 \cdot 2 \cdot \delta_{f,s} \cdot (1 + \frac{H_p}{B_p}) + \Delta_n} = \frac{1.35 \cdot f_{u,as} \cdot \frac{B}{s} \cdot \Delta_n}{0.95 \cdot 2 \cdot \delta_{f,s} \cdot (1 + \frac{H_p}{B_p}) + \Delta_n} \tag{3.19}$$

In Equation 3.19, B_p and H_p are the width and the height of the sheathing panel, respectively, s is the fastener spacing. The parameters $a_0 = 1.35$ and $b_0 = 0.95$ provide the best fit to the values obtained experimentally. The wall is considered to reach the serviceability limit state for a fastener slip of approximately $\delta_{f,s} = 0.2[mm]$. The racking displacement of the wall due to the nail slip Δ_n can be estimated using the proposal made by Stewart [92] and Deam [18], given in Equation 3.11. Equation 3.19 describes the wall behaviour sufficiently well, including the wall stiffness and degradation rate, up to the point of maximum displacement and strength as presented in Figure 3.40.

In addition to the tests conducted in Europe, in the USA by McMullin et al. (2002), reported [64], Knvinde (2006) [52] and Deierlein (2003) [19] have tested LFTWs sheathed with GFB. In the CUREE CalTech program, the seventeen wall tests conducted at San Jose State University by McMullin and Merrick (2001) have been used to develop an analytical model for LFTWs with GFB sheathing. Three different power and exponential functions have been proposed as backbone curves to capture the wall response to monotonic loading. The best fit was achieved using an exponential model with an unloading slope, labeled as Model 3. An attempt was made to capture the hysteretic behaviour of the wall containing pinching effects and strength degradation without involving a hysteretic model of a single fastener. The results were not adequate.

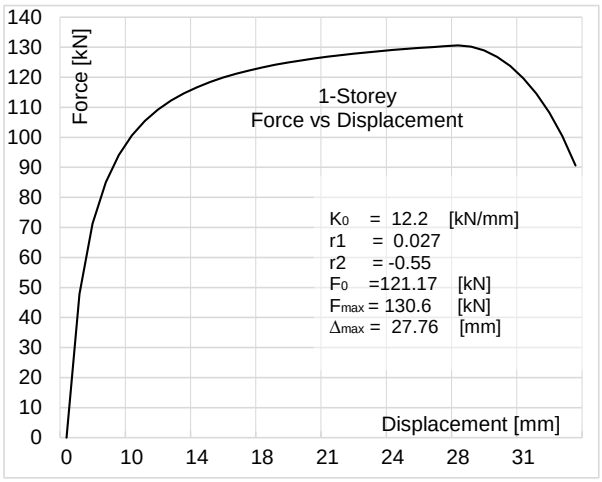

Fig. 3.40: Response of the LFTW both sides sheathed with GFB according to equation 3.19. For comparison see test results presented in 3.42(b)

Experimental testing of LFTW sheathed with GFB subjected to monotonic and cyclic loading

In this thesis, 4 walls sheathed with GFB have been tested at the Structural Research Laboratory of Empa. Two monotonic and two cyclic tests have been carried out, with one- or two-sided sheathing. The specimen length and width were the same (see Figure 3.34) as those used in the NRP 66 project. The production drawing and the photo of the specimen are presented in Figures 3.41(a) and 3.41(b). The monotonic loading applied was in accordance with ISO 21581:210.

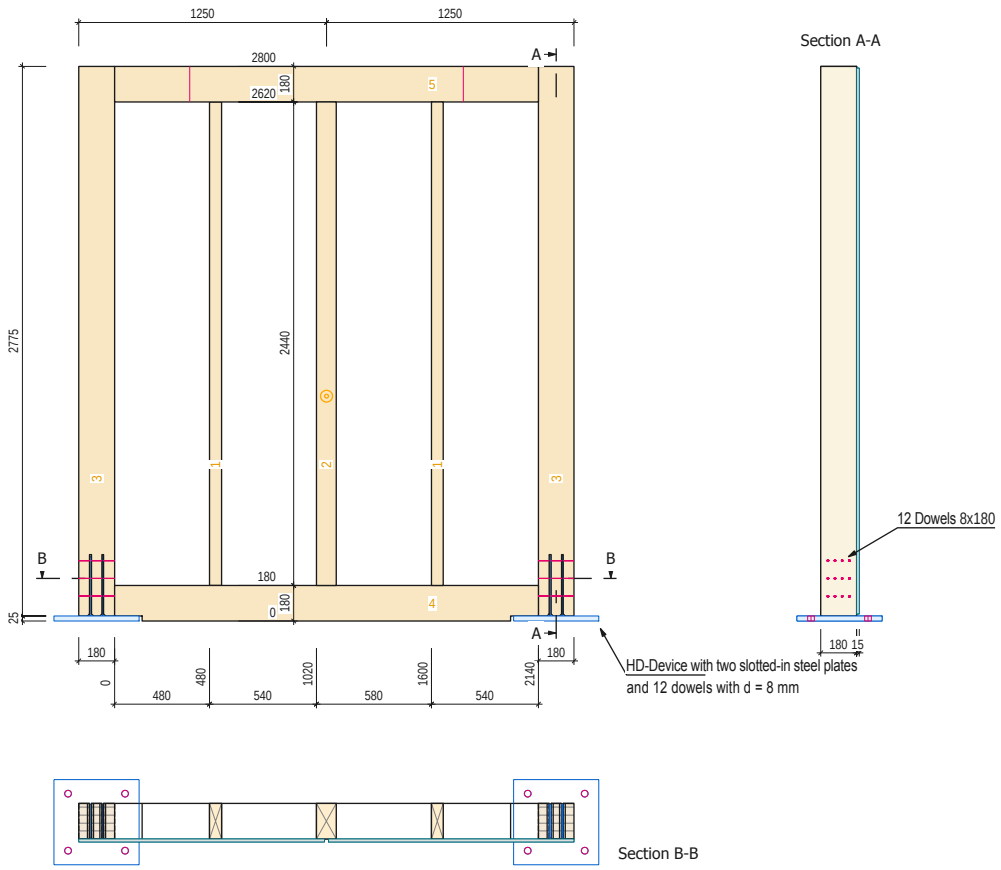

(a)

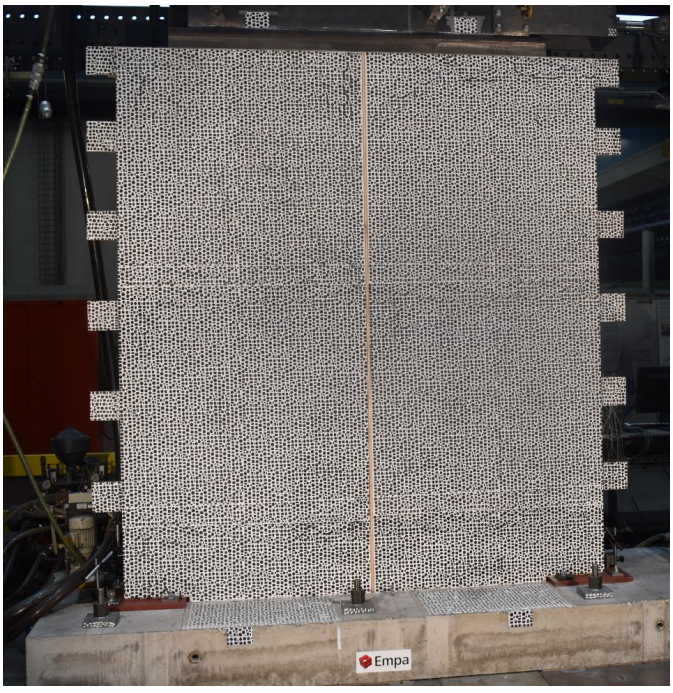

(b)

Fig. 3.41: Production drawing of the wall specimen sheathed with GFB 3.41(a) on one side: Photo of the specimen during testing at the Structural Engineering Research Laboratory of Empa 3.41(b)

The wall length was $B = 2500[mm]$, the wall height $H = 2800[mm]$ and the thickness of the GFB sheathing material was $t_p = 15[mm]$. The frame was made of GL24h and the cross-section of the two edge studs were $180 \cdot 180[mm]$, the center stud was $100 \cdot 180[mm]^2$, and the two internal studs were $60 \cdot 180[mm]^2$.

The monotonic force-displacement relationship of the shear wall element, sheathed with GFB, was estimated using a numerical model in MCASHEW. The results are presented in Figures 3.43(b) and 3.43(a), and the test results are presented in Figures 3.42(a) and 3.42(b).

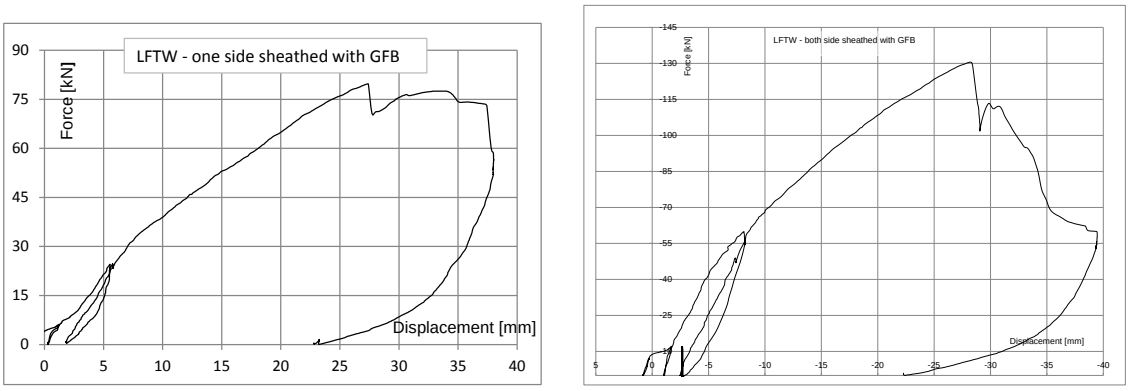

(a) (b)

Fig. 3.42: Response of the LFTW sheathed on one side with GFB, tested under monotonic loading 3.42(a): Response of the LFTW sheathed on both sides with GFB, tested under monotonic loading 3.42(b)

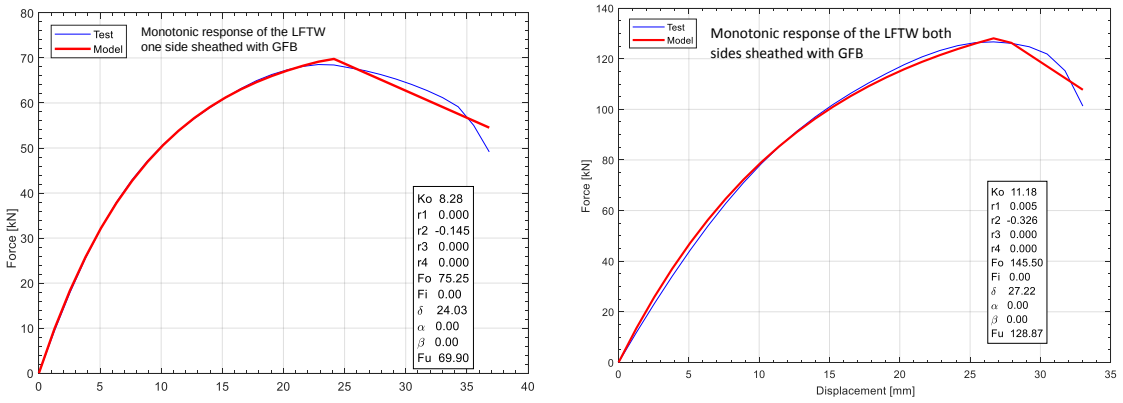

(a) (b)

Fig. 3.43: Response according to the numerical model of the LFTW sheathed on one side with GFB under monotonic loading 3.43(a): Response according to the numerical model of the LFTW sheathed on both sides with GFB under monotonic loading 3.43(b)

The numerical model underestimates the maximal strength response of the LFTW by approximately 1.7% for the two-sided sheathing case and by approximately 14.5%, for the one-side sheathing case. In terms of displacements, the results are almost exactly within the range of

±5% for both the tests and the numerical model. Considering the monotonic response of the LFTW as an envelope for the cyclic response presented in Figures 3.46(a) and 3.46(b), the numerically estimated backbone curve is considered to be sufficiently accurate.

3.5 Behaviour of LFTWs Sheathed with GFB under Cyclic Loading

As previously mentioned, the ISO 21581:210 loading protocol, presented in Figure 3.45, has been used for testing the LFTW sheathed with GFB. This choice was made to avoid potential brittle and sudden failure, due to the large steps between two subsequent amplitudes which is the characteristic of the Mergos-Beyer loading protocol. In this way, the maximum displacement associated with the corresponding load level has been recorded properly. Strictly speaking, this is inconsistent with the effort to estimate the response of a structure situated in a region of low to moderate seismicity, for which the Mergos-Beyer loading protocol is particularly suitable. This inconsistency will be addressed by using the Mergos-Beyer loading protocol in the numerical analysis.

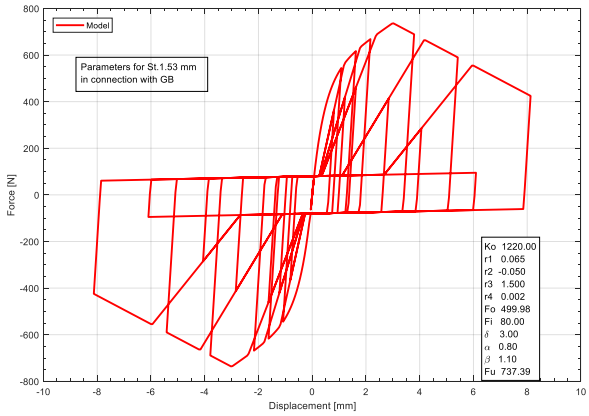

Fig. 3.44: Hysteretic model of staple $d = 1.53[mm]$ connecting GFB panel with a timber frame member

As seen in Figure 3.46(b), the response of the tested wall element is a typical hysteresis, which is stable in both directions up to the maximum displacement capacity. Little strength degradation is observed for cycles repeated within the same displacement amplitudes. The most loaded fasteners, placed in the corners of the sheathing experienced the highest forces. When they were ripped out, the bearing capacity decreased slightly, and the displacement increased. Unexpectedly, after the brittle failure of the outer fasteners occur, the next fastener took over the associated force, enabling the wall element to develop an increase in displacement accompanied with little strength degradation. This effect can be described as a zipper fastener effect. In the displacement controlled tests it provides a quasi-ductile behaviour. However, the maximum displacement capacity of a LFTW sheatehed with GFB is significantly smaller than that of a LFTW sheathed with OSB panels. For more details, see Figures 3.46(a) and 3.46(b), in which the response of the wall element obtained during cyclic testing is presented. Figures

3.47(a) and 3.47(b) show the response of the LFTW with one-side sheathing obtained analytically. Figures 3.48(a) and 3.48(b) show the response obtained analytically of the LFTW with two-sided sheathing. The numerical analysis using the ISO loading protocol overestimates the experimentally obtained average force of the positive and negative cycles by approximately 1.1% and 7.8% fore one- and two-sided sheathing, respectively. The displacement is underestimated by approximately 0.4% and 6.5% for one- and two-sided sheathing, respectively. The numerical model predicts the behaviour reasonably well, with an error range of approximately 1% for displacements and 8% for maximum strength. The model of a single staple with $d = 1.53[mm]$, presented in Figure 3.44, will be used in further modeling of LFTWs sheathed with GFB.

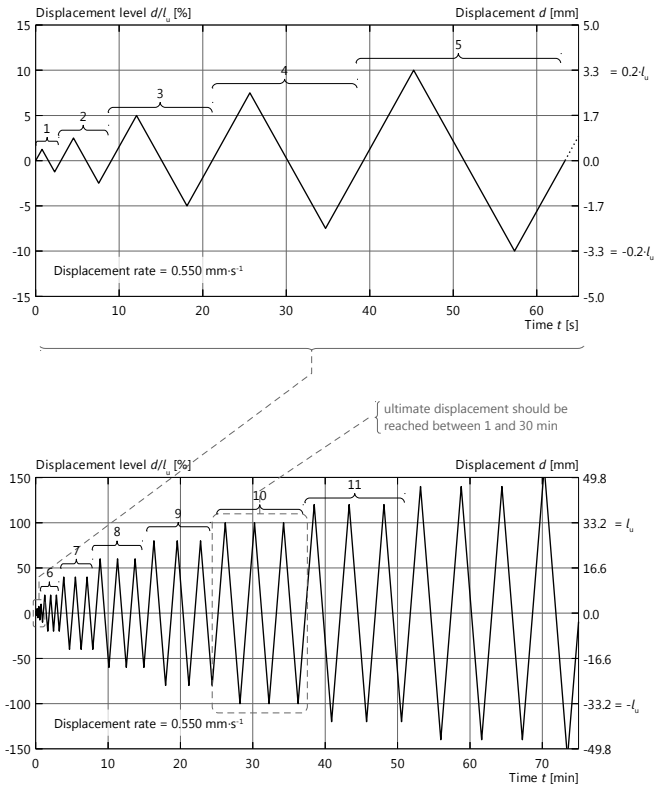

Fig. 3.45: Loading protocol ISO 21581:210, used for cyclic testing of LFTW sheathed with GFB

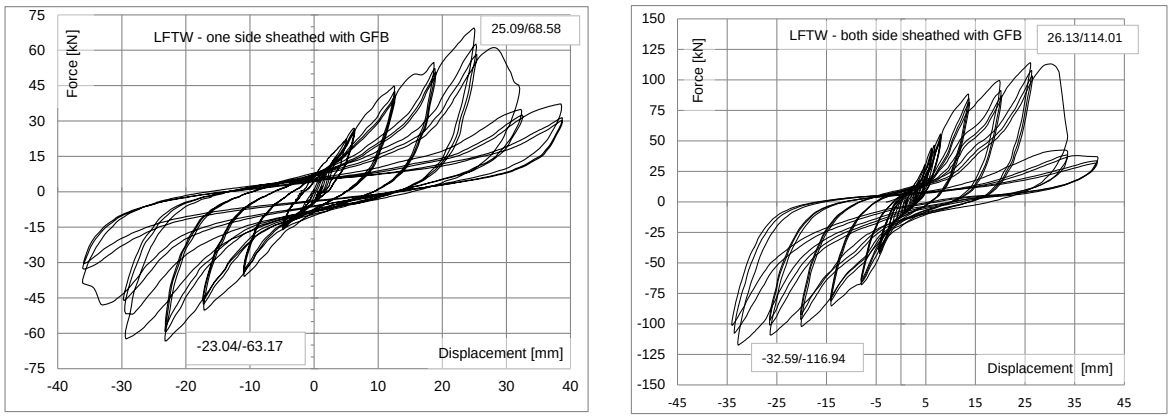

(a) (b)

Fig. 3.46: Response of the LFTW sheathed on one side with GFB to the cyclic loading 3.46(a): Response of the LFTW sheathed on both sides with GFB to the cyclic loading 3.46(b)

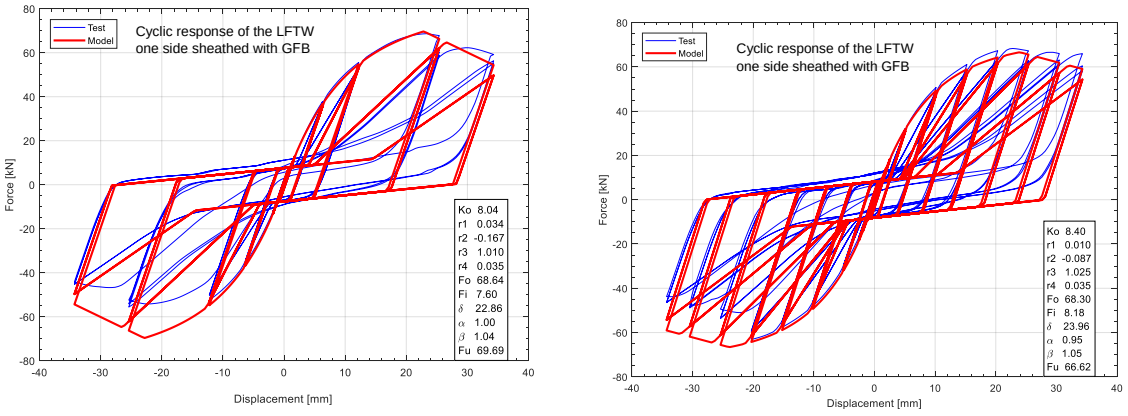

(a) (b)

Fig. 3.47: Response according to the numerical model of the LFTW sheathed on one side with GFB to the Mergos-Beyer cyclic loading 3.47(a): Response according to the numerical model of the LFTW sheathed on one sides with GFB to the ISO cyclic loading 3.47(b)

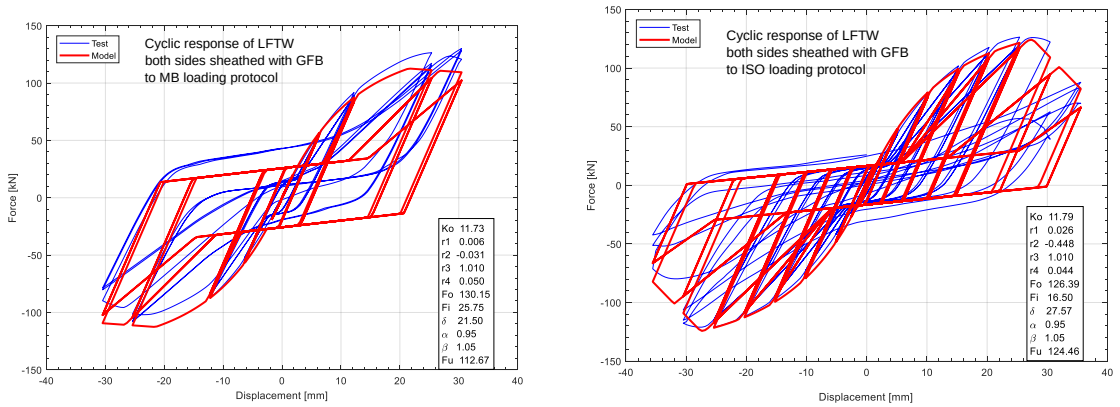

(a) (b)

Fig. 3.48: Response according to the numerical model of the LFTW sheathed on both sides with GFB to the Mergos-Beyer cyclic loading 3.48(a): Response according to the numerical model of the LFTW sheathed on both sides with GFB to the ISO cyclic loading 3.48(b)

Tab. 3.14: Estimated parameters of the Stewart hysteresis for a wall length of 2400$[mm]$, wall height of 2800$[mm]$, single and double sheathed wall with GFB, $t_p = 15[mm]$, fastener: staple $d = 1.53[mm]$, spacing 35$[mm]$, fastener hysteresis according to table 3.13

GFB	K_0	R_1	R_2	R_3	R_4	F_0	F_i	Δ_{max}	α	β	F_{max}
#	[kN/mm]	[-]	[-]	[-]	[-]	[kN]	[kN]	[mm]	[-]	[-]	[kN]
CASHEW monotonic loading											
1	6.64	0.015	-0.28	-	-	55.5	-	25.07	-	-	55.53
2	9.0	0.075	-0.85	-	-	102.5	-	28.25	-	-	111.5
CASHEW Mergos-Beyer loading protocol											
1	6.48	0.029	-0.251	1.038	0.047	55.6	9.3	22.52	0.95	1.05	55.5
2	11.36	0.082	-0.218	1.01	0.048	84.1	24.0	22.8	0.95	1.05	100.6
CASHEW ISO 21581 loading protocol											
1	6.46	0.146	-0.255	1.027	0.086	38.0	10.4	21.25	0.75	1.05	56.5
2	8.5	0.071	-0.28	1.01	0.117	108.6	16.2	26.25	0.95	1.05	108.4
McCutcheon energy based approach											
1	9.54	0.022	-0.28	-	-	57.6	-	24.1	-	-	62.5
2	11.72	0.031	-0.53	-	-	115.1	-	28.3	-	-	125.4

Tab. 3.15: Estimated parameters of the Stewart hysteresis for a wall length of 3000[mm], wall height of 2800[mm], single and double sheathed wall with GFB, $t_p = 15[mm]$, fastener: staple $d = 1.53[mm]$, spacing 35[mm], fastener hysteresis according to table 3.13

GFB	K_0	R_1	R_2	R_3	R_4	F_0	F_i	Δ_{max}	α	β	F_{max}
#	[kN/mm]	[-]	[-]	[-]	[-]	[kN]	[kN]	[mm]	[-]	[-]	[kN]
CASHEW monotonic loading											
1	8.042	0.043	-0.144	-	-	68.5	-	23.65	-	-	72.0
2	10.2	0.084	-0.275	-	-	135.1	-	29.33	-	-	142.8
CASHEW Mergos-Beyer loading protocol											
1	7.85	0.037	-0.21	1.03	0.03	70.8	9.3	22.23	0.95	1.05	70.7
2	10.09	0.07	-0.262	1.01	0.09	139.6	17.6	28.65	0.80	1.1	139.7
CASHEW ISO 21581 loading protocol											
1	7.92	0.068	-0.298	1.009	0.06	62.9	8.9	21.50	0.95	1.05	69.6
2	10.03	0.074	-0.295	1.01	0.088	139.6	17.7	28.71	0.95	1.05	140.3
McCutcheon energy based approach											
1	12.13	0.022	-0.327	-	-	72.0	-	21.56	-	-	78.4
2	14.49	0.030	-0.65	-	-	145.4	-	25.91	-	-	156.7

Tab. 3.16: Estimated parameters of the Stewart hysteresis for a wall length of 3600[mm], wall height of 2800[mm], single and double sheathed wall with GFB, $t_p = 15[mm]$, fastener: staple $d = 1.53[mm]$, spacing 35[mm], fastener hysteresis according to table 3.13

GFB	K_0	R_1	R_2	R_3	R_4	F_0	F_i	Δ_{max}	α	β	F_{max}
#	[kN/mm]	[-]	[-]	[-]	[-]	[kN]	[kN]	[mm]	[-]	[-]	[kN]
CASHEW monotonic loading											
1	9.92	0.034	-1.04	-	-	79.7	-	26.0	-	-	84.9
2	13.77	0.044	-1.106	-	-	169.5	-	29.93	-	-	171.3
CASHEW Mergos-Beyer loading protocol											
1	9.53	0.041	-0.148	1.053	0.042	79.5	10.9	21.51	0.95	1.05	81.3
2	13.27	0.058	-0.218	1.01	0.087	165.4	22.4	26.67	0.95	1.05	164.1
CASHEW ISO 21581 loading protocol											
1	9.7	0.16	-0.298	1.015	0.066	51.5	14.8	20.7	0.95	1.05	81.8
2	13.23	0.062	-0.286	1.01	0.086	164.9	23.1	22.2	0.95	1.05	152.2
McCutcheon energy based approach											
1	13.32	0.023	-0.30	-	-	86.3	-	24.6	-	-	94.1
2	16.11	0.032	-0.57	-	-	172.7	-	29.2	-	-	188.1

Tab. 3.17: Estimated parameters of the Stewart hysteresis for a wall length of 4200[mm], wall height of 2800[mm], single and double sheathed wall with GFB, $t_p = 15[mm]$, fastener: staple $d = 1.53[mm]$, spacing 35[mm], fastener hysteresis according to table 3.13

GFB	K_0	R_1	R_2	R_3	R_4	F_0	F_i	Δ_{max}	α	β	F_{max}
#	[kN/mm]	[-]	[-]	[-]	[-]	[kN]	[kN]	[mm]	[-]	[-]	[kN]
CASHEW monotonic loading											
1	12.17	0.04	-0.135	-	-	96.5	-	23.2	-	-	102.0
2	17.38	0.062	-0.485	-	-	195.7	-	27.56	-	-	205.9
CASHEW Mergos-Beyer loading protocol											
1	11.61	0.037	-0.217	1.058	0.04	100.3	13.2	22.9	0.95	1.05	102.2
2	16.82	0.066	-0.5751	1.01	0.081	199.2	31.7	24.93	0.95	1.05	199.1
CASHEW ISO 21581 loading protocol											
1	11.84	0.082	-0.212	1.007	0.049	83.6	13.2	21.65	0.95	1.05	99.7
2	16.48	0.065	-0.25	1.01	0.083	199.0	36.0	24.13	0.95	1.05	199.1
McCutcheon energy based approach											
1	15.49	0.025	-0.33	-	-	100.7	-	22.88	-	-	109.7
2	18.33	0.059	-0.66	-	-	201.4	-	27.77	-	-	219.4

Tab. 3.18: Estimated parameters of the Stewart hysteresis for a wall length of 4800[mm], wall height of 2800[mm], single and double sheathed wall with GFB, $t_p = 15[mm]$, fastener: staple $d = 1.53[mm]$, spacing 35[mm], fastener hysteresis according to table 3.13

GFB	K_0	R_1	R_2	R_3	R_4	F_0	F_i	Δ_{max}	α	β	F_{max}
#	[kN/mm]	[-]	[-]	[-]	[-]	[kN]	[kN]	[mm]	[-]	[-]	[kN]
CASHEW monotonic loading											
1	12.73	0.026	-1.583	-	-	108.0	-	25.8	-	-	110.8
2	18.92	0.051	-0.29	-	-	212.3	-	29.03	-	-	222.4
CASHEW Mergos-Beyer loading protocol											
1	12.38	0.028	-0.114	1.042	0.037	109.3	13.7	24.08	0.95	1.05	110.0
2	18.59	0.067	-0.177	1.01	0.063	201.1	32.0	24.614	0.95	1.05	208.3
CASHEW ISO 21581 loading protocol											
1	12.63	0.015	-0.26	1.052	0.035	108.3	15.4	21.25	0.95	1.05	102.9
2	18.16	0.052	-0.164	1.01	0.082	216.7	30.3	27.41	0.95	1.05	218.2
McCutcheon energy based approach											
1	16.63	0.028	-0.33	-	-	113.7	-	24.6	-	-	125.4
2	19.74	0.039	-0.64	-	-	227.4	-	29.8	-	-	250.8

3.6 On robustness of the LFTWs sheathed with OSB and GFB

The SIA260 regulations [75] postulates that the structures generally must satisfy the bearing capacity and serviceability requirements. Moreover, the structures should be designed in a cost-effective way and provide robustness and durability. In the context of LFTWs sheathed with GFB and OSB, exposed to earthquake loading, durability and robustness deserve special attention. While the bearing capacity and serviceability can be estimated analytically, the robustness and durability cannot be quantified. The code [75] describes robustness as the ability of the entire structure or its structural components to limit the extent of the damage to a reasonable proportion in accordance to their cause. The robustness could be described as the opposite of vulnerability. An analytical estimation of the robustness and durability is possible as part of the specific risk analysis. Nevertheless, the increase of the structural durability and robustness can be achieved by different measures stipulated within the code such as:

- redundancy
- reliability
- ductility
- deformability
- adaptability

For gravity loads the robustness requirement could be achieved by increasing strength or stiffness. In the sense of earthquake engineering an increase of strength and stiffness is a path in the opposite direction, since an increase in strength and stiffness consequently reduces the natural period of vibration and enhances the induced lateral earthquake forces. The LFTWs are highly redundant, deformable and have a pronounced ductility due to the large number of connectors. As presented in Chapter 3, the specific aim of this thesis is to develop a reliable mechanical model for the analysis of the LFTWs exposed to earthquake loading. From the nature of the material used it is obvious that the LFTWs sheathed with OSB can develop much higher deformations and provide higher ductility ratios when compared with LFTWs sheathed with GFB (see also section 3.5). However, the LFTWs sheathed with GFB are suitable to be used as parts of lateral load resisting systems in timber structures, capable of providing sufficient structural robustness due to their characteristics which satisfy the requirements specified above. Nevertheless, the robustness of the lateral load resisting system within the timber structures can be affected most efficiently by means of conceptual considerations such as the arrangement of LFTWs in the building, symmetry in the plan and a constant geometry over the height of the structure.

3.7 Conclusions

The application of the shear field theory to the LFTWs by means of simple hand calculations have been presented. The simple elastic shear field theory has been demonstrated for modeling and

analyzing multi-storey shear wall elements. The cyclic loading test results of fasteners, using the Mergos-Beyer and CUREE loading protocols, have been shown. Using the MCASHEW software package, the fitting of the numerical mechanical model to the results obtained by testing has been conducted and the 10-parameter mechanical models of single fasteners have been established. For the wall lengths used in this thesis, mechanical models of wall elements sheathed on one and both sides with OSB and GFB, have been derived. The derived mechanical models are the basis for the parameter study, conducted later in this thesis.

Chapter 4

Seismic Analysis of MDOF System

In the previous section, the mechanical models for single-storey LFTWs of different lengths and two different sheathing materials have been developed. The response of the wall elements is nonlinear, even for small displacements. Based on the mechanical models established in previous chapter this chapter will show how the seismic analysis of nonlinear multi-degree-of-freedom systems will be conducted within this thesis.

4.1 Analyzes and Design Concepts used in the Thesis

Strictly speaking, the best method for the seismic analysis is a nonlinear-time-history analysis (NLTHA), because it provides the "correct" results from the theoretical point of view. Despite its accuracy and the delivery of the complete structural response it seems to be a "black box" because the analysis is performed numerically within an "invisible" procedure. In order to make all steps transparent, the standard modal analysis, pushover analysis and capacity-spectra analysis procedures have always been performed in addition to NLTHA, in order to visualize the design procedure and to compare the results of different analyzes. The procedures as well as the outcomes of the analyses used within this thesis are schematically presented in Figure 4.1.

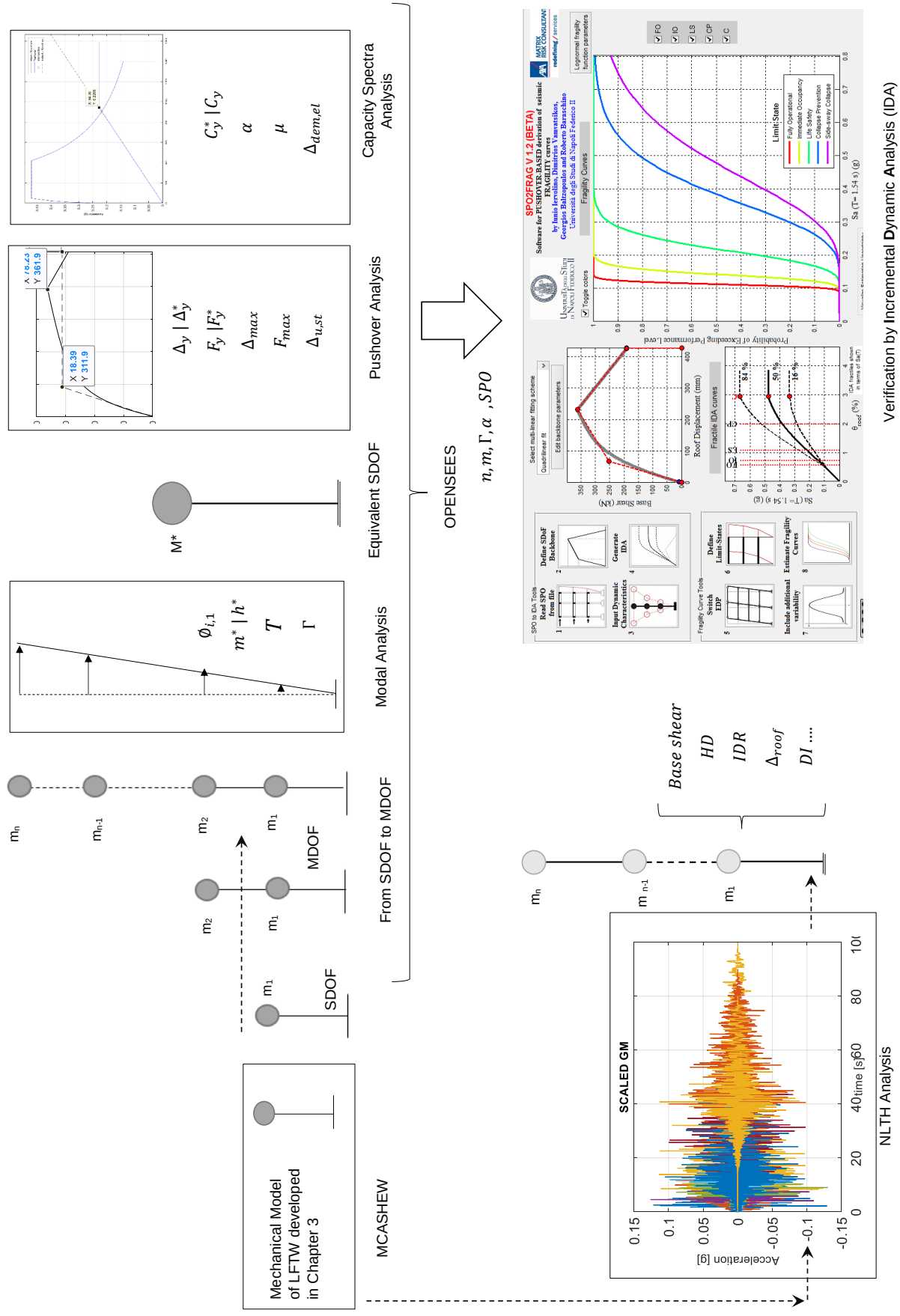

Fig. 4.1: Analyzes and design concepts used in the thesis

4.1.1 Modal analysis

The modal analysis is based on the analytical response estimation of an undamped elastic multi-degree of freedom (MDOF) system. Let us consider an undamped 4-storey shear wall element with lumped masses at each storey, as presented in Figure 4.2. The equation of motion can be obtained from the free body diagram and written according to Equation 4.1[1].

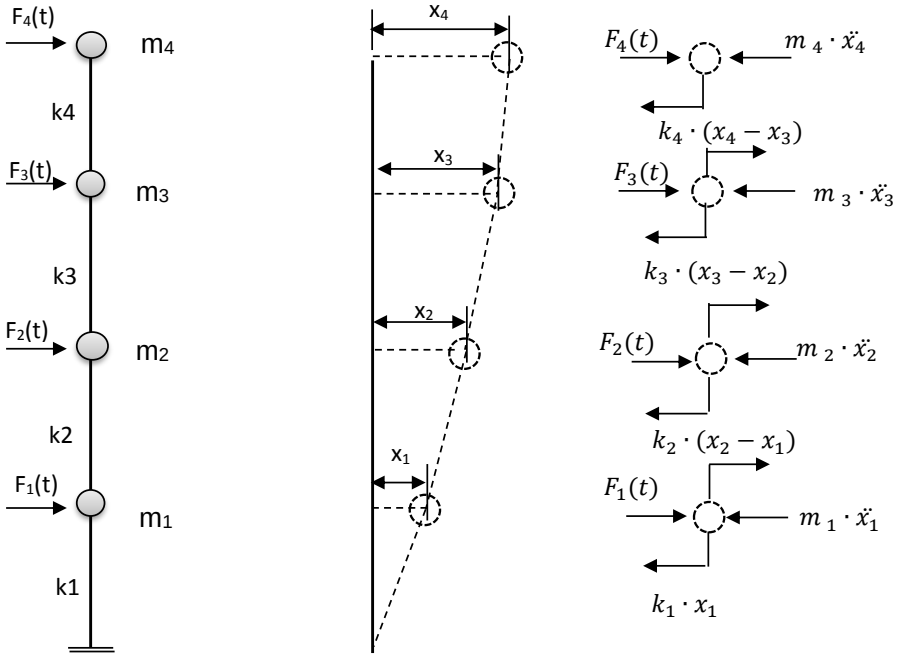

Fig. 4.2: Shear-wall presentation (left) and free body diagram (right)

$$\begin{aligned} m_1 \cdot \ddot{x_1} + k_1 \cdot x_1 - k_2 \cdot (x_2 - x_1) - F_1(t) = 0 \\ m_2 \cdot \ddot{x_2} + k_2 \cdot (x_2 - x_1) - k_3 \cdot (x_3 - x_2) - F_2(t) = 0 \\ m_3 \cdot \ddot{x_3} + k_3 \cdot (x_3 - x_2) - k_4 \cdot (x_4 - x_3) - F_3(t) = 0 \\ m_4 \cdot \ddot{x_4} + k_4 \cdot (x_4 - x_3) - F_4(t) = 0 \end{aligned} \tag{4.1}$$

Equation 4.1 is reorganized and written in matrix form as follows:

$$\begin{bmatrix} m_1 & 0 & 0 & 0 \\ 0 & m_2 & 0 & 0 \\ 0 & 0 & m_3 & 0 \\ 0 & 0 & 0 & m_4 \end{bmatrix} \cdot \begin{Bmatrix} \ddot{x_1} \\ \ddot{x_2} \\ \ddot{x_3} \\ \ddot{x_4} \end{Bmatrix} + \begin{bmatrix} k_1 + k_2 & -k2 & 0 & 0 \\ -k_2 & k_2 + k_3 & -k_3 & 0 \\ 0 & -k_3 & k_3 + k_4 & -k_4 \\ 0 & 0 & -k_4 & k_4 \end{bmatrix} \cdot \begin{Bmatrix} x_1 \\ x_2 \\ x_3 \\ x_4 \end{Bmatrix} - \begin{Bmatrix} F_1(t) \\ F_2(t) \\ F_3(t) \\ F_4(t) \end{Bmatrix} = \begin{Bmatrix} 0 \end{Bmatrix} \tag{4.2}$$

[1]The modal analysis is a topic of many books on structural dynamics. In this chapter the book on structural dynamics by Mario Paz (2012) [82] have been used

In the case of free vibrations, there are no external forces, $F_i(t) = 0$, so Equation 4.2 can be written as follows:

$$\Big[M\Big] \cdot \Big\{\ddot{X}\Big\} + \Big[K\Big] \cdot \Big\{X\Big\} = \Big\{0\Big\} \tag{4.3}$$

When analyzing the free vibration of undamped structures, the solution is of the form $x_i = \phi_i \cdot sin(\omega \cdot t - \phi_p)$ for $i = 1.....n$, where n is number of degrees of freedom. The substitution in Equation 4.3 gives:

$$\Big[\Big[K\Big] - \omega^2 \cdot \Big[M\Big]\Big] \cdot \Big\{\Phi\Big\} = \Big\{0\Big\} \tag{4.4}$$

Equation 4.4 is called an eigenproblem, which cannot be solved in closed mathematical form. It has a non-trivial solution if the determinant $[K] - \omega^2 \cdot [M]$ is equal to zero.

$$\Big|\Big[K\Big] - \omega^2 \cdot \Big[M\Big]\Big| = \Big\{0\Big\} \tag{4.5}$$

The solution to Equation 4.5 is a polynomial of degree n which is satisfied for n values of ω^2. For each of the values of ω, which satisfy Equation 4.5, Equation 4.4 can be solved for ϕ_1, ϕ_2 ... ϕ_n. These solutions have the form of normalized column vectors, known as modes. The normalization is necessary to be able to solve for ϕ. Usually, the normalization is performed so that the value ϕ_{ni} is set equal to 1.

In this thesis, complete modal response is not conducted and is not required. This can be justified by the fact that in the modal analysis of elastic systems the mode orthogonality applies. Thus, the complete response of an elastic system is expressed as combination of all modal contributions. However, it is well known that the LFTWs respond predominantly nonlinearly. Therefore, only the first mode is generally considered.

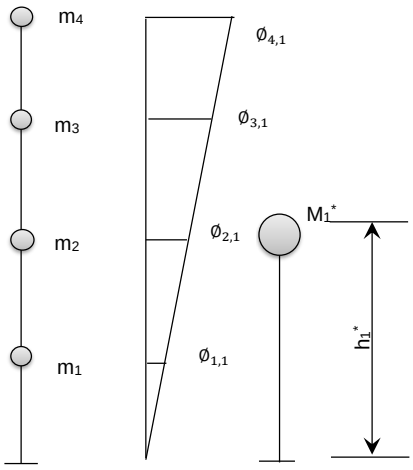

Fig. 4.3: MDOF and its equivalent SDOF representation

In this thesis (see also Figure 4.3), the modal analysis has been performed to estimate the first mode shape Φ_{i1}, the modal mass participating in the first mode m_1^*, the equivalent modal height

h_1^*, the equivalent modal mass M_1^*, the period of vibration T_1, the modal mass participation factor Γ_1 and the mass participation factor α_1, as follows:

$$m_1^* = \sum m_i \cdot \phi_{i,1} \tag{4.6}$$

$$M_1^* = \frac{(\sum m_i \cdot \phi_{i,1})^2}{\sum m_i \cdot \phi_{i,1}^2} \tag{4.7}$$

$$\Gamma_1 = \frac{\sum m_i \cdot \phi_{i,1}}{\sum m_i \cdot \phi_{i,1}^2} \tag{4.8}$$

$$\alpha_1 = \frac{\Gamma_1 \cdot m_1^*}{\sum m_i} \tag{4.9}$$

$$h_1^* = \frac{\sum m_i \cdot \phi_{i,1} \cdot h_i}{\sum m_i \cdot \phi_{i,1}} \tag{4.10}$$

The results of the modal analysis are extensively used in further analyses for the response and capacity spectra, as presented in the following section.

4.1.2 Response spectra concept

The response of a real structure subjected to a time-dependent loading can be estimated by analytically or numerically solving the equitation of motion. See for example Equation 4.20 and 4.21. The results obtained are time-dependent responses in terms of displacements, velocities and accelerations for each degree of freedom under consideration. For the seismic design of the structure, it is not always necessary to know the "exact" response of the structure at each time instance throughout the duration of the earthquake. Instead, only the maximum responses of the structure are typically used in order to design the structure for the maximum action induced by an earthquake excitation. A response spectrum (RS) enables estimation of the maximum quantities as a function of the natural period of vibration and the seismic hazard level for a given structural damping. The response spectra represent envelopes of the maximum responses of SDOF systems for natural periods of vibration within the range of approximately 0 to 4 seconds. The natural periods of vibration longer then 4 seconds have no practical relevance for the problems analyzed within this thesis. The RS are developed for a constant damping coefficient of 5%, different hazard levels ($0.6, 1.0, 1.3$ and 1.6 $[m/s^2]$) and soil conditions prescribed by the national codes. They are representations of seismic demand (see Equations 4.13 - 4.16) for the given seismicity, and, vice versa, they represent the required structural strength for an elastic response of a structure to the design earthquake. Thus, the RS for a certain seismicity (hazard level) is usually called an elastic RS. The RS can be developed for accelerations, velocities or displacements and can be represented in different formats. The relationship between the spectral quantities: pseudo acceleration S_a, pseudo velocity S_v and pseudo displacement S_d, is given in Equations 4.11 and 4.12.

$$S_a = \omega_n^2 \cdot S_d; S_v = \omega_n \cdot S_d \tag{4.11}$$

whereby,

$$\omega_n^2 = \frac{k}{m} \tag{4.12}$$

In this thesis, the response spectra defined in [3] have been used. The definition of the RS is given as follows:

$$S_a = \gamma_f \cdot \frac{a_{gd}}{g} \cdot S \cdot [0.67 + (\frac{2.5}{q} - 0.67) \cdot \frac{T}{T_B}], (0 \leqslant T \leqslant T_B) \tag{4.13}$$

$$S_a = 2.5 \cdot \gamma_f \cdot \frac{a_{gd}}{g} \cdot \frac{S}{q}, (T_B \leqslant T \leqslant T_C) \tag{4.14}$$

$$S_a = 2.5 \cdot \gamma_f \cdot \frac{a_{gd}}{g} \cdot S \cdot \frac{T_C}{T \cdot q}, (T_C \leqslant T \leqslant T_D) \tag{4.15}$$

$$S_a = 2.5 \cdot \gamma_f \cdot \frac{a_{gd}}{g} \cdot S \cdot \frac{T_C \cdot T_D}{T^2 \cdot q} \geqslant 0.1 \cdot \gamma_f \cdot \frac{a_{gd}}{g}, (T_D \leqslant T) \tag{4.16}$$

In Equations 4.13 to 4.16, γ_f is importance factor that is assumed to be equal 1.0 in this study, a_{gd} is ground acceleration of the considered hazard zone, and q is the behaviour factor, which accounts for the nonlinear response of the structure. If $q = 1.0$, the RS is elastic. T_A, T_B and T_C are characteristic periods, which separate the acceleration-, velocity- and displacement-sensitive regions. The elastic RS for all hazard zones, represented by ground accelerations of 0.6, 1.0, 1.3 and 1.6 $[m/s^2]$, are presented in Figure 4.4. The RS format is referred to as the Acceleration Displacement Response Spectra (ADRS) format and is derived using relations given by Equations 4.11 and 4.12.

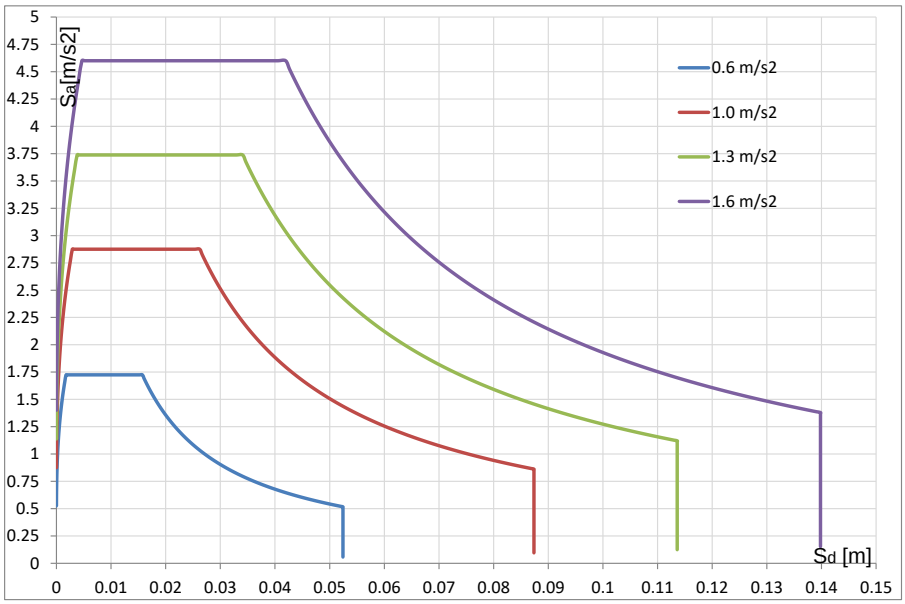

Fig. 4.4: Elastic Response Spectra for hazard zones $0.6, 1.0, 1.3$ and $1.6[m/s^2]$ in ADRS format

4.1.3 Capacity spectra concept

In the Figure 4.4, the seismic demand is presented for the hazard zones considered. The capacity spectrum concept superimposes the seismic demand, represented by a RS, and the capacity of the structure, represented by the capacity curve, in the same graphical presentation enabling a clear comparison between demand and capacity. The procedure to transform the pushover curve into a bi-linear approximation and then in the capacity curve is presented in Figure 4.5. First, the pushover curve is approximated by a bi-linear curve using the Equal Energy Elastic Plastic (EEEP) approach. In the next step, the bearing capacity of the structure, represented by F_y, is divided by the modal mass participating in the first mode in order to transform the force into an acceleration. The result is the capacity curve, which can be directly superimposed on the RS, as presented in Figure 4.5. The initial stiffness used in the presentation of the capacity spectrum (see Equation 4.19) is the inelastic initial stiffness.

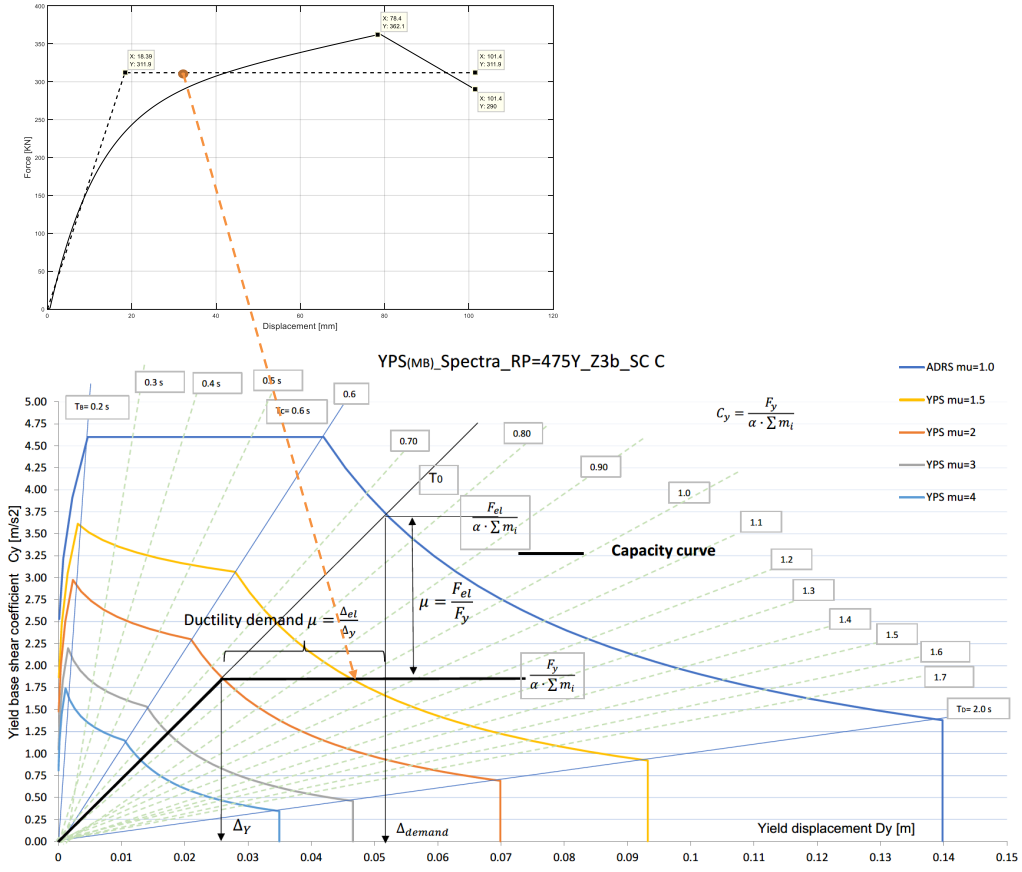

Fig. 4.5: Capacity curve derived from static pushover curve and introduced in Yield Point Spectra in ADRS format

The intersection between the stiffness, represented by the fundamental inelastic period of vibration, with the RS is the elastic demand in terms of both the displacement and the required elastic bearing capacity. The yield point gives the required real strength of the structure and the corresponding ductility demand. In the YPS both, the base shear coefficient (force) and

the displacement have the same ductility demand μ related to the intersection point between initial stiffness and elastic RS. In this thesis, the capacity curve is always derived from the static pushover curve and superimposed on the RS, providing the results needed for further analyzes, such as:

$$\Delta_y^* = \frac{\Delta_y}{\Gamma_1} \tag{4.17}$$

$$C_y^* = \frac{F_y}{\alpha_1 \cdot \sum m \cdot g} \tag{4.18}$$

$$T^* = 2 \cdot \pi \cdot \sqrt{\frac{\Delta_y^*}{C_y^* \cdot g}} \tag{4.19}$$

4.1.4 Representation in yield point spectra (YPS)

As previously mentioned, the PBE approach applied herein is based on NLTHA. However, the results of the NLTHA are not always self-evident and may require some interpretation. Thus, a graphical interpretation is sometimes useful and necessary in order to illustrate the estimated results in a more transparent manner. The results of the nonlinear static analysis are usually presented by response spectra with a superimposed capacity curve. In EC8, the method referred to as N2, proposed by Fajfar, Gašperšič and Fišinger, is implemented. Within this thesis, N2 is modified into yield point spectra (YPS) presentation. The motivation to use YPS can be justified by the ability to present the fulfillment of multiple performance objectives in a single graph, if they are stated as limits on peak displacement and system ductility. For more information, see [4]. The modification to the YPS has been made to take scaling of the spectral displacements along an abscissa. The spectral displacements are divided by their corresponding ductility coefficient and they are plotted directly as yield displacement in the YPS. The YPS enables an engineer to have direct control over the strength and the stiffness provided to the structure and to determine, if necessary, the combination of strength and stiffness needed to satisfy certain performance objectives. Additionally the peak displacement demand can easily be estimated from the plot and compared with the displacement capacity. The $R-\mu-T$ relationship used in this thesis is the same as that used within the N2 method, with the difference in the acceleration sensitive region. Here, to maintain consistency with the mechanical model used, the $R-\mu-T$ relationship proposed by Mergos-Beyer (2015) in [66] is applied. In the velocity sensitive region,the $R-\mu-T$ relationship according to Mergos-Beyer and the N2 proposal are equal . The maximum mass, which can be applied to the system, often leads to periods of vibrations falling in the velocity sensitive region, characterized by periods larger than T_C, with values of approximately 0.5-0.6 [s].

Figure 4.6 schematically shows the feasibility region within YPS defined by a red dashed line in which all combinations of strength and stiffness would satisfy the performance objectives. The representation by means of YPS is intensively used in Chapter 8, while establishing the differences between PBE and FB seismic design.

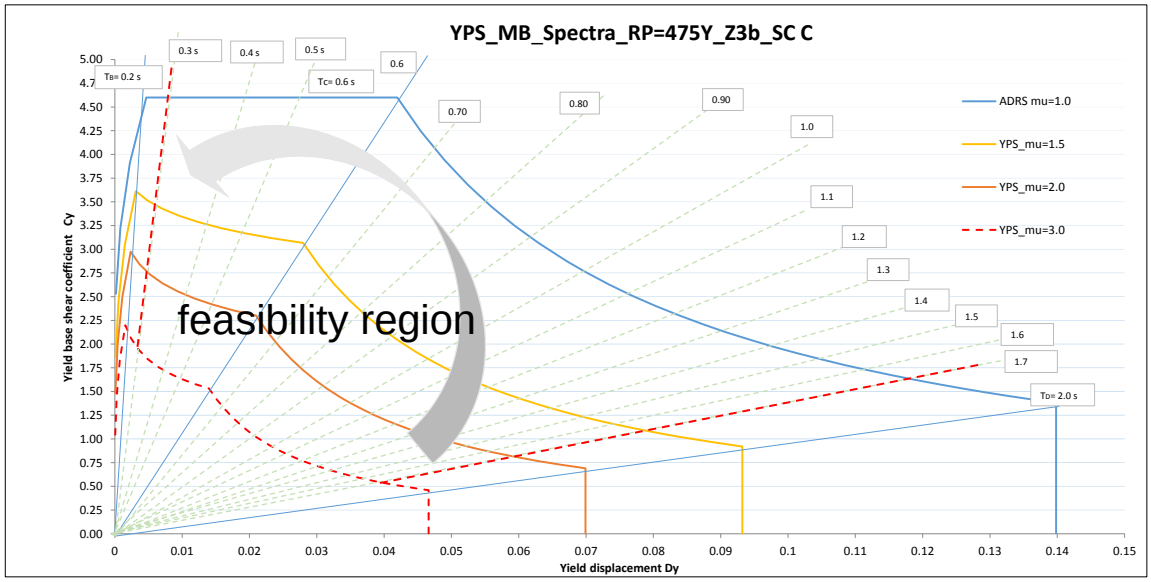

Fig. 4.6: YPS with characteristic feasibility region in which all combinations of strength and stiffness enclosed by dashed red lines satisfy the performance objectives

4.1.5 Non Linear Time History Analysis

Theoretical background

The dynamic analysis of an arbitrary real structure is based on the dynamic equilibrium. The structure can response in a linear elastic or a nonlinear manner. In the literature (see for example [9]), the theoretical explanations of how the structure responds to a transient loading starts with a single-degree-of-freedom (SDOF) system, represented in Figure 4.7, being extended to the response of a multi-degree-of-freedom (MDOF) structure. However, an analytical solution to the equation of motion Equation 4.20 is not possible if the excitation arbitrarily varies with respect to time or the system is nonlinear. In these cases a step-by-step integration is necessary. The equation of motion for a SDOF system can be written as follows:

$$m \cdot \ddot{x} + c \cdot \dot{x} + f_{s(x,\dot{x})} = p(t) - m \cdot \ddot{x_g}(t) \tag{4.20}$$

where m is the mass of the system, c is the damping ratio provided by the system, $f_{s(x,\dot{x})}$ is the inelastic force induced in the system at the considered time increment, and x, $\dot{x}$ and $\ddot{x}$ are the relative displacement, relative velocity and relative acceleration of the mass, respectively. $\ddot{x_g}(t)$ is the ground acceleration introduced at the base of the structure. The equation of motion for a MDOF system has a similar form to Equation 4.20 if the physical quantities are written as corresponding matrices:

$$\left[M\right] \cdot \left\{\ddot{X}\right\} + \left[C\right] \cdot \left\{\dot{X}\right\} + \left\{F_{s(x,\dot{x})}\right\} = \left\{P(t)\right\} - \left[M\right] \cdot \left\{\imath\right\} \cdot \left\{\ddot{X}_g(t)\right\} \tag{4.21}$$

where the capital letters M, C and F_s denote the mass, damping and force matrices, respectively. The displacements X, velocities $\dot{X}$ and accelerations $\ddot{X}$ are one-dimensional column

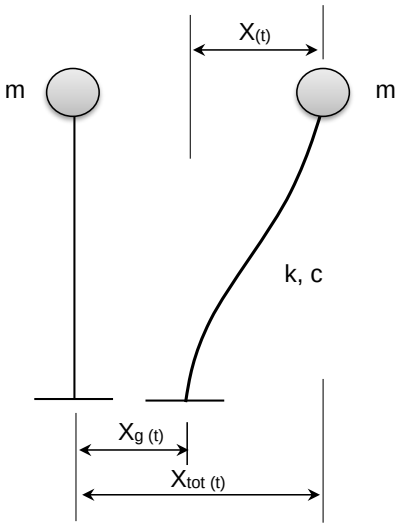

Fig. 4.7: Response of the single-degree-of-freedom system to the arbitrarily ground displacement

matrices, i.e. vectors. If the external forces do not exist, $P(t) = 0$. The $\imath$ is the vector representing the influence of a unit ground displacement on the displacements of the storey masses. In the case that all of the storey masses and ground displacements are oriented in the same direction, which applies for planar 2D- systems, the vector $\imath$ becomes a unit column vector 1. However, due to the transient disturbance of an earthquake excitation as well as the material non-linearity, a numerical integration is required. There are a number of numerical integration methods available, but the most powerful one is the Newmark's integration method. In the OpenSees software platform, the interpolation of the excitation function uses an average, trapezoidal acceleration. The main requirements for a numerical integration method are convergence, stability and accuracy. The details of how the Newmark step-by-step integration is performed can be seen in more detail in [9]. Within this thesis, the integration algorithm implemented in the OpenSees software platform uses this same approach when performing NLTHA.

Newmark's integration method is unconditionally stable for:

$$\frac{\Delta_t}{T_n} \leqslant \frac{1}{\pi \cdot \sqrt{2}} \cdot \frac{1}{\sqrt{\gamma - 2 \cdot \beta}} \tag{4.22}$$

but conditionally stable for $\frac{\Delta_t}{T_n} \leqslant 0.551$. The parameters γ and β define the variation of the acceleration over a time step, controlling the stability of the method. Parameter γ is typically selected to be 0.5, and parameter β is tipically in the range $0.167 \leqslant \beta \leqslant 0.25$. From Equation 4.22, it can be seen that an important contribution to the stability of the NLTHA is the choice of the integration time step, which is set to be $0.0025[s]$ in this thesis. The convergence of the iterations within each incremental time step is ensured by means of the Newton-Rapson iteration approach.

4.1.6 Ground motion input

Selection and Scaling of Ground Motion Records

A simple way to perform THA is to use modal response analysis by applying the modal superposition procedure, a method applicable to linear elastic systems. Since the response of a LFTW is nonlinear over the entire displacement range, nonlinear time history analysis, referred to as the direct dynamic integration method is more appropriate to be used in performance based engineering (PBE). Furthermore, the excitation term on the right side of the equation of motion, 4.20 which in NLTHA has to be solved directly by using appropriate numerical integration methods, is represented by an acceleration time series of real ground motions. Real ground motion records have a natural frequency, duration and energy content which affect the response of the structure under earthquake action regardless the seismic hazard zone the structure is located in. The main task related to utilization of unique ground motions recorded in the original form is how to make them representative for design of the structures in a specific hazard zone. Thus, for each ground motion, the corresponding response spectra are to be estimated first. In the second step, the RS of an individual record is to be "adjusted" by scaling its amplitude for a given fundamental vibration period of the structure. This is done in such way as to provide the best fit to the elastic response spectra stipulated by the seismic provisions for the corresponding hazard zone. The scaling of amplitudes to match the elastic response spectra has, among other scaling procedures, the main advantage in retaining the original frequency while the damage energy content and amplitude will be changed. Since the response spectra are derived as an envelope of responses of all SDOF systems, a single record can never meet the elastic response spectra over all vibration periods. In the selection of the ground motion magnitude range, the distance to the fault as well as the soil conditions should be taken into account. Some papers and even practical guidelines (see for example [49] and [100]), deal with the selecting and scaling of ground motions for nonlinear response analysis. The researchers still have different opinions about which criteria are crucial for the selection of ground motions and how the records should be selected. Iervolino et al. reported (2008) in [42] about critical issues in selection and scaling of ground motions as well as the best practice in Europe. The authors were concerned with finding ground motions which would match the spectra stipulated in EC8 without scaling. Such records have not been found. In any case, the requirements related to the earthquake selection and scaling given in EC8 [1] are as follows:

- A minimum of three accelerograms should be used. The most unfavourable value of the response should be used as the design value of the action.
- If the response is obtained from 7 nonlinear time history analyses, the average of the response quantities should be used as the design value of the action.
- In the range of periods between $0.2 \cdot T_1$ and $2 \cdot T_1$, where T_1 is the fundamental period, no value of the mean 5% damped elastic spectrum calculated from all time histories should be less than 90% of the corresponding value of the elastic spectrum.

The period range $(0.2 - 1.0) \cdot T_1$ takes into account the higher mode contribution since the periods of the second and the third mode are usually in the range $(\frac{1}{5} - \frac{1}{3})$ of T_1. The period range of $(1.0 - 2.0) \cdot T_1$ takes into account the fact that the period corresponding to the elastic system (beginning of the loading path) increases when the system is transitioning into the inelastic response regime [90].

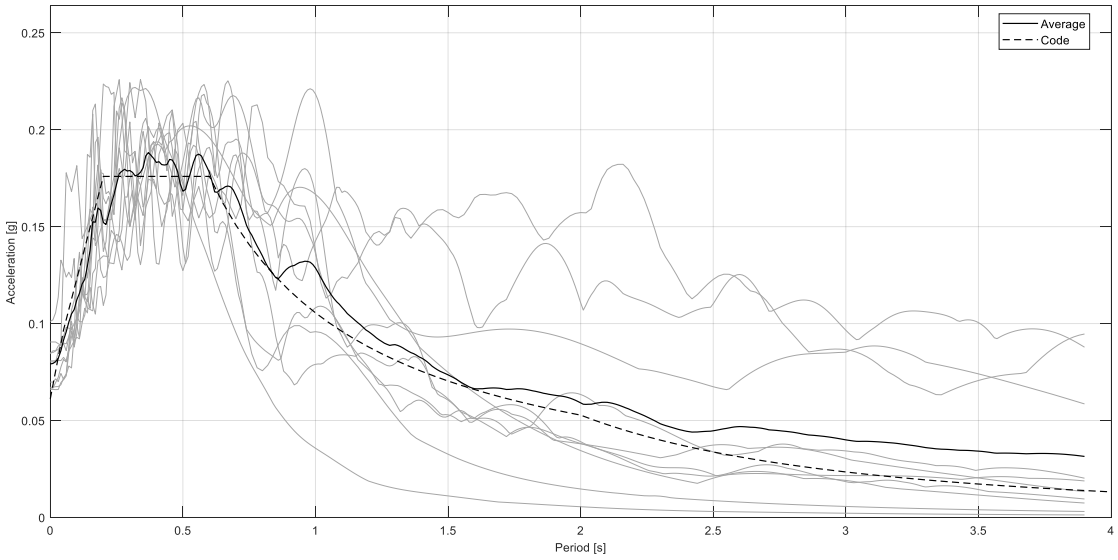

Fig. 4.8: Resultant mean value of 10 selected earthquake ground accelerations scaled to the hazard level of Zone $Z1$ - soil class C according [3].

Within this thesis, the NGA database has been used as source of real ground motions recorded worldwide in different soil conditions and with different magnitudes, frequency contents, fault distances, source mechanisms and durations. The data set consists of the currently freely available 3551 three-component records covering the magnitude range between 4.2 to 7.9. More details regarding the NGA database are given in [8].

Using the MatLab code written by Gabriele Garnello, PhD candidate at the University of Canterbury, New Zealand, the NGA database has been searched for earthquakes, which are scaled to the levels of the four hazard zones characterized by ground accelerations of 0.6, 1.0, 1.3 and 1.6 $[\frac{m}{s^2}]$. The earthquakes must also have a scaling factor with an amplitude of $0.3 < k_0 < 4$ (see [90]), and the difference between the peak amplitude and plateau-value must be $\frac{a_{record}}{a_{plato}} < 1.4$ in the range of $T_A < T_n < T_C$. For each hazard zone (Z1, Z2, Z3a and Z3b [3]) as well as for all soil conditions (A, B, C, D and E [3]), approximately 150 to 200 records that satisfy the given conditions have been extracted. Note that, for each earthquake consisting of two orthogonal direction amplitude components a_1 and a_2, a resulting amplitude given by $\sqrt{a_1^2 + a_2^2}$ has been considered. After selection and scaling the records for each zone and soil condition, 10 appropriate earthquakes have been chosen manually so that the mean value of the 10 records is the best fit to the code-prescribed, 5% damped elastic response spectrum. For illustration, the mean response spectrum obtained by selecting and scaling real records is presented in Figure 4.8 for the hazard Zone Z1 and soil condition C. It can be seen that the

resultant mean RS oversteps the elastic RS for almost the entire period range, regardless of the fundamental period of the structure. In Figure 4.9, the resultant mean RS for the hazard zone $Z2$ and soil class C is presented. In the range of approximately $0.47 - 0.7[s]$, the resultant mean value underestimates the elastic RS, but not by more than 10%, as required by the EC8. For vibration periods between $0.7 - 4[s]$, the resultant mean value has overstepped the elastic code spectrum. Additionally, in Figures 4.10 and 4.11, the selected and scaled records are presented. From Figure 4.10, it can be seen that, strictly speaking, the 10% rule in the short period range between 0.55 - 0.6 [s] is not satisfied, underestimating the required value by approximately 12%. Nevertheless, it has been considered as acceptable since all the results of the parameter study said to be of practical relevance will additionally be checked by IDA. The mean value of the scaled records spectra has been over the required value for periods $0.65[s] < T_n < 2.0[s]$. In the parameter study, the average values of the response quantities have been used. A minimum of 7 records must converge. Otherwise the record selection was repeated to replace the records that did not converge. For the great majority of cases, the THA could have been successfully performed for all 10 records.

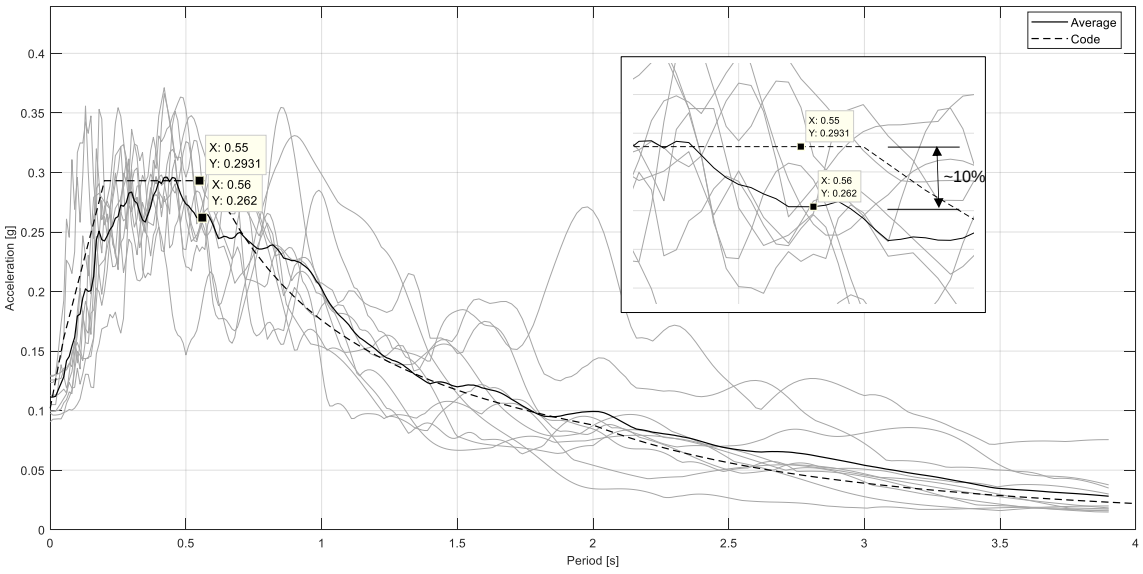

Fig. 4.9: Resultant mean value of 10 selected earthquake ground accelerations scaled to the hazard level of Zone $Z2$ - soil class C according [3].

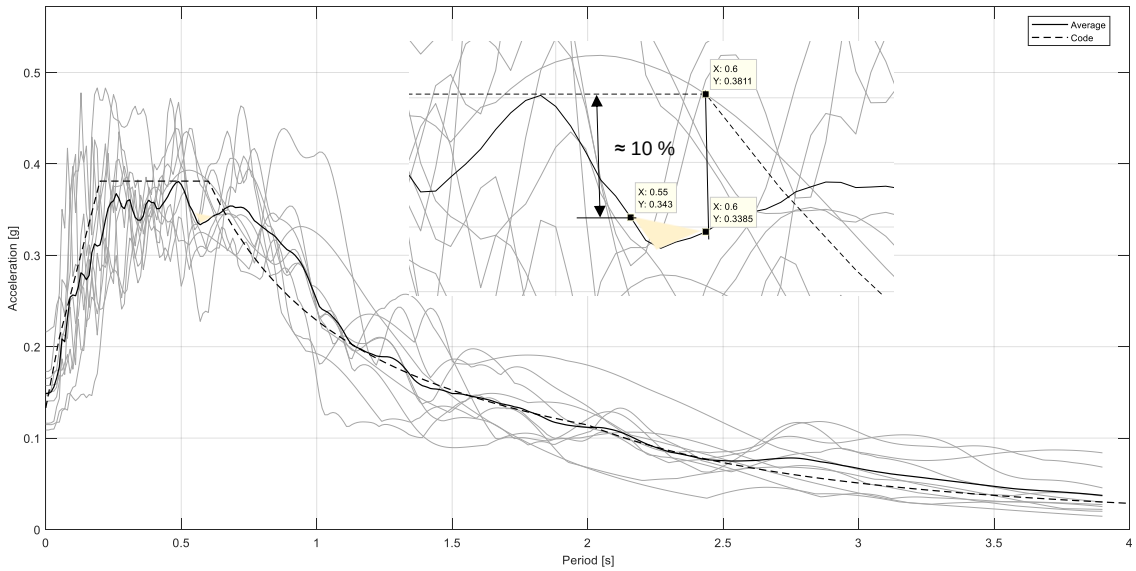

Fig. 4.10: Resultant mean value of 10 selected earthquake ground accelerations scaled to the hazard level of Zone $Z3a$ - soil class C according [3].

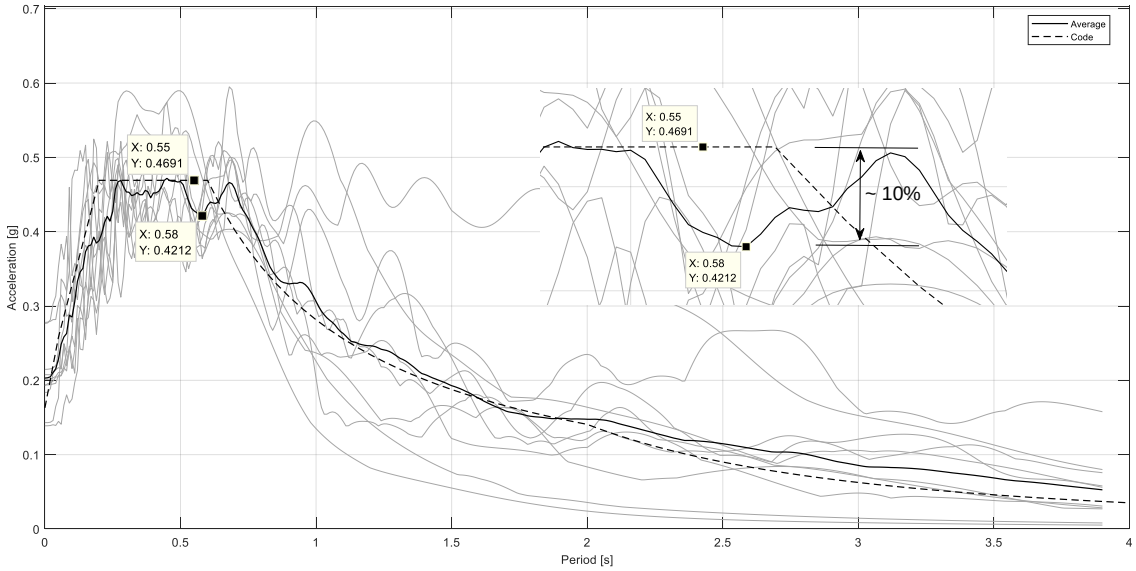

Fig. 4.11: Resultant mean value of 10 selected earthquake ground accelerations scaled to the hazard level of Zone $Z3b$ - soil class C according [3].

SAWS - Shear spring material in OPENSEES

The parametric study performed in this thesis has been carried out by using the software framework provided by the Open System for Earthquake Engineering Simulation (OpenSees) platform. This software offers more than 160 different element types, 220 material types, 15 solution algorithms, 40 integration strategies and 30 solver types (see [62] and *http* : *//opensees.berkeley.edu/*). The software enables one to build an appropriate model using appropriate materials and to per-

form gravity, static pushover and dynamic analyses. Within the software library, a uniaxial SAWS material, which can be understood as a shear spring element, is available. The material implements the well-known Stewart 10-parameter hysteretic model, as presented in Figure 4.12 and described in Table 2.1. The model has been developed in the CUREE CalTech project (see [32]), and represents the response of the LFTW to the static and dynamic lateral loading. The parameters which describe different LFTWs considered within this thesis are listed in Tables 3.8 to 3.12 for wall elements sheathed with OSB panels and in Tables 3.14 to 3.18 for LFTWs sheathed with GFB, respectively. The SAWS material can be represented by a zero length element, implying that the response of the entire wall element to the static and cyclic loading can be "reproduced" by specific points (zero-length-elements), mutually connected by rigid truss elements with large axial stiffnesses.

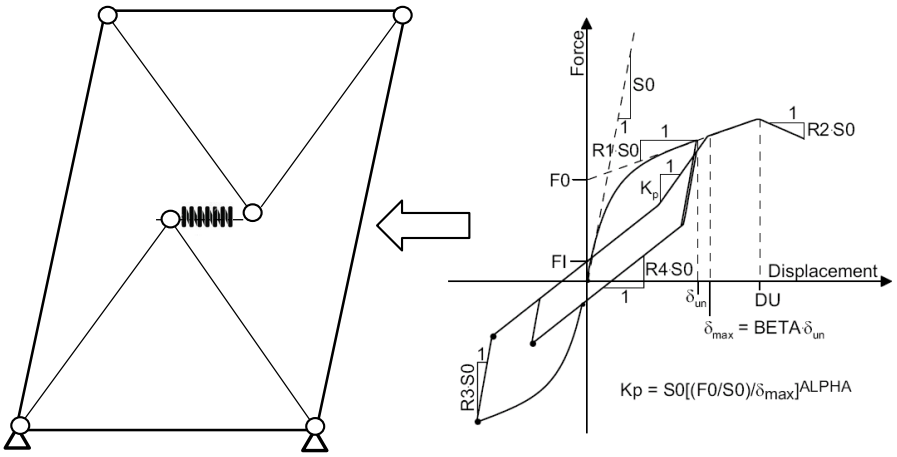

Fig. 4.12: Representation of the SAWS material by a zero-length-element [60]

Transition from a SDOF to a MDOF system

All the features of a single LFTW element, including the compliance of the hold-downs, are entirely contained in the SAWS material, representing the response of the LFTW as a nonlinear shear spring element. In order to shift from a SDOF to a MDOF model, it is necessary to stack the elements on top of each other, as presented in Figure 4.13. As already mentioned, the mechanical characteristics along the height remain constant, i.e., the structure is built of identical elements.

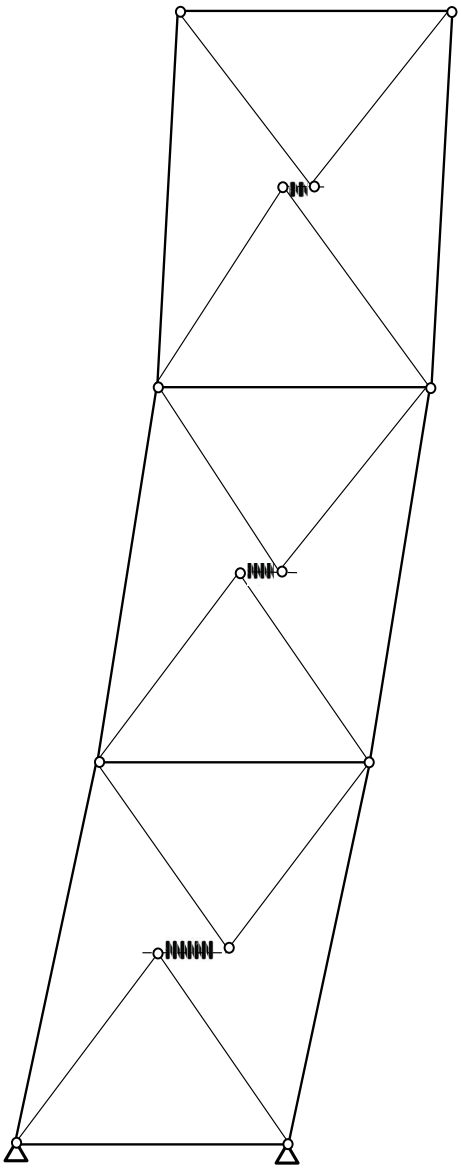

Fig. 4.13: Transition from a SDOF to a MDOF system by using identical SAWS material representation at each storey level

4.1.7 Damping in OpenSees

The NLTHA uses Rayleigh damping as a linear combination of the damping proportional to the mass in the range of low and to the stiffness in the range of the high frequencies. The Rayleigh damping matrix can be expressed as:

$$[C] = a_{r0} \cdot [M] + a_{r1} \cdot [K_0] \tag{4.23}$$

$$\xi_n = \frac{a_{r0}}{2\omega_n} + \frac{a_{r1} \cdot \omega_n}{2} \tag{4.24}$$

where

$$a_{r0} = \frac{2 \cdot \xi \cdot \omega_1 \cdot \omega_2}{\omega_1 + \omega_2} \tag{4.25}$$

and

$$a_{r1} = \frac{2 \cdot \xi}{\omega_1 + \omega_2} \tag{4.26}$$

The circular frequencies ω_1 and ω_2 are the first and the second frequencies with an assumed damping coefficient of 5%.

In [11] the authors refer to the fact that the Rayleigh damping may lead to results which are not physically plausible. However, the forces associated to the part of the Rayleigh damping model proportional to the stiffness cause unbalanced joint forces, which are referred to as *spurious* forces in the column-beam frame connection. It has been shown that the unbalanced forces, stemming from the Rayleigh damping model, can be significantly reduced or entirely eliminated by using the tangent stiffness, see Equation 4.27, instead of the initial stiffness in Equation 4.23. Although this option is available in OpenSees, in [11] Chopra and McKenna have proposed to use superposition of modal damping matrices for NLTHA within the software platform OpenSees. The software has been extended in this way to allow the formulation of the damping as a sum of the damping matrices associated with the modes which significantly contribute to the response of the structure. The number of the modes is not prescribed and depends on the contribution of the higher vibration modes to the overall structural response. In this thesis the inconvenience caused by *spurious* forces can largely be relativized, since the analyses are performed on the simple cantilever model. Nevertheless, the options to model the damping within NLTHA as a sum of modal damping matrices, offered by the software have been extensively used within this presented work. The modal damping coefficient is assumed to be 5%.

$$[C] = a_{r0} \cdot [M] + a_{r1} \cdot [K_T] \tag{4.27}$$

Analysis algorithm used in OpenSees

In the OpenSees software framework, object-oriented NLTHA is implemented, allowing for a flexible software architecture. According to [59], the main modules that OpenSees is comprised of, are given in Figure 4.14, including the components of the analysis itself. The procedures used in each single analysis component are marked in Figure 4.14. The integration step considered within the analysis has been chosen as $\Delta_T = 0.0025[s]$. The stability and convergence of the analysis has been ensured by using the Newmark integration method [60]. In the case of not reaching convergence, the time step is automatically reduced within the analysis in the next iteration by a factor of 20. As already mentioned, from the total of 10 earthquake records used for every NLTH analysis, predominantly all, or at least 7 of them have always converged, as required by EC 8.

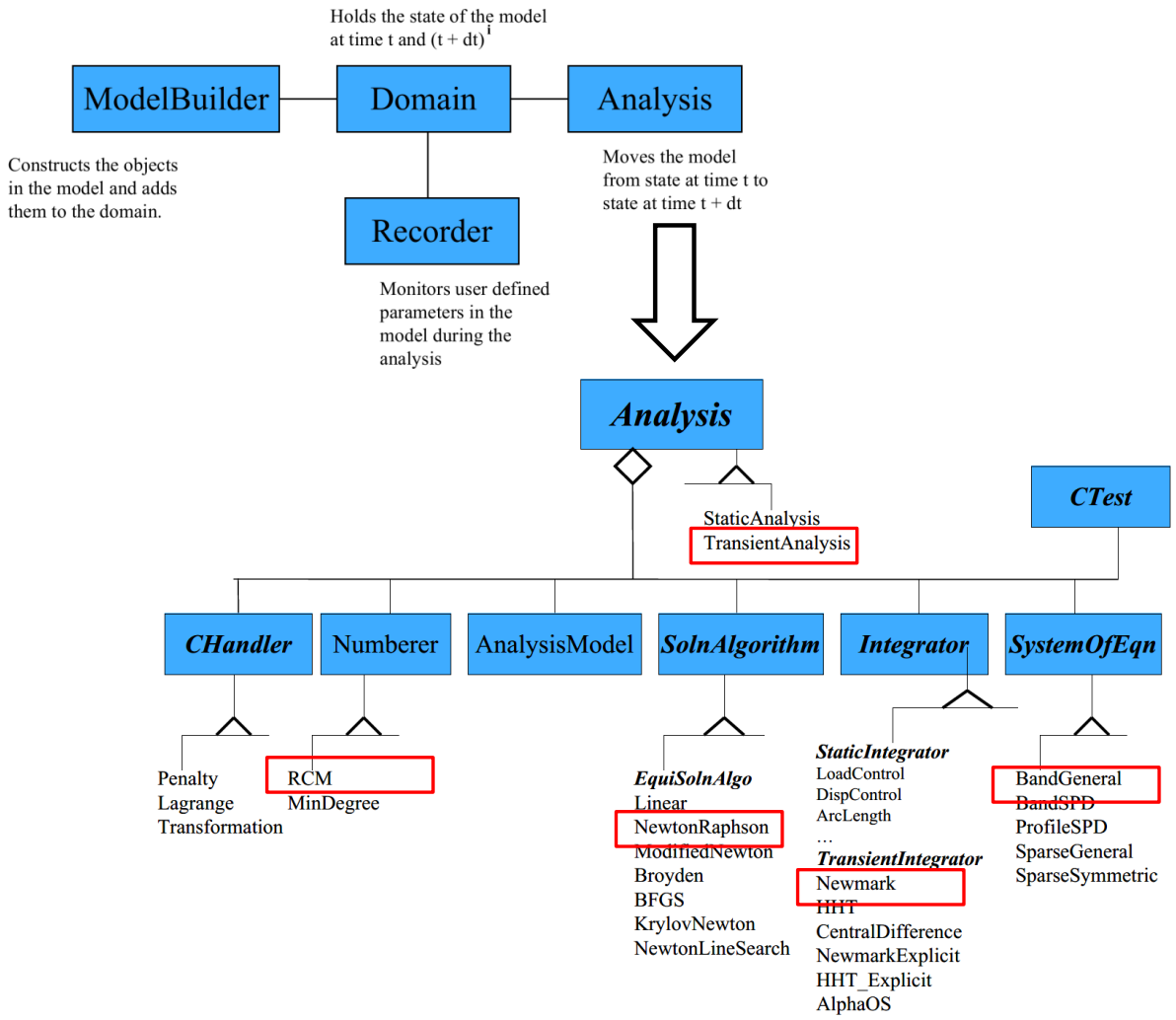

Fig. 4.14: The main modules and analysis objects according to [59] in an overview

4.1.8 Incremental dynamic analysis (IDA)

The damage index analysis, described in the next chapter, is more comprehensive than a simple displacement analysis based on nonlinear static pushover analysis, and therefore more appropriate to be used as a structural performance indicator. The probabilistic part of the analysis is limited to the suite of 10 earthquakes scaled to the certain hazard level that the damage index is computed for. The hazard levels are the seismic zones Z1, Z2, Z3a and Z3b, prescribed in the SIA 261 [3] provisions. In order to conduct a probability-based estimation over all of the stages the structure experiences, i.e., from the elastic part of the response to the inelastic part and finally to collapse, all earthquakes should be scaled in a way to produce failure of the structure, while simultaneously accounting for the uncertainty arising from the structural bearing and displacement capacity. To do so, a deterministic structural model can be subjected to a sample of earthquakes, which will be gradually scaled in amplitude until collapse of the structure occurs, while simultaneously recording the corresponding response of the structure. The scaling

of the ground motion amplitudes and the analysis of the structure up to failure is referred to as Incremental Dynamic Analysis (IDA), presented in detail in [96] and [97]. In the case where a deterministic numerical model of the structure is subjected to a sample of earthquakes, the distribution of the structural responses reflects the record-to-record variability arising from the ground motion records contained in the sample. If a NLTHA using multiple ground motion records is performed on a structure represented by a nonlinear SDOF system, the procedure is referred to as a SPO2FRAG procedure, proposed (2016) by Iervolino, Baltzopoulos, Vamvatsikos and Baraschino. This is presented in [41], based on the former work of Vamvatsikos, referred to as SPO2IDA (2003), also contained in [96]. The IDA analysis is characterized by intensive computational efforts, thus the simplification provided by the SPO2FRAG approach is appreciated in terms of reducing the computational time, while retaining the same accuracy. In this thesis, both procedures, implemented in a MatLab based, freely available software SPO2IDA and SPO2FRAG, will be used for performance level validation of the structure analyzed within the parameter study.

4.1.9 Incremental dynamic analysis framework

The Incremental Dynamic Analysis (IDA) is a comprehensive tool for reliable prediction of both seismic demand and structural capacity in terms of Damage Measure (DM) and Intensity Measure (IM). DM is represented by a scalar value, which defines the required performance demand, such as the inter-storey drift ratio (IDR). In the literature this is also referred to as engineering demand parameter (EDP). The IM used in this thesis is the first mode spectral acceleration of the 5% damped SDOF system $S_{a(T_1)}$. The aim of the procedure is to provide a probability based estimation of fragility curves, which reflect the conditional likelihood of exceedance of a certain IM, given DM or vice versa. The distribution of the IDA curves is plotted in accordance with the Gaussian normal distribution with, mean $\pm$ standard deviation ($\mu_m \pm 1 \cdot \sigma$), resulting in 16, 50 and 84% IDA fractile curves.

As mentioned before, the IDA analysis will be conducted on a deterministic structural model, represented by a nonlinear SDOF system. From the variable chosen to represent the seismic intensity, it is clear that the derivation of the fragility functions is IM oriented, where the given limit state is an additional condition, whose exceedance is understood as approaching failure. Under these circumstances, the fragility function, according to [41], can be written as the probability of the random, lognormal distributed variable IM.

$$P[IM_f^{LS} \leq \ im] = \Phi[\frac{ln(im) - \eta}{\zeta}] \tag{4.28}$$

In equation 4.28, Φ is the standard Gaussian function, and η and ζ are the logarithmic mean and standard deviation, respectively. These are estimated automatically while performing performance of the IDA procedure. For more details, see [41] and [96]. In the SPO2FRAG software, an additional uncertainty, resulting from the structural model, and its transformation from a MDOF into a SDOF system, denoted as β_{yo} and β_{y,T_2}, respectively, could be taken into account without having an influence on the median fractile IDA curves.

The first parameter accounts for an early non-linear behaviour and the second one accounts for a higher-mode contribution to the yield strength variability. Both of them have been assumed to be 0.5 resulting in a variability of the nominal yield strength due to the higher mode effects of $\beta_{y,tot} = \sqrt{\beta_{yo}^2 + \beta_{y,T_2}^2} = 0.71$. Additionally, the logarithmic standard deviation, required for the Monte-Carlo simulation for estimation of the yield strength variability, is set to be in the same range of 0.5 similar as in [77]. The additional uncertainties that are taken into account affect only the distribution width without impacting the median fractile IDA curves.

The procedure, how the IM will be estimated for defined DM within IDA analysis is presented in Figure 4.15

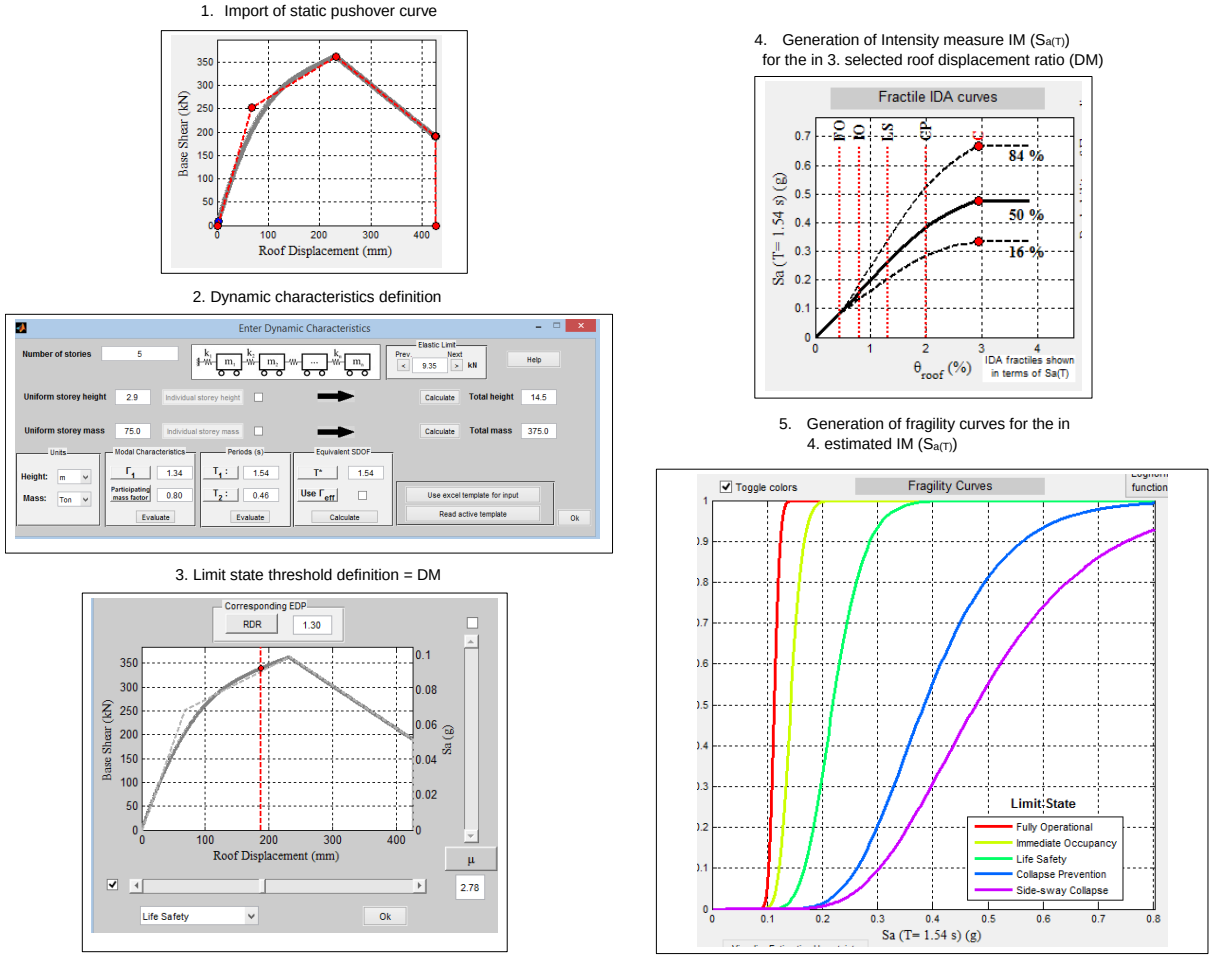

Fig. 4.15: IDA procedure used as controll and validation of results of the parametric study

4.2 Conclusions

In this chapter, the general seismic engineering methods have been presented with a special focus on the features used in this thesis. The general concepts of modal analysis, the capacity spectrum and the response spectrum have been presented as the commonly-used methods in seismic engineering. In the second part of the chapter, the concepts of the non-linear time

history analysis and the incremental dynamic analysis have been presented. The selection and scaling of earthquake records as the input transient loading in the THA have been introduced. The concepts presented give a general overview of the methods used in this thesis, emphasizing their strengths and weaknesses. The outcomes of all of the methods have been extensively used in this work. Due to its accuracy the results of the NLTHA have been considered to be decisive.

Chapter 5

Limit State Definition

In this chapter, the performance objectives for the serviceability, live safety and collapse prevention limit states for LFTWs sheathed with OSB and GFB are defined in terms of two performance indices, namely, the inter-storey drift ratio (IDR) and the damage index (DI). The performance objectives for the life safety limit state are based on the damage index, proposed by Park and Ang, as the linear combination of the displacements and the hysteretic energy disipated during an earthquake excitation. Since no data from the literature is available for LFTWs sheathed with GFB, the analytically estimated physically observed damage intensities during testing are related to the corresponding IDRs in order to establish performance objectives within the considered performance limit states. The relative energy input used in the Park-Ang approach is estimated according to the Uang-Bertero proposal, extended to MDOF systems. An independent probability-based procedure, referred to as the incremental dynamic analysis (IDA), is shown to be applicable to control and validate the results obtained by the parameter study based on a NLTHA.

5.1 Introduction

As outlined in Chapter 2, Eurocode 8 sets the general requirements related to performance based seismic design, prescribing that two limit states should be checked, serviceability (Damage Limitation State) and collapse (Ultimate Limit State). However, detailed information about how to satisfy the requirements is not specified. As a result, performance based design has rarely been implemented by practitioners. Since the N2 method, proposed by Fajfar, Fišinger and Vidić and adopted in EC8, is based on the capacity curve, which is an approximation of the nonlinear force-displacement relationship, the performance level is likely to be expressed relative to displacement. This approach is not capable of accounting for structural damage to timber shear walls, their strength degradation and energy dissipation due to the earthquake loading. Thus, for reliable performance level definition, two inherently different methodologies are available. The first one is the quasi-deterministic approach, referred to as the Damage Index Analysis (DI). This is an approach which represents a linear combination of the displacement capacity and the dissipated energy during a specific earthquake excitation. The damage index is a non-

negative scalar value $\leq$ 1.0, which expresses the degree of damage. The damage index also contains a probabilistic component, which accounts for the variance of the structural response. It is expressed in terms of the maximum displacement under a specific earthquake excitation, and the uncertainty related to the ground motion, expressed in terms of the dissipated energy during a specified earthquake. The second methodology, referred to as Incremental Dynamic Analysis (IDA) is a probabilistic estimation of safety margins and accounts for the uncertainty arising from both variability in the ground motions and the mechanical characteristics of timber shear walls. In order to narrow down the limit states, seismic damage analysis will first be performed. After the damage indexes are established for both the SLS and ULS in terms of the corresponding inter-storey drift ratio (IDR), the IDR will be expressed as the damage measure (DM) within a fragility analysis.
Finally, a fragility function will be generated through an IDA in terms of the first mode ground acceleration as a conditional intensity measure (IM) for the stipulated DM. The results of the IDA are fractile curves in terms of prescribed drift ratios and corresponding spectral accelerations, which have a 50 % probability of exceedence.

5.2 Seismic Damage Analysis of LFTWs Sheathed with OSB

5.2.1 Analytical model according to the Park-Ang proposal

A simple analytical relationship for structural damage estimation, which accounts for the maximum displacement imposed by an earthquake, the displacement capacity of the shear wall element, as well as the amount of dissipated energy during an earthquake event has been proposed for reinforced concrete structures in [80] by Y. Park and H.S. Ang (1985).

$$DI = \frac{\Delta_{resp}}{\Delta_{u,st}} + \frac{\beta_{DI}}{F_y \cdot \Delta_{u,st}} \cdot \int dE \tag{5.1}$$

where Δ_{resp} is the maximum deformation due to an earthquake, $\Delta_{u,st}$ is the ultimate deformation capacity under static loading, F_y is the yield strength, $\int dE$ is the absorbed hysteretic energy and β_{DI} is the structural coefficient, which is estimated experimentally and accounts for the cyclic loading effects. According to the damage model of Park, Reinhorn and Kunnath (1988) presented in [79], parameter β_{DI} reflects the rate of strength degradation caused by the incremental increase of the normalized maximum response, $\frac{d\Delta_{resp}}{\Delta_{u,st}}$ to the normalized incremental hysteretic energy, $\frac{d\int dE}{\Delta_{u,st}}$. The physical meaning of the parameter listed can be understood from Figures 5.1 and 5.2 where the yield force, the displacement capacity and the maximal response of the structure due to a specific earthquake are presented. The complete collapse of the structure is associated with a Damage Index $DI \geq 1.0$.

The displacement capacity denoted $\Delta_{u,st}$ obeys the widely accepted convention, related to the definition of the maximum available (ultimate) displacement given by R. Park (1989) in [78]. However this point does not mean that the structure will definitely experience collapse at this displacement stage. From Equation 5.1, it follows that, to a certain damage grade, a

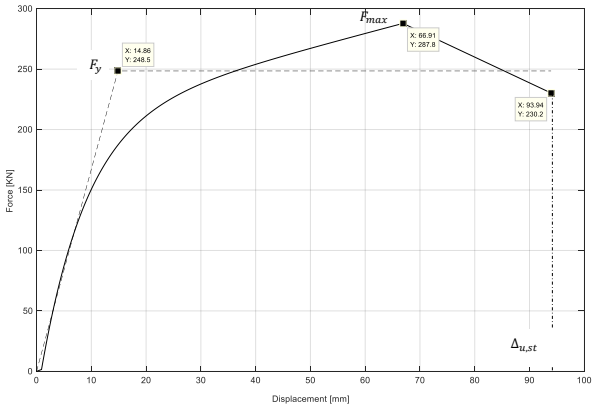

Fig. 5.1: Static yield strength F_y and ultimate deformation capacity $\Delta_{u,st}$

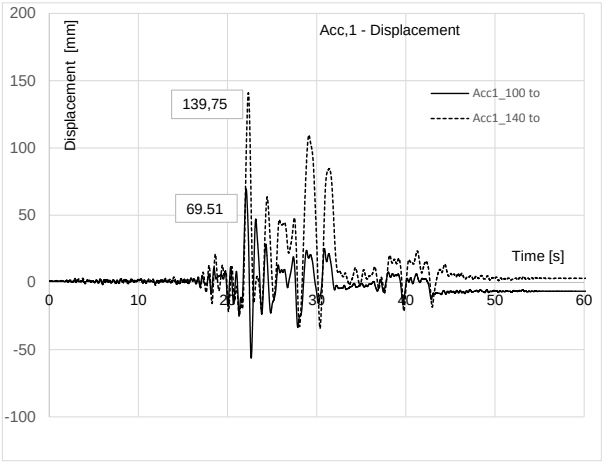

Fig. 5.2: Maximal displacement response to the specific ground motion Δ_{resp}

corresponding earthquake intensity characterized by Δ_{resp} and $\int dE$, can be associated. Hence, each earthquake can be scaled in such a way as to cause collapse of the structure producing damage index equal to 1.0. Since the damage index can take the value of 1.0, the rearrangement of equation 5.1 enables writing of parameter β_{DI} as follows:

$$\beta_{DI} = \frac{F_y \cdot (\Delta_{u,st} - \Delta_{resp})}{\int dE} \tag{5.2}$$

5.2.2 Estimation of the parameter β_{DI} for LFTW sheathed with OSB

Equation 5.2 implies that the parameter β_{DI} is constant, estimated for the conditions in which the structure is close to or has already reached the total damage stage. In this case the damage index ratio is equal to 1.0. It is reasonable to assume that the same conditions can also be captured by cyclic testing. Thus, the parameter β_{DI} can be estimated by evaluating the cyclic tests, provided the structure tested has been driven to collapse.

In Section 3, the hysteretic wall parameters have been estimated numerically for single storey wall elements with lengths $2.4, 3.0, 3.6, 4.2$ or $4.8[m]$. They have been estimated by using the

CASHEW model, which is also capable of modeling the collapsed wall conditions including the energy dissipated up to the point of collapse. From Figure 5.1, it can be seen that the F_y and $\Delta_{u,st}$ are values that depend on the wall configuration and the wall geometry. Therefore, these two values, which appear in Equation 5.1, are constant for a certain wall length. The values Δ_{resp} and $\int dE$ depend on the specific earthquake or the imposed loading protocol. In order to account for the variability of the loading protocols used, parameter β_{DI} for both the Mergos-Beyer and the CUREE loading protocols have been estimated and averaged. The values of parameter β_{DI}, estimated for all shear wall configurations considered within this thesis, are summarized in Table 5.1.

Tab. 5.1: Estimation of coefficient β_{DI} from the CASHEW hysteretic and static pushover analysis

OSB	L_w	$\Delta_{u,st}$	F_y	$\Delta_{resp_{CE}}$	$\Delta_{resp_{MB}}$	$\int dE_{CE}$	$\int dE_{MB}$	β_{CE}	β_{MB}	β_{DI}
#	[m]	[mm]	[kN]	[mm]	[mm]	[kNm]	[kNm]	[-]	[-]	[-]
1	2.4	110.6	85.0	76.8	90.3	65.16	73.6	0.044	0.023	0.034
2		102.8	163.0	87.68	87.64	124.7	110.7	0.02	0.022	0.021
1	3.0	134.3	113.4	66.81	62.63	71.72	72.15	0.107	0.113	0.11
2		103.9	220.8	67.35	72.85	133.5	159.7	0.061	0.043	0.052
1	3.6	101.1	136.6	72.25	74.68	113.6	102.6	0.035	0.035	0.035
2		119.3	265.0	71.98	74.85	181.12	178.0	0.069	0.062	0.067
1	4.2	111.6	168.8	55.35	66.93	101.4	124.8	0.094	0.060	0.077
2		176.5	318.0	65.77	78.31	211.3	224.5	0.1645	0.1371	0.15
1	4.8	92.5	174.5	76.24	76.63	170	114.5	0.017	0.024	0.02
2		155.5	369.7	75.21	76.81	260.5	270.1	0.114	0.108	0.11

The parameters Δ_{respCE} and Δ_{respMB}, needed for estimation of the parameter β_{DI}, have been taken from Tables 3.8 to 3.12. The parameters $\int dE_{CE}$ and $\int dE_{MB}$ have been calculated separately for each individual wall and have been summarized in Table 5.1.
As an example, the calculated cumulative energy dissipated during the MB cyclic loading of a wall with two-sided sheathing and a length of $3.6[m]$ is presented in Figure 5.3. Parameters $\Delta_{u,st}$ and F_y have been obtained from the static pushover curve, as presented in Figure 5.4, for the same wall element.
The values of parameter β_{DI} range from 0.02 to 0.15. Such low values of parameter β_{DI} imply quite small contribution of strength and stiffness deterioration, which is characteristic for the deformation range far beyond the displacement corresponding to the maximum force value, to the entire degree of damage. Thus, the predominant damage amount contained in the damage index is due to the first term in Equation 5.1, coming from the maximum static response to the cyclic excitation related to the displacement capacity of the shear wall element. In other words, the energy dissipated by hysteresis is less than the energy dissipated by the forces causing the monotonic backbone response. This monotonic backbone response envelopes the cyclic hysteretic response.

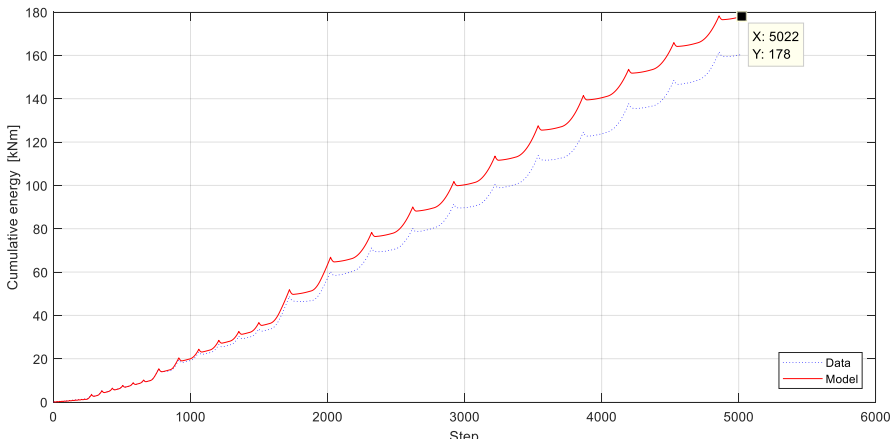

Fig. 5.3: Cumulative energy dissipated by cyclic loading of a shear wall with a length of $L_w = 3.6[m]$ sheathed on both sides.

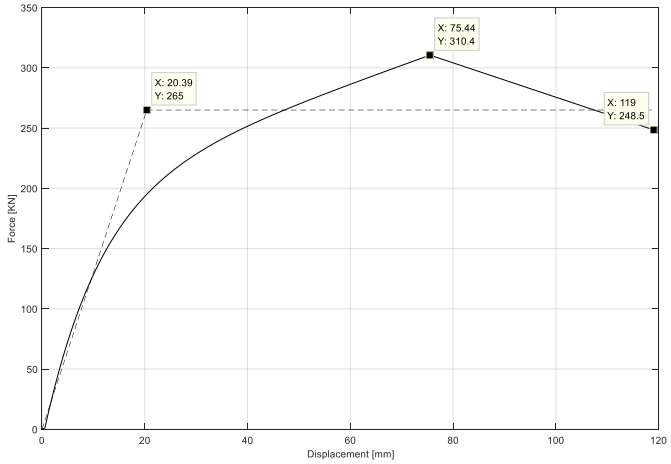

Fig. 5.4: Yield force and ultimate displacement of a shear wall with a length of $L_w = 3.6[m]$ sheathed on both sides. Wall parameters according to Table 3.10.

Once the parameter β_{DI} has been estimated, the next step in the estimation of the damage index is made. The expected drift corresponding to each performance level is given in FEMA 356, Chapter 8 (2000) and ASCE/SEI-41, [13] and summarized here in Table 5.2.

The principle of estimating the damage index will be described for a three storey structure. Figures 5.5(a) and 5.5(b) show a pushover curve for a $3.6[m]$ long shear wall element in a one- and three storey building, respectively, with schematically identified drift limits, as proposed in[13].

The 2% drift limit is associated with the design earthquake (DE) with a probability of exceedance of 10% in 50 years and corresponds to the Life Safety (LS) limit state. According to Figure 5.5(a), a drift limit of 2% appears to underestimate the displacement associated with the LS limit state because the maximum force and the maximum displacement are not yet reached at this stage. A drift limit of 4% seems to be appropriate with respect to the Collapse Prevention (CP) performance objective, corresponding almost exactly to the limit introduced

Tab. 5.2: Performance expectations according to ASCE/SEI-41 [13]

Performance level	Design level	Seismic hazard	Return Period	Performance Expectations	
				Inter-storey Drift Limit	Non-exceedance Probabaility
Level 1	IO	50% in 50Y	72Y	1%	50%
Level 2	LS	10% in 50Y	475Y	2%	50%
Level 3	CP	2% in 50Y	2475Y	4%	50%

IO - Immediate Occupancy
LF - Life Safety
CP - Collapse Prevention

by Park in [78]. Note that, as explicitly shown in Table 5.2, the drift limits are referred to as inter-storey drift ratios and cannot apply to the entire height of a multi-degree of freedom system (for example, see Figure 5.5(b)). However, if the drift limits are applied to a MDOF system, as presented in Figure 5.5(b), one can see that the drift limit of 2% applies for the LS limit state. From the Figure 5.5(b) follows that the drift limit of 4%, associated to CP limit state, is accompanied by a strength reduction to approximately 30% of F_{max} and 45% of F_y, cannot be achieved without losing structural stability.
It is well known that the displacement capacity of a structure is an inherent characteristic of the structural system with a strong dependence on the structural material. The previous discussion shows that general statements related to displacement capacities are not always the best way to define the performance objectives. The displacements alone, as absolute or normalized values, are not appropriate measures for performance level definition. In performance based seismic design, multiple objectives must be checked and satisfied simultaneously.
The damage index analysis consisted of simultaneous checking the absolute roof displacement, the inter-storey drift ratio and the corresponding damage intensity. In the next step, NLTHA will be performed for the structural system represented by the pushover curve in Figure 5.5(b). A sample of 10 earthquake records will be selected and scaled to achieve inter-storey drifts of 1%, 2%, 2.5%, 3.0% and 4% measured at the first storey level. For each of the 10 records, the energy absorbed during the earthquake and the maximum displacement response of the shear wall element at the first storey level will be extracted for the purpose of computing the corresponding DI for each single earthquake. The key results are summarized in the Table 5.3 .

5.2.3 Energy input and energy dissipation

The current seismic design procedures use either inelastic strength principles (Force Based Design) or inelastic displacement capacity principles (Displacement Based Design) in order to

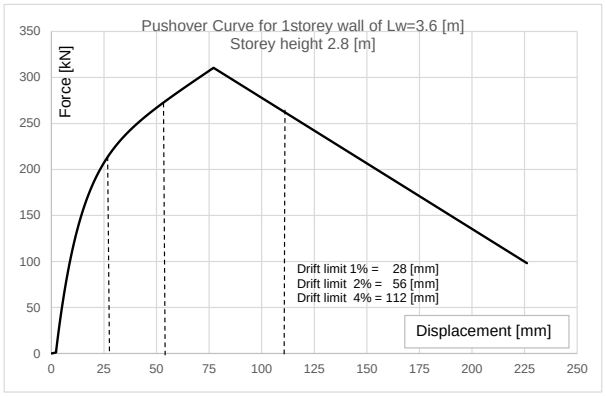

(a)

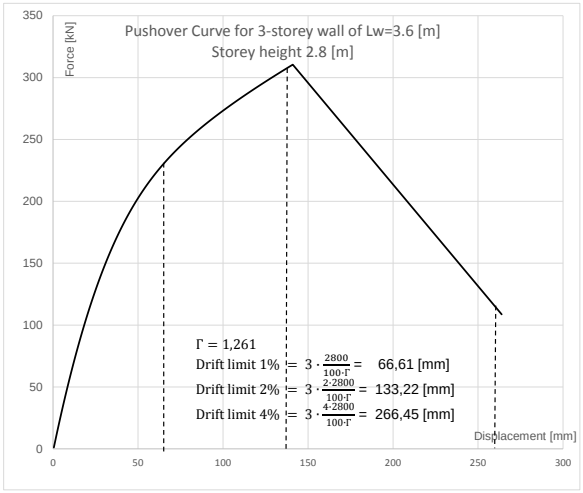

(b)

Fig. 5.5: Drift limits marked on the pushover curve of a 1-storey wall with a length of 3.6 [m] 5.5(a): Drift limits marked on the pushover curve of a 3-storey wall with a length of 3.6 [m] 5.5(b)

achieve the desired structural bahaviour under seismic action. In both of these design concepts, neither the duration of the earthquake nor the hysteretic behaviour of the structure are considered. An alternative energy based approach was proposed by G.W. Housner (1956) in [40]. The proposal follows a simple physical rule, that the *energy demand* during an earthquake can be predicted and the *energy capacity* provided by a structure or a structural element can be established. The design outcome is satisfactory when the energy capacity is larger than the energy demand (see [95]). Based on the work of G.W. Housner, some researchers (see for example [63], [55], [72]) have investigated the influence that the fundamental period, the yield strength, the damping and the ratio between the maximum hysteretic and input energy have on the response of SDOF systems. Uang and Bertero (1990) in [95] investigated the differences that the absolute and relative energy inputs have on the response of SDOF systems. A relevant discussion about this issue can also be seen in [53] and [50]. It is recognized nowadays that the relative and absolute energies differ only for very rigid and very flexible structures. In the flexible structures, the

mass tends to preserve its original position while the ground moves. In this case, the absolute energy approaches zero. For the rigid structures, the relative displacement of the mass is small, so the relative energy amount is also small, while the absolute energy may build up. Uang and Bertero extended their investigation from SDOF to MDOF systems (see [95]). The results show that the absolute and relative input energies for constant displacement ductility are very close in the period range of practical interest between 0.3 and 5[s]. Since only the displacements and the accelerations relative to the ground cause forces in the structure, only the energy dissipated by the work of the mass on the displacements relative to the ground will be taken into account (see [9] and [53]) within this thesis.

SDOF system

The general equation of motion, given for example in [9], is re-written by Uang and Bertero in [95] as follows:

$$\int m \cdot \ddot{x} \cdot \dot{x} \cdot dt + \int c \cdot \dot{x} \cdot \dot{x} \cdot dt + \int f \cdot \dot{x} \cdot dt = -\int m \cdot \ddot{x_g} \cdot \dot{x} \cdot dt \tag{5.3}$$

where m is the mass, c is the damping coefficient, f is the restoring force, and x is the relative displacement of the SDOF system. respectively. $\dot{x}$ is the velocity, $\ddot{x}$ is the acceleration of the mass relative to the ground and $\ddot{x_g}$ is the ground acceleration.

For simplicity, Equation 5.3 can also be written as follows:

$$E_k + E_{da} + E_{st} = E_{in,r} \tag{5.4}$$

where E_k is the relative kinetic energy, E_{da} is the damping energy and E_{st} is the sum of the elastic and the hysteretic portion of the energy stored in the system. The last term, $E_{in,r}$, denotes the relative input energy.

MDOF system

In this thesis, general MDOF systems are of primary interest. Figure 5.6 shows how the total energy input is distributed over the structure. The general equation of motion, written for a SDOF system, can be re-written for a MDOF systems as follows:

$$\int m_i \cdot \ddot{x_i} \cdot \dot{x_i} \cdot dt + \int c_i \cdot \dot{x_i} \cdot \dot{x_i} \cdot dt + \int f_i \cdot \dot{x_i} \cdot dt = -\int m_i \cdot \ddot{x_g} \cdot \dot{x_i} \cdot dt \tag{5.5}$$

In the equation of motion 5.5, the first and the second term, $\int m_i \cdot \ddot{x_i} \cdot \dot{x_i} \cdot dt$ and $\int c \cdot \dot{x_i}^2 \cdot dt$ represent the kinetic and damping energy, respectively. The third term $\int f_i \cdot \dot{x_i} \cdot dt$ represents the elastic and hysteretic energy dissipated at each level.

The equation of motion expanded to MDOF systems can also be written in matrix form, as follows:

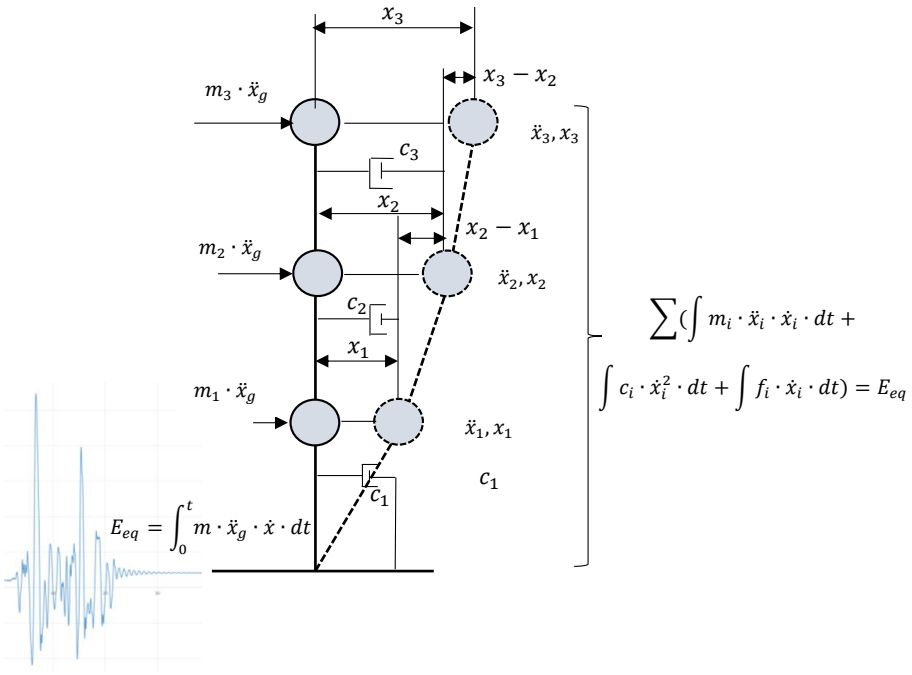

Fig. 5.6: Energy input and energy distribution along the height of the structure

$$\int \left[M\right] \cdot \left\{\ddot{X}\right\} \cdot \left\{\dot{X}\right\} \cdot dt + \int \left[C\right] \cdot \left\{\dot{X}\right\}^2 \cdot dt + \int \left\{F_{s(x,\dot{x})}\right\} \cdot \left\{\dot{X}\right\} \cdot dt = -\int \left[M\right] \cdot \left\{\imath\right\} \cdot \left\{\ddot{X}_g(t)\right\} \cdot \left\{\dot{X}\right\} \cdot dt \tag{5.6}$$

The right-hand-side of Equation 5.6 denotes the relative energy input and can be written as:

$$E_{in,r} = -\int \left[M\right] \cdot \left\{\imath\right\} \cdot \left\{\ddot{X}_g\right\} \cdot \left\{\dot{X}\right\} \cdot dt = \int \sum_{i=1}^{n} m_i \cdot \ddot{x_g} \cdot \dot{x_i} \cdot dt \tag{5.7}$$

Finally, the equation for the relative input energy can be written as the sum of the work done by the equivalent static forces on the corresponding relative displacements at each level as follows:

$$E_{in,r} = \sum_{i=1}^{n} m_i \cdot \ddot{x_g} \cdot x_i \cdot \frac{\Delta_i^2}{2} \tag{5.8}$$

Equation 5.8 presents the entire work on the structure done by the equivalent static forces ($m_i \cdot \ddot{x_g}(t)$) on the corresponding storey displacements. The work done by the equivalent static forces can also been written as the sum of the relative work done at each storey for all of the stories. From Figure 5.6, it can be seen that all masses above the ground level experience a displacement.

$$E_{in,r} = E_{in,r,1} + E_{in,r,2} + ... + E_{in,r,n-1} + E_{in,r,n} = (\sum_{i=1}^{n} m_i \cdot \ddot{x_g} \cdot x_1 + \sum_{i=2}^{n} m_i \cdot \ddot{x_g} \cdot x_2 + \\ + ... \sum_{i=n-1}^{n} m_i \cdot \ddot{x_g} \cdot x_{n-1} + m_n \cdot \ddot{x_g} \cdot x_n) \cdot \frac{\Delta_t^2}{2} = \tag{5.9}$$

In Equation 5.9, the term $m \cdot \ddot{x_g} \cdot x_i$ can be positive or negative depending on whether the ground acceleration and storey displacements are in-phase or out-of-phase. The distribution of the relative input energies along the height of the structure is schematically shown on the displaced structure correlated to the first vibration mode, as presented in Figure 5.7.

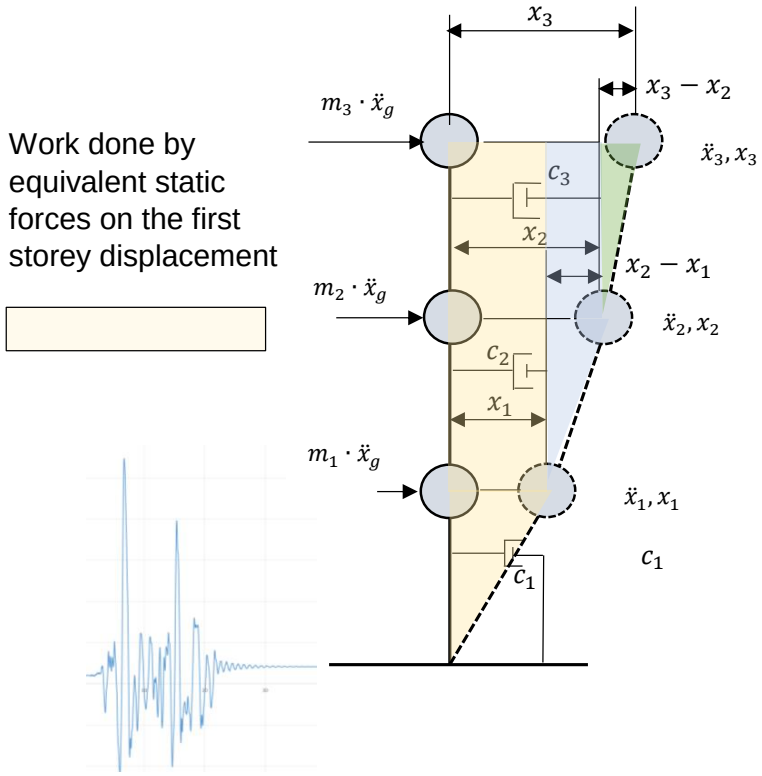

Fig. 5.7: Relative input energy dissipated at different floor levels, exemplarily shown for the first vibration mode

Since work done by the equivalent static forces and thus the relative energy input at the first storey is of the particular interest, it can be written as follows:

$$E_{in,r,1} = \sum_{i=1}^{n} m_i \cdot \ddot{x_g} \cdot x_1 \cdot \frac{\Delta_t^2}{2} = m_{total} \cdot \ddot{x_g} \cdot x_1 \cdot \frac{\Delta_t^2}{2} \tag{5.10}$$

where $E_{in,r,1}$ is the amount of relative energy input introduced at the 1^{st} storey level. By dividing $E_{in,r,1}$ by the mass, the normalized relative energy input can be estimated for each degree of freedom as follows:

$$\frac{E_{in,r,1}}{m_{total}} = -\int \ddot{x_g} \cdot \dot{x_1} \cdot dt = \ddot{x_g} \cdot x_1 \cdot \frac{\Delta_t^2}{2} \tag{5.11}$$

An example of the energy dissipated during nonlinear displacements of the shear wall in the first floor is presented in Figure 5.8, whereby the cumulative energy amount have been normalized by unit mass.

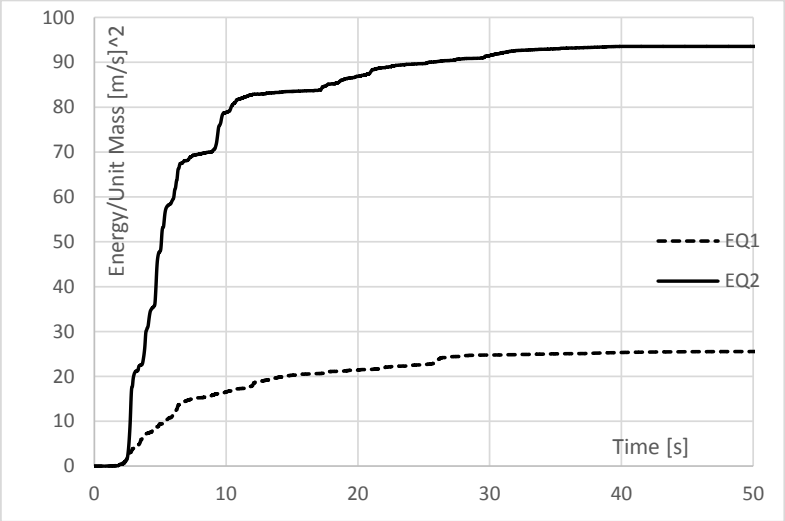

Fig. 5.8: Energy dissipated by nonlinear displacements of the first level shear wall under two selected earthquakes with low (EQ1) and high (EQ2) energy content, see also table 5.3

In order to estimate DI of a selected structure for different IDR, 10 earthquakes have been selected and scaled to the seismic hazard level of 10% in 50Y for Soil Category C, and both Zones 3a and 3b. A mass of 80$[t]$ per storey has been applied to the structure. 1.05% and 2.27% median inter-storey drift ratios at the first level and calculated average values of damage index of $DI = 0.28$ and 0.65 have been obtained for Zones Z3a 3b, respectively. In order to investigate whether there is some regularity in the relationship between the inter-storey drift ratios and the damage indexes, the soil conditions A, B and C with corresponding earthquake suites as well as number of storeys, masses and hazard levels have been varied until IDR′s of 2.0, 2.5, 3.0 and 3.5% have been reached. The results with the corresponding DI are summarized in Table 5.3.

When comparing the IDR and DI, given in Table 5.3, a certain regularity can be recognized. The different earthquake intensities produce different IDR-s and thus different damage indexes, so the IDR-s of 1, 2, 3, and 3.5% correspond approximately to DI of $0.3, 0.6, 0.9$ and $DI > 1$, respectively. Additional analyses, which have been performed for the same structure by varying the mass, led to IDR of 2.5 %, providing a corresponding DI of 0.7.

According to Figure 5.5(a), which can be considered as representative for all single storey walls studied in this thesis, it is obvious that the immediate occupancy and life safety limit states hold for the associated IDRs of 1% and 2.5% and the corresponding DIs of 0.3 and 0.7, respectively. Since the maximum structural strength is achieved at the 2.5% displacement level, it is reasonable to assume that the damage expected at this stage is still in a moderate range. Beyond this

Tab. 5.3: Damage index estimation for a three-storey structure. Constitutive wall element with a length of 3.6 [m], with a displacement capacity of $\Delta_{u,st} = 119.3[mm]$, yield force $F_y = 265[kN]$ and parameter $\beta_{DI} = 0.067$ for an earthquake suite scaled in such way to produce an average IDR of 1%, 2%, 3% and 3.5% corresponding to the IO, LS and CP limit states

EQ	IDR 1%			IDR 2.0%			IDR 3%			IDR 3.5%		
	Δ_{resp}	$\int dE$	DI	Δ_{resp}	$\int dE$	DI	Δ_{resp}	$\int dE$	DI	Δ_{resp}	$\int dE$	DI
No.	[mm]	[kNm]	[-]	[mm]	[kNm]	[-]	[mm]	[kNm]	[-]	[mm]	[kNm]	[-]
1	22.94	16.93	0.23	43.73	26.60	0.42	32.84	27.12	0.33	86.21	141.29	1.02
2	35.18	12.00	0.32	24.0	38.90	0.28	167.7	145.7	1.78	21.95	48.68	0.29
3	36.87	22.62	0.36	18.37	5.23	0.17	196.7	1.3	78.0	26.11	0.71	
4	20.35	34.44	0.24	24.4	4.37	0.21	30.08	73.1	0.41	20.23	38.48	0.817
5	25.60	6.41	0.23	26.38	17.52	0.26	199.77	149.2	2.0	27.23	20.06	0.27
6	6.88	3.08	0.06	42.58	15.53	0.39	131.5	160.1	1.44	38.06	18.27	0.36
7	21.60	14.93	0.21	236.85	70.73	2.1	28.83	23.1	0.29	309.43	no co.	> 2.6
8	40.49	24.66	0.39	73.45	23.01	0.66	34.2	48.4	0.39	242.43	217.07	2.49
9	30.51	17.15	0.29	42.70	77.5	0.52	27.82	10.98	0.26	85.03	705.98	2.2
10	54.72	22.36	0.51	25.92	57.42	0.34	75.55	n.c.	> 0.63	72.36	128.20	0.88
average	29.51	17.46		55.84	33.68		83.3	92.7		98.2	149.4	
Average Damage Index			0.28			0.54			0.88			1.16

displacement level, the damage becomes increasingly severe. Similarly, for an IDR approaching 3%, accompanied by a DI of approximately 0.9-1.0, the damage intensity approaches failure. Finally, for an IDR of about 3.5% and a corresponding damage index of $DI \geq 1.0$, collapse of the structure is to be expected.

Liang et al. (2011) [56], have proposed a relationship between damage index and observed damage for wood-frame buildings. Their damage description associated with the damage index is given in Table 5.4.

If the DI range proposed by Liang in [56] is applied to the structure under consideration, the wall will experience minor damage at the first storey for a DI estimated within the range of $0.25 \leq DI = 0.30 < 0.4$, moderate damage for a DI estimated within the range of $0.4 \leq DI = 0.60 < 0.7$, severe damage in the range of $0.7 \leq DI = 0.9 < 1.0$ and total collapse in the range of $DI \geq 1.0$. This matches the DI ranges given in Table 5.4. Thus, the performance expectations given by the ASCE provisions in Table 5.2 have been confirmed for the IO limit state with an IDR of 1%. The LS limit state underestimates the admissible IDR as 2% instead of 2.5%. The drift limit of 4% associated with the CP performance objective seems to be too large and overestimates the displacement capacity of the structure. An IDR of 3.25%, providing the damage index of approximately 1.0, seems to be a more appropriate drift limit for the CP limit state. Note that the drift limits are not consistently defined across literature. For moment resisting systems, they are conveniently expressed as percentage values normalized by the entire height of the structure. For structures with a pronounced similarity to the shear beam behaviour,

Tab. 5.4: Relationship between damage index and damage observed for wood-frame buildings after [56]

Degree of damage	Damage description	Damage Index range
Collapse	Total or partial collapse of the building	$DI \geq 1.0$
Severe	Partial or complete failure of any structural component, severe cracks in walls, separation of sheathing from studs, building is hardly repairable	$0.7 \leq DI < 1.0$
Moderate	Extensive cracking in walls, evidence of permanent deflection, damage is repairable	$0.4 \leq DI < 0.7$
Minor	Main structural components are essentially undamaged, only minor repairs are required	$0.25 \leq DI < 0.4$
None	no visible damage	$DI < 0.25$

such as LFTWs, the drift ratio at the ground floor level governs the design. This is because the maximum shear forces and shear displacements are concentrated in the first storey. Thus, in order to control the drifts of LFTWs, we primarily look at the displacements, IDRs and DIs at the first storey level.

Comment

If in the analysis the contribution of the energy dissipation at the specific point would be neglected while estimating the damage index, the methodology would fall back to the performance-based design. The remaining criterion would still be the IDR, which is a measurement for the structural exploitation due to a specific earthquake. It is in the engineer's hands to quantify the damage extend as a performance objective associated with the specific IDR,using for example equivalent ductility factors, (see [26]). Furthermore, the estimation of the DI can be entirely suppressed. In this case, an appropriate IDR should be established as proper performance objective. Finally, neglection of the energy contribution in the estimation of the DI would not cause essential modification in the results presented in the tabular format. Nevertheless, an important indicator for the fulfillment of the set criteria would be omitted, which would have a negative impact on the quality of the performed seismic analysis.

5.2.4 Damage limit states for LFTW based on damage index estimation

Considering the findings in the previous chapter, a proposal for performance limit states based on damage index analysis can be made. Although EC8 defines only two performance limit states, namely damage control and collapse prevention, the introduction of the life safety limit state seems to be useful and widely accepted. In Table 5.7, a proposal for performance levels based on

damage analysis is given. In the damage index analysis the inter-storey drift limit is provided as additional information. The damage index, reflecting a combination of a deterministic (the given mechanical model of the LFTW) and a probabilistic (varaibility in considered earthquake motions) approach, is more extensive and more reliable for limit state definition. In this thesis, in addition to the inter-storey drift limits, the damage index DI will be estimated for all structures analyzed.

5.3 Seismic Fragility Analysis of LFTWs Sheathed with OSB

In order to compare the performance expectations obtained by the damage index analysis with those estimated by the IDA analysis, the same three-storey structure consisting of a shear wall with a length of 3.6 [m], will be considered. Direct comparison is not possible because the damage index analysis and the IDA do not operate in the same space. The damage index is obtained using earthquake records scaled to the prescribed hazard levels, which can be represented by appropriate response spectra. The response spectra are defined by spectral accelerations, spectral displacements or periods of vibration of a certain seismicity i.e., a certain hazard level. If the fractile of the IDA curves is generated using spectral accelerations as the intensity measure and roof drift or inter-storey drift as the damage measure, DI and IDA could be linked to each other. To do so, the original roof-displacement - base-shear relationship of the structure is imported into the SPO2FRAG software. The original format of the backbone curve is presented in Figure 5.5(b) before and Figure 5.10(a) after input into the software. The pushover curve follows the original nonlinear form. The software uses a quadri-linear fit to the curve, which enables better approximation of the overall structural behaviour. Considering the physical meaning of the structural response to the lateral loading represented by the backbone curve, the limit states have been directly introduced into the curve representing the roof drift. This divides the response into characteristic ranges with specific limit states, as presented in Figure 5.9.

Figure 5.10(b) shows the dispersion of the IDA curves for the IM expressed as spectral acceleration S_a, given DMs of 1%, 1.7% and 2.13% roof drift ratios in accordance with Figure 5.9, for the structure analyzed in the previous section. As shown in Figures 5.10(b) and 5.11, the suite of all earthquake records should be scaled to the intensity levels of $S_a = 0.195 \cdot g$; $S_a = 0.35 \cdot g$ and $S_a = 0.39 \cdot g$ in order to produce 1%, 1.79 % and 2.13% roof drift ratios corresponding to the predefined performance levels IO, LS and CP, respectively. Based on the quadri-linear approximation of the pushover curve and modal mass participation factor Γ, the inelastic vibration period T^* is within IDA procedure estimated to be $T^* = 1.21[s]$. For the IM of $S_{a(T=1.21s)}$, all limit states have the same probability of exceedance of 50%. The IDA fractile and fragility curves are the results characteristic of the structure under consideration. They remain constant because they depend only on the structural characteristics such as its nonlinear force-displacement relationship and its dynamic properties. Unlike the results of the IDA analysis, represented by the fractile curve, which remain constant, the damage index changes, i.e., increases with increasing seismicity. Thus, two representations can be combined, provided both of them are presented in the same format with respect to spectral accelerations and spectral

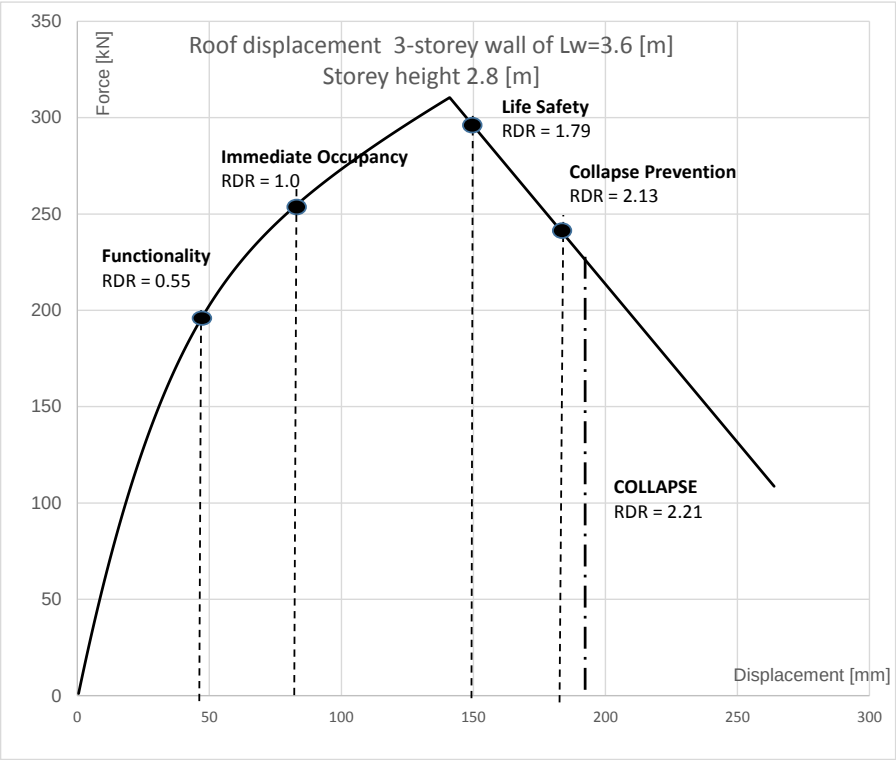

Fig. 5.9: Drift limits defined direct on the roof-displacement - base-shear backbone curve, see also 5.10(a)

displacements. To do so, the fractile IDA curve is superimposed on the response spectra. With increasing seismicity, the response spectra glide along the unchanging curve representing the IDA fractile. The IDA fractile, estimated for the roof drift ratio DM, according to Figure 5.9 and the response spectra with increasing intensity, produces increasing roof displacements of the structure considered in this example. The results are presented in Figure 5.13(a), 5.13(b) and 5.13(c), where the IO limit state corresponds to the service level response spectra (RS) with return period (RP) =72Y, the LS limit state with the design level RS with RP=475Y and CP with the maximum credible earthquake RS with RP =2475Y, respectively.

Ideally, the point which represents a certain limit state on the IDA curve, should lie at the intersection with the corresponding elastic response spectra. Thus, the elastic response spectra, representing the design earthquake with a RP of 475Y with Probability of Exceedance (PoE) of 10% in 50Y should intersect the IDA fractile curve at the point which characterizes the LS limit state and the maximum credible earthquake RS with a RP of 2475Y with PoE of 2% in 50Y should intersect the IDA fractile curve at the point which characterizes the CP limit state, as presented in Figures 5.13(b) and 5.13(c). The points representing the LS and CP limit states in Figures 5.13(b) and 5.13(c), lie quite far beyond the intersection of the elastic spectra and the IDA representation, indicating that the structure subjected to the chosen seismicity, i.e., hazard level, will not exhibit the roof displacements of 1.0, 1.79 and 2.13 %, as stipulated in Figure 5.9 in accordance with the limit state definition in SPO2IDA. Additionally, it means that the drift

limit points on the roof displacements - base shear curve do not reflect the drift magnitude at the ground storey level, which governs the structural behaviour. Furthermore, the DI, which is estimated for the IDR instead of the roof displacement ratio cannot be directly introduced in the graphical presentation with the roof displacement curve. Thus, a better agreement between the DI and IDA results has been achieved when spectral displacements based on the IDR as the DM have been superimposed on the corresponding RS, where, for each chosen seismicity level, the corresponding damage index has been estimated, as presented in Figures 5.14(a), 5.14(b) and 5.14(c). In this representation, the displacements arising from the IDR are located on the same IDA fractile curve and lie closer to the intersection with the elastic response spectra.

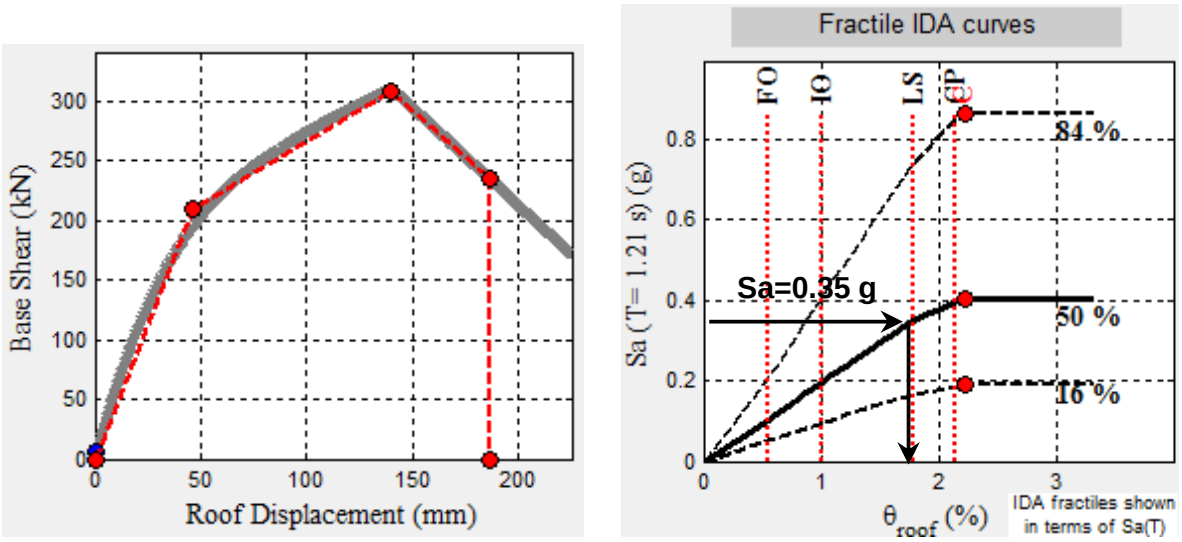

(a) (b)

Fig. 5.10: Quadri-linear fit of nonlinear base shear roof- displacement relationship of the three storey shear wall with a length of 3.6$[m]$ 5.10(a): Fractile IDA curves in format roof drift as DM vs intensity measure (IM) represented by $S_{a(T=1.21s)} \cdot g$ 5.10(b)

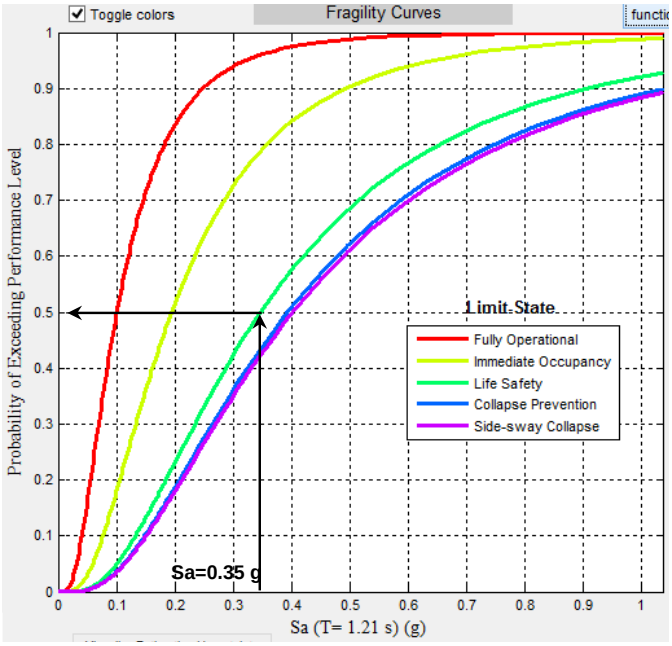

Fig. 5.11: Fragility curves for different performance levels in terms of intensity measure (IM) represented by the first-mode spectral acceleration $S_{a,T_1}5\%$ and probability of exceedance of the specified performance level

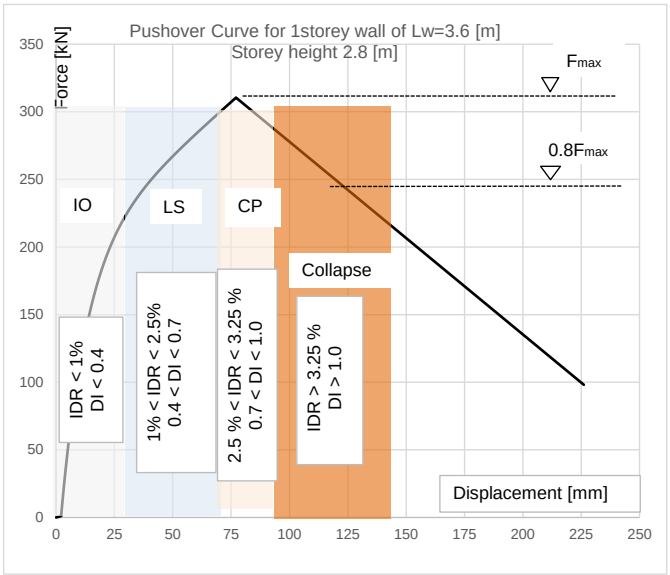

Fig. 5.12: Performance levels with corresponding Inter-storey Drift Ratio (IDR) and Damage Index (DI) range, identified on the pushover curve of a single storey LFTW element

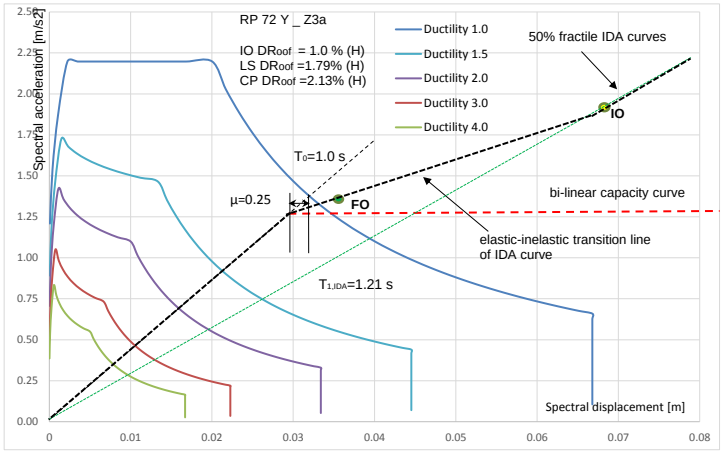

(a)

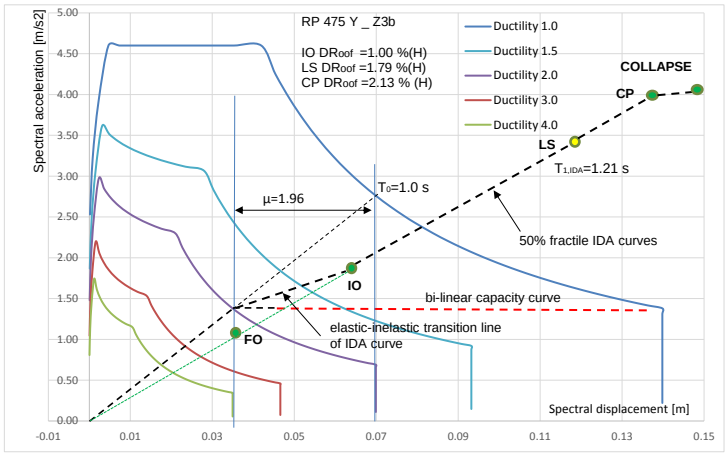

(b)

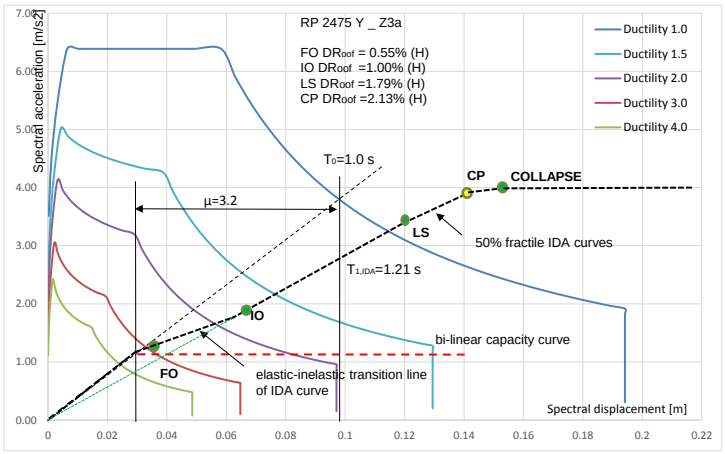

(c)

Fig. 5.13: IDA curve superimposed on the response spectra representing seismicity of $0.77[\frac{m}{s^2}]$ (Zone Z3a and RP 72Y), 5.13(a): seismicity of $1.6[\frac{m}{s^2}]$ (Zone Z3b and RP 475Y), 5.13(b): seismicity of $2.22[\frac{m}{s^2}]$ (Zone Z3a and RP 2475Y), 5.13(c)

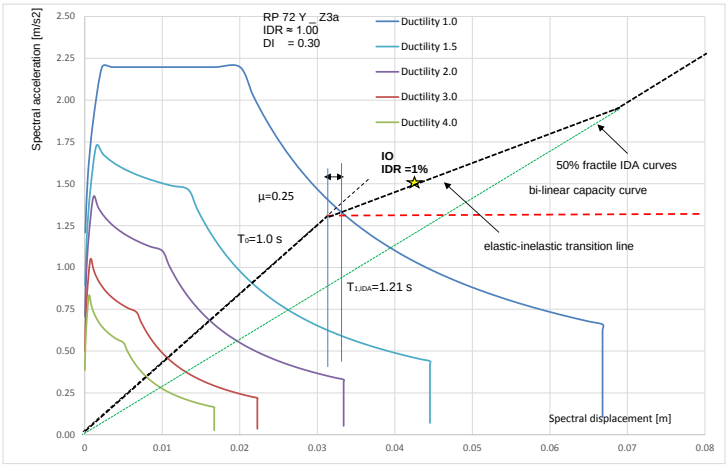

(a)

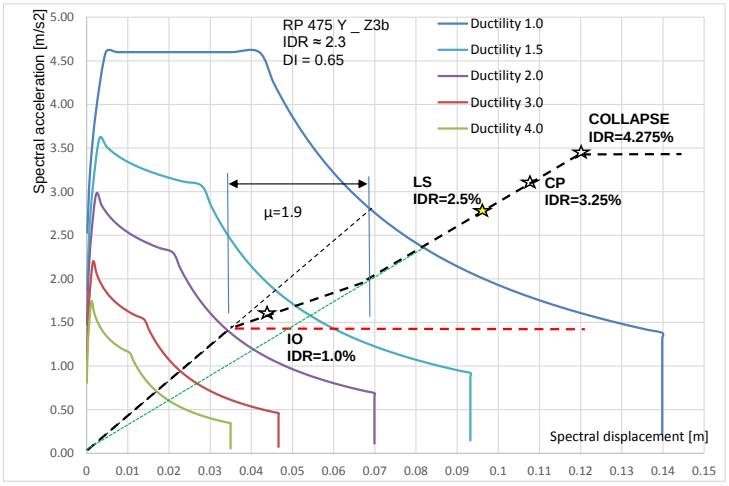

(b)

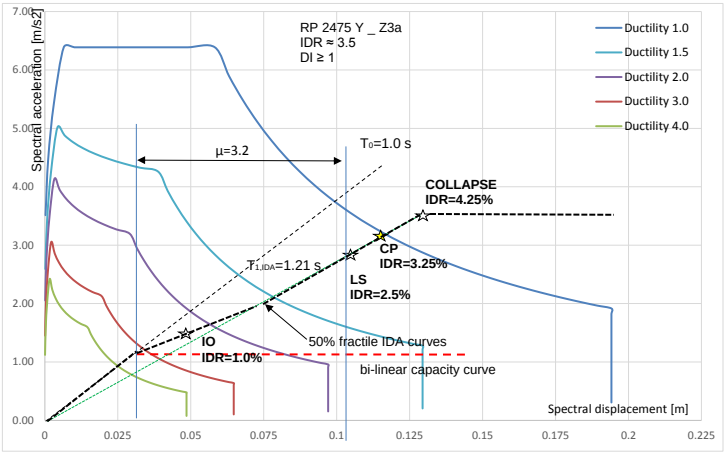

(c)

Fig. 5.14: IDA curve superimposed on the response spectra representing seismicity of $0.77[\frac{m}{s^2}]$ (Zone Z3a and RP 72Y), producing IDR of 1% and DI of approximately 0.3, 5.14(a): seismicity of $1.6[\frac{m}{s^2}]$ (Zone Z3b and RP 475Y), producing IDR of 2.3% and DI of approximately 0.65, 5.14(b): seismicity of $2.22[\frac{m}{s^2}]$ (Zone Z3a and RP 2475Y), producing IDR of 3.5% and $DI > 1.0$, 5.14(c)

From Figures 5.14(a), 5.14(b) and 5.14(c), it can be seen follows that the structure subjected to the three different hazard levels experiences damages of DI = 0.3, DI = 0.65 and $D > 1$, with a good match between the IDA and the elastic response spectra. In the case of the CP limit state, the IDA analysis governs the assessment of the seismic demand, providing an even smaller IM than the elastic spectrum. By looking at the IDR value for which the $DI > 1$ has been estimated, one will see that the $IDR = 3.5$, which increases the stipulated limits of 3.25% and the corresponding $DI = 1.16 > 1.0$. At the same time, an overstepping of the maximum ductility demand $\mu = 3.2 > \mu = 3.0$ has been observed. Hence, the DI, which is $D = 1.16 > 1.0$, $\mu = 3.2 > 3.0$ and the IDA result, where the DM is expressed through $IDR = 3.5 > 3.25\%$ have overstepped the stipulated performance limit state almost simultaneously.
The IO limit states for both IDA related damage measures lie on the IDA representation close to the elastic limit of the capacity curve. This implies that, for this range, the yielding displacement has not yet been achieved. Thus, the structure will experience minor damages which is consistent with the IO performance objective.
Finally, it can be stated that both the damage index and IDA analysis methods, are consistent. They provide similar results in terms of damage indexes for the corresponding limit states, as shown in Table 5.7.
In the parameter study within this thesis, in addition to the maximum periods of vibration, the maximum hold down forces and the ductility demand, the range of the DI will simultaneously be checked.

5.4 Seismic Damage Analysis of LFTWs Sheathed with GFB

5.4.1 Introduction

As shown in Chapter 3, the behaviour of LFTW sheathed with GFB is similar to that of LFTW sheathed with OSB plates. Nevertheless, there is a significant difference. The displacement capacity of shear walls sheathed with OSB is approximately 2.5-3.0 times lager compared to the displacement capacity of shear walls sheathed with GFB. Consequently, the damage to walls sheathed with GFB caused by cyclic loading will occur at much lower displacement magnitudes. For DI estimation according to Equation 5.1, the corresponding parameter β_{DI} should be estimated first.

5.4.2 Estimation of parameter β_{DI} for shear walls sheathed with GFB

By rearranging Equation 5.1 to obtain a DI value =1, implying total collapse of the structure, Equation 5.2 results. Parameters $\Delta_{respISO}$ and Δ_{respMB}, needed for the estimation of the parameter β_{DI}, have been taken from Tables 3.14 to 3.18. Parameters $\int dE_{ISO}$ and $\int dE_{MB}$ have been calculated for each individual wall and have been recorded in Table 5.5. For illustration, the calculated cumulative energy dissipated during the Mergos-Beyer cyclic loading of a wall element sheathed on both sides with a length of 3.6[m] is presented in Figure 5.15. Parameters $\Delta_{u,st}$ and F_y have been obtained from the static pushover curve, as presented in Figure 5.16.

Tab. 5.5: Estimation of coefficient β_{DI} from the CASHEW hysteretic and static pushover analysis of shear walls sheathed with GFB

GFB	L_w	$\Delta_{u,st}$	F_y	$\Delta_{resp_{ISO}}$	$\Delta_{resp_{MB}}$	$\int dE_{ISO}$	$\int dE_{MB}$	β_{ISO}	β_{MB}	β_{DI}
#	[m]	[mm]	[kN]	[mm]	[mm]	[kNm]	[kNm]	[-]	[-]	[-]
1	2.4	29.75	47.71	21.25	22.52	10.038	8.85	0.038	0.039	0.039
2		31.25	85.74	26.25	22.8	15.98	17.92	0.027	0.04	0.033
1	3.0	31.06	60.75	21.5	22.23	11.79	10.92	0.049	0.049	0.049
2		39.52	119.2	28.71	28.65	16.83	11.55	0.077	0.112	0.095
1	3.6	33.3	70.1	20.65	21.5	17.8	12.48	0.05	0.066	0.058
2		38.31	140.5	22.2	26.67	25.96	18.63	0.087	0.0878	0.087
1	4.2	31.2	87.92	21.65	22.86	15.92	13.94	0.053	0.053	0.053
2		29.3	167.9	24.13	24.93	37.32	28.53	0.023	0.026	0.024
1	4.8	39.88	95.62	21.25	24.08	20.53	15.16	0.087	0.099	0.093
2		37.53	179.1	27.41	26.62	34.9	26.58	0.052	0.074	0.063

Due to the low value of the β parameters estimated for the shear walls sheathed with GFB the stiffness and strength deterioration under cyclic loading in the range beyond the maximum displacement contributes less to the energy dissipation and thus, to the entire DI ratio. The energy dissipated through the hysteretic process into the shear walls sheathed with GFB is even less than that dissipated by the shear walls sheathed with OSB panels.

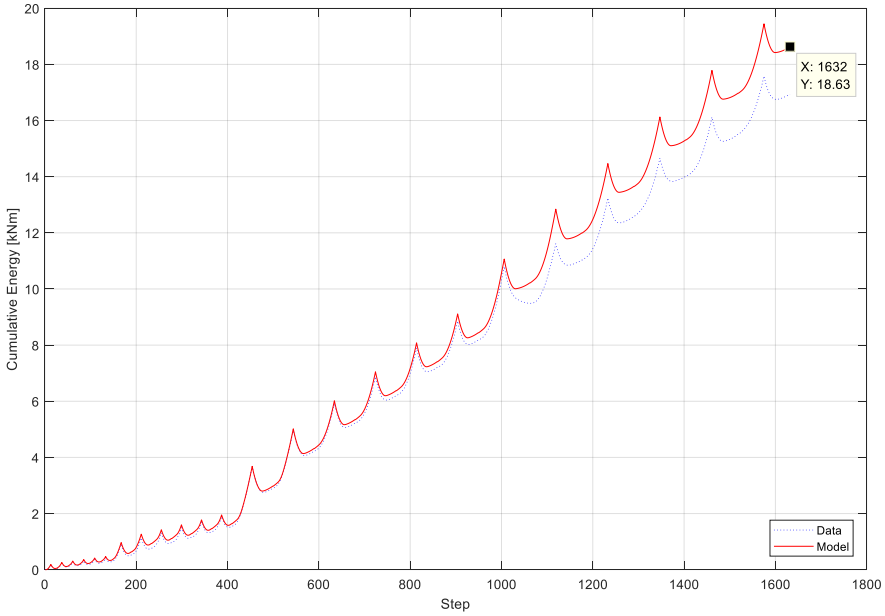

Fig. 5.15: Cumulative energy dissipated by cyclic loading of a shear wall with a length of $L_w = 3.6[m]$, sheathed on both sides with GFB.

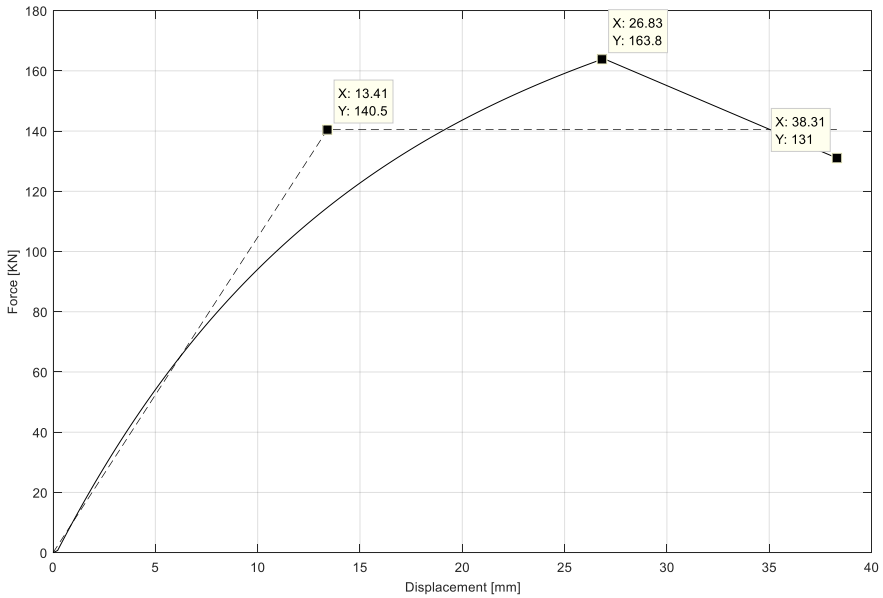

Fig. 5.16: Force-displacement curve of one storey shear wall with a length of $L_w = 3.6[m]$ sheathed with GFB on both sides. Wall parameters according to table 3.10

5.4.3 Experimental damage estimation of shear walls sheathed with GFB

The LFTWs sheathed with GFB have been tested at the Structural Research Laboratory of Empa under monotonic and cyclic loading as described in Chapter 3 and presented in Figures 3.41(a) and 3.41(b). The wall displacements have been captured by using a digital image correlation (DIC) system. The DIC enables visualization of the deformation and strain changes on the panel surface in all displacement stages, providing precise data for what exactly happens during the testing. The pictures were taken with only one camera. Thus, only 2D correlation has been feasible. Consequently, out of plane displacements could be measured. Moreover, during the monotonic tests, the pictures were taken manually at approximately each $1.0[mm]$ step. The pictures during the cyclic testing were taken automatically at a rate of approximately 1 picture per second. Thus the monotonic tests are captured by 30 images, while the cyclic tests are captured by 260 images.

The results are presented in Figures 5.17 to 5.25, where Figures 5.17 to 5.20 show the monotonic test results, and Figures 5.22 to 5.25 present the cyclic test results. From Figures 5.18 and 5.20, it can be seen that during the monotonic loading up to approximately $IDR = 0.5$, no cracking occurred. Any micro cracks that might have occurred in this stage were not detected by DIC. Cracking started at displacements of approximately $15[mm]$ and continued propagating up to an IDR = 0.75. This is within the corresponding displacement range of approximately $20[mm]$ with a cracking length of approximately $600[mm]$ (Test 1) or a sudden diagonal crack appearance in the edge of the panel (Test 2). At displacement of approximately $25[mm]$ and a corresponding IDR = 0.9, cracking took place along almost half of the panel height (Test 1). In Test 2, at displacement magnitude of $25[mm]$, a crack propagated at the right panel corner on

the bottom edge. The degradation process characterized by propagation of cracking along the fastener line on the panel edge was finished for displacements of approximately 30[mm], which corresponds to an IDR of 1.1%. In terms of damage index analysis, an IDR of 0.5 is characterized by no visible cracking and can be associated with full serviceability and immediate occupancy limit state. $0.5 < IDR \leq 0.75$ corresponds to moderate damage and can be associated with life safety limit state. For inter-storey drift ratios between $0.75 < IDR \leq 1.0$, severe damages, characterized by the collapse prevention limit state, have been observed. Displacements in the range of $IDR \geq 1.0$ indicate that the structure is close to the collapse stage.

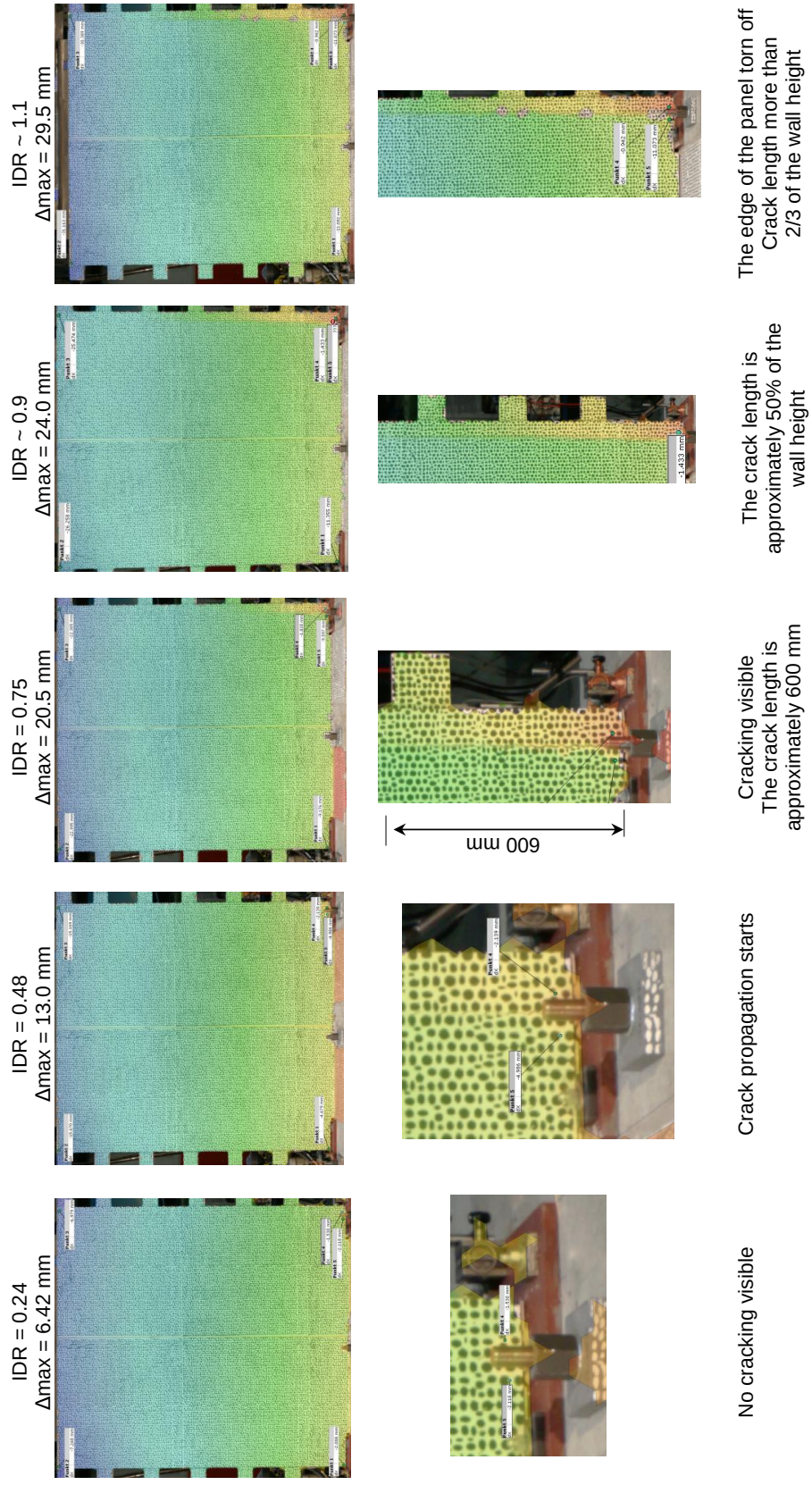

Fig. 5.17: Shear wall sheathed on both sides with GFB under monotonic loading in terms of Inter-storey Drift Ratios (IDR) and corresponding damage pattern and damage intensity.

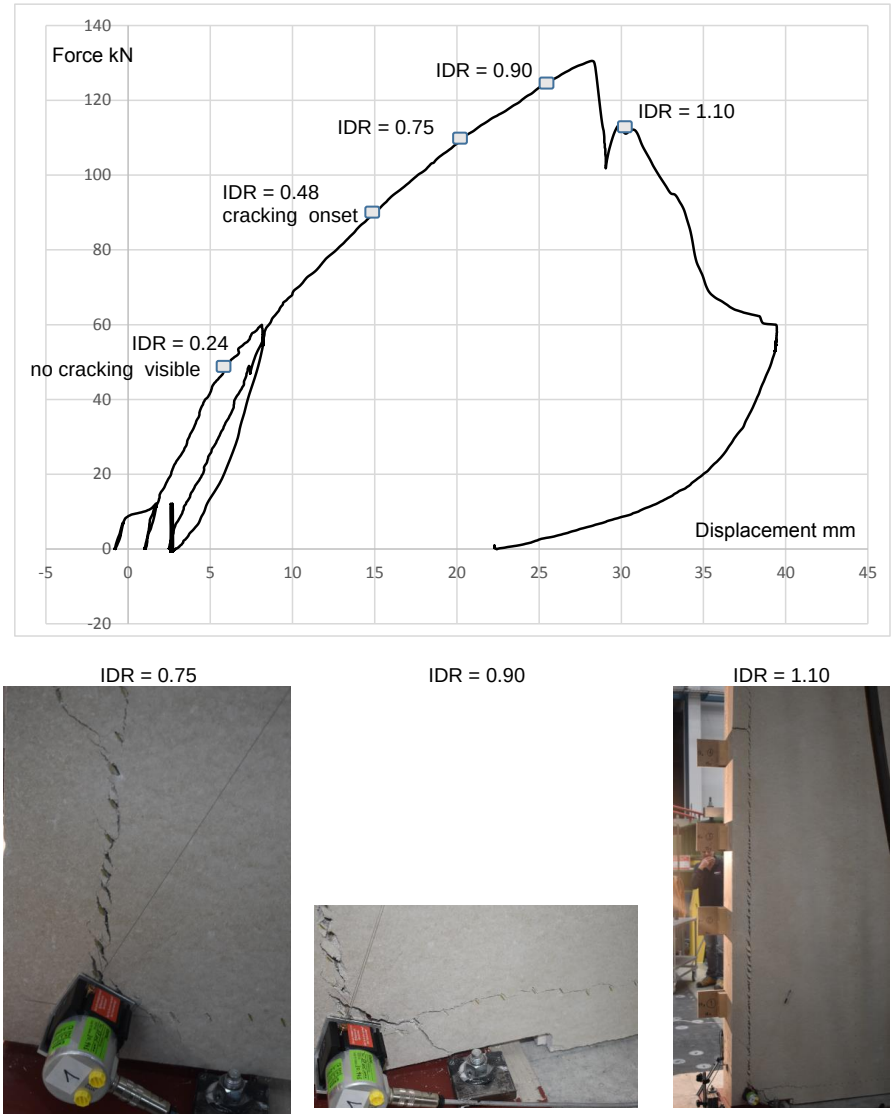

Fig. 5.18: Force-displacement relationship of the shear wall, sheathed on both sides with GFB, under monotonic loading with introduced IDR according to the figure 5.17 and corresponding damage pattern and damage intensity

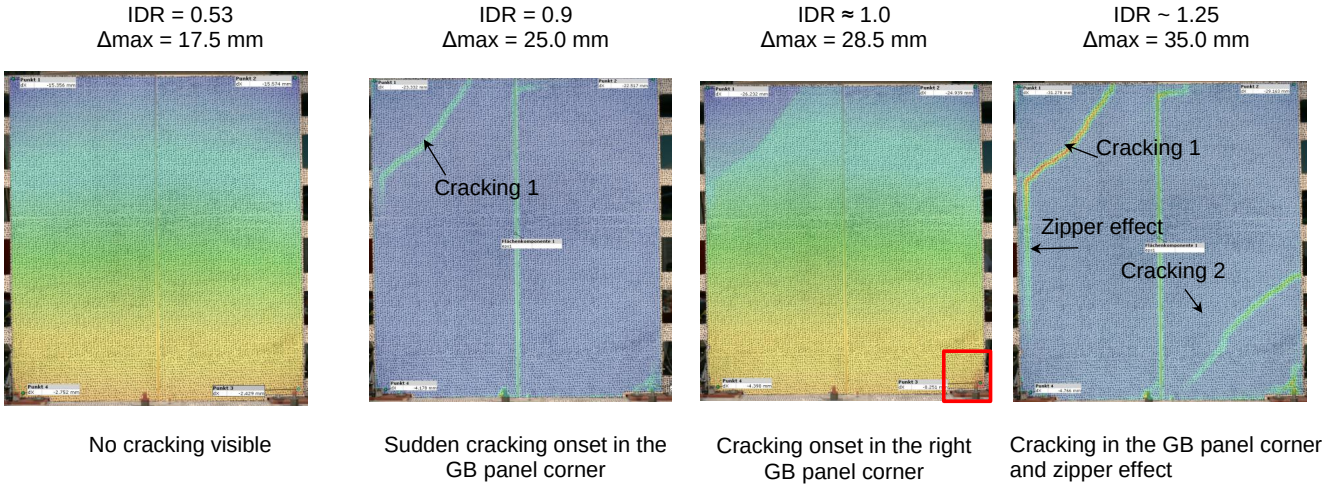

Fig. 5.19: Shear wall sheathed on one side with GFB under monotonic loading in terms of Inter-Storey Drift Ratios (IDR) and corresponding damage pattern and damage propagation.

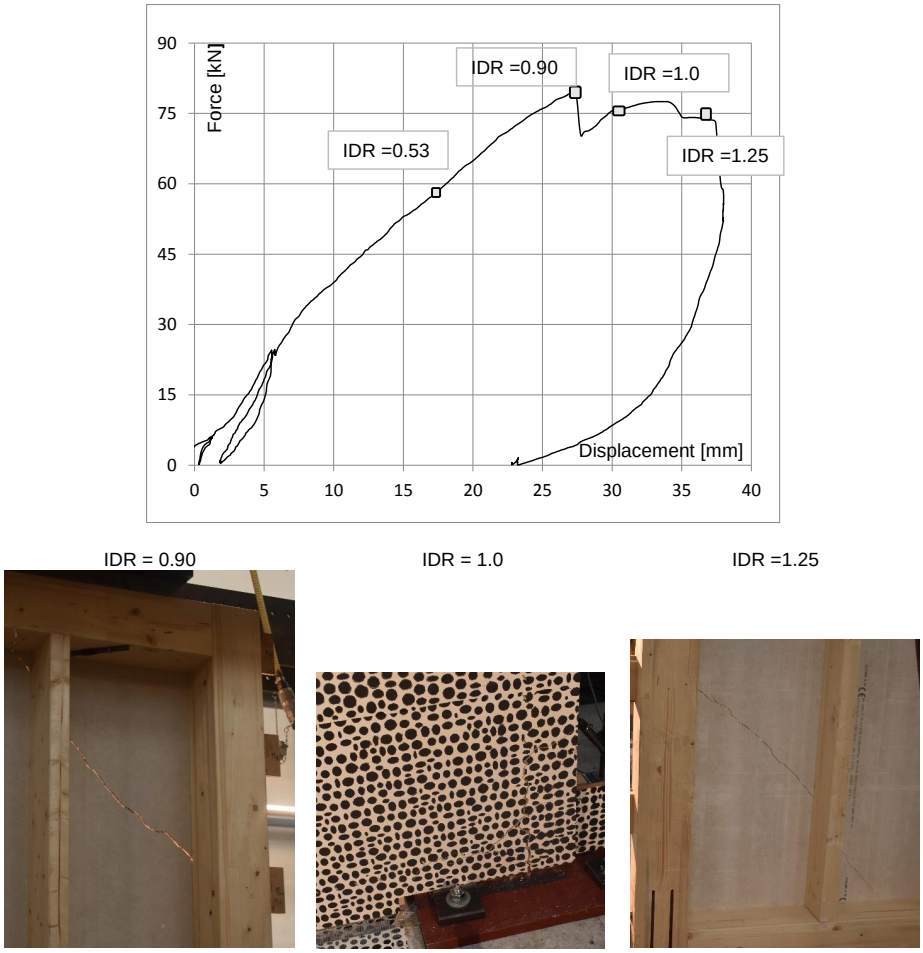

Fig. 5.20: Force-displacement relationship of the shear wall, sheathed on one side with GFB, under monotonic loading with introduced IDR according to Figure 5.19

Remarks:

Although the sheathing panels had been designed to have enough space around them to enable free rotation while testing, they were produced with only a few [mm] space on the bottom side. Since the GFB was trimmed around the HD devices, this insufficiency was not apparent before testing. By closely looking at the displacement profile presented in Figure 5.21, the sheathing panels can be seen to develop different displacements. The left side is unrestrained free and developed vertical displacement of approximately 4.7$[mm]$. The right side is restrained, performing and displaces only 1.1$[mm]$ vertically. This can explain the brittle failure observed at low displacements. Additionally, the stiffness of the wall seems to be affected by this production error. The consequence are: a) the structure is stiffer and b) the displacement quantity is probably smaller than it would be in the case of unrestrained rotations. On the other hand, the numerical model is not affected by this uncertainty. The real displacement capacity is larger. The decision to restrain the IDR to 0.8% is conservative. Due to the fact that the GFB is a rather brittle material, the limiting IDR and DI seem to be acceptable. Note that the numerical model is not calibrated using the experimental results.

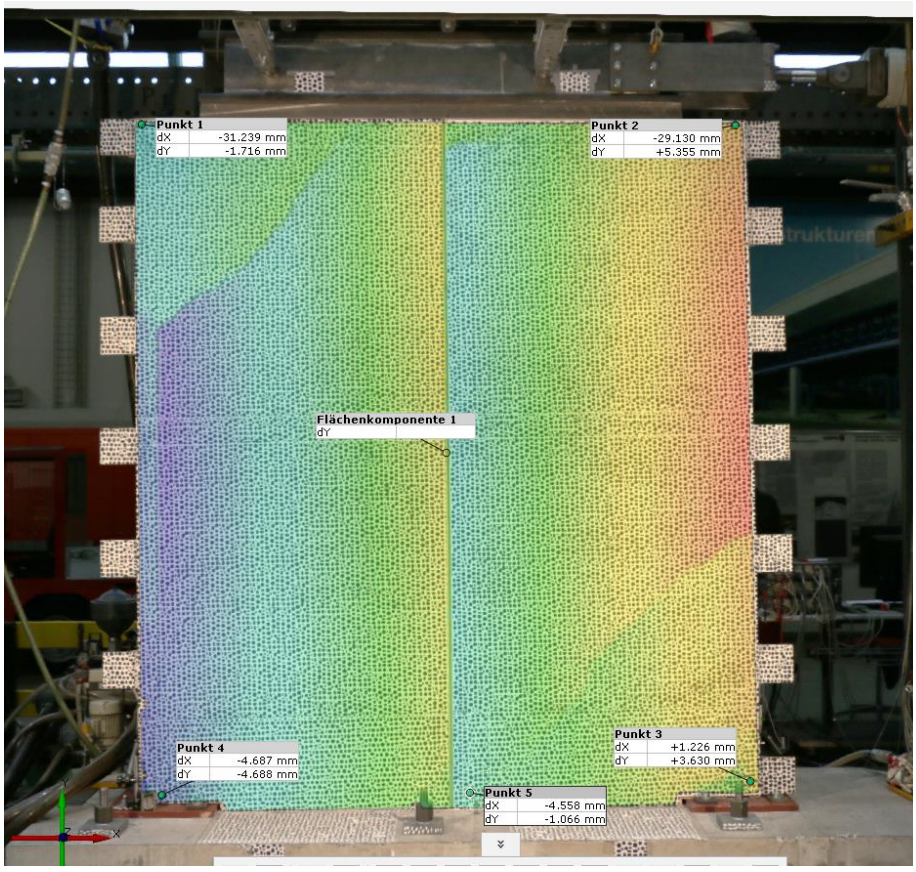

Fig. 5.21: Displacement of the panel has been unintentionally restraint, leading to brittle cracking at low displacement levels

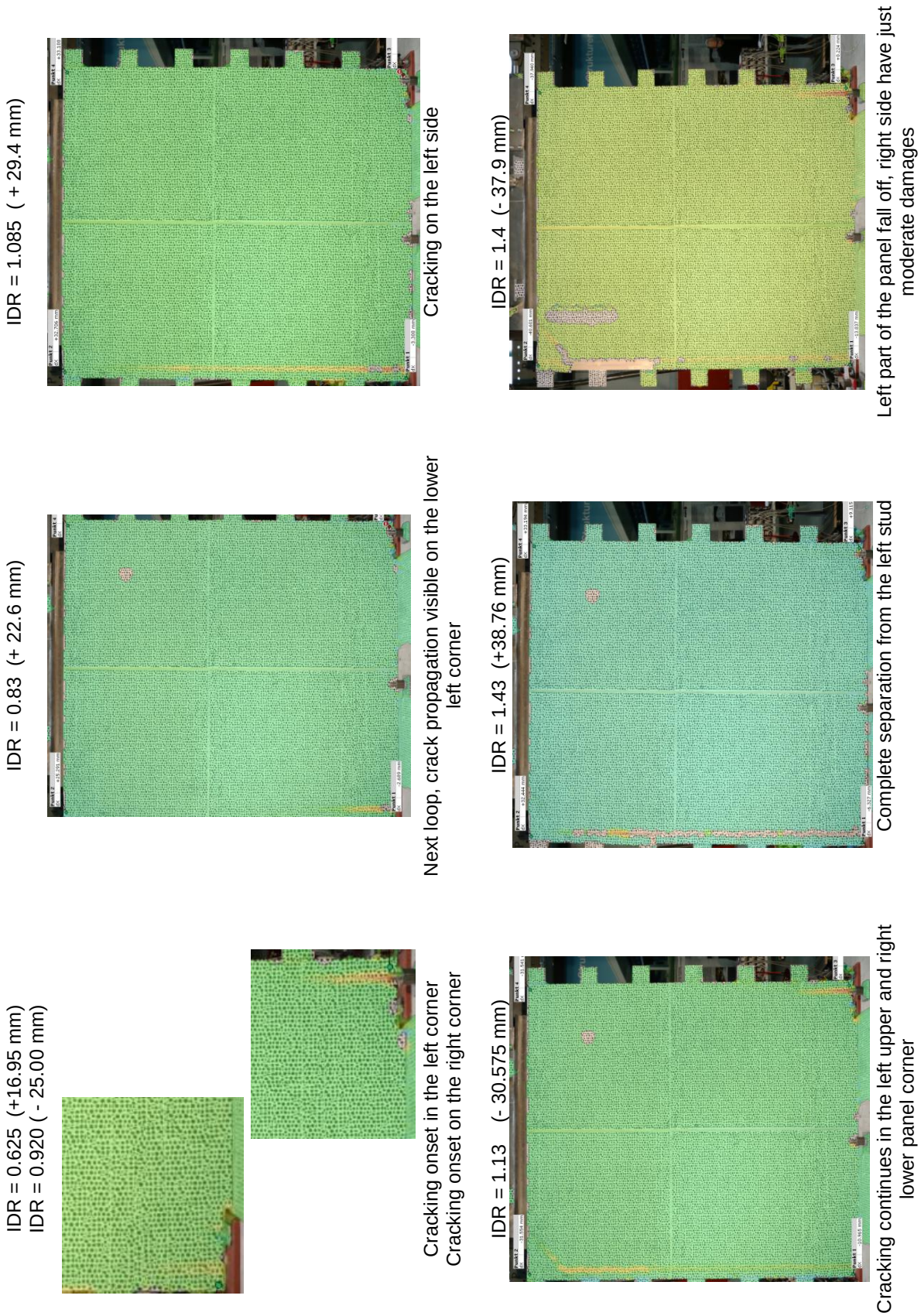

Fig. 5.22: Damage stages under cyclic loading of the shear wall, both sides sheathed with GFB in accordance with figure 5.23

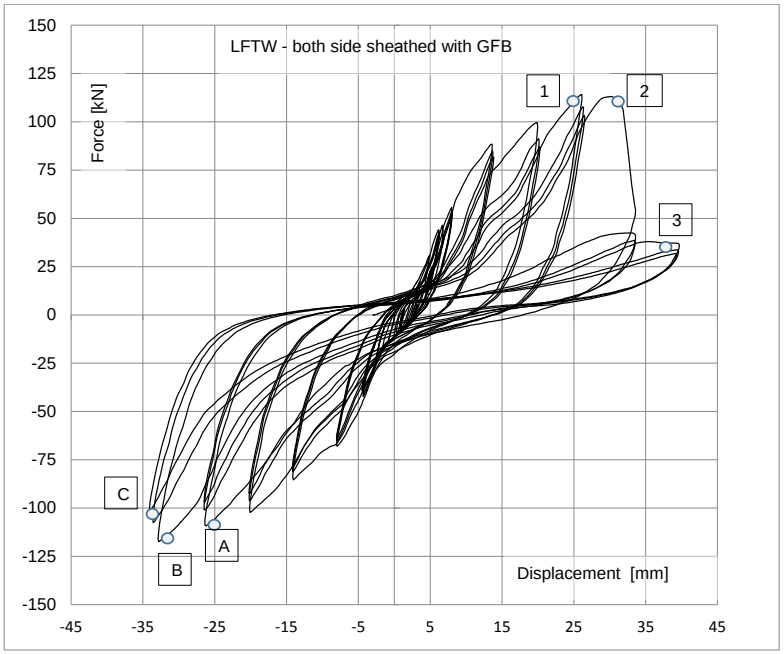

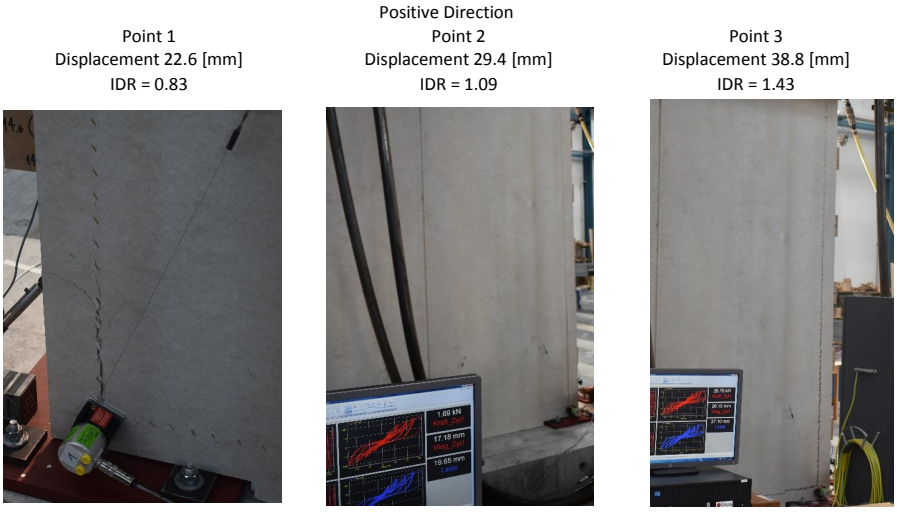

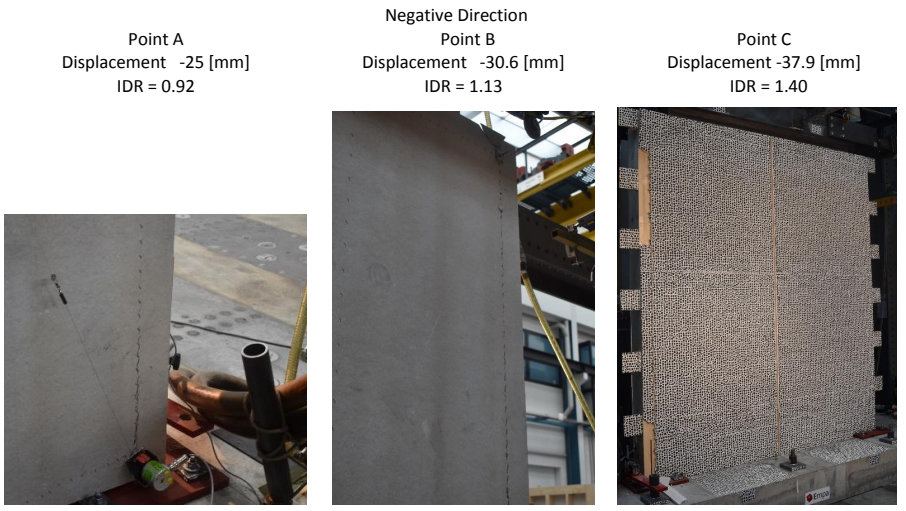

Fig. 5.23: Hysteresis of the shear wall, sheathed on both sides with GFB, under cyclic loading with introduced IDR according to the figure 5.22 and corresponding damage pattern and damage intensity

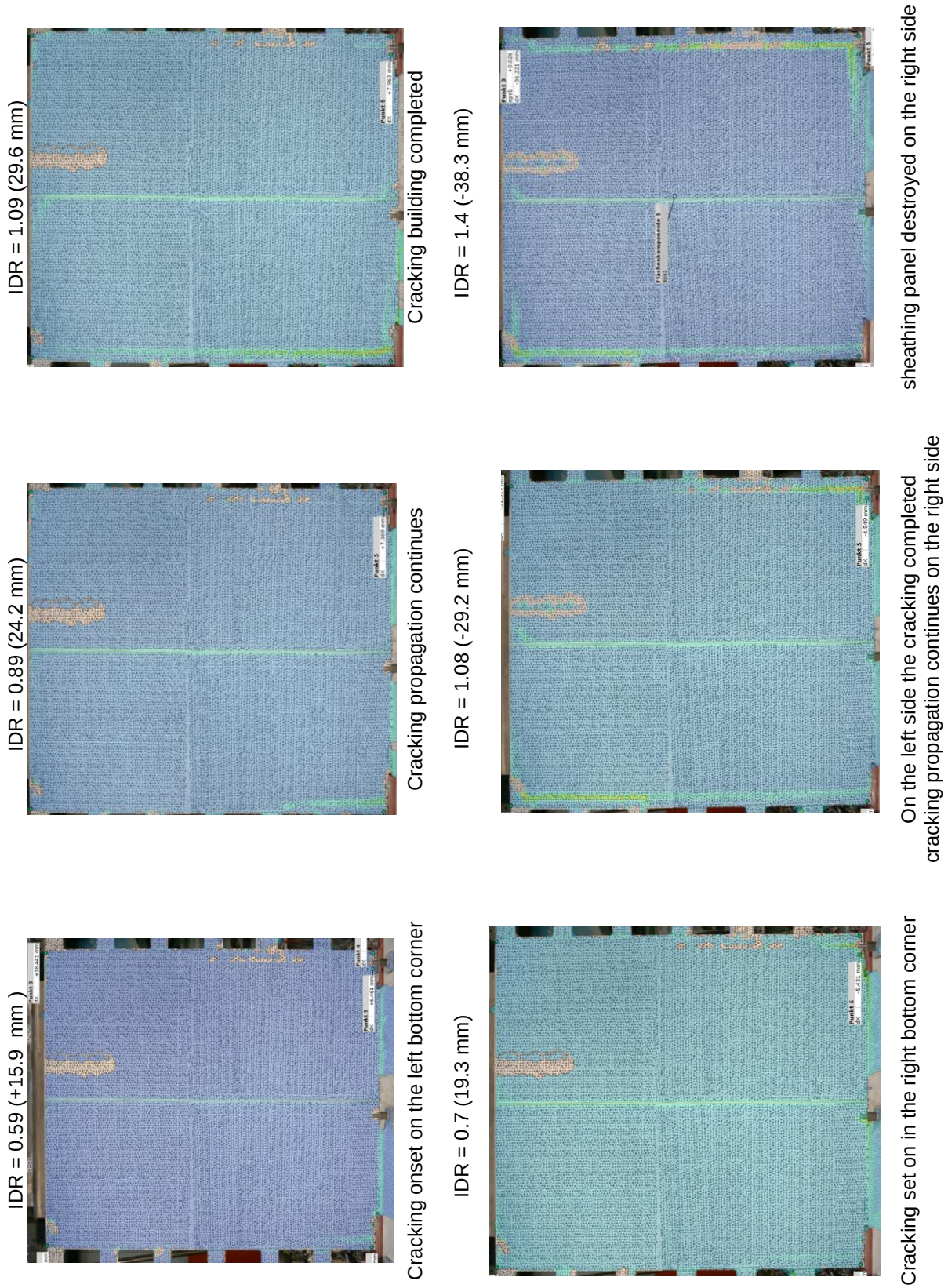

Fig. 5.24: Damage stages under cyclic loading of the shear wall, sheathed on one side with GFB in accordance with figure 5.25

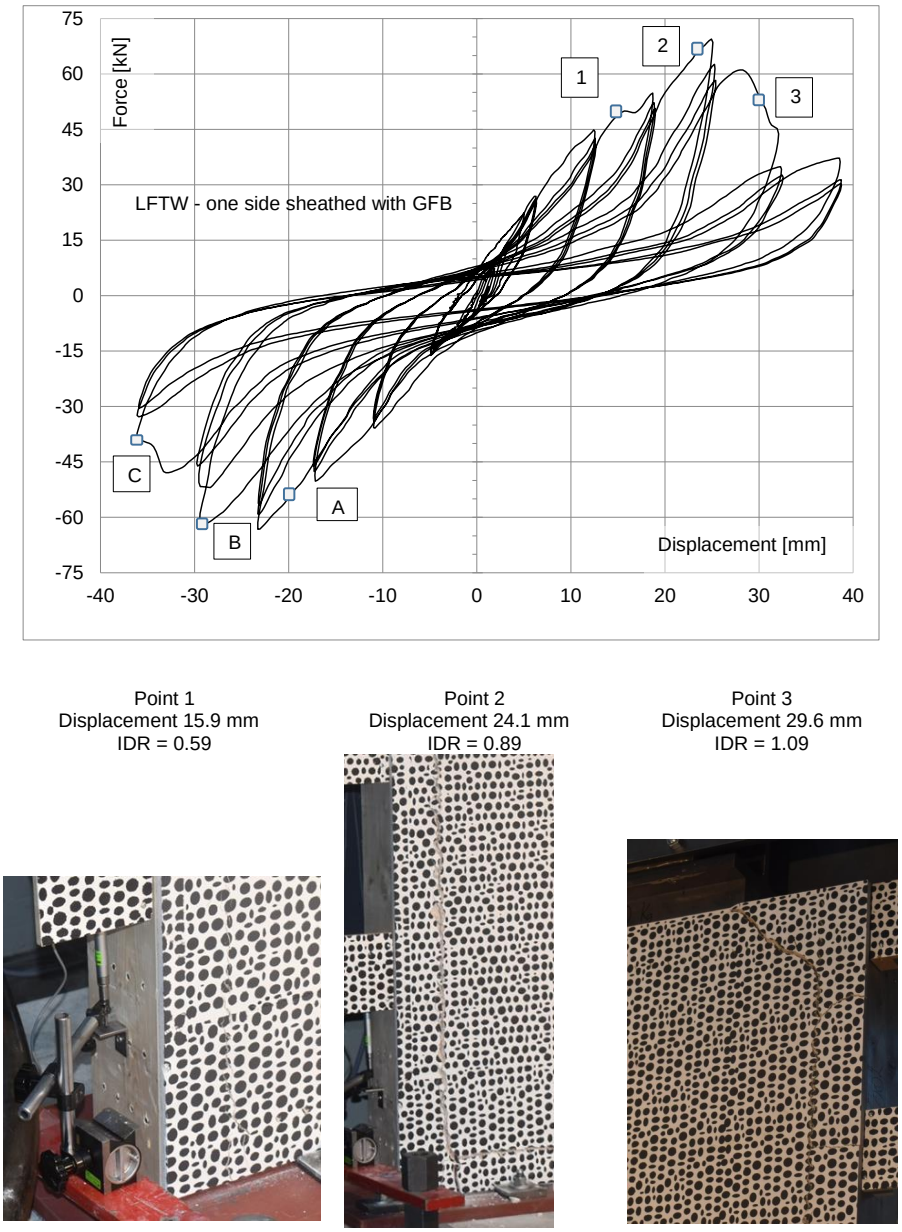

Fig. 5.25: Hysteresis of the shear wall, sheathed withon one side with GFB, under cyclic loading with introduced IDR according to the Figure 5.24 and corresponding damage pattern and damage intensity

Figures 5.22 to 5.25 show the damage pattern under cyclic loading. Despite the brittle failure of the single staple-GFB connection, the walls tested under cyclic loading developed a typical pinched hysteresis, and have been stable while experiencing displacements of approximately IDR=1%. The value of IDR =1% is five times the serviceability requirement of $IDR = 0.2\% = h_{st}/500$ according to Swiss code SIA260 [75]. The displacement ranges for monotonic loading expressed as inter-storey drift ratios, could also be applied for the cyclic loading, as stipulated in Table 5.8.

The drift limits and the performance expectations stated above are based on experimental testing. For general use, numerical models, which are able to reproduce similar drift ranges

with corresponding damage indices are necessary. In Chapter 3, a mechanical model has been established for the LFTW sheathed with GFB. The same mechanical model will be used for numerically based damage analysis.

5.4.4 Numerical damage estimation of shear walls sheathed with GFB

As stated in the previous chapter, the displacement capacity of LFTWs sheathed with GFB is limited. Nevertheless, the wall can develop hysteretic behaviour, providing a controlled failure mechanism under cyclic loading occurs. In the following section, the numerically based correlation between the damage index for the stipulated IDR will be investigated. To do so a structure consisting of a wall with length of 3.6 m and mechanical characteristics in accordance with Table 3.16 will be analyzed under seismic intensities causing IDRs of 0.45%, 0.65%, 0.85% and 1.1 %. From the results, summarized in Table 5.6, it can be concluded that the numerical model provides a very good agreement between the numerically estimated DI with the corresponding IDR and the real damage observed during the testing.

Tab. 5.6: Damage Index Estimation for a three-storey structure. Constitutive wall element of length 3.6 [m] with displacement capacity $\Delta_{u,st} = 38.8[mm]$, yield force $F_y = 140.5[kN]$ and parameter $\beta_{DI} = 0.087$ for an earthquake sute scaled in such way to produce average IDR of 0.45%, 0.65%, 0.85% and 1.1% corresponding to the IO, LS and CP limit states

EQ	IDR 0.45%			IDR 0.65%			IDR 0.85%			IDR 1.1%		
	Δ_{resp}	$\int dE$	DI	Δ_{resp}	$\int dE$	DI	Δ_{resp}	$\int dE$	DI	Δ_{resp}	$\int dE$	DI
No.	[mm]	[kNm]	[-]	[mm]	[kNm]	[-]	[mm]	[kNm]	[-]	[mm]	[kNm]	[-]
1	18.36	19.11	0.77	22.07	3.56	0.62	9.87	3.53	0.31	18.48	6.67	0.58
2	15.85	8.12	0.54	6.31	1.22	0.18	36.66	16.59	1.20	21.74	19.1	0.87
3	10.76	1.49	0.30	13.2	5.45	0.43	24.44	10.57	0.80	15.43	15.16	0.64
4	12.41	4.9	0.40	12.61	3.22	0.38	22.36	15.12	0.82	19.51	6.06	0.60
5	11.27	4.75	0.37	27.42	8.35	0.84	13.87	9.96	0.52	26.201	6.05	0.77
6	11.29	5.75	0.38	33.17	37.87	1.46	43.91	28.18	1.58	41.05	9.48	1.21
7	12.72	4.96	0.41	12.98	5.94	0.43	18.46	13.47	0.69	93.83	27.14	> 2.85
8	9.95	2.71	0.30	14.82	6.651	0.49	20.03	23.37	0.89	26.82	21.68	1.04
9	15.0	6.85	0.50	27.78	40.25	1.36	18.98	10.09	0.65	19.56	8.82	0.64
10	10.32	3.24	0.32	13.15	7.92	0.46	25.66	20.46	0.99	18.56	11.48	0.66
average	12.79	6.19		18.35	12.04		23.42	15.13		30.12	13.17	
Average Damage Index			0.43			0.67			0.85			0.99

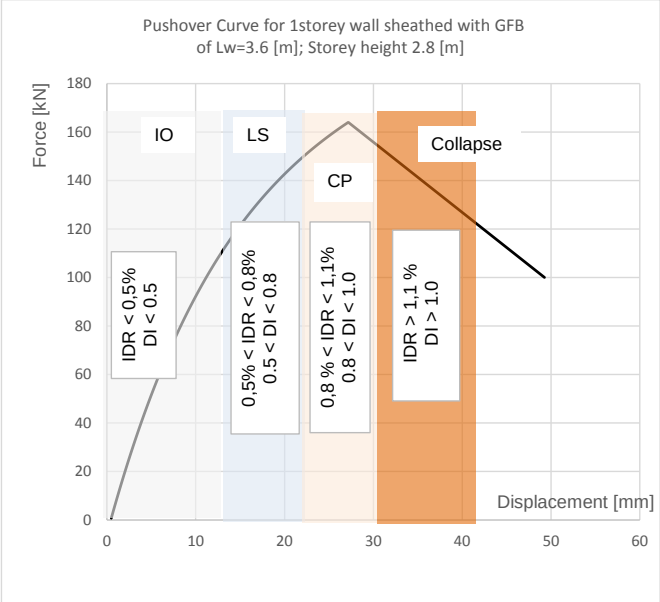

Fig. 5.26: Performance levels with corresponding Inter-storey Drift Ratio (IDR) and Damage Index (DI) range, presented on pushover curve of single storey LFTW element sheathed with GFB

5.5 Seismic Fragility Analysis of LFTWs Sheathed with GFB

5.5.1 Introduction

The information in the previous chapter for the IDA analysis of LFTWs sheathed with OSB analogously applies to the LFTWs sheathed with GFB. In this section, the consistency between the results obtained by the DI and IDA analyses will be checked by superimposing the IDA fractile curve on the corresponding response spectra. The same three storey structure, consisting of a 3.6 [m] long LFTW element sheathed with GFB, used for the DI analysis, will be also examined using IDA analysis. The static pushover curves, which represent responses of one storey and three storey structures are presented in Figures 5.16 and 5.27, respectively.

Figure 5.28(b) shows the dispersion of the IDA curves for the IM expressed as a spectral acceleration S_a, given DMs of 0.3%, 0.6% and 0.74% roof drift ratios in accordance also with Figure 5.27. As shown in Figures 5.28(b) and 5.29, the suite of all earthquake records should be scaled to the intensity levels of $S_a = 0.05 \cdot g$; $S_a = 0.106 \cdot g$ and $S_a = 0.125 \cdot g$ in order to produce 0.3%, 0.6 % and 0.74% roof drift ratios of the system with inelastic natural vibration period $T^* = 1.32[s]$ corresponding to predefined performance levels of IO, LS and CP, respectively. Note that the inelastic period of vibration is estimation based on the quadri-linear approximation of the pushover curve within IDA procedure and differ slightly from the period estimated on the bases of EEEP approach. For the IM of $S_{a(T=1.32s)}$, all limit states have the same probability of exceedance of 50%. As previously discussed the IDA fractile and fragility curves are the characteristic results for the structure under consideration. They remain constant since they depend

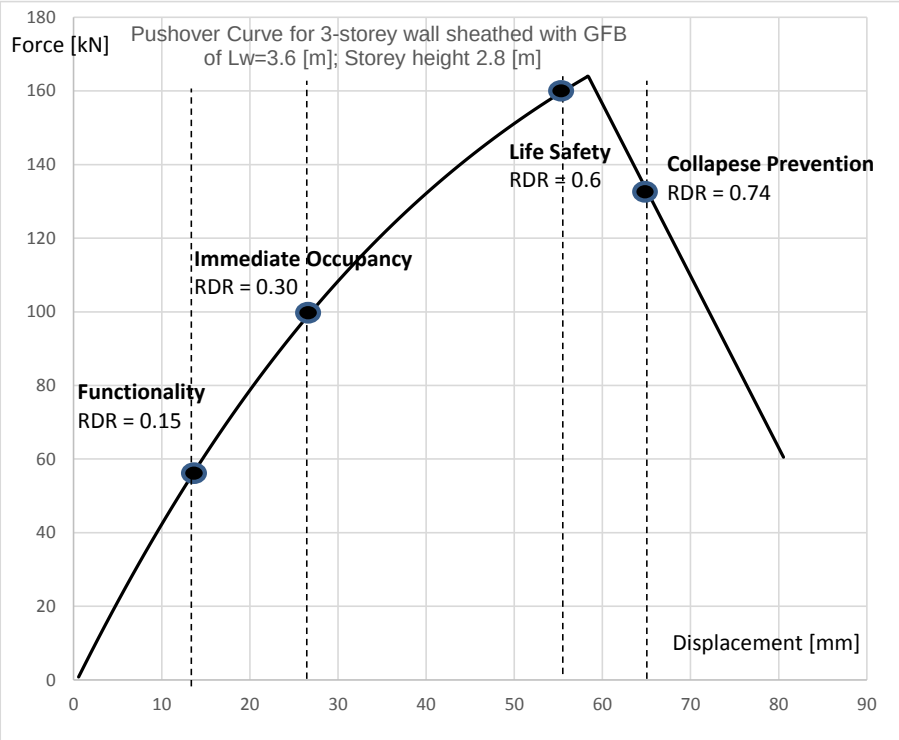

Fig. 5.27: Drift limits defined on the roof-displacement - base-shear backbone curve, see also 5.28(a)

only on the structural characteristic including the nonlinear force-displacement relationship and the dynamic properties including the structural mass and stiffness i.e., the period of vibration.

Again, the objective is to put both the DI and IDA representations together in order to verify their consistency related to how they define the performance expectations for the LFTW sheathed with GFB. For this purpose, the IDA fractile curve will be superimposed on the response spectra representing different hazard levels. The response spectrum with a return period of 72Y and a PoE of 50% in 50Y should intersect the IDA fractile curve at the point which represents the IO limit state. The response spectra with a return period of 475Y and PoE 10% in 50Y should intersect the IDA fractile curve at the point representing the LS limit state. The response spectra with a return period of 2475Y and a PoE of 2% in 50Y, should intersect the IDA fractile curve at the point represents CP limit state.

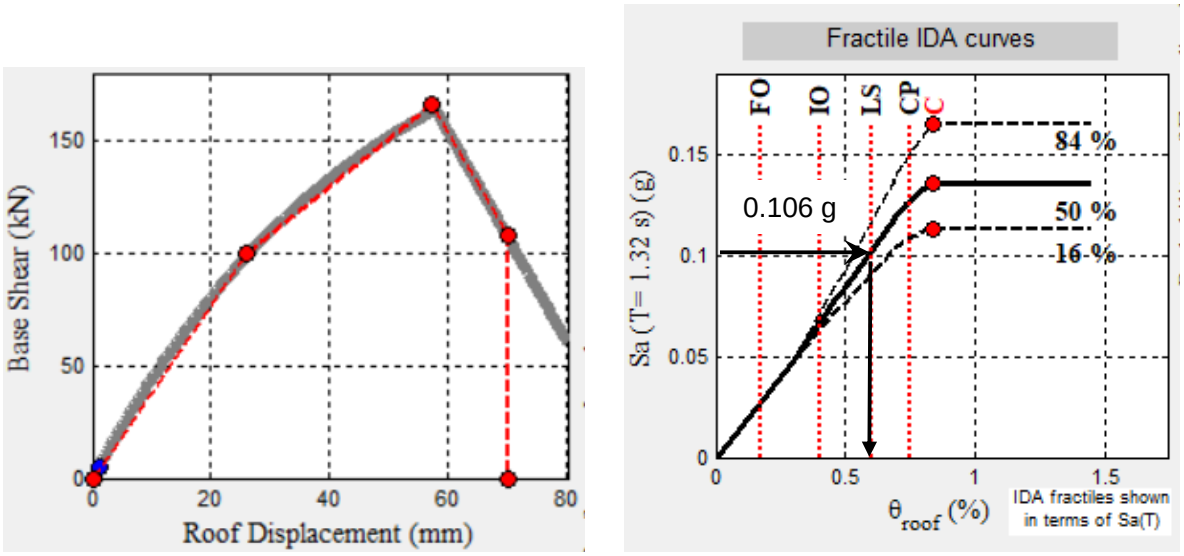

(a) (b)

Fig. 5.28: Quadri-linear fit of nonlinear relationship between base shear and roof top displacement of the three storey on both sides with GFB sheathed shear wall of length 3.6[m] 5.28(a): Fractile IDA curves probability distribution of performance demand represented by roof drift ratio vs intensity measure (IM) represented by $S_{a(T=1.32s)} \cdot g$ 5.28(b)

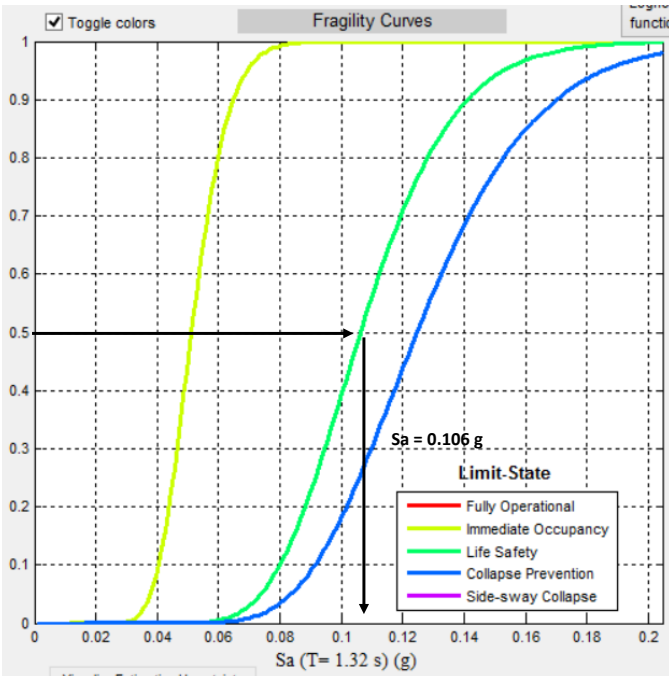

Fig. 5.29: Fragility curves for different performance levels in terms of intensity measure (IM) represented by first-mode spectral acceleration $S_{a,T_1}5\%$ and probability of exceedance of the specified performance level

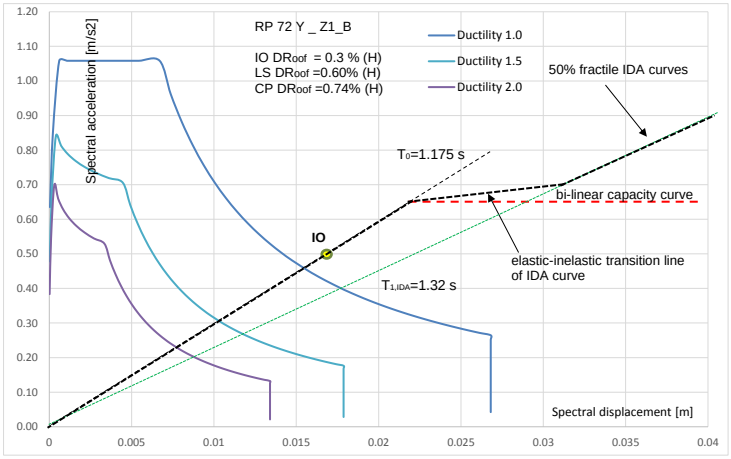

(a)

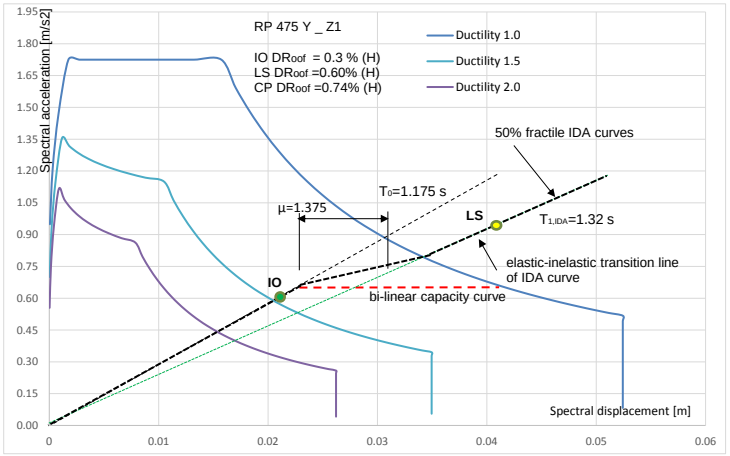

(b)

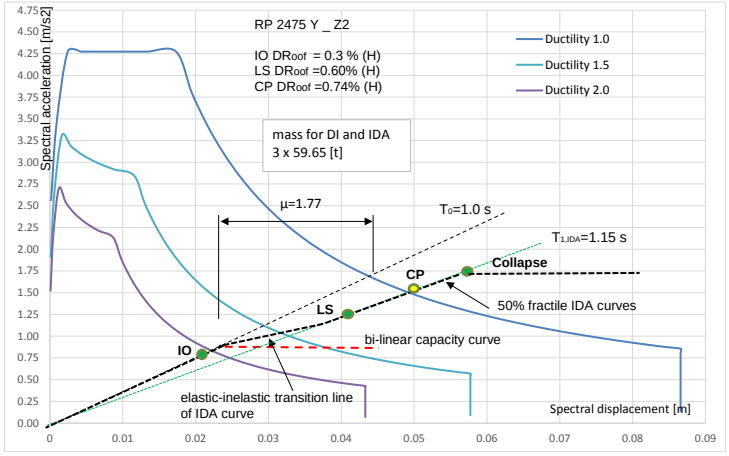

(c)

Fig. 5.30: IDA curve superimposed on the response spectra representing seismicity of $0.354[\frac{m}{s^2}]$ (Zone Z1 and RP 72Y), 5.30(a): seismicity of $0.6[\frac{m}{s^2}]$ (Zone Z1 and RP 475Y), 5.30(b): seismicity of $1.71[\frac{m}{s^2}]$ (Zone Z2 and RP 2475Y), 5.30(c)

Figures 5.30(a) and 5.30(b) show the intersection between the corresponding RS and IDA fractile curve based on the roof drift ratio, where the corresponding DIs estimated by means of NLTHA have the values of 0.45 and 0.65, respectively. The mass applied to the model was 80 [t] on each storey. Figure 5.30(c) shows the intersection between the RS representing a MCE with a RP of 2475Y and the IDA fractile curve, for a mass of 59.7 [t] applied to each storey. The DI estimated for the system is 0.91.

The LFTWs sheathed with GFB can not satisfy the ductility demand of approximately $\mu > 1.85$. In order to satisfy this condition at the MCE hazard level, the storey-mass had to be reduced to 59.7 [t] for the given system, resulting in a DI = 0.91 corresponding to the CP limit state, (see also Figure 5.30(c)).

Furthermore, Figures 5.31(a), 5.31(b) and 5.31(c), shows the IDA fractile curves with the IDR as the DM, confirming the agreement with the DI estimated for the same IDR.

From Figures 5.30(a), 5.30(b) and 5.30(c), as well as from Figures 5.31(a), 5.31(b) and 5.31(c), it can be alleged that the DI and IDA analysis results are consistent and conform to with the performance expectation ranges given in Table 5.8.

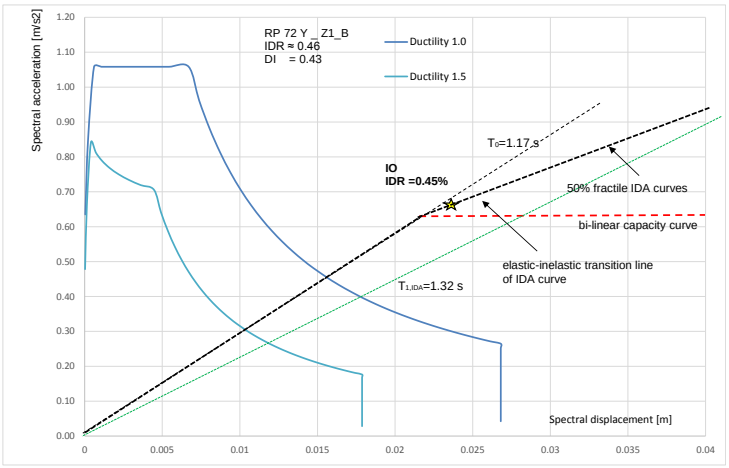

(a)

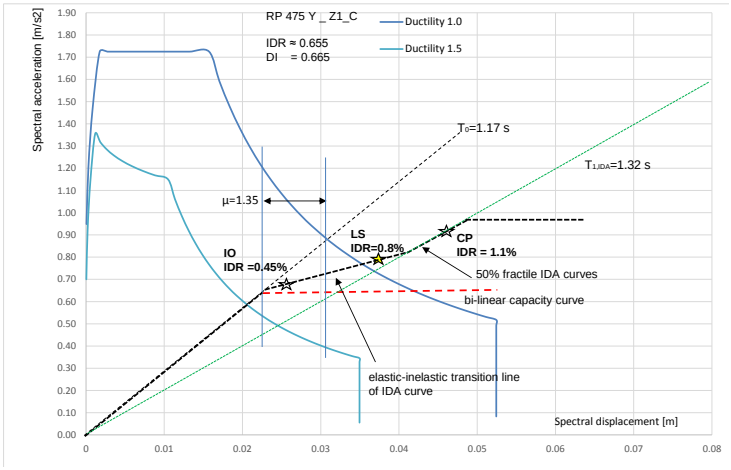

(b)

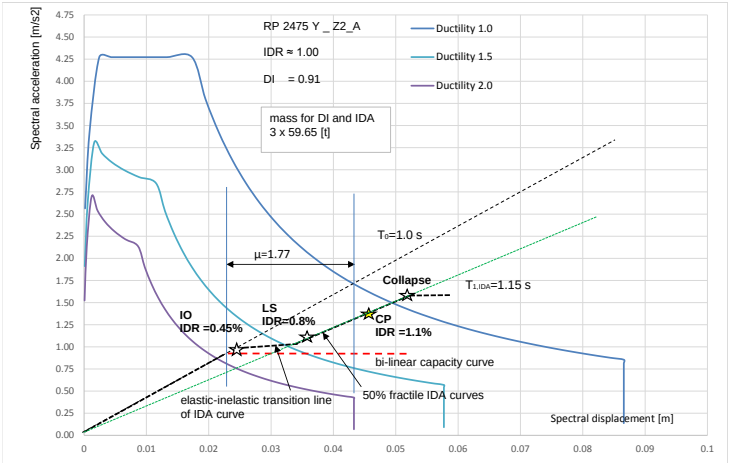

(c)

Fig. 5.31: IDA curve superimposed on the response spectra representing seismicity of $0.354[\frac{m}{s^2}]$ (Zone Z1 and RP 72Y), 5.31(a): seismicity of $0.6[\frac{m}{s^2}]$ (Zone Z1 and RP 475Y), 5.31(b): seismicity of $1.71[\frac{m}{s^2}]$ (Zone Z2 and RP 2475Y), 5.31(c)

5.6 Proposal for Limit State Definition of LFTW

5.6.1 General remarks

Performance based engineering (PBE) is a relatively new approach among seismic design philosophies. It posed a remarkable shift from traditional deterministic seismic design concepts, such as force and displacement based seismic design towards probability based methods, which will dominate the future earthquake design in Europe. PBE deals with real nonlinear responses far beyond the yield point and hysteretic energy dissipated during an earthquake event. It accounts for variability in mechanical response as well as in the earthquake record uncertainty. The method aims to quantify the desired performance objective by mapping the design with expected damage to the structure for a given seismic demand. In order to perform a design based on the PBE method, performing a NLTHA is indispensable.

The Eurocode 8: Design of structures for earthquake resistance - Part 1 [1] defines two performance requirements which should be met with adequate degree of reliability: the damage limitation and the no-collapse requirement. Unfortunately, the limit states are not defined clearly. Moreover, the corresponding hazard levels are partly inconsistent. Regarding timber structures of any kind, there is indication in EC8 as to what performance objectives should be met by means of adequate structural design. Therefore, in this thesis first the limit states of LFTW structures were defined. Additionally, it was recognized that the collapse prevention limit state, required by EC8, is associated with large displacements and damage indexes close to 1, which is inappropriate for design purposes. More appropriate performance limits, capable of covering design requirements have to be introduced. In accordance with the widely-accepted nomenclature, the additional limit state, used in the previous section, is the Life Safety limit state. It is related to design earthquake spectra having a PoE of 10% in 50Y and a corresponding RP of 475Y.

5.6.2 Literature review related to damage description based on damage observations

The damage analysis approach evaluates the damage index as a value which is a linear combination of maximum deformation and absorbed hysteretic energy. The concept has been originally developed for reinforced concrete structures, as presented in [80]. The methodology is material independent and will be used for damage index evaluation for light frame timber structures. Park and Ang (1985) have summarized in [80] the damages observed during the 1971 San Fernando earthquake in the USA and the 1978 Miyagiken-Oki earthquake in Japan. The damage observed on RC structures has been divided into 5 classes: slight, minor, moderate, severe and collapse. Each class has a corresponding description and Damage Index, ranging from DI = 0.25 for minor, DI = 0.25 - 0.70 for moderate to DI = 0.8 - 1.0 for severe damage. Damages in minor and moderate ranges are considered as reparable.
Okada and Takai (2004) [76] tried to describe the damage rate for wood frame dwellings and RC

buildings, concerning building damage in the Kobe area after the Hanschin-Awaji earthquake in 1995 by developing a damage index function. They specified the damage indices for wooden frame dwellings in the range of DI = 0.1, 0.3, 0.5, 0.7 to 0.9 for slight, moderate, heavy, very heavy and destructive damages, respectively. In [25] (2004) Ellingwood et all. have investigated the fragility of light frame wood construction subjected to wind and earthquake. Within the fragility assessment of LFTW due to earthquake excitation, the limit states and performance objectives have been used in accordance with nomenclature used in the USA, i.e. IO, LS and CP. The damage and damage prediction for wood shear walls subjected to simulated earthquake loads have been investigated by J.W. van de Lindt and Guapta (2006) and presented in [98]. The mechanical damage model is based on the Park-Ang proposal, focusing primary on the local damage phenomena, such as nail pull out and sheathing separation. Additionally, the damage descriptions based on an IDA analysis have been given. In the previously mentioned work of Liang at all (2011) [56], damage limit state critera, based on observed local damage mechanisms for LFTWs sheathed with OSB and GFB have been established in accordance with the Park-Ang proposal, presented in [80].

5.6.3 Limit state evaluation

The limit state identification is to be made based on the observed damage pattern and damage intensity. The decision about which degree of damage is acceptable, and thus, which performance objective should be required, is in general up to the society. According to the experiences after the last strong earthquakes, for example in Christchurch 2011 and 2017, the investors are nowadays not only interested in preventing collapse of the structure, but also in minimizing damage as well as down time of the building and hence mitigation of financial losses. Thus, the desired performance objective, which should be met through proper design of the structure, can be for all intents and purposes a protection objective arranged with investors, insurances or other parties involved in the decision making process. From the engineering point of view, the description of damage intensities which could be related to the different protection grades, which is also an insurance matter, should be established. Thus, the people, the institutions and the entire society are encouraged to choose between different performance objectives, adequately related to increasing damage grades. The performance evaluation should be established by technicians.

Collapse prevention limit state

In order to illustrate how the specific performance levels are evaluated the displacements at the collapse prevention limit state are presented in Figure 5.32 directly on an pushover curve of a SDOF system. The collapse prevention limit state was chosen to represent setting of drift limits since, at this specific stage, the displacement limits are given by the nominal strength of the structure at poinz which corresponds to 80% of F_{max}, The damage index of DI = 1.0 was

estimated by means of NLTHA for corresponding IDR of 3.25%. A few observations can be made:

- The nominal strength due to the monotonic loading is defined as the bearing capacity at the displacement corresponding to a force of $0.8 \cdot F_{max}$, (see [78]). At this stage, the corresponding IDR is approximately 4.3%.
- The structure exposed to a random earthquake excitation reaches the collapse stage for a damage index of 1.0 and a corresponding IDR of approximately 3.25%. The difference between the drift limits due to the monotonic loading and the random earthquake excitation is approximately 25%.
- The damage index can be divided into two contributing parts. Both parts together yield the damage index of 1.0 and thus to collapse. The contribution of normalized displacements is in the range of up to approximately 75% and the contribution of normalized hysteretic energy is in the range of up to approximately 25%.
- Regarding DI analysis the drift limit for DI = 1.0 is set to the corresponding IDR of 3.25% for the CP limit state

The same derivation can be made for LFTWs sheathed with GFB, (see Figures 5.18, 5.19, 5.23 and 5.25).

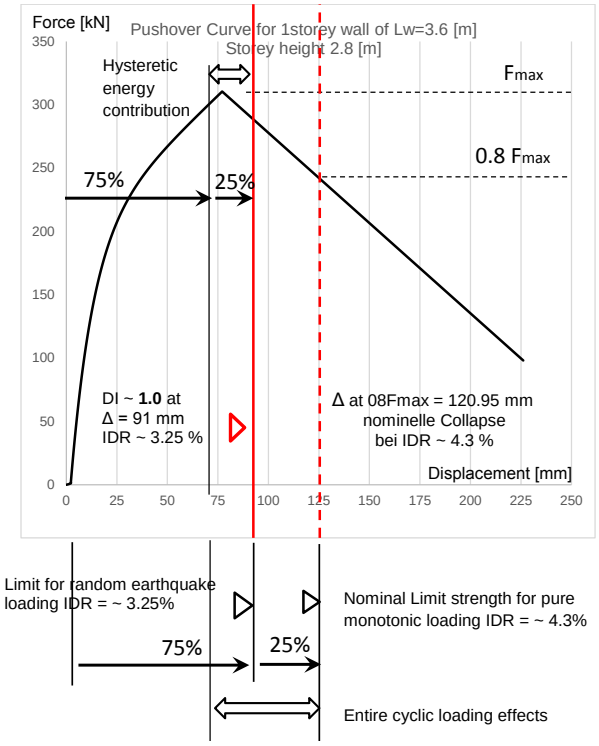

Fig. 5.32: Drifts at the CP limit state for damage index DI = 1.0 consisting of displacement part, absorbed hysteretic energy part in comparison with nominal IDR at collapse

Life safety limit state

The LS limit state is the most relevant one for design. In contrast to the CP limit state, there are no specific limits which could be extracted from the mechanical model of the structure to represent the ranges of the LS limit state. Thus, the definition is entirely a matter of engineer's judgment. The drift limit should be set while accounting for DI estimated by means of the NLTHA. Thus, the LS limit should be in a range significantly smaller than 1.0. In order to narrow down the reasonable range for the LS limit state, one should focus on the extent of damage for a specific level of drift. From observations based on tests and the damage description given in the literature listed above, the repairable damages occurs up to the damage grades of DI = 0.7, (see [80] and [56]). The damage intensity is referred to as minor to moderate, covering damage indices between $0.25 < DI < 0.7$. The drift limit in terms of LFTWs sheathed with OSB, which can be associated with the LS limit state, is roughly between $1\% < IDR < 2.5\%$. The corresponding damage index is between $0.25 < DI < 0.7$, as proposed in literature [56]. An important, additional argument to keep the upper value of the DI in the moderate range of 0.7 for the LS limit state is the requirement that the structure should be able to sustain aftershocks, which regularly accompany the main earthquake events. In order to fulfill the sustainability requirement regarding aftershocks, the structure has to possess enough residual bearing capacity, following the first shock of the main earthquake.
Regarding damage development in terms of LFTWs sheathed with GFB, the IDR associated with reparable damage is in the range between $0.5\% < IDR < 0.8\%$, and the corresponding damage index is between $0.5 < DI < 0.8$. The observations made through testing of LFTW sheathed with GFB associate an IDR up to 0.8% with reparable damage. This can be seen from Point A and Point 1 in Figure 5.23, and in Figures 5.22, 5.19 and 5.18.

The drift limits associated with LS limit state are presented with vertical red lines in Figure 5.33 for both OSB and GFB sheathing material.
An overview related to the general displacement capability of different construction materials is given in Figure 5.34. The displacement capability of LFTWs sheathed with GFB is twice that of unreinforced masonry [85]. Masonry is a material which is very often used in Europe for low rise buildings up to approximately four storeys. On the other hand the LFTWs sheathed with OSB have similar displacement capacities as ductile RC walls.

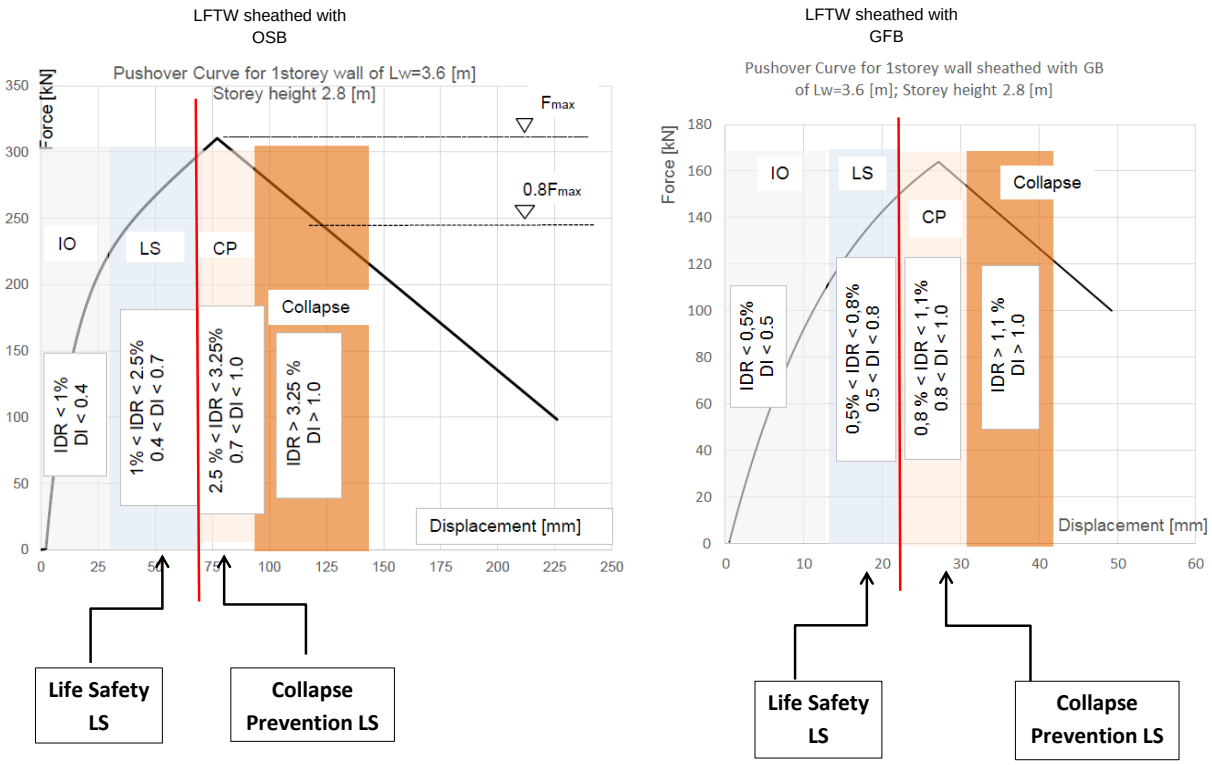

Fig. 5.33: Drifts at the LS limit state for damage index $0.25 < DI \leq 0.7$ for LFTW sheathed with OSB and $0.5 < DI \leq 0.8$ for LFTW sheathed with GFB, respectively

Comment

The acceptable range of the IDR have been proposed for different hazard levels separately for LFTWs sheathed with OSB and GFB. Since the IDR for LFTWs sheathed with GFB does not exceed the value of 0.8% for the life safety limit state, which corresponds to a displacement of approximately 24.0$[mm]$ for the standard storey height of 3.0$[m]$. LFTWs sheathed with OSB can perform displacements of up to $IDR = 2.0 - 2.5\%$ for the same hazard level. Here, the displacement amounts between 60 to 75$[mm]$. It is obvious that the non-structural elements must be capable of performing this deformation without failure. It means that partition walls, ventilation cables, installation pipes and building equipment should be designed and constructed in such a way to be able to sustain the displacements imposed by a design earthquake. Particular attention must be paid to the fastening of the facade construction to the load-bearing structure.

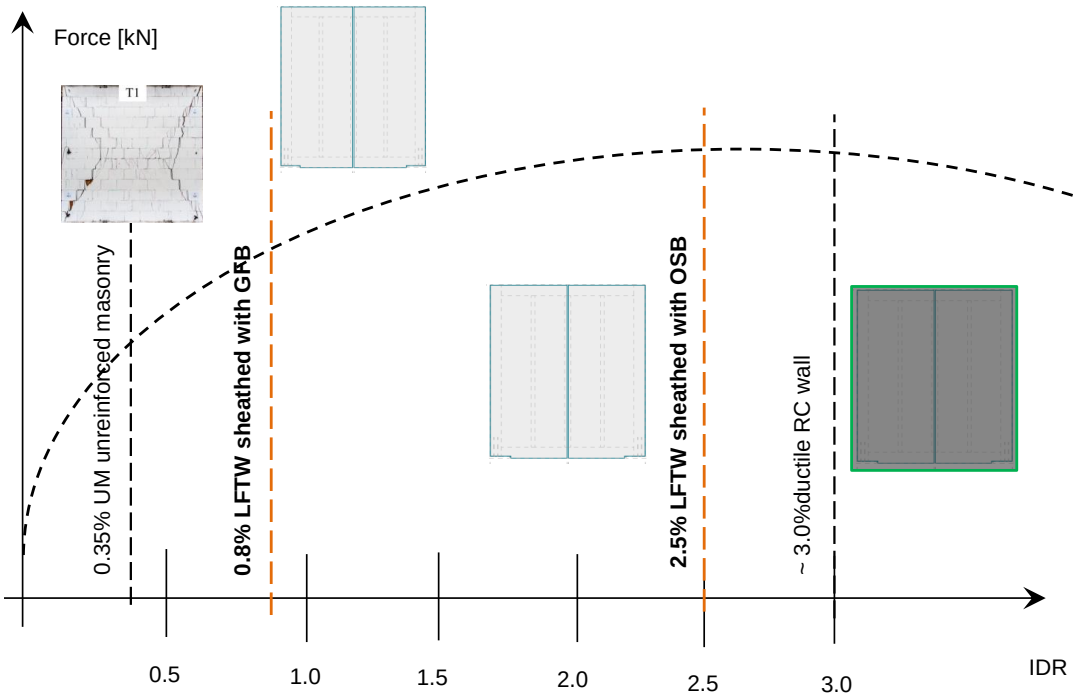

Fig. 5.34: The upper drift limits at LS limit state for materials: unreinforced masonry, LFTW sheathed with GFB, LFTW shethed with OSB and ductile RC walls, with corresponding damage index of $0.25 < DI < 0.7$.

Immediate occupancy limit state

The immediate occupancy limit state is linked with serviceability of the structure. This means that frequent earthquakes cause negligible damage. Thus, only slight damages occurs at this performance level related to an $IDR < 1.0\%$ and $IDR < 0.5\%$ for LFTWs sheathed with OSB and GFB, respectively. The corresponding DI are $DI < 0.4$ and $DI < 0.5$ for LFTWs sheathed with OSB and GFB, respectively.

The proposal for nomenclature in terms of PBE with respect to the design level and seismic hazard definition as well as for inter-storey drift limits and damage indexes are summarized in Tables 5.7 and 5.8 for LFTWs sheathed with OSB and GFB, respectively.

Tab. 5.7: Performance expectations and drift limits for LFTW sheathed with OSB

Design level	EC8 nomenclature	Seismic hazard PoE	Return Period	Performance expectations		
				Inter-storey Drift Limit	Non-exceedance Probabaility	Damage Index
IO	Damage control	50% in 50Y	72Y	1%	50%	
	Description	The structure is slightly damaged. The structural elements preserve their strength and stiffness. Damages are reparable in an economic way.				≤ 0.4
LS	Life safety	10% in 50Y	475Y	$(1.0 - 2.5)$%	50%	
	Description	The structure is moderately to significantly damaged. Moderate permanent drifts are present. Damages are likely to be reparable.				$0.4 < DI \leq 0.7$
CP	Collapse prevention	2% in 50Y	2475Y	$(2.5 - 3.25)$%	50%	
	Description	The structure is heavily damaged. Large permanent drifts are present. Damages are likely irreparable. The structure could probably not survive another earthquake, even of a moderate intensity.				$0.7 < DI \leq 1.0$

IO - Immediate Occupancy
LF - Life Safety
CP - Collapse Prevention
PoE - Probability of Exceedance

Tab. 5.8: Performance Expectations Proposal for Light Frame Shear Timber Walls Sheathed with GFB

Design level	EC8 nomenclature	Seismic hazard PoE	Return Period	Performance Expectations		
				Inter-storey Drift Limit	Non-exceedance Probabaility	Damage Index
IO	Damage control	50% in 50Y	72Y	$< 0.5\%$	50%	
	Description	The structure is lightly damaged. The structural elements preserve their strength and stiffness. The damages are reparable in an economic way.				≤ 0.5
LS	Life safety	10% in 50Y	475Y	$(0.5 - 0.8)\%$	50%	
	Description	The structure is moderate to significantly damaged. Moderate permanent drifts are present. The damages are likely to be reparable.				$0.5 < DI \leq 0.8$
CP	Collapse prevention	2% in 50Y	2475Y	$(0.8 - 1.1)\%$	50%	
	Description	The structure is heavily damaged. Large permanent drifts are present. The damages are likely not to be reparable. The structure could probably not survive an another earthquake, even of moderate intensity.				$0.8 < DI \leq 1.0$

IO - Immediate Occupancy
LF - Life Safety
CP - Collapse Prevention
PoE - Probability of Exceedance

5.7 Conclusions

The damage index as the performance indicator for LFTWs has been introduced for different limit states. The DI is separately derived for LFTWs sheathed with OSB and GFB. The DIs for LFTWs sheathed with GFB have been compared to the damage rates observed during the testing at the Empa laboratory. It has been shown that the analytically estimated DI and the DI resulting from physical testing correlate very well for both LFTWs sheathed with GFB and OSB. Finally, the performance objectives in accordance with the limit states considered have

been established. Additionally, the IDA methodology has been introduced. It has been shown that the intensity measure, given the damage measure, can be used as a consistent control procedure to validate the results obtained using NLTHA.

Chapter 6

Fundamentals of the Parameter Study

In this chapter, the main assumptions on which the whole parameter study is based, are discussed using a prototype building. The limitations of the key parameters considered are assessed. The decision not to consider gravity loads in the seismic analysis is justified. The limiting vibration period is set to give the minimum required stiffness in order to satisfy serviceability requirements arising from wind loads. The influence of HD and inter-storey connection devices on the overall behaviour of LFTWs subjected to the seismic loading is examined. The geometry of LFTWs as well as the detailing of HD and inter-storey connection devices is presented. The mass corresponding to the typical ceiling configuration is estimated, giving a practically relevant range of the mass estimated by the parameter study. Finally, the algorithms for deriving results within the parameter study are assessed and the validation procedure using IDA is presented.

6.1 Introduction

The objective of this thesis is to estimate the range of applicability of LFTWs in regions of low to moderate seismicity. In order to perform this feasibility estimation, an advanced mechanical model, which takes into account the nonlinear force-displacement relationship, the stiffness and the strength degradation as well as the pinching effects under reversed cyclic loading, has been developed for the most commonly used wall configurations in Switzerland (presented in Chapter 3). The chosen wall configurations have been adopted in accordance with the current Swiss practice, which is similar to the practice in many other European countries. The feasibility estimation has been based on a parameter study, which focuses on estimation of the maximum range of applicability of the LFTW structure by satisfying all the limiting requirements given by the performance-based engineering (PBE) approach, described in Chapter 5. Analysis has been conducted as NLTHA.

In a conventional design process, the seismic demand is estimated first. In the next step, the structure is designed to meet the design requirements. In this thesis, the problem has been approached from the other direction. The structure, with all its corresponding mechanical char-

acteristics, has been regarded as given. The range of applicability of the given structure has been the topic of investigation. The advanced mechanical model used for the analysis was activated and exploited all the hidden load-bearing resources in the structure.
Among the vast amount of parameters, which could be varied with respect to both the structural configuration of the shear wall element and the seismic demand, an attempt has been made to determine which parameters should be kept constant throughout all the analysis in order to make the analysis feasible and representative. The motivation in performing the parameter study has been to show how efficient the LFTW is as a lateral load resisting system. The outcome of the estimation of the applicability range of LFTWs should encourage practitioners to use timber structures beyond the currently used range.

6.2 Prototype building

In order to justify the decisions relating to the limiting parameter quantities used in this thesis, a 5-storey prototype building is considered. The building is of the same type as the building introduced in Chapter 1 and analyzed in Chapter 9 (see also [6]), with some modifications introduced in order to discuss the parameter choices. The structure is symmetric. The walls are 4.2 m long and arranged so that walls W1 are carrying the gravity loads and simultaneously acting as part of the lateral load resisting system. The walls W2 are also part of the lateral load resisting system, but they do not carry any vertical loads. The geometry of the prototype building is presented in Figure 6.1. The slab is a hybrid type structure often used in Switzerland, consisting of a timber pile and a concrete layer.

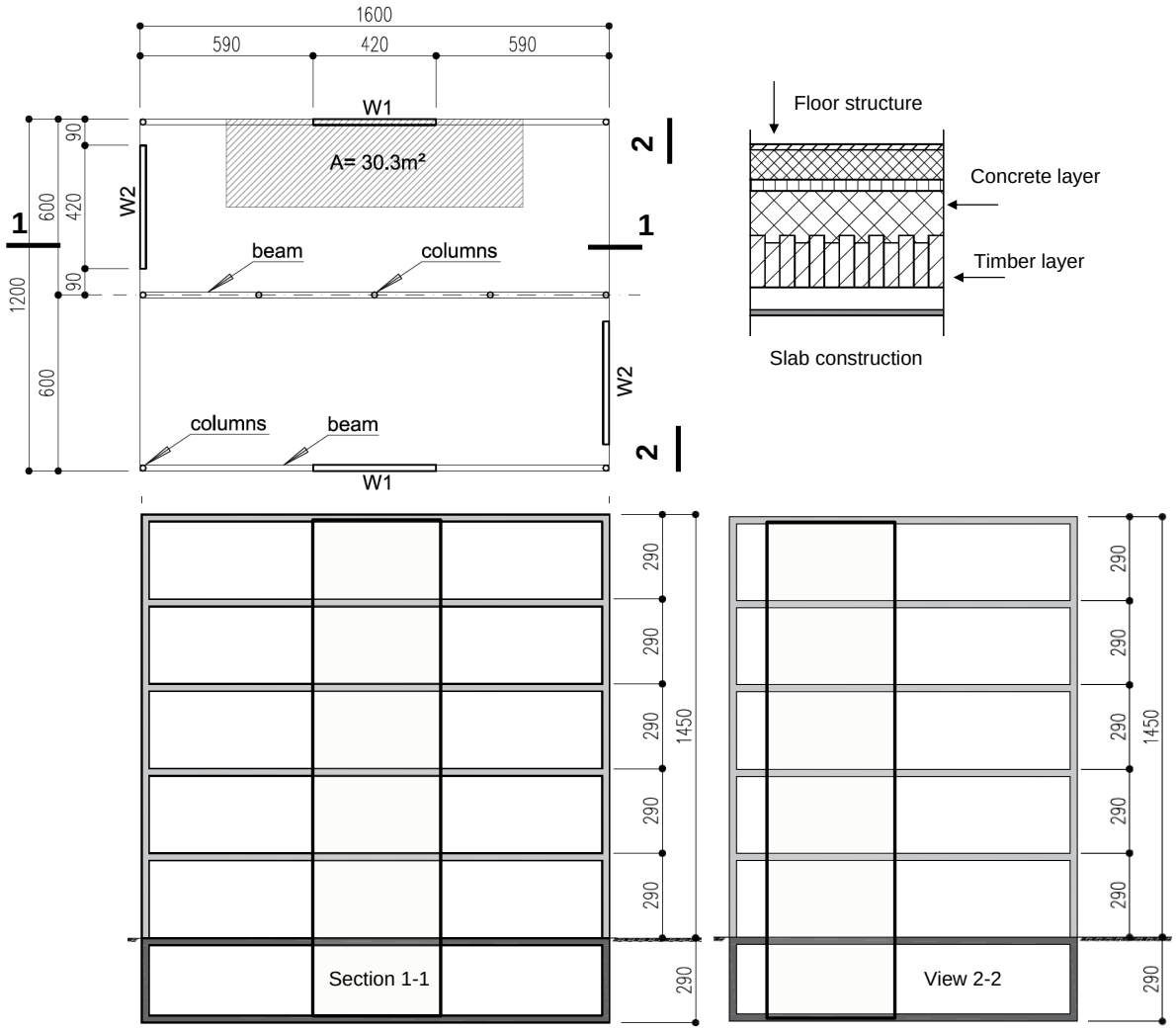

Fig. 6.1: LFTW with a length of 4200 [mm]

The tributary area for the estimation of the gravity loads is: $(4.2 + 5.9) \cdot 3 = 30.3[m^2]$. According to [6], the dead load of the slab is 5.83 $[kN/m^2]$, the live load is 2.0 $[kN/m^2]$, and the internal walls have been taken into account with 0.5 $[kN/m^2]$ distributed over the entire flat surface. The bearing walls have a weight of 1.05 $[kN/m^2]$.

$$\begin{aligned} N_{storey} = (g + g_{w0}) \cdot (4.2 + 5.9) \cdot 3 = (5.83 + 0.5) \cdot 30.3 = 191.80[kN] \\ (\psi \cdot p) \cdot (4.2 + 5.9) \cdot 3 = 0.3 \cdot 2.0 \cdot 30.3 = 18.18[kN] \\ g_w \cdot l_w \cdot h_w = 1.05 \cdot 4.2 \cdot 2.9 = 12.8[kN] \\ = 223[kN] \end{aligned} \tag{6.1}$$

$$\begin{aligned} N_{roof} = N_{storey} - [g_{w0} \cdot 30.3 \cdot 0.5 + g_w \cdot 4.2 \cdot 2.9 \cdot 0.5] \\ = 210[kN] \end{aligned} \tag{6.2}$$

The force on the top of the building, due to the missing walls in the last storey, is estimated to be 210$[kN]$:

6.2.1 Behaviour of the wall subjected to the gravity loads

In the Figure 6.1, the structure presented has a storey mass of 150$[t]$, which is the quantity also estimated in [6]. Since the structure is symmetrical, the storey mass which is sustained by one single wall is 75$[t/storey]$. The earthquake force, which is equal to the bearing capacity of the wall W1, has been distributed over the structure according to the first vibration mode, producing shear forces in each storey as presented in Figure 6.2.

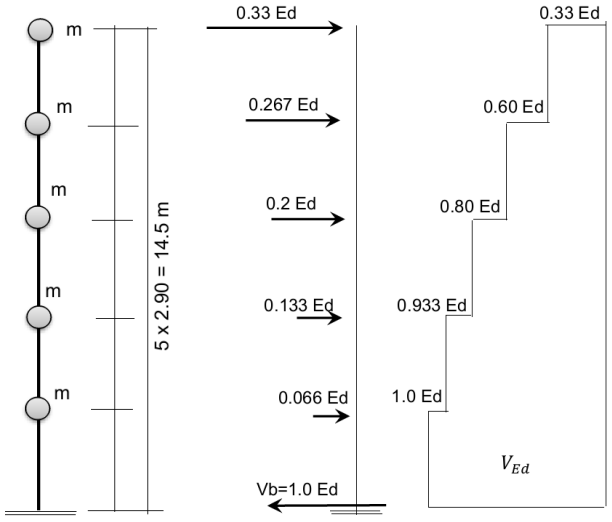

Fig. 6.2: Earthquake force distribution along the height of the structure

The pushover curve of a single-storey shear wall used in the five-storey building, is presented in Figure 6.3.

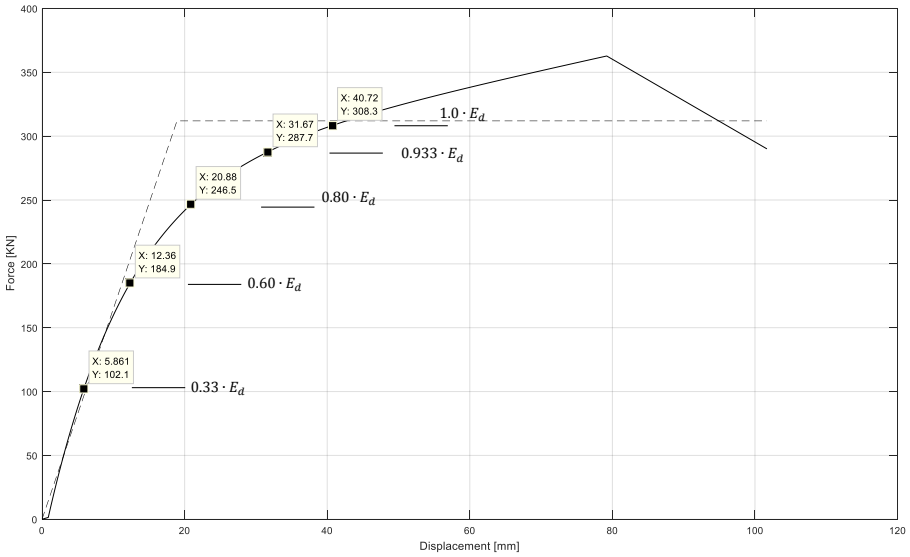

Fig. 6.3: Displacements of the single storey, 4.2 [m] long wall at different load levels

By introducing the displacements in each storey caused by the corresponding earthquake forces and the vertical loads acting on the corresponding levels, the structure experiences additional bending due to the eccentricity imposed by the lateral loads. The additional bending moments are given in Figure 6.4.

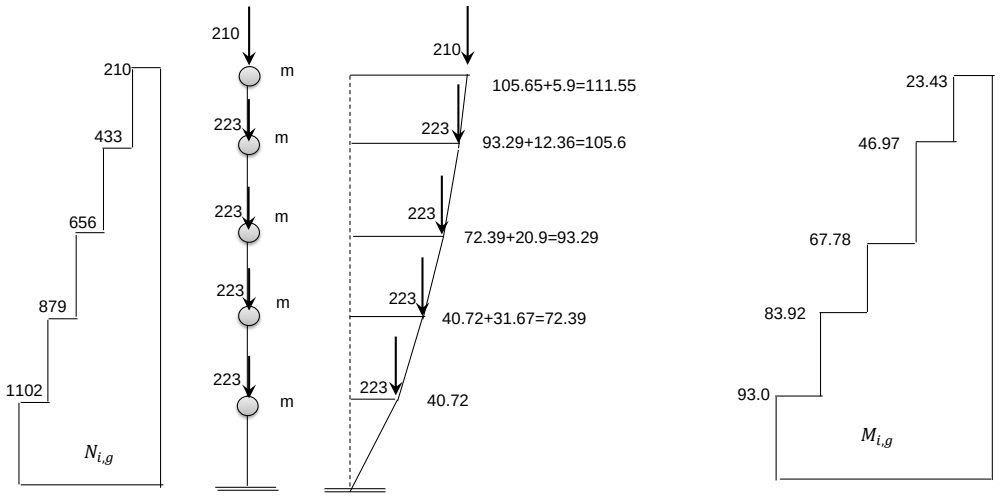

Fig. 6.4: Additional bending moments due to the eccentricity of the gravity loads

The bearing capacity of the 4.2 [m] LFTW sheathed with OSB panels is 308.3 [kN], as presented in Figure 6.5.

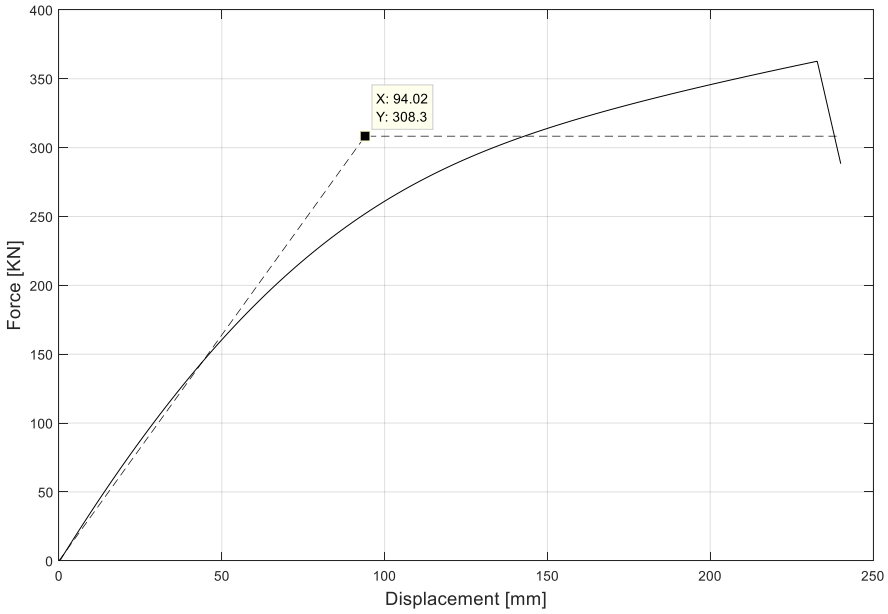

Fig. 6.5: Pushover curve of a five-storey wall element with length 4.2[m]

Finally, considering the normal forces in the wall, the total bending moments and resulting forces in the hold-down devices are presented in Figure 6.6.

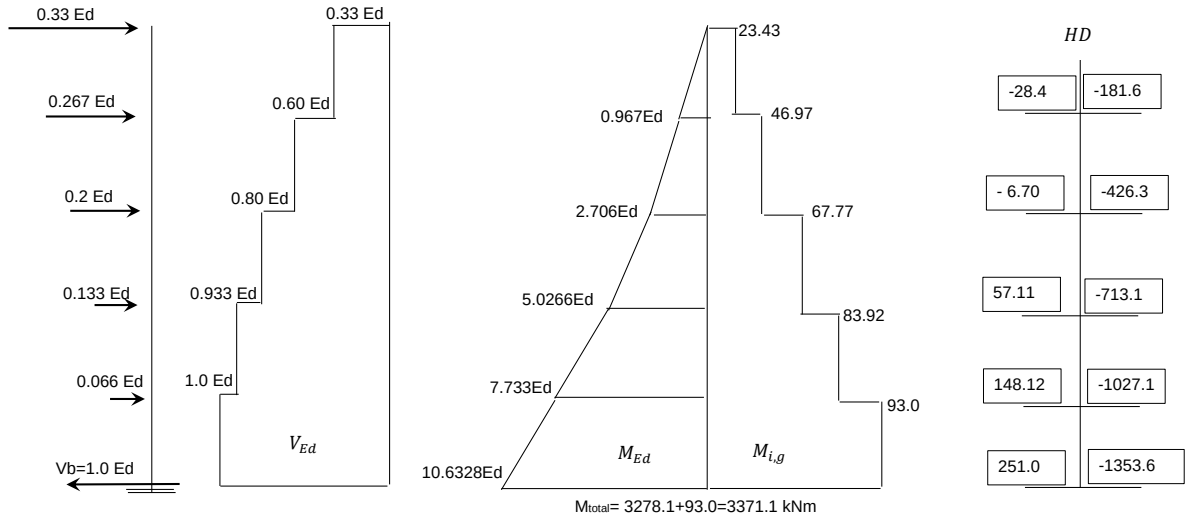

Fig. 6.6: Total bending moments in the wall W1 and resulting forces in HD-devices

For comparison, the HD forces for Wall W2, which does not carry any gravity loads but has to sustain the same lateral loads are: $3278.1/4.2 = 780[kN]$. The tension forces estimated for Wall W1 are 251 = approximately 32% of $780[kN]$. (Note that the HD forces estimated by means of NLTHA are on the order of magnitude of $657.5[kN]$ or $\approx 84.3\%$ of $780.0[kN]$ for a max base shear force of $280.2[kN]$ or $\approx 90\%$ of $308.3[kN]$. The roof displacement according to the NLTHA is $116.5[mm]$ or $\approx 104\%$ of $111.6[mm]$, estimated in Figure 6.4).

6.2.2 Impact of the vertical load to the hysteretic response of LFTW to the lateral monotonic and cyclic loading

In the previous section, it has been outlined that the gravity load stabilizes the LFTWs if subjected to the lateral loading. Hence, for the seismic analysis of the LFTW in a building assembly the contribution of the gravity load should be neglected. Since the mechanical model of LFTWs presented in section 3.3 and 3.5 have been derived without impact of the gravity load, the question arose whether the same mechanical model of the shear spring can also be used to model a LFTW subjected to the vertical load. If this is the case, the mechanical model of the LFTWs evaluated in Chapter 3 can be used for both LFTWs carrying and LFTWs not carrying vertical gravity loads. In order to compare the hysteresis of the LFTWs, three vertical load levels have been applied to the LFTW with the length of $3.6[m]$, namely: $q = 5.0$, 50.0 and 100.0 $[kN/m]$, respectively. The analyses have been performed in MCASHEW. The wall element is sheathed on one side with an OSB panel with $t = 15[mm]$. Nails are used as fasteners, with $d = 2.87[mm]$ spaced in $30[mm]$. Figures 6.7(a), 6.7(b), 6.8(a), 6.8(b), 6.9(a) and 6.9(b) each show the monotonic response of the structure with the maximum displacement and maximum force being highlighted, as well as the hysteretic response of the wall with the corresponding hysteretic parameters generated within the MCASHEW program.

As one can see, the parameters which define the response of the LFTW to the monotonic and cyclic loading are within the same range, only differing by some percent. It seems to be plausible, since the vertical loads are carried by the frame columns, without affecting the sheathing panels and fasteners, which are responsible for transfering the horizontal loads to the basement. It has been shown that the same mechanical model of LFTWs under lateral earthquake loading can be used for LFTWs subjected and those which are not subjected to the vertical gravity loads.

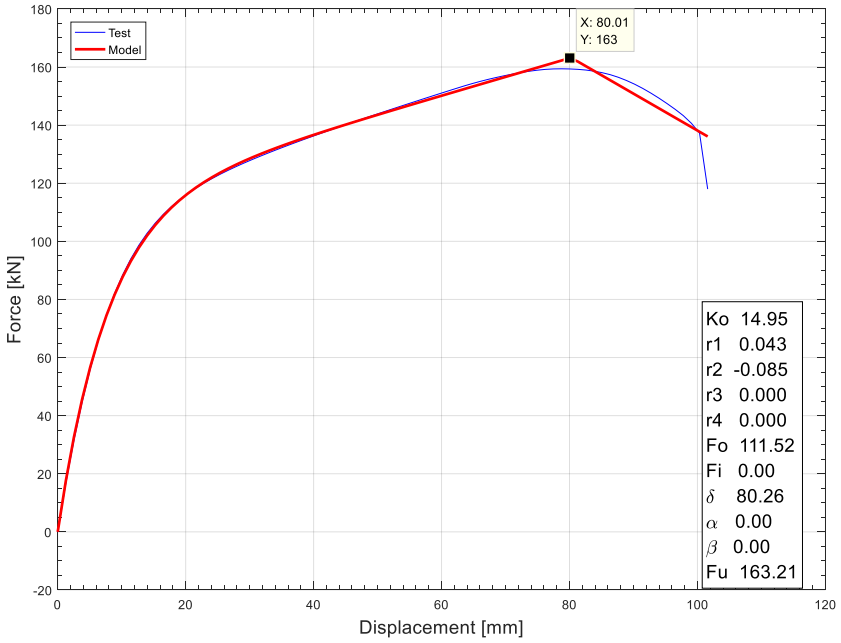

(a)

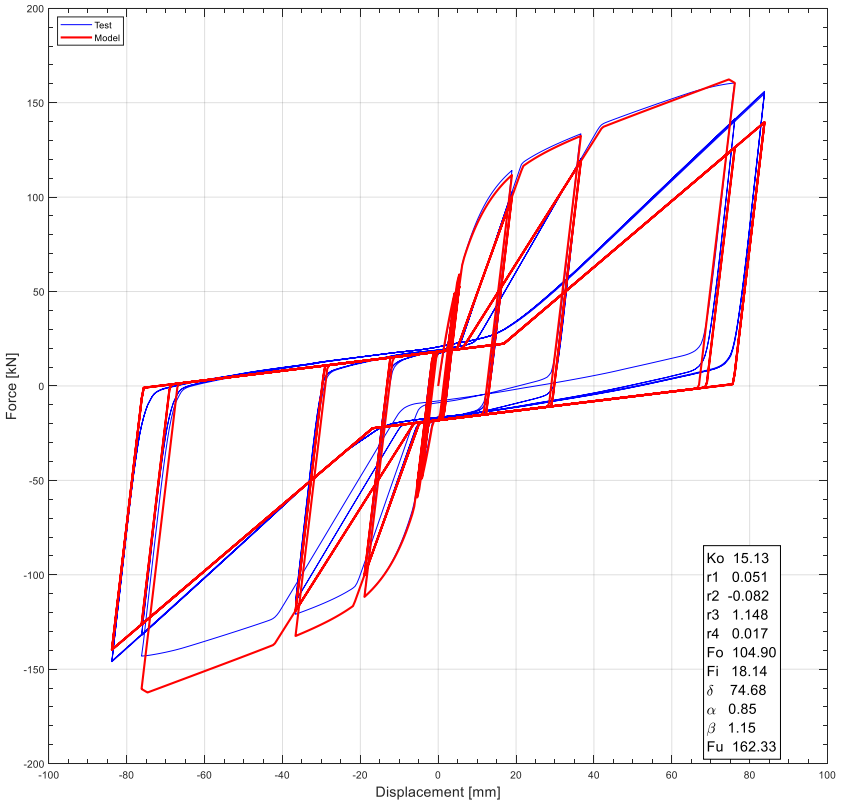

(b)

Fig. 6.7: Monotonic response of the structure subjected by 5.0$[kN/m]$ gravity load, 6.7(a): Hysteretic response of the structure subjected by 5.0$[kN/m]$ gravity load, 6.7(b)

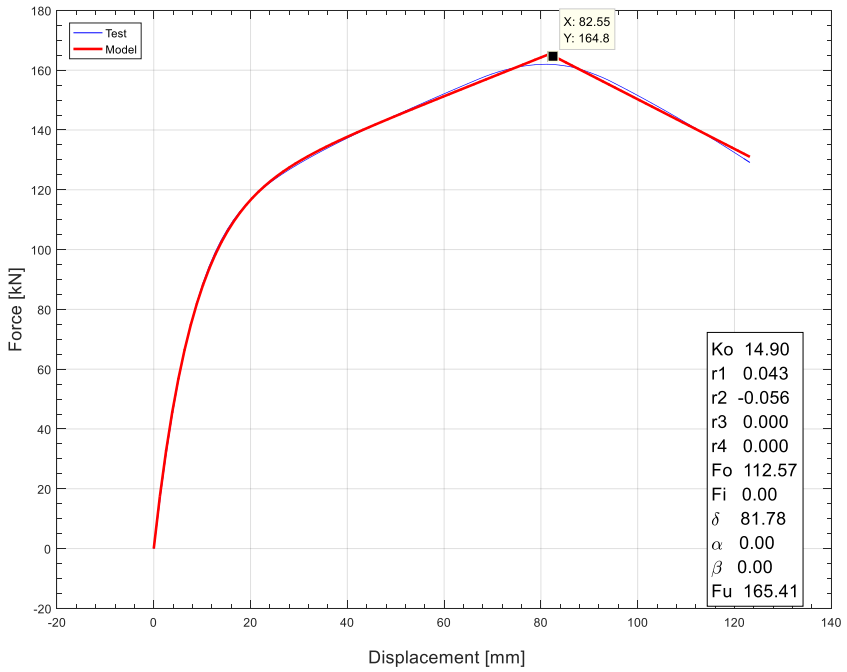

(a)

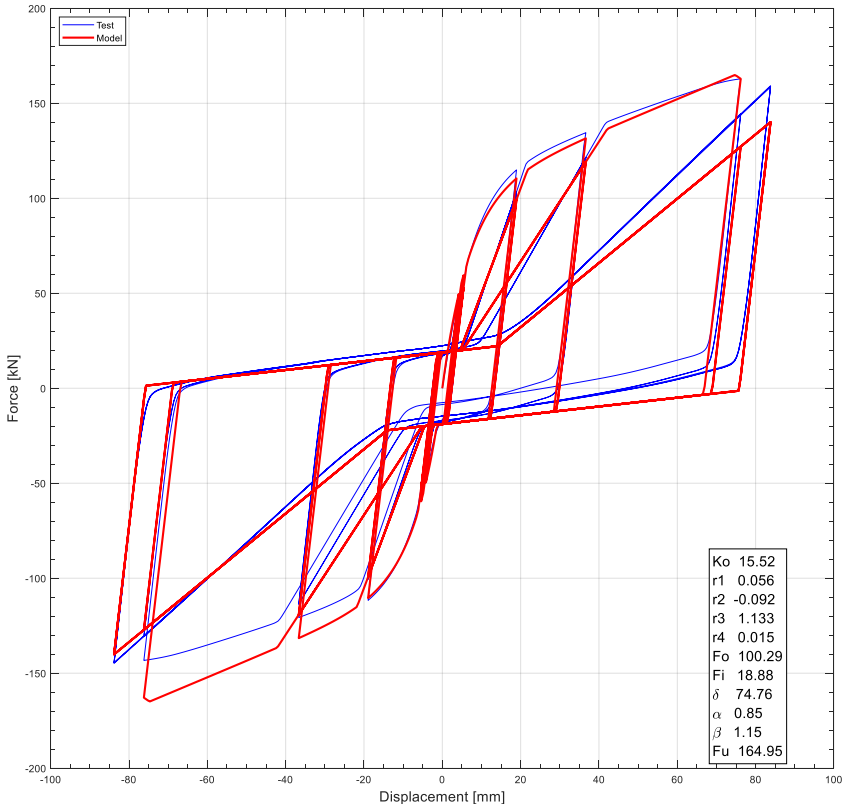

(b)

Fig. 6.8: Monotonic response of the structure subjected by 50.0$[kN/m]$ gravity load, 6.8(a): Hysteretic response of the structure subjected by 50.0$[kN/m]$ gravity load, 6.8(b)

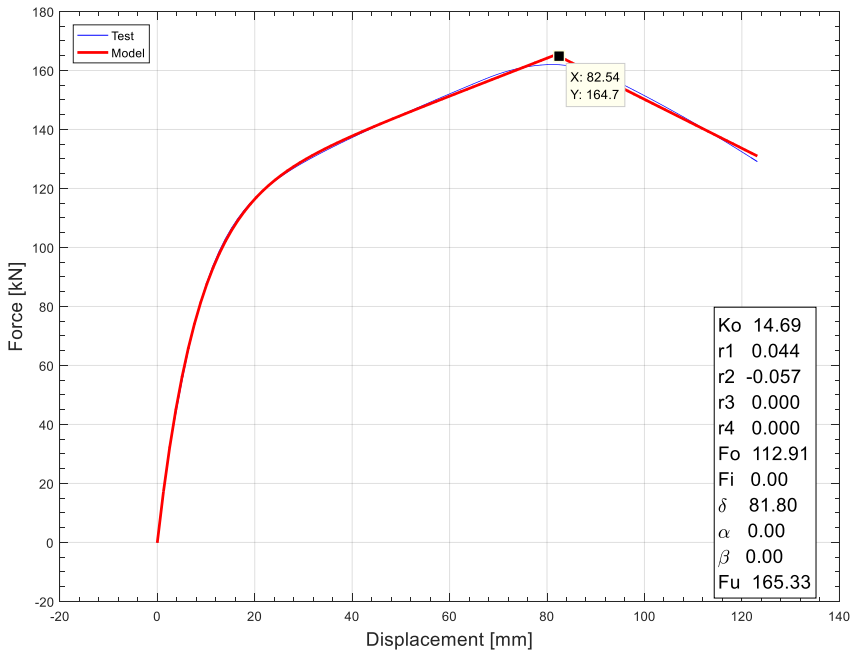

(a)

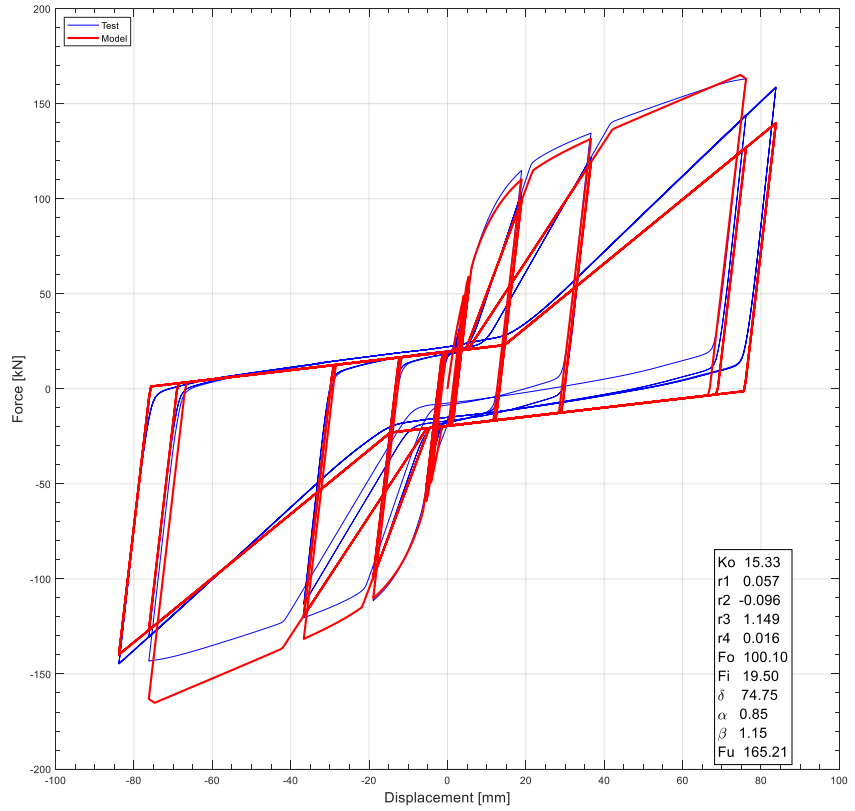

(b)

Fig. 6.9: Monotonic response of the structure subjected by 100.0$[kN/m]$ gravity load, 6.9(a): Hysteretic response of the structure subjected by 100.0$[kN/m]$ gravity load, 6.9(b)

P-Δ effects - conclusion

Although the wall elements analyzed within this thesis can sustain both gravity and lateral loads, the walls which do not bear vertical loads, but have to sustain the same lateral loads, are more vulnerable. The decrease of vulnerability can be related to the stabilizing effects of the vertical loads. Although, the geometrical non-linearity contribute to an increase of the overturning moment, the contribution of the vertical load to the overall stability is predominant. A similar observation has also been made also during testing (see for example [87]).

Therefore, the wall elements considered within this thesis have been analyzed without the beneficial influence of the vertical loads.

The parameters selected for the parameter study are summarized in Table 6.6. In the subsequent sections, the analysis process and the corresponding model parameters are described in more detail.

6.2.3 Period of vibration as limit criteria

Sensitivity to wind loads

In the seismic design of the structures, the period is not limited. If one would keep the mass and the stiffness of the structure constant, the fundamental period of vibration would increase with increasing building height. Tall buildings have a fundamental period of several seconds. Since the periods of vibration is directly related to the stiffness of the structure, overly flexible structures could experience undesired displacements even under service wind loads. To investigate how the stiffness of the structure affects the behaviour of the structure under service wind loads, the structure presented in Figure 6.1 is considered. In order to achieve an increase of vibration period while keeping the height and the stiffness of the structure constant, the mass of the structure must change. The change of the mass is achieved by "stretching" or "shortening " the building width which simultaneously changes the surface area of the facade exposed to the wind loads. The masses of the structure are chosen to achieve periods of vibration of 1.5, 1.7 and 1.9$[s]$. The masses of the structure corresponding to $T^* = 1.5$, 1.7 and 1.9 $[s]$ are 62.5, 80, and 100 $[t/storey]$, respectively. The floor mass is estimated to be 150$[t/storey]$ for floor dimensions of 12 by 16 $[m]$. The depth and the height of the building is kept constant as 12$[m]$ and 14.5$[m]$, respectively. In order to change the storey mass, only the width of the structure may change. The corresponding change of the facade surface can be estimated as follows:

$$l_{new} = \frac{m_{new}}{75} \cdot 8; for$$

$$m = 62.5[t/storey]; \rightarrow l_{new} = 6.667[m]; \rightarrow A_{fac} = 6.667 \cdot 14.5 = 96.67[m^2]$$

$$m = 80.0[t/storey]; \rightarrow l_{new} = 8.533[m]; \rightarrow A_{fac} = 8.533 \cdot 14.5 = 123.73[m^2]$$

$$m = 100.0[t/storey]; \rightarrow l_{new} = 10.667[m]; \rightarrow A_{fac} = 6.667 \cdot 14.5 = 154.67[m^2]$$

The wind load estimation follows the procedure given in SIA 261. According to section 6.2, the wind pressure is a function of the height and shape of the building, surface levelness and placement of the building in the landscape. Due to the large number of parameters which could vary significantly, a reference wind pressure of $1.0[kN/m^2]$ has been adopted for the analyses in this section. Note that this value is often the outcome of the "real" wind load analysis. Hence, the wind loads can now be estimated in accordance with the change of the facade surface area caused by the change of the storey mass as follows:

$$m = 62.5[t/storey]; \rightarrow F_{wind} = 97[kN]; \rightarrow F_{wind} = 19.4[kN/storey]$$
$$m = 80.0[t/storey]; \rightarrow F_{wind} = 124[kN]; \rightarrow F_{wind} = 24.8[kN/storey]$$
$$m = 100.0[t/storey]; \rightarrow F_{wind} = 155[kN]; \rightarrow F_{wind} = 31.0[kN/storey]$$

For simplicity, the wind loads are assumed to be equally distributed along the height of the structure. Their distribution, as well as the corresponding displacements, are summed over the height of the structure as shown in Figure 6.10. The values for the displacements corresponding to each wind load intensity have been obtained from a corresponding pushover curve of a one-storey structure. See Tables 6.1, 6.2, 6.3, which provides similar information as presented in Figure 6.4.

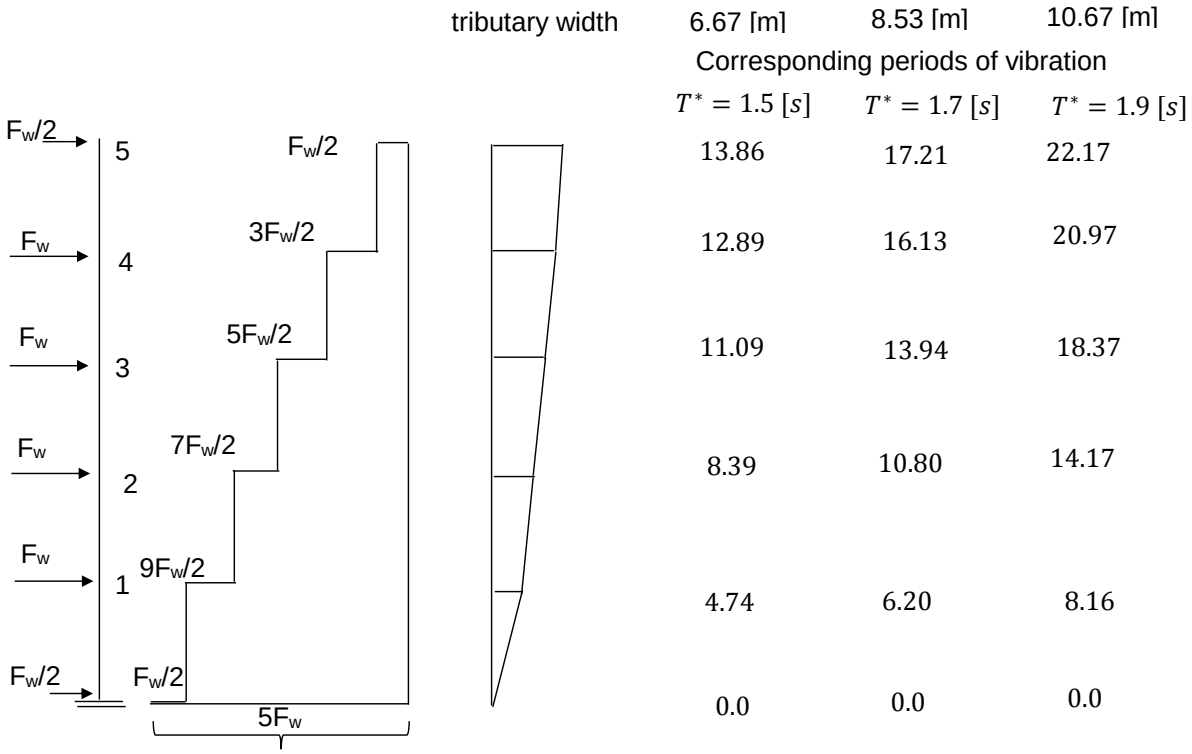

Fig. 6.10: Service wind load distributed along the height of the structure with corresponding displacements for three different tributary widths

In Tables 6.1, 6.2, 6.3, the relative and absolute displacements due to the different wind load levels and the corresponding earthquake excitation have been presented. The wind loads correspond to the service level and thus the serviceability requirements should be satisfied. According to code provisions [75], the admissible deflection of each storey is defined as $h_{st}/500$ for buildings with brittle nonstructural elements and/or sensitive equipment in the building. For buildings with standard requirements, the allowable horizontal deflection is $h_{st}/300$. The displacements due to the earthquake excitation are not quantified, except if the building is of high importance. As seen from the analyzes presented in Tables 6.1, 6.2 and 6.3, the inter-storey drift in the first storey for a structure with a period of vibration $T^* = 1.5[s]$ is $h_{st}/611$. The service wind loads would produce deflection of 4.74 [mm], which seems to be too conservative, if set as limiting condition. The wind loads produce an IDR of 6.2 [mm], which is equal to $h_{st}/467$, for the structure with a period of vibration of $T^* = 1.7[s]$. Thus, the requirement postulated in [75] as $h_{st}/500$, would be slightly violated, but the requirement of $h_{st}/300$ would be easily satisfied. Finally, the service wind loads would produce a storey deflection of $8.16[mm]$ or an IDR of $h_{st}/355$ on the structure with a period of vibration of $T^* = 1.9[s]$. Thus, the stricter requirement for an IDR of $h_{st}/500$, prescribed in [75], is clearly not satisfied, whereas that of $h_{st}/300$ is satisfied.

Tab. 6.1: Displacement due to the wind load corresponding to the mass of $62.5[t/storey]$; $T^* = 1.5[s]$, F_{wind}=19.4 [kN/storey], $\sum F_{w,1st} = 87.3[kN]$

	Displacement due to wind load			Displacement due to EQ load		
Storey	relative	IDR	absolute	relative	IDR	absolute
	[mm]		[mm]	[mm]		[mm]
5th	0.97	$h_{st}/2990$	13.86	13.53	$h_{st}/214$	103.8
4th	1.80	$h_{st}/1610$	12.89	17.64	$h_{st}/164$	90.27
3th	2.70	$h_{st}/1074$	11.09	21.05	$h_{st}/138$	72.63
2nd	3.65	$h_{st}/795$	8.39	21.27	$h_{st}/136$	51.58
1st	4.74	$h_{st}/611$	4.74	30.01	$h_{st}/97$	30.01

Tab. 6.2: Displacement due to the wind load corresponding to the mass of $80.0[t/storey]$; $T^* = 1.7[s]$, F_{wind}=24.8 [kN/storey], $\sum F_{w,1st} = 111.33[kN]$

	Displacement due to wind load			Displacement due to EQ load		
Storey	relative	IDR	absolute	relative	IDR	absolute
	[mm]		[mm]	[mm]		[mm]
5th	1.08	$h_{st}/2685$	17.21	14.80	$h_{st}/195$	115.7
4th	2.19	$h_{st}/1324$	16.13	18.36	$h_{st}/158$	100.9
3th	3.14	$h_{st}/924$	13.94	23.01	$h_{st}/126$	82.54
2nd	4.60	$h_{st}/630$	10.80	25.02	$h_{st}/116$	59.43
1st	6.20	$h_{st}/467$	6.20	34.41	$h_{st}/84$	34.41

Tab. 6.3: Displacement due to the wind load corresponding to the mass of 100.0$[t/storey]$; $T^* = 1.9[s]$, F_{wind}=31.0 [kN/storey], $\sum F_{w,1st} = 139.17[kN]$

	Displacement due to wind load			Displacement due to EQ load		
Storey	relative	IDR	absolute	relative	IDR	absolute
	[mm]		[mm]	[mm]		[mm]
5th	1.20	$h_{st}/2417$	22.17	18.8	$h_{st}/154$	136.2
4th	2.6	$h_{st}/1115$	20.97	24.43	$h_{st}/119$	117.4
3th	4.2	$h_{st}/690$	18.37	26.32	$h_{st}/110$	92.97
2nd	6.01	$h_{st}/483$	14.17	28.04	$h_{st}/103$	66.65
1st	8.16	$h_{st}/355$	8.16	38.61	$h_{st}/75$	38.61

After examining the sensitivity of the structure to service wind loads in this section, there are not sacrosanct evidence for the choice of the period limits. Judging by the applicability to structures with brittle nonstructural elements, the criterion for an IDR of $h_{st}/500$ seems to be better satisfied if the combination of the storey mass and stiffness of the structure result in a period of vibration equal to 1.7$[s]$. This value has been chosen as the limiting vibration period for all structures in the following parameter study. The differences in the response of the structure can be presented graphically by means of a YPS. Since the YPS-presentation uses only the inelastic stiffness presented by T^*, the displacements caused by the wind loads are applied on the capacity curve related to the inelastic system. However, the service wind loads act on the system that behaves predominantly elastically. Thus, the displacements obtained from the YPS-inelastic system are overestimated by approximately a factor of two (see Figure 6.11) when compared with more realistic quantities, estimated from an effective pushover curve, i.e. a system with a "real" stiffness, given in Tables 6.1, 6.2 and 6.3.

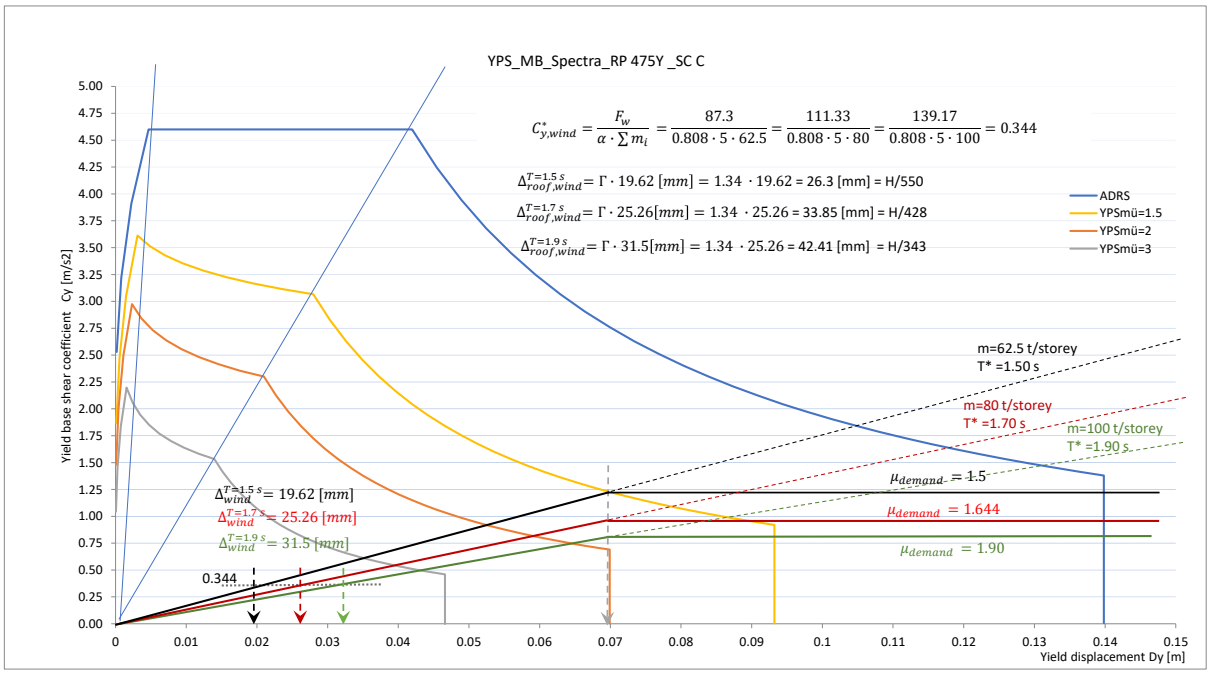

Fig. 6.11: Presentation of all three models with mass $62.5, 80$ and $100[t/storey]$ in the YPS, including wind action with related displacements on inelastic structure

The previous discussion is based on a wall length of $4.2[m]$. Since the structural sensitivity to the corresponding equivalent wind load is not intuitively known, an analysis has been performed in the same way for all wall lengths. The height and depth of the prototype building have been kept constant, resulting in different facade surfaces exposed to the wind. The distributed loads i.e. floor mass per m^2 are assumed to be $700kg/m^2$. In this way, the corresponding width of the facade has been estimated as follows: $m/(12 \cdot 0.7)$, resulting in a total wind force as follows: $m/[(12 \cdot 0.7) \cdot 14.5]$, where 12 and 14.5 are the depth and height of the prototype building, respectively (see Figure 6.1). The results are summarized in Tables 6.4 and 6.5 and Figure 6.12.

Tab. 6.4: Correlation between periods of vibration and serviceability requirements due to corresponding equivalent wind loads of prototype building, estimated for wall length 2.4 and $3.0[m]$

	Wall length 2.4 [m]			Wall length 3.0 [m]		
	$T^* = 1.5[s]$	$T^* = 1.7[s]$	$T^* = 1.9[s]$	$T^* = 1.5[s]$	$T^* = 1.7[s]$	$T^* = 1.9[s]$
mass [t/storey]	27.0	35.0	44.0	42.0	54.0	68.0
corresp. width [m]	3.20	4.16	5.24	5.00	6.42	8.10
$F_w[kN]$	46.50	60.32	76.00	72.50	93.20	117.30
$F_w/storey[kN]$	9.30	12.06	13.68	14.50	18.64	23.47
$\frac{9 \cdot F_w}{2}$	41.85	54.28	68.4	65.24	84.0	105.6
Displacement [mm]	4.20	5.63	7.54	4.32	5.84	7.98
IDR	$h_st/690$	$h_st/515$	$h_st/385$	$h_st/670$	$h_st/496$	$h_st/363$

Tab. 6.5: Correlation between periods of vibration and serviceability requirements due to corresponding equivalent wind loads of prototype building, estimated for wall length 3.6 and 4.8$[m]$

	Wall length 3.6 [m]			Wall length 4.8 [m]		
	$T^* = 1.5[s]$	$T^* = 1.7[s]$	$T^* = 1.9[s]$	$T^* = 1.5[s]$	$T^* = 1.7[s]$	$T^* = 1.9[s]$
mass [t/storey]	47.50	60.50	76.0	69.0	87.0	110.0
corresp. width [m]	5.65	7.20	9.05	8.21	10.35	13.1
$F_w[kN]$	82.0	104.43	131.22	119.1	150.0	190.0
$F_w/storey[kN]$	16.39	20.88	26.25	23.82	30.0	38.0
$\frac{9 \cdot F_w}{2}$	73.73	93.96	118.12	107.20	135.0	171.0
Displacement [mm]	4.88	6.48	8.71	5.314	6.99	9.50
IDR	$h_st/594$	$h_st/446$	$h_st/332$	$h_st/550$	$h_st/414.5$	$h_st/305$

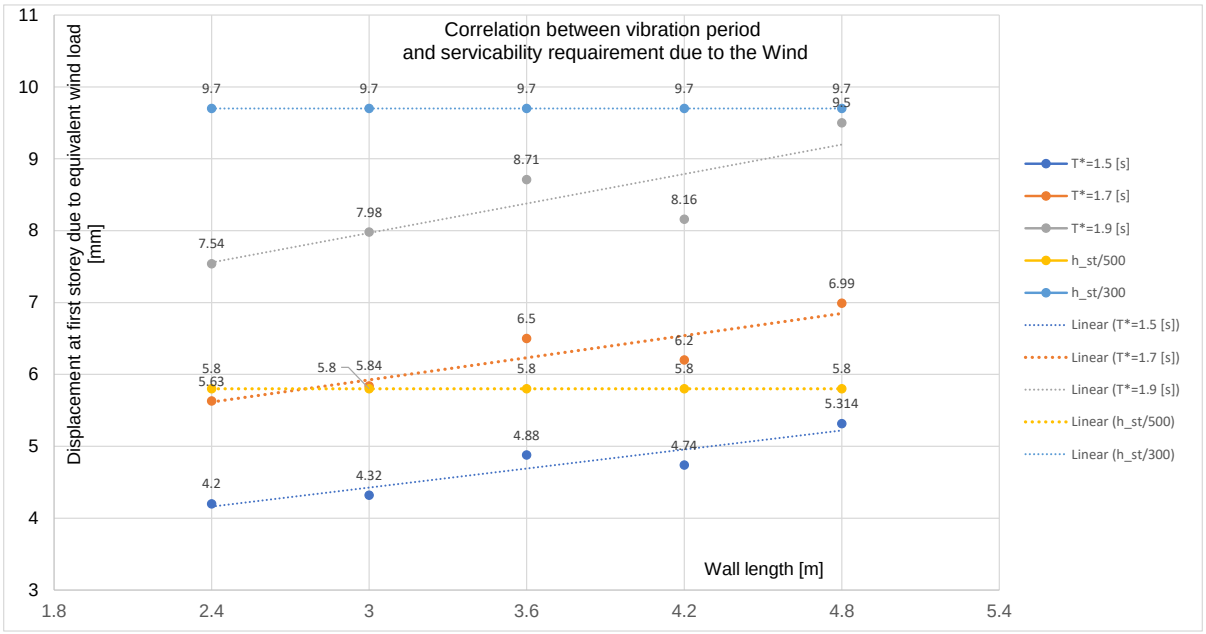

Fig. 6.12: Correlation between vibration periods and serviceability requirement due to corresponding equivalent wind loads

As one can see from Figure 6.12, the results for wall lengths of 2.4 and 3.0 [m] satisfy the serviceability requirement for $T^* = 1.7[s]$ exactly. The walls with lengths of 3.6 and 4.2[m] violate the serviceability requirement for 0.7 and 0.4 [mm], which correspond to 12, and 7%, respectively. The most significant divergence of 20% is estimated for wall with the length of 4.8 [m]. However, the structures with a period of vibration of $T^* = 1.7[s]$ satisfied the serviceability requirements sufficiently well, as stated previously.

Vibration period - conclusion

Among other results, the natural period of vibration is an important outcome of any dynamic analysis. The natural period is the first, rough indicator about how the structure will respond, if subjected to lateral loading. It is proportional to the stiffness and inversely proportional to the mass of the structure. A larger period of vibration will lead to larger displacements. The natural period of vibration for stiff and squat structures is in the low range between 0.3 and 0.5 [s], while for tall timber buildings, it is in the range of up to a number of seconds. Within this study, a middle range period has been considered. The limiting period prevents a structural response that is too "soft" and thus vulnerable to wind action. In other words, the period of vibration and thus the stiffness of the structure are searched, for which the structure exposed to the wind load still responds in the elastic range with reasonably small drifts at the first storey. Such a minimum required stiffness leads to a minimum required spectral acceleration and finally to a maximum desirable period of vibration. The natural period of vibration characteristic for mid-rise buildings, which still ensure enough stiffness to sustain the wind loads predominantly in the elastic range, satisfying serviceability condition $IDR < h_s t/500$, is shown to be approximately 1.7 [s]. In PBE, multiple performance objectives must be satisfied simultaneously, primarily the damage index and the corresponding IDR, defined in the previous chapter. For buildings in the range of 5 - 10 storeys, the period of vibration and the hold-down forces are the governing limitations within seismic analysis, rather than IDR and thus the DI. In order to meet the wind load-related serviceability condition while performing the seismic analysis, the period of vibration is limited to $T^* = 1.7[s]$.

6.2.4 Hold-down and inter-storey connection devices

The constitutive parts of the LFTW elements are HD devices and inter-storey connectors, which are used to ensure a connection with the basement and the two subsequent storeys, respectively. The design of the HD or inter-storey devices is a simple issue, if the forces, which should be captured by devices, are known. For this purpose, the diagrams in Chapter 3, Figures 3.4, 3.5 and 3.6 as well as Table 3.1 can be used. However, the HD and inter-storey devices are assumed to behave elastically and do not affect the response of the LFTW in the inelastic range. This assumption is true if the HD or inter-storey connectors are designed so that their displacements are in the range of less than 2 [mm], which is approximately the displacement range in which the devices behave elastically (see Figure 6.15). Moreover, the mechanical model developed in Chapter 3, inherently includes a part of a linear elastic HD-response. Considering the Wall W2 subjected to earthquake loads only, the force distribution along the height of the structure, the corresponding bending moments and the hold-down forces are presented in 6.13.

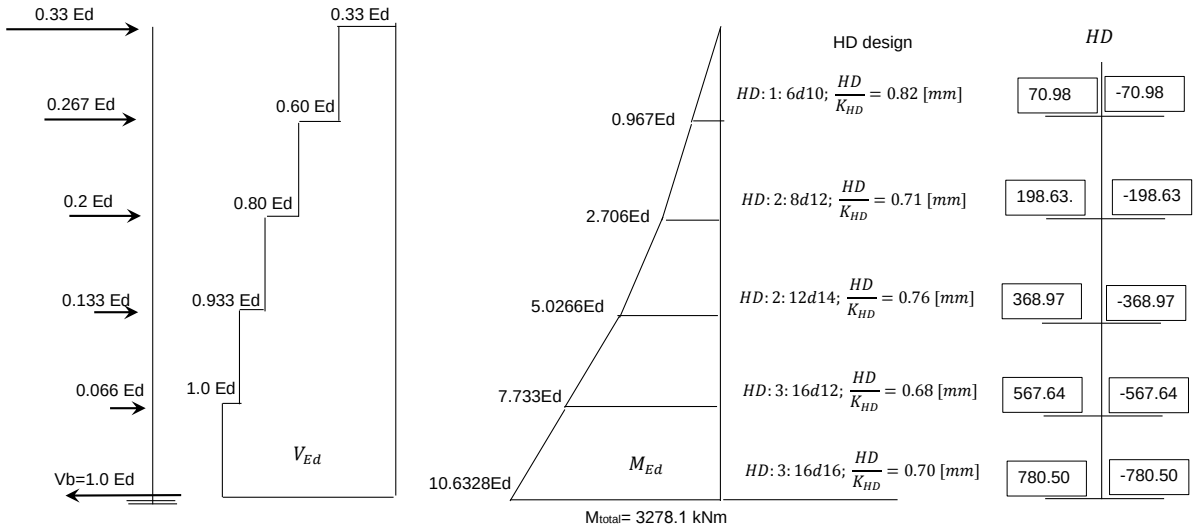

Fig. 6.13: Total bending moments in the wall W1 and resulting forces in HD-devices

In the same figure, the design of the HD-devices for the corresponding HD-forces is performed. The HD, or inter-storey connectors, chosen are labeled with the number of slotted in steel plates, the required dowel diameter and the number of dowels in the connection. The inter-storey connections have two devises, so the deformation, which arises from the connection, is multiplied by 2 at each storey. However, the displacements which arise from the HD or inter-storey connectors are less then 1 [mm]. The impact of the displacements, stemming from the HD and inter-storey connector devices, on the displacement profile of the wall can be seen in Figure 6.14.

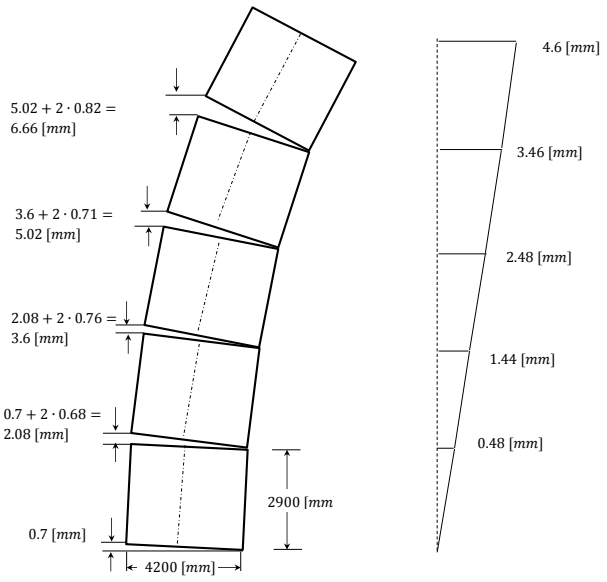

Fig. 6.14: Displacement profile arising from HD and inter-storey devices

Again, if the displacements arising from HD and inter-storey devices would be added to the earthquake displacements, one would obtain 111.55 + 4.6 = 116.15 [mm], which is an increase of approximately 4%. At the first-storey level, this increase would be 40.72+0.48 = 41.2 $[mm]$, which is an increase of approximately 1%.

There have been numerous tests carried out on bracket angle hold-downs worldwide, but there have only been few of them (see e.g. [24] and [102]), conducted on strong HD devices adopted in this work. In [102] strong hold-down devices have been investigated experimentally and numerically for timber with a density of $\rho = 450\frac{kg}{m^3}$ and a dowel diameter of d = 16 mm. In addition, the bearing capacity of the connection investigated in [102] has been estimated by using Johansen's model, also called the European Yielding Model (EYM), implemented in [17] with Equation 6.3. The test results, as well as the values of the bearing capacity estimated analytically by EYM, are summarized in Figure 6.15. Considering that a hole slip of 1 [mm] exists due to the tolerance in production practice, the experimentally estimated stiffness of the HD connection has been compared with the stiffness according to [17]. The elastic limit has been assumed to be equal to the analytically estimated bearing capacity divided by 1.35, which is also approximately the partial safety coefficient $\gamma_M = 1.3$ according to EC5.

$$F_{v,R} = min \begin{cases} f_{h,1,k} \cdot t_1 \cdot d \\ f_{h,1,k} \cdot t_1 \cdot d \cdot [\sqrt{2 + \frac{4 \cdot M_{y,R}}{f_{h,1,k} \cdot t_1^2 \cdot d}} - 1] \\ 2.3 \cdot \sqrt{f_{h,1,k} \cdot M_{y,R} \cdot d} \end{cases} \tag{6.3}$$

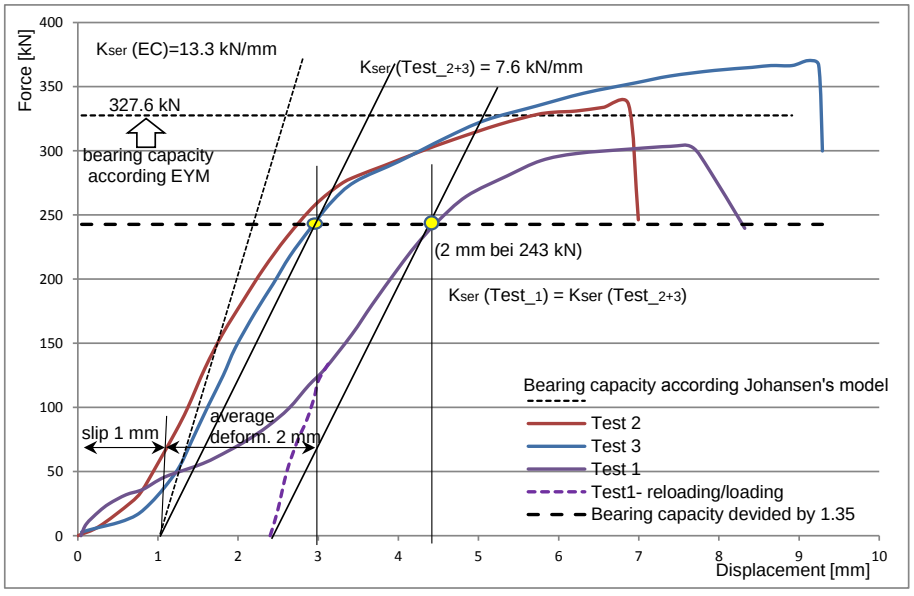

Fig. 6.15: HD Test according to [102] with limits of elastic response

Hold-down and inter-storey connection devices - conclusion

The bearing capacities of the HD devices considered within this work, with one, two or three slotted in steel plates, are given in Figures 3.4, 3.5 and 3.6. It has been shown in Chapter 3

that the HD device can be designed in such a way as to behave in the elastic range, without significantly contributing to the inelastic displacements of the LFTW. The applicability range for the HD devices presented in Figures 3.4, 3.5 and 3.6, which operate in the elastic range, is between ($\frac{86}{1.35} = 64[kN]$) for one slotted in steel plate and 6 bolts with d = 8 [mm] up to ($\frac{1038}{1.35} = 769[kN]$) [1] for three slotted in steel plates and 16 bolts with d = 16 [mm]. In the example in chapter 3, it is shown that the horizontal displacement arising from the HD devices acting in the elastic range is about 1.0%, and, thus this has little influence on the decrease of the stiffness when the structure is responding in the inelastic range. The same statement can be made for the inter-storey connection devices, which are to be designed in the same manner. Furthermore, given that all elements along the height of the building, including the inter-storey connection devices, have been the same, the structure considered within this thesis has not exhibited changes of stiffness and strength along its height. The influence of the hold down-devices on the stiffness of the shear wall element has been inherently taken into account sufficiently well by the MCASHEW mechanical model developed in Chapter 3, and hence it has not been additionally taken into account in modeling of the multi-storey structure.

Tab. 6.6: List of parameters subjected to the parameter study

Parameter		Status	
		varied	kept constant
Geometry of the wall	Length	X	
	Height of 2.90 [m]		X
Fastener	OSB: Nail d=2.87 [mm]		X
	Spacing 30 [mm]		X
	GFB: Staple 1.53 [mm]		X
	Spacing 35 [mm]		X
Sheathing material	OSB/GFB	X	
	Thickness		X
	Aspect ratio (H_w/L_w)	X	
	Both sides sheathed		X
Mass	Per storey	X	
	Distribution along height		X
Seismic hazard zone	Z1, Z2, Z3a and Z3b	X	
Soil category	A, B, C, D, E	X	
Earthquake records	Hazard zone and Soil category	X	

[1] In the parameter study presented in Chapters 6 and 7, the HD force has never exceeded the level of approximately 670 [kN].

6.3 Modeling Parameters

6.3.1 Geometry of LFTW

The shear wall element is defined by its length L_w and its height H_w. The sheathing material, its thickness, as well as the fasteners and the spacing of the fasteners used to connect the sheathing panel with the timber frame, are the components needed to define the element completely. Figures 6.16, 6.17, 6.18, 6.19 and 6.20 show different wall configurations with different number of sheathing panels, different number of intermediate studs and different panel aspect ratios. All shear wall elements considered within this thesis have sheathing panels on both sides. The thickness of the sheathing material used is $15[mm]$ for both OSB and GFB.

The strength class of the timber frame is GL24h, density $\rho = 380[N/mm^2]$. The dimension of the timber frame differ from $200 \cdot 200$, and $240 \cdot 240$ up to $300 \cdot 300[mm^2]$, respectively for low, moderate and high force levels in the frame studs.
The HD-devices required to sustain corresponding forces are with one, two or three slotted-in steel plates as presented in 6.21. The dowel-type connectors have diameters between 8 and 16 [mm], with a strength $f_u = 510[N/mm^2]$. For the design of HD devices the diagrams according Figures 3.4, 3.5 and 3.6 can be used. The steel plates are S235 of the strength $f_y = 235[N/mm^2]$ and thickness $t_p = d/2$ in [mm]. Figure 6.21 shows the anchorage of the wall into the sub-ground by means of hold-down devices. Figures 6.22 and 6.23 show the construction details, characteristic for the walls which support and those which do not support, a slab structure.

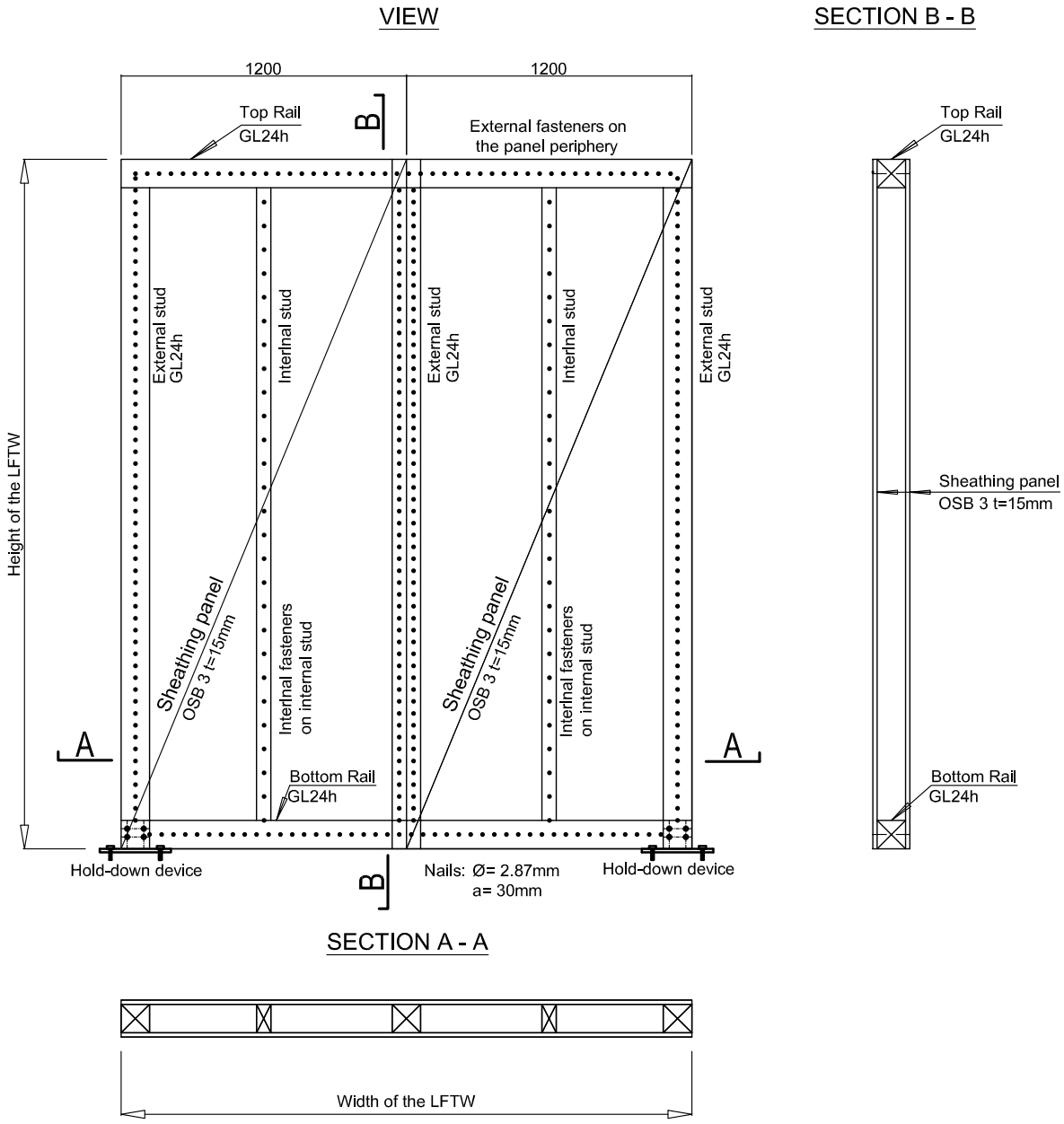

Fig. 6.16: LFTW with a length of 2400 [mm] subjected to the parameter study

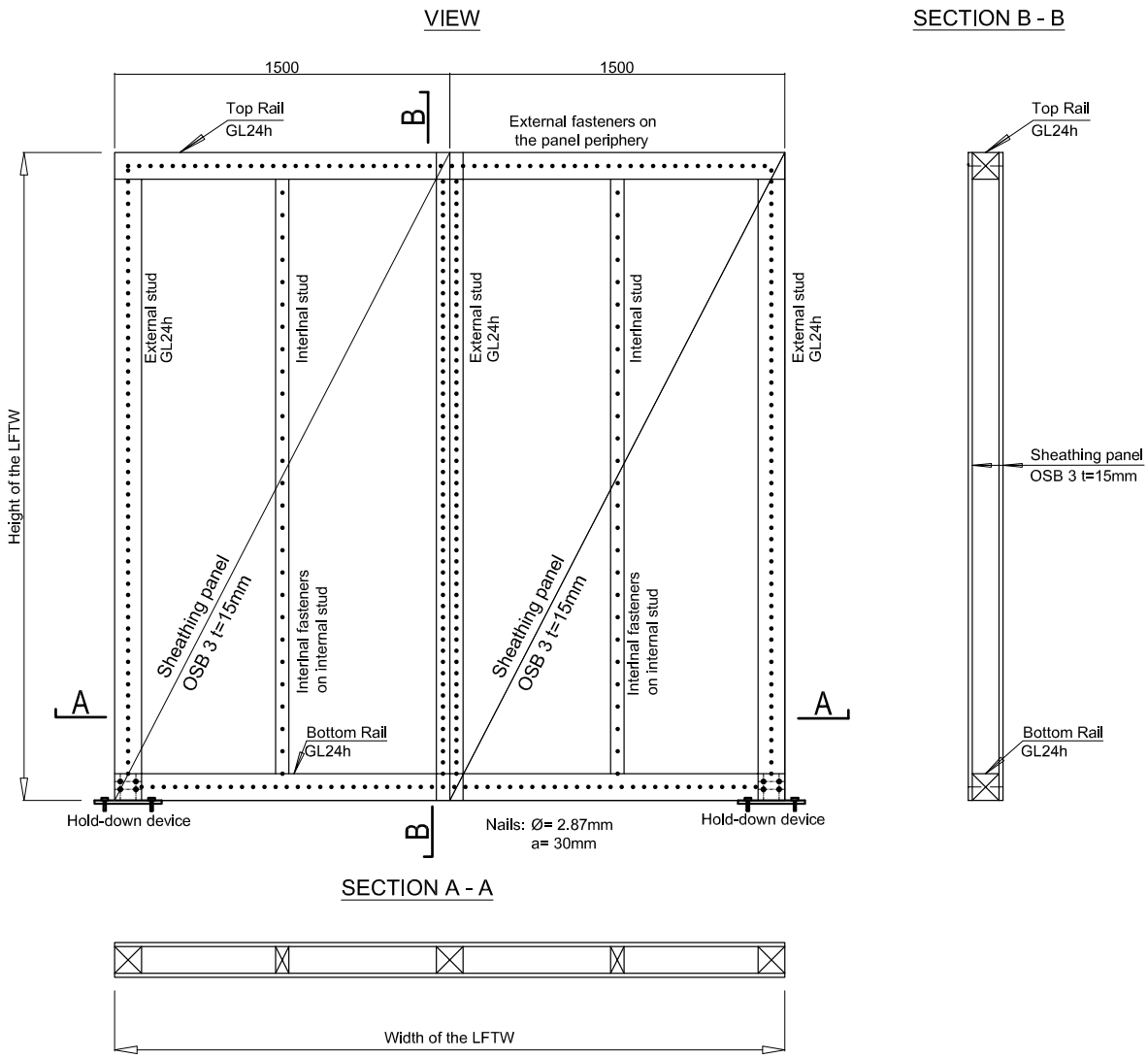

Fig. 6.17: LFTW with a length of 3000 [mm] subjected to the parameter study

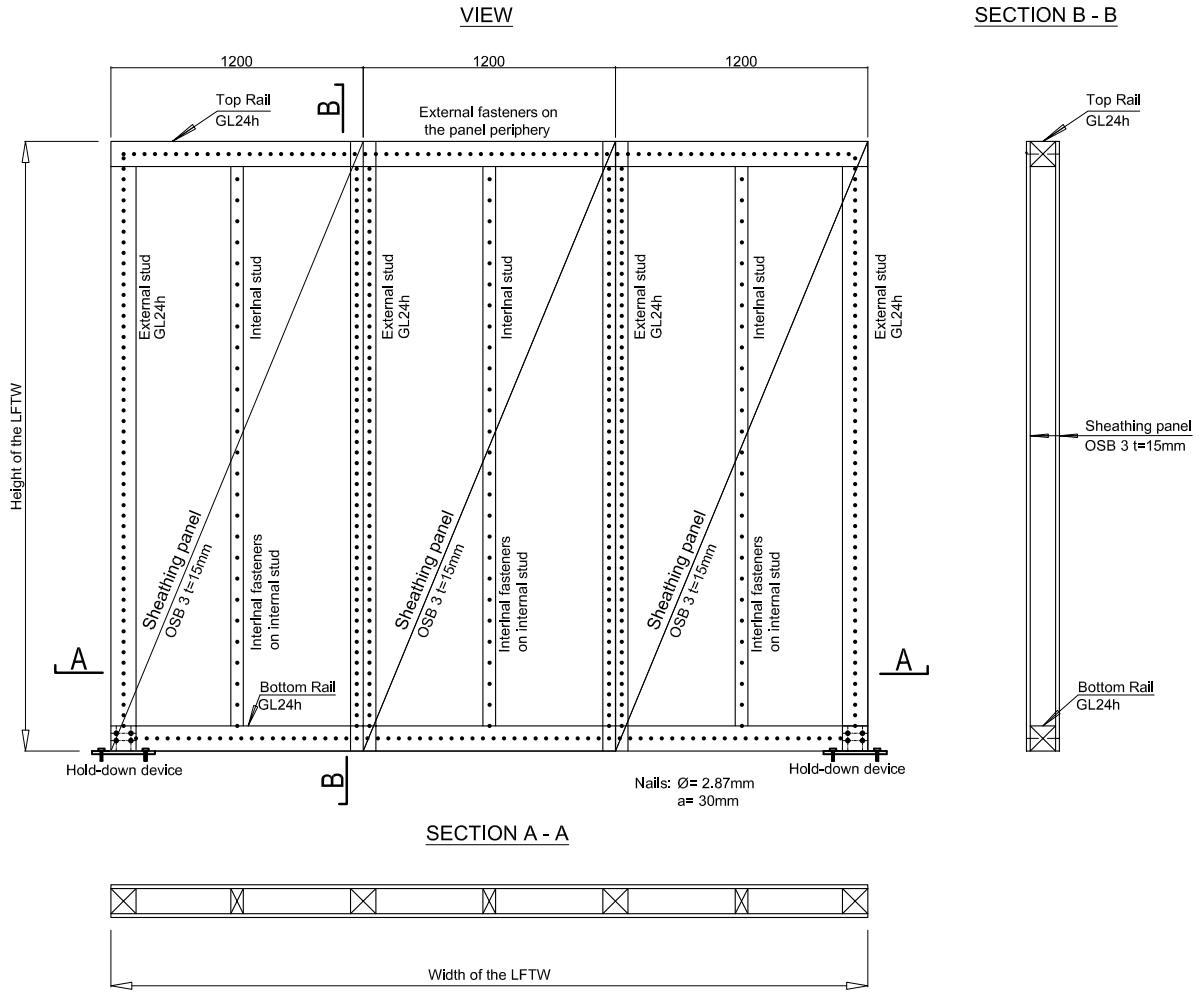

Fig. 6.18: LFTW with a length of 3600 [mm] subjected to the parameter study

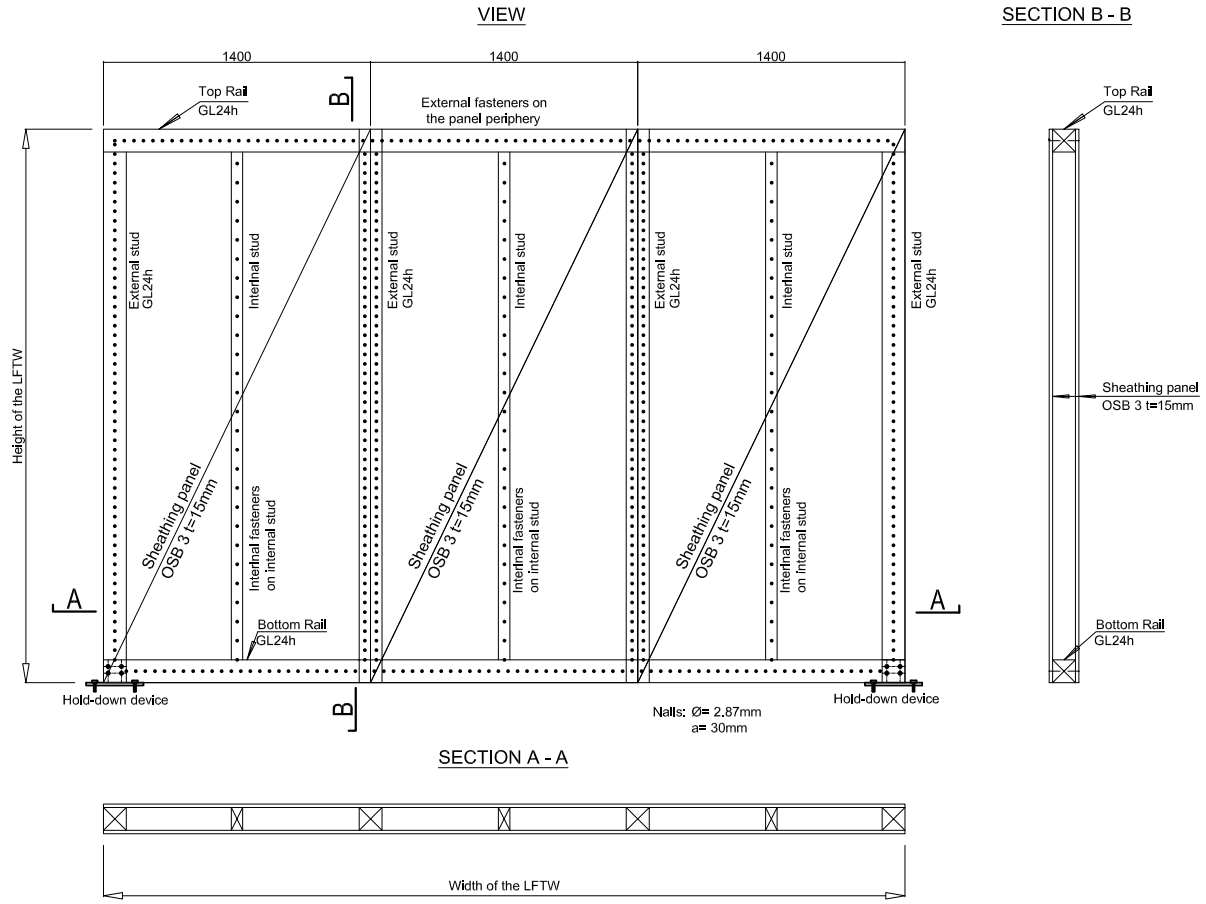

Fig. 6.19: LFTW with a length of 4200 [mm] subjected to the parameter study

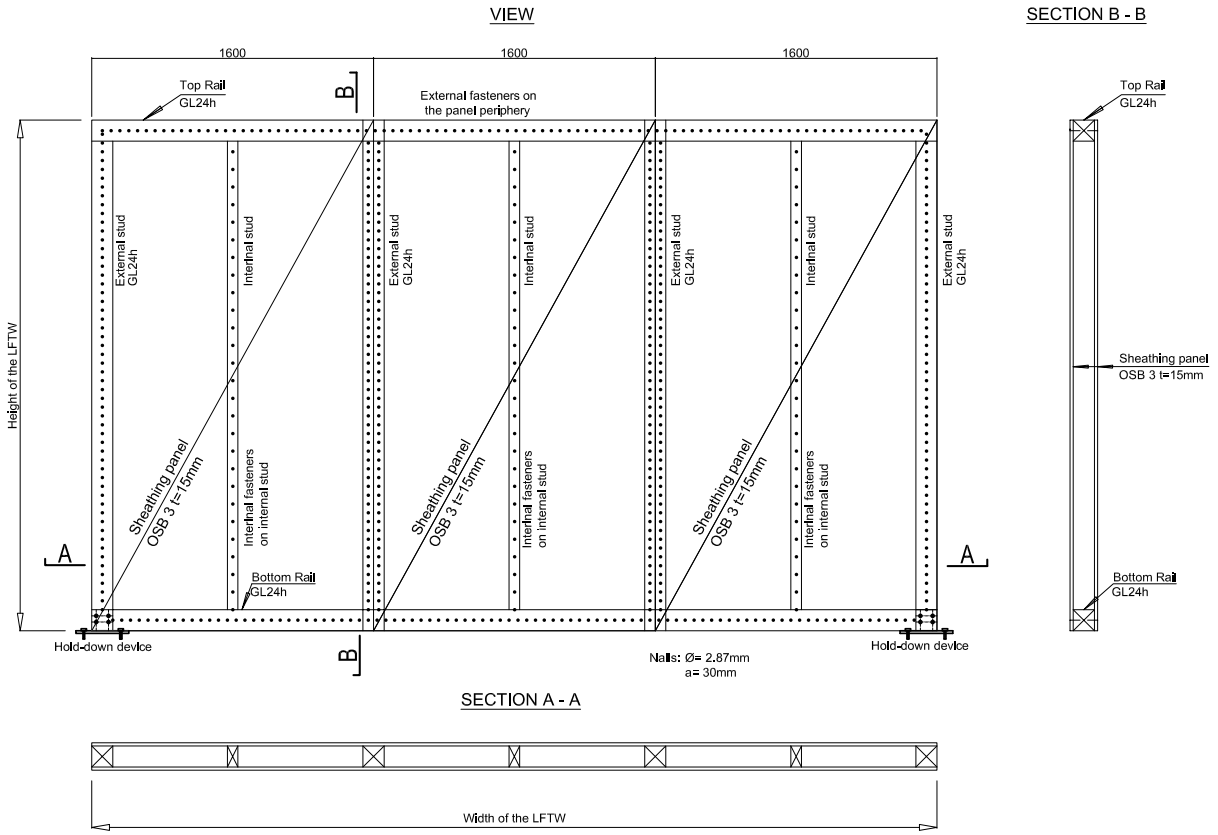

Fig. 6.20: LFTW with a length of 4800 [mm] subjected to the parameter study

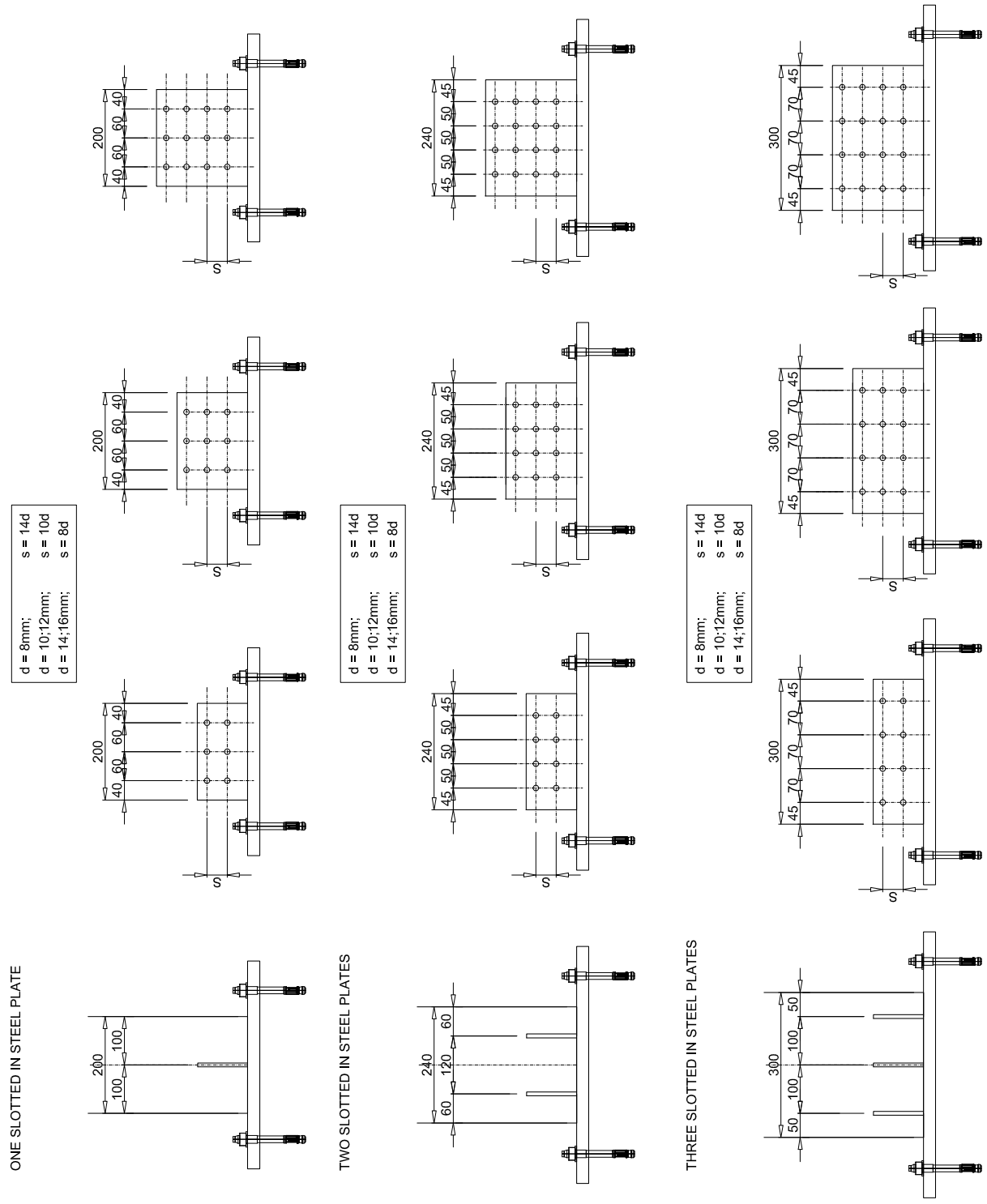

Fig. 6.21: HD Devices involved in the parameter study

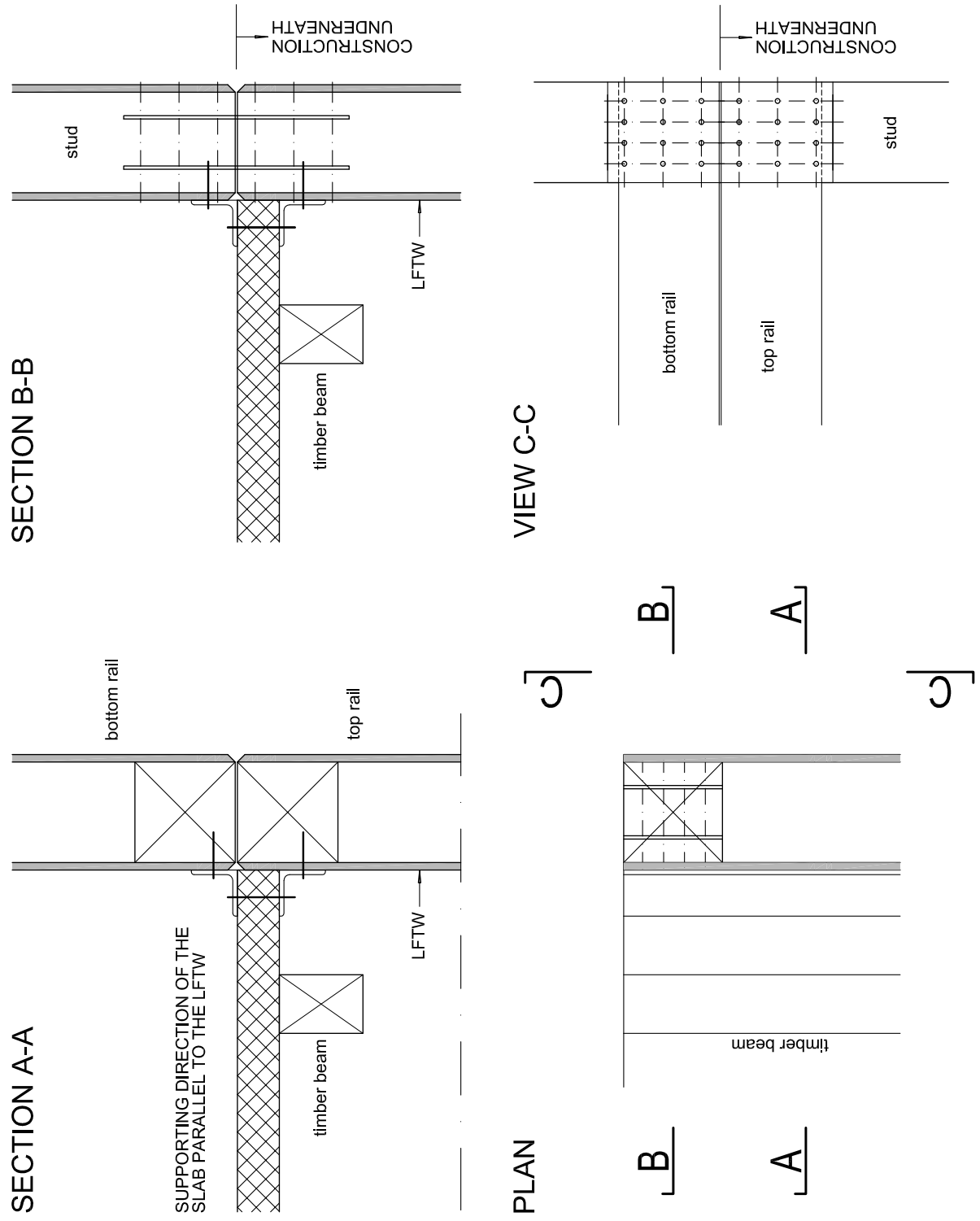

Fig. 6.22: LFTW that does not support a slab structure

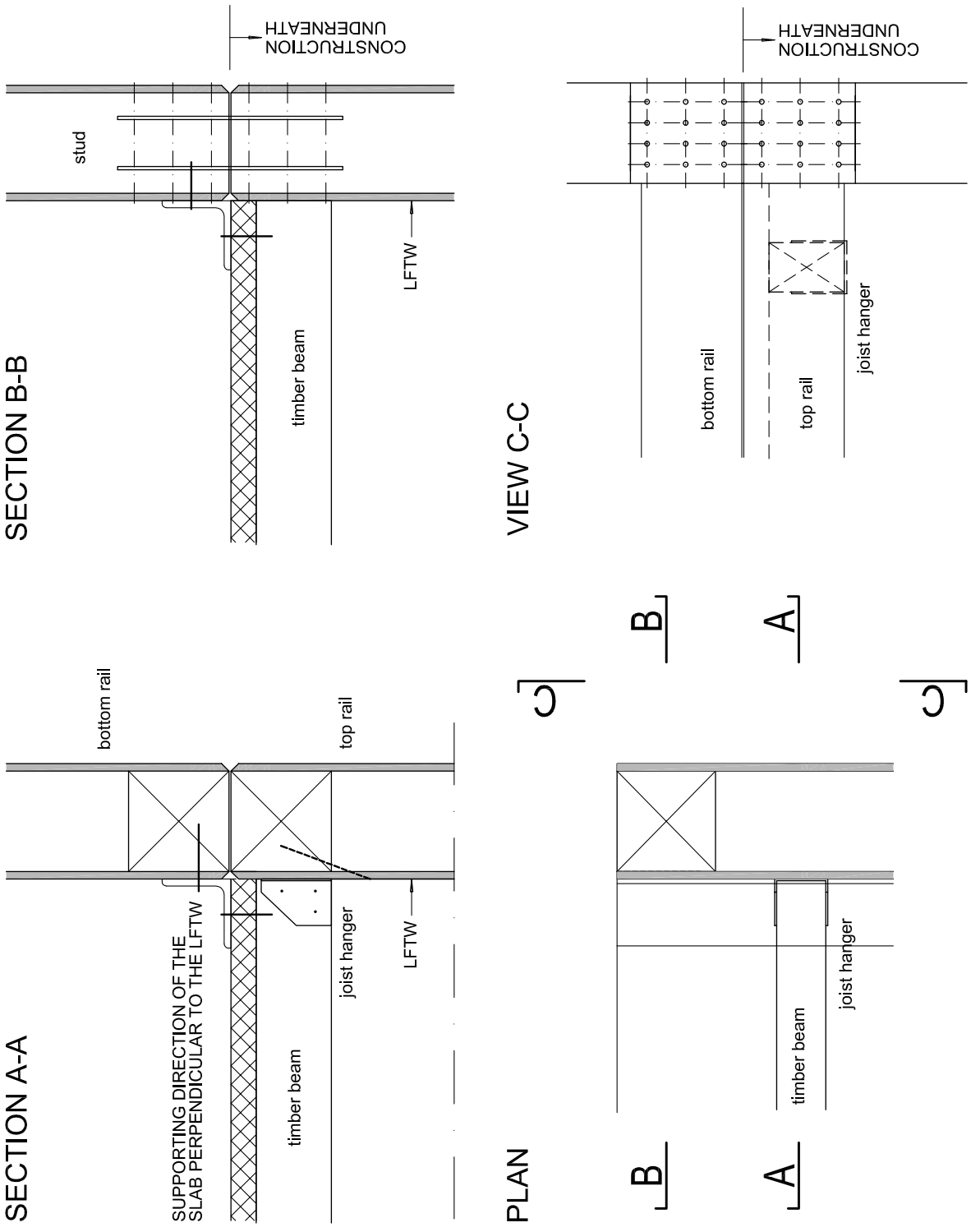

Fig. 6.23: The LFTW that supports a slab structure

6.3.2 Torsion due to asymmetry

The analytical model presented herein is two dimensional. It is not capable of accounting for influences of torsion. Nevertheless, the torsional effects can be estimated easily by statics, since torsion affects the distribution of forces, depending on their bending and shear stiffness. In Chapter 9, the results obtained by using PBE are compared with the results obtained by the frequently used force-based seismic design. The comparison is based on the example worked out in [6]. The elevation of the example building is simple. The structure is symmetric in the Y-direction and asymmetric in the X-direction due to the different wall lengths. This leads to eccentricity and thus to torsion if the structure is subjected to lateral loads. In the example worked out in [6], torsional effects have been taken into account. Providing that the wall elements are designed in the same manner and the only difference arises from the element length, one can easily estimate the additional force due to eccentricity and transform it into a mass acting on the wall under consideration. For more details, see Chapter 9.

6.3.3 Mass and mass distribution

In the present work, a regular structure is considered. This means that the stiffness, the height and the masses are the same and constant along the height of the structure. Usually, the mass of the top storey is different from the masses in the underlying levels because of different requirements, such as structure-borne noise and thermal insulation. The roof is sometimes conceived as a green area with additional loads for the plants. Additionally, the roof area is used for different kinds of installations, such as ventilation, cooling or photo-voltaic systems. The requirements to use the roof surface for different purposes are always present. Therefore, the model considered within this thesis uses equally distributed masses along the entire height of the structure.

In the parameter study, presented in Chapters 7 and 8, the theoretically admissible masses have been estimated, regardless their practical relevance. The practical relevance can be estimated if the weight of the timber ceiling is known. There are a number of different typical construction configurations of timber ceilings which have inherently different masses. Figure 6.24 shows some typical timber ceilings. The mass estimated from the dead load of a ceiling typically used as the level separation in multi-storey buildings (Figure 6.24(a)), is 460 $[\frac{kg}{m^2}]$. The ceiling typically used for roofs (Figure 6.24(b)) has a mass of 245 $[\frac{kg}{m^2}]$ including extensive roof greening. The ceiling typically used as the base element in the ground floor (Figure 6.24(c)) has a mass of 295 $[\frac{kg}{m^2}]$. If the contribution of the live load is considered, one can estimate the average mass of a timber ceiling to the range between 355 $[\frac{kg}{m^2}]$ $(295 + \psi \cdot 200 = 295 + 0.3 \cdot 200)$ and 520 $[\frac{kg}{m^2}]$ $(490 + 0.3 \cdot 200)$, for a ceiling with and without a concrete layer, respectively. Therefore, an average mass of 450 $[\frac{kg}{m^2}]$ has been considered within this thesis, when the tributary area is estimated. If the real masses of an actual project are known, the practical relevance can easily be derived from the results of the parameter study performed in Chapters 7 and 8.

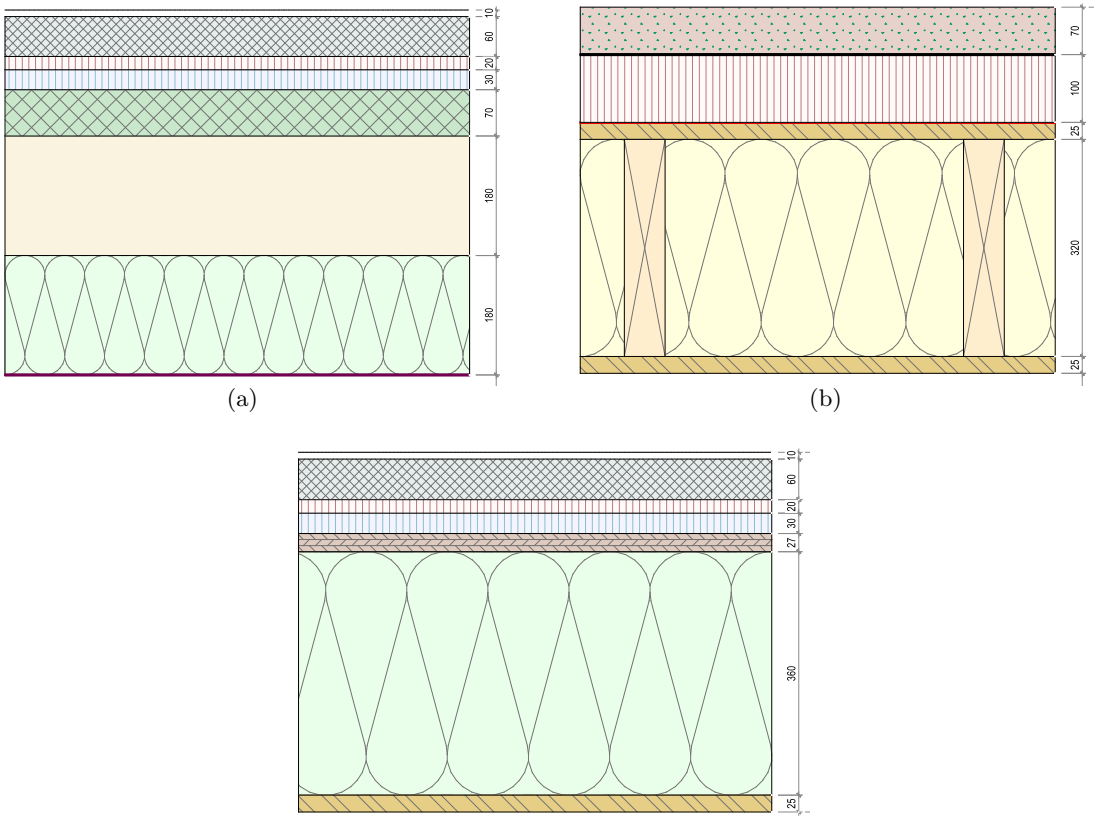

Fig. 6.24: Timber ceiling structure with a concrete layer, typically used as a separation between two storeys in apartment houses, 6.24(a): Timber ceiling structure, typically used for roofs, 6.24(b): Timber ceiling structure, typically used for ground floors without the requirement for sufficient structure-borne sound insulation, 6.24(c)

6.3.4 Damping

All vibration processes which occur in real conditions are connected with some kind of energy dissipation. The dissipation mechanisms have different origins, such as internal friction effects, transformation of strain energy into thermal energy, damaging effects such as cracking and plastic deformations in the cases of RC and steel structures or yielding of fasteners within light frame timber structures. The parameter which accounts for the energy dissipation mechanisms and the diminishing of the vibration amplitudes during the vibration process is the equivalent viscose damping. The damping coefficient is expressed as a fraction of the critical damping. It is different for different materials and types of the structure.

An accurate estimation of the damping is difficult and still unresolved, due to the variety of damping sources and absence of reliable physical models. Summarizing the sources of damping in LFTW-structures from a literature review, Jayamon at al. (2018) have specified the sources of energy dissipation which can be expressed as damping in [45] as follows:

- Viscous damping in wood materials which is amplitude-independent and frequency dependent
- Damping due to the friction on the contact surface between connected components which is amplitude dependent and frequency-independent
- Hysteretic damping due to the deformations and damages in nail connections which is path-dependent
- Damping due to the deformation of other structural and non-structural components which can not be included in mathematical model of the damping.

In [45] the damping in would structures have been grouped in four classes:

- Damping in wood material
- Damping in wood-shear wall assemblies
- Damping in horizontal diaphragm assemblies and
- Damping in multi-storey wood-frame shear wall buildings

The values for damping evaluated in the past, which are given back in [45] in Tables 1, 2 and 4, are of relevance for this work. So, the damping produced in the wood material is different for various wood species. The damping ratio is low and lies between 0.2% and 1.68%. See Table 1 in[45]. The damping measured in wood-frame shear walls is in the range between 5% and 14% up to values of 40%, see Table 2 in [45], for lower and higher levels of wall deformations, respectively. Finally, the damping ratios measured in shear wall buildings, see Table 4 in [45] are between 2% to 4% and 15% to 20%, or even 34% to 40% for lover and higher levels of deformations, respectively.

The damping ratios are commonly estimated by cyclic loading tests. If test results are not available, the Equation 6.4 gives a good approximation of damping ratio (see e.g. Chopra (2007), [9]). The equivalent viscose damping ξ is then expressed in a general form using Equation 6.4, proposed by Clough and Penzien (1993) (see [12]).

$$\xi = \frac{1 \cdot E_{loop}}{2 \cdot \pi \cdot K_s \cdot \Delta_{max}^2} \tag{6.4}$$

An attempt to determine the damping coefficient using the Equation 6.4 can be found in [77], Pang et al. In this specific case the obtained damping coefficient is $\xi = 0.27$. Furthermore, Equation 6.5 in [77] is proposed as a function for estimating the damping ratio, as a function of the secant and initial stiffness ratios. The damping ratio referred to as hysteric damping, lies in a range between 9% and 32%.

$$\xi_{hyst} = 0.32 \cdot e^{-1.38 \cdot \frac{K_s}{K_0}} \tag{6.5}$$

LFTW structures are capable of developing quite high equivalent viscose damping ratios, if they are responding in the nonlinear range. Nevertheless, the design spectra in many seismic codes are given for a damping ratio of 5%. In order to enable comparison with traditionally used design concepts and to allow direct use of the response spectra stipulated by code, a damping ratio of 5% has been used within the parameter study of this thesis. Please note, that the damping ratio is considered within capacity spectra design by using 5% damped response spectra. Within NLTHA performed in OpenSees the modal damping assumption is introduced in the Rayleigh damping model, which is expressed as the linear combination of the damping proportional to the mass and stiffness. So, for small vibration frequencies the damping proportional to the mass is predominant. For high vibration frequencies, the damping proportional to the stiffness is predominant. The response of the structure is quite sensitive to the assumption of the modal damping. In order to check how it affects results of the NLTHA, a 1-storey, 2-storey, 3-storey and 4-storey structure consisting of the LFTWs with a length of 3.6 [m], sheathed with OSB will be examined using two different modal damping coefficients $\xi = 3.0\%$ and $\xi = 5.0\%$. The results are compared in Table 6.7.

Tab. 6.7: Comparison of the NLTHA results obtained for 1-4 storey structures with the wall length of 3.6$[m]$ analyzed for modal damping coefficients $\xi = 3.0\%$ and $\xi = 5.0\%$ in the seismic Zone Z2 with $a_g = 1.0[m/s^2]$

Storey	Mass	Modal damping coefficient $\xi = 3.0\%$					Modal damping coefficient $\xi = 5.0\%$				
number	m	μ	HD force	Δ_{roof}	IDR	DI	μ	HD force	Δ_{roof}	IDR	DI
	$[t/st]$	[-]	[kN]	[mm]	[%]	[-]	[-]	[kN]	[mm]	[%]	[-]
1	576.0	2.38	219.2	60.41	2.10	0.73	2.35	218.9	57.26	1.97	0.70
		Mass correction for $\xi = 3.0\%$									
	535.0	2.33	220.6	58.9	2.0	0.70					
2	362.0	2.67	367.0	79.0	2.10	0.72	2.64	359.4	73.8	1.95	0.70
		Mass correction for $\xi = 3.0\%$									
	326.0	2.53	361.6	78.96	2.1	0.70					
3	172.5	1.79	433.0	78.7	1.40	0.46	1.76	425.8	75.94	1.28	0.43
4	100.0	1.35	469.0	81.7	0.94	0.30	1.32	460.6	79.87	0.95	0.30

As one can see in Table 6.7, all parameters increase slightly across all of the examined structures. The maximum increase in roof displacement and IDR is experienced by the one- and two-storey structures. The increase of the roof displacement is approximately 7.0%. The increase of the DI is in the range of 3% - 4%. The increase has no consequences for the structures higher than two stories, since for those structures the vibration period becomes the limiting criterion. The maximum admissible mass estimated for the structures with the modal damping coefficient $\xi = 5.0\%$ should be reduced for the structures with the modal damping coefficient $\xi = 3.0\%$, by approximatelly 7.0% for 1-storey and by 10% for 2-storey structures, in order to satisfy the required performance objectives.

Unfortunaltely, the discussion about the correct range of modal damping does not lead to an end, because of the lack of a physically based mathematical model for the damping coefficient. Since for the modal damping coefficient the value of 5% is widely used in the standard dynamics of structures, and supported by the results reported in [45], the modal damping assumption seems to be acceptable. The influence of higher or lower damping ratios on the nonlinear dynamic response of the structures and the possible adjustment of the presented parameter study could be the matter of a further investigation.

6.3.5 Ductility

LFTWs are said to be ductile, with a ductility ratio of up to $\mu = 5$ for DCH structures. See, for example, [1]. This apply for LFTWs sheathed with OSB panels (see e.g. [101] or [37]). A reference value for LFTWs sheathed with GFB does not exists. The LFTWs respond in a nonlinear manner, even under very low lateral loads. A pronounced yield point does not exist. Thus, the ductility ratio is a matter of judgement and despite the clear physical meaning, it is not always easy to be estimated for LFTWs. Moreover, in the study presented herein, the ductility demand, not the ductility coefficient, has been estimated as the consequence of the displacement demand and displacement capacity within the nonlinear pushover analysis. Especially in the case of LFTWs sheathed with GFB, the ductility demand governs the design. In the parameter study presented in Chapters 7 and 8, the ductility demand of the LFTWs sheathed with OSB panels has been set to $\mu = 3.0$, which is set to be the maximum ductility coefficient allowed. This maximum value could have been exceeded in the study, considering that ductility ratios of up to $\mu = 3.5$ have been obtained for squat walls, but such results are practically irrelevant (masses are too large, as will be shown in the parameter study). On the other hand, the ductility demand of approximately $\mu = 2.0 - 2.5$, regarded as the maximum available in the case of LFTWs sheathed with GFB, could not always be provided. Squat 1-storey LFTWs sheathed with GFB are able to provide a ductility up to 2.5. 2- and 3-storey LFTWs sheathed with GFB are only capable of providing a ductility of up to 1.8, as will be shown in the parameter study. Due to the low values of the ductility factor provided by the LFTWs sheathed with GFB ductility factors have not been restricted in this study. The ductility coefficients obtained in the parameter study have exceeded the value of approximately $\mu = 2.0$ very seldomly, even for 1-storey structures. Typical definition of the ductility as well as the ductility limit of $\mu = 3.0$ adopted in this thesis are presented in Figure 6.25.

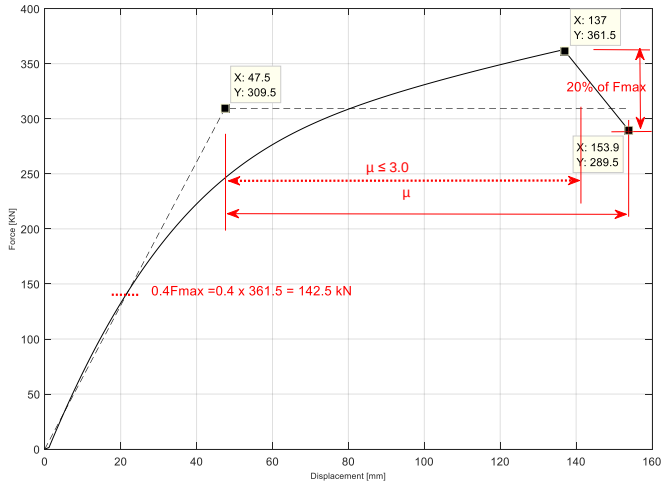

Fig. 6.25: The ductility definition as well as the ductility limitation presented on a pushover curve

6.3.6 Wind

Beside earthquake excitation, the wind load is an additional load case, which has to be taken into account within any structural analysis especially when designing the lateral load resisting system. However, a structure subjected to wind loads should respond in the elastic range in terms of both displacements and strength. The estimation of the wind load is a simple issue in practice. Within this thesis, the magnitude of the wind action has been controlled by assuming that the normalized wind load of 1.0 $[\frac{kN}{m^2}]$ acting perpendicularly to the facade surface will not exceed 55% of the LFTW's yield strength. Figure 6.26 shows an example of a pushover curve of a three storey LFTW element with a length of $4.2[m]$. The characteristic points which reflect the yield strength, the maximum strength and the ultimate displacement are depicted in the figure. By restricting the wind load so that it does not exceed the limit of 55% of F_y, the response is entirely in the elastic range and the serviceability of the structure is preserved with a deflection magnitude of $26.4[mm]$, corresponding to a lateral displacement of approximately $\frac{H}{330}$. Note that this condition is related to the effective strength of the LFTW element, enabling estimation of the admissible facade area exposed to the wind load. The admissible displacements caused by wind load should be estimated separately.

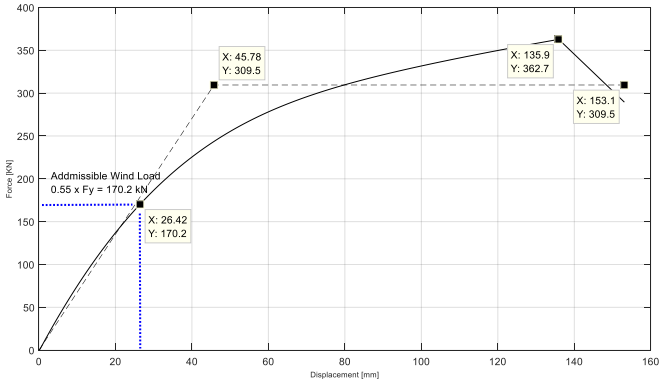

Fig. 6.26: Wind load limitation calculated from 6.7 compared with yield strength of the LFTW sheathed on both sides with OSB panels

Using the assumptions related to the normalized wind pressure and the admissible magnitude of the wind load, the width of the facade surface the wind pressure is acting on can be estimated as follows:

$$F_{wind} = q_w \cdot width \cdot H_w < 0.55 \cdot F_y \tag{6.6}$$

$$width = \frac{0.55 \cdot F_y}{n_{storey} \cdot h} \tag{6.7}$$

Using Equation 6.7, the admissible facade width would be $width = \frac{0.55 \cdot 309.5}{2.9 \cdot 3} = 19.5[m]$, which seems to be quite practice irrelevant, as the tributary facade width is normally up to $12[m]$. In this particular case, the wind load is probably governing design, because the admissible seismic mass is in the range of $155 - 223[t/storey]$, see also Table 7.4, thus the analysis reduces to the design due to the wind loads. Once the width of the facade is estimated, a direct comparison with the earthquake forces can be made.

6.4 On Economic Efficiency

6.4.1 Stiffness invariant

Chapter 1 mentioned that some assumptions are necessary to be able to conduct this parameter study. A constant stiffness along the height of the structure is assumed. A question which could arise is, which consequences could this have for companies in the practice in terms of competition? Since the stiffness of LFTWs is mainly due to the number of fasteners used to connect the sheathing material to the timber frame, the answer could be rather simple. The production in Switzerland and other European countries is fully automatic nowadays. The machines, often robots, are provided with nails or staples, which are automatically driven into the timber frame. Changing the algorithm to accomodate a different number of fasteners in the machine is often more time consuming than the material savings. Moreover, if a large number of the same elements should be produced, then it is reasonable to make them identical, in order

to prevent mistakes and to simplify assembly at the construction site. This is not related to the inter-storey connectors, which can provide the same stiffness, even when produced differently. Thus, the material savings in terms of inter-storey connectors are economically relevant. The savings are possible without an extra effort. The saving related to the number of fasteners is not justified in terms of economic savings.

6.5 Procedure of the parameter study

6.5.1 Input and analysis

In Chapter 3, the mechanical models of single-storey LFTWs, which can be presented as corresponding SDOF systems, have been derived for different wall lengths. In Chapter 4, the seismic analyses methods used in this thesis have been introduced and finally in this Chapter 6, the decision related to the limits of the critical parameter quantities have been outlined. The fundamentals for the parameter study, which is performed in the next two chapters, have been prepared. A flow diagram shows the input (Figure 6.27), analyses types, some of expected results, (Figure 6.28) and the check procedure whether the specified limits have been met. In Figure 6.30, the flow chart of the IDA procedure as presented in [41], is shown.

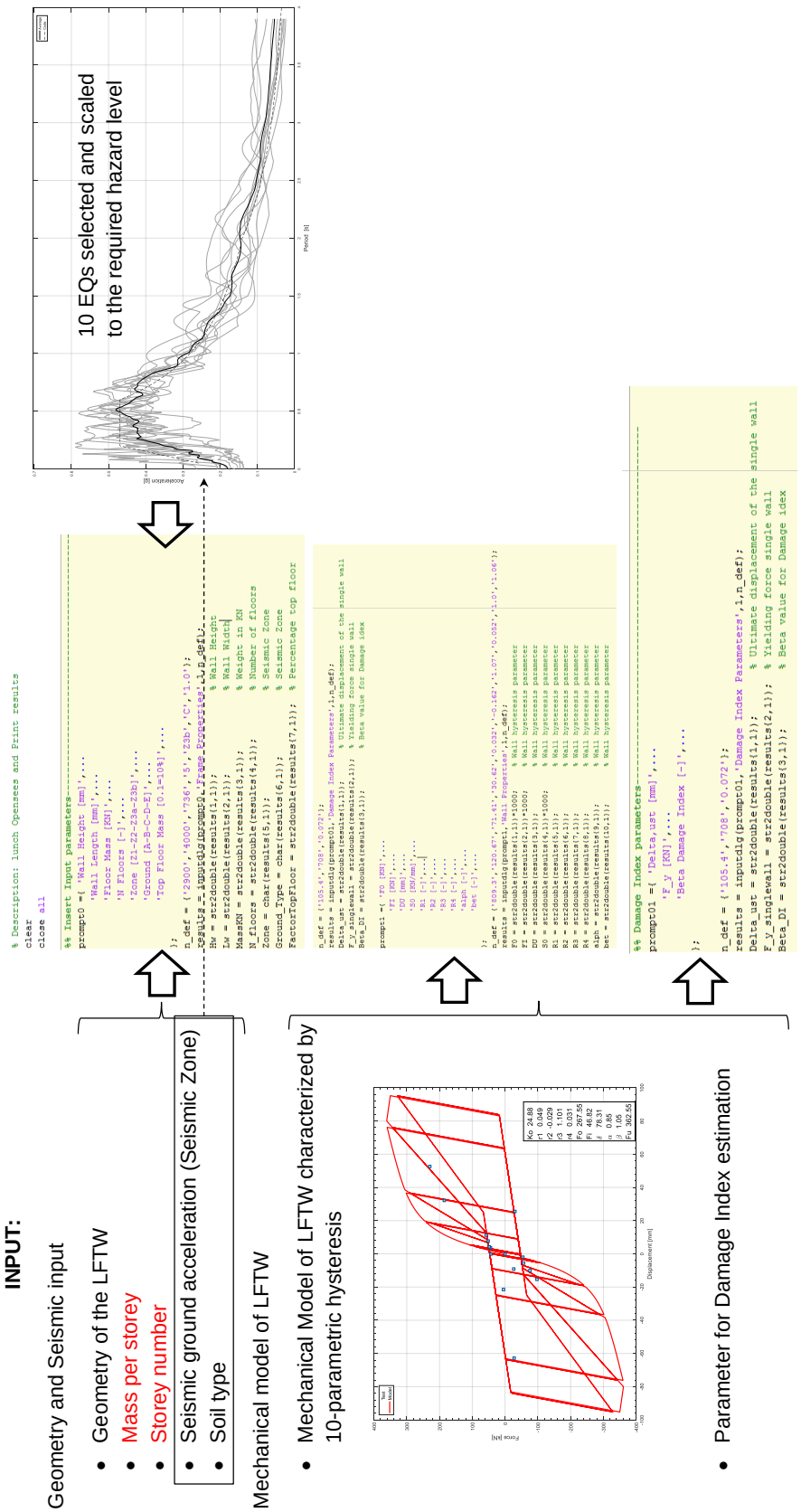

Fig. 6.27: Flow chart of the input steps

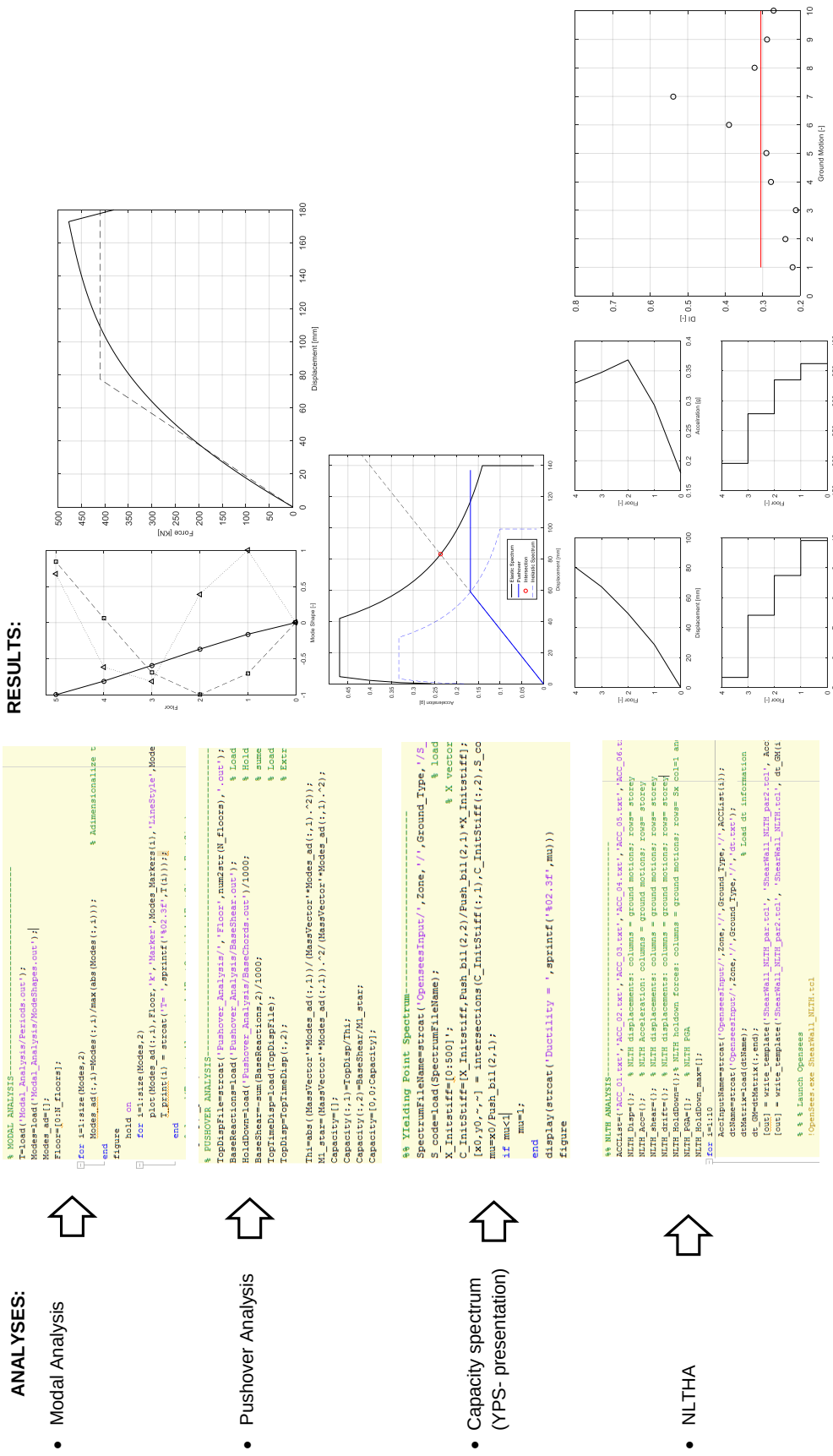

Fig. 6.28: Analyses performed within the parameter study and results of the analyses

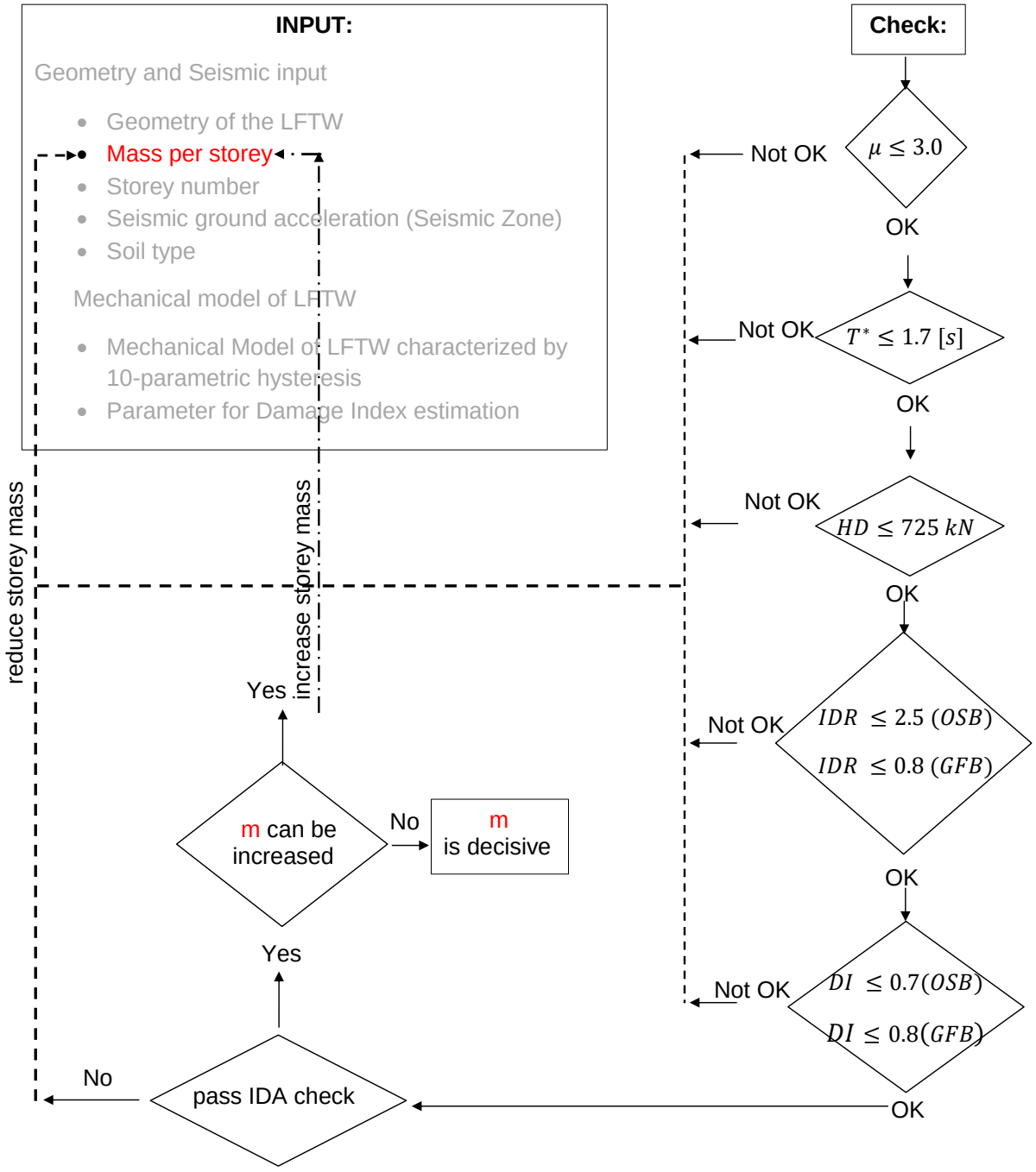

Fig. 6.29: Check if prescribed limits have been met

6.5.2 Check of the results

Generally speaking, the check procedure can end with a decision to reduce the input mass, as a consequence of the fact that one or more of the selected criteria have not been satisfied. It can also lead to the decision to increase the input mass if all selected criteria have been satisfied, and the structure has also passed the IDA check. The IDA check ends positively, if the estimated

intensity measure (IM), given the damage measure (DM), increases the elastic demand for a considered hazard level (see Figures 6.33 and 6.34).

6.5.3 IDA procedure

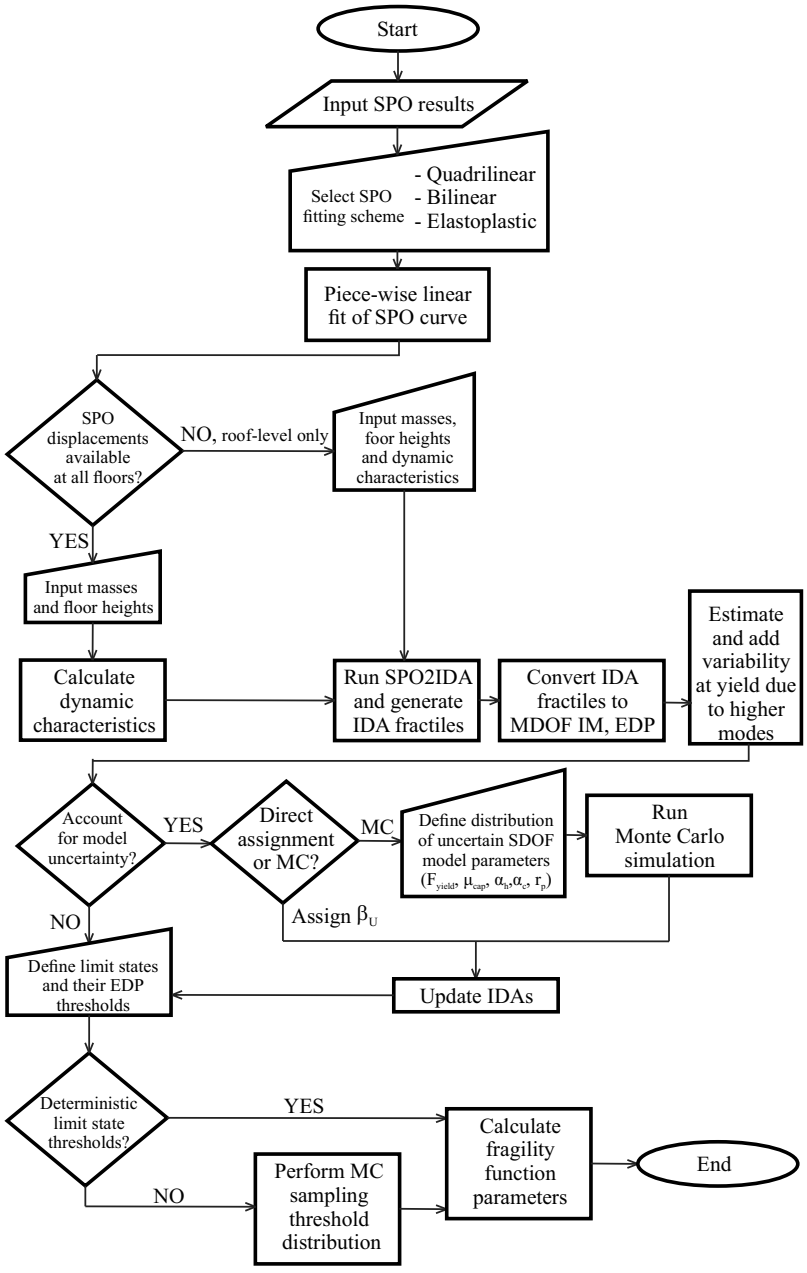

Fig. 6.30: Flowchart of IDA procedure according [41]

The following section shows how the check within the IDA procedure works. At the beginning, the static pushover curve, estimated within the parameter analysis, is introduced into the SPO2FRAG MATLAB-based program. Subsequently, the corresponding dynamic characteris-

tics of the system under consideration are estimated. Afterwards, a damage measure, e.g. roof drift ratio, is defined. For a given damage measure, IDA 16%, 50% and 84% fractile curves are generated. As Figure 6.31 indicates, 84% of all earthquakes should be scaled to the level of $S_{a(T)} = 0.175 \cdot g$, 50% to the level of $0.217 \cdot g$ and 16% of all earthquakes should be scaled to the level of $0.28 \cdot g$ in order to produce the specified RDR of 1.17%, set as the limiting displacement corresponding to the life safety limit state. In this thesis, the intensity measures corresponding to the 50% fractile IDA curve are adopted for validation of the parameter study.

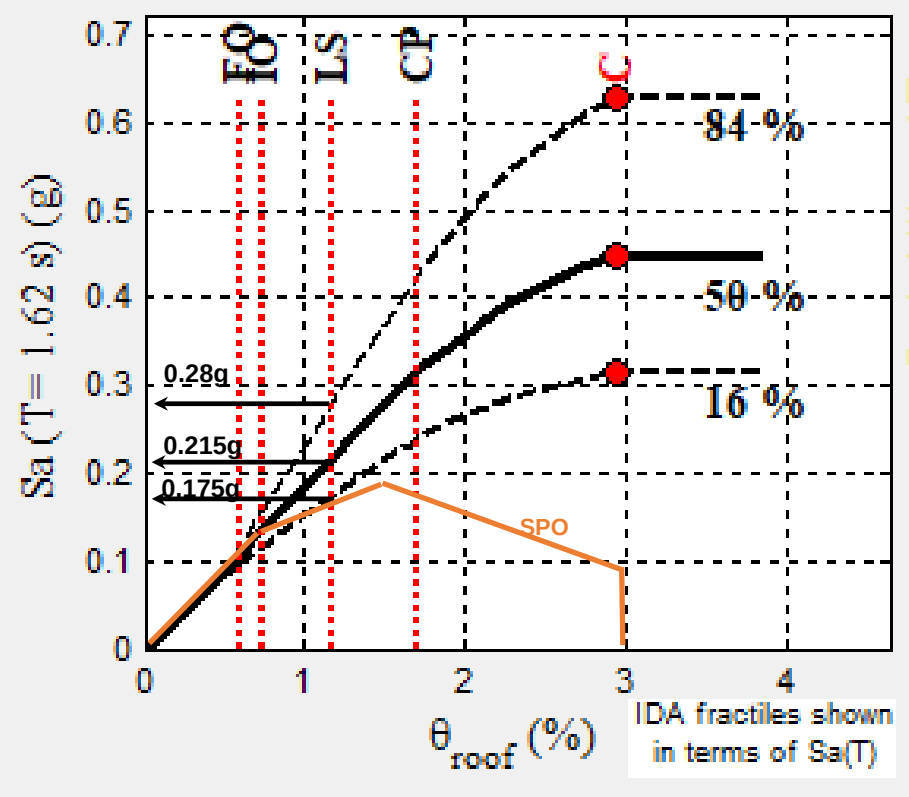

for RDR of 1.17% = 169.7 [mm]

84% of all earthquakes must be scaled to 0.175g in order to cause RDR of 1.17%
50% of all earthquakes must be scaled to 0.215g in order to cause RDR of 1.17%
16% of all earthquakes must be scaled to 0.280g in order to cause RDR of 1.17%

Fig. 6.31: Correlation between SPO and IDA- curves for 84%, 50% and 16% Fractile with corresponding IM, given DM

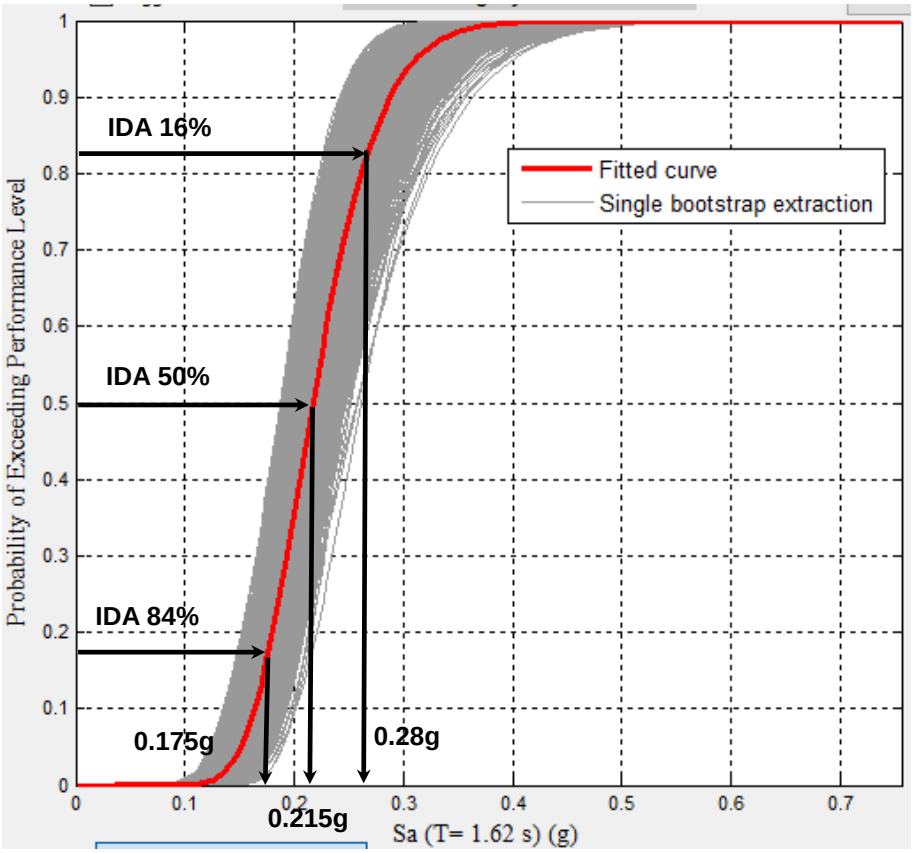

Fig. 6.32: Fragility curve with corresponding probability of exceedance of ID, given DM

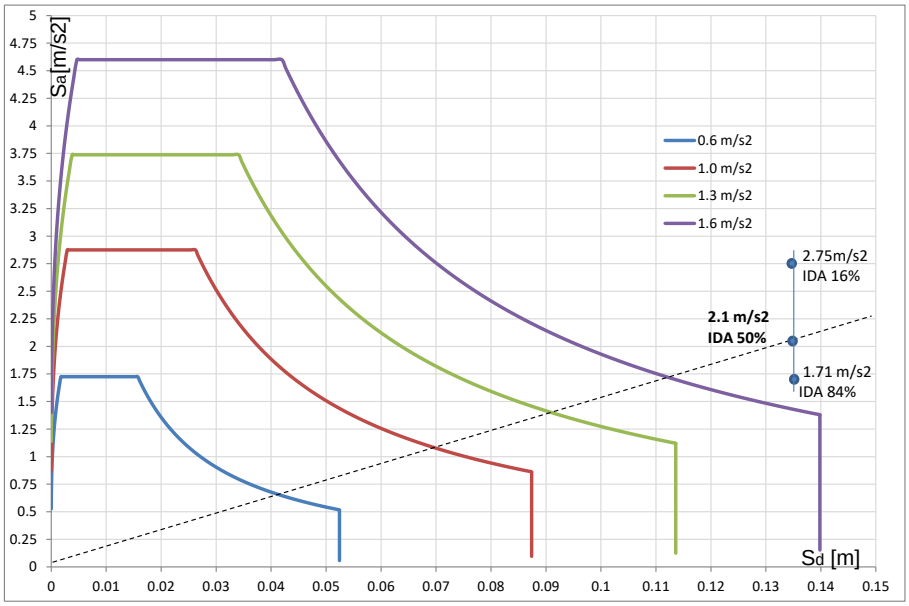

Fig. 6.33: Visualized check procedure within IDA for a 5-storey building with 16, 50 and 84 % IDA -fractile quantities superimposed in RS

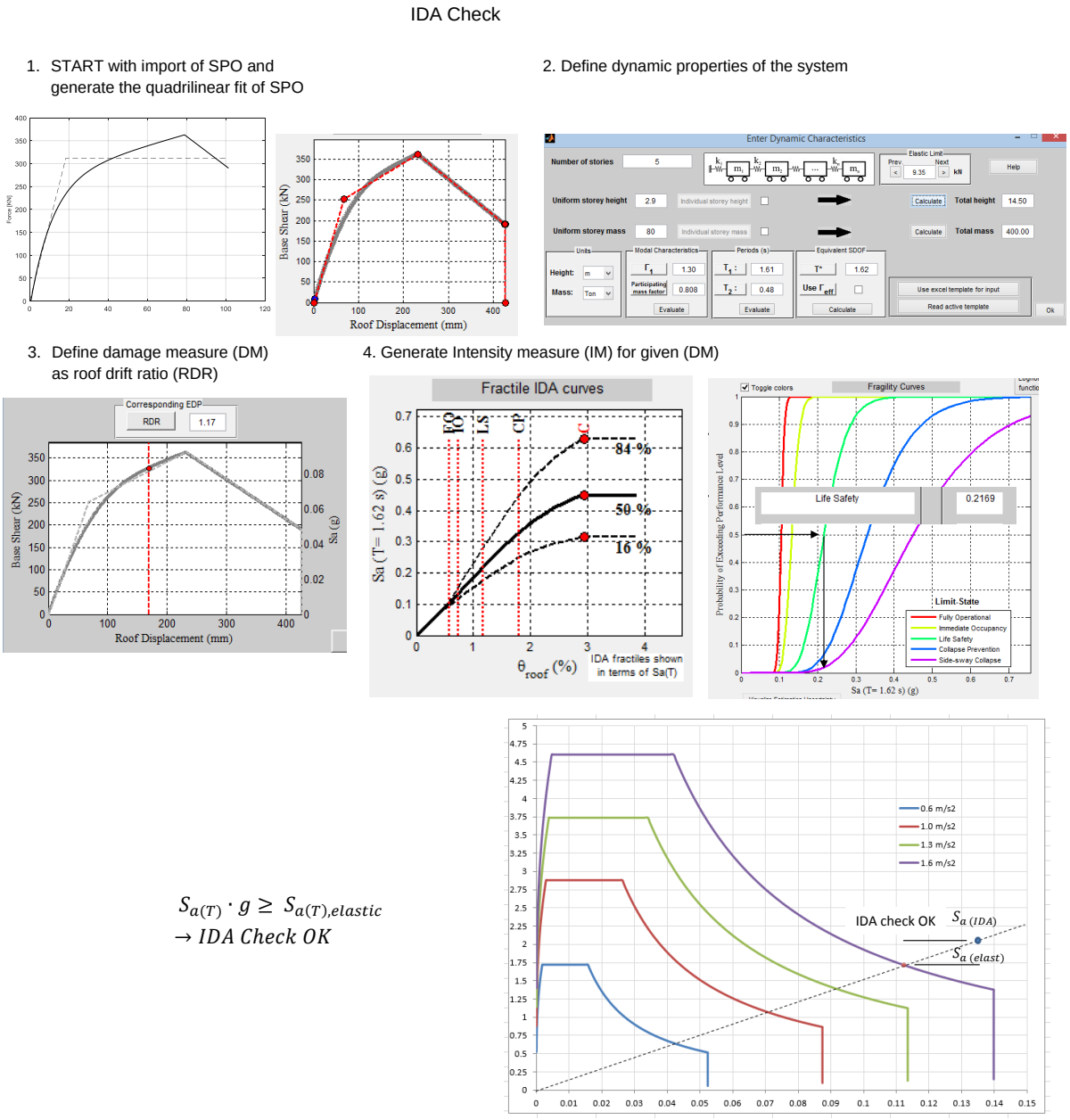

Fig. 6.34: Visualized check procedure within IDA in accordance with Figure 6.30

The procedure presented here is repeated for every run of the parameter study. The results are summarized in tabular and graphical form and discussed in Chapters 7 and 8. Note that the IDR and DI are correlated and thus coupled to each other. However, if the IDR should slightly overstep the maximum value stipulated in advance, which rarely occurs, the DI is considered to be the governing criterion.

6.6 Conclusions

The main assumptions related to the parameter quantities can be confirmed. Thus, the analysis of the prototype building has shown that the gravity loads contribute to the reduction of HD forces despite driving effects arising from geometric non-linearity. For this reason, the parameter study should be performed by neglecting the gravity loads. The serviceability requirements related to the brittle nonstructural elements are best satisfied if the maximum period of vibration is $T^* \leq 1.7[s]$. The overall behaviour of LFTWs is negligibly affected by the resiliency of the HD and inter-storey connection devices. Due to the lack of physical model for the proper mathematical description of damping in HRW, the most commonly used modal damping coefficient of 5% will also be used in the present parameter study. To control the extent of the damage intensity, the ductility demand limit is set in advance to be $\mu \leq 3.0$. The configuration of the LFTWs as well as the economical consequences related to setting the stiffness as constant along building height have been discussed. The steps within the process of the parameter study as well as the validation process using IDA have been shown by means of a flow diagram.

Chapter 7

Parameter Study of LFTW Sheathed with OSB

7.1 Introduction

In this chapter, the parameter study for LFTWs sheathed with OSB is performed. The results of the parameter study are summarized in tabular and graphical form. The IDA analysis is performed for each run in parallel. The mass, which satisfies all conditions, is recognised as decisive.

Within the parameter study performed in this chapter, the mechanical model of LFTW sheathed with OSB developed in Chapter 3 and summarized in Tables 3.8 to 3.12 has been used. The analyses have been performed for all wall elements, characterized by their lengths of $2.4, 3.0, 3.6, 4.2$ or $4.8[m]$ and seismic hazard zones characterized by ground accelerations $0.6, 1.0, 1.3$ or $1.6\frac{m}{s^2}$ corresponding to hazard zones $Z1, Z2, Z3a$ or $Z3b$, as stipulated in the SIA code [3]. The LFTWs are sheathed on both sides with OSB panels. The panel thickness is $t_p = 15[mm]$. Nails with $d = 2.87[mm]$, spaced at $30[mm]$, were used as fasteners to connect the OSB panels with the timber frame.
Only soil category C has been considered in this chapter. Soil conditions C have been chosen for the parameter study because soil rock / dense soils are often found in European regions. Furthermore, the amplification and the plateau periods are in the median range. The results for additional soil categories A (stiff soil) and E (soft soil) are attached in Appendix B. The outcome of the parameter analysis is the maximum mass applicable at each storey of the structure under consideration so that all the performance limits for the life safety (LS) limit state, derived in Chapter 5, are satisfied. The analyses are based on the parameters briefly described in Chapter 6.

7.2 Parameter Study

7.2.1 General considerations

The outcome of the parameter study is presented in both tabular and chart format. The results in the tabular format are divided into the following sub-analysis parts:

- Check by means of IDA analysis
- Modal analysis
- Pushover analysis
- NLTHA

All results of the parametric study have been also subsequently checked by means of IDA-analysis, as presented in Chapter 5 and 6, see e.g. Figure 6.34. For illustration some of the results are presented graphically. See also Subsection 7.3.6. The damage index (DI) in the damage index analysis has been performed using the parameter β_{DI} according to Table 5.1.

7.2.2 Tabular and graphical presentation for LFTW with a length of $2.4[m]$ sheathed on both sides with OSB

The results of the parametric study of the 2.4 [m] long LFTW element sheathed with OSB panels on both sides are summarized in Table 7.1. A typical, graphical presentation is given in Figure 7.1

Tab. 7.1: Results of the parameter study of the LFTW with a length of 2.4 [m] sheathed on both sides with OSB

Zone	Mass	IDA	Modal analysis			Pushover analysis				NLTH analysis			
a_g	m	check	T	T^*	Γ	Δ_y	F_y	μ	$\Delta_{u,st}$	HD force	Δ_{roof}	IDR	DI
$\frac{m}{s^2}$	[t]		[s]	[s]	[-]	[mm]	[kN]	[-]	[mm]	[kN]	[mm]	[-]	[-]
1- storey structure													
0.6	500.0	✓	1.26	1.70	1.0	24.22	163.7	1.85	105.2	170.6	57.88	2.0	0.65
1.0	408.0	✓	1.14	1.50				2.85		202.5	62.67	2.20	0.70
1.3	255.0	✓	0.90	1.14				3.00		197.5	56.23	1.94	0.60
1.6	153.0	✓	0.70	0.86				3.00		210.7	62.97	2.17	0.65
2- storey structure													
0.6	230.0	✓	1.47	1.70	1.189	34.4	162.4	1.59	126.4	254.4	45.74	1.16	0.38
1.0	230.0	✓	1.47	1.70				2.65		339.0	74.52	1.90	0.62
1.3	173.0	✓	1.28	1.47				3.00		326.5	69.50	1.72	0.53
1.6	112.0	✓	1.03	1.18				3.00		341.1	77.30	2.02	0.62

Zone	Mass	IDA	Modal analysis			Pushover analysis				NLTH analysis			
a_g	m	check	T	T^*	Γ	Δ_y	F_y	μ	$\Delta_{u,st}$	HD force	Δ_{roof}	IDR	DI
$\frac{m}{s^2}$	[t]		[s]	[s]	[-]	[mm]	[kN]	[-]	[mm]	[kN]	[mm]	[-]	[-]
3- storey structure													
0.6	110.0	✓	1.57	1.70	1.266	52.39	161.7	1.08	158.6	286.4	47.79	0.8	0.35
1.0	110.0	✓	1.52	1.70				1.80		403.0	78.3	1.26	0.40
1.3	110.0	✓	1.52	1.70				2.33		421.0	83.36	1.37	0.43
1.6	110.0	x	1.52	1.70				2.88		496.5	118.8	2.02	0.65
	85.0	✓	1.34	1.49				2.53		463.2	100.7	1.75	0.55
4- storey structure													
0.6	60.0	✓	1.57	1.70	1.3184	80.01	162.4	1.0	217.4	292.4	50.99	0.54	0.17
1.0	60.0	✓	1.57	1.70				1.23		429.7	82.59	0.87	0.17
1.3	60.0	✓	1.57	1.70				1.60		451.0	87.36	1.0	0.31
1.6	60.0	✓	1.57	1.70				1.97		555.3	119.4	1.50	0.47
5- storey structure													
0.6	35.0	✓	1.61	1.70	1.357	117.5	162.3	1.0	283.8	272.6	50.75	0.44	0.13
1.0	35.0	✓	1.61	1.70				1.0		409.3	83.96	0.67	0.20
1.3	35.0	✓	1.61	1.70				1.1		439.4	91.03	0.78	0.23
1.6	35.0	✓	1.61	1.70				1.40		516.9	113.4	1.10	0.33
6- storey structure													
0.6	21.5	✓	1.61	1.70	1.386	168.6	163.0	1.0	368.3	240.1	52.16	0.40	0.10
1.0	21.5	✓	1.61	1.70				1.0		387.8	87.73	0.61	0.15
1.3	21.5	✓	1.61	1.70				1.0		414.0	95.97	0.67	0.19
1.6	21.5	✓	1.61	1.70				1.0		499.0	115.4	0.81	0.25

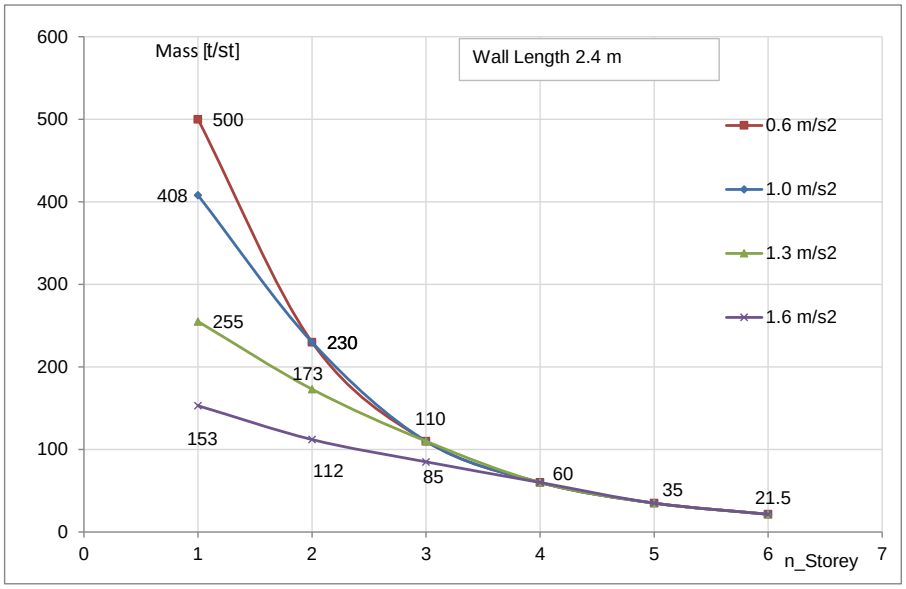

Fig. 7.1: Outcome of the parameter study of the 2.4 [m] LFTW element sheathed on both sides with OSB, see also Table 7.1

7.2.3 Tabular and graphical presentation of LFTW with a length of $3.0[m]$ sheathed on both sides with OSB

The results of the parametric study of the 3.0 [m] long LFTW element sheathed with OSB panels on both sides are summarized in Table 7.2. A typical, graphical presentation is given in Figure 7.2.

Tab. 7.2: Results of the parameter study of theLFTW with a length of 3.0 [m] sheathed on both sides with OSB

Zone	Mass	IDA	Modal analysis			Pushover analysis				NLTH analysis			
a_g	m	check	T	T^*	Γ	Δ_y	F_y	μ	$\Delta_{u,st}$	HD force	Δ_{roof}	IDR	DI
$\frac{m}{s^2}$	[t]		[s]	[s]	[-]	[mm]	[kN]	[-]	[mm]	[kN]	[mm]	[-]	[-]
1- storey structure													
0.6	630.0	✓	1.14	1.70	1.0	25.82	216.5	1.72	108.0	191.7	48.1	1.66	0.66
1.0	408.0	✓	0.92	1.28				2.48		219.9	56.0	1.93	0.70
1.3	331.5	✓	0.83	1.120				3.00		220.2	55.23	1.90	0.64
1.6	200.0	✓	0.64	0.82				3.00		234.6	60.61	2.10	0.67
2- storey structure													
0.6	345.0	✓	1.45	1.70	1.187	29.68	219.9	1.78	124.4	305.9	52.99	1.55	0.63
1.0	307.5	✓	1.37	1.59				2.8		353.7	64.1	1.74	0.66
1.3	206.5	✓	1.12	1.30				3.00		356.1	66.23	1.71	0.58
1.6	135.0	✓	0.90	1.04				3.00		372.9	76.84	2.08	0.69

Zone	Mass	IDA	Modal analysis			Pushover analysis				NLTH analysis			
a_g	m	check	T	T^*	Γ	Δ_y	F_y	μ	$\Delta_{u,st}$	HD force	Δ_{roof}	IDR	DI
$\frac{m}{s^2}$	[t]		[s]	[s]	[-]	[mm]	[kN]	[-]	[mm]	[kN]	[mm]	[-]	[-]
3- storey structure													
0.6	165.0	✓	1.50	1.70	1.266	47.08	216.3	1.21	153.0	329.6	49.20	0.87	0.32
1.0	165.0	✓	1.50	1.70				2.02		465.5	76.1	1.70	0.51
1.3	165.0	✓	1.50	1.70				2.63		479.6	86.11	1.46	0.53
1.6	136.5	x	1.36	1.53				2.91		532.4	103.5	1.84	0.67
	125.0	✓	1.30	1.47				2.83		504.3	98.0	1.79	0.63
4- storey structure													
0.6	92.0	✓	1.57	1.70	1.318	70.32	219.1	1.0	204.1	350.3	52.0	0.62	0.22
1.0	92.0	✓	1.57	1.70				1.40		507.71	84.81	0.95	0.34
1.3	92.0	✓	1.57	1.70				1.82		522.5	87.95	1.11	0.38
1.6	92.0	✓	1.57	1.70				2.23		577.7	119.7	1.62	0.56
5- storey structure													
0.6	54.0	✓	1.61	1.70	1.357	102.5	218.2	1.0	256.3	334.5	53.29	0.45	0.16
1.0	54.0	✓	1.61	1.70				1.0		486.5	84.36	0.70	0.24
1.3	54.0	✓	1.61	1.70				1.28		526.4	91.53	0.84	0.28
1.6	54.0	✓	1.61	1.70				1.58		576.7	111.1	1.17	0.38
6- storey structure													
0.6	33.5	✓	1.64	1.70	1.386	146.0	218.2	1.0	319.6	299.9	53.59	0.40	0.12
1.0	33.5	✓	1.64	1.70				1.0		483.9	88.25	0.60	0.19
1.3	33.5	✓	1.64	1.70				1.0		504.61	97.34	0.70	0.22
1.6	33.5	✓	1.64	1.70				1.58		576.7	111.1	1.17	0.38
7- storey structure													
0.6	21.75	✓	1.67	1.70	1.41	202.4	218.2	1.0	405.3	269.8	57.77	0.39	0.09
1.0	21.75	✓	1.67	1.70				1.0		424.5	91.65	0.56	0.14
1.3	21.75	✓	1.67	1.70				1.0		458.3	101.1	0.63	0.16
1.6	21.75	✓	1.67	1.70				1.0		580.7	134.8	0.80	0.24

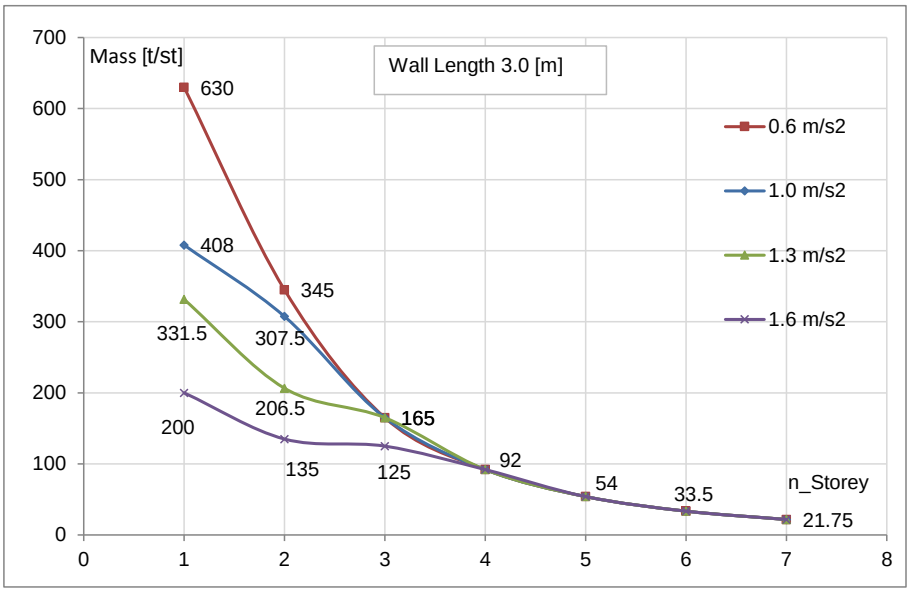

Fig. 7.2: Outcome of the parameter study of the 3.0 [m] LFTW element sheathed on both sides with OSB, see also Table 7.2

7.2.4 Tabular and graphical presentation of LFTW with a length of $3.6[m]$

The results of the parametric study of the 3.6 [m] long LFTW element sheathed with OSB panels on both sides are summarized in Table 7.3. The typical, graphical presentation is given in Figure 7.3

Tab. 7.3: Results of the parameter study of the LFTW with a length of 3.6 [m]

Zone	Mass	IDA	Modal analysis			Pushover analysis				NLTH analysis			
a_g	m	check	T	T^*	Γ	Δ_y	F_y	μ	$\Delta_{u,st}$	HD force	Δ_{roof}	IDR	DI
$\frac{m}{s^2}$	[t]		[s]	[s]	[-]	[mm]	[kN]	[-]	[mm]	[kN]	[mm]	[-]	[-]
1- storey structure													
0.6	632.0	✓	1.148	1.70	1.0	31.47	266.0	1.44	124.3	179.0	39.43	1.36	0.48
1.0	576.0	✓	1.10	1.60				2.35		218.9	57.26	1.97	0.70
1.3	510.0	✓	1.03	1.47				2.93		218.5	61.25	2.10	0.70
1.6	250.0	✓	0.72	0.95				2.76		225.9	65.13	2.25	0.70
2- storey structure													
0.6	367.0	✓	1.47	1.70	1.184	33.25	263.9	1.59	142.2	269.4	47.13	1.33	0.49
1.0	362.0	✓	1.46	1.69				2.64		359.4	73.80	1.95	0.70
1.3	290.0	x	1.30	1.50				3.0		360.6	72.33	1.70	0.56
	285.0	✓	1.30	1.50				3.0		357.8	71.80	1.70	0.56
1.6	183.5	x	1.04	1.20				3.0		365.4	80.53	2.0	0.63
	177.5	✓	1.02	1.18				2.95		356.6	74.35	1.93	0.62

Zone	Mass	IDA	Modal analysis			Pushover analysis				NLTH analysis			
a_g	m	check	T	T^*	Γ	Δ_y	F_y	μ	$\Delta_{u,st}$	HD force	Δ_{roof}	IDR	DI
$\frac{m}{s^2}$	[t]		[s]	[s]	[-]	[mm]	[kN]	[-]	[mm]	[kN]	[mm]	[-]	[-]
3- storey structure													
0.6	172.5	✓	1.51	1.70	1.256	53.19	262.9	1.06	180.6	292.3	44.97	0.81	0.28
1.0	172.5	✓	1.51	1.70				1.76		425.8	75.94	1.28	0.43
1.3	172.5	✓	1.51	1.70				2.29		446.1	81.72	1.39	0.45
1.6	172.5	x	1.51	1.70				2.820		529.3	114.20	2.0	0.67
	160.0	✓	1.43	1.63				2.720		513.0	103.2	1.80	0.56
4- storey structure													
0.6	100.0	✓	1.54	1.70	1.305	73.68	256.5	1.0	190.1	320.5	50.19	0.60	0.20
1.0	100.0	✓	1.54	1.70				1.32		460.6	79.87	0.95	0.30
1.3	100.0	✓	1.54	1.70				1.72		491.9	84.36	1.10	0.34
1.6	100.0	✓	1.54	1.70				2.12		570.5	111.70	1.46	0.44
5- storey structure													
0.6	60.0	✓	1.57	1.70	1.343	105.6	260.8	1.0	274.3	297.0	48.05	0.46	0.14
1.0	60.0	✓	1.57	1.70				1.0		458.4	80.60	0.68	0.22
1.3	60.0	✓	1.57	1.70				1.23		492.0	87.14	0.82	0.24
1.6	60.0	✓	1.57	1.70				1.51		598.3	115.8	1.09	0.32
6- storey structure													
0.6	39.0	✓	1.61	1.70	1.373	144.7	259.7	1.0	334.2	281.0	48.91	0.38	0.11
1.0	39.0	✓	1.61	1.70				1.0		430.7	82.15	0.56	0.17
1.3	39.0	✓	1.61	1.70				1.0		459.2	88.65	0.70	0.20
1.6	39.0	✓	1.61	1.70				1.13		593.2	123.3	0.98	0.29
7- storey structure													
0.6	26.0	✓	1.64	1.70	1.397	194.2	259.7	1.0	397.2	259.6	52.51	0.35	0.09
1.0	26.0	✓	1.64	1.70				1.0		405.5	84.30	0.52	0.14
1.3	26.0	✓	1.64	1.70				1.0		444.9	94.28	0.57	0.16
1.6	26.0	✓	1.64	1.70				1.0		561.1	125.0	0.78	0.23

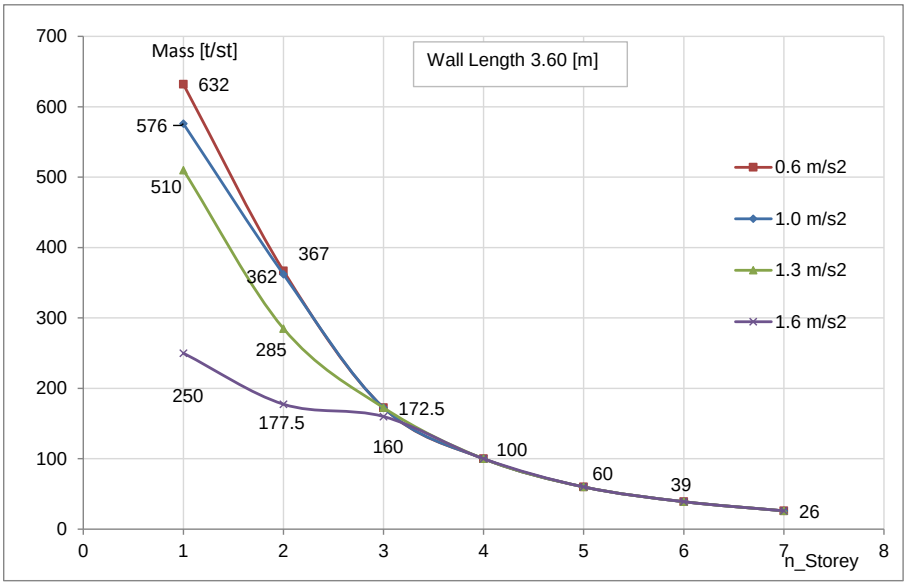

Fig. 7.3: Outcome of the parameter study of the 3.6 [m] LFTW element sheathed on both sides with OSB, see also Table 7.3

7.2.5 Tabular and graphical presentation of LFTW with a length of $4.2[m]$ sheathed on both sides with OSB

The results of the parametric study of the 4.20 [m] long LFTW element sheathed with OSB panels on both sides are summarized in Table 7.4. The typical, graphical presentation is given in Figure 7.4

Tab. 7.4: Results of the parameter study of the LFTW with a length of 4.2 [m] sheatehd on both sides with OSB

Zone	Mass	IDA	Modal analysis			Pushover analysis				NLTH analysis			
a_g	m	check	T	T^*	Γ	Δ_y	F_y	μ	$\Delta_{u,st}$	HD force	Δ_{roof}	IDR	DI
$\frac{m}{s^2}$	[t]		[s]	[s]	[-]	[mm]	[kN]	[-]	[mm]	[kN]	[mm]	[-]	[-]
1- storey structure													
0.6	734.0	✓	1.09	1.70	1.0	32.31	319.2	1.39	182.3	188.4	39.45	1.36	0.46
1.0	719.0	✓	1.08	1.68				2.30		224.4	60.0	2.07	0.70
1.3	693.5	x	1.06	1.64				2.97		226.0	64.72	2.22	0.70
	535.0	✓	0.93	1.37				2.76		222.5	59.68	2.06	0.57
1.6	367.0	x	0.77	1.06				3.00		239.3	71.25	2.46	0.66
	335.0	✓	0.74	1.0				2.90		238.4	68.05	2.35	0.60
2- storey structure													
0.6	512.5	✓	1.54	1.70	1.183	29.23	316.8	1.84	194.8	300.3	53.9	1.65	0.65
1.0	441.0	✓	1.42	1.58				2.83		380.7	73.17	1.97	0.70
1.3	300.0	✓	1.18	1.32				3.00		373.8	67.73	1.71	0.49
1.6	204.0	✓	0.97	1.09				3.00		383.3	78.73	2.1	0.55

Zone	Mass	IDA	Modal analysis			Pushover analysis				NLTH analysis			
a_g	m	check	T	T^*	Γ	Δ_y	F_y	μ	$\Delta_{u,st}$	HD force	Δ_{roof}	IDR	DI
$\frac{m}{s^2}$	[t]		[s]	[s]	[-]	[mm]	[kN]	[-]	[mm]	[kN]	[mm]	[-]	[-]
3- storey structure													
0.6	223.0	✓	1.48	1.70	1.255	47.77	307.0	1.17	136.8	355.2	46.55	0.89	0.29
1.0	223.0	✓	1.48	1.70				1.95		459.7	73.15	1.36	0.40
1.3	223.0	✓	1.48	1.70				2.53		468.4	80.42	1.42	0.41
1.6	186.0	x	1.33	1.55				2.86		530.6	99.75	1.81	0.52
	156.0	✓	1.24	1.41				2.61		523.8	94.36	1.73	0.48
4- storey structure													
0.6	132.0	✓	1.56	1.70	1.30	66.23	307.0	1.00	180.2	347.4	49.62	0.66	0.23
1.0	132.0	✓	1.56	1.70				1.46		480.6	71.37	0.85	0.25
1.3	132.0	✓	1.56	1.70				1.90		530.3	84.84	1.17	0.32
1.6	132.0	✓	1.56	1.70				2.34		628.3	101.70	1.17	0.29
5- storey structure													
0.6	80.0	✓	1.59	1.70	1.332	95.52	313.2	1.00	314.9	344.7	50.03	0.50	0.14
1.0	80.0	✓	1.59	1.70				1.04		519.0	82.18	0.73	0.21
1.3	80.0	✓	1.59	1.70				1.36		548.4	88.30	0.88	0.23
1.6	80.0	✓	1.59	1.70				1.67		662.3	115.7	1.19	0.31
6- storey structure													
0.6	51.5	✓	1.61	1.70	1.37	128.7	308.1	1.0	294.2	317.9	49.45	0.40	0.11
1.0	51.5	✓	1.61	1.70				1.00		480.7	82.14	0.60	0.16
1.3	51.5	✓	1.61	1.70				1.03		520.4	89.86	0.75	0.18
1.6	51.5	✓	1.61	1.70				1.27		644.6	122.0	1.02	0.25
7- storey structure													
0.6	34.5	✓	1.64	1.70	1.395	173.2	308.2	1.00	367.1	293.8	51.52	0.34	0.08
1.0	34.5	✓	1.64	1.70				1.00		452.6	84.46	0.52	0.13
1.3	34.5	✓	1.64	1.70				1.00		502.1	93.60	0.60	0.14
1.6	34.5	✓	1.64	1.70				1.00		631.7	124.7	0.84	0.20
8- storey structure													
0.6	24.0	✓	1.64	1.70	1.415	229.1	309.4	1.00	452.9	281.4	55.94	0.32	0.06
1.0	24.0	✓	1.64	1.70				1.00		436.8	88.70	0.48	0.10
1.3	24.0	✓	1.64	1.70				1.00		502.1	93.60	0.60	0.14
1.6	24.0	✓	1.64	1.70				1.00		631.7	124.7	0.84	0.20

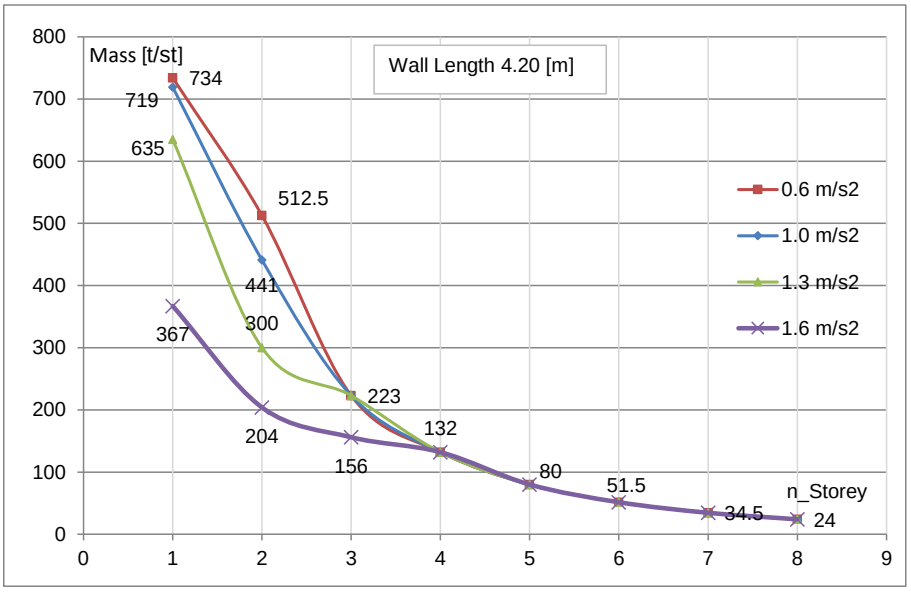

Fig. 7.4: Outcome of the parameter study of the 4.2 [m] LFTW element sheathed on both sides with OSB, see also Table 7.4

7.2.6 Tabular and graphical presentation of LFTW with a length of $4.8[m]$ sheathed on both sides with OSB

The results of the parametric study of the 4.8 [m] long LFTW element sheathed with OSB panels on both sides are summarized in Table 7.5. A typical, graphical presentation is given in Figure 7.5.

Tab. 7.5: Results of the parameter study of the LFTW with a length of 4.8 [m]sheazhed on both sides with OSB

Zone	Mass	IDA	Modal analysis			Pushover analysis				NLTH analysis			
a_g	m	check	T	T^*	Γ	Δ_y	F_y	μ	$\Delta_{u,st}$	HD force	Δ_{roof}	IDR	DI
$\frac{m}{s^2}$	[t]		[s]	[s]	[-]	[mm]	[kN]	[-]	[mm]	[kN]	[mm]	[-]	[-]
1- storey structure													
0.6	775.0	✓	1.1	1.70	1.0	35.33	371.1	1.27	162.2	182.6	38.69	1.33	0.40
1.0	775.0	✓	1.1	1.70				2.10		225.1	60.22	2.08	0.65
1.3	775.0	x	1.1	1.70				2.75		229.4	64.48	2.22	0.67
	600.0	✓	0.97	1.42				2.55		224.1	59.63	2.06	0.56
1.6	464.0	x	0.85	1.20				2.89		244.8	73.83	2.55	0.70
	377.5	✓	0.77	1.05				2.69		242.0	67.28	2.32	0.59
2- storey structure													
0.6	555.0	✓	1.55	1.70	1.18	30.53	366.8	1.73	176.7	287.4	51.78	1.60	0.55
1.0	525.0	✓	1.50	1.65				2.80		376.9	74.76	2.05	0.70
1.3	367.0	✓	1.26	1.40				3.0		358.7	69.45	1.80	0.51
1.6	247.0	✓	1.03	1.16				3.0		382.9	77.48	2.00	0.54

Zone	Mass	IDA	Modal analysis			Pushover analysis				NLTH analysis			
a_g	m	check	T	T^*	Γ	Δ_y	F_y	μ	$\Delta_{u,st}$	HD force	Δ_{roof}	IDR	DI
$\frac{m}{s^2}$	[t]		[s]	[s]	[-]	[mm]	[kN]	[-]	[mm]	[kN]	[mm]	[-]	[-]
3- storey structure													
0.6	232.5	✓	1.45	1.70	1.25	52.36	353.9	1.07	160.2	312.0	45.52	0.9	0.29
1.0	232.5	✓	1.45	1.70				1.78		448.1	75.62	1.30	0.38
1.3	232.5	✓	1.45	1.70				2.31		464.5	80.69	1.40	0.40
1.6	214.0	x	1.45	1.70				2.74		527.5	99.94	1.79	0.52
	184.5	✓	1.30	1.50				2.55		495.5	94.13	1.80	0.49
4- storey structure													
0.6	140.0	✓	1.50	1.70	1.295	69.96	355.0	1.00	198.4	339.9	48.42	0.67	0.19
1.0	140.0	✓	1.50	1.70				1.38		493.4	79.72	0.98	0.28
1.3	140.0	✓	1.50	1.70				1.79		515.2	83.34	1.16	0.31
1.6	140.0	✓	1.50	1.70				2.21		602.4	110.0	1.49	0.37
5- storey structure													
0.6	87.0	✓	1.59	1.70	1.331	97.66	356.9	1.00	247.50	323.9	46.86	0.50	0.13
1.0	87.0	✓	1.59	1.70				1.01		488.4	77.58	0.74	0.20
1.3	87.0	✓	1.59	1.70				1.32		532.1	86.25	0.88	0.23
1.6	87.0	✓	1.59	1.70				1.62		630.1	111.7	1.10	0.27
6- storey structure													
0.6	57.5	✓	1.59	1.70	1.36	130.2	355.3	1.0	301.1	306.2	47.23	0.40	0.11
1.0	57.5	✓	1.59	1.70				1.00		476.93	80.32	0.62	0.17
1.3	57.5	✓	1.59	1.70				1.01		523.0	88.45	0.75	0.21
1.6	57.5	✓	1.59	1.70				1.25		647.8	119.9	01.0	0.25
7- storey structure													
0.6	38.0	✓	1.61	1.70	1.386	172.5	356.7	1.00	370.8	288.0	49.31	0.34	0.09
1.0	38.0	✓	1.61	1.70				1.00		442.4	80.85	0.50	0.13
1.3	38.0	✓	1.61	1.70				1.00		486.0	89.45	0.60	0.15
1.6	38.0	✓	1.61	1.70				1.00		618.7	121.3	0.80	0.19
8- storey structure													
0.6	27.5	✓	1.64	1.70	1.41	223,7	356.7	1.00	453.4	267.6	51.37	0.31	0.07
1.0	27.5	✓	1.64	1.70				1.00		423.5	84.04	0.46	0.11
1.3	27.5	✓	1.64	1.70				1.00		467.8	93.18	0.50	0.12
1.6	27.5	✓	1.64	1.70				1.00		598.2	126.3	0.670	0.17

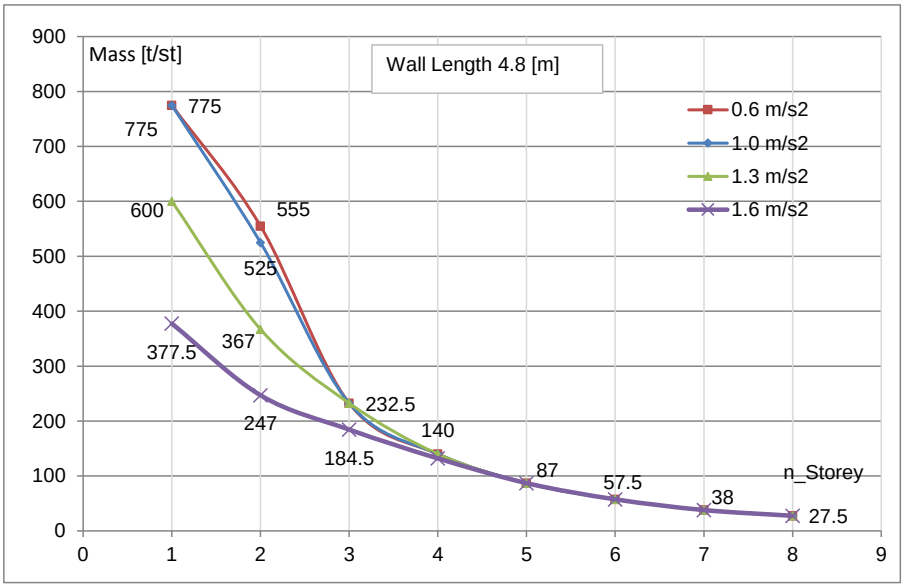

Fig. 7.5: Outcome of the parameter study of the 4.8 [m] LFTW element sheathed on both sides with OSB, see also table 7.5

7.3 Discussion

7.3.1 General considerations

LFTWs sheathed with OSB are used in timber structures in seismically prone regions due to their deformability and large ductility. The analyses performed and presented within this chapter show illustratively that, in all hazard zones, LFTWs sheathed with OSB can be used for structures with up to 7 or even 8 storeys. From Figures 7.1, 7.2, 7.3, 7.4 and 7.5, it can be seen that all LFTWs have the same admissible masses from 4- up to 8-storeys. This is due to the fact that the limiting period of $T^* = 1.7[s]$ is reached as soon as the structure has attained a height of 4-storeys and more. The admissible mass for a 4-storey structure is 60 and 140 [t/storey] for wall lengths of 2.4 [m] and 4.8 [m], respectively.

7.3.2 Inter-Storey Drift Ratio (IDR) and Damage Index (DI)

Similar to the squat LFTWs sheathed with GFB, low-rise LFTWs sheathed with OSB are also forced to develop larger IDRs and DIs than taller walls. The admissible mass decreases and the vibration period increases, with the structure height, resulting in continued reduction of IDR and DI.

From Tables 7.1 to 7.5, it can be seen that the limiting $IDR \leq 2.5$ and $DI \leq 0.7$, stipulated in Chapter 5, (see Table 5.7), have been estimated only for 1- and 2-storey structures in hazard zones Z1 and Z2. In hazard zones Z3a and Z3b, the limiting ductility demand $\mu = 3.0$ has been reached first. For all structures with 2- to 8-storeys, IDR and DI decrease rapidly with increasing structure height and decreasing the admissible masses.

7.3.3 Admissible mass and mass distribution

As discussed previously in Chapter 6, Section 6.3.3, the average evenly distributed storey mass active during an earthquake is assumed to be $450[\frac{kg}{m^2}]$. The admissible mass estimated for all LFTW elements decreases with increasing height of the structure, exhibiting the maximum value in the case of the 1-storey structures. Within the parameter study presented herein, the number of storeys is increased until the admissible mass reaches approximately 25 [t/storey]. The admissible mass value of 25 [t/storey] corresponds to a surface area of approximately A=25/0.45 = 56 $[m^2]$, which is considered to be in the lower range of practical applicability.
On the other hand, the average surface area of a housing unit is in the range of 120 and 150 $[m^2]$. Between two housing units, wall elements are commonly used as a physical separation. Thus, it is reasonable to assume that, the required physical separation can be constructed by using LFTWs able to sustain the lateral loads induced by winds and earthquakes. The mass induced from these areas and subjected to a single wall element is then approximately $(120 \div 150) \cdot 0.45 = 54 \div 67.5[t/storey]$, which is considered to be in the optimum range of practical applicability.

The admissible masses, estimated during the parameter study, presented in this chapter, reaching the values of approximately $70 \div 100[t/storey]$ are considered to be in the upper range of practical applicability. The corresponding surface area is defined by side dimensions of approximately $12 \div 15$ by $12 \div 15[m]$. The way the mass is distributed over each individual wall length is discernible, but a general statement that applies to all elements is not possible.

Walls with a length of 2.4 [m]

From Table 7.1 and Figure 7.1, it can be seen that the admissible mass $m_{adm} \geq 100[\frac{t}{storey}]$ has been estimated for 1- to 3-storey structures in seismic zones Z1, Z2 and Z3a, and for 2-storey structures in seismic zone Z3b. One can see that, due to the large admissible mass, even in the case of a short wall length of 2.4 [m], the earthquake excitation will not be the limiting criteria for the applicability of LFTWs in structures of up to three storeys. Furthermore, the optimum range of applicability of the 2.4 [m] LFTW is for structures of up to 4-storeys. Due to the limitation provided by the inelastic period of vibration T^* =1.7 [s], the same admissible mass of $60[t/storey]$ has been estimated for 4-storey structures in all hazard zones. The use of 2.4[m] LFTWs for 5- and 6-storey structures is not in the optimum range from an economical point of view, but quite possible regarding the technical aspect.

Walls with a length of 3.0 [m]

From Table 7.2 and Figure 7.2, it can be seen that admissible masses of $m_{adm} \geq 100[\frac{t}{storey}]$ have been estimated for 1- to 3-storey structures in all seismic zones. The optimum range of applicability of 3.0 [m] LFTWs is for structures with up to 5-storeys, with a corresponding

admissible mass of 54.0 [t/storey]. The 3.0 [m] long LFTWs could be used for structures up to 6 storeys with a corresponding admissible mass of 33.5 [t/storey].

Due to the limitation provided by the inelastic period of vibrations T^* =1.7 [s], the same admissible masses for all hazard zones have been estimated for all structures with 4 and more storeys.

Walls with a length of 3.6 [m]

From Table 7.3 and Figure 7.3, it can be seen that the admissible masses $m_{adm} \geq 100[\frac{t}{storey}]$ have been estimated for 1- to 4-storey structures in all seismic zones. The optimum range of applicability of 3.6 [m] LFTWs is for structures of up to 5-storeys, with a corresponding admissible mass of 60.0 [t/storey]. The 3.6 [m] long LFTWs could be used up to 7 storeys with a corresponding admissible mass of 26 [t/storey].

Due to the limitation provided by the inelastic period of vibrations T^* =1.7 [s], the same admissible masses for all hazard zones have been estimated for all structures with 4 and more storeys.

Walls with a length of 4.2 [m]

From Table 7.4 and Figure 7.4, it can be seen that the admissible masses $m_{adm} \geq 100[\frac{t}{storey}]$ have been estimated for 1- to 4-storey structures in all seismic zones. The optimum range of applicability of 4.2 [m] LFTW is for strcutures of up to 6-storeys, with corresponding admissible mass of 51.5 [t/storey]. The 4.2 [m] long LFTWs could be reasonably used for structures of up to 7 storeys with a corresponding admissible mass of 34.5 [t/storey]. From the technical point of view, the 4.2 [m] LFTWs could be used even for 8-storey structures, with an admissible mass of merely 24.0 [t/storey].

Due to the limitation provided by the inelastic period of vibrations T^* =1.7 [s], the same admissible masses for all hazard zones have been estimated for all structures with 4 and more storeys.

Walls with a length of 4.8 [m]

From Table 7.5 and Figure 7.5, it can be seen that the admissible masses $m_{adm} \geq 100[\frac{t}{storey}]$ have been estimated for 1- to 4-storey structures in all seismic zones. The optimum range of applicability of 4.8 [m] long LFTWs is for structures of up to 6-storeys, with a corresponding admissible mass of 57.5 [t/storey]. The 4.8 [m] long LFTWs could be reasonably used for structures of up to 7 storeys with corresponding admissible mass of 38.0 [t/storey]. From the technical point of view, the 4.8 [m] LFTWs could also be used even for 8-storey structures, with an admissible mass of merely 27.5 [t/storey].

Due to the limitation provided by the inelastic period of vibrations T^* =1.7 [s], the same admissible masses for all hazard zones have been estimated for all structures with 4 and more storeys.

7.3.4 Ductility demand

Since the LFTWs which behave in the inelastic range even in the case of small displacements, the definition of ductility is not an easy issue. In the parameter study performed and presented in this chapter, the ductility has been estimated by using the Equal-Energy-Elastic-Plastic (EEEP) bi-linear approximation [22] for estimation of the yield displacement and the yield force in the pushover analysis. The initial stiffness has been defined through the point on the pushover curve at $0.4F_{max}$ (see also Figure 6.25). Within the parameter study presented, it has been observed that the limitation of the ductility demand governs the design for all wall lengths in the cases of 1- and 2-storey structures in hazard zones Z3a and Z3b. In all other cases, the ductility demand is $\mu \leq 3.0$.

7.3.5 Hold-Down forces

As already observed for the LFTWs sheathed with GFB, the hold-down forces vary little with respect to the number of storeys for all wall lengths and hazard zones. So, the HD force for the 1- storey LFTW element is in the range between 170 and 210 [kN]. The HD forces for the wall lengths of 2.4[m] and 4.8 [m] are 183 and 242 [kN], respectively. Maximum HD forces have been estimated in the range between 560 and 660 [kN] in the cases of 5- and 6-storey structures of all wall lengths. According to Chapter 3, the required bearing capacity of the HD-devices is between 760 and 890 [kN], in order to continue to respond in the elastic range. Hence, HDs with three slotted in steel plates and 12 or 16 dowels with d=16 [mm] are required. Studs proportioned to $300 \cdot 300[mm]$ have been used.

7.3.6 Control of parameter study using IDA analysis

The parameter study performed within this chapter is based on the pushover and NLTHA analyses. The pushover analysis provides yield displacement and yield force, as well as maximum displacement capacity (see also Figure 6.25). The NLTHA provides HD-forces, roof displacements, inter-storey drift ratios, storey accelerations and displacements, and damage indexes. During the parameter study, measures were taken to ensure that all pre-defined conditions are satisfied. Only the results which have satisfied the limitations defined in advance, have been adopted as valid outcomes of the deterministic parameter analyses. Let us consider, for example, the results obtained by analyzing a 1-storey structure with a 2.4 [m] wall length. The limitation given by the inelastic period of vibrations $T^* = 1.7[s]$ is reached first for seismic zone Z1 and a mass of 500 [t]. The limiting $IDR = 2.0 \leq 2.5$ and $DI = 0.65 \leq 0.7$, as well as HD forces are not reached yet. For the structure in seismic zone Z2 with a mass of 408 [t], maximum DI of 0.7 is reached first, while the ductility, the period of vibration, the HD-forces as well as the IDR are still below the corresponding limit values. In the seismic zones Z3a and Z3b, the maximum ductility demand $\mu = 3.0$ is reached first, while the other control parameters are still below the corresponding limit values. An additional, independent model, capable of validating the results obtained from the pushover and the NLTHA analyses has been used to control the outcomes

of the parameter study. The probabilistic method used for this control is incremental dynamic analysis (IDA), introduced in Chapter 4. A great majority of all analyses performed by means of NLTHA have passed the IDA check. However, some of them failed. The analyses failing the IDA check have been marked in Tables 7.1 to 7.5 by the failure sign "×" and have been analyzed further within the IDA-analysis framework until passing the IDA check. Unlike the IDA check for the LFTWs sheathed with GFB, where the maximum estimated admissible masses have differed significantly for different wall lengths and hazard zones, the LFTWs sheathed with OSB behave similarly in the cases of all wall lengths and structures with over 4-storeys in all seismic hazard zones. The results of the IDA analysis for 4-storey structures for all hazard zones and the corresponding wall lengths are presented in this section.

Figure 7.6 shows the check for a 4-storey structure in all hazard zones for the same admissible mass of 60 [t/storey]. This mass is considered to be in the optimum range for the 2.4 [m] LFTWs. In Figure 7.6, it can be seen that the damage measure for the life safety limit state, defined as a roof drift of 168 [mm], which is 1.45% of the total building height, will be reached for a spectral acceleration of $S_{a,T=1.7[s]}$ of 1.9 $[m/s^2]$. This acceleration is much higher then the accelerations which are to be expected in Zone Z1 (0.6 $[m/s^2]$), Z2 (1.0 $[m/s^2]$); Z3a (1.31 $[m/s^2]$) and Z3b (1.62 $[m/s^2]$). Thus, the structure has passed the IDA check for all seismic hazard zones, characterized by ground accelerations 0.6, 1.0, 1.3 and 1.6 $[m/s^2]$.

Figure 7.7 presents the check for a 4-storey structure in all hazard zones for the same admissible mass of 92 [t/storey]. This mass has been considered to be in the upper range for the 3.0 [m] LFTWs. From Figure 7.7, it is evident that the damage measure for the life safety limit state, defined as a roof drift of 158 [mm], which is 1.36% of the total building height, will be reached for a spectral acceleration of $S_{a,(T=1.68[s])}$ of 1.83 $[m/s^2]$. This acceleration is much higher than the accelerations which are to be expected in zones Z1 (0.62 $[m/s^2]$), Z2 (1.03

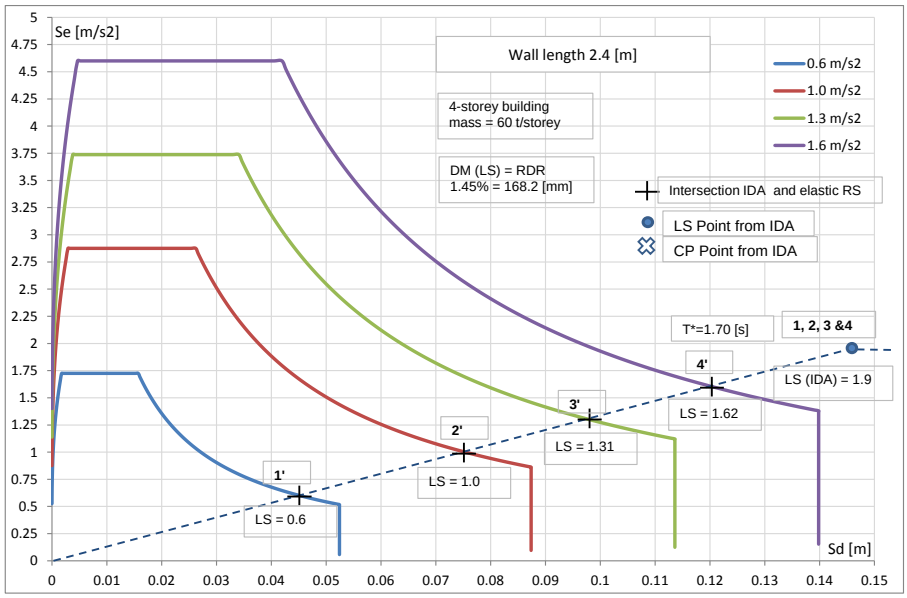

Fig. 7.6: IDA-control of the 4-storey 2.4 [m] LFTW for a mass of 60 [t/storey]

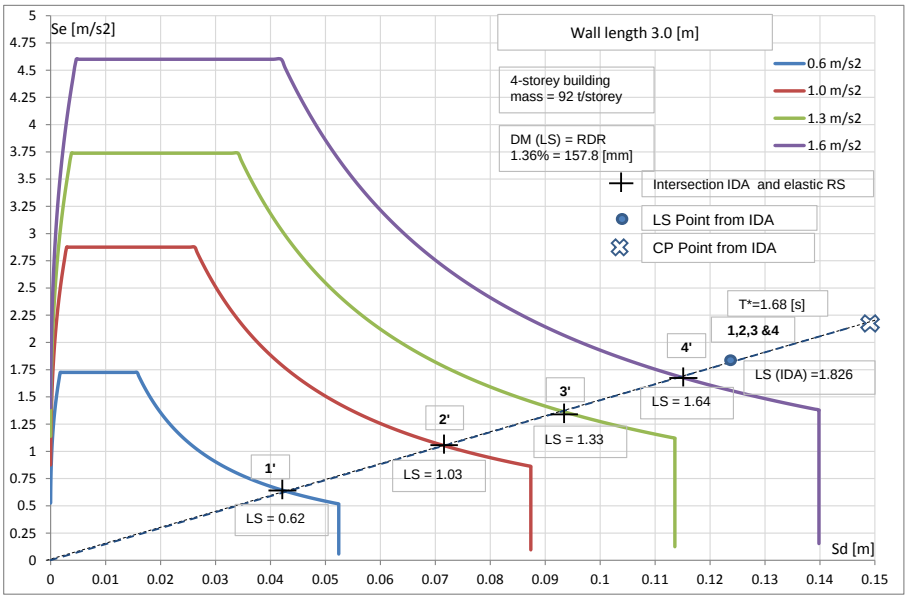

Fig. 7.7: IDA-control of the 4-storey 3.0 [m] LFTW for a mass of 92 [t/storey]

$[m/s^2]$); Z3a (1.33 $[m/s^2]$) and Z3b (1.64 $[m/s^2]$). Note that the inelastic period of vibration estimated within the IDA by a quadrilinear fit of the pushover curve is $T^* = 1.68[s]$. This is slightly less then $T^* = 1.70[s]$, estimated by using the EEEP rule within the pushover analysis carried out in the parameter study.

Figure 7.8 shows the check for a 4-storey structure in all hazard zones for the same admissible mass of 100 [t/storey]. This mass is considered to be within the upper limit of the upper range for the 3.6 [m] LFTWs. From Figure 7.8, it can be seen that the damage measure for the life safety limit state, defined as a roof drift of 150 [mm], which is 1.30% of the total building height,

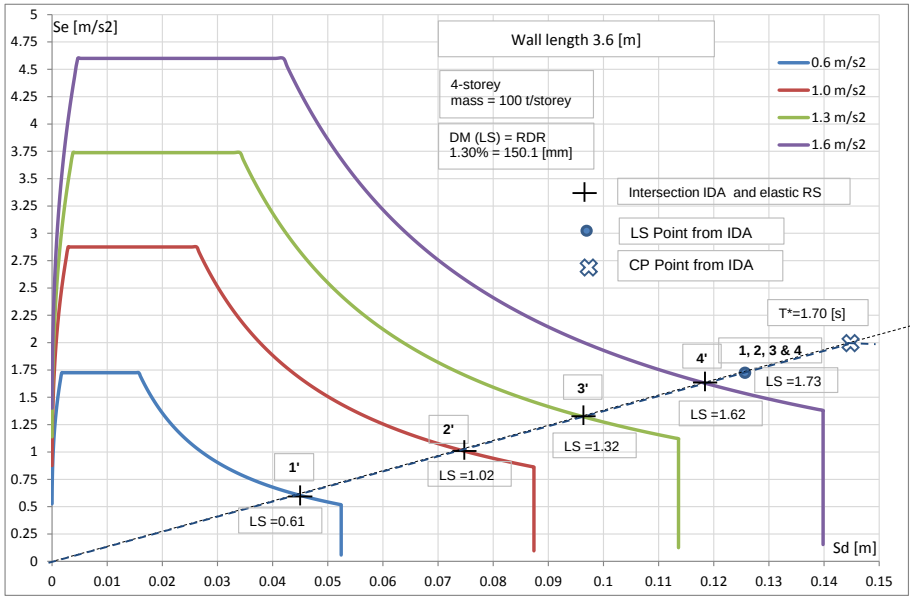

Fig. 7.8: IDA-control of the 4-storey 3.6 [m] LFTW for a mass of 100 [t/storey]

will be reached for a spectral acceleration of $S_{a,(T=1.70[s])}$ of 1.73 $[m/s^2]$. This acceleration is much higher than the accelerations which can be expected in zones Z1 (0.61 $[m/s^2]$), Z2 (1.02 $[m/s^2]$); Z3a (1.32 $[m/s^2]$) and Z3b (1.62 $[m/s^2]$). Note that the inelastic period of vibration, estimated within the IDA Analysis by a quadrilinear fit of the pushover curve, is $T^* = 1.70[s]$. This is equal to the period estimated by using the EEEP rule within the pushover analysis performed in the parameter study.

Figure 7.9 presents the check for a 4-storey structure in all hazard zones for the same admissible mass of 132 [t/storey]. This mass is considered to be above the upper range for the 4.2 [m] LFTWs, giving a corresponding wall surface area of approximately 293 $[m^2]$, defined as a surface with side dimensions of approximately 17 by 17 [m]. In Figure 7.9, it is evident that the damage measure for the life safety limit state, defined as a roof drift of 150 [mm], which is 1.30% of the total building height, will be reached for a spectral acceleration of $S_{a,(T=1.69[s])}$ of 1.75 $[m/s^2]$. This acceleration is more than the accelerations which are to be expected in zones Z1 (0.61 $[m/s^2]$), Z2 (0.1.02 $[m/s^2]$); Z3a (1.33 $[m/s^2]$) and Z3b (1.63 $[m/s^2]$). Note that the inelastic period of vibration estimated within the IDA by a quadrilinear fit of the pushover curve is $T^* = 1.69[s]$. This is slightly smaller than the period of $T^* = 1.70[s]$, estimated by use of the EEEP rule within the pushover analysis conducted in the parameter study.

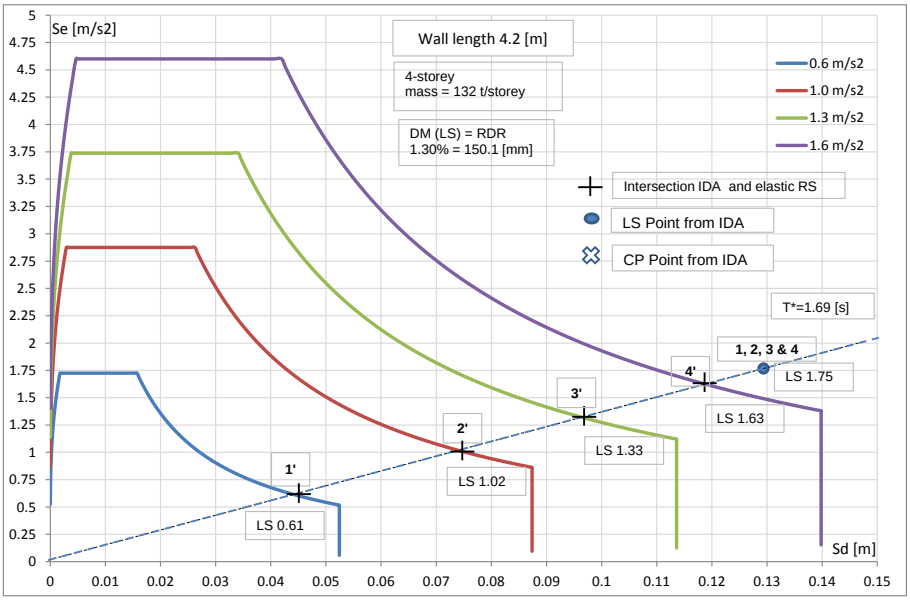

Fig. 7.9: IDA-control of the 4-storey 4.2 [m] LFTW for a mass of 132 [t/storey]

Figure 7.10 presents the check for a 4-storey structure in all hazard zones for the same admissible mass of 140 [t/storey]. This mass has been considered to be above the upper range for the 4.8 [m] LFTWs, giving a corresponding wall surface area of approximately 311 $[m^2]$, defined as a surface with side dimensions of approximately 17.6 by 17.6 [m]. In Figure 7.10, it is obvious that the damage measure for the life safety limit state, defined as a roof drift of 150 [mm], which is 1.30% of the total building height, will be reached for spectral acceleration of $S_{a,(T=1.68[s])}$ of 1.75 $[m/s^2]$. This acceleration exceeds the accelerations which are to be expected

in zones Z1 (0.61 $[m/s^2]$), Z2 (0.1.02 $[m/s^2]$); Z3a (1.33 $[m/s^2]$) and Z3b (1.63 $[m/s^2]$). Note that the inelastic period of vibration $T^* = 1.68[s]$ estimated within the IDA by a quadrilinear fit of the pushover curve is slightly below the period of $T^* = 1.70[s]$, estimated by using of the EEEP rule within the pushover analysis carried out in the parameter study.

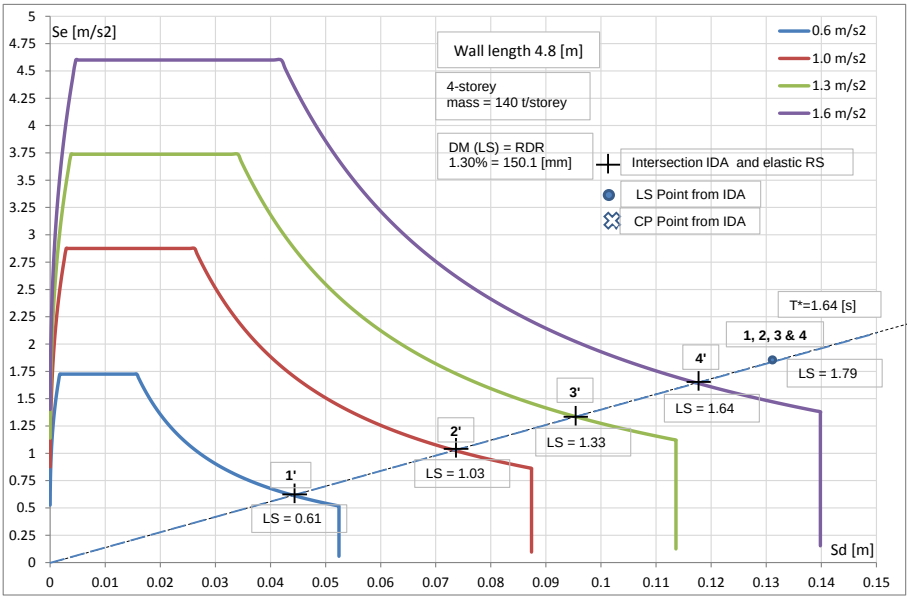

Fig. 7.10: IDA-control of the 4-storey 4.8 [m] LFTW for a mass of 140 [t/storey]

Chapter 8

Parameter Study of LFTW Sheathed with GFB

In this chapter, the parameter study for LFTWs sheathed with GFB is performed. The results of the parameter study are summarized in tabular and graphical form. The IDA analysis is performed for each run in parallel. The mass, which satisfies all conditions, is adopted.

8.1 Introduction

Within the parameter study presented in this chapter, the mechanical model of the LFTW sheathed on both sides with GFB developed in Chapter 3 and summarized in Tables 3.14 to 3.18 has been used. Sheathing panels have a thickness of $t_p = 15[mm]$. Staples with d = 1.53[mm], spaced at 35[mm], have been used as fasteners to connect the GFB with the timber frame. The analyses have been performed for all wall elements, characterized by their lengths of $2.4, 3.0, 3.6, 4.2$ or $4.8[m]$, and seismic hazard zones, characterized by design ground accelerations of $0.6, 1.0, 1.3$ or $1.6[\frac{m}{s^2}]$, corresponding to the hazard zones $Z1, Z2, Z3a$ or $Z3b$, as stipulated by the SIA code [3].
Only soil category C will be considered in this chapter. Soil conditions C have been chosen for the parameter study because the peak amplification and the edge periods on the plateau are in the median range for dense soils. The results for soil categories A (stiff soil) and E (soft soil) are attached in Appendix A. The outcome of the parameter analysis is the maximum mass applicable at each storey of the structure under consideration so that all the performance limits for the life safety (LS) limit state, derived in Chapter 5, are satisfied. The analyses are based on parameters described in Chapter 6.

8.2 Parameter Study

8.2.1 General considerations

The outcome of the parameter study is presented in both tabular and chart format. The results in the tabular format are divided into the following sub-analysis parts:

- Check by means of IDA analysis
- Modal analysis
- Pushover analysis
- NLTHA

All the results of the parametric study have been subsequently also checked by means of IDA- analysis, as presented in Chapter 5. Only the results relevant for application in practice are presented graphically. See also subsection 6.3.6.
The damage index (DI) as the result of the damage analysis has been estimated by using the parameter β_{DI} according to Table 5.5.

8.2.2 Tabular and graphical presentation of LFTW with a length of $2.4[m]$ sheathed on both sides wirh GFB

The results of the parametric study for a 2.4 [m] long LFTW element sheathed on both sides with GFB are summarized in Table 8.1. The typical, graphical presentation is given in Figure 8.1

Tab. 8.1: Results of the parameter study of a LFTW with a length of 2.4 [m] sheathed on both sides with GFB

Zone	Mass	IDA	Modal analysis			Pushover analysis				NLTH analysis			
a_g	m	check	T	T^*	Γ	Δ_y	F_y	μ	$\Delta_{u,st}$	HD force	Δ_{roof}	IDR	DI
$[\frac{m}{s^2}]$	[t]		[s]	[s]	[-]	[mm]	[kN]	[-]	[mm]	[kN]	[mm]	[-]	[-]
1- storey structure													
0.6	138.0	✓	0.70	0.85	1.0	11.52	86.06	1.94	31.95	106.8	22.21	0.77	0.79
1.0	72.5	✓	0.52	0.61				2.50		119.1	23.19	0.80	0.80
1.3	57.0	✓	0.45	0.52				2.49		118.3	23.74	0.82	0.80
1.6	39.0	x	0.38	0.43				2.10		120.5	24.0	0.83	0.80
	36.0	✓	0.36	0.41				1.93		116.1	21.88	0.75	0.73
2- storey structure													
0.6	67.8	✓	0.83	0.93	1.19	17.8	85.0	1.63	41.48	152.2	27.04	0.67	0.69
1.0	43.3	✓	0.67	0.75				2.19		183.2	31.96	0.80	0.80
1.3	28.5	✓	0.55	0.60				2.31		183.7	31.25	0.75	0.73
1.6	22.0	x	0.48	0.53				2.20		190.0	33.59	0.82	0.80
	19.5	✓	0.45	0.49				1.96		181.9	29.89	0.72	0.70

Zone	Mass	IDA	Modal analysis			Pushover analysis				NLTH analysis			
a_g	m	check	T	T^*	Γ	Δ_y	F_y	μ	$\Delta_{u,st}$	HD force	Δ_{roof}	IDR	DI
$[\frac{m}{s^2}]$	[t]		[s]	[s]	[-]	[mm]	[kN]	[-]	[mm]	[kN]	[mm]	[-]	[-]
3- storey structure													
0.6	47.4	✓	1.05	1.14	1.26	27.86	83.17	1.35	52.9	208.8	35.5	0.62	0.63
1.0	31.6	x	0.86	0.93				1.85		239.5	42.99	0.74	0.75
	28.5	✓	0.81	0.88				1.76		228.6	39.36	0.65	0.66
1.3	18.4	✓	0.65	0.71				1.83		232.2	37.79	0.60	0.58
1.6	12.24	✓	0.53	0.58				1.77		233.7	38.01	0.58	0.57
4- storey structure													
0.6	47.4	✓	1.46	1.55	1.31	42.58	83.67	1.25	76.64	226.3	44.42	0.71	0.77
1.0	24.80	✓	1.06	1.12				1.50		281.8	53.63	0.80	0.80
1.3	18.35	x	0.94	0.99				1.73		292.0	55.52	0.65	0.64
	17.5	✓	0.89	0.94				1.65		276.6	51.22	0.60	0.60
1.6	12.24	x	0.74	0.79				1.69		302.8	57.85	0.74	0.73
	11.0	✓	0.70	0.74				1.62		291.3	54.88	0.69	0.68
5- storey structure													
0.6	32.6	✓	1.63	1.69	1.35	63.73	83.89	1.0	103.1	241.5	50.43	0.47	0.50
1.0	20.1	✓	1.28	1.32				1.23		291.0	62.96	0.58	0.60
1.3	15.8	✓	1.13	1.17				1.42		322.0	69.5	0.64	0.63
1.6	9.2	✓	0.86	0.89				1.33		316.7	67.6	0.68	0.67

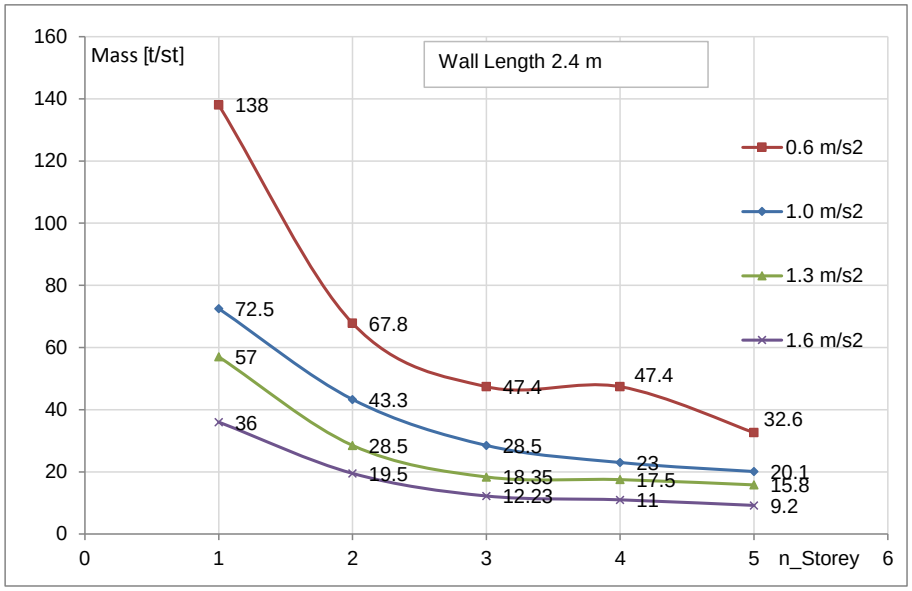

Fig. 8.1: Result of the parameter study of the LFTW sheathed on both sides with GFB with a length of 2.4 [m], see also Table 8.1

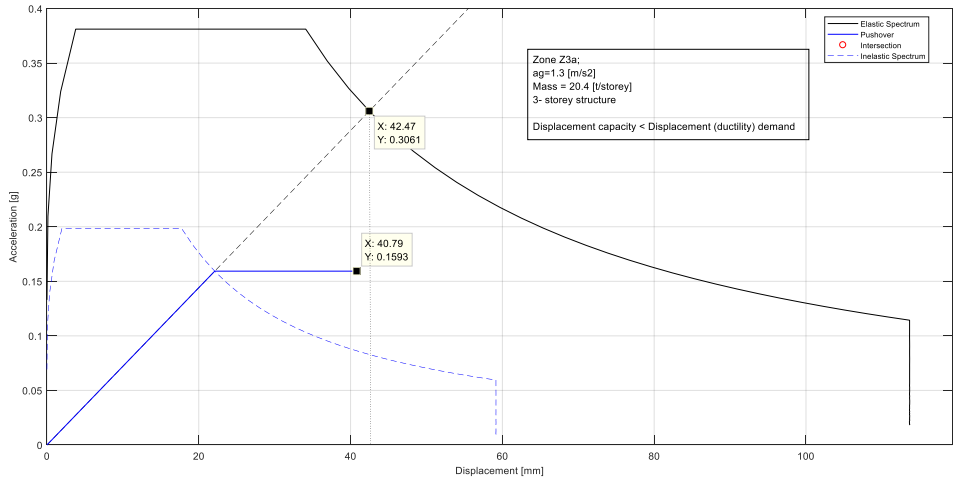

(a)

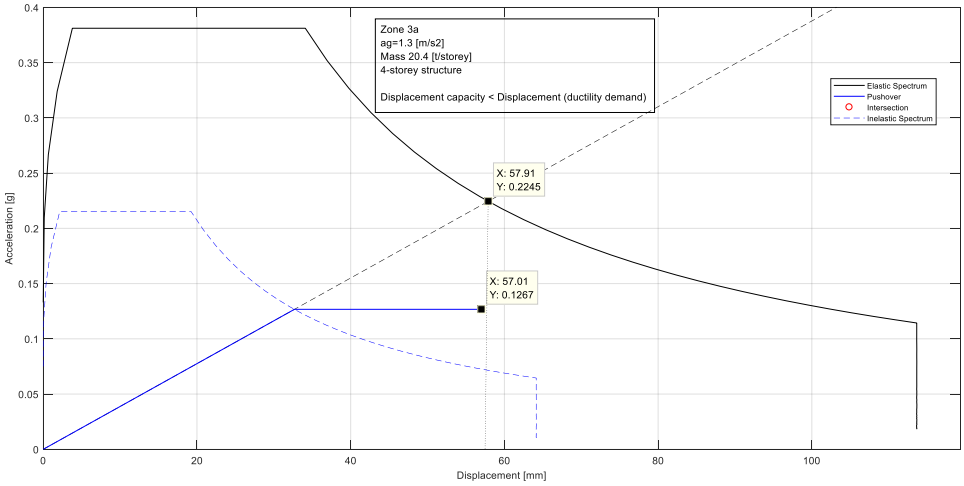

(b)

Fig. 8.2: YPS- representation of displacement capacity and displacement (ductility) demand for a 3-storey structure with a mass of 20.4 [t] at each storey 8.2(a): Displacement capacity and displacement (ductility) demand for a 4-storey structure with a mass of 20.4 [t] in each storey 8.2(b)

8.2.3 Tabular and graphical presentation of LFTW with a length of $3.0[m]$ sheathed on both sides with GFB

The results of the parametric study for a 3.0 [m] long LFTW element sheathed on both sides with GFB are summarized in Table 8.2. The typical, graphical presentation is given in Figure 8.3

Tab. 8.2: Results of the parameter study of a LFTW with a length of 3.0 [m] sheathed on both sides with GFB

Zone	Mass	IDA	Modal analysis			Pushover analysis				NLTH analysis			
a_g	m	check	T	T^*	Γ	Δ_y	F_y	μ	$\Delta_{u,st}$	HD force	Δ_{roof}	IDR	DI
$[\frac{m}{s^2}]$	[t]		[s]	[s]	[-]	[mm]	[kN]	[-]	[mm]	[kN]	[mm]	[-]	[-]
1- storey structure													
0.6	139.0	✓	0.75	0.88	1.0	16.83	119.6	1.37	40.41	114.9	24.9	0.86	0.80
1.0	78.0	x	0.55	0.64				1.77		128.7	26.5	0.90	0.80
	65.0	✓	0.51	0.58				1.57		121.1	23.07	0.80	0.72
1.3	58.6	x	0.48	0.55				1.84		129.8	27.8	0.95	0.80
	50.0	✓	0.44	0.50				1.57		124.5	24.72	0.85	0.72
1.6	43.3	x	0.42	0.47				1.67		130.9	27.5	0.95	0.80
	40.0	✓	0.40	0.45				1.54		130.1	27.15	0.94	0.80
2- storey structure													
0.6	88.0	✓	1.0	1.08	1.19	25.3	118.1	1.33	44.57	188.7	35.3	0.80	0.78
1.0	46.0	✓	0.71	0.78				1.60		201.9	39.33	0.86	0.77
1.3	35.7	x	0.63	0.69				1.84		210.7	41.17	0.91	0.77
	30.0	✓	0.58	0.63				1.69		206.8	40.0	0.85	0.73
1.6	24.5	✓	0.52	0.57				1.78		214.8	42.48	0.90	0.77
3- storey structure													
0.6	73.4	✓	1.3	1.43	1.25	38.0	115.1	1.23	64.52	217.2	42.72	0.68	0.71
1.0	37.7	✓	0.94	1.02				1.48		266.1	53.34	0.84	0.78
1.3	30.0	✓	0.83	0.90				1.71		258.9	50.49	0.82	0.71
1.6	16.8	✓	0.63	0.68				1.58		279.2	55.05	0.86	0.73
4- storey structure													
0.6	52.5	✓	1.50	1.60	1.3	54.79	116.4	1.0	91.36	234.3	48.85	0.56	0.60
1.0	32.0	✓	1.17	1.25				1.29		305.3	66.47	0.78	0.76
1.3	27.5	x	1.08	1.16				1.56		318.8	70.12	0.9	0.8
	25.5	✓	1.04	1.11				1.5		323.4	69.75	0.84	0.79
1.6	14.8	✓	0.78	0.85				1.4		316.2	67.56	0.81	0.71
5- storey structure													
0.6	36.0	✓	1.60	1.69	1.33	75.94	116.1	1.0	119.6	243.1	54.71	0.48	0.53
1.0	27.0	✓	1.39	1.46				1.12		331.6	77.32	0.66	0.68
1.3	24.5	✓	1.32	1.39				1.39		346.7	84.05	0.76	0.65
1.6	11.5	✓	0.89	0.94				1.16		342.7	78.66	0.77	0.67
6- storey structure													
0.6	23.5	✓	1.63	1.69	1.36	103.4	116.6	1.0	157.0	219.0	55.23	0.42	0.42
1.0	23.5	✓	1.63	1.49				1.0		346.4	90.53	0.68	0.62
1.3	21.5	✓	1.56	1.61				1.21		352.9	92.84	0.69	0.67

1.6	8.0	✓	0.96	0.99		1.0	347.6	88.06	0.65	0.56

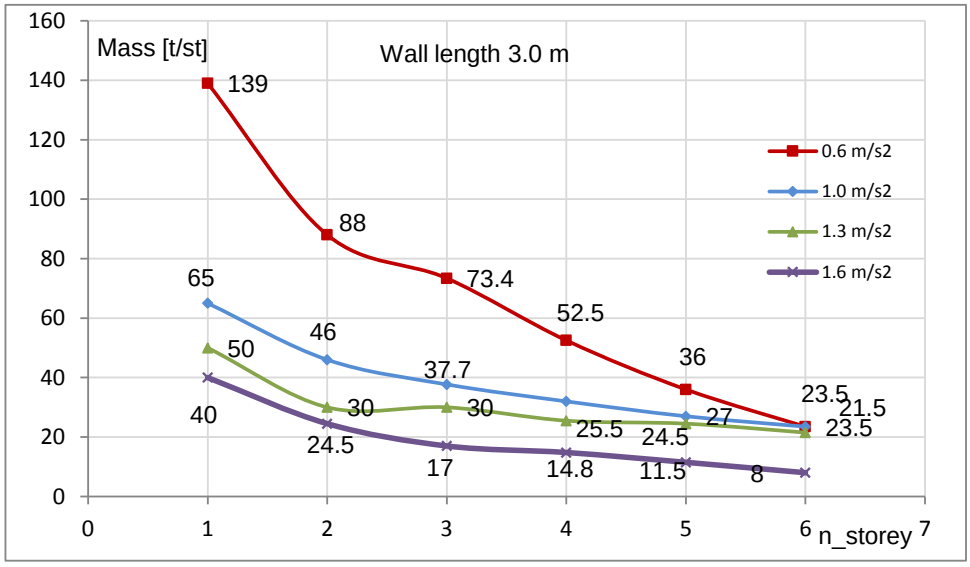

Fig. 8.3: Result of the parameter study of the 3.0 [m] LFTW element sheathed with GFB on both sides, see also Table 8.2.

8.2.4 Tabular and graphical presentation of LFTW with a length of $3.6[m]$ sheathed on both sides with GFB

The results of the parametric study for a 3.6 [m] long LFTW element sheathed on both sides with GFB are summarized in Table 8.3. The typical, graphical presentation is given in Figure 8.4

Tab. 8.3: Results of the parameter study of a LFTW with a length of 3.6 [m]. sheathed on both sides with GFB

Zone	Mass	IDA	Modal analysis			Pushover analysis				NLTH analysis			
a_g	m	check	T	T^*	Γ	Δ_y	F_y	μ	$\Delta_{u,st}$	HD force	Δ_{roof}	IDR	DI
$[\frac{m}{s^2}]$	[t]		[s]	[s]	[-]	[mm]	[kN]	[-]	[mm]	[kN]	[mm]	[-]	[-]
1- storey structure													
0.6	178.5	✓	0.73	0.90	1.0	16.39	141.0	1.45	39.62	113.8	23.14	0.80	0.77
1.0	98.0	x	0.54	0.64				1.87		127.1	25.31	0.87	0.8
	95.0	✓	0.54	0.63				1.85		126.4	24.43	0.84	0.77
1.3	73.5	x	0.47	0.54				1.95		127.6	26.41	0.91	0.79
	71.0	✓	0.46	0.53				1.89		127.3	25.37	0.87	0.76
1.6	54.0	✓	0.4	0.46				1.77		129.5	26.48	0.91	0.80

Zone	Mass	IDA	Modal analysis			Pushover analysis				NLTH analysis			
a_g	m	check	T	T^*	Γ	Δ_y	F_y	μ	$\Delta_{u,st}$	HD force	Δ_{roof}	IDR	DI
$[\frac{m}{s^2}]$	[t]		[s]	[s]	[-]	[mm]	[kN]	[-]	[mm]	[kN]	[mm]	[-]	[-]
2- storey structure													
0.6	107.0	✓	0.94	1.04	1.18	22.44	139.3	1.43	50.16	188.0	33.17	0.75	0.77
1.0	58.0	✓	0.70	0.76				1.76		205.5	37.22	0.83	0.78
1.3	46.0	x	0.62	0.68				2.04		211.0	40.09	0.89	0.79
	36.5	✓	0.55	0.60				1.82		201.6	35.14	0.78	0.67
1.6	31.0	x	0.51	0.56				1.92		217.2	40.93	0.89	0.8
	25.0	✓	0.46	0.50				1.54		121.5	32.33	0.72	0.62
3- storey structure													
0.6	91.7	✓	1.27	1.39	1.25	34.45	138.2	1.31	58.83	225.9	41.52	0.70	0.78
1.0	46.0	✓	0.89	0.97				1.56		26.3	49.95	0.82	0.79
1.3	38.75	x	0.82	0.90				1.87		267.2	49.95	0.87	0.78
	31.0	✓	0.74	0.8				1.67		260.0	46.11	0.73	0.65
1.6	21.5	x	0.61	0.66				1.71		283.4	52.93	0.88	0.78
	17.0	✓	0.55	0.59				1.54		252.6	43.84	0.66	0.58
4- storey structure													
0.6	66.0	✓	1.45	1.56	1.29	48.18	137.2	1.1	80.49	245.4	46.92	0.60	0.64
1.0	40.8	✓	1.13	1.22				1.43		316.5	63.58	0.77	0.79
1.3	30.0	x	0.98	1.04				1.60		318.7	62.18	0.72	0.66
	27.0	✓	0.93	0.99				1.52		306.8	54.4	0.66	0.61
1.6	18.86	✓	0.77	0.83				1.56		332.3	65.31	0.83	0.76
5- storey structure													
0.6	48.8	✓	1.62	1.70	1.327	65.95	136.4	1.0	106.6	262.7	54.43	0.50	0.58
1.0	32.6	✓	1.33	1.39				1.22		342.6	74.1	0.69	0.72
1.3	28.5	✓	1.22	1.3				1.49		357.1	78.49	0.78	0.74
1.6	13.75	✓	0.85	0.90				1.27		353.2	72.31	0.71	0.65
6- storey structure													
0.6	32.0	✓	1.63	1.70	1.356	89.14	136.9	1.0	138.6	245.8	55.44	0.43	0.47
1.0	31.1	✓	1.6	1.68				1.12		358.2	86.92	0.66	0.72
1.3	25.0	✓	1.43	1.50				1.3		370.6	86.98	0.62	0.63
1.6	10.0	✓	1.91	0.96				1.03		363.7	81.21	0.59	0.54
7- storey structure													
0.6	22.0	✓	1.64	1.70	1.38	117.6	136.9	1.0	177.5	227.8	55.93	0.38	0.37
1.0	22.0	✓	1.65	1.70				1.0		355.3	91.54	0.38	0.58
1.3	22.0	✓	1.65	1.70				1.14		380.5	100.1	0.69	0.68
1.6	8.0	✓	1.0	1.04				1.0		386.1	94.94	0.57	0.51

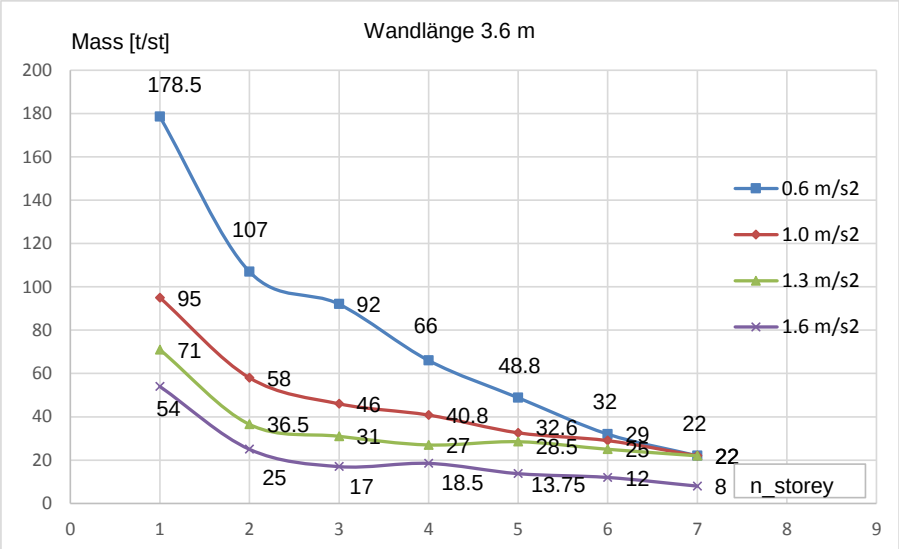

Fig. 8.4: Result of the parameter study of the 3.6 [m] LFTW element sheathed with GFB on both sides, see also Table 8.3

8.2.5 Tabular and graphical presentation of LFTW with a length of $4.2[m]$ sheathed on both sides with GFB

The results of the parametric study for a 4.2 [m] long LFTW element sheathed on both sides with GFB are summarized in Table 8.4. The typical, graphical presentation is given in Figure 8.5

Tab. 8.4: Results of the parameter study of a LFTW with a length of 4.2 [m]sheathed on both sides with GFB

Zone	Mass	IDA	Modal analysis			Pushover analysis				NLTH analysis			
a_g	m	check	T	T^*	Γ	Δ_y	F_y	μ	$\Delta_{u,st}$	HD force	Δ_{roof}	IDR	DI
$[\frac{m}{s^2}]$	[t]		[s]	[s]	[-]	[mm]	[kN]	[-]	[mm]	[kN]	[mm]	[-]	[-]
1- storey structure													
0.6	180.0	✓	0.66	0.82	1.0	15.24	168.6	1.36	30.55	117.0	20.21	0.70	0.73
1.0	112.0	x	0.51	0.61				1.86		129.8	21.96	0.75	0.8
	95.0	✓	0.48	0.56				1.63		120.4	19.02	0.66	0.68
1.3	83.3	x	0.44	0.52				1.85		131.3	22.6	0.78	0.80
	71.0	✓	0.41	0.48				1.58		119.2	18.9	0.65	0.67
1.6	58.5	x	0.37	0.42				1.6		130.4	22.4	0.77	0.80
	56.0	✓	0.37	0.42				1.54		127.6	21.38	0.73	0.75

Zone	Mass	IDA	Modal analysis			Pushover analysis				NLTH analysis			
a_g	m	check	T	T^*	Γ	Δ_y	F_y	μ	$\Delta_{u,st}$	HD force	Δ_{roof}	IDR	DI
$[\frac{m}{s^2}]$	[t]		[s]	[s]	[-]	[mm]	[kN]	[-]	[mm]	[kN]	[mm]	[-]	[-]
2- storey structure													
0.6	110.5	✓	0.85	0.92	1.18	20.56	165.8	1.40	40.35	179.8	27.74	0.65	0.7
1.0	67.0	x	0.66	0.72				1.81		207.3	33.52	0.76	0.80
	62.0	✓	0.64	0.70				1.74		201.4	31.05	0.70	0.74
1.3	46.0	x	0.55	0.60				1.94		211.2	34.18	0.76	0.78
	43.0	✓	0.53	0.58				1.82		201.8	31.97	0.72	0.74
1.6	33.0	✓	0.46	0.51				1.72		206.3	33.05	0.76	0.78
3- storey structure													
0.6	91.8	✓	1.12	1.24	1.25	32.52	165.0	1.24	55.19	240.0	37.89	0.63	0.69
1.0	52.0	✓	0.84	0.92				1.58		272.4	45.33	0.74	0.78
1.3	36.0	✓	0.84	0.92				1.58		272.4	45.33	0.74	0.78
1.6	25.5	✓	0.55	0.60				1.67		270.0	43.76	0.67	0.70
4- storey structure													
0.6	76.5	✓	1.37	1.47	1.29	44.82	164.9	1.11	74.83	247.7	42.75	0.52	0.6
1.0	39.5	✓	0.98	1.06				1.33		316.7	54.59	0.60	0.69
1.3	29.5	✓	0.85	0.91				1.50		304.7	50.4	0.67	0.70
1.6	18.0	✓	0.66	0.71				1.43		336.4	57.18	0.68	0.71
5- storey structure													
0.6	63.0	✓	1.60	1.70	1.33	61.68	164.8	1.0	99.16	279.4	52.97	0.52	0.59
1.0	38.0	✓	1.24	1.32				1.25		356.6	67.76	0.61	0.67
1.3	28.5	✓	1.07	1.14				1.40		374.6	69.64	0.75	0.79
1.6	16.5	✓	0.81	0.86				1.30		361.3	67.45	0.62	0.64
6- storey structure													
0.6	41.5	✓	1.63	1.70	1.35	82.55	165.6	1.0	128.5	263.9	53.02	0.42	0.48
1.0	30.6	✓	1.37	1.44				1.05		361.2	75.12	0.54	0.57
1.3	28.5	✓	1 .35	1.41				1.32		399.6	83.50	0.62	0.66
1.6	12.5	✓	0.9	0.93				1.07		378.5	75.62	0.56	0.58
7- storey structure													
0.6	28.35	✓	1.64	1.70	1.38	109.0	166.4	1.0	164.1	252.5	54.23	0.36	0.40
1.0	28.35	✓	1.64	1.70				1.0		385.0	88.48	0.55	0.57
1.3	25.5	✓	1.56	1.61				1.16		400.0	92.58	0.58	0.63
1.6	9.2	✓	0.93	0.97				1.0		378.8	81.54	0.48	0.48

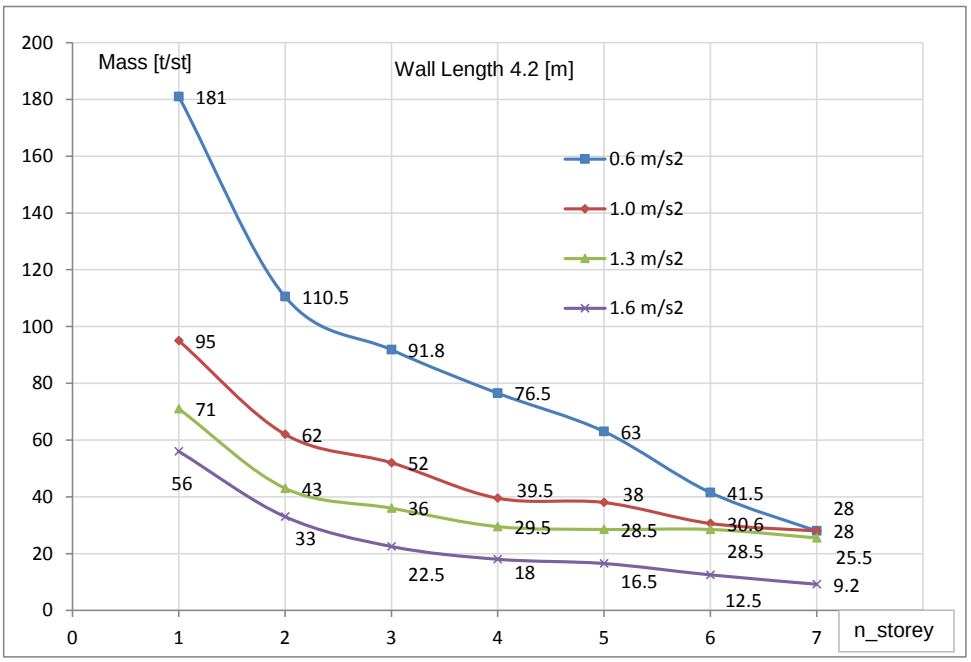

Fig. 8.5: Result of the parameter study of the 4.2 [m] LFTW element sheathed with GFB on both sides, see also Table 8.4

8.2.6 Tabular and graphical presentation of LFTW with a length of $4.8[m]$ sheathed on both sides with GFB

The results of the parametric study for a 4.8 [m] long LFTW element sheathed on both sides with GFB are summarized in Table 8.5. The typical, graphical presentation is given in Figure 8.6

Tab. 8.5: Results of the parameter study of a LFTW with a length of 4.8 [m]

Zone	Mass	IDA	Modal analysis			Pushover analysis				NLTH analysis			
a_g	m	check	T	T^*	Γ	Δ_y	F_y	μ	$\Delta_{u,st}$	HD force	Δ_{roof}	IDR	DI
$[\frac{m}{s^2}]$	[t]		[s]	[s]	[-]	[mm]	[kN]	[-]	[mm]	[kN]	[mm]	[-]	[-]
1- storey structure													
0.6	245.0	✓	0.72	0.95	1.0	16.82	180.1	1.48	39.53	109.4	24.73	0.85	0.80
1.0	139.7	x	0.55	0.67				2.0		124.5	25.77	0.89	0.80
	122.5	✓	0.51	0.62				1.90		119.4	22.35	0.77	0.69
1.3	105.0	x	0.47	0.57				2.19		123.8	26.94	0.93	0.80
	92.5	✓	0.44	0.53				1.93		120.1	23.27	0.80	0.68
1.6	76.5	x	0.4	0.47				1.97		124.0	26.87	0.93	0.80
	74.0	✓	0.40	0.47				1.90		124.2	26.23	0.9	0.78

Zone	Mass	IDA	Modal analysis			Pushover analysis				NLTH analysis			
a_g	m	check	T	T^*	Γ	Δ_y	F_y	μ	$\Delta_{u,st}$	HD force	Δ_{roof}	IDR	DI
$[\frac{m}{s^2}]$	[t]		[s]	[s]	[-]	[mm]	[kN]	[-]	[mm]	[kN]	[mm]	[-]	[-]
2- storey structure													
0.6	140	✓	0.9	0.99	1.178	19.23	176.7	1.57	47.66	179.3	33.63	0.83	0.79
1.0	84.0	x	0.70	0.76				2.00		199.2	36.4	0.87	0.80
	62.5	✓	0.61	0.66				1.73		179.7	28.91	0.66	0.58
1.3	64.0	x	0.56	0.65				2.27		202.8	38.7	0.89	0.80
	46.0	✓	0.52	0.57				1.82		185.6	31.1	0.70	0.60
1.6	42.5	x	0.50	0.55				2.06		205.4	39.6	0.90	0.79
	37.0	✓	0.46	0.51				1.80		273.9	34.15	0.76	0.66
3- storey structure													
0.6	112.0	✓	1.16	1.30	1.243	30.75	172.2	1.39	53.17	226.6	39.57	0.71	0.71
1.0	63.23	x	0.88	0.97				1.76		256.9	47.73	0.84	0.78
	60.0	✓	0.85	0.94				1.72		258.4	46.65	0.77	0.71
1.3	37.73	x	0.68	0.74				1.78		252.6	42.65	0.69	0.59
	34.0	✓	0.64	0.71				1.70		252.8	41.6	0.65	0.55
1.6	25.0	✓	0.55	0.60				1.79		256.5	44.05	0.68	0.60
4- storey structure													
0.6	89.23	✓	1.38	1.49	1.28	40.93	172.2	1.23	70.79	238.7	44.81	0.67	0.70
1.0	55.0	✓	1.09	1.18				1.61		310.1	58.87	0.81	0.78
1.3	37.22	✓	0.90	0.97				1.73		304.2	54.58	0.69	0.62
1.6	24.5	✓	0.72	0.78				1.72		332.5	61.18	0.81	0.71
5- storey structure													
0.6	71.0	✓	1.58	1.70	1.317	56.47	173.8	1.03	96.29	270.4	52.75	0.64	0.68
1.0	45.89	✓	1.27	1.36				1.39		338.3	68.75	0.76	0.75
1.3	36.2	✓	1.13	1.21				1.61		358.2	71.57	0.82	0.73
1.6	19.38	✓	0.83	0.88				1.45		355.9	68.45	0.81	0.72
6- storey structure													
0.6	48.0	✓	1.61	1.70	1.346	73.36	172.4	1.0	118.4	263.3	53.22	0.44	0.48
1.0	42.83	✓	1.52	1.61				1.29		374.7	80.32	0.71	0.72
1.3	35.7	✓	1.39	1.46				1.53		373.3	81.23	0.76	0.72
1.6	14.78	✓	0.90	0.94				1.25		379.6	77.82	0.74	0.65
7- storey structure													
0.6	33.0	✓	1.63	1.70	1.37	95.39	172.8	1.0	149.1	248.2	53.82	0.37	0.38
1.0	33.0	✓	1.63	1.70				1.07		374.2	87.04	0.67	0.67
1.3	30.6	✓	1.56	1.64				1.34		393.2	92.19	0.76	0.72
1.6	12.0	✓	0.97	1.01				1.02		392.0	87.96	0.68	0.60

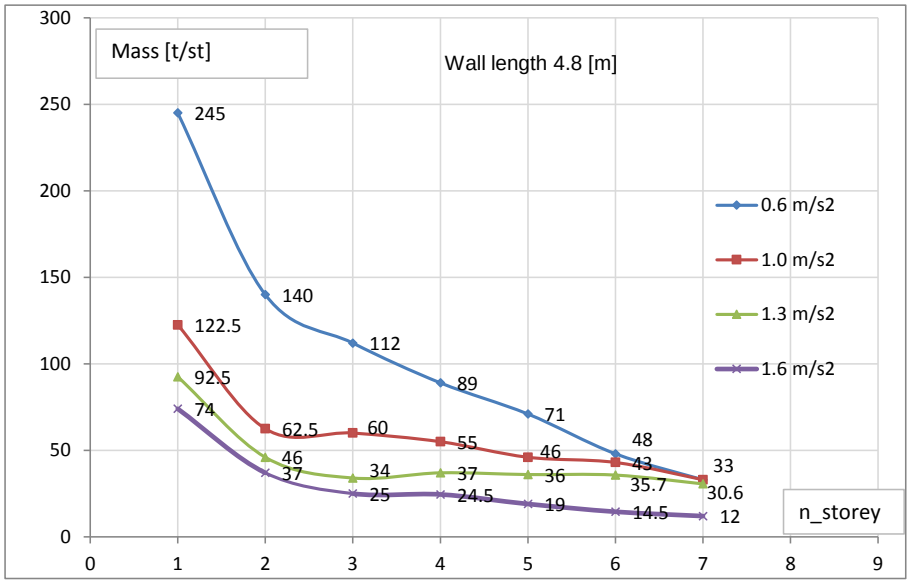

Fig. 8.6: Result of the parameter study of the 4.8 [m] LFTW element sheathed with GFB on both sides, see also Table 8.5

8.3 Discussion

8.3.1 General considerations

LFTWs sheathed with GFB are intuitivly considered to be inappropriate to sustain seismic lateral loads due to their low ductility and quite high sensitivity to cracking. The analyses performed and presented within this chapter show illustratively that, in the hazard zone Z1 with a ground acceleration of 0.6 $[\frac{m}{s^2}]$, the walls sheathed with GFB can be reasonably used for structures of up to 6 storeys. Even the LFTW with a length of 2.4 [m] can sustain the loads associated with the mass of 47.4 [t/storey] in the case of structures of up to 4 storeys. Under assumption that the avearge evenly distributed laod of a slab during an earthquake is 4.5 $[\frac{kg}{m^2}]$, (see also explanations related to ths assumption in Chapter 6, section 6.3.3) the area associated with the wall element is approximately $47.4/0.45 = 105[m^2]$, which is approximatelly 10 by 10 [m]. In hazard zone Z2, defined by a ground acceleration of 1.0 $[\frac{m}{s^2}]$, the walls with length of 4.8 [m], sheathed on both sides with GFB, can be reasonably used for structures of up to 5 storeys with an mass of 46 $[t/st]$ and an area associated with the wall element of approximately 10 by 10 [m]. Presuming the mass of 450 $[\frac{kg}{m^2}]$ evenly distributed over storey surface, in hazard zone Z3a, defined by a ground acceleration of 1.3 $[\frac{m}{s^2}]$, the LFTWs sheathed with GFB can also be used economically for structures of up to 5 storeys, with an area associated to the wall of approximately $36/0.45 = 80[m^2]$ which is approximately area of 9 by 9 [m]. In the hazard zone Z3b, defined by a ground acceleration 1.6 $[\frac{m}{s^2}]$, and under the same assumption related to the evenly distributed load of 450 $[\frac{kg}{m^2}]$ the LFTWs sheathed with GFB can be only used predominantly for 1 and 2 storey structures.

8.3.2 Inter-Storey Drift Ratio (IDR) and Damage Index (DI)

Generally, low-rise structures are forced to develop larger IDR and DI than the taller ones. This is because the admissible masses decrease and the vibration periods increase with height, resulting in a continuous reduction of IDR and DI. Since it has not been possible to make a conclusion related to the IDR and DI which generally applies to all structures, these have been estimated consecutively for all wall elements individually. In the following subsection, the behaviour of the LFTW elements regarding IDR and DI will be described.

Walls with a length of 2.4 [m]

From Table 8.1, it can be seen that the values for both the IDR and DI correspond very well to the range associated with the LS limit state. The one- and two-storey wall elements are in the upper range of approximately 0.7 - 0.8, implying that the structural bearing capacity is highly exploited. Examples of the expected damage in this range of IDR and DI are shown in Figures 5.23 and 5.25. Structures with three to five storeys respond with moderate IDR and DI in the range between 0.58 - 0.68. The damage associated with this DI range can be seen in Figures 5.18 and 5.19. Only the five-storey structure in seismic zone Z1 with an admissible mass of $32.6[t]$ assigned at each storey, has shown an IDR in the lower range of 0.47 and a DI of 0.5. In this specific case, the maximum vibration period of $T^* = 1.7[s]$ has almost been reached, leading to the lower seismic loads and thus to lower IDR and DI ratios.

Walls with a length of 3.0 [m]

From Table 8.2, it can be seen that structures of up to three storeys, under the masses applied, develop IDRs in the range of 0.8 to 0.95, exceeding the value proposed in Table 5.8 as the limit value $IDR = 0.8$. The parameter study has been primarily oriented to satisfy the limit value of $DI \leq 0.8$, i.e., the value for which the admissible masses have been estimated. Similar to the 2.4 [m] LFTW, the bearing capacity of the elements of the structures with up to three storeys has been highly exploited in the study. The structures in the range between 4 and 6 storeys respond with moderate DIs. This implies that the damage potential decreases with increasing building height due to both the reduction of the admissible masses and increasing of the vibration periods.

Walls with a length of 3.6 [m]

In Table 8.3, it can be seen that structures of up to three storeys develop IDRs in the range of 0.8 to 0.91, exceeding the limit value of 0.8 given in Table 5.8. The DIs are always kept below the limit value proposed in Table 5.8. As observed for the 2.4 [m] and the 3.0 [m] LFTW, the 3.6 [m] wall elements also respond with moderate IDR and DI in the case of structures with up to 5 storeys (range 0.5 - 0.78), and low IDR and DI in the case of structures with up to seven storeys (range 0.37 - 0.69).

Walls with a length of 4.2 [m]

The IDR and DI values are consistently within the expected range of $IDR = DI \leq 0.8$, decreasing continuously with increasing building height up to 7 storeys. See also Table 8.4.

Walls with a length of 4.8 [m]

The IDR values for structures of up to two storeys are in the range between 0.83 - 0.93. The DI is kept at the proposed maximum level of $DI \leq 0.8$. See Table 8.5. Structures with 3 - 5 storeys and structures with 6 - 7 storeys respond with moderate and low DI and IDR, respectively.

8.3.3 Admissible masses and mass distribution

The admissible mass which can be applied to the structure at each storey is the main focus of the parameter study. In Figures 8.1, 8.3, 8.4, 8.5 and 8.6, the admissible masses applied at each storey have been estimated for different hazard levels. The values listed in the tables have been estimated in such a way that all limiting conditions, specified in advance, have been satisfied. If one assumes that the realistic, evenly distributed floor load in a traditional timber structure is approximately $q_{st} = 4.5[\frac{kN}{m^2}]$, the area associated with the shear wall can be easily estimated as $A = \frac{m}{g_{st}}$, regardless of whether the shape of the area is quadratic or rectangular.

Walls with a length of 2.4 [m]

For the relatively short wall length of 2.4 m and the average evenly distributed load of $q_{st} = 4.5[\frac{kN}{m^2}]$, the surface area associated with the shear wall element of approximately 7 by 7 $[m]$ seems to be realistic. However, this surface area of approximately 50 $[m^2]$ and the admissible masses of $22.5[\frac{t}{storey}]$ are at the lower boundary of practical relevance. From this simple observation, it can be easily concluded that the $2.4[m]$ long LFTW sheathed with the GFB can be reasonably used in hazard zone Z1 for structures of up to 5 storeys, in hazard zone Z2 for structures of up to 4 storeys and in hazard zones Z3a and Z3b for structures of up to 2 storeys. The results discussed here are all related to soil conditions C. Moreover, it has been observed that, in the transition zone between 3 and 4 storeys, the same or almost the same admissible masses have been estimated for both 3 and 4 storey structures. This indicates that for structures of up to 3 storeys, the IDR and the ductility demands, which can not be satisfied for larger masses, are the predominant limitations. Both the ductility demand and the IDR are attenuated with increasing height and vibration period and hence lead to a decrease of the lateral loads induced by earthquakes.

Walls with a length of 3.0 [m]

Using the same criteria as in the previous discussion about the 2.4 [m] wall element, from Table 8.2, it can be concluded that the 3.0 [m] wall element with applied masses of up to $30.0[\frac{t}{storey}]$ can be reasonably used for structures of up to 5 storeys in Zone 1, 4 storeys in Zone 2, 3 storeys in Zone 3a and 1 storey in Zone 3b. The associated area is then approximately 8.0 by 8.0 [m].

Note that the results obtained by using NLTHA will be checked by means of IDA analysis and are discussed in a separate section "Control of parameter study results by IDA".

Walls with a length of 3.6 [m]

The same admissible mass of $30.0[\frac{t}{storey}]$ applied to a 3.6 [m] wall element can be reasonably used for structures of up to 6-storeys in hazard zones Z1 and Z2, structures of up to 3 storeys in hazard zone Z3a and structures of up to 2-storeys in hazard zone Z3b.

Walls with a length of 4.2 [m]

Applying the criteria that the mass which can be applied to the 4.2 [m] wall element is in the range $> 30.0[\frac{t}{storey}]$, one can conclude from Table 8.4, that the 4.2 [m] wall element can reasonably be used for structures of up to 6 storeys in hazard zone Z1, structures of up to 5 storeys in hazard zone Z2, structures of up to 3-storeys in hazard zone Z3a, and structures of up to 2 storeys in hazard zone Z3b. The area related to the mass of $33.0[\frac{t}{storey}]$ is then approximately 8.5 by 8.5 [m].

Walls with a length of 4.8 [m]

Applying the criteria that the mass which can be applied to the 4.8 [m] wall element is in the range of $> 35.0[\frac{t}{storey}]$, one can conclude from Table 8.5, that the 4.8 [m] wall element can reasonably be used for structures of up to 6 storeys in hazard zone Z1 and Z2, structures of up to 5-storeys in hazard zone Z3a, and structures of up to 2 storeys in hazard zone Z3b. The area related to the mass of $35.0[\frac{t}{storey}]$ is then approximately 8.8 by 8.8 [m]. Please note that the admissible mass for a 7 storey structure in hazard zones Z1 and Z2 is $33.0[\frac{t}{storey}]$ because the inelastic period of vibration $T^* = 1.7[s]$ has been reached. The check with IDA has revealed that the mass of $35.0[\frac{t}{storey}]$ is realistic with a related period of $T^* = 1.69[s]$. The differences in the vibration periods estimated within the IDA and the pushover analysis within the parameter study are due to the better quadrilinear fit of the pushover curve within the IDA analysis when compared with the EEEP approximation used in the parameter study. Additionally, by taking a closer look at Table 8.5, one can see that the admissible mass in hazard zone 3a is almost constant for a 3 and 6-storey structure, ranging from 35.7 to 37.7 $[\frac{t}{storey}]$. All these values have been confirmed with the IDA analysis. Thus, the maximum admissible mass in hazard zone Z3a is approximately 35 $[\frac{t}{storey}]$ for all structures between 3 and 6 storeys.

8.3.4 Ductility demand

The displacement capacity of LFTW sheathed with GFB is quite small. Nevertheless, the structure is able to satisfy ductility demands of up to 2.5, depending on the period of vibration and the requirements imposed by the hazard zone. It has been observed that the ductility demand governs the design of LFTW sheathed with GFB in the range of up to 3-storeys. This

is the reason why the mass for low rise structures is still a moderate value, remaining almost constant also for structures with more than 3 storeys.

From Table 8.1, referring to 3 and 4 storey structures and hazard zone 3a, it can be seen that the admissible mass is surprisingly larger (or equal for some other hazard zones) for the 4 storey structure, which seems to be incomprehensible at first sight. In Figures 8.2(a) and 8.2(b), the displacement capacity, displacement demand (and thus the ductility demand) are presented for a mass of 20.4 [t] assigned at each floor, of both 3-storey and 4-storey structures, which is slightly more mass than that which satisfied the given condition. In both cases, the ductility demand governs the design. If the mass applied to the storey gives a period of vibration that satisfies the condition related to the ductility demand, NLTHA analysis is to be performed. In this case, the IDR and DI are sometimes much smaller than the limiting value of approximately 0.8, since the ductility demand governs the design. Similar observations have also been made for the 4.8 [m] wall element, as discussed in the previous section about admissible mass and mass distribution.

8.3.5 Hold-Down forces

As expected, the hold-down forces increase with increasing building height, covering the range of approximately 100 to 375 [kN]. Despite huge differences in admissible masses, feasible storey number and element length, the HD forces change only slightly, given a specific number of storeys as well as a certain hazard zone. The HD force for one storey structures and all lengths of wall elements is in the range between 106 and 130 [kN]. In the case of 5 storey structures, the HD forces differ approximately 50 [kN] within the same hazard zone. According to Figure 3.4, the hold-down devices with one slotted in steel plate and either 9 or 12 dowels, would be sufficient for structures with up to 3 storeys. The 5 storey structures require two slotted in steel plates and connections with 8 or 12 dowels. See Figure 3.5. The maximal HD-force in the case of a specific solution of practical relevance is approximately 373 [kN]. This is for a 4.6 [m] wall in a 6 storey structure in Zone 3a. Hence, a HD-device with two slotted-in plates and 12 dowels is needed. In summary, structures with up to 3 storeys require stud dimensions of 200 x 200 [mm] with one slotted in steel plate, while the structures with 4 to 7-storeys require stud dimensions of 240x240 [mm] and two slotted-in steel plates.

8.3.6 Wind loads

The influence of the wind load upon a structure in terms of an earthquake analysis is described in Chapter 6 in more detail. It has been concluded that the wind load influence is a rather easy to estimate by simple checking if the requirement given by Equation 6.6 is satisfied. Since the check as to whether the wind loads govern the design is a straightforward issue, which is not the subject of the presented work, it has not been considered in more details in the subsequent sections.

8.3.7 Control of parameter study results by IDA

As already mentioned in Section 8.2.1, the results obtained by the parameter study based on NLTHA have been checked by incremental dynamic analysis (IDA), which is an independent procedure presented in Chapter 4. In the parameter analysis, the theoretically admissible masses for all wall elements and hazard zones have been estimated, regardless their practical relevance. The minimum mass estimated for mid-rise buildings with 5 -7 storeys for hazard zone 3b is in the range of 8 to 12 $[\frac{t}{storey}]$. This is irrelevant for practical applications due to the relatively small surface area that results from the admissible masses for the assumed evenly distributed load of 4.5$[\frac{kN}{m^2}]$. These surface areas are being in the range of 4.2 by 4.2 [m] and 5.1 by 5.1 [m] for 5 and 7 storeys, respectively. The minimum admissible masses considered relevant in practice have been estimated for surfaces with minimum side dimensions between 7.0 by 7.0 up to 8.8 by 8.8 [m] for the 2.4 and 4.8 [m] wall element, respectively. Hence, the minimum admissible masses considered as practically relevant are in the range between 22.5 and 35 $[\frac{t}{storey}]$. A detailed review related to the practice-relevance of the masses estimated in the parametric study is given in the previous Section 8.3.3 "Admissible Masses and Mass Distribution". The relevant results of the parameter study for practical applicability have been checked by IDA analysis. A short overview related to the results obtained by IDA is the subject of this section.
Note that all results obtained within the parameter study have been checked by IDA. Structures that have passed the control have been assigned a positive check-mark (✓) in the table. Those that have not passed the check have been assigned negative ×-mark. The IDA analysis has been repeated until the structure passed the check for given damage measure (DM).

Wall with length of 2.4 [m]

Figure 8.7 shows the IDA-check for 5-, 4-, 2-, and 1-storey buildings located in hazard zones Z1, Z2, Z3a and Z3b. The satisfaction of the LS performance objectives, given by the damage measure as an inter-storey drift ratio (IDR) or roof drift ratio (RDR), as stipulated in Chapter 5, is represented by the intersection of the 50%-fractile IDA curve and the elastic response spectrum of the corresponding hazard zone. These intersection points are labeled 1 - 4. For all cases where points 1 - 4, representing the LS limit state on the IDA curve, lie beyond the intersection with the elastic RS, the structure has passed the IDA-check. As seen in Figure 8.7, the admissible masses meet the conditions well. Thus, the results of the parameter analysis for the 2.4 [m] wall element have been confirmed by IDA. For illustration, in the case of 1-storey structure, in hazard Zone 3b, the admissible mass obtained in the parameter study has not been confirmed by the IDA analysis. The IDA result has been adopted, as presented in Figure 8.7. Note that IDA analysis is based on the pushover curve and depends strongly on the chosen intensity of the damage measure, herein called a roof drift ratio, which has been specified for all structures in accordance with Figure 5.27. Generally, smaller masses as resulting from NLTHA or IDA analysis have been accepted as decisive and introduced in the graphical representation.

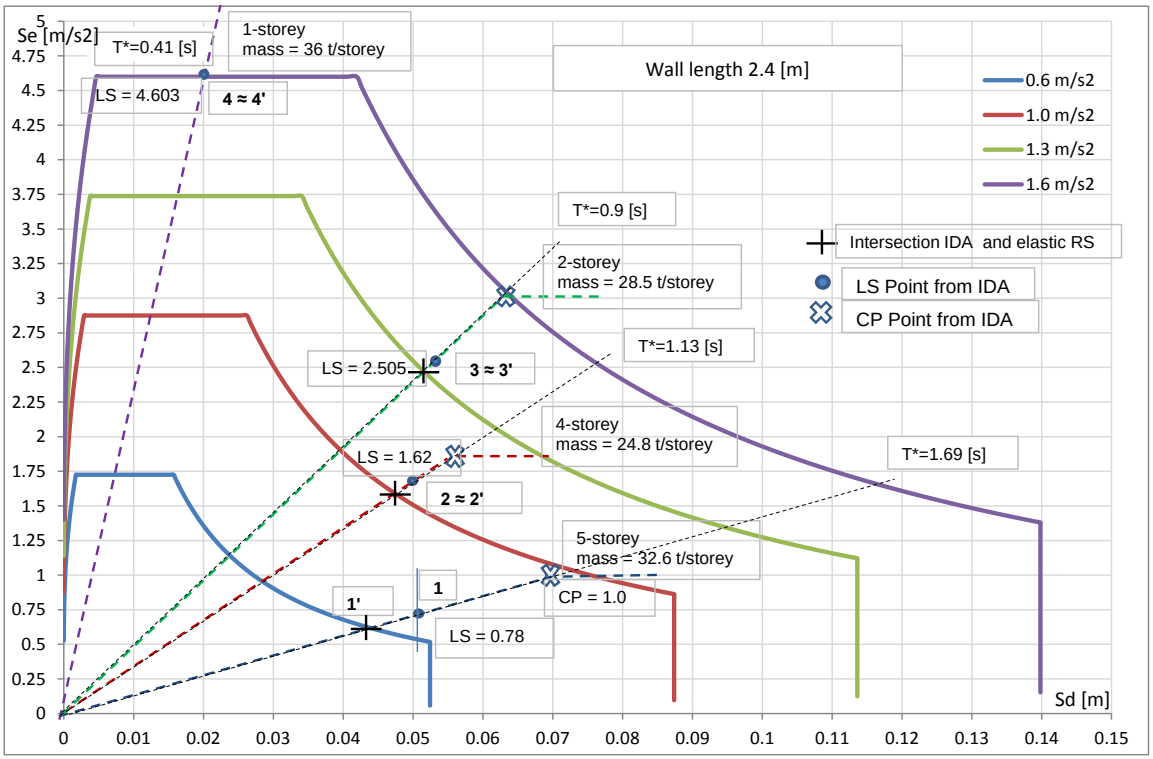

Fig. 8.7: Control of the results of the parameter study by incremental dynamic analysis (IDA) for masses of practice-relevance superimposed in YPS for the 2.4 [m] LFTW element, see also Table 8.1

Wall with a length of 3.0 [m]

Figure 8.8 shows the IDA-check for 5-, 4-, 3-, and 1-storey buildings situated in hazard zones Z1, Z2, Z3a and Z3b. As shown in Figure 8.8, the admissible masses meet the conditions well in hazard zones Z3a and Z3b, implying that the structural capacity is highly utilized. The distances between points 1 and 1' as well as 2 and 2', representing buildings in hazard zones Z1 and Z2, implies, that the structural capacity is entirely utilized. Nevertheless, an increase in the admissible masses is not possible since another limiting criterion has been reached first. In this case, the limiting criteria are the ductility demand and the period of vibration T^* for Z2 and Z1, respectively. Thus, the results of the parameter analysis for the 3.0 [m] wall element have been confirmed by IDA.

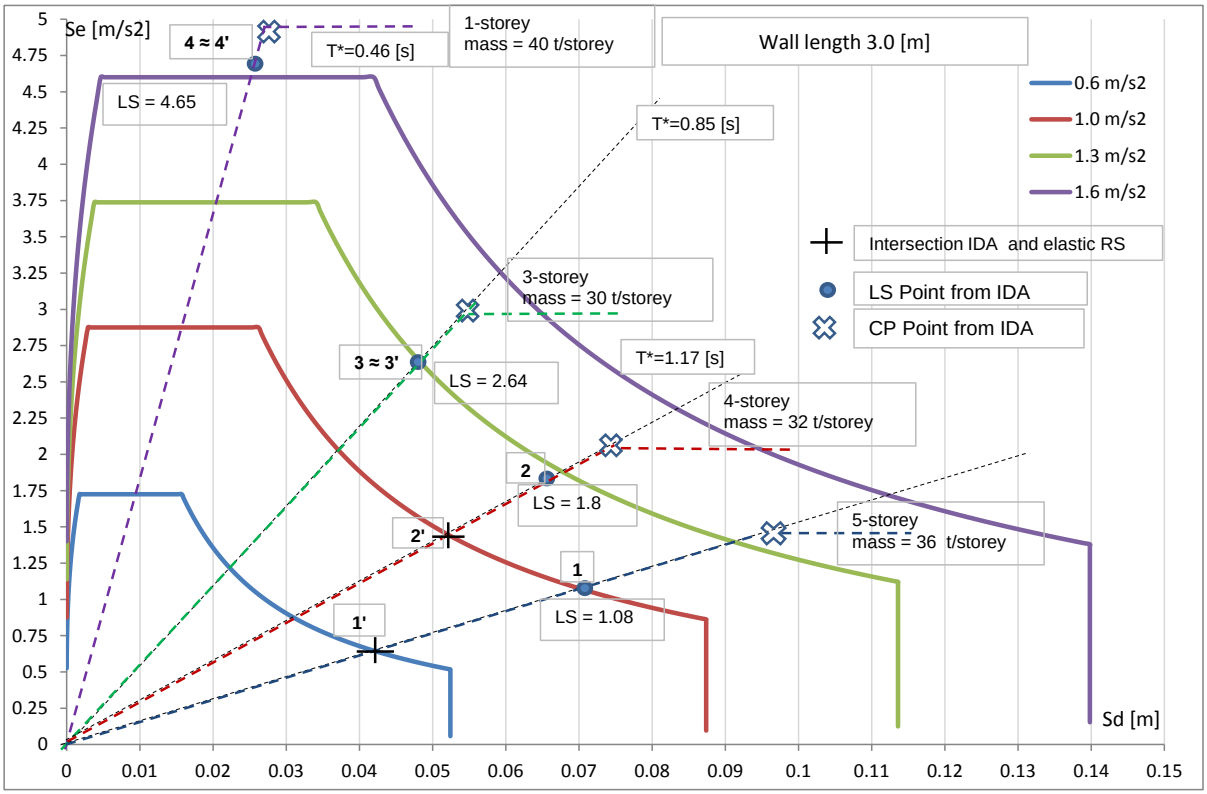

Fig. 8.8: Control of the results of the parameter study by incremental dynamic analysis (IDA) for masses of practice-relevance superimposed in YPS for the 3.0 [m] LFTW element, see also Table 8.2

Wall with a length of 3.6 [m]

Figure 8.9 shows the IDA-check for 6-, 3- and 1-storey buildings located in hazard zones Z1, Z2, Z3a and Z3b. In Figure 8.9, one can see that the admissible masses for the 6-storey structure in zones Z1 and Z2 are equal. The points 1 and 1' as well 2 and 2' which represent the LS limit states on the 50% fractile IDA curve, are on the same curve. This is due to the same period of vibration which is limiting for both structures. The results of the parameter analysis for the 3.6 [m] wall element have been confirmed by IDA.

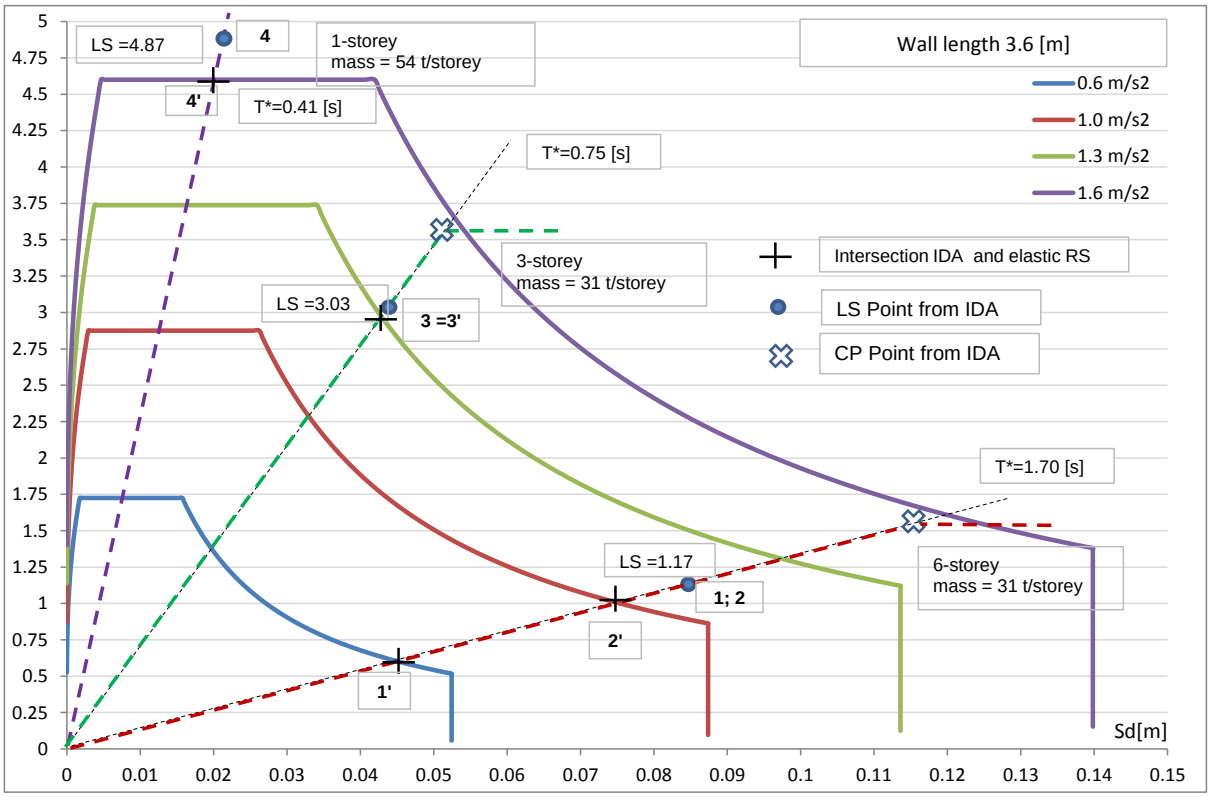

Fig. 8.9: Control of the results of the parameter study by incremental dynamic analysis (IDA) for masses of practice-relevance superimposed in YPS for the 3.6 [m] LFTW element, see also Table 8.3

Wall with a length of 4.2 [m]

Figure 8.10 shows the IDA-check for 6-, 4- and 2-storey buildings located in hazard zones Z1, Z2, Z3a and Z3b. One can see from Figure 8.10 that the admissible masses for the 6-storey structure in zone Z1 and Z2 differ, leading to different periods of vibrations. In any case, points 1 and 1' as well 2 and 2', which represent the LS limit states on the 50% fractile IDA curve, lie beyond the intersection with the elastic RS. Again, the results of the parameter analysis for the 4.2 [m] wall element have been confirmed by IDA.

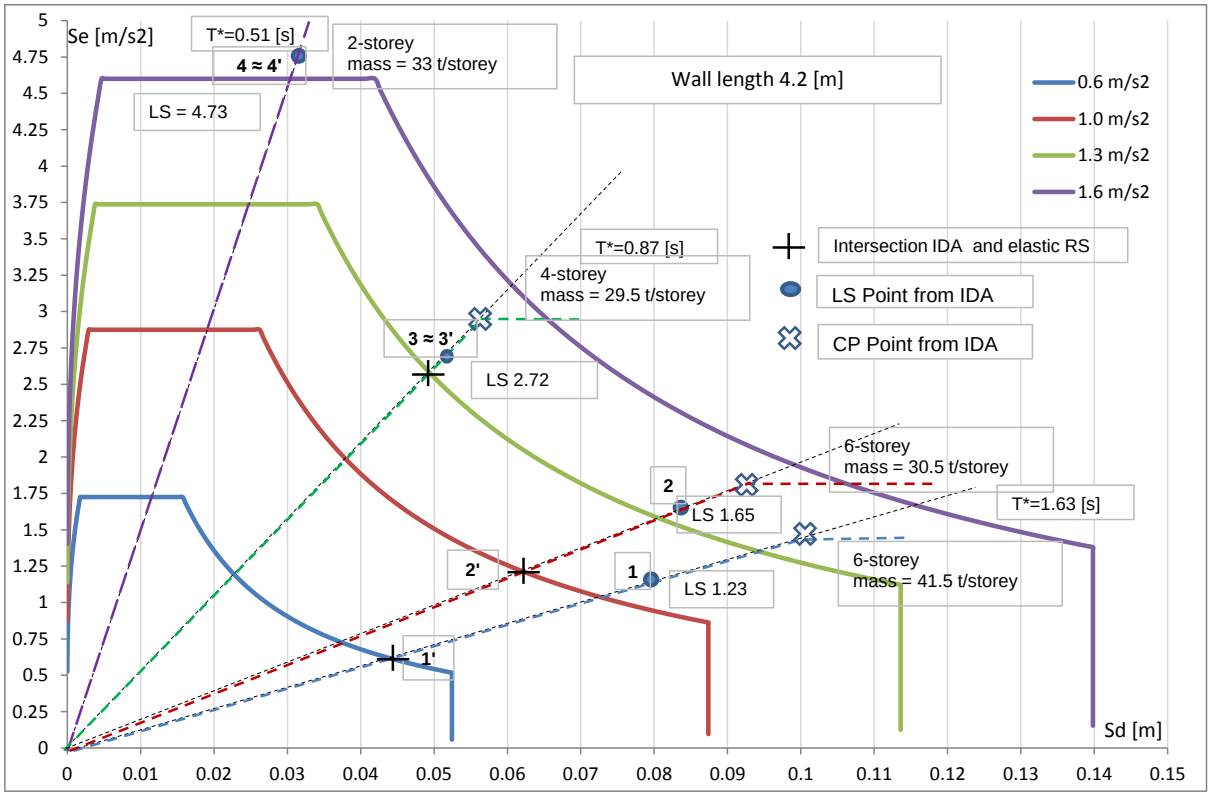

Fig. 8.10: Control of the results of the parameter study by incremental dynamic analysis (IDA) for masses of practice-relevance superimposed in YPS for the 4.2 [m] LFTW element, see also Table 8.4

Wall with a length of 4.8 [m]

Figure 8.11 shows the IDA-check for 7-, 6- 3- and 2-storey buildings situated in hazard zones Z1, Z2, Z3a and Z3b. One can see from Figure 8.11 that the admissible masses for the 6-storey structure in zones Z1 and Z2 differ, leading to different periods of vibrations. In any case, points 1 and 1' as well 2 and 2', which represent the LS limit states on the 50% fractile IDA curve lie, beyond the intersection with the elastic RS. The results of the parameter analysis for the 4.8 [m] wall element have been confirmed by IDA.

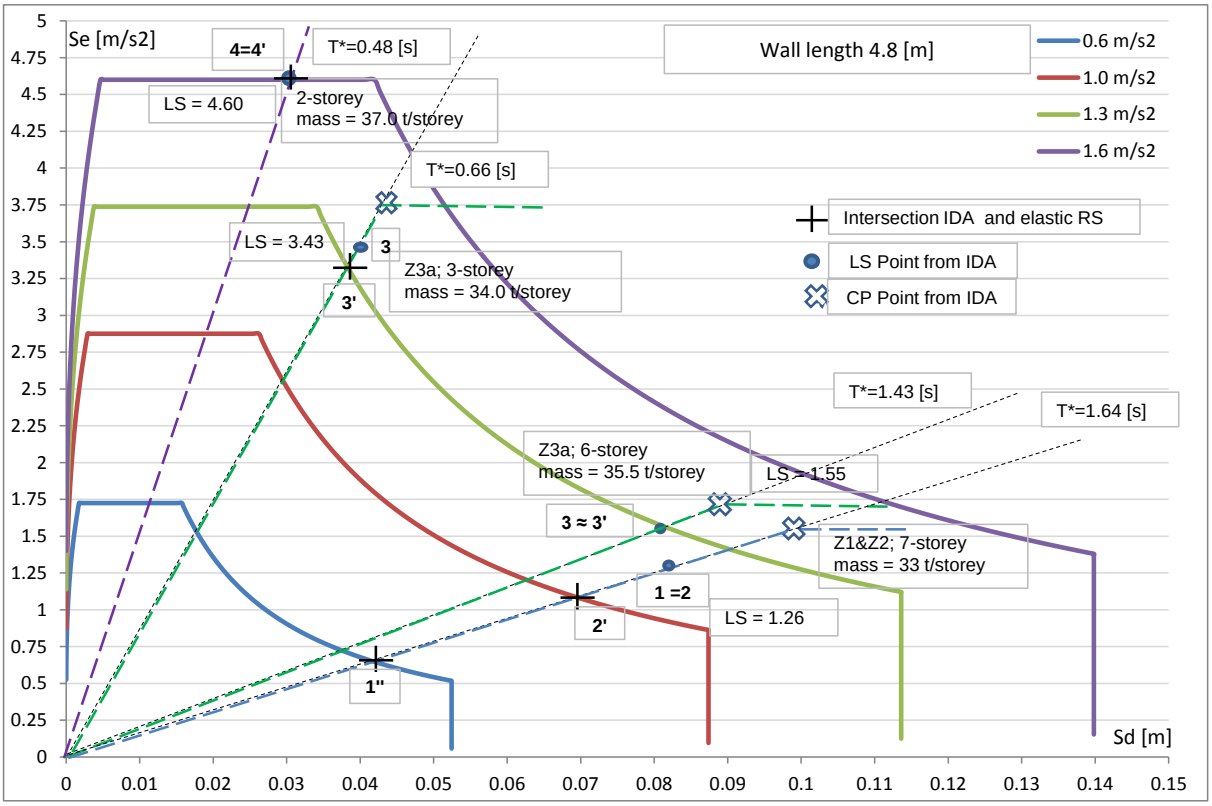

Fig. 8.11: Control of the results of the parameter study by incremental dynamic analysis (IDA) for masses of practice-relevance superimposed in YPS for the 4.8 [m] LFTW element, see also Table 8.5

8.4 Comparison of the LFTWs Sheathed with OSB and GFB Panels

Although, the GFB is a material which does not behave in a ductile way under tension and shear loading, the response of the LFTWs sheathed with GFB to the cyclic loading is a stable, closed hysteresis, as has been observed during the testing. The results presented in the previous section are related to the seismic analysis of structures being placed in regions with type C subsoil conditions. The results for subsoil conditions of type A and E are given in Appendix A1 and A2 for LFTWs sheathed with GFB and B1 and B2 for LFTWs sheathed with OSB. In Appendix C, the results for all examined wall lengths have been compared for soil conditions A,

C and E for both sheathing materials. In general, it can be stated that the *best* performance of LFTWs sheathed with GFB lies under the *worst* performance of the LFTWs sheathed with OSB.The *best* performance means the maximum admissible storey mass, estimated steadily for the hazard zone with the lowest design ground acceleration Z1, and *worst* means the maximum admissible storey mass estimated steadily for the hazard zone with the maximum design ground acceleration Z3b.

8.4.1 Comparison of LFTWs sheathed with OSB and GFB for soil conditions of type A

Depending on the wall length the LFTWs sheathed with GFB can reasonably be used in structures of up to 5 storeys, including in the hazard zone Z3b. Even LFTWs with wall lengths of 2.4 [m] can be used in the buildings up to 4 storeys in the hazard zones Z1 and Z2. Curiously, the admissible masses per storey estimated for the LFTWs sheathed with OSB are represented by the same curve for all hazard zones. This is due to the inelastic vibration period, the limiting criterion reached in each analysis, despite varying hazard zones and the storey numbers. The LFTWs sheathed with OSB can reasonably be used in the structures of up to six storeys, (see also Figures C.1 to C.5).

8.4.2 Comparison of LFTWs sheathed with OSB and GFB for soil conditions of type C

The use of LFTWs sheathed with GFB in the structures situated in regions with subsoil conditions of type C have been discussed in the previous section in more detail. From Figures C.6 to C.10 it is apparent that the LFTWs sheathed with GFB can be reasonably used for up to 5 and 4 storeys in the hazard Zones Z1 and Z2, respectively. In the hazard zones Z3a and Z3b the use of the LFTWs sheathed with GFB is limited to 1 and 2 storey structures. Again, due to the limiting vibration period reached in each analysis of the structures with more than four storeys, the LFTWs sheathed with OSB can be used in structures of up to 6 storeys, independent of the hazard zone.

8.4.3 Comparison of LFTWs sheathed with OSB and GFB for soil conditions of type E

The LFTWs sheathed with GFB built in the regions with the soil conditions E can be reasonably used in structures of up to 5 storeys in the hazard zones Z1 and Z2. In the hazard zones Z3a and Z3b, the LFTWs sheathed with GFB can be rationally used for 1-storey structures only. The use of the LFTWs sheathed with OSB can be justified for structures of up to six storeys, (see Figures C.11 to C.15).

Chapter 9

Comparison of FBD vs PBE

Using a prototype building, analyzed in the literature and currently used as a guideline for seismic design of timber structures in Switzerland, the differences between force based design and performance based engineering are evaluated. The comparison points out that stiff and strong structures do not necessarily have higher levels of protection than weaker and more flexible ones. Furthermore, it is shown that the real behaviour of the structure designed using FBD are for the most part unknown in contrast to the structures designed using PBE, which enables attaining full control of the structural behaviour under seismic excitation.

9.1 Introduction

The behaviour of LFTWs sheathed with GFB or OSB panels is inelastic, even in the case of quite small displacements. Because of fastener distortion at the connection with the timber material, LFTW elements sheathed with OSB PANELS have large displacement capacities, and consequently large displacement ductility. The estimation of the ductility of the LFTWs is not simple to define because a pronounced yield point does not exist. In order to enable estimation of a quasi yield-point and introduce a unified nomenclature, national codes (see e.g. [91], [20] or [39]) have adopted the proposal presented in Figure 9.1. The bearing capacity is estimated by using a simple equation based on the shear field theory (see also Chapter 3 and [91]). The strength estimation is based on the code requirements. In the analysis, a force-displacement relationship covering the entire displacement range up to failure is not required, and it is generally unknown. The bearing capacity of a single fastener and hence of the entire wall element is at the design level R_d.

The procedure is used for estimation of some characteristic points and has little in common with the real shear wall behaviour. Despite the fact that the code-based estimation of the strength and displacement is a straightforward procedure, literature dealing with lateral load resisting systems composed of LFTWs is rare. A significant attempt to address the design of shear walls subjected to seismic loads has been made recently by a group of Swiss professionals, who have worked out a document, presented in [6]. It has been used in Switzerland as the guidelines for earthquake design of timber structures. The brochure gives a comprehensive

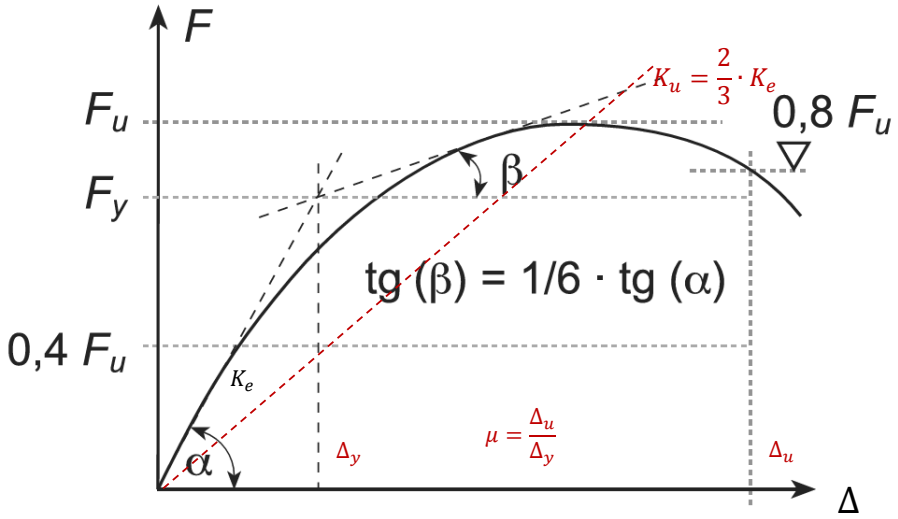

Fig. 9.1: The definition of yield point, yield force and ductility ratio in the Swiss standard SIA 265 [91] and DIN EN 12512 [20]

overview of the mechanical characteristics of timber connections, the main configurations of LFTWs, as well as a review related to seismic actions, ductility estimation, code requirements and capacity design. The analysis used is force-based. In order to compare the performance-based engineering (PBE) procedure presented in this work with the results obtained using the force-based seismic design (FBD), the wall element $TWX1$ (see Figure: 9.2), designed in [6], is chosen as the subject of comparison.

9.2 Geometry of the Prototype Building

The prototype building, proposed in [6], is used as a model for introducing the design of LFTWs subjected to earthquake loads. It is presented in Figure 9.2.

The structure represents a 4-storey residential building with plan-view dimensions of 12 by 16 [m]. The basement storey, constructed of reinforced concrete, is considered to be infinitely stiff and therefore it is neglected in the further analysis. The storey height is 2.9 [m] and remains constant over the building height. The floor masses are the same for all the storeys. They are calculated for an evenly distributed dead load of $g_c = 6.33[\frac{kN}{m^2}]$ and a live load of $q_c = 2.0[\frac{kN}{m^2}]$. The contribution of the live load in the earthquake scenario is taken into account by using a reduction factor for the quasi-static loads of $\psi_2 = 0.3$. This gives a reduced live load of $\psi_2 \cdot q_c = 0.3 \cdot 2.0 = 0.6[\frac{kN}{m^2}]$. The roof mass is estimated to be approximately 50% of the storey mass. It is calculated for evenly distributed dead loads of $g_{ch} = 3.54[\frac{kN}{m^2}]$. No additional live loads acting at the roof level are considered. The total mass estimated is $m_1 = m_2 = m_3 = 150[t]$, and $m_4 = 77[t]$ at the roof level. In Figures 9.2 and 9.3, the plan view of the building and a typical wall configuration are shown. The lateral load resisting system consists of two 4.0 [m] LFTWs oriented in the Y-direction and one 3.0 [m] and one 4.0 [m] long LFTW element oriented in the X direction. Thus, the lateral load resisting system is symmetric with respect to the Y direction

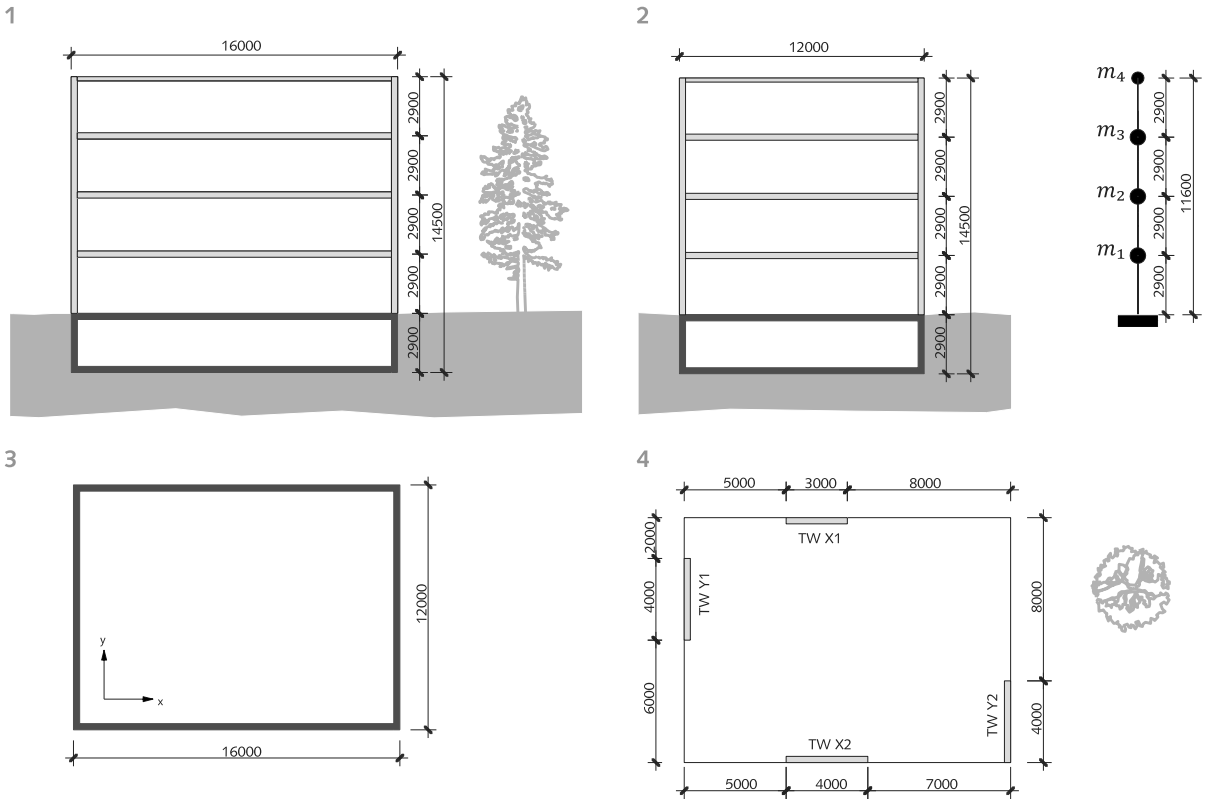

Fig. 9.2: Plan view of the prototype building analyzed in [6]

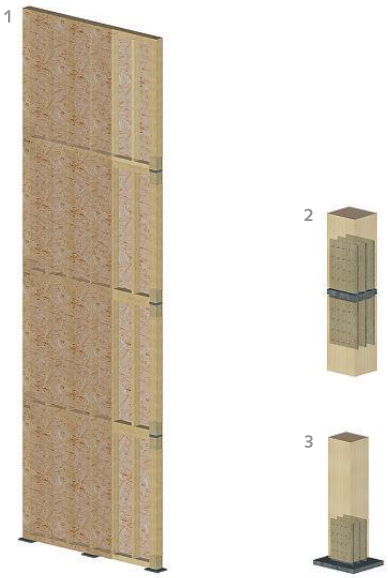

Fig. 9.3: Typical wall configuration of LFTWs as well as HD devices and inter-storey connectors used for the prototype building analyzed in [6]

and asymmetric with respect to the X direction. The building is situated in hazard zone *Z3b* with soil conditions C and importance class I. The behaviour factor in design has been taken as $q = 3.0$, which is equal to the ductility ration of $\mu = 3$ in the velocity sensitive region of RS, characterieted with periods of vibration between 0.6 and 2.0 [s], which is to be expected in this specific case. For more details, see [6].

9.3 Outcome of the Force-Based Analysis Conducted in [6]

In [6], the basic assumptions, the procedure for estimating the equivalent stiffness and model properties, the modal analysis, the estimation of the torsion effects as well as the estimation of the number of fasteners and their arrangement are described in detail.

The geometry, the main assumptions related to the seismic impact as well as the results of the force-based seismic analysis are summarized in Tables 9.1, 9.2 and 9.3.

Tab. 9.1: Geometry of the wall TWX_1

Wall length	Storey number	Storey height	Building height	Storey mass	Roof mass	OSB thickness	Staple diameter	Staple spacing	Row number
[m]	[-]	[m]	[m]	[t]	[t]	[mm]	[mm]	[mm]	[-]
3.0	4	2.90	11.6	75	37.5	15.0	1.53	24.0	2

Tab. 9.2: Seismic hazard: input data

Hazard zone	Ground acceleration	Soil category	Edge period T_C	Coefficient S	Building class	Coefficient γ_f	Ductility
[-]	$[m/s^2]$	[-]	[s]	[-]	[-]	[-]	[-]
Z3b	1.60	C	0.6	1.15	1.0	I	3.0

Tab. 9.3: Results of the force-based analysis conducted in [6]

Period of vibrations T_1	Base shear according SIA161 (2013)	Base shear calculated translation	$P-\Delta$	torsion	total	Bearing capacity after [6]
[s]		[kN]	[kN]	[kN]	[kN]	[kN]
1.51	$2.5 \cdot \frac{a_{gd}}{g \cdot q} \cdot \gamma_f \cdot S \cdot \frac{T_C}{T_1}$	141.4*	32.35*	24.3*	198.0	238.0

*) values in accordance with Figure 79, distributed in accordance with Figure 92 in [6]. Shear force estimation in accordance with calculation presented on page 83 in [6].

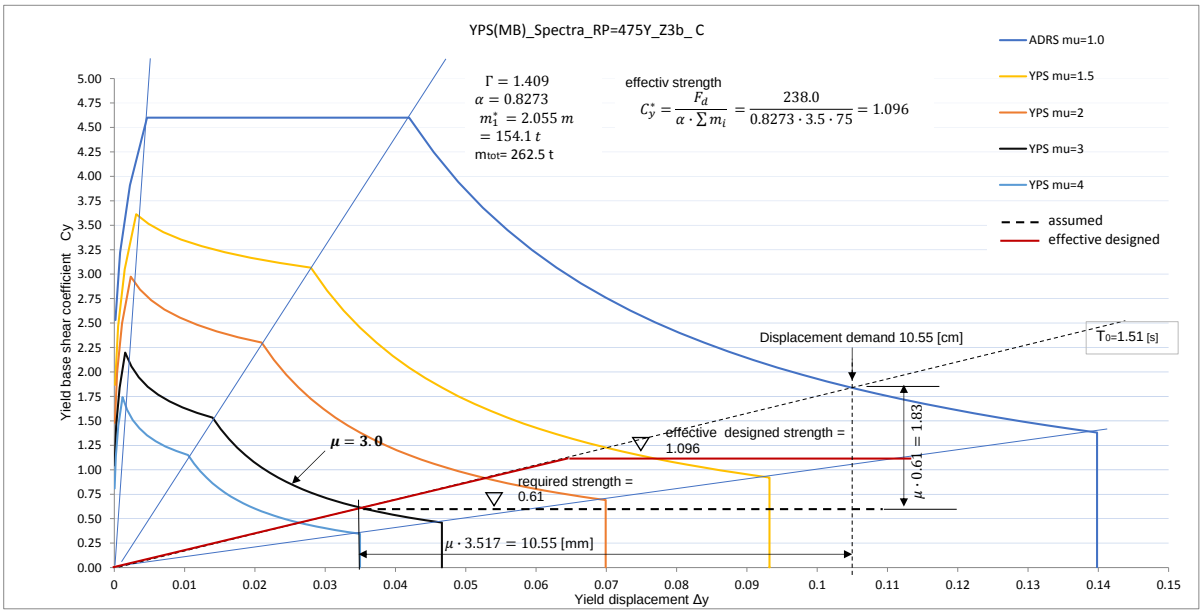

Fig. 9.4: Results obtained by force-based seismic design after [6], summarized and presented in yield point response spectra

In Figure 9.4, the ductility assumption of $\mu = 3.0$ and the result of the analysis based on an equivalent elastic beam element, represented by the period of vibration $T_0 = 1.51[s]$ are superimposed on the response spectra, resulting in the required strength expressed as yield base shear coefficient $C_y^* = 0.61[m/s^2]$. Wall TWX_1 is designed in such a way to provide strength of $C_y^* = 1.096[m/s^2]$ with the corresponding effective ductility demand of $\mu = 1.67$. Note that the mass participation factor α has been estimated within the modal analysis (see also the next section). The displacement demand of the equivalent SDOF system, represented in the RS in Figure 9.4, is $106[mm]$. The corresponding roof displacement capacity demand is then $\Delta_{roof} = \Gamma \cdot \Delta_{el} = 1.409 \cdot 106 = 149[mm]$

No iteration has been performed following the effective design. Strictly speaking, the increase in strength and stiffness has consequences for the ductility demand as well as for the period of vibrations and hence, the base shear coefficient. The assumed strength is $133[kN]$, and the effective strength is $238[kN]$. This is an increase by 80%.

During the design process, it is stated that the rules of capacity design can be applied. This means that the material overstrength in the "plastic hinge" can be exploited. Thus the staples behave in the inelastic range, developing plastic deformations, while all other elements behave elastically. According to the specification in the Swiss standard for the design of timber structures SIA265 [91] the elements subjected to shear (OSB panels) should be over dimensioned by approximately 20% in order to avoid brittle failure.

9.4 Performance Based Engineering (PBE)

9.4.1 Different wall length combinations and torsion effects

This chapter compares the results of two different seismic design procedures. At the same time, a description is provided about how the elements with different wall lengths and stiffnesses can be combined within a structure in order to enable use of the results presented in this thesis.

Structures which are perfectly symmetric in plan view are rare. It is much more common, that the lateral load resisting systems contain walls of different lengths in an asymmetrical arrangement. Consequently, the center of stiffness moves away from the center of mass towards the elements with larger flexural or shear rigidity. This produces torsion effects if a structure is subjected to lateral loads or an earthquake excitation. Additionally, as a result of the increasing large deformation along the height of the structure, the eccentricity increases with increasing building height. Moreover, the codes [3] and [1] require an increase of eccentricity due to random eccentricity and possible random collapse patterns. It is difficult to consider all of these effects in an analysis of a 2D-model. Nowadays, structures are generally analyzed using 3D linear elastic models. Thus, the estimation of the load distribution between different bearing elements is generally not a big problem. In the brochure [6], the eccentricity has been estimated by using a 3D beam model based on an equivalent elastic beam element. Although in computer based FE analysis, the distribution of the lateral loads, including an asymmetric arrangement of LFTWs,

is a straightforward issue, a simplified handling of this problem is briefly presented in this section for completeness.

9.4.2 Asymmetric wall arrangement

In Figure 9.5, a lateral load resisting system consisting of 4 LFTWs, 2 in each direction, is presented. Due to the different wall lengths of wall TWX_1, 3.0[m] and wall TWX_2, 4.0[m] along the X-axis, the centers of stiffness and mass do not lie on the axis of symmetry. The position of the center of rigidity is load independent, since it is a function of the structural properties. On the other side the earthquake forces act at the center of mass with the consequence that in addition to bending, torsion effects occur as well. The total displacement vector can be expressed as a linear combination of the translation (work done by shear forces) and the rotation (work done by torsion) within the floor plane.

$$F_i = \frac{k_{i,x}}{\Sigma k_{i,x}} \cdot E_d + M_{Td,n} \cdot \frac{k_{i,x} \cdot y_{c,i}}{\sum(k_{x,i} \cdot y_{ci}^2 + k_{y,i} \cdot x_{ci}^2)} \tag{9.1}$$

Translation

The lateral load is distributed over the bearing elements proportional to their lateral stiffness. This is expressed as follows:

$$F_i = \frac{k_{i,x}}{\Sigma k_{i,x}} \cdot E_d \tag{9.2}$$

where F_i is the force in wall i and E_d is the total earthquake load acting at the center of mass.

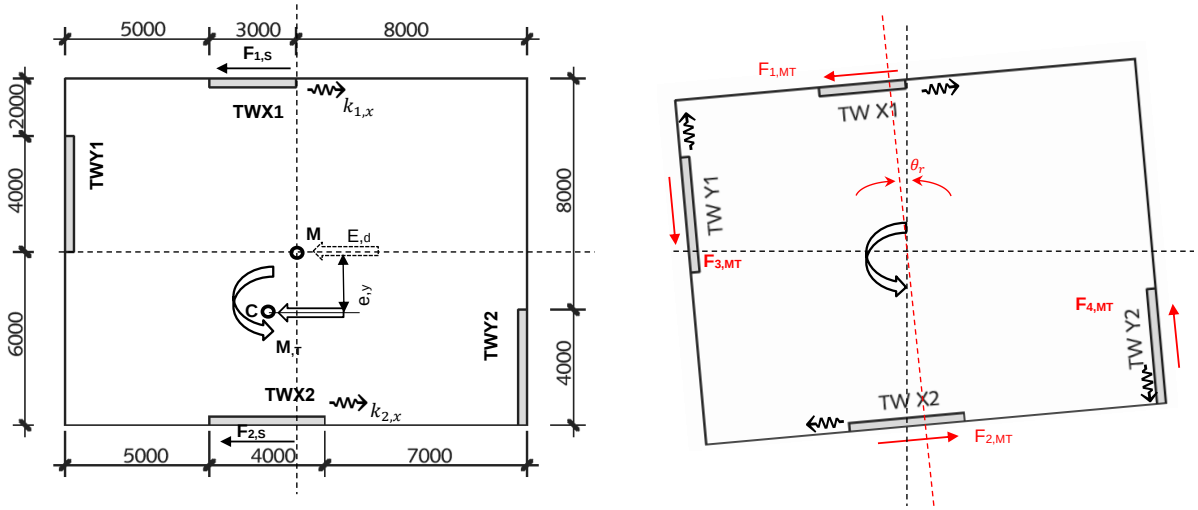

Fig. 9.5: Lateral load resisting system at plan view with mass and stiffness centroid (left), distribution of the shear force due to translation (left) and torsion (right)

In Figure 9.6, the total earthquake force, induced by masses m_1 and m_2, is sustained by walls TWX_1 and TWX_2. The total mass of the system is $m = m_1 + m_2$. For uncoupled, separately

acting systems applies $\omega_1^2 = \frac{k_1}{m_1}$ and $\omega_2^2 = \frac{k_2}{m_2}$. Taking into account only translation, following applies for a coupled system: $\omega_1 = \omega_2$, and thus $\frac{k_1}{m_1} = \frac{k_2}{m_2}$. The mass, and hence the force distribution, is proportional to stiffness $\frac{k_1}{k_2} = \frac{m_1}{m_2}$, the fact reflected in Equation 9.2.

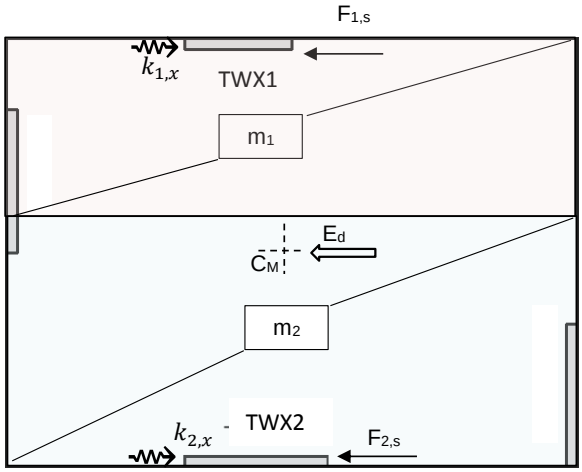

Fig. 9.6: Distribution of lateral load due to translation

Torsion

In order to estimate the load distribution on the individual walls due to torsion, the stiffness center should be estimated, and the eccentricity over the building height should be estimated in accordance with the wall stiffnesses. Since the structure is asymmetric for earthquake forces along the x- axis, only the eccentricity along y-axis will be investigated. From simple statics, the stiffness center can be estimated as follows:

$$y_s = \frac{\sum k_{i,x} \cdot y_i}{\sum k_{i,x}} \tag{9.3}$$

Equation 9.3 is related to the stiffness distribution in plane. The stiffness distribution along the height of the structure is estimated using a static pushover curve. The results are summarized in Table 9.4. See also Figure 9.7.

Tab. 9.4: Stiffness of W_1 and W_2 for 1-, 2- 3- and 4-storey building

storey	Wall with length $3[m]$ (TWX_1)			Wall with length $4[m]$ (TWX_2)		
	Δ_y $[mm]$	F_y $[kN]$	$k_{1,n}$ $[kN/mm]$	$\Delta_y[mm]$	F_y $[kN]$	$k_{2,n}[kN/mm]$
1	28.81	495.7	17.206	30.68	708.1	23.08
2	51.33	491.87	9.58	52.4	702.6	13.4
3	85.51	488.0	5.70	85.04	697.1	8.197
4	133.0	482.0	3.62	128.1	694.2	5.419

The position of the stiffness center in each storey is to be estimated separately:

$$y_s, 1st = \frac{k_{1,x} \cdot y_1 + k_{2,x} \cdot y_2}{k_{1,x} + k_{2,x}} = \frac{17.206 \cdot 12 + 23.08 \cdot 0}{17.206 + 23.08} = 5.125[m]$$
$$y_s, 2st = \frac{9.58 \cdot 12 + 13.4 \cdot 0}{9.58 + 13.4} = 5.00[m]$$
$$y_s, 3st = \frac{5.70 \cdot 12 + 8.197 \cdot 0}{5.70 + 8.197} = 4.922[m]$$
$$y_s, 4st = \frac{3.62 \cdot 12 + 5.419 \cdot 0}{3.62 + 5.419} = 4.806[m]$$

so, the eccentricity along the height of the structure is:

$$e1, y = 6.0 - 5.125 = 0.875[m]$$
$$e2, y = 6.0 - 5.00 = 1.0[m]$$
$$e3, y = 6.0 - 4.922 = 1.078[m]$$
$$e4, y = 6.0 - 4.806 = 1.194[m]$$

In Figure 9.7, the distribution of the earthquake forces along the height of the structure is presented. The eccentricity at the considered level is influenced not only by the forces acting at this level, but also by the forces acting at the levels above. For example, on the forth storey-level, only forces on this level affect the eccentricity here. On the first level, all forces above the first level contribute to an increase of the eccentricity here. This can be expressed as follows:

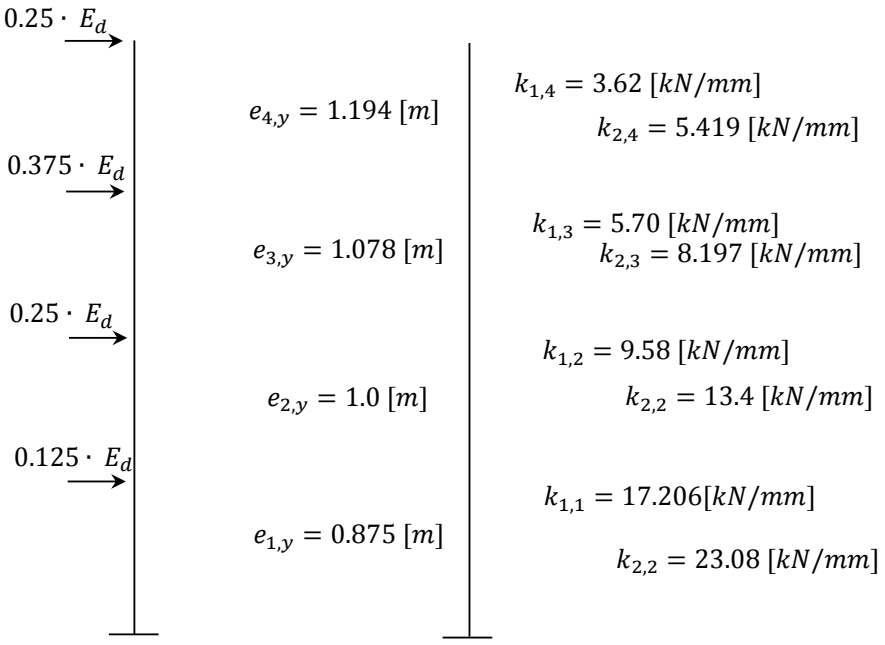

Fig. 9.7: Distribution of lateral load along the height of the structure with corresponding eccentricities and stiffness

$$e_{eff,n} = \frac{\sum (E_{d,n} \cdot e_{n,y})}{\sum E_{d,n}}$$

$$e_{eff,1} = \frac{0.25 \cdot 1.194 + 0.375 \cdot 1.078 + 0.25 \cdot 1.0 + 0.125 \cdot 0.875}{0.25 + 0.375 + 0.25 + 0.125} = \frac{1.062}{1.0} = 1.062[m]$$

$$e_{eff,2} = \frac{0.25 \cdot 1.194 + 0.375 \cdot 1.078 + 0.25 \cdot 1.0}{0.25 + 0.375 + 0.25} = \frac{0.95275}{0.875} = 1.089[m]$$

$$e_{eff,3} = \frac{0.25 \cdot 1.194 + 0.375 \cdot 1.078}{0.25 + 0.375} = \frac{0.70275}{0.625} = 1.124[m]$$

$$e_{eff,4} = \frac{0.25 \cdot 1.194}{0.25} = \frac{0.2985}{0.25} = 1.194[m]$$

The values of the effective eccentricity, estimated above on the basis of the structural properties, are the real eccentricities. In order to take into account a random failure, the torsion moment acting at each level should be increased as required by the code (see [3]), leading to the design quantities of the eccentricity, as follows:

$$e_{d,n} = \lambda \cdot e_{eff,n} + \Delta e_y = 1.5 \cdot e_{eff,n} + 0.05 \cdot b$$

$$e_{d,1} = 1.5 \cdot 1.062 + 0.05 \cdot 12 = 1.593 + 0.6 = 2.193[m]$$

$$e_{d,2} = 1.5 \cdot 1.089 + 0.05 \cdot 12 = 1.633 + 0.6 = 2.234[m]$$

$$e_{d,3} = 1.5 \cdot 1.124 + 0.05 \cdot 12 = 1.686 + 0.6 = 2.286[m]$$

$$e_{d,4} = 1.5 \cdot 1.194 + 0.05 \cdot 12 = 1.791 + 0.6 = 2.391[m]$$

where $\lambda = 1.5$ for an analysis based on an equivalent lateral load and $\lambda = 1.0$ for an analysis based on a response spectrum. Note that, in the following analyses, the value $\lambda = 1.5$ is used in order to enable comparison with the analyses conducted in [6].

The design torsion moments are distributed as follows:

$$M_{Td,n} = \sum E_{d,n} \cdot e_{d,n}$$

$$M_{Td,1} = E_d \cdot 2.193 = 2.193 \cdot E_d[kNm]$$

$$M_{Td,2} = 0.875 \cdot E_d \cdot 2.234 = 1.955 \cdot E_d[kNm]$$

$$M_{Td,3} = 0.625 \cdot E_d \cdot 2.286 = 1.429 \cdot E_d[kNm]$$

$$M_{Td,4} = 0.25 \cdot E_d \cdot 2.391 = 0.598 \cdot E_d[kNm]$$

For completion of Equation 9.1, $\sum(k_{x,i} \cdot y_{ci}^2 + k_{y,i} \cdot x_{ci}^2)$ should be estimated.

The total force distribution on the first storey can be estimated as a linear combination of the translation and the torsion as follows:

$$F_i, n = \frac{k_{i,x}}{\Sigma k_{i,x}} \cdot E_{d,n} + M_{Td,n} \cdot \frac{k_{i,x} \cdot y_{c,i}}{\sum(k_{x,i} \cdot y_{ci}^2 + k_{y,i} \cdot x_{ci}^2)}$$

$$F_1 = \frac{E_d \cdot 17.206}{(17.206 + 23.08)} + 2.193 \cdot E_d \cdot \frac{17.206 \cdot 6.875}{4374.0} = 0.427 \cdot E_d + 0.0593 \cdot E_d = 0.486 \cdot E_d$$

Tab. 9.5: Estimation of the torsional stiffness

storey	Walls in x-direction				Walls in y-directiontran		
	$k_{1,x}$	$y_{c,1}$	$k_{2,x}$	$y_{c,2}$	$k_{2,y}$	$x_{c,2}$	$\sum(k_{i,x} \cdot y_{ci}^2 + k_{i,y} \cdot x_{c,i}^2)$
	$[kN/mm]$	$[m]$	$[kN/mm]$	$[m]$	$[kN/mm]$	$[m]$	$[kNm]$
1	17.206	6.875	23.08	5.125	23.08	8.0	4374.0
2	9.58	7.0	13.4	5.0	13.4	8.0	2520.0
3	5.70	7.078	8.197	4.922	8.197	8.0	1533.0
4	3.62	7.194	5.419	4.806	5.419	8.0	1006.0

For the purposes of comparison, the total mass is distributed between walls W_1 and W_2 in a ratio of 50% : 50% for all storeys, Thus the mass subjected to the wall 1 is $m_{1...3} = 75\ [t/storey]$, and mass on the roof is $m_4 = 37.5[t]$.

9.5 Analysis Based on PBE

9.5.1 One storey shear wall

Geometry and constitutive modeling

The basic constitutive element of the model is the mechanical model of a 1 storey shear wall. For this purpose, a wall with a length of 3.0 [m] is created and analyzed in MCASHEW [31]. The main geometrical and mechanical properties of the model are presented in Figure 9.8. The fasteners used to connect the OSB panels with the timber frame are staples with a diameter of

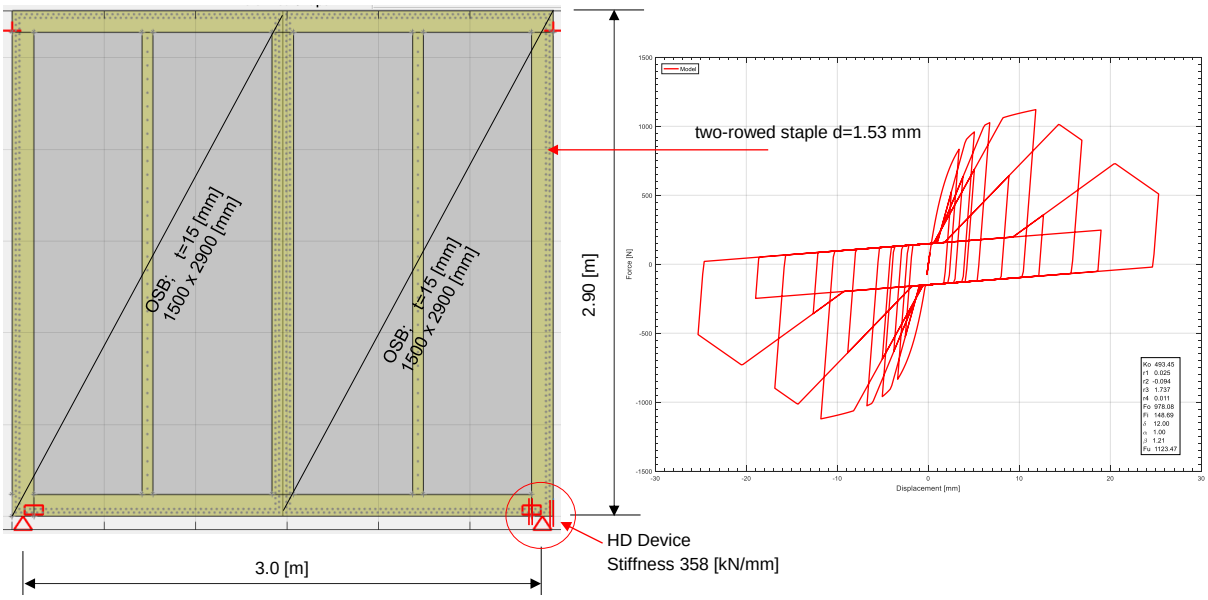

Fig. 9.8: Geometrical properties and constitutive components of the model of a one-storey 3.0 [m] shear wall element

$d = 1.53[mm]$ araringed in two rows. The fastener behaviour is represented by its hysteresis, characterized by the 10 Stewart parameters (see also Table 3.6). The wall element is sheathed with OSB panels with $t_p = 15[mm]$ on both sides. The HD devices behave predominantly elastically with a stiffness of 358 [kN/mm]. This is approximately 50% of the stiffness provided by a HD device consisting of 16 dowel-type connectors with d=10 [mm] and 3 slotted-in steel plates. This stiffness is estimated as $K_{HD} = 7.22 \cdot 16 \cdot 6 = 693[kN/mm]$ (see also Table 3.1). With 50% of the effective stiffness provided by the HD devices, the stiffnesses of the inter-storey connectors have been accounted for.

Hysteresis

The mechanical characteristics of two wall elements used in the analysis of prototype building are estimated for monotonic, Mergo-Beyer and CUREE loading protocols. The hysteresis are presented in graphical form in Figure 9.9 and 9.10, as well in tabular form in Tables 9.6 and 9.7 for LFTWs with length 3.0 and 4.0[m], respectively.

The parameters estimated by using the Mergos-Beyer loading protocol are used in further PBE analyses, for both considered wall lengths.

Tab. 9.6: Estimated parameters of the Stewart hysteresis for a wall length of 3000[mm], wall height of 2900[mm]; both sides sheathed with OSB3, $t_p = 15[mm]$; fasteners: two-rowed staples with $d = 1.53[mm]$, spacing 24[mm]; fastener hysteresis according to Table 3.6

OSB	K_0	R_1	R_2	R_3	R_4	F_0	F_i	Δ_{max}	α	β	F_{max}
#	[kN/mm]	[-]	[-]	[-]	[-]	[kN]	[kN]	[mm]	[-]	[-]	[kN]
CASHEW monotonic loading											
2	23.53	0.045	-0.438	-	-	531.14	-	71.21	-	-	580.70
CASHEW Mergos-Beyer loading protocol											
2	23.01	0.028	-0.132	1.009	0.050	569.19	79.51	67.20	1.0	1.01	571.70
CASHEW CUREE loading protocol											
2	23.33	0.018	-0.150	1.065	0.04	569.14	70.34	67.63	1.0	1.11	560.30

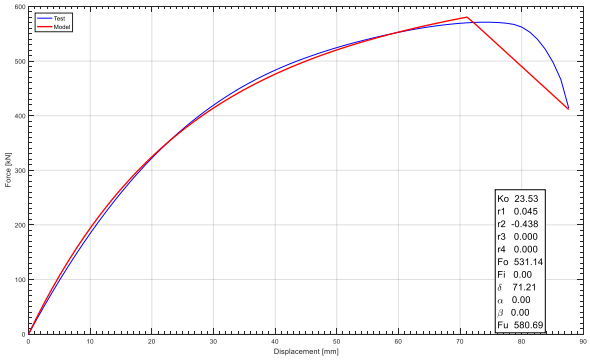

(a)

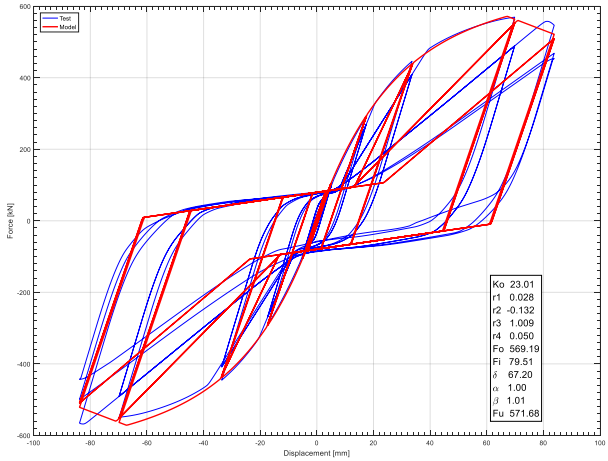

(b)

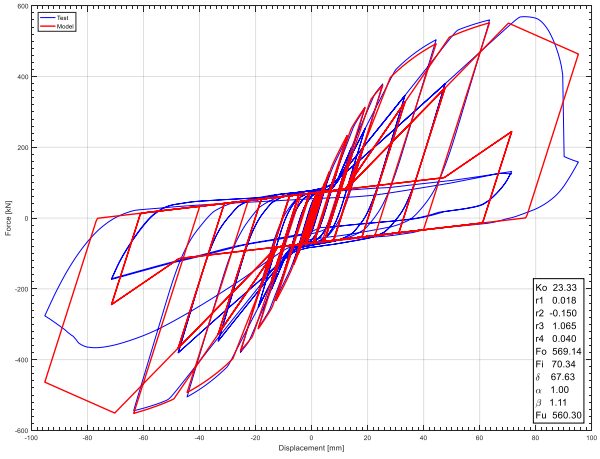

(c)

Fig. 9.9: Hysteretic parameters of the 3.0 [m] LFTW, estimated under monotonic loading 9.9(a): under the Mergos-Beyer loading protocol, 9.9(b): under the CUREE loading protocol, 9.9(c)

Tab. 9.7: Estimated parameters of the Stewart hysteresis for a wall length of 4000[mm], wall height of 2900[mm]; both sides sheathed with OSB3, $t_p = 15[mm]$; fasteners: two- rowed staples with $d = 1.53[mm]$, spacing 24[mm]; fastener hysteresis according to Table 3.6

OSB	K_0	R_1	R_2	R_3	R_4	F_0	F_i	Δ_{max}	α	β	F_{max}
#	[kN/mm]	[-]	[-]	[-]	[-]	[kN]	[kN]	[mm]	[-]	[-]	[kN]
CASHEW monotonic loading											
2	31.826	0.020	-0.295	-	-	824.31	-	74.77	-	-	825.73
CASHEW Mergos-Beyer loading protocol											
2	30.62	0.032	-0.162	1.07	0.052	809.3	120.68	71.42	1.0	1.06	820.04
CASHEW CUREE loading protocol											
2	30.89	0.022	-0.350	1.137	0.035	820.21	95.53	65.46	0.95	1.05	790.30

Parameters needed for damage index (DI) analysis

In order to be able to perform complete damage analysis, parameter β should be estimated according to Equation 5.2. For this purpose, the energy dissipated during both the Mergos-Beyer and the CUREE loading protocols has been estimated. In Figure 9.12 and 9.11, the dissipated energy is presented for LFTWs with length 3.0 and 4.0[m] respectively.

Tab. 9.8: Estimation of coefficient β_{DI} from the CASHEW hysteretic and static pushover analysis performed for the 3.0 and 4.0 [m] LFTW, presented schematically in Figure 9.8

OSB	L_w	$\Delta_{u,st}$	F_y	$\Delta_{resp_{CE}}$	$\Delta_{resp_{MB}}$	$\int dE_{CE}$	$\int dE_{MB}$	β_{CE}	β_{MB}	β_{DI}
#	[m]	[mm]	[kN]	[mm]	[mm]	[kNm]	[kNm]	[-]	[-]	[-]
2	3.0	106.5	495.7	67.63	67.20	226.4	253.7	0.0851	0.0768	0.081
2	4.0	105.4	708.1	65.46	71.41	290.4	357.7	0.098	0.067	0.083

9.5.2 Four storey shear wall

A four-storey structure is created by stacking equivalent 1-storey LFTW elements on top of each other and connecing them.

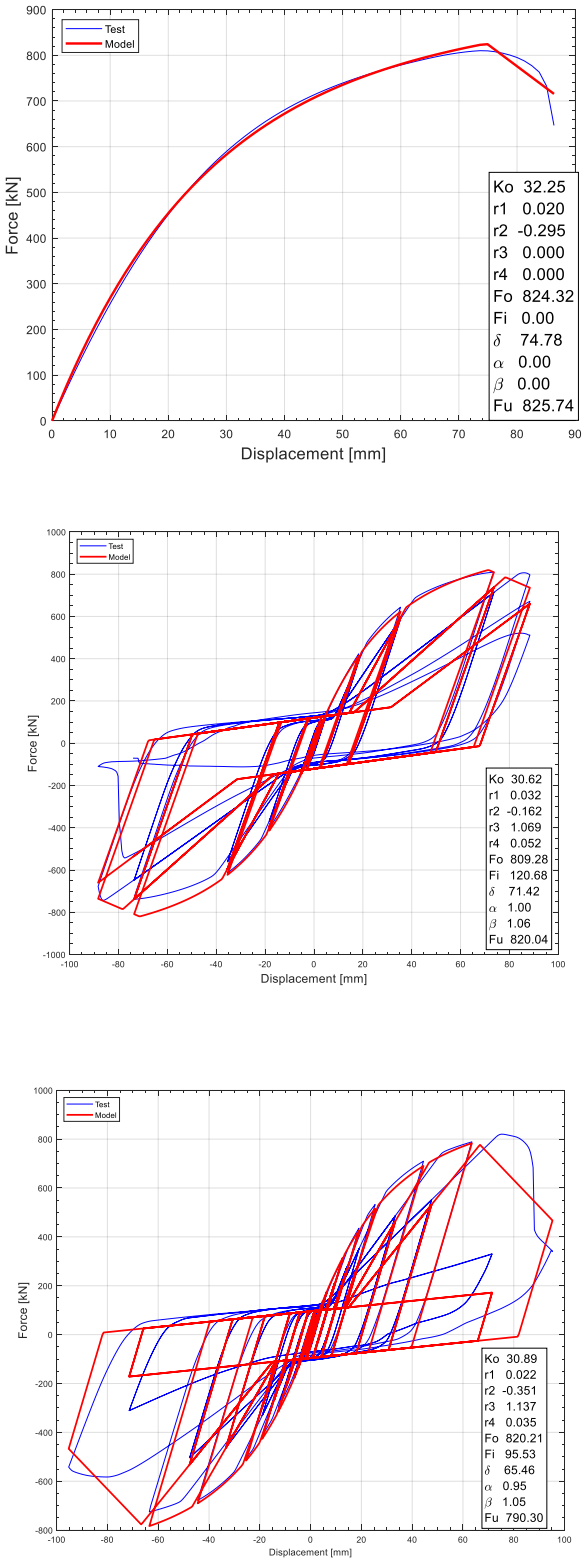

Fig. 9.10: Mechanical model of the LFTW with the length of 4[m], response to monotonic loading, Mergos-Beyer and CUREE laoding protocol.

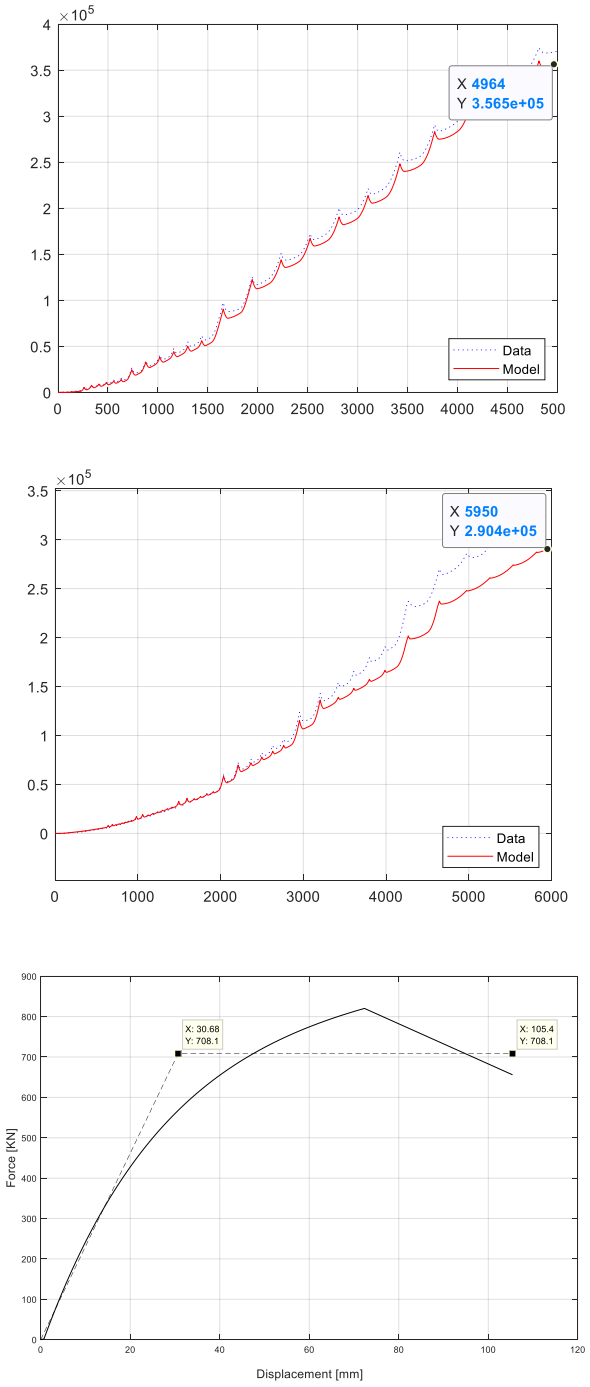

Fig. 9.11: Numerical energy dissipation due to the Mergos-Beyer and CUREE loading protocol, estimated for LFTW with length of $4[m]$

In the first step, a modal analysis is performed. The mass of 75 [t], estimated in the previous section is constant for all residential floors. The mass on the top of the building is 37.5 [t]. The stiffness of the single-storey element used to build the four-storey structure is constant along the height of the building.

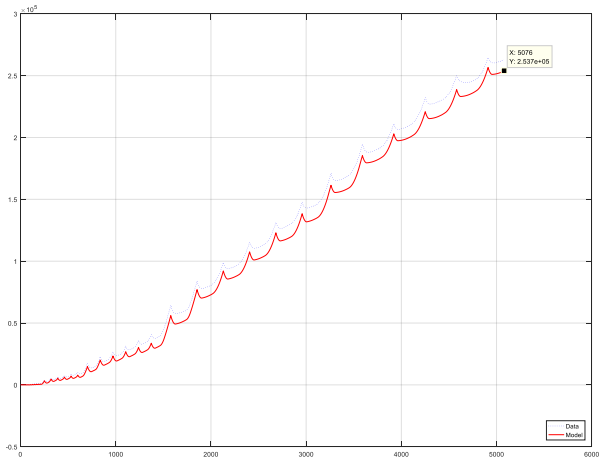

(a)

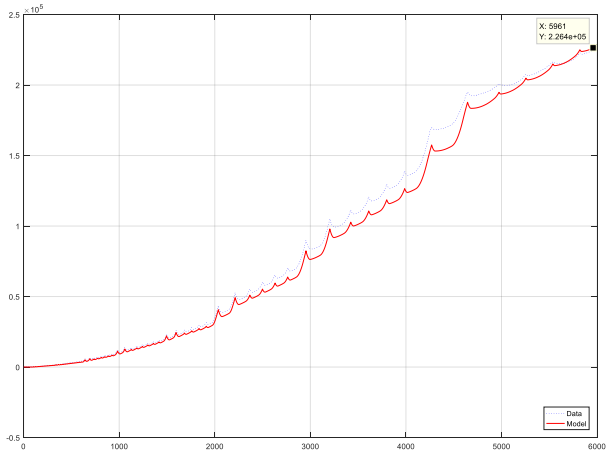

(b)

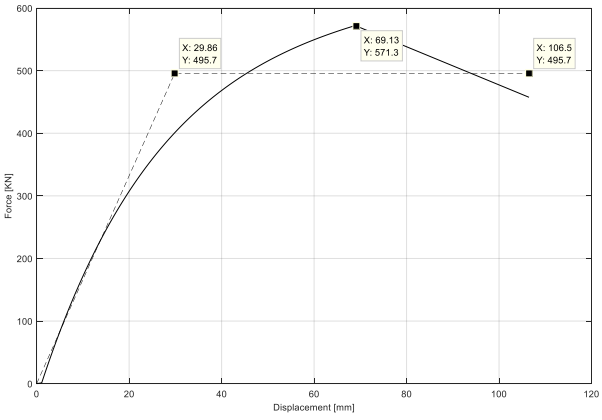

(c)

Fig. 9.12: Energy dissipated during the Mergos-Beyer loading protocol, 9.12(a): under the CUREE loading protocol, 9.12(b): pushover curve of the one-storey LFTW with a length of 3.0 [m], 9.12(c)

Modal analysis

In Figure 9.13 (right), the first three mode shapes of a 3.0 [m] long LFTW are shown.
The modal mass, the modal mass participation factor Γ_i, the periods of vibration and the mass participation factor α_i can be estimated as follows:

$$m^* = \Sigma m_i \cdot \phi_{ij} = 75 \cdot (0.238 + 0.522 + 0.795) + 37.5 \cdot 1.0 = 154.125[t] = 2.055 \cdot m$$

for the first mode applies:

$$\Gamma_1 = \frac{\sum m_1 \cdot \phi_{i,1}}{\sum m_1 \cdot \phi_{i,1}^2} = \frac{2.052}{1.45628} = 1.409$$

$$\alpha_1 = \frac{\Gamma_1 \cdot m^*}{\sum m_i} = \frac{1.409 \cdot 2.055}{3.5} = 0.8273$$

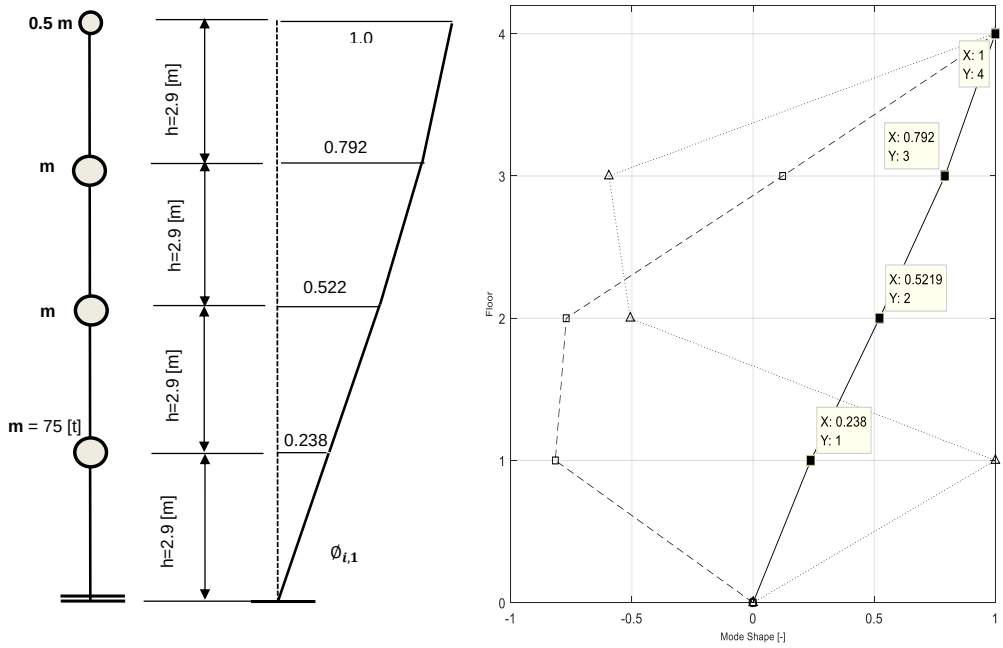

Fig. 9.13: Four storey-model, the first mode shape extracted (left) and shapes of the first three modes (right)

Pushover analysis

In Figure 9.14, the pushover curve for the 4-storey structure is presented. From the figure, it can be seen that the yield force and the yield displacement are 482 [kN] and 133 [mm], respectively. The displacement capacity at the roof level is 223.7 [mm] (see Figure 9.14).

$$\Delta_y^* = \frac{\Delta_y}{\Gamma_1} = \frac{133}{1.409} = 94.4[mm], \text{ see also Figure 9.15}$$

$$C_y = \frac{F_y}{\sum m \cdot g} = \frac{482}{3.5 \cdot 75 \cdot 9.81} = 0.1872 \cdot g = 1.84[m/s^2]$$

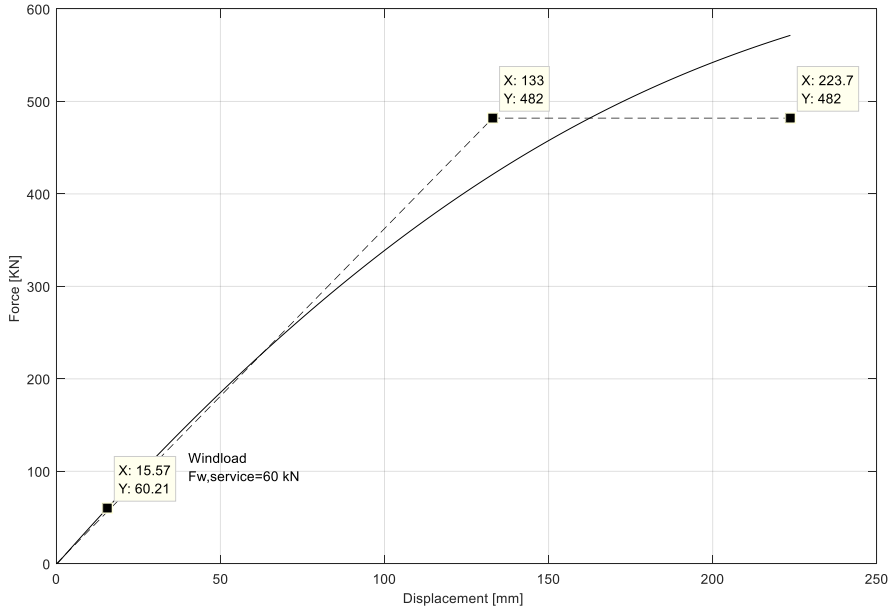

Fig. 9.14: Pushover curve (force-roof-displacement relationship) for the 3.0 [m], 4-storey LFTW

$C_y^* = \frac{F_y}{\alpha_1 \cdot \sum m \cdot g} = \frac{482}{0.8273 \cdot 3.5 \cdot 75 \cdot 9.81} = 0.2266 \cdot g = 2.22[m/s^2]$, see also Figure 9.15

$T^* = 2 \cdot \pi \cdot \sqrt{\frac{\Delta_y^*}{C_y^* \cdot g}} = 2 \cdot \pi \cdot \sqrt{\frac{94.39}{0.2266 \cdot 9810}} = 1.29[s]$

The pushover curve shows an almost linear rising branch up to the maximum bearing capacity of 572 [kN]. The yield force and the yield displacement are estimated by using the EEEP approach. At the same time, a service-level wind load of $60[kN] = 12 \cdot 0.5 \cdot 4 \cdot 2.9 \cdot q_{wind} = 69.6[m^2] \cdot 0.862[kN/m^2]$ is superimposed on the pushover curve. The wind load is about 12.5% of the yield strength of the wall, so the wind is not likely to govern the design.

Ductility demand

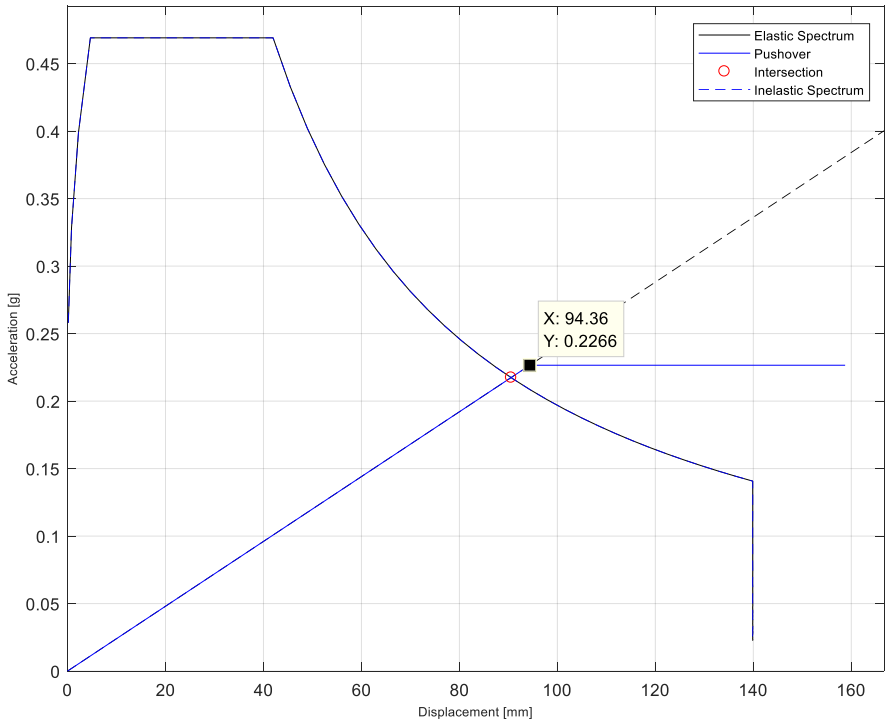

Fig. 9.15: Response spectra for hazard zone Z3b and capacity curve of the wall

The pushover curve is transformed into a capacity curve and is superimposed on the RS in Figure 9.15. Since the yiled point characterized by displacement of 94.6$[mm]$ lies beyond elastic spectra, it can be seen that the ductility demand is 1.0, and the structure responde elastically in the case of an design earthquake excitation with the displacement demand of 90.2$[mm]$, which is the intersection point of the capacity curve and the RS for $T^* = 1.29[s]$. At the intersection point between the capacity curve and the RS, the base shear coefficient is 2.14, resulting in an earthquake force of 464.64 [kN]. This implies that the earthquake lateral load is less than the elastic strength of the structure.

9.5.3 Damage index analysis

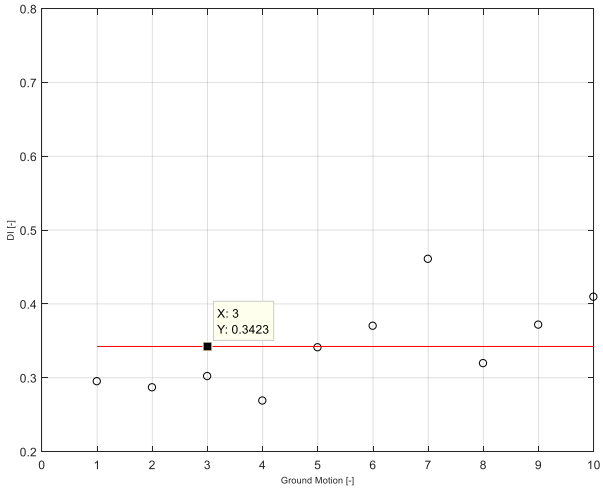

Fig. 9.16: Average Damage Index estimated from 10 earthquake records

The damage index has been estimated using Equation 5.1, as presented in Figure 9.16. The value of $D = 0.34 < 0.4$ reveals that, according to Table 5.7, the structure would experience slight damage and the elements would preserve their strength and stiffness. This response better applies to the immediate occupancy limit state than the life safety limit state.

9.5.4 The results of the NLTHA

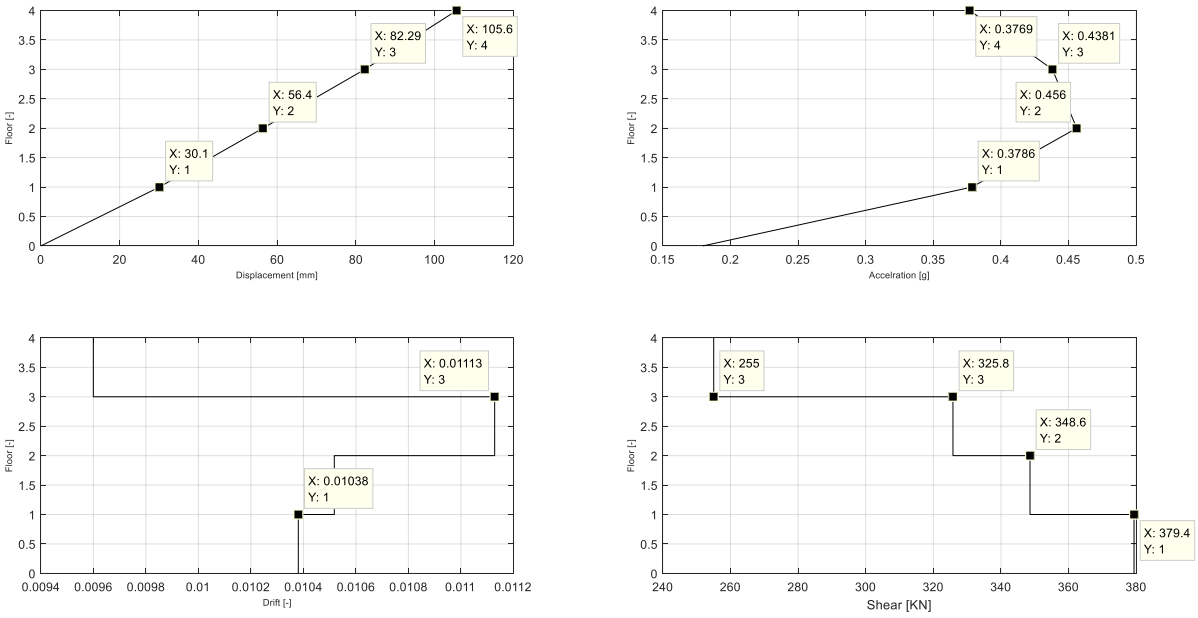

Fig. 9.17: Average displacements, accelerations, IDR and shear forces estimated from 10 earthquake records scaled to the Z3b hazard level

Figure 9.17 shows the results obtained by NLTHA. The maximum estimated shear force is $F_{BS,NLTHA} = 379[kN]$, which is approximately 79% of the yield strength (see Figures 9.14 and 9.20). The maximum roof displacement is $106[mm]$, corresponding to a RDR= 0.91% and a maximum IDR of approximately 1.11%. The IDR of 1%, estimated for the first storey level is, according to Table 5.7, the threshold value between the IO and the LS limit state.

9.5.5 Tabular results presentation for prototype LFTW

Similar to the parameter study performed in Chapters 6 and 7 for LFTWs sheathed with GFB and OSB, the results of the IDA, modal, pushover and NLTH analyses are summarized in Table 9.9 and 9.10 for walls with length 3.0 and $4.0[m]$, respectively.
As can be seen from the table 9.9 and 9.10, no limit parameter values used in the parameter study have been exceeded, except the hold-down forces, which are in the range of $927[kN]$ and $940.5[kN]$. It is significant to note that, even for hazard zone 3b, the system still behaves in the linear elastic range, with a ductility demand of $\mu = 1.0$. The consequences are discussed later in this chapter.

Tab. 9.9: Results of PBE analysis performed for a prototype 4-storey LFTW with a length of 3.0 [m]

Zone	Mass	IDA	Modal analysis			Pushover analysis				NLTH analysis			
a_g	m	check	T	T^*	Γ	Δ_y	F_y	μ	$\Delta_{u,st}$	HD force	Δ_{roof}	IDR	DI
$[\frac{m}{s^2}]$	[t]		[s]	[s]	[-]	[mm]	[kN]	[-]	[mm]	[kN]	[mm]	[-]	[-]
4- storey structure													
1.6	75.0/37.5	✓	1.16	1.29	1.41	133.0	482.0	1.0	223.7	926.7	105.6	1.11	0.34

Tab. 9.10: Results of PBE analysis performed for a prototype 4-storey LFTW with a length of 4.0 [m]

Zone	Mass	IDA	Modal analysis			Pushover analysis				NLTH analysis			
a_g	m	check	T	T^*	Γ	Δ_y	F_y	μ	$\Delta_{u,st}$	HD force	Δ_{roof}	IDR	DI
$[\frac{m}{s^2}]$	[t]		[s]	[s]	[-]	[mm]	[kN]	[-]	[mm]	[kN]	[mm]	[-]	[-]
4- storey structure													
1.6	75.0/37.5	✓	0.96	1.08	1.39	128.1	694.2	1.0	234.0	940.5	90.34	0.95	0.30

9.5.6 IDA analysis

IDA analysis has been performed by using the pushover curve presented in Figure 9.14. The dynamic analysis is based on a quadrilinear fit of the inserted pushover curve and the yielding period of vibration of $T^* = 1.24[s]$. This period is slightly different from $T^* = 1.29[s]$ estimated by using the EEEP approach within the pushover analysis.

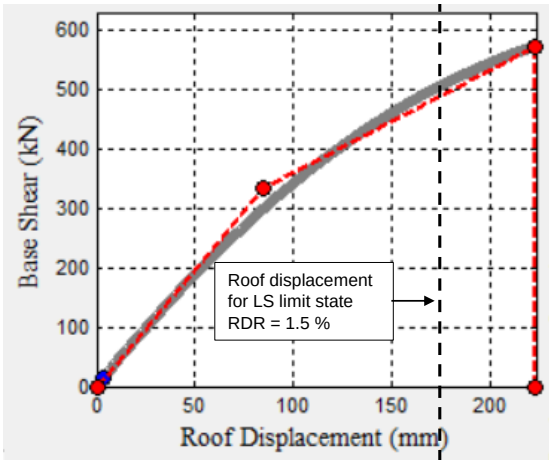

(a)

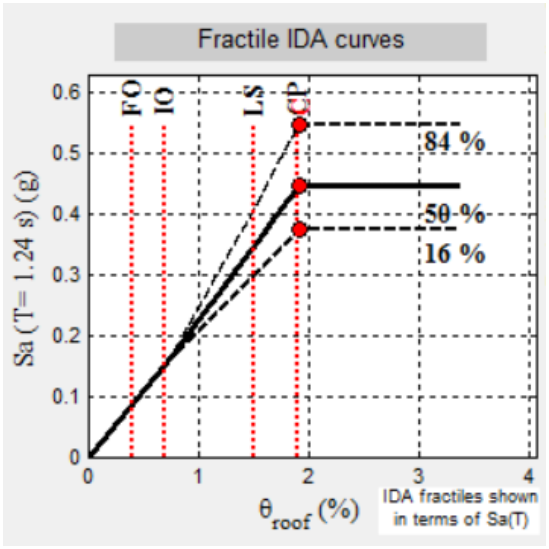

(b)

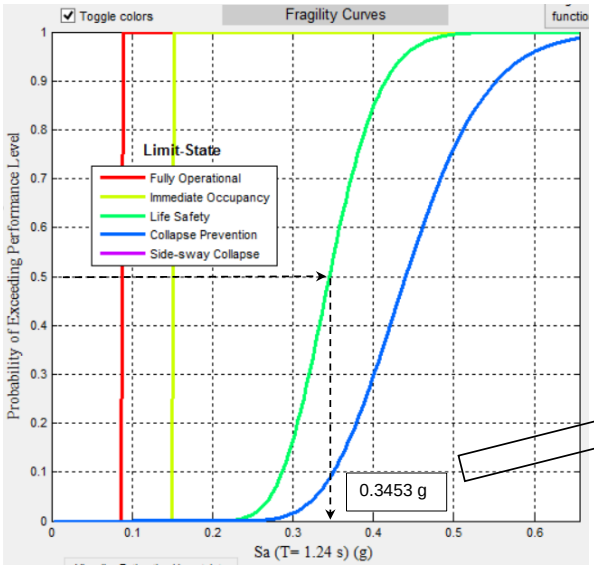

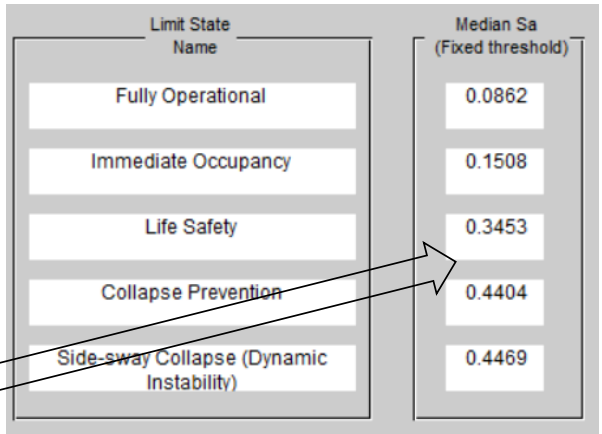

(c)

Fig. 9.18: Roof drift ratio of 1.5% as a damage measure (DM), selected directly from the quadrilinear fit of the pushover curve, 9.18(a): Fractile IDA curves for a roof drift ratio of 1.5% as a damage measure (DM), in terms of spectral acceleration $S_{a,(T=1.24[s]}$ as an intensity measure (IM), 9.18(b): Fragility curve for spectral acceleration as an intensity measure for $T = 1.24[s]$, 9.18(c)

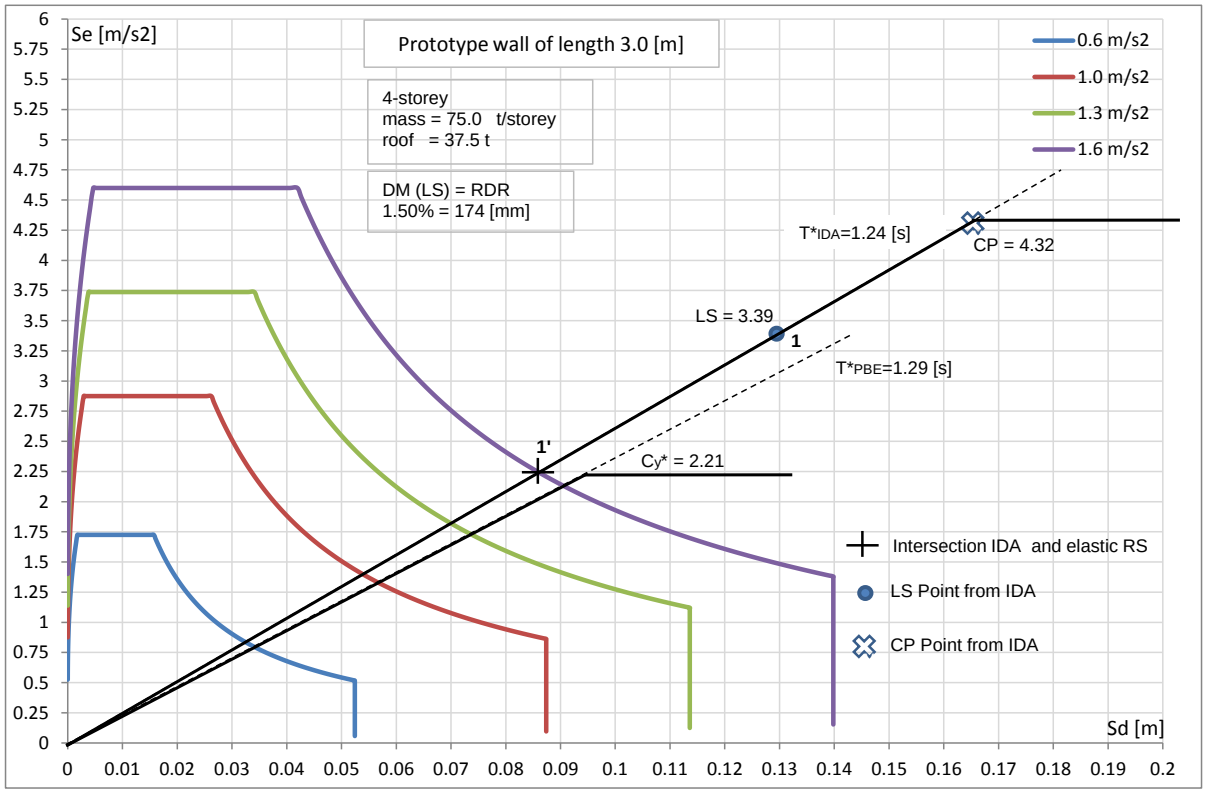

Fig. 9.19: 50% fractile IDA-curve estimated for $DM = RDR$ of 1.5% in terms of the spectral acceleration $S_{a(T)}$ used as the intensity measure for vibration period of $T = 1.24[s]$ superimposed on YPS for hazard zone Z3b

The damage measure (DM) corresponding to the life safety limit state is chosen to be a roof drift ratio of $RDR = 1.5\% = 174[mm]$ (see also Figure 9.18. The intensity measure (IM) for which the DM will be reached is estimated to be a spectral acceleration of $S_a = 0.3453 \cdot g = 3.39[m/s^2]$ at $T^* = 1.24[s]$, see Figure 9.18. The results obtained using the pushover and the IDA analyses are summarized in Figure 9.19. The intersection point between the elastic RS and the IDA fractile curve, illustrated by $1'$, is at the spectral acceleration of $2.23 < 3.39[m/s^2]$. This implies that the bearing capacity of the system is not entirely exploited, according to the IDA analysis. Another calculation, which is not given here, shows that a spectral acceleration of $S_{a,T=1.24[s]} = 0.2238 \cdot g$ produces a roof drift ratio, and hence DM of = 1%, characteristic of the IO limit state. The corresponding roof displacement is $116[mm]$, which is also evidence of a stiff structure.

9.5.7 Discussion

Earthquake forces and ductility demand

In Figure 9.20, the results of the force based seismic design performed in [6] and the results of the pushover analysis of the LFTW TWX_1 are summarized. The assumption, made in advance, is that the ductility provided by the system is $\mu = 3.0$. Independent of the analysis method used for estimation of the earthquake forces, the ductility factor, and hence the behaviour factor in the velocity sensitive region of the RS, is always understood as a reduction coefficient, which defines the required strength of the structure. See also Figure 9.4.

From Figure 9.4, the earthquake force, defined as the intersection point with the elastic RS for the given period of vibration $T_1 = 1.51[s]$, is $E_{d,el} = 1.83 \cdot 0.8273 \cdot 3.5 \cdot 75 = 397[kN]$. The required strength is only $R_{d,req} = 0.61 \cdot 0.8273 \cdot 3.5 \cdot 75 = 132.5[kN]$, provided the structure can exhibit a displacement of $\Gamma \cdot 10.55[cm] = 148.6[mm]$, as required by the equal displacement rule.

As it is typical for force-based seismic design, the structure is designed in a way to provide a bearing capacity larger than the assumed earthquake force. Consequently, the strength ($238[kN]$) and stiffness, and hence the ductility demand ($\mu = 1.96$) are modified without an impact on the design. At this point, it is clear that the condition for applicability of the capacity design ($\mu = q \geq 3.0$ required for the DCH structural class), does not apply.

The capacity curve, estimated by carrying out a pushover analysis, reveals that the period of vibration of $T_1 = 1.29[s]$ leads to a moderate increase of the shear base coefficient from 1.83 to 2.14, which is an increase of 17%. Moreover, the pushover analysis gives a system strength larger than the earthquake force. Consequently, the earthquake force, estimated as $E_{d,el} = 2.14 \cdot 0.8273 \cdot 3.5 \cdot 75 = 464.7[kN]$, is less than the structural yield strength, estimated

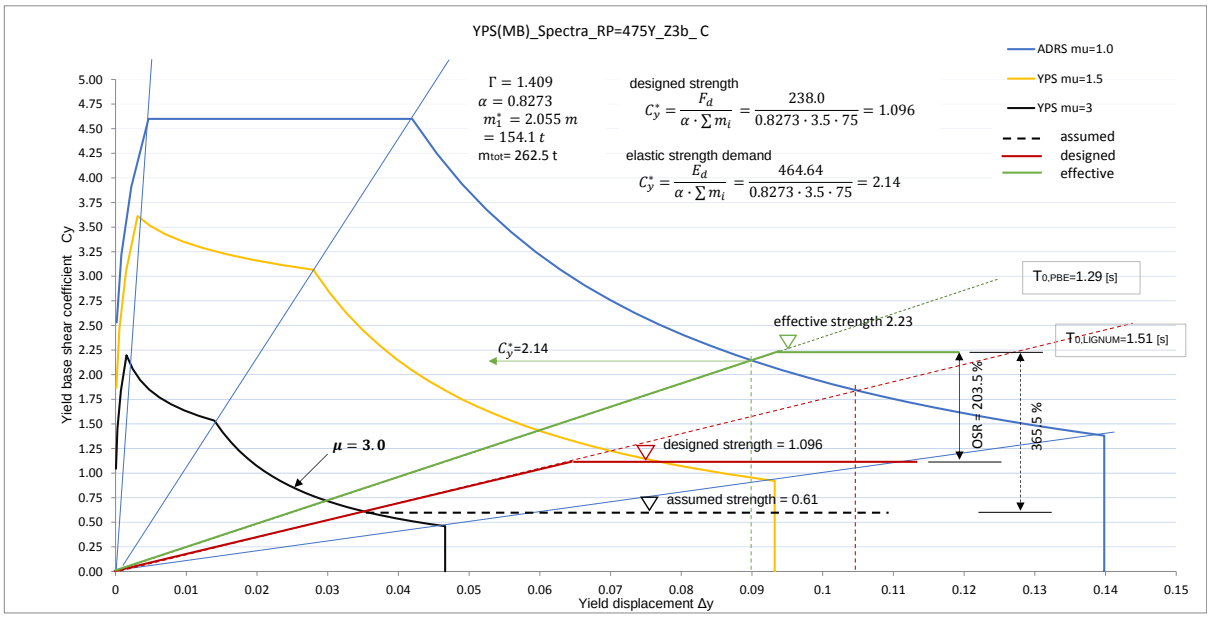

Fig. 9.20: Results of the FB analysis performed in [6] and the pushover analysis for wall TWX_1 superimposed on the yield point response spectra

at $R_y = 482[kN]$, leading to elastic behaviour of the system.
Conclusion:
In capacity design, the ratio of the effective strength to the design strength is called the overstrength ratio. In this case the overstrength ratio $OSR = 2.0$, and the ratio of the effective strength to the required strength is 3.6. The assumption about the ductility ratio, which is the ductility demand achieved by effective design, differs significantly from the real ductility demand estimated by pushover analysis. It can be said that the design process started with assuming a ductile structure and ended with an non-ductile structure in reality.

Generally, the design of the structure does not meet the requirements, since neither ductility nor strength are estimated properly. The stiffness however, is estimated sufficiently well.

Considering how the structure is constructed, one can say that the system does not behave in the desired manner, but thanks to its rigidity and strength, it provides enough safety for both people and properties. The truth of this statement will be evaluated in the next section.

Overall behaviour

The overall behaviour of the designed prototype structure can be examined based on the results obtained by the NLTHA. The values of $IDR = 1\%$, $DI = 0.34$ and a roof displacement of $\Delta roof = 105.6[mm]$ indicate a fairly stiff structure, which would experience small deformations and only slight damage if subjected to the designed earthquake associated with hazard zone Z3b. On the other hand, the high strength of the structure, even with the unchanging stiffness,

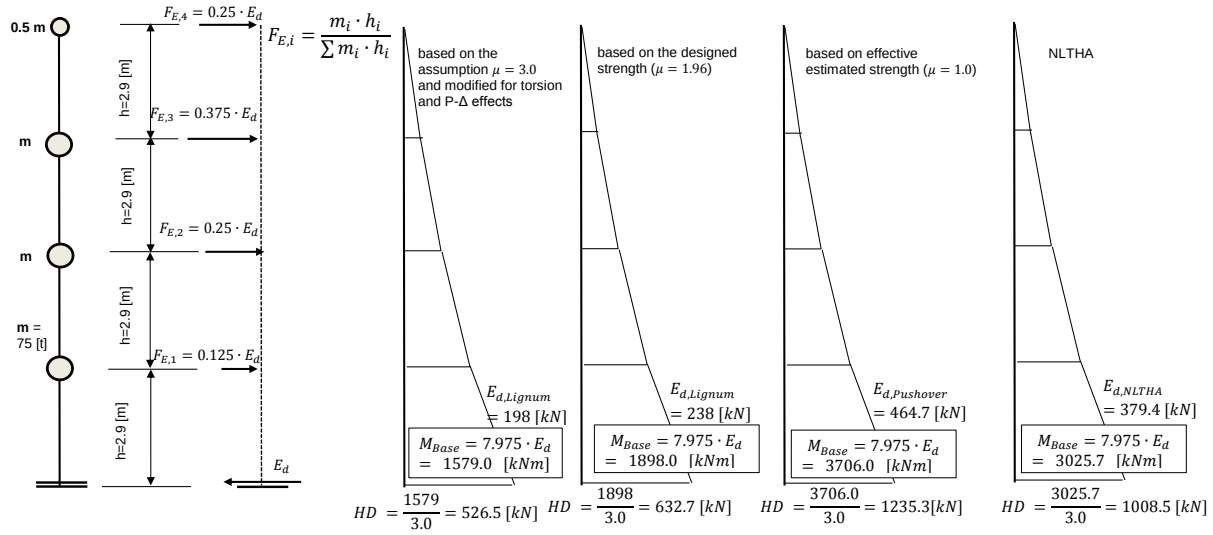

Fig. 9.21: Distribution of earthquake forces estimated using the ductility assumption $\mu = 3.0$, the designed strength of the wall element (see [6]), the effective strength and the base shear force estimated by performing NLTHA over the building height, as well as the clamping moment and corresponding HD-forces

"attracts" larger inertial forces, producing an increase in the HD-forces, as can be seen from the NLTHA. A closer look into the response of the structure with an increased strength will provide answers to whether the increase in strength causes any consequences for the HD devices.
In Figure 9.21, four different earthquake forces, estimated using the basic ductility assumption, designed strength, effective strength as well as the base shear force of 379.4[kN], see Figure 9.17 estimated by the NLTHA, are distributed along the height of the building in accordance with the first mode shape. The corresponding clamping moments and HD-forces are estimated. The "exact" value of the HD-force is estimated by means of the NLTHA $HD_{NLTHA} = 926.7[kN]$ (see also Table 9.9). It is less than the HD force obtained from simple distribution of the force 379.4[kN] over the building height in accordance with the first mode shape.
From the results presented in Figure 9.21, it can be seen that the increase in strength causes an increase in the force-response to the earthquake excitation and hence, an increase of the HD-forces. It can be concluded that the rigid structure attracts significantly larger earthquake forces, which cannot be sustained by the HD devices, as stipulated within this thesis. Although the structure is considered to be ductile, in fact, the structure has been built as non-ductile, attracting significantly larger seismic forces than presumed. The weakest elements have suddenly become not the fasteners, but the HD devices, which would either behave inelastically or would rupture. This would cause a kind of an uncontrolled rocking mode, while the entire overlying structure would still remain stiff and elastic over the entire building height.

9.5.8 Design according results of the parameter study presented in previous chapter

The previous section has concluded that the structure of the prototype building analyzed in this section would probably fail, due to the overloading of the HD devices. Regarding the example discussed here, one can ask what would be an appropriate result of the design procedure according to PBE, as presented in previous chapters. For this purpose, the results of the parameter study of LFTWs sheathed with OSB panels are recalled. In Table 7.2, the 4-storey LFTW with a length of 3.0[m] has reached the limiting period of vibration of $T^* = 1.7[s]$ for a storey mass of 92[t] at each level. Note that nails with $d = 2.87[mm]$ have been used here instead of staples with $d = 1.53[mm]$. The structure has a strength of 220[kN], which is of the same order of magnitude as the strength of 238[kN] of the wall designed in [6]. From Table 7.2, it can be seen that the ductility demand for the structure under consideration is $\mu = 2.23$, the HD force is 577.7[kN], the roof displacement is 119.7[mm], the $IDR = 1.62$ and the $DI = 0.56$. All limit criteria specified in the parametric study are satisfied, even for larger storey masses of $92[t] > 75[t]$. Furthermore, the wall of length 4.0 [m], can be replaced with a length of 3.0 [m], which would optimize the structure for both directions. This would have the additional benefit of eliminating the torsional effects. Despite material savings and the elimination of the torsional effects, the most beneficial effect would be gaining of the control over the overall behaviour of the structure in an earthquake excitation. The analysis of the same wall for an effective storey

mass of $75[\frac{t}{storey}]$ revealed $T^* = 1.406[s]$, a ductility demand $\mu = 1.96$, a roof displacement $104.5[mm]$, $IDR = 1.37$ and $DI = 0.45$.

The design according PBE has clearly pointed out that not the assumed ductility and the designed strength, but the effective ductility demand, the effective strength and the displacement capacity govern the seismic design. Hence, it can be concluded that, in the case of an earthquake event, stronger structures do not necessarily behave better than weaker ones, provided a displacement capacity is available and provided certain damage can be accepted.

By using the over-strength ratio (OSR), the current seismic design practice confirms the awareness that the structures have larger load-bearing capacities than calculated. This is inconsistent at least with regard to two points. First, with an increase of the bearing capacity, which will be presumed by considering the OSR, the earthquake loads also increase, with the consequence that the overturning moment and thus the HD-forces increase simultaneously. This fact is suppressed within the constant period design procedure (FBD). The second consequence is the change in ductility demand, which violates a major assumption of the FBD. Finally, the design loses clearity and consistency, providing unreliable results. For these reasons, it is strongly recommended to use PBE or at least PBD as a design procedure for seismic design of timber structures.

9.6 Conclusion

By comparing the results obtained by using the force-based seismic design and the performance-based engineering, the following conclusions can be made:

- The drawbacks of the force-based seismic design, as described in Chapter 2, section 2.3.1, have been confirmed.
- The properties of the effective designed structural member have not been questioned and thus have not been compared with the assumptions made at the beginning of the design process.
- The actual behaviour of the system designed by use of the force-based seismic design is unknown.
- The safety factor of the structure designed by use of the force-based seismic design is basically unknown, see also [5].
- The collapse of the structure cannot be predicted sufficiently well.
- The weakest member in the structure can not be satisfactorily determined.
- Within the capacity design, the mechanical overstrength cannot be applied without accounting for the corresponding ductility and stiffness.

- Due to the strength underestimation, the force-based seismic design leaves an erroneous impression that an extra safety margin exists.
- The force-based seismic design is due to the poor prediction of both strength and ductility demand, inappropriate for the design of LFTWs.

Comment:

It is outside the scope of this thesis to suggest improvements to the force-based seismic design of timber structures. In the author's opinion, the results of both analyses would have probably been in the same range, if the estimation of strength had been more realistic within the force-based analysis. This can be achieved in two different ways:

- Since the strength of a LFTW depends on the strenrth of a single fastener, its strength estimation should be more realistic, and that means not necessary code-based so called design strength. It is more appropriate to use the characteristic strength instead. Chapter 3 shows how to estimate the more realistic bearing capacity of a fastener by using Johansen's failure mechanism, corrected by a regression function, fitted to the test results.
- An additional approach within the force based seismic design could be to consider the overstrength ratio, which has been a constitutive part of the capacity design from the very beginning. In the literature, the overstrength ratios are said to be in the range between 1.5 and 2.2 (see for example [86], [88] and [36]). So, the design value of the fastener capacity could be multiplied by the OSR in order to estimate the strength and the corresponding ductility demand more realisticaly. The estimation of the stiffness can still be based on an equivalent elastic beam element, as presented in [6].

Chapter 10

Summary and further developments

10.1 Summary

For decades, the requirements of the fire protection regulations have limited the use of timber structures In Switzerland to buildings of up to only 5-storeys. Since new fire provisions have been adpted in January 2015 [51], this limitation has been lifted. At the same time, the question arose weather traditionally-used lateral load resisting systems in timber structures can still be used to sustain earthquake loads in structures with a height of more than 5-storeys. An estimation of the applicability range of both LFTWs sheathed with GFB and OSB is required.
In order to estimate the realistic properties of LFTW, reliable and effective mechanical models are required. To find out whether LFTWs can be used in an economic way in seismic regions of low to moderate seismicity, a reasonable combination of both powerful mechanical models as well as appropriate seismic design philosophy is necessary.
The behaviour of a LFTW depends on the behaviour of a single fastener within the timber connection under monotonic and cyclic loading [16], [91], [74]. Therefore, a mechanical model of a single fastener has first been estimated by testing. After characterizing the response of the single fastener by Stewart's 10-parameter hysteresis [92], the numerical model of the LFTW element is created and analyzed in the MatLab based program, MCASHEW [31]. The LFTW element consists of a timber frame, sheathing panels, hold-down devices and fasteners, where every single fastener used to connect the sheathing panels with the timber frame is considered. The numerical response of the LFTW-model is validated by means of testing. Finally, each wall element, sheathed with GFB or OSB panels, with a length of 2.4, 3.0, 3.6, 4.2 or 4.8 m has been defined by Stewart's 10-parameter hysteresis.

Since force-based seismic design is stipulated as inappropriate for reliable performance estimation of LFTWs, performance based seismic engineering, based on a nonlinear static (pushover) analysis and a NLTHA analysis is performed. Moreover, the design standards SIA265 and Eurocode 8 do not provide precise information with respect to the definition of the performance limits or how to apply performance-based seismic design to timber structures. Therefore, the performance limits: Immediate Occupancy (IO), Life Safety (LS) and Collapse Prevention (CP),

are proposed within this thesis for both LFTWs sheathed with GFB and OSB panels. The proposal has been based on damage index analysis.

The feasibility range, represented by the admissible mass applied to the LFTW at each storey is estimated by simultaneously fulfilling multiple performance objectives: limiting the period of vibration ($T^* \leq 1.7[s]$), limiting the ductility demand ($\mu \leq 3.0$), HD-forces $HD \leq 725[kN]$. The following objects apply to LFTWs sheathed with GFB and OSB, respectively, $IDR \leq 0.8$, $DI \leq 0.8$ and $IDR \leq 2.5$ and $DI \leq 0.7$.

Furthermore, the outcome of the parametric analysis is checked and verified by the probability-based Incremental Dynamic Analysis (IDA).

It have been shown that the LFTWs sheathed with GFB and OSB can perform IDRs of 0.8% and 2.5% of the storey height, experiencing moderate damages. At the same time, the partition walls, ventilation cables, installation pipes and building equipment should be designed and constructed in such a way to be capable of sustaining the displacements imposed by a design earthquake. Particular attention must be paid to the fastening of the facade construction to the load-bearing structure.

The efficiency and transparency of PBE have been demonstrated using an example in which the results of the seismic design procedure presented within this work are compared to those of the traditionally-used force-based seismic design.

The main contributions of this thesis can be summarized as follows:

- reliable mechanical models for both LFTWs sheathed with OSB and GFB have been established
- the methodology for how to perform Performance Based Seismic Engineering and how to apply it to Light Frame Timber Walls has been developed
- the set of major parameters which affect the performance of LFTWs have been defined and justified in advance
- the performance objectives and performance limits for both LFTWs sheathed with OSB and GFB have been proposed
- a comprehensive parameter study of LFTWs sheathed with OSB and GFB, with different wall lengths for regions of low to moderate seismicity, has been performed
- reliable results of the parameter study narrow down the applicability range of LFTWs in regions of low to moderate seismicity
- a set of easy-to-use diagrams and tables suitable for practical use have been established

- the design procedure starts with previously designed elements, with known characteristics, behaviour and performance
- the reliable design results supply engineers with verified data supporting them in the use of LFTWs as the lateral load resisting system for mid-rise buildings up to eight storeys

Regarding the type of the LFTW, soil conditions and seismic hazard zone, it can be stated that:

- The LFTWs sheathed with GFB can be used in an economic way for structures up to 5 and 6 storeys in seismic zones Z1 and Z2, and 1-2 storeys and 5 to 6 storeys for seismic zones Z3a and Z3b, depending on the soil conditions.
- The LFTWs sheathed with OSB can be used in an economic way for structures up to 6 and 8 storeys depending on the soil class but independent of the seismic zone.

10.2 Further developments

10.2.1 Mechanical modeling

The main objective of this study is to narrow the scope of application of traditionally used LFTWs, sheathed with GFB and OSB panels and exposed to earthquake excitation in regions of low to moderate seismicity. To achieve this goal, reliable mechanical models of the LFTW elements used have been developed.

The behaviour of LFTWs depends on the behaviour of the individual fasteners used to connect the sheathing panels to the timber frames. In order to obtain a realistic response of a single fastener to cyclic loading, a few fastener types have been investigated experimentally. For more data about the fastener response to the cyclic loading, comprehensive investigation into different fastener types is recommended. Some investigations, which cover a huge spectrum of fasteners used in Switzerland, have already been carried out within a NRP 66 project [37].

Within this thesis, mechanical models of LFTW elements with minimal fastener spacing have been derived. An additional study of LFTWs with fasteners attached at a moderate spacing of 50 or 75$[mm]$ as well as two-rowed fasteners at a minimal spacing of 30 or 35$[mm]$ would provide information about how the applicability of LFTWs changes with the change of stiffness and strength.

Strong and robust hold-down devices have not been investigated within the presented work. In order to consider the contribution of the hold-down devices to the overall response of the LFTWs to lateral loading, the stiffness and strength proposed by the code [91] are used. There are some indications that the real stiffness and strength of dowel type connections with slotted-in steel plates are not in accordance with those obtained by use of the code provisions [91].

Although the contribution of HD devices to the overall response, even in the case of a multi-storey structure, is rather small, experimental investigations on hold-down devices and inter-storey connectors with slotted-in steel plates are recommended.

10.2.2 Geometry

In the first step, LFTWs with five different wall lengths, ranging between 2.4 and 4.8$[m]$, are analyzed. The LFTW elements are sheathed on both sides, have no openings and remain constant along the building height. A mechanical model for a LFTWs sheathed on one side has been developed and is presented in Chapter 3, but analyses for these LFTW elements have not been conducted. LFTW elements sheathed only on one side are extensively used in practice for facade walls. Often a combination of OSB (outside) and GFB (inside) appears in real structures. In order to close this gap, a feasibility study for LFTWs sheathed on one side would be benefical.

A wall length of 6$[m]$ and more, without windows or door openings , is not common for practical reasons. Further investigations should take into account the influence of the openings on the overall behaviour of shear wall elements. The combination of wall elements with different lengths should also be investigated.

10.2.3 Basic analysis parameters

At the beginning of the presented work, the parameters related to the ductility demand μ, the inelastic vibration period T^* and the hold-down forces have been fixed. The main idea behind fixing these analysis parameters was to avoid producing structures that are too weak. However, it would be interesting to see how the applicability of LFTWs would change with changing these parameters. The ductility demand could be assumed to be $\mu = 3.5$, and the inelastic vibration period could increase to a value of $T^* = 2.0[s]$, which seems to be realistic.
Moreover, the inter-storey drift ratio for LFTWs sheathed with OSB panels and GFB is assumed to be $IDR \leq 2\%$ and $IDR \leq 0.8\%$, respectively. Within the damage analysis, the IDR as the limiting displacement for LFTWs sheathed with OSB panels, has been modified to the value of $IDR = 2.5\%$. The IDR for LFTWs sheathed with GFB is estimated in accordance with the damage index analysis, based on experimental testing. The IDR for LFTWs sheathed with OSB is not yet confirmed by testing. Although an $IDR = 2.5\%$ has no practical relevance, validation of the assumed IDR-limit for LFTWs sheathed with OSB, based on the results of experimental testing, is necessary.

NLTHA has been performed for soil condition C. In Appendices A and B, the results of the NLTHA for soil conditions A and E are presented. Additional analyses for soil conditions B and D should be performed for completion.

10.2.4 Applicability and codification of LFTWs

The results of the presented work showed that LFTWs can be used in an economic way in structures with up to 5 storeys in LFTWs sheathed with GFB and 8 storeys in LFTWs sheathed with OSB. It has been shown that the limits for the usage of the LFTWs are artificially influenced by the lack of knowledge about how the LFTWs actually perform and by the analysis method applied. The force based-seismic design, which has not been upgraded for more than 30 years, is still mainly used in seismic design of structures in Switzerland and Europe. Regarding the definition of appropriate performance limit states the presented study revealed have outlined that regulations in the actual Swiss design code do not exist and that those in Eurocode 8 are insufficient. In the future code development, the focus should be on performance-based design, for new buildings in general and in particular for analysis of existing structures.

Nomenclature

Abbreviations

CASHEW	Cyclic Analysis of Shear Walls, Software provided by Floz and Filiatrault
CUREE	Consortium of Universities for Research in Earthquake Engineering
DCH	Ductility Class High
DCL	Ductility Class Low
DCM	Ductility Class Middle
DI	Damage Index
DIA	Damage Index Analysis
DL	Damage Limitation
EEEP	Equivalent Energy Elastic Plastic
EI	Stiffness
EYM	European Yield Model
FBD	Force Based Seismic Design
FEMA	Federal Emergency Management Agency
GFB	Gipsum Board
IDA	Incremental Dynamic Analysis
IDR	Inter-storey Drift Ratio
LFTW	Light Frame Timber Wall
MDOF	Multi Degree of Freedom
NC	Near Collapse
NLTHA	Nonlinear Time History Analysis
OPENSEES	Open Source for Earthquake Engineering
OSB	Oriented Strand Board

PBD	Performance Based Design
PBE	Performance Based Engineering
PoE	Probability of Exceedance
RP	Repeat Period
RS	Response Spectra
SAWS	Seismic Analysis of Woodframe Structures
SD	Significant Damage
SDOF	Single Degree of Freedom
SLS	Serviceability Limit State
SPO	Static pushover
ULS	Ultimate Limit State

Upper-case roman letters

A^*	Effective shear cross section area
A_0	Asymptotic wall element strength
A_{st}	Stud cross section area
B	Width of the wall element
B_p	Width of the sheathing panel
B_0	Measure of elastic-plastic wall response to the lateral loading
E_k	Kinetic energy
E_0	Young's modulus parallel to the grain
$E_\perp$	Modulus of elasticity perpendicular to the grain
E_{da}	Damping energy
E_d	Equivalent earthquake load
$E_{in,r,i}$	Relative input energy in i-th storey
$E_{in,r}$	Relative input energy
E_{loop}	Energy dissipated in one cycle of loading
E_{st}	Strain energy
F	Force
$F_{(t)}$	Time depending force
F_0	Force at intersection point between asymptotic line and force axis

$F_{R,wall}$	Ultimate shear wall strength
F_{stud}	Stud force
F_{wall}	Force of a wall element
F_{wind}	Wind load
G	Shear modulus
H	Height of the wall element
H_p	Height of the sheathing panel
K_0	Initial stiffness of a wall element
K_1	Asymptotic, post-yielding stiffness of a wall element
K_2	Decreasing stiffness of a wall element
K_f	Geometric constant accounts for fastener arrangement on panel periphery
$K_{HD,ser}$	HD device stiffness
$K_{HD,ser}$	Stiffness of the hold-down device
K_{rot}	Rotational spring stiffness
K_s	Secant stiffness
K_T	Tangent stiffness of a wall element
M	Moment, Moment area
M'	Moment area due to the unit force
$M_{y,R}$	Yield moment of the fastener
N_{roof}	Axial force at roof level
N_{storey}	Axial force per storey level
R_1	Asymptotic stiffness
R_2	Descending stiffness
R_3	Unloading stiffness
R_4	Reloading stiffness
R_1	Asymptotic stiffness of a wall element as percentage of initial wall stiffness
R_2	Decreasing stiffness of a wall element as percentage of initial wall stiffness
$R_{ch,calc}$	Calculated characteristic bearing strength
S_a	Spectral acceleration
S_d	Spectral displacement
S_v	Spectral velocity

T	Elastic vibration period
T^*	Inelastic vibration period
T_0	Fundamental, elastic vibration period
W_{eq}	Equivalent section modulus of inertia

Lower-case roman letters

a_0	Asymptotic fastener strength
a_{r0}	mass-proportional damping coefficient
a_{r1}	stiffness-proportional damping coefficient
b_0	Measure of elastic-plastic fastener response to the lateral loading
d	Diameter of dowel-type fastener
d_{eq}	Equivalent staple diameter
d_{st}	Staple diameter
f_n	Nail force
f_s	Staple force
f_0	Fastener force at intersection point between asymptotic line and force axis
$f_{c,0,k}$	Compression strength parallel to the grain
$f_{c,90,k}$	Compression strength perpendicular to the grain
f_{fast}	Individual fastener force
$f_{h,1,k}$	Embedment strength strength parallel to the grain
$f_{h,2,k}$	Embedment strength perpendicular to the grain
f_{max}	Maximum individual fastener force
$f_{u,as}$	Asymptotic fastener strength
f_{uk}	Characteristic value of steel tensile strength
h^*	Equivalent height
k	Stiffness
k_g	Shear cross section coefficient
k_i	i-th storey stiffness
m	Mass
n_c	Number of loading steps
r_1	Asymptotic stiffness of a fastener as percentage of initial stiffness

r_2	Decreasing stiffness of a fastener as percentage of initial stiffness
s	Spacing
t_p	Thickness of the sheathing panel
t_w	Thickness of the wall

Upper-case greek letters

Δ_{max}	Maximum displacement corresponding to maximum force
Δ_n	Wall displacement due to the fastener slip
Δ_{resp}	Maximum response of the wall element due to the earthquake loading
$\Delta_{u,st}$	Ultimate displacement of the wall element due to the monotonic loading
Γ_i	Modal participation factor
Φ_j	Mode shape
Q	Shear force
Q'	Shear force diagram due to unit shear force

Lower-case greek letters

α	Parameter which controls the stiffness degradation
α_c	Coefficient which controls the best fit between rough and smooth amplitudes of a loading protocol
β	Parameter which controls the stiffness degradation related to the previous cycle
β_{DI}	Strength degradation ratio
β_{y,T_2}	Parameter which controls the variability in transition from the SDOF to the MDOF system
β_{yo}	Parameter which controls the variability in yield strength of the mechanical model
$\ddot{x_g}$	Ground acceleration
$\ddot{x}$	Acceleration of the storey mass
δ	Displacement of a fastener
δ_1	Flexural deformation of the timber frame
δ_2	Shear deformation of the sheathing panel
δ_3	Rigid body deformation of the frame
δ_4	Deformation due to the fastener slip

$\delta_{f,max}$	Maximum displacement of a fastener
$\delta_{f,s}$	Fastener distortion at service level
$\delta_{HD,ten}$	Elongation of the Hold-down device
δ_n	Fastener distortion
$\delta_{st,comp}$	Compression of the stud
δ_{stud}	Deformation of the stud
δ_{ult}	Ultimate displacement of a fastener
$\dot{x_g}$	Ground velocity
$\dot{x}$	Velocity of the storey mass
η	Logarithmic mean deviation
μ	Ductility ratio
μ_m	Mean deviation
ω_n	natural circular frequency
$\phi_{i,j}$	Value at position i, in Mode shape j
ψ_2	Quasi-permanent gravity load coefficient
ρ	Density
ξ	equivalent viscose damping
ξ_n	critical damping ratio
ζ	Logarithmic standard deviation
$m*$	Equivalent mass
q	Behaviour factor
q_w	Evenly distributed wind load
x	Displacement of the storey mass
x_g	Ground displacement

Bibliography

[1] Eurocode 8: Design of structures for earthquake resistance-part 1: General rules, seismic actions and rules for buildings. *Brussels: CEN European Committee for Standardization*, 2005.

[2] DIN EN 14081-4 - Timber structures - Strength graded structural timber with rectangular crosssection - Part 4: Machine grading - Grading machine settings for machine controlled systems; German version, 2009.

[3] Schweizerischer Ingenieur-und Architektenverein. Sia 261: 2014. einwirkungen auf tragwerke, 2014.

[4] Mark Aschheim and Edgar F Black. Yield point spectra for seismic design and rehabilitation. *Earthquake Spectra*, 16(2):317–336, 2000.

[5] Hugo Bachmann. *Erdbebensicherung von Bauwerken.* Springer-Verlag, 2013.

[6] Roland Brunner, Pirmin Jung, René Steiger, Thomas Wenk, and Niklaus Wirz. *Erdbebengerechte mehrgeschossige Holzbauten.* Lignum, Holzwirtschaft Schweiz, 2010.

[7] Daniele Casagrande, Paolo Grossi, and Roberto Tomasi. Shake table tests on a full-scale timber-frame building with gypsum fibre boards. *European Journal of Wood and Wood Products*, 74(3):425–442, 2016.

[8] Brian Chiou, Robert Darragh, Nick Gregor, and Walter Silva. Nga project strong-motion database. *Earthquake Spectra*, 24(1):23–44, 2008.

[9] Anil K Chopra. *Dynamics of structures: theory and applications to earthquake engineering.* Number Pearson Prentice Hall. 2007.

[10] Anil K Chopra and Rakesh K Goel. Direct displacement-based design: use of inelastic vs. elastic design spectra. *Earthquake Spectra*, 17(1):47–64, 2001.

[11] Anil K Chopra and Frank McKenna. Modeling viscous damping in nonlinear response history analysis of buildings for earthquake excitation. *Earthquake Engineering & Structural Dynamics*, 45(2):193–211, 2016.

[12] Ray W Clough and Joseph Penzien. Dynamics of structures. 1993. *Applied Mechanics & Materials*, 1993.

[13] ASCE/SEI Seismic Rehabilitation Standards Committee et al. Seismic rehabilitation of existing buildings (asce/sei 41-06). *American Society of Civil Engineers, Reston, VA*, 2007.

[14] David Countryman. Lateral tests on plywood sheathed diaphragms. *Douglas Fir Plywood Association (DFPA), Tacoma, WA*, 1952.

[15] Raymond A Currier. *Strength Tests on Full-scale Plywood-sheathed Wall Sections*. Oregon Forest Products Laboratory, State Board of Forestry and School of Forestry, Oregon State College, 1956.

[16] CEN-Comité Européen de Normalisation. Timber structures test methods-cyclic testing of joints with mechanical fasteners. *EN TC*, 124.

[17] Comité Européen de Normalisation. Eurocode 5–design of timber structures–part 1-1: General rules and rules for buildings. Technical report, prEN 1995-1-1. Bruxelles, Belgium, 2003.

[18] Bruce Lindsay Deam. *The seismic design and behaviour of multi-storey plywood sheathed timber framed shearwalls*. PhD thesis, 1996.

[19] GG Deierlein and AM Kanvinde. Seismic performance of gypsum walls–analytical investigation, curee publication no. *W-23, Richmond, CA, USA*, 2003.

[20] EN DIN. 12512: Prüfverfahren, zyklische prüfungen von anschlüssen mit mechanischen verbindungsmitteln. *Ausgabe August*, 2002.

[21] David W Dinehart and Harry W Shenton III. Comparison of static and dynamic response of timber shear walls. *Journal of Structural Engineering*, 124(6):686–695, 1998.

[22] James Daniel Dolan. *The dynamic response of timber shear walls*. PhD thesis, University of British Columbia, 1989.

[23] JD Dolan and B Madsen. Monotonic and cyclic nail connection tests. *Canadian Journal of Civil Engineering*, 19(1):97–104, 1992.

[24] Michael Dorn, Karin de Borst, and Josef Eberhardsteiner. Experiments on dowel-type timber connections. *Engineering structures*, 47:67–80, 2013.

[25] Bruce R Ellingwood, David V Rosowsky, Yue Li, and Jun Hee Kim. Fragility assessment of light-frame wood construction subjected to wind and earthquake hazards. *Journal of Structural Engineering*, 130(12):1921–1930, 2004.

[26] Peter Fajfar. Equivalent ductility factors, taking into account low-cycle fatigue. *Earthquake Engineering & Structural Dynamics*, 21(10):837–848, 1992.

[27] Peter Fajfar and Peter Gašperšič. The n2 method for the seismic damage analysis of rc buildings. *Earthquake Engineering & Structural Dynamics*, 25(1):31–46, 1996.

[28] A Filiatrault. Static and dynamic analysis of timber shear walls. *Canadian Journal of Civil Engineering*, 17(4):643–651, 1990.

[29] Maurizio Follesa, Chun Ni, Marjan Popovski, and Erol Karacabeyli. Blind prediction of the seismic response of the neeswood capstone building. In *Proceedings of 10th World Conference on Timber engineering WTCE. Riva del Garda*, pages 543–548, 2010.

[30] B Folz and A Filiatrault. Saws-version 1.0: A computer program for seismic analysis of woodframe buildings. *Rep. No. SSRP-2001*, 9, 2001.

[31] Bryan Folz and Andre Filiatrault. *CASHEW: Computer Program for the Cyclic Analysis of Wood Shear Walls*. CUREE Publications, 2001.

[32] Bryan Folz and André Filiatrault. *A computer program for seismic analysis of woodframe structures*. Consortium of Universities for Research in Earthquake Engineering, 2002.

[33] Bryan Folz and Andre Filiatrault. Seismic analysis of woodframe structures. i: Model formulation. *Journal of Structural Engineering*, 130(9):1353–1360, 2004.

[34] Ricardo O Foschi. Analysis of wood diaphragms and trusses. part i: Diaphragms. *Canadian Journal of Civil Engineering*, 4(3):345–352, 1977.

[35] Kip Gatto and Chia-Ming Uang. Effects of loading protocol on the cyclic response of woodframe shearwalls. *Journal of Structural engineering*, 129(10):1384–1393, 2003.

[36] Martin Geiser, Simon Meier, Gunther Ratsch, Mareike Vogel, and Ein Bericht im Auftrag des Bundesamtes. Duktile erdbebenbemessung von holzbauwerken. 2019.

[37] Research group consisting of researchers from the Empa HEIG-VD and EPFL institutes within the framework of an NRP66 research project on "Resource Wood". Earthquake-resistant timber systems for multi-storey buildings. Unpublished article, 2017.

[38] Ajaya K Gupta and George P Kuo. Behavior of wood-framed shear walls. *Journal of Structural Engineering*, 111(8):1722–1733, 1985.

[39] Andreas Heiduschke, Peer Haller, and Bo Kasal. Zum tragverhalten textilbewehrt-verdichteter holz-rahmenecken unter zyklischer beanspruchung. *Bautechnik*, 81(8):658–662, 2004.

[40] George W Housner. Limit design of structures to resist earthquakes. In *Proc. of 1st WCEE*, pages 5–1, 1956.

[41] Iunio Iervolino, Georgios Baltzopoulos, Dimitrios Vamvatsikos, and Roberto Baraschino. Spo2frag v1. 0: software for pushover-based derivation of seismic fragility curves. In *Proceedings of the VII European congress on computational methods in applied sciences and engineering, ECCOMAS, Crete Island, Greece*, pages 5–10, 2016.

[42] Iunio Iervolino, Giuseppe Maddaloni, and Edoardo Cosenza. Eurocode 8 compliant real record sets for seismic analysis of structures. *Journal of Earthquake Engineering*, 12(1):54–90, 2008.

[43] Rafik Y Itani and Sergio A Obregon. Nonlinear racking analysis of nailed walls. *Wood and Fiber Science*, 16(3):454–465, 2007.

[44] Rafik Y Itani, Roger L Tuomi, and William J McCutcheon. Methodology to evaluate racking resistance of nailed walls. *Forest Products Journal*, 32(1):30–36, 1982.

[45] Jeena R Jayamon, Philip Line, and Finley A Charney. *State-of-the-art review on damping in wood-frame shear wall structures.* PhD thesis, American Society of Civil Engineers, 2018.

[46] KW Johansen. Theory of timber connections. *Int Assoc Bridge and Struct Eng*, 9:249–262, 1949.

[47] André Johannes Maria Jorissen. *Double shear timber connections with dowel type fasteners.* Delft University Press Delft, The Netherlands, PhD Thesis, 1998.

[48] Johnn P Judd and Fernando S Fonseca. Analytical model for sheathing-to-framing connections in wood shear walls and diaphragms. *Journal of Structural Engineering*, 131(2):345–352, 2005.

[49] Erol Kalkan and Anil K Chopra. Practical guidelines to select and scale earthquake records for nonlinear response history analysis of structures. *US geological survey open-file report*, 1068(2010):126, 2010.

[50] Erol Kalkan and Sashi K Kunnath. Relevance of absolute and relative energy content in seismic evaluation of structures. *Advances in Structural Engineering*, 11(1):17–34, 2008.

[51] Vereinigung kantonaler Feuerversicherungen and VKF Schweizerische Brandschutzvorschriften. gültig seit 01.01. 2005. *VKF, Bern.*

[52] Amit M Kanvinde and Gregory G Deierlein. Analytical models for the seismic performance of gypsum drywall partitions. *Earthquake Spectra*, 22(2):391–411, 2006.

[53] Payam Khashaee, Bijan Mohraz, Fahim Sadek, Hai S Lew, and John L Gross. *Distribution of earthquake input energy in structures.* Diane Publishing Company, 2003.

[54] Helmut Krawinkler, Francisco Parisi, Luis Ibarra, Ashraf Ayoub, and Ricardo Medina. *Development of a testing protocol for woodframe structures*, volume 102. CUREe Richmond, CA, 2001.

[55] Hitoshi Kuwamura, Yasunori Kirino, and Hiroshi Akiyama. Prediction of earthquake energy input from smoothed fourier amplitude spectrum. *Earthquake engineering & structural dynamics*, 23(10):1125–1137, 1994.

[56] Hao Liang, Yi-Kwei Wen, and Greg C Foliente. Damage modeling and damage limit state criterion for wood-frame buildings subjected to seismic loads. *Journal of structural engineering*, 137(1):41–48, 2010.

[57] Wei Yuen Loo, Pierre Quenneville, and Nawawi Chouw. A numerical approach for simulating the behaviour of timber shear walls. *Structural Engineering and Mechanics*, 42(3):383–407, 2012.

[58] Abdollah Sadeghi Marzaleh, Stella Nerbano, Andrea Sebastiani Croce, and René Steiger. Osb sheathed light-frame timber shear walls with strong anchorage subjected to vertical load, bending moment, and monotonic lateral load. *Engineering Structures*, 173:787–799, 2018.

[59] Silvia Mazzoni, Frank McKenna, Michael H Scott, and Gregory L Fenves. The open system for earthquake engineering simulation (opensees) user command-language manual. 2006.

[60] Silvia Mazzoni, Frank McKenna, Michael H Scott, Gregory L Fenves, et al. Opensees command language manual. *Pacific Earthquake Engineering Research (PEER) Center*, 264, 2006.

[61] William J McCutcheon. Racking deformations in wood shear walls. *Journal of Structural Engineering*, 111(2):257–269, 1985.

[62] Frank McKenna. Opensees: a framework for earthquake engineering simulation. *Computing in Science & Engineering*, 13(4):58–66, 2011.

[63] WE McKevitt, DL Anderson, and S Cherry. Hysteretic energy spectra in seismic design. In *Proceeding of the Seventh World Conference on Earthquake Engineering*, pages 487–494, 1980.

[64] Kurt M McMullin and Dan Merrick. *Seismic performance of gypsum walls: Experimental test program.* Consortium of Universities for Research in Earthquake Engineering, 2002.

[65] Kenneth Medearis. Static and dynamic characteristics of composite structures. *Bulletin of the Seismological Society of America*, 57(5):913–933, 1967.

[66] Panagiotis Mergos and Katrin Beyer. Displacement-based seismic design of symmetric single-storey wood-frame buildings with the aid of n2 method. *Frontiers in Built Environment*, 1:10, 2015.

[67] Panagiotis E Mergos and Katrin Beyer. Loading protocols for european regions of low to moderate seismicity. *Bulletin of earthquake engineering*, 12(6):2507–2530, 2014.

[68] Adolf Meyer. Die tragfähigkeit von nagelverbindungen bei statischer belastung. *HOLZ als Roh-und Werkstoff*, 15(2):96–109, 1957.

[69] R Mohamad and A Bernasconi. Nailed panel-to-timber connections. Unpublished article, 2016.

[70] R Mohamad and A Bernasconi. Stapled panel-to-timber connections. Unpublished article, 2017.

[71] Williams Muñoz, M Mohammad, A Salenikovich, and Pierre Quenneville. Determination of yield point and ductility of timber assemblies: in search for a harmonised approach. *Engineered Wood Products Association*, 2008.

[72] Masayoshi Nakashima, Kazuhiro Saburi, and Bunzo Tsuji. Energy input and dissipation behaviour of structures with hysteretic dampers. *Earthquake engineering & structural dynamics*, 25(5):483–496, 1996.

[73] RH Neisel and JF Guerrera. Racking strength of fiberboard sheathing. *Tappi*, 39(9):625–628, 1956.

[74] SIA Norm. 265/1. *Holzbau–Ergänzende Festlegungen, Schweizerischer Ingenieur-und Architektenverein, Zürich*, 2009.

[75] SIA Norm. 260: Grundlagen der projektierung von tragwerken. *Schweizerischer Ingenieur- und Architekten-Verein, Zürich*, page 44, 2013.

[76] Shigeyuki Okada and Nobuo Takai. Damage index functions of wooden buildings and reinforced buildings for seismic risk management. In *Proc. 13th World Conf. on Earthquake Engineering*, 2004.

[77] Weichiang Pang, David V Rosowsky, Shiling Pei, and John W van de Lindt. Simplified direct displacement design of six-story woodframe building and pretest seismic performance assessment. *Journal of structural engineering*, 136(7):813–825, 2010.

[78] R Park. Evaluation of ductility of structures and structural assemblages from laboratory testing. *Bulletin of the New Zealand national society for earthquake engineering*, 22(3):155–166, 1989.

[79] Young J Park, Andrei M Reinhorn, and Sashi K Kunnath. Idarc: Inelastic damage analysis of reinforced concrete frame-shear-wall structures. 1987.

[80] Young-Ji Park, Alfredo H-S Ang, and Yi Kwei Wen. Seismic damage analysis of reinforced concrete buildings. *Journal of Structural Engineering*, 111(4):740–757, 1985.

[81] Marcia Patton-Mallory and William J McCutcheon. Predicting racking performance of walls sheathed on both sides. *Forest products journal*, 37(9):27–32, 1987.

[82] Mario Paz. *Structural dynamics: theory and computation*. Springer Science & Business Media, 2012.

[83] MJN Priestley, GM Calvi, and MJ Kowalsky. Direct displacement-based seismic design. In *2005 NZSEE Conference*, pages 33–43, 2007.

[84] Alexander J Salenikovich. *The racking performance of light-frame shear walls.* PhD thesis, Virginia Tech, 2000.

[85] Amir Hosein Salmanpour, Nebojša Mojsilović, and Joseph Schwartz. Displacement capacity of contemporary unreinforced masonry walls: an experimental study. *Engineering Structures*, 89:1–16, 2015.

[86] M Schick, T Vogt, and W Seim. Connections and anchoring for wall and slab elements in seismic design. *CIB Working Commission W18-Timber Structures, Vancouver, Canada*, 2013.

[87] Peter Seaders, Rakesh Gupta, and Thomas H Miller. Monotonic and cyclic load testing of partially and fully anchored wood-frame shear walls. *Wood and Fiber Science*, 41(2):145–156, 2009.

[88] Werner Seim, Tobias Vogt, Michael Schick, and Gabriel Höflich. Experimentelle und rechnerische untersuchungen zur praxisgerechten verankerung von holzrahmenwänden. In *International Wood Construction Conference (Holzbau-Forum)*, 2013.

[89] G Solomos, A Pinto, and S Dimova. A review of the seismic hazard zonation in national building codes in the context of eurocode 8. *Support to the Implementation, Harmonization and Further Development of the Eurocodes, JRC European Commission*, 2008.

[90] New Zealand Standard. Nzs 1170.5: 2004 structural design actions part 5: Earthquake actions–new zealand. *Wellington, New Zealand: Standards New Zealand*, 2004.

[91] Swiss Timber Standard. Norm sia 265 (2012): Holzbau. *Schweizerischer Ingenieur und Architektenverein, Zürich.*

[92] Wayne Stewart. *The seismic design of plywood sheathed shear walls.* PhD thesis, 1987.

[93] Stuart J Thurston and AB King. *Full-sized House Cyclic Racking Test.* BRANZ, 2002.

[94] Roger L Tuomi and William J McCutcheon. Racking strength of light-frame nailed walls. 104(7):1131–1140, 1978.

[95] Chia-Ming Uang and Vitelmo V Bertero. Evaluation of seismic energy in structures. *Earthquake Engineering & Structural Dynamics*, 19(1):77–90, 1990.

[96] Dimitrios Vamvatsikos and C Allin Cornell. Incremental dynamic analysis. *Earthquake Engineering & Structural Dynamics*, 31(3):491–514, 2002.

[97] Dimitrios Vamvatsikos and Michalis Fragiadakis. Incremental dynamic analysis for estimating seismic performance sensitivity and uncertainty. *Earthquake engineering & structural dynamics*, 39(2):141–163, 2010.

[98] John W van de Lindt and Rakesh Gupta. Damage and damage prediction for wood shearwalls subjected to simulated earthquake loads. *Journal of performance of constructed facilities*, 20(2):176–184, 2006.

[99] JW Van de Lindt. Damage-based seismic reliability concept for woodframe structures. *Journal of Structural Engineering*, 131(4):668–675, 2005.

[100] NEHRP Consultants Joint Venture. Selecting and scaling earthquake ground motions for performing response-history analyses. *NIST GCR*, pages 11–917, 2011.

[101] Tobias Vogt. *Entwicklung eines Berechnungsmodells zur Beschreibung des Trag-und Verformungsverhaltens von Holzrahmenwänden unter Berücksichtigung lokaler Effekte*, volume 6. kassel university press GmbH, 2015.

[102] BH Xu, A Bouchaïr, M Taazount, and EJ Vega. Numerical and experimental analyses of multiple-dowel steel-to-timber joints in tension perpendicular to grain. *Engineering Structures*, 31(10):2357–2367, 2009.

Appendix

Appendix A

Parameter Study of LFTWs Sheathed with GFB

A.1 Soil Conditions A

Figures A.1 to A.4 show the resultant means of 10 earthquake records, selected and scaled to the hazard Zone Z1, Z2, Z3a and Z3b for soil conditions A.

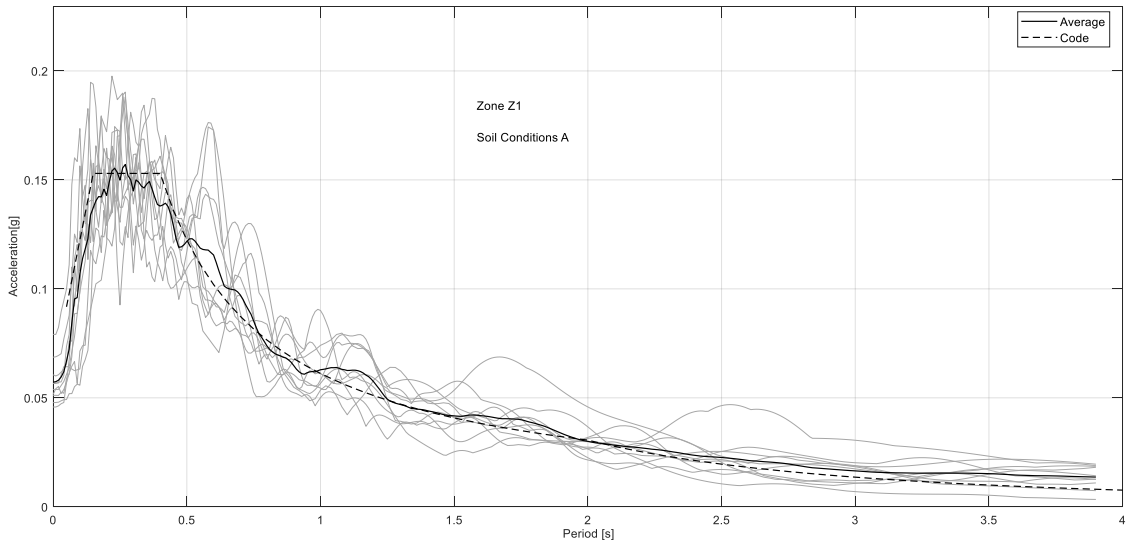

Fig. A.1: Resultant average of 10 earthquake records selected and scaled to the hazard level of Zone $Z1$ for soil conditions A superimposed on elastic RS.

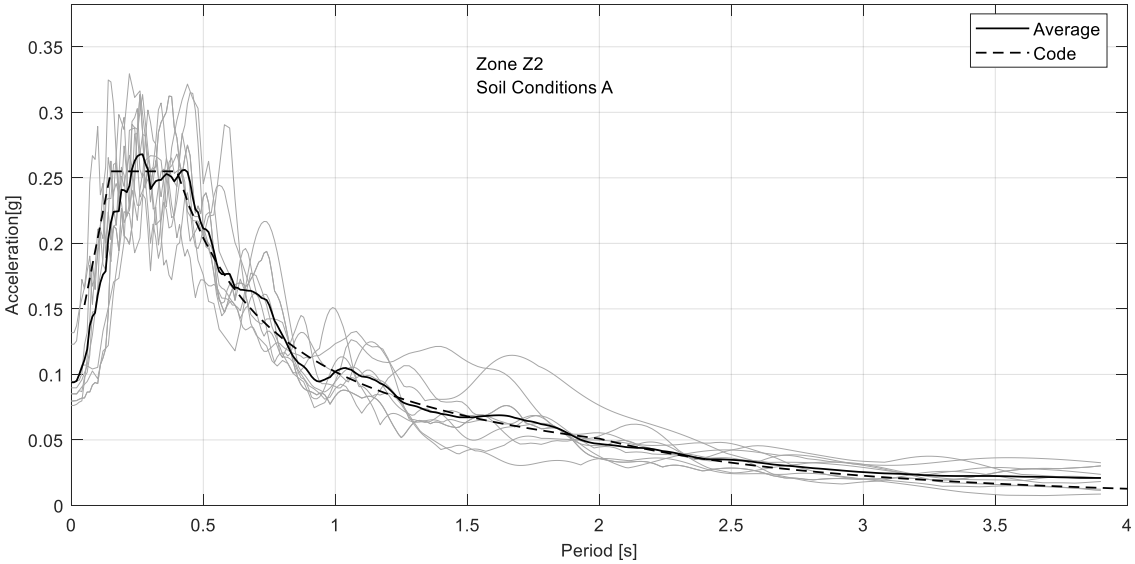

Fig. A.2: Resultant average of 10 earthquake records selected and scaled to the hazard level of Zone $Z2$ for soil conditions A superimposed on elastic RS..

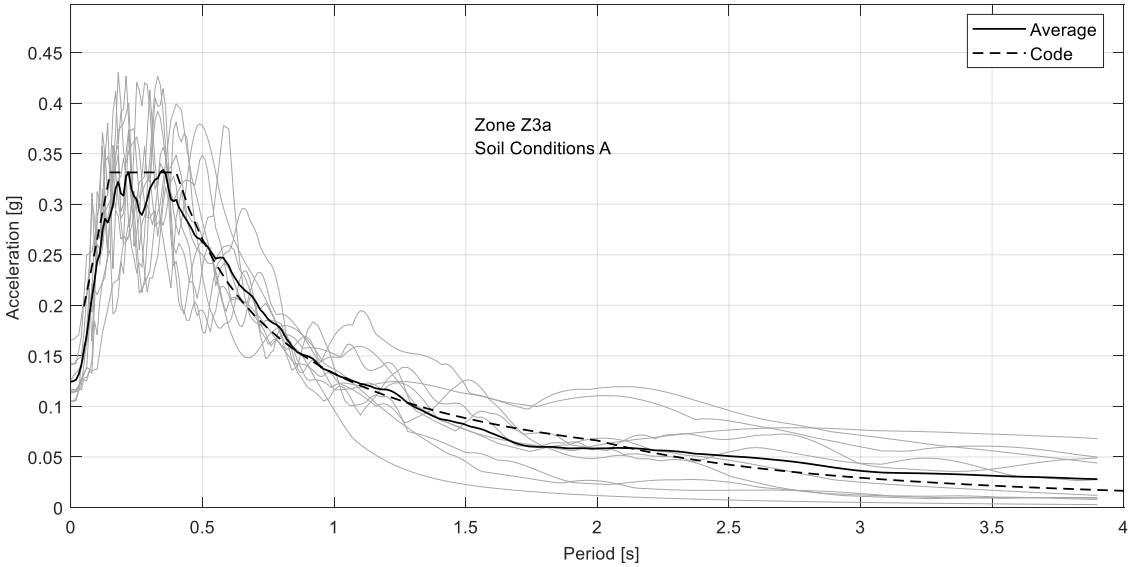

Fig. A.3: Resultant average of 10 earthquake records selected and scaled to the hazard level of Zone $Z3a$ for soil conditions A superimposed on elastic RS..

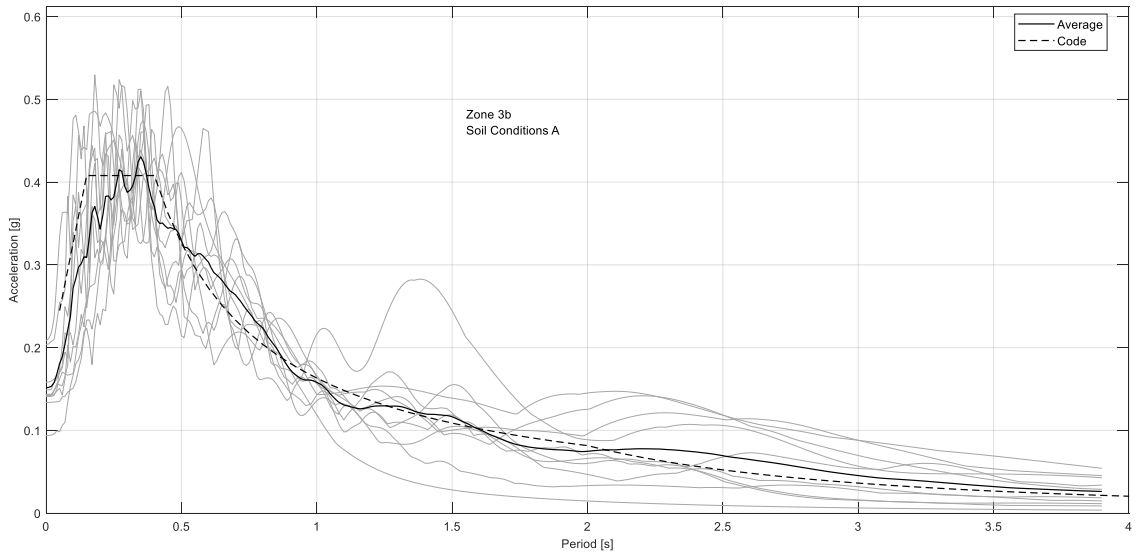

Fig. A.4: Resultant average of 10 earthquake records selected and scaled to the hazard level of Zone *Z3b* for soil conditions *A* superimposed on elastic RS..

A.1.1 Tabular and graphical presentation for LFTW of a length $2.4[m]$ sheathed on both sides with GFB

The results of the parametric study for a 2.4 [m] long LFTW element sheathed with GFB on both sides are summarized in Table A.1. The typical, graphical presentation is given in Figure A.5

Tab. A.1: Results of the parameter study of a LFTW with a length of 2.4 [m] sheathed on both sides with GFB

Zone	Mass	IDA	Modal analysis			Pushover analysis				NLTH analysis			
a_g	m	check	T	T^*	Γ	Δ_y	F_y	μ	$\Delta_{u,st}$	HD force	Δ_{roof}	IDR	DI
$[\frac{m}{s^2}]$	[t]		[s]	[s]	[-]	[mm]	[kN]	[-]	[mm]	[kN]	[mm]	[-]	[-]
1- storey structure													
0.6	418.0	✓	1.228	1.70	1.0	15.0	86.40	1.71	31.95	105.9	18.49	0.66	0.72
1.0	194.0	x	0.83	1.04				2.16		111.4	21.66	0.75	0.80
	140.0	✓	0.70	0.86				1.89		107.7	17.11	0.59	0.62
1.3	127.5	x	0.68	0.82				2.36		116.0	22.7	0.78	0.80
	78.0	✓	0.53	0.62				1.90		109.4	17.11	0.59	0.62
1.6	96.0	x	0.59	0.69				2.57		117.3	22.8	0.79	0.80
	49.0	✓	0.42	0.48				1.90		102.6	15.7	0.54	0.53

Zone	Mass	IDA	Modal analysis			Pushover analysis				NLTH analysis			
a_g	m	check	T	T^*	Γ	Δ_y	F_y	μ	$\Delta_{u,st}$	HD force	Δ_{roof}	IDR	DI
$[\frac{m}{s^2}]$	[t]		[s]	[s]	[-]	[mm]	[kN]	[-]	[mm]	[kN]	[mm]	[-]	[-]
2- storey structure													
0.6	210.0	✓	1.48	1.69	1.186	18.66	85.0	1.62	41.89	142.9	21.86	0.54	0.61
1.0	122.0	x	1.13	1.27				2.19		183.2	31.96	0.80	0.80
	100	✓	1.0	1.14				1.91		154.4	25.5	0.63	0.67
1.3	75.0	x	0.88	0.98				2.15		178.6	30.5	0.77	0.79
	61.5	✓	0.80	0.89				1.96		169.9	27.73	0.7	0.7
1.6	56.0	x	0.80	0.89				2.31		184.3	31.3	0.75	0.76
	40.0	✓	0.65	0.71				1.95		169.0	26.15	0.61	0.61
3- storey structure													
0.6	105.0	✓	1.56	1.70	1.263	28.57	83.96	1.15	53.45	83.96	22.73	0.42	0.46
1.0	100.0	✓	1.52	1.66				1.87		208.4	37.22	0.64	0.75
1.3	59.0	✓	1.17	1.27				1.88		232.5	39.41	0.61	0.65
1.6	38.5	✓	0.95	1.0				1.88		216.4	37.74	0.65	0.66
4- storey structure													
0.6	57.0	✓	1.60	1.70	1.31	42.68	83.67	1.0	74.66	86.3	24.09	0.35	0.37
1.0	57.0	✓	1.60	1.70				1.33		222.9	40.04	0.51	0.57
1.3	42.5	✓	1.4	1.46				1.5		242.8	44.66	0.61	0.63
1.6	35.5	x	1.26	1.34				1.68		251.0	49.15	0.67	0.7
	29.0	✓	1.14	1.21				1.52		248.5	47.77	0.58	0.60
5- storey structure													
0.6	34.0	✓	1.64	1.70	1.353	62.52	83.92	1.0	101.6	162.7	27.78	0.29	0.30
1.0	34.0	✓	1.64	1.70				1.0		202.8	40.94	0.43	0.47
1.3	30.5	✓	1.55	1.62				1.16		244.5	50.95	0.60	0.60
1.6	26.5	✓	1.43	1.49				1.31		262.3	57.04	0.61	0.63

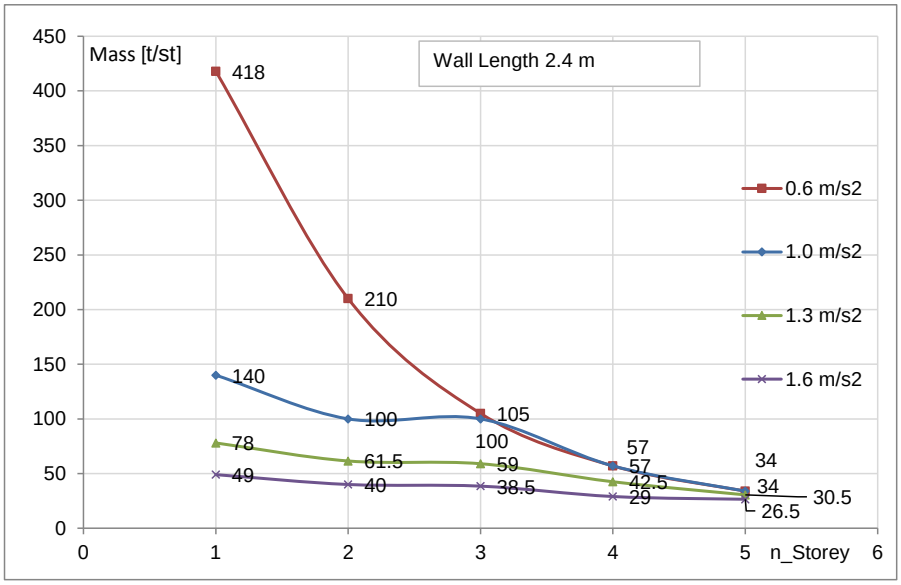

Fig. A.5: Outcome of the parameter study of the LFTW sheathed on both sides with GFB with a length of 2.4 [m], see also Table A.1

A.1.2 Tabular and graphical presentation for LFTW of a length $3.0[m]$ sheathed on both sides with GFB

The results of the parametric study for a 3.0 [m] long LFTW element sheathed with GFB on both sides are summarized in Table A.2. The typical, graphical presentation is given in Figure A.6

Tab. A.2: Results of the parameter study of a LFTW with a length of 3.0 [m] sheathed on both sides with GFB

Zone	Mass	IDA	Modal analysis			Pushover analysis				NLTH analysis			
a_g	m	check	T	T^*	Γ	Δ_y	F_y	μ	$\Delta_{u,st}$	HD force	Δ_{roof}	IDR	DI
$[\frac{m}{s^2}]$	[t]		[s]	[s]	[-]	[mm]	[kN]	[-]	[mm]	[kN]	[mm]	[-]	[-]
1- storey structure													
0.6	385.0	✓	1.24	1.62	1.0	20.82	120.1	1.19	42.17	112.2	21.79	0.75	0.80
1.0	181.0	✓	0.85	1.02				1.48		117.4	23.3	0.80	0.80
1.3	137.7	x	0.74	0.87				1.71		122.5	25.27	0.87	0.80
	126.0	✓	0.70	0.83				1.65		120.0	23.47	0.81	0.73
1.6	89.0	x	0.60	0.68				1.73		127.3	26.1	0.90	0.80
	79.0	✓	0.56	0.64				1.65		123.7	24.39	0.84	0.73
2- storey structure													
0.6	212.0	✓	1.53	1.70	1.186	25.91	118.1	1.18	53.19	156.8	25.97	0.65	0.70
1.0	122.0	✓	1.16	1.28				1.5		169.3	30.8	0.74	0.80
1.3	87.0	✓	0.98	1.08				1.66		196.5	37.1	0.84	0.8
1.6	69.0	✓	0.87	0.96				1.82		197.4	37.65	0.81	0.78

Zone	Mass	IDA	Modal analysis			Pushover analysis				NLTH analysis			
a_g	m	check	T	T^*	Γ	Δ_y	F_y	μ	$\Delta_{u,st}$	HD force	Δ_{roof}	IDR	DI
$[\frac{m}{s^2}]$	[t]		[s]	[s]	[-]	[mm]	[kN]	[-]	[mm]	[kN]	[mm]	[-]	[-]
3- storey structure													
0.6	103.0	✓	1.55	1.70	1.25	38.42	115.6	1.0	64.65	154.2	26.21	0.48	0.50
1.0	92.0	✓	1.46	1.60				1.33		212.8	41.92	0.72	0.80
1.3	76.5	✓	1.36	1.46				1.58		228.4	45.44	0.77	0.78
1.6	49.0	✓	1.07	1.16				1.56		236.0	48.3	0.73	0.71
4- storey structure													
0.6	59.0	✓	1.60	1.70	1.295	54.81	116.4	1.0	91.36	147.0	27.43	0.38	0.37
1.0	59.0	✓	1.60	1.70				1.02		206.9	42.4	0.60	0.64
1.3	55.5	✓	1.53	1.65				1.28		248.2	53.57	0.82	0.79
1.6	44.5	✓	1.37	1.47				1.42		286.6	61.24	0.76	0.77
5- storey structure													
0.6	36.5	✓	1.64	1.70	1.331	76.01	116.1	1.0	119.3	140.1	27.77	0.32	0.30
1.0	36.5	✓	1.64	1.70				1.0		208.6	46.03	0.46	0.47
1.3	36.5	✓	1.64	1.70				1.0		255.3	57.87	0.61	0.6
1.6	33.0	✓	1.54	1.62				1.15		294.4	69.85	0.75	0.73
6- storey structure													
0.6	23.5	✓	1.63	1.70	1.36	103.4	116.1	1.0	157.0	135.3	29.73	0.27	0.24
1.0	23.5	✓	1.63	1.70				1.0		201.0	47.23	0.37	0.37
1.3	23.5	✓	1.63	1.70				1.0		238.8	58.08	0.47	0.43
1.6	23.5	✓	1.63	1.70				1.0		288.3	73.4	0.61	0.58

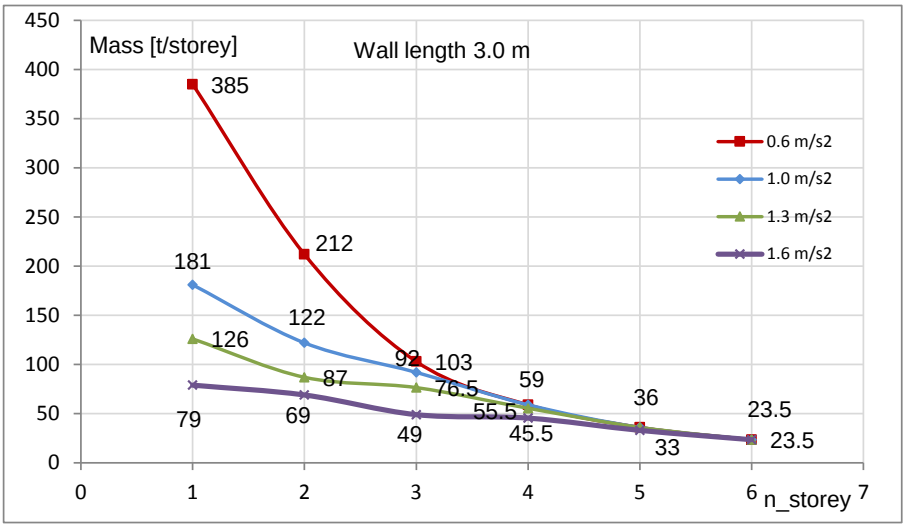

Fig. A.6: Outcome of the parameter study of the LFTW sheathed on both sides with GFB with a length of 3.0 [m], see also Table A.2

A.1.3 Tabular and graphical presentation for LFTW of a length $3.6[m]$ sheathed on both sides with GFB

The results of the parametric study for a 3.6 [m] long LFTW element sheathed with GFB on both sides are summarized in Table A.3. The typical, graphical presentation is given in Figure A.7.

Tab. A.3: Results of the parameter study of a LFTW with a length of 3.6 [m] sheathed on both sides with GFB

Zone	Mass	IDA	Modal analysis			Pushover analysis				NLTH analysis			
a_g	m	check	T	T^*	Γ	Δ_y	F_y	μ	$\Delta_{u,st}$	HD force	Δ_{roof}	IDR	DI
$[\frac{m}{s^2}]$	[t]		[s]	[s]	[-]	[mm]	[kN]	[-]	[mm]	[kN]	[mm]	[-]	[-]
1- storey structure													
0.6	460.0	✓	1.18	1.66	1.0	20.76	142.1	1.16	41.57	105.8	21.18	0.73	0.80
1.0	227.0	✓	0.83	1.05				1.53		117.6	22.59	0.80	0.80
1.3	171.0	✓	0.72	0.88				1.79		121.0	24.8	0.85	0.80
1.6	115.0	✓	0.59	0.70				1.86	115.0	25.2	0.87	0.8	
2- storey structure													
0.6	280.0	✓	1.54	1.69	1.18	22.59	139.3	1.34	50.23	160.65	25.39	0.68	0.79
1.0	148.0	✓	1.16	1.22				1.63		177.3	29.73	0.73	0.79
1.3	107.0	x	0.95	1.04				1.80		196.0	35.56	0.84	0.80
	100.0	✓	0.92	1.0				1.74		191.1	34.46	0.82	0.77
1.6	81.0	x	0.85	0.93				2.0		201.6	36.27	0.81	0.79
	65.0	✓	0.72	0.8				1.73		188.8	31.6	0.72	0.66

Zone	Mass	IDA	Modal analysis			Pushover analysis				NLTH analysis			
a_g	m	check	T	T^*	Γ	Δ_y	F_y	μ	$\Delta_{u,st}$	HD force	Δ_{roof}	IDR	DI
$[\frac{m}{s^2}]$	[t]		[s]	[s]	[-]	[mm]	[kN]	[-]	[mm]	[kN]	[mm]	[-]	[-]
3- storey structure													
0.6	135.0	✓	1.54	1.70	1.248	35.72	138.2	1.0	66.56	166.9	26.4	0.52	0.56
1.0	114.5	✓	1.42	1.56				1.41		223.5	40.62	0.70	0.80
1.3	94.0	x	1.28	1.41				1.67		237.8	44.05	0.78	0.80
	90.0	✓	1.25	1.38				1.64		243.0	43.32	0.73	0.75
1.6	68.0	x	1.08	1.18				1.74		256.9	48.94	0.79	0.80
	60.0	✓	1.03	1.13				1.67		261.5	45.64	0.72	0.71
4- storey structure													
0.6	78.0	✓	1.57	1.69	1.292	48.51	137.2	1.0	80.73	150.1	26.59	0.40	0.41
1.0	78.0	✓	1.57	1.69				1.15		221.1	41.97	0.59	0.67
1.3	69.0	✓	1.48	1.59				1.40		258.9	51.86	0.8	0.8
1.6	56.5	✓	1.35	1.44				1.56		292.5	57.84	0.78	0.8
5- storey structure													
0.6	49.0	✓	1.60	1.70	1.327	66.12	136.4	1.0	106.6	154.5	27.77	0.34	0.33
1.0	49.0	✓	1.60	1.70				1.0		224.7	45.74	0.46	0.50
1.3	49.0	✓	1.6	1.7				1.13		272.0	56.62	0.68	0.67
1.6	42.0	✓	1.48	1.57				1.28		299.0	64.8	0.76	0.74
6- storey structure													
0.6	32.0	✓	1.63	1.70	1.36	89.18	136.9	1.0	150.78	138.6	29.24	0.28	0.27
1.0	32.0	✓	1.63	1.70				1.0		218.3	46.33	0.39	0.40
1.3	32.0	✓	1.63	1.70				1.0		264.5	58.28	0.49	0.47
1.6	32.0	✓	1.63	1.70				1.05		306.8	72.74	0.76	0.73
7- storey structure													
0.6	21.75	✓	1.65	1.70	1.38	117.6	136.9	1.0	177.5	149.3	32.1	0.24	0.22
1.0	21.75	✓	1.65	1.70				1.0		205.0	47.22	0.34	0.33
1.3	21.75	✓	1.65	1.70				1.0		242.9	59.03	0.42	0.39
1.6	21.75	✓	1.65	1.70				1.0		296.3	74.26	0.5	0.49

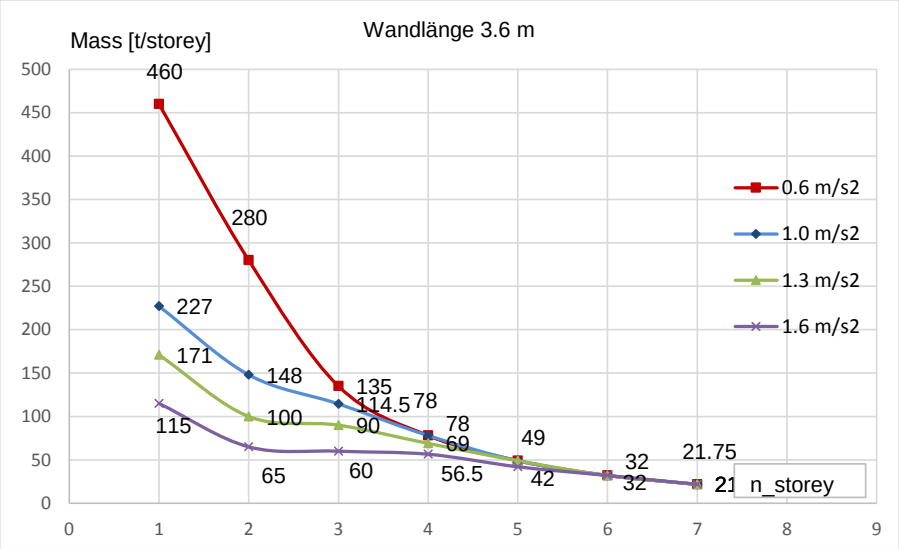

Fig. A.7: Outcome of the parameter study of the LFTW sheathed on both sides with GFB with a length of 3.6 [m], see also Table A.3

A.1.4 Tabular and graphical presentation for LFTW of a length $4.2[m]$ sheathed on both sides with GFB

The results of the parametric study for a 4.2 [m] long LFTW element sheathed with GFB on both sides are summarized in Table A.4. The typical, graphical presentation is given in Figure A.8.

Tab. A.4: Results of the parameter study of a LFTW with a length of 4.2 [m] sheathed on both sides with GFB

Zone	Mass	IDA	Modal analysis			Pushover analysis				NLTH analysis			
a_g	m	check	T	T^*	Γ	Δ_y	F_y	μ	$\Delta_{u,st}$	HD force	Δ_{roof}	IDR	DI
$[\frac{m}{s^2}]$	[t]		[s]	[s]	[-]	[mm]	[kN]	[-]	[mm]	[kN]	[mm]	[-]	[-]
1- storey structure													
0.6	540.0	✓	1.13	1.69	1.0	23.1	167.9	1.11	33.99	116.2	23.1	0.71	0.80
1.0	273.0	✓	0.80	1.05				1.53		121.5	21.2	0.73	0.80
1.3	187.0	x	0.67	0.83				1.73		127.5	21.95	0.75	0.8
	175.0	✓	0.64	0.8				1.68		126.8	21.36	0.74	0.77
1.6	110.0	✓	0.50	0.61				1.71		126.1	21.6	0.75	0.77
2- storey structure													
0.6	324.0	✓	1.46	1.56	1.18	20.02	1165.08	1.4	40.1	24.36	0.69	0.79	
1.0	171.0	✓	1.06	1.15				1.68		181.4	28.09	0.73	0.80
1.3	110.0	✓	0.85	0.92				1.75		195.9	30.4	0.76	0.8
1.6	89.5	x	0.77	0.84				1.94		200.0	31.79	0.75	0.8
	82.5	✓	0.73	0.8				1.86		198.9	30.93	0.72	0.75

Zone	Mass	IDA	Modal analysis		Pushover analysis					NLTH analysis			
a_g	m	check	T	T^*	Γ	Δ_y	F_y	μ	$\Delta_{u,st}$	HD force	Δ_{roof}	IDR	DI
$[\frac{m}{s^2}]$	[t]		[s]	[s]	[-]	[mm]	[kN]	[-]	[mm]	[kN]	[mm]	[-]	[-]
3- storey structure													
0.6	170.0	✓	1.52	1.70	1.246	33.3	165.0	1.0	55.57	179.2	25.44	0.52	0.59
1.0	124.0	✓	1.30	1.44				1.39		208.0	434.02	0.66	0.75
1.3	107.0	✓	1.3	1.35				1.68		256.8	41.71	0.70	0.76
1.6	57.0	✓	0.88	0.97				1.53		238.7	38.67	0.64	0.67
4- storey structure													
0.6	102.5	✓	1.59	1.70	1.289	44.91	164.9	1.0	74.88	173.0	26.4	0.43	0.48
1.0	102.5	✓	1.59	1.70				1.24		245.9	41.87	0.60	0.71
1.3	77.0	✓	1.37	1.48				1.40		276.1	46.82	0.69	0.74
1.6	59.0	✓	1.0	1.29				1.50		297.6	49.41	0.70	0.71
5- storey structure													
0.6	63.0	✓	1.60	1.70	1.325	61.63	164.8	1.0	99.13	154.5	27.77	0.34	0.33
1.0	63.0	✓	1.60	1.70				1.0		247.2	43.99	0.48	0.54
1.3	60.0	✓	1.56	1.66				1.18		286.9	54.44	0.7	0.76
1.6	48.0	✓	1.40	1.48				1.29		312.5	59.11	0.63	0.68
6- storey structure													
0.6	41.5	✓	1.63	1.70	1.354	82.59	165.6	1.0	128.5	167.3	28.66	0.31	0.33
1.0	41.5	✓	1.63	1.70				1.0		233.8	45.24	0.42	0.46
1.3	41.5	✓	1.63	1.70				1.0		291.2	57.76	0.51	0.55
1.6	35.5	✓	1.50	1.58				1.04		317.4	64.45	0.55	0.60
7- storey structure													
0.6	28.5	✓	1.65	1.70	1.38	109.0	166.4	1.0	164.1	168.5	32.29	0.26	0.28
1.0	28.5	✓	1.65	1.70				1.0		225.8	45.5	0.36	0.39
1.3	28.5	✓	1.65	1.70				1.0		268.8	57.56	0.44	0.46
1.6	28.5	✓	1.65	1.70				1.0		322.9	72.46	0.55	0.59
8- storey structure													
0.6	20.0	✓	1.68	1.70	1.40	141.3	167.0	1.0	206.5	165.1	34.75	0.23	0.24
1.0	20.0	✓	1.68	1.70				1.0		221.5	50.0	0.31	0.33
1.3	20.0	✓	1.68	1.70				1.0		246.8	57.83	0.37	0.39
1.6	20.0	✓	1.68	1.70				1.0		303.0	74.07	0.46	0.49

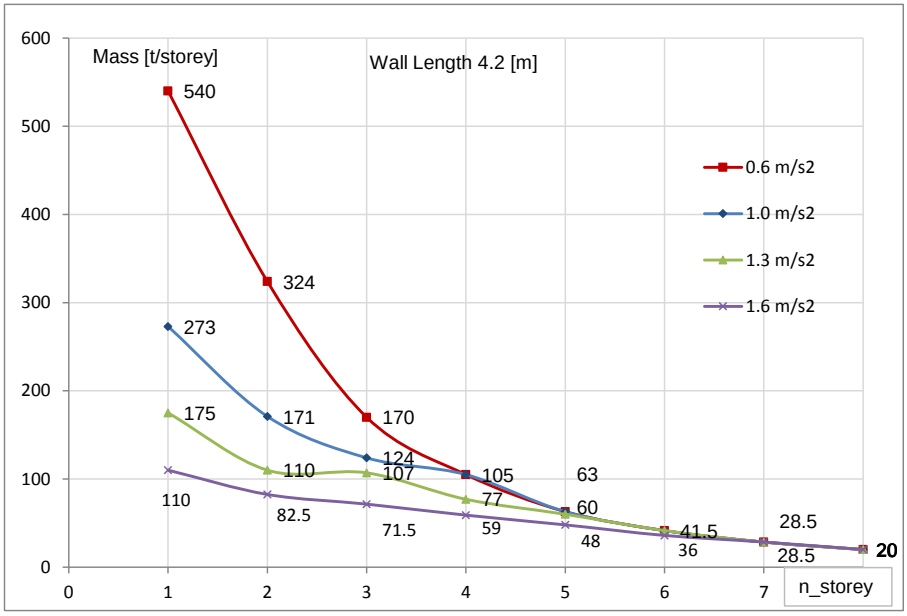

Fig. A.8: Outcome of the parameter study of the LFTW sheathed on both sides with GFB with a length of 4.2 [m], see also Table A.4

A.1.5 Tabular and graphical presentation for LFTW of a length $4.8[m]$ sheathed on both sides with GFB

The results of the parametric study for a 4.8 [m] long LFTW element sheathed with GFB on both sides are summarized in Table A.5. The typical, graphical presentation is given in Figure A.9.

Tab. A.5: Results of the parameter study of a LFTW with a length of 4.8 [m] sheathed on both sides with GFB

Zone	Mass	IDA	Modal analysis			Pushover analysis				NLTH analysis			
a_g	m	check	T	T^*	Γ	Δ_y	F_y	μ	$\Delta_{u,st}$	HD force	Δ_{roof}	IDR	DI
$[\frac{m}{s^2}]$	[t]		[s]	[s]	[-]	[mm]	[kN]	[-]	[mm]	[kN]	[mm]	[-]	[-]
1- storey structure													
0.6	550.0	✓	1.10	1.70	1.0	23.14	182.9	1.10	42.31	104.0	20.2	0.70	0.71
1.0	323.5	x	0.84	1.14				1.57		115.5	23.59	0.81	0.80
	310	✓	0.81	1.11				1.55		115.5	22.56	0.78	0.75
1.3	235.0	x	0.71	0.92				1.83		117.1	25.29	0.87	0.79
	190.0	✓	0.64	0.80				1.7		117.1	21.66	0.75	0.67
1.6	150.0	x	0.6	0.75				2.0		122.8	25.47	0.88	0.79
	120.0	✓	0.51	0.61				1.74		122.8	21.58	0.74	0.65

Zone	Mass	IDA	Modal analysis			Pushover analysis				NLTH analysis			
a_g	m	check	T	T^*	Γ	Δ_y	F_y	μ	$\Delta_{u,st}$	HD force	Δ_{roof}	IDR	DI
$[\frac{m}{s^2}]$	[t]		[s]	[s]	[-]	[mm]	[kN]	[-]	[mm]	[kN]	[mm]	[-]	[-]
2- storey structure													
0.6	367.0	✓	1.47	1.53	1.178	19.07	176.7	1.53	47.59	163.1	24.71	0.72	0.80
1.0	200.0	✓	1.06	1.15				1.68		181.4	28.09	0.73	0.80
1.3	152	x	0.95	1.018				2.06		190.9	33.89	0.86	0.8
	120	✓	0.82	0.89				1.78		180.0	29.27	0.75	0.67
1.6	120.0	x	0.84	0.90				2.24		196.4	35.25	0.85	0.80
	76.0	✓	0.67	0.73				1.77		184.3	29.76	0.67	0.59
3- storey structure													
0.6	183.5	✓	1.49	1.70	1.243	31.8	172.2	1.0	53.67	163.6	24.5	0.53	0.56
1.0	153.0	✓	1.36	1.54				1.55		211.9	37.78	0.71	0.78
1.3	107.0	✓	1.14	1.27				1.71		236.6	40.49	0.66	0.64
1.6	73.5	✓	0.94	1.05				1.76		232.8	40.24	0.65	0.61
4- storey structure													
0.6	115.0	✓	1.57	1.70	1.284	40.95	172.2	1.0	70.8	164.6	25.83	0.46	0.47
1.0	115.0	✓	1.57	1.70				1.35		229.7	40.9	0.63	0.70
1.3	93.8	✓	1.42	1.54				1.59		269.2	50.31	0.80	0.77
1.6	73.5	✓	1.26	1.36				1.73		283.0	53.2	0.72	0.71
5- storey structure													
0.6	71.0	✓	1.58	1.70	1.317	656.55	173.5	1.0	96.33	160.7	25.85	0.36	0.36
1.0	71.0	✓	1.58	1.70				1.0		247.2	43.99	0.48	0.54
1.3	69.0	✓	1.56	1.67				1.28		276.2	54.8	0.77	0.73
1.6	57.0	✓	1.42	1.52				1.44		305.2	60.0	0.75	0.72
6- storey structure													
0.6	47.5	✓	1.60	1.70	1.346	73.4	172.4	1.0	118.8	154.4	26.46	0.31	0.29
1.0	47.5	✓	1.60	1.70				1.0		233.8	45.24	0.42	0.46
1.3	47.5	✓	1.60	1.70				1.03		284.2	57.85	0.56	0.53
1.6	44.5	✓	1.55	1.64				1.22		308.3	67.71	0.78	0.72
7- storey structure													
0.6	33.0	✓	1.64	1.70	1.37	95.42	172.8	1.0	149.1	172.8	29.48	0.27	0.25
1.0	33.0	✓	1.64	1.70				1.0		224.0	45.97	0.37	0.3.6
1.3	33.0	✓	1.64	1.70				1.0		271.0	58.19	0.45	0.41
1.6	33.0	✓	1.64	1.70				1.0					
8- storey structure													
0.6	23.75	✓	1.65	1.70	1.392	122.4	173.7	1.0	186.6	162.1	32.33	0.24	0.21
1.0	23.75	✓	1.65	1.7				1.0		216.3	47.83	0.32	0.30

1.3	23.75	✓	1.65	1.70	1.0	252.8	57.93	0.35	0.38
1.6	23.75	✓	1.65	1.70	1.0	304.7	72.92	0.48	0.44

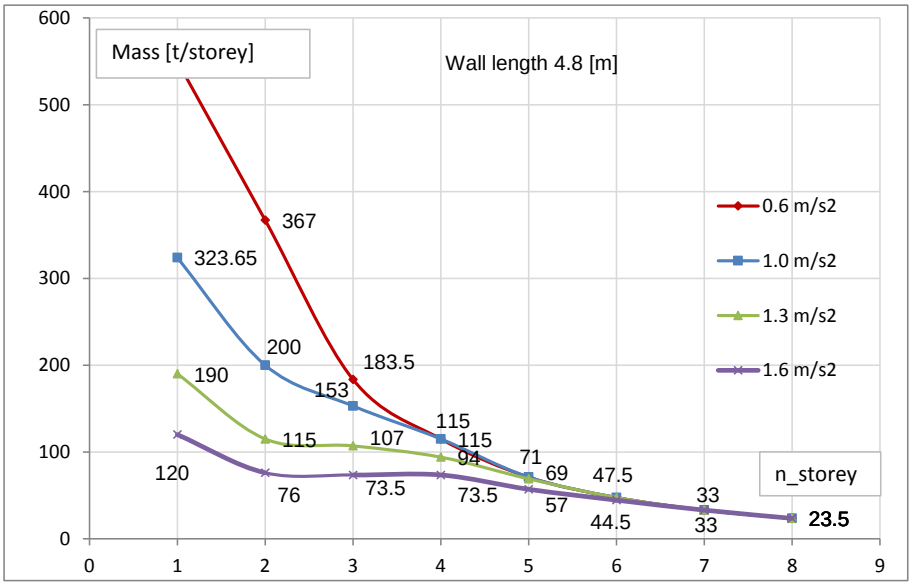

Fig. A.9: Outcome of the parameter study of the LFTW sheathed on both sides with GFB with a length of 4.8 [m], see also Table A.5

A.2 Soil conditions E

Figures A.10 to A.13 show the different resultant means of 10 earthquake records, selected and scaled to the hazard Zone Z1, Z2, Z3a and Z3b for soil conditions E.

Note that the scaled earthquake record samples for hazard zones Z3a and Z3b do not satisfy 90%-condition required by Eurocode 8 for all vibration periods. The period-range where the condition is not satisfied is rather narrow, being less than 0.25 and 0.4 [s] for Zone Z3a and Z3b, respectively. Thus, it was decided to use the sample in further analysis, because the 90%-condition is satisfied in the remaining period range. Moreover, the non-conservative solutions will be checked and where necessary corrected by means of IDA analysis, (see for e.g. A.6 with period range up to 0.5 [s]).

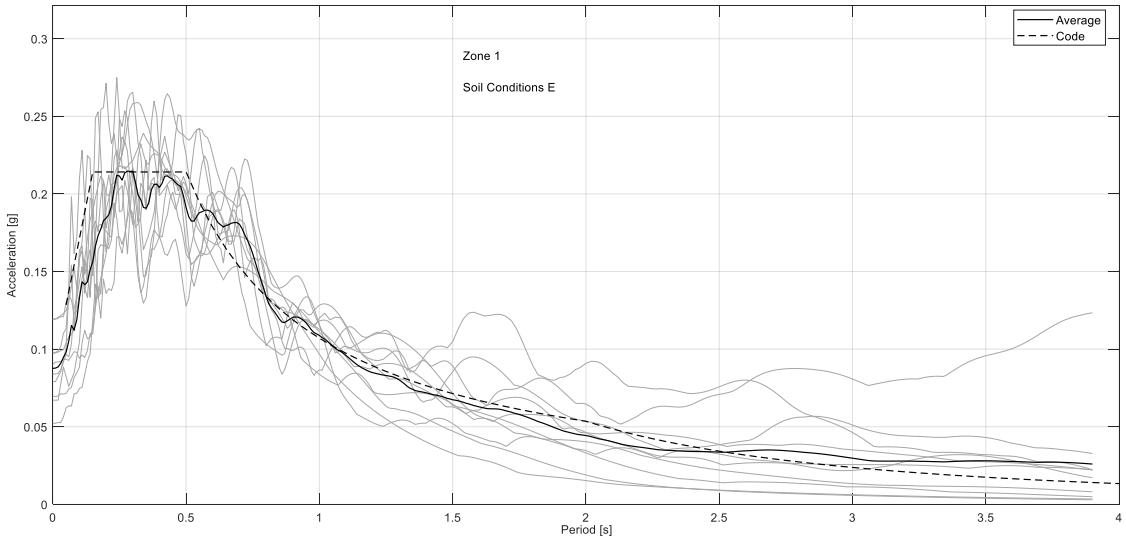

Fig. A.10: Resultant average of 10 earthquake records selected and scaled to the hazard level of Zone $Z1$ for soil conditions E superimposed on elastic RS..

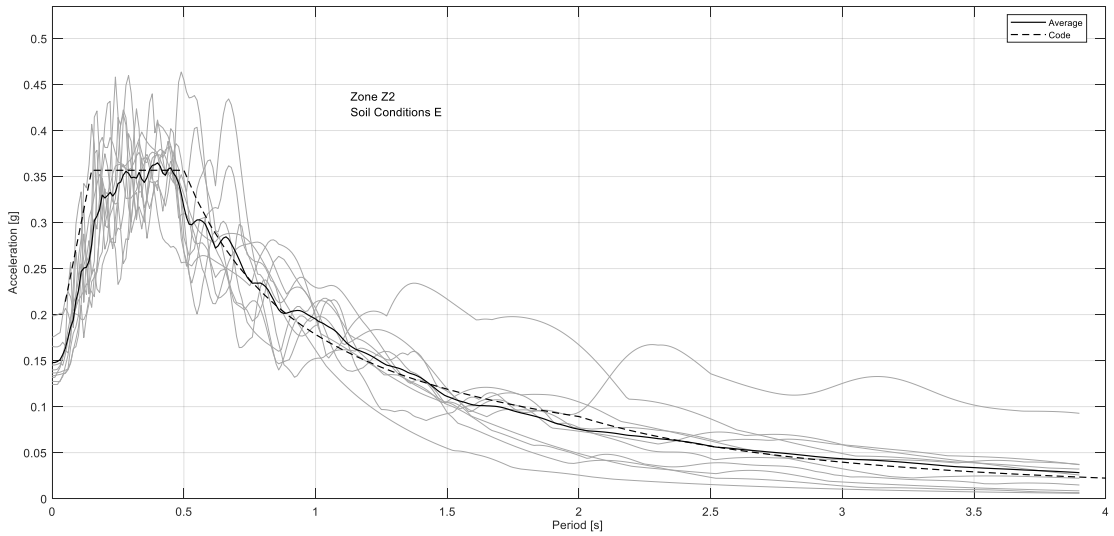

Fig. A.11: Resultant average of 10 earthquake records selected and scaled to the hazard level of Zone $Z2$ for soil conditions E superimposed on elastic RS..

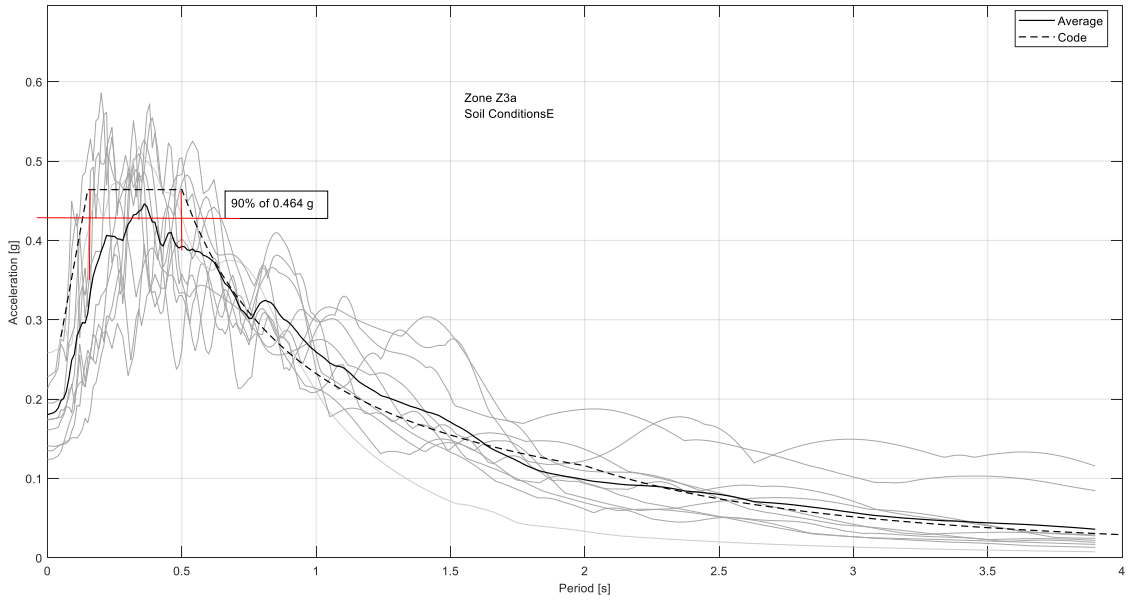

Fig. A.12: Resultant average of 10 earthquake records selected and scaled to the hazard level of Zone *Z3a* for soil conditions *E* superimposed on elastic RS..

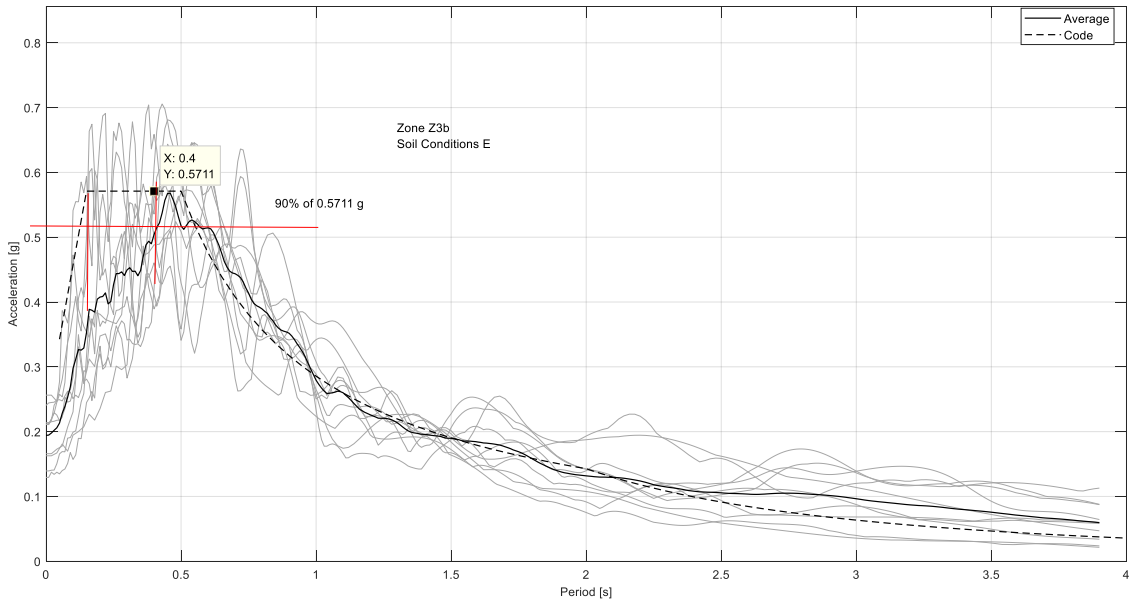

Fig. A.13: Resultant average of 10 earthquake records selected and scaled to the hazard level of Zone *Z3b* for soil conditions *E* superimposed on elastic RS..

A.2.1 Tabular and graphical presentation for LFTW of a length $2.4[m]$ sheathed on both sides with GFB

The results of the parametric study for a 2.4 [m] long LFTW element sheathed with GFB on both sides are summarized in Table A.6. The typical, graphical presentation is given in Figure A.14

Tab. A.6: Results of the parameter study of a LFTW with a length of 2.4 [m] sheathed on both sides with GFB

Zone	Mass	IDA	Modal analysis			Pushover analysis				NLTH analysis			
a_g	m	check	T	T^*	Γ	Δ_y	F_y	μ	$\Delta_{u,st}$	HD force	Δ_{roof}	IDR	DI
$[\frac{m}{s^2}]$	[t]		[s]	[s]	[-]	[mm]	[kN]	[-]	[mm]	[kN]	[mm]	[-]	[-]
1- storey structure													
0.6	173.0	x	0.79	0.97	1.0	11.95	86.06	2.17	33.53	118.6	22.29	0.77	0.79
	130.0	✓	0.68	0.82				1.92		111.9	19.16	0.66	0.67
1.0	70.5	x	0.50	0.59				2.45		109.6	23.49	0.81	0.8
	46.0	✓	0.40	0.47				1.88		105.7	16.46	0.57	0.55
1.3	46.0	x	0.4	0.47				2.46		120.0	23.28	0.8	0.79
	35.0	✓	0.36	0.41				1.86		105.0	16.43	0.57	0.55
1.6	35.0	x	0.36	0.41				2.3		119.2	23.42	0.81	0.8
	28.0	✓	0.31	0.36				1.83		103.2	15.75	0.54	0.53
2- storey structure													
0.6	107.0	x	1.06	1.18	1.19	18.0	85.0	2.07	41.58	178.4	29.78	0.76	0.80
	100.0	✓	1.02	1.14				2.0		179.1	28.49	0.70	0.72
1.0	45.0	x	0.68	0.75				2.24		183.8	32.46	0.8	0.8
	33.0	✓	0.59	0.65				1.94		176.4	27.58	0.65	0.65
1.3	25.5	x	0.51	0.57				2.22		187.8	33.74	0.81	0.8
	20.5	✓	0.46	0.51				2.0		176.7	27.53	0.62	0.61
1.6	16.5	✓	0.41	0.46				2.02		179.4	29.52	0.71	0.70
3- storey structure													
0.6	72.0	✓	1.29	1.40	1.263	28.05	83.17	1.69	52.9	202.0	35.63	0.67	0.71
1.0	29.5	x	0.83	0.90				1.83		239.0	40.78	0.62	0.62
	27.0	✓	0.79	0.86				1.73		236.6	38.97	0.59	0.58
1.3	16.0	✓	0.6	0.65				1.73		229.3	38.49	0.63	0.6
1.6	10.0	✓	0.48	0.52				1.67		213.0	34.41	0.6	0.58
4- storey structure													
0.6	55.0	✓	1.57	1.67	1.31	42.58	83.67	1.37	74.66	213.9	39.26	0.62	0.66
1.0	29.0	✓	1.14	1.21				1.66		268.4	52.69	0.7	0.71
1.3	18.5	x	0.9	0.96				1.72		315.8	63.52	0.72	0.72
	17.5	✓	0.89	0.94				1.68		313.7	62.13	0.71	0.71
1.6	11.50	✓	0.72	0.77				1.70		301.2	58.0	0.78	0.77

Zone	Mass	IDA	Modal analysis			Pushover analysis				NLTH analysis			
a_g	m	check	T	T^*	Γ	Δ_y	F_y	μ	$\Delta_{u,st}$	HD force	Δ_{roof}	IDR	DI
$[\frac{m}{s^2}]$	[t]		[s]	[s]	[-]	[mm]	[kN]	[-]	[mm]	[kN]	[mm]	[-]	[-]
5- storey structure													
0.6	34.0	✓	1.65	1.70	1.35	62.5	83.92	1.0	101.6	217.1	42.24	0.42	0.43
1.0	33.0	✓	1.60	1.67				1.6		317.0	71.83	0.68	0.72
1.3	19.5	✓	1.24	1.29				1.61		346.4	77.68	0.71	0.74
1.6	11.5	✓	0.96	1.0				1.54		338.3	73.94	0.64	0.64

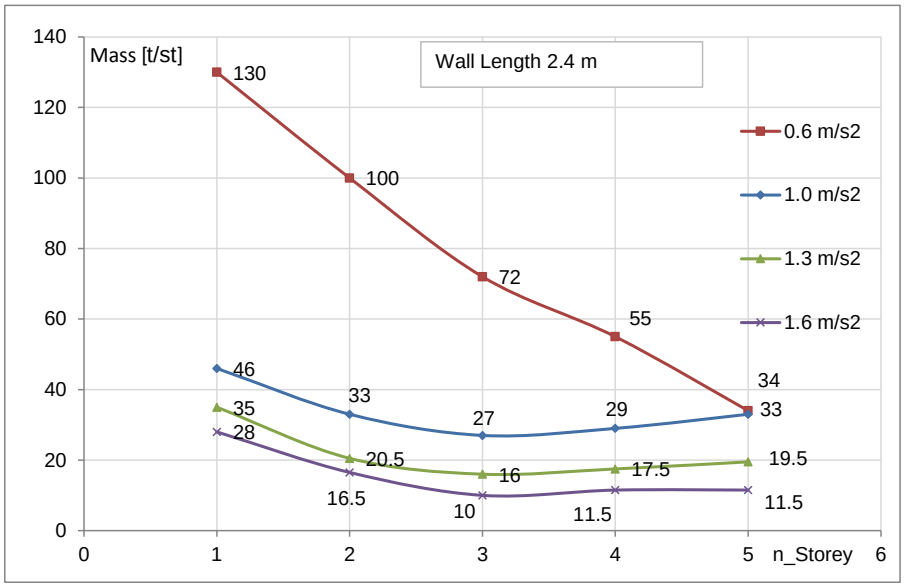

Fig. A.14: Outcome of the parameter study of the LFTW sheathed on both sides with GFB with a length of 2.4 [m], see also Table A.6

A.2.2 Tabular and graphical presentation for LFTW of a length $3.0[m]$ sheathed on both sides with GFB

The results of the parametric study for a 3.0 [m] long LFTW element sheathed with GFB on both sides are summarized in Table A.7. The typical, graphical presentation is given in Figure A.15

Tab. A.7: Results of the parameter study of a LFTW with a length of 3.0 [m] sheathed on both sides with GFB

Zone	Mass	IDA	Modal analysis			Pushover analysis				NLTH analysis			
a_g	m	check	T	T^*	Γ	Δ_y	F_y	μ	$\Delta_{u,st}$	HD force	Δ_{roof}	IDR	DI
$[\frac{m}{s^2}]$	[t]		[s]	[s]	[-]	[mm]	[kN]	[-]	[mm]	[kN]	[mm]	[-]	[-]
1- storey structure													
0.6	173.0	✓	0.83	1.0	1.0	17.37	119.6	1.52	40.66	123.2	25.0	0.86	0.80
1.0	78.5	✓	0.55	0.64				1.77		128.8	26.67	0.92	0.80
1.3	50.0	✓	0.45	0.50				1.9		130.0	27.54	0.95	0.80
1.6	37.5	✓	0.39	0.43				1.76		130.3	27.64	0.95	0.80
2- storey structure													
0.6	120.0	✓	1.15	1.27	1.181	25.53	118.1	1.57	53.01	183.6	33.41	0.81	0.80
1.0	52.5	✓	1.76	1.14				1.74		207.5	39.92	0.92	0.80
1.3	30.5	✓	0.59	0.64				1.73		208.5	40.82	0.95	0.8
1.6	20.0	✓	0.47	0.5				208.5	40.39	0.95	0.8		
3- storey structure													
0.6	92.0	✓	1.46	1.60	1.25	38.17	115.1	1.39	64.6	207.0	41.21	0.75	0.80
1.0	45.5	✓	1.03	1.12				1.64		273.6	56.18	0.87	0.80
1.3	28.5	✓	0.8	0.89				1.70		300.7	59.82	0.87	0.8
1.6	16.5	✓	0.62	0.67				1.58		277.1	55.14	0.86	0.69
4- storey structure													
0.6	60.0	✓	1.60	1.70	1.295	54.6	116.4	1.08	89.41	212.2	42.44	0.53	0.57
1.0	32.0	✓	1.17	1.25				1.3		286.0	61.09	0.79	0.71
1.3	25.0	✓	1.03	1.10				1.5		351.0	78.42	0.82	0.79
1.6	18.5	✓	0.88	0.94				1.59		339.6	73.44	0.81	0.77
5- storey structure													
0.6	36.5	✓	1.61	1.70	1.331	75.95	116.1	1.0	119.6	208.8	44.25	0.44	0.44
1.0	36.5	✓	1.61	1.70				1.32		333.2	79.96	0.70	0.66
1.3	26.5	✓	1.37	1.44				1.46		284.0	94.88	0.81	0.8
1.6	17.5	✓	1.11	1.17				1.46		388.8	91.5	0.77	0.79
6- storey structure													
0.6	23.75	✓	1.64	1.70	1.36	103.4	116.1	1.0	157.0	195.6	46.0	0.38	0.35
1.0	23.75	✓	1.64	1.70				1.0		326.0	75.98	0.63	0.52
1.3	23.75	✓	1.64	1.70				1.29		389.5	107.9	0.78	0.78
1.6	14.0	✓	1.26	1.31				1.22		419.1	111.2	0.77	0.78

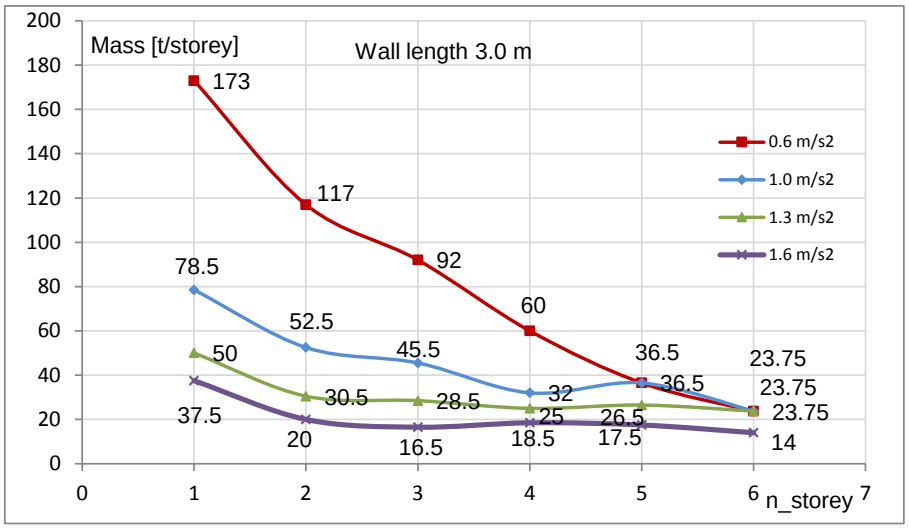

Fig. A.15: Outcome of the parameter study of the LFTW sheathed on both sides with GFB with a length of 3.0 [m], see also Table A.7

A.2.3 Tabular and graphical presentation for LFTW of a length $3.6[m]$

The results of the parametric study for a 3.6 [m] long LFTW element sheathed with GFB on both sides are summarized in Table A.8. The typical, graphical presentation is given in Figure A.16

Tab. A.8: Results of the parameter study of a LFTW with a length of 3.6 [m]

Zone	Mass	IDA	Modal analysis			Pushover analysis				NLTH analysis			
a_g	m	check	T	T^*	Γ	Δ_y	F_y	μ	$\Delta_{u,st}$	HD force	Δ_{roof}	IDR	DI
$[\frac{m}{s^2}]$	[t]		[s]	[s]	[-]	[mm]	[kN]	[-]	[mm]	[kN]	[mm]	[-]	[-]
1- storey structure													
0.6	219.0	✓	0.81	1.02	1.0	17.21	141.6	1.59	39.97	124.3	24.55	0.85	0.80
1.0	99.0	x	0.54	0.64				1.90		128.3	26.24	0.90	0.80
	54.0	✓	0.50	0.59				1.78		124.9	24.14	0.830	0.71
1.3	63.5	x	0.44	0.50				2.0		129.1	27.02	0.93	0.80
	62.0	✓	0.43	0.5				2.0		128.6	26.39	0.91	0.78
1.6	47.5	✓	0.38	0.43				1.9		129.4	26.89	0.93	0.8
2- storey structure													
0.6	144.0	✓	1.10	1.20	1.18	22.47	139.3	1.69	50.17	185.9	31.55	0.80	0.79
1.0	66.0	x	0.74	0.81				1.90		211.0	38.66	0.89	0.80
	56.0	✓	0.69	0.75				1.76		198.4	34.36	0.80	0.71
1.3	38.0	x	0.57	0.62				1.89		211.0	39.16	0.91	0.80
	31.5	✓	0.51	0.56				1.71		195.6	34.75	0.80	0.68
1.6	25.0	x	0.45	0.5				1.88		206.3	38.54	0.94	0.8
	23.75	✓	0.45	0.49				1.79		203.0	36.8	0.88	0.75

Zone	Mass	IDA	Modal analysis			Pushover analysis				NLTH analysis			
a_g	m	check	T	T^*	Γ	Δ_y	F_y	μ	$\Delta_{u,st}$	HD force	Δ_{roof}	IDR	DI
$[\frac{m}{s^2}]$	[t]		[s]	[s]	[-]	[mm]	[kN]	[-]	[mm]	[kN]	[mm]	[-]	[-]
3- storey structure													
0.6	112.0	✓	1.40	1.55	1.248	34.22	138.2	1.47	65.86	223.3	40.22	0.75	0.80
1.0	57.0	x	1.0	1.09				1.76		281.7	53.73	0.83	0.78
	50.0	✓	0.90	1.02				1.65		275.8	50.61	0.75	0.68
1.3	35.0	x	0.79	0.86				1.8		298.2	56.08	0.86	0.79
	30.0	✓	0.72	0.78				1.67		283.5	51.19	0.81	0.72
1.6	19.5	✓	0.58	0.63				1.66		278.9	51.09	0.82	0.72
4- storey structure													
0.6	78.5	✓	1.58	1.70	1.292	48.21	137.2	1.20	84.4	226.1	41.63	0.57	0.62
1.0	58.0	✓	1.36	1.46				1.73		309.8	65.95	0.79	0.80
1.3	30.0	✓	0.97	1.04				1.62		361.7	74.4	0.85	0.80
1.6	20.5	✓	0.8	0.86				1.65		338.2	67.16	0.8	0.74
5- storey structure													
0.6	49.0	✓	1.60	1.70	1.327	66.06	136.4	1.0	106.6	223.6	43.27	0.45	0.47
1.0	49.0	✓	1.60	1.70				1.32		333.2	79.96	0.70	0.66
1.3	31.5	✓	1.29	1.36				1.59		399.0	88.39	0.78	0.80
1.6	21.5	x	1.07	1.13				1.62		402.8	87.0	0.76	0.78
	20.5	✓	0.9	1.1				1.57		398.7	85.1	0.74	0.74
6- storey structure													
0.6	32.0	✓	1.62	1.70	1.36	89.15	136.9	1.0	138.6	215.0	45.31	0.41	0.39
1.0	32.0	✓	1.62	1.70				1.15		350.0	81.35	0.60	0.56
1.3	29.5	✓	1.57	1.64				1.43		411.8	102.7	0.78	0.78
1.6	18.5	✓	1.24	1.29				1.40		436.9	106.4	0.76	0.80
7- storey structure													
0.6	21.75	✓	1.64	1.70	1.38	117.6	136.9	1.0	177.5	202.1	46.71	0.33	0.32
1.0	21.75	✓	1.62	1.70				1.0		328.1	83.99	0.46	0.45
1.3	21.75	✓	1.57	1.64				1.15		411.7	107.1	0.62	0.62
1.6	17.0	✓	1.45	1.50				1.25		437.0	117.8	0.70	0.75

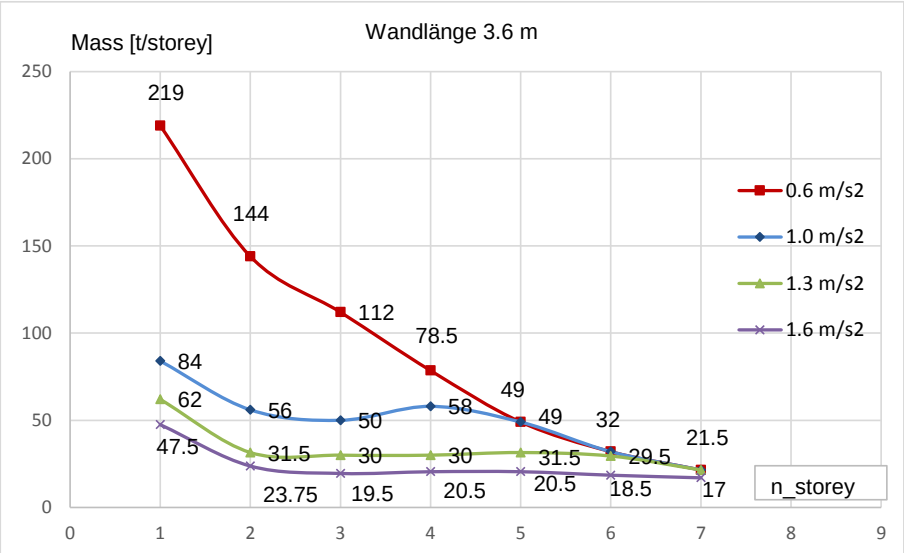

Fig. A.16: Outcome of the parameter study of the LFTW sheathed on both sides with GFB with a length of 3.6 [m], see also Table A.8

A.2.4 Tabular and graphical presentation for LFTW of a length $4.2[m]$ sheathed on both sides with GFB

The results of the parametric study for a 4.2 [m] long LFTW element sheathed with GFB on both sides are summarized in Table A.9. The typical, graphical presentation is given in Figure A.17

Tab. A.9: Results of the parameter study of a LFTW with a length of 4.2 [m] sheathed on both sides with GFB

Zone	Mass	IDA	Modal analysis			Pushover analysis				NLTH analysis			
a_g	m	check	T	T^*	Γ	Δ_y	F_y	μ	$\Delta_{u,st}$	HD force	Δ_{roof}	IDR	DI
$[\frac{m}{s^2}]$	[t]		[s]	[s]	[-]	[mm]	[kN]	[-]	[mm]	[kN]	[mm]	[-]	[-]
1- storey structure													
0.6	243.0	✓	0.76	0.98	1.0	17.03	167.9	1.53	31.31	127.1	21.91	0.75	0.80
1.0	98.4	x	0.48	0.57				1.80		128.7	22.46	0.77	0.80
	90.0	✓	0.46	0.54				1.72		12.5	20.54	0.71	0.72
1.3	71.0	x	0.41	0.48				1.92		130.3	22.49	0.78	0.8
	68.5	✓	0.40	0.47				1.86		128.0	21.48	0.74	0.76
1.6	54.0	✓	0.36	0.41				1.80		129.3	22.59	0.78	0.8
2- storey structure													
0.6	161.0	✓	1.02	1.11	1.18	20.43	165.8	1.71	40.42	193.0	29.65	0.75	0.80
1.0	67.0	x	0.66	0.72				1.83		204.3	32.27	0.77	0.80
	64.0	✓	0.65	0.71				1.79		200.4	31.03	0.75	0.77
1.3	39.0	✓	0.50	0.55				1.81		208.1	33.85	0.78	0.8

1.6	28.0	✓	0.43	0.47				1.79		208.7	33.52	0.78	0.8
Zone	Mass	IDA	Modal analysis			Pushover analysis				NLTH analysis			
a_g	m	check	T	T^*	Γ	Δ_y	F_y	μ	$\Delta_{u,st}$	HD force	Δ_{roof}	IDR	DI
$[\frac{m}{s^2}]$	[t]		[s]	[s]	[-]	[mm]	[kN]	[-]	[mm]	[kN]	[mm]	[-]	[-]
3- storey structure													
0.6	125.5	✓	1.31	1.46	1.246	32.95	165.0	1.47	55.40	230.4	36.35	0.66	0.72
1.0	60.0	x	0.90	0.99				1.71		282.8	46.83	0.72	0.76
	54.0	✓	0.86	0.94				1.63		272.3	44.01	0.70	0.73
1.3	33.5	x	0.68	0.74				1.68		289.7	47.92	0.77	0.80
	30.5	✓	0.65	0.71				1.60		280.4	45.94	0.75	0.78
1.6	22.75	x	0.56	0.61				1.71		288.0	47.30	0.76	0.80
	18.0	✓	0.50	0.54				1.52		261.6	40.82	0.68	0.70
4- storey structure													
0.6	94.0	✓	1.52	1.63	1.29	44.88	164.90	1.25	74.86	239.5	40.39	0.8	0.64
1.0	54.0	✓	1.36	1.46				1.73		309.8	65.95	0.79	0.80
1.3	26.5	✓	0.80	0.87				1.44		3339.2	56.57	0.65	0.67
1.6	17.0	✓	0.64	0.69				1.42		336.2	56.46	0.66	0.68
5- storey structure													
0.6	62.5	✓	1.60	1.70	1.325	61.7	164.8	1.0	99.17	242.7	42.44	0.48	0.53
1.0	33.8	✓	1.17	1.24				1.19		323.9	60.6	0.75	0.79
1.3	22.0	✓	0.95	1.0				1.25		390.2	73.34	0.63	0.66
1.6	17.0	✓	0.83	0.88				1.35		385.2	68.73	0.61	0.64
6- storey structure													
0.6	41.5	✓	1.62	1.70	1.353	82.53	165.6	1.0	128.5	228.1	43.7	0.41	0.44
1.0	41.5	✓	1.62	1.70				1.24		378.2	79.83	0.60	0.62
1.3	20.5	✓	1.14	1.19				1.13		408.6	85.0	0.59	0.63
1.6	21.0	x	1.15	1.21				1.41		436.9	94.43	0.65	0.71
	18.0	✓	1.07	1.12				1.31		427.0	86.24	0.59	0.62
7- storey structure													
0.6	28.5	✓	1.65	1.70	1.38	108.9	166.4	1.0	164.1	218.8	45.48	0.36	0.38
1.0	28.5	✓	1.65	1.70				1.0		359.7	81.25	0.36	0.38
1.3	28.0	✓	1.63	1.69				1.23		435.0	103.5	0.66	0.68
1.6	19.5	✓	1.38	1.42				1.28		469.0	111.6	0.70	0.75

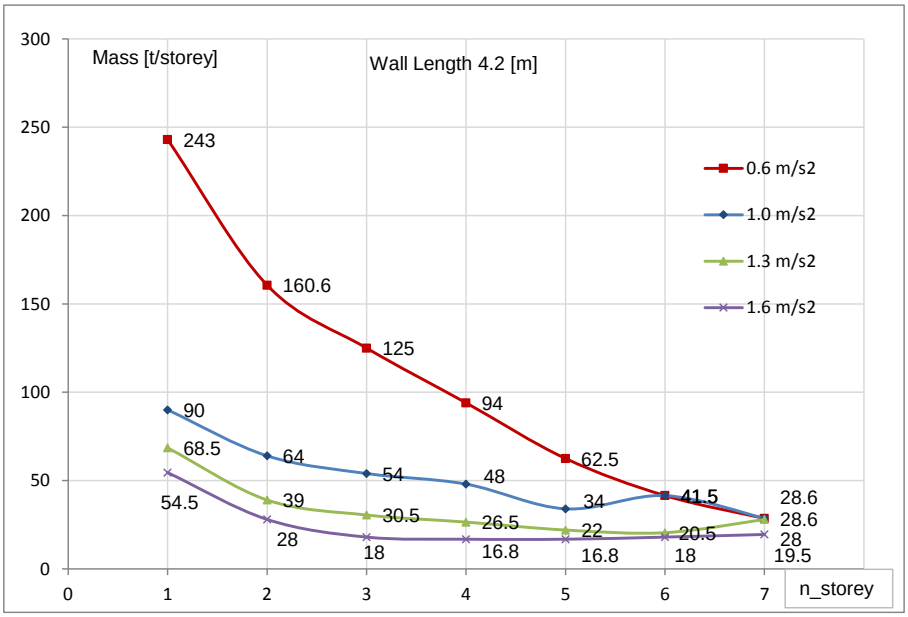

Fig. A.17: Outcome of the parameter study of the LFTW sheathed on both sides with GFB with a length of 4.2 [m], see also Table A.9

A.2.5 Tabular and graphical presentation for LFTW of a length $4.8[m]$ sheathed on both sides with GFB

The results of the parametric study for a 4.8 [m] long LFTW element sheathed with GFB on both sides are summarized in Table A.10. The typical, graphical presentation is given in Figure A.18

Tab. A.10: Results of the parameter study of a LFTW with a length of 4.8 [m] sheathed on both sides with GFB

Zone	Mass	IDA	Modal analysis			Pushover analysis				NLTH analysis			
a_g	m	check	T	T^*	Γ	Δ_y	F_y	μ	$\Delta_{u,st}$	HD force	Δ_{roof}	IDR	DI
$[\frac{m}{s^2}]$	[t]		[s]	[s]	[-]	[mm]	[kN]	[-]	[mm]	[kN]	[mm]	[-]	[-]
1- storey structure													
0.6	306.0	x	0.81	1.10	1.0	17.12	180.1	1.62	39.55	119.8	24.87	0.86	0.80
	260.0	✓	0.75	0.99				1.54		117.0	21.91	0.75	0.69
1.0	138.0	x	0.54	0.66				2.02		124.1	26.52	0.91	0.80
	105.0	✓	0.48	0.57				1.80		117.1	21.87	0.75	0.64
1.3	89.0	x	0.43	0.52				2.19		125.0	27.25	0.94	0.80
	80.0	✓	0.42	0.49				2.04		122.7	24.0	0.83	0.70
1.6	66.0	x	0.38	0.44				2.07		124.4	27.33	0.94	0.80
	64.0	✓	0.37	0.43				2.0		124.1	26.0	0.90	0.76

Zone	Mass	IDA	Modal analysis			Pushover analysis				NLTH analysis			
a_g	m	check	T	T^*	Γ	Δ_y	F_y	μ	$\Delta_{u,st}$	HD force	Δ_{roof}	IDR	DI
$[\frac{m}{s^2}]$	[t]		[s]	[s]	[-]	[mm]	[kN]	[-]	[mm]	[kN]	[mm]	[-]	[-]
2- storey structure													
0.6	203.0	X	1.09	1.17	1.178	19.09	176.7	1.94	47.59	181.3	30.81	0.84	0.80
	177.5	✓	1.02	1.1				1.80		180.5	29.57	0.77	0.72
1.0	93.0	x	0.74	0.80				2.14		203.7	37.94	0.91	0.80
	55.0	✓	0.57	0.62				1.64		171.0	26.72	0.66	0.56
1.3	53.0	x	0.56	0.61				2.1		201.9	38.45	0.93	0.80
	37.0	✓	0.47	0.51				1.75		181.9	29.48	0.65	0.55
1.6	34.5	x	0.45	0.49				2.04		197.5	37.62	0.95	0.8
	29.5	✓	0.41	0.46				1.75		188.9	0.41	0.46	
3- storey structure													
0.6	144.0	✓	1.32	1.50	1.243	31.21	172.7	1.58	53.39	220.7	38.62	0.77	0.77
1.0	62.0	x	0.86	0.96				1.77		258.9	44.97	0.69	0.62
	56.0	✓	0.82	0.91				1.69		257.0	43.06	0.69	0.60
1.3	37.0	x	0.67	0.73				1.78		272.1	47.48	0.78	0.68
	29.5	✓	0.60	0.66				1.60		249.4	41.31	0.68	0.57
1.6	24.0	x	0.54	0.59				1.78		268.7	46.12	0.77	0.66
	21.0	✓	0.50	0.55				1.67		253.2	42.08	0.73	0.62
4- storey structure													
0.6	109.0	✓	1.53	1.65	1.29	44.88	164.90	1.284	74.86	239.5	40.39	0.8	0.64
1.0	61.0	x	1.15	1.24				1.73		307.7	57.89	0.86	0.78
	56.0	✓	1.10	1.19				1.65		309.7	56.90	0.74	0.67
1.3	36.0	x	0.88	0.95				1.73		351.0	67.11	0.85	0.75
	31.0	✓	0.81	0.88				1.60		331.9	58.41	0.68	0.61
5- storey structure													
0.6	71.5	✓	1.58	1.70	1.317	56.48	173.4	1.05	96.30	234.9	41.82	0.48	0.49
1.0	65.0	x	1.52	1.63				1.69		352.9	73.47	0.81	0.78
	54.5	✓	1.39	1.48				1.54		334.9	67.75	0.69	0.65
1.3	39.0	x	1.17	1.26				1.70		390.3	79.62	0.76	0.72
	30.0	✓	1.03	1.10				1.49		385.0	76.11	0.73	0.67
1.6	26.0	x	0.96	1.03				1.71		400.0	79.43	0.74	0.70
	19.0	✓	0.84	0.88				1.46		366.0	68.11	0.64	0.57
6- storey structure													
0.6	48.0	✓	1.61	1.70	1.346	73.4	172.4	1.0	119.1	227.8	43.38	0.42	0.41
1.0	48.0	✓	1.61	1.70				1.38		368.2	78.39	0.58	0.57
1.3	37.5	x	1.42	1.50				1.59		415.9	94.05	0.80	0.78
	28.0	✓	1.23	1.30				1.38		401.8	84.58	0.64	0.60

1.6	25.0	x	1.18	1.24				1.62		427.3	95.19	0.78	0.78
	18.0	✓	0.99	1.04				1.36		398.8	81.13	0.57	0.53
					7- storey structure								
0.6	33.0	✓	1.63	1.70	1.37	95.42	172.8	1.0	149.1	217.4	44.92	0.36	0.34
1.0	33.0	✓	1.63	1.70				1.08		355.9	79.89	0.50	0.48
1.3	33.0	✓	1.63	1.70				1.41		429.0	106.4	0.76	0.74
1.6	26.5	x	1.46	1.52				1.55		450.8	110.2	0.73	0.77
	21.5	✓	1.31	1.37				1.40		454.0	107.8	0.69	0.69

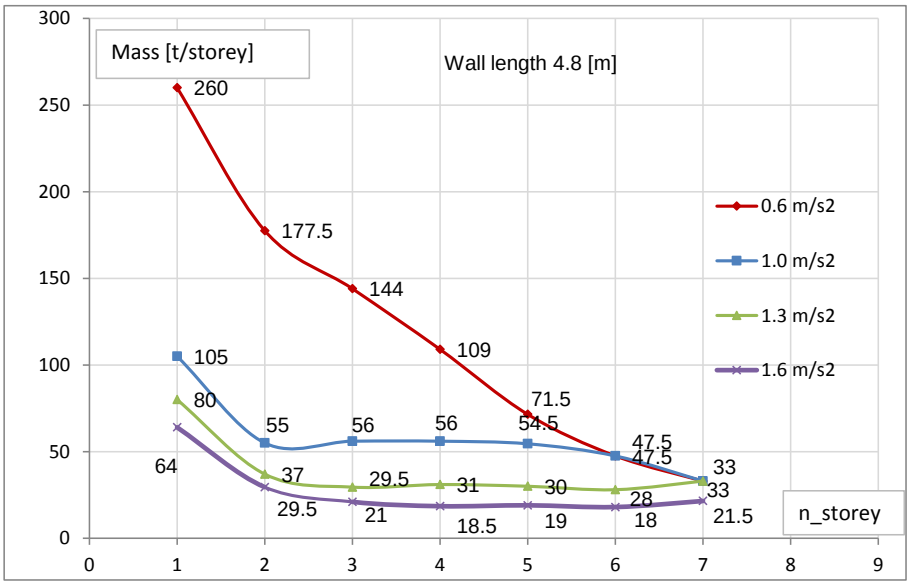

Fig. A.18: Outcome of the parameter study of the LFTW sheathed on both sides with GFB with a length of 4.8 [m], see also Table A.10

Appendix B

Parameter Study of LFTWs Sheathed with OSB

B.1 Soil conditions A

B.1.1 Tabular and graphical presentation for LFTW of a length $2.4[m]$ sheathed on both sides with OSB

The results of the parametric study for a 2.4 [m] long LFTW element sheathed with OSB on both sides are summarized in Table B.1. The typical, graphical presentation is given in Figure B.1

Tab. B.1: Results of the parameter study of a LFTW with a length of 2.4 [m] sheathed on both sides with OSB

Zone	Mass	IDA	Modal analysis			Pushover analysis				NLTH analysis			
a_g	m	check	T	T^*	Γ	Δ_y	F_y	μ	$\Delta_{u,st}$	HD force	Δ_{roof}	IDR	DI
$[\frac{m}{s^2}]$	[t]		[s]	[s]	[-]	[mm]	[kN]	[-]	[mm]	[kN]	[mm]	[-]	[-]
1- storey structure													
0.6	500.0	✓	1.27	1.71	1.0	19.98	163.0	1.08	103.2	145.5	20.01	0.69	0.21
1.0	500.0	✓	1.27	1.71				1.79		174.4	20.01	0.69	0.21
1.3	500.0	✓	1.27	1.71				2.32		187.2	49.3	1.70	0.54
1.6	500.0	✓	1.27	1.71				2.86		197.2	60.51	2.09	0.67
2- storey structure													
0.6	230.0	✓	1.47	1.70	1.188	33.48	162.4	1.0	125.8	189.1	22.50	0.54	0.17
1.0	230.0	✓	1.47	1.70				1.54		260.7	37.51	0.90	0.29
1.3	230.0	✓	1.47	1.70				2.00		280.7	52.99	1.34	0.41
1.6	230.0	✓	1.47	1.70				2.46		297.5	68.07	1.80	0.57

Zone	Mass	IDA	Modal analysis			Pushover analysis				NLTH analysis			
a_g	m	check	T	T^*	Γ	Δ_y	F_y	μ	$\Delta_{u,st}$	HD force	Δ_{roof}	IDR	DI
$[\frac{m}{s^2}]$	[t]		[s]	[s]	[-]	[mm]	[kN]	[-]	[mm]	[kN]	[mm]	[-]	[-]
3- storey structure													
0.6	110.0	✓	1.53	1.70	1.267	52.76	161.7	1.0	158.6	188.4	23.14	0.41	0.12
1.0	110.0	✓	1.53	1.70				1.04		268.6	38.4	0.66	0.21
1.3	110.0	✓	1.53	1.70				1.35		321.4	54.37	0.92	0.28
1.6	110.0	✓	1.53	1.70				1.67		369.1	71.32	1.30	0.39
4- storey structure													
0.6	60.0	✓	1.58	1.70	1.318	79.92	162.4	1.0	217.4	176.2	24.59	0.31	0.09
1.0	60.0	✓	1.60	1.70				1.0		265.3	41.42	0.46	0.14
1.3	60.0	✓	1.60	1.70				1.0		319.9	54.43	0.68	0.21
1.6	60.0	✓	1.60	1.70				1.14		369.6	71.21	0.94	0.28
5- storey structure													
0.6	35.0	✓	1.62	1.70	1.357	117.5	162.3	1.0	283.7	168.9	27.17	0.25	0.08
1.0	35.0	✓	1.62	1.70				1.0		240.9	43.27	0.38	0.11
1.3	35.0	✓	1.62	1.70				1.0		299.3	54.39	0.48	0.14
1.6	35.0	✓	1.62	1.70				1.0		356.7	69.72	0.66	0.20
6- storey structure													
0.6	22.0	✓	1.65	1.70	1.386	168.6	163.0	1.0	368.3	158.7	31.06	0.21	0.06
1.0	22.0	✓	1.65	1.70				1.0		214.5	45.76	0.37	0.09
1.3	22.0	✓	1.65	1.70				1.0		254.5	54.69	0.44	0.11
1.6	22.0	✓	1.65	1.70				1.0		318.9	72.24	0.54	0.14

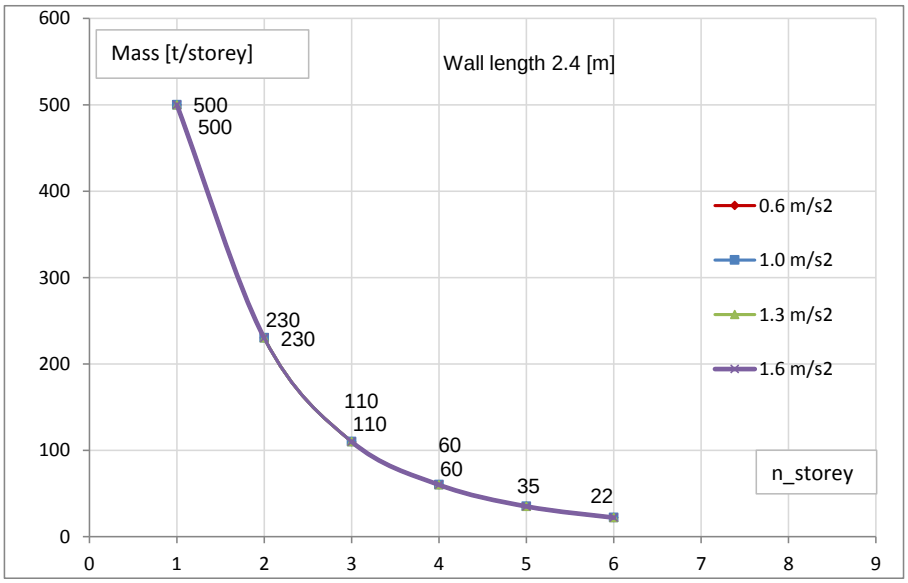

Fig. B.1: Outcome of the parameter study of the LFTW sheathed on both sides with OSB with a length of 2.4 [m], see also Table B.1

B.1.2 Tabular and graphical presentation for LFTW of a length $3.0[m]$ sheathed on both sides with OSB

The results of the parametric study for a 3.0 [m] long LFTW element sheathed with OSB on both sides are summarized in Table B.2. The typical, graphical presentation is given in Figure B.2

Tab. B.2: Results of the parameter study of a LFTW with a length of 3.0 [m] sheathed on both sides with OSB

Zone	Mass	IDA	Modal analysis			Pushover analysis				NLTH analysis			
a_g	m	check	T	T^*	Γ	Δ_y	F_y	μ	$\Delta_{u,st}$	HD force	Δ_{roof}	IDR	DI
$[\frac{m}{s^2}]$	[t]		[s]	[s]	[-]	[mm]	[kN]	[-]	[mm]	[kN]	[mm]	[-]	[-]
1- storey structure													
0.6	622.0	✓	1.13	1.70	1.0	25.8	220.8	1.0	103.9	157.4	20.24	0.70	0.24
1.0	622.0	✓	1.13	1.70				1.66		187.8	33.27	1.1	0.42
1.3	622.0	✓	1.13	1.70				2.16		206.4	47.05	1.6	0.58
1.6	570.0	✓	1.09	1.59				2.59		216.1	56.87	2.0	0.70
2- storey structure													
0.6	352.0	✓	1.46	1.71	1.188	29.33	219.9	1.04	120.5	230.7	23.5	0.66	0.23
1.0	352.0	✓	1.46	1.71				1.73		298.2	38.45	1.0	0.38
1.3	352.0	✓	1.46	1.71				2.25		314.4	53.88	1.43	0.51
1.6	352.0	✓	1.46	1.71				2.77		329.1	68.15	1.93	0.70

Zone	Mass	IDA	Modal analysis			Pushover analysis				NLTH analysis			
a_g	m	check	T	T^*	Γ	Δ_y	F_y	μ	$\Delta_{u,st}$	HD force	Δ_{roof}	IDR	DI
$[\frac{m}{s^2}]$	[t]		[s]	[s]	[-]	[mm]	[kN]	[-]	[mm]	[kN]	[mm]	[-]	[-]
3- storey structure													
0.6	167.0	✓	1.51	1.70	1.266	46.89	219.0	1.0	156.8	220.8	23.58	0.47	0.16
1.0	167.0	✓	1.51	1.70				1.17		320.6	40.57	0.75	0.27
1.3	167.0	✓	1.51	1.70				1.51		371.1	55.55	1.0	0.34
1.6	167.0	✓	1.51	1.70				1.86		422.6	73.02	1.37	0.47
4- storey structure													
0.6	92.0	✓	1.57	1.70	1.318	70.21	219.1	1.0	200.1	214.5	25.3	0.37	0.12
1.0	92.0	✓	1.57	1.70				1.0		303.8	40.98	0.52	0.18
1.3	92.0	✓	1.57	1.70				1.05		385.7	56.47	0.76	0.25
1.6	92.0	✓	1.57	1.70				1.30		438.8	74.12	1.06	0.34
5- storey structure													
0.6	54.0	✓	1.61	1.70	1.357	102.5	218.2	1.0	252.5	203.7	27.6	0.30	0.093
1.0	54.0	✓	1.62	1.70				1.0		291.7	43.7	0.41	0.14
1.3	54.0	✓	1.62	1.70				1.0		363.9	56.39	0.55	0.17
1.6	54.0	✓	1.62	1.70				1.0		413.8	71.4	0.73	0.23
6- storey structure													
0.6	34.0	✓	1.65	1.70	1.386	145.9	218.1	1.0	316.8	201.2	30.96	0.23	0.07
1.0	34.0	✓	1.65	1.70				1.0		268.1	48.42	0.33	0.11
1.3	34.0	✓	1.65	1.70				1.0		319.0	55.81	0.44	0.14
1.6	34.0	✓	1.65	1.70				1.0		402.7	74.62	0.53	0.17
7- storey structure													
0.6	22.0	✓	1.67	1.70	1.409	202.4	218.1	1.0	316.8	187.5	34.13	0.20	0.06
1.0	22.0	✓	1.67	1.70				1.0		238.7	48.41	0.27	0.085
1.3	22.0	✓	1.67	1.70				1.0		289.8	57.4	0.35	0.108
1.6	22.0	✓	1.67	1.70				1.0		370.7	77.43	0.44	0.134

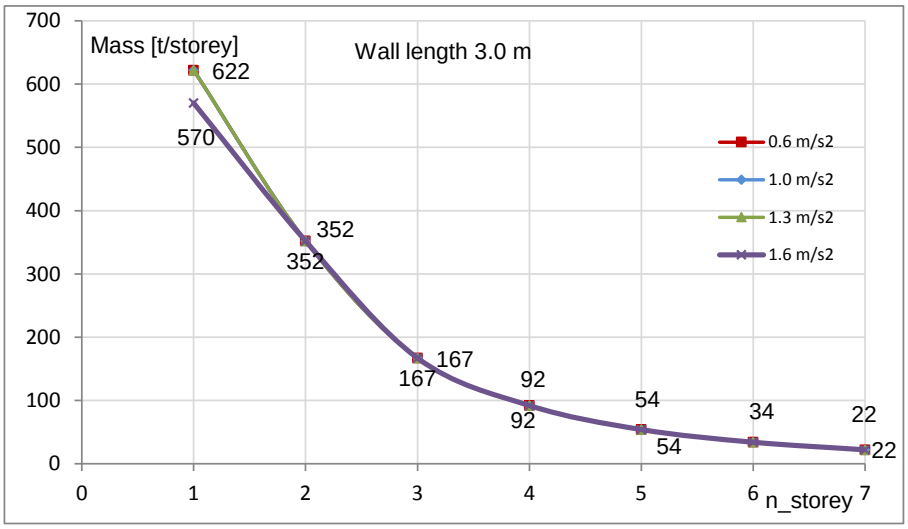

Fig. B.2: Outcome of the parameter study of the LFTW sheathed on both sides with OSB with a length of 3.0 [m], see also Table B.2

B.1.3 Tabular and graphical presentation for LFTW of a length $3.6[m]$ sheathed on both sides with OSB

The results of the parametric study for a 3.6 [m] long LFTW element sheathed with OSB on both sides are summarized in Table B.3. The typical, graphical presentation is given in Figure B.3

Tab. B.3: Results of the parameter study of a LFTW with a length of 3.6 [m] sheathed on both sides with OSB

Zone	Mass	IDA	Modal analysis			Pushover analysis				NLTH analysis			
a_g	m	check	T	T^*	Γ	Δ_y	F_y	μ	$\Delta_{u,st}$	HD force	Δ_{roof}	IDR	DI
$[\frac{m}{s^2}]$	[t]		[s]	[s]	[-]	[mm]	[kN]	[-]	[mm]	[kN]	[mm]	[-]	[-]
1- storey structure													
0.6	635.0	✓	1.15	1.70	1.0	30.36	260.8	1.0	98.83	140.6	20.57	0.70	0.22
1.0	635.0	✓	1.15	1.70				1.43		173.9	33.09	1.1	0.38
1.3	635.0	✓	1.15	1.70				1.85		193.3	45.11	1.6	0.50
1.6	635.0	✓	1.15	1.70				2.28		209.3	57.65	1.99	0.65
2- storey structure													
0.6	367.5	✓	1.47	1.70	1.183	32.73	258.7	1.0	117.0	196.5	22.3	0.66	0.21
1.0	352.0	✓	1.47	1.71				1.56		266.6	36.57	1.0	0.33
1.3	352.0	✓	1.47	1.71				2.03		297.2	52.98	1.40	0.46
1.6	352.0	✓	1.47	1.71				2.49		312.3	67.48	1.9	0.64
3- storey structure													
0.6	173.0	✓	1.48	1.70	1.256	52.6	258.7	1.0	155.5	194.8	22.21	0.48	0.15
1.0	173.0	✓	1.48	1.70				1.04		279.6	36.89	0.68	0.23
1.3	173.0	✓	1.48	1.70				1.35		338.0	51.92	0.96	0.29

1.6	173.0	✓	1.48	1.70				1.66		393.7	69.63	1.26	0.38
Zone	Mass	IDA	Modal analysis			Pushover analysis				NLTH analysis			
a_g	m	check	T	T^*	Γ	Δ_y	F_y	μ	$\Delta_{u,st}$	HD force	Δ_{roof}	IDR	DI
$[\frac{m}{s^2}]$	[t]		[s]	[s]	[-]	[mm]	[kN]	[-]	[mm]	[kN]	[mm]	[-]	[-]
4- storey structure													
0.6	100.0	✓	1.58	1.70	1.305	73.95	257.7	1.0	198.2	180.4	22.54	0.38	0.11
1.0	100.0	✓	1.58	1.70				1.0		276.5	39.09	0.55	0.17
1.3	100.0	✓	1.58	1.70				1.0		348.3	53.51	0.74	0.22
1.6	100.0	✓	1.58	1.70				1.22		403.7	71.09	0.98	0.29
5- storey structure													
0.6	60.5	✓	1.61	1.70	1.343	104.3	257.7	1.0	249.0	187.9	25.63	0.31	0.09
1.0	60.5	✓	1.62	1.70				1.0		260.7	40.51	0.45	0.13
1.3	60.5	✓	1.62	1.70				1.0		337.7	53.55	0.56	0.16
1.6	60.5	✓	1.62	1.70				1.0		391.6	67.79	0.69	0.20
6- storey structure													
0.6	39.0	✓	1.61	1.70	1.373	143.5	257.5	1.0	315.8	190.7	28.63	0.27	0.07
1.0	39.0	✓	1.65	1.70				1.0		246.8	43.77	0.38	0.11
1.3	39.0	✓	1.65	1.70				1.0		303.6	54.02	0.45	0.12
1.6	39.0	✓	1.65	1.70				1.0		363.7	67.41	0.53	0.15
7- storey structure													
0.6	26.0	✓	1.67	1.70	1.397	194.2	258.6	1.0	397.2	187.0	32.03	0.23	0.06
1.0	26.0	✓	1.67	1.70				1.0		237.8	45.78	0.31	0.09
1.3	26.0	✓	1.67	1.70				1.0		280.0	54.6	0.37	0.1
1.6	26.0	✓	1.67	1.70				1.0		345.1	71.42	0.45	0.13

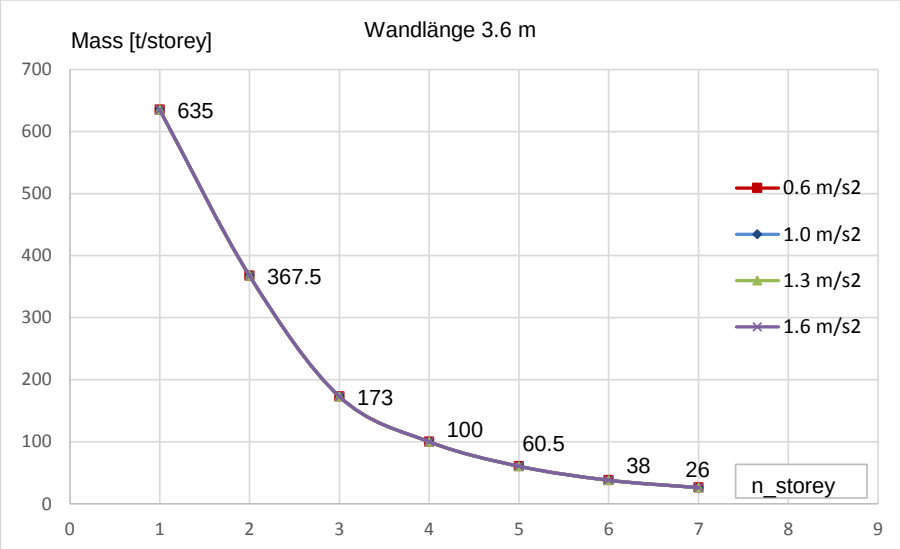

Fig. B.3: Outcome of the parameter study of the LFTW sheathed on both sides with OSB with a length of 3.6 [m], see also Table B.3

B.1.4 Tabular and graphical presentation for LFTW of a length $4.2[m]$ sheathed on both sides with OSB

The results of the parametric study for a 4.2 [m] long LFTW element sheathed with OSB on both sides are summarized in Table B.4. The typical, graphical presentation is given in Figure B.4

Tab. B.4: Results of the parameter study of a LFTW with a length of 4.2 [m] sheathed on both sides with OSB

Zone	Mass	IDA	Modal analysis			Pushover analysis				NLTH analysis			
a_g	m	check	T	T^*	Γ	Δ_y	F_y	μ	$\Delta_{u,st}$	HD force	Δ_{roof}	IDR	DI
$[\frac{m}{s^2}]$	[t]		[s]	[s]	[-]	[mm]	[kN]	[-]	[mm]	[kN]	[mm]	[-]	[-]
1- storey structure													
0.6	730.0	✓	1.1	1.70	1.0	31.34	314.4	1.0	107.3	157.1	21.9	0.75	0.20
1.0	730.0	✓	1.1	1.70				1.36		188.5	33.64	1.16	0.34
1.3	730.0	✓	1.1	1.70				1.77		204.7	44.38	1.53	0.43
1.6	730.0	✓	1.1	1.70				2.18		218.0	56.04	1.93	0.56
2- storey structure													
0.6	510.0	✓	1.53	1.70	1.183	28.48	310.7	1.08	119.9	198.66	23.18	0.8	0.25
1.0	510.0	✓	1.53	1.70				1.81		294.3	37.43	1.1	0.41
1.3	510.0	✓	1.53	1.70				2.35		315.3	54.0	1.52	0.49
1.6	510.0	✓	1.53	1.70				2.90		336.0	68.73	2.06	0.68

Zone	Mass	IDA	Modal analysis		Pushover analysis					NLTH analysis			
a_g	m	check	T	T^*	Γ	Δ_y	F_y	μ	$\Delta_{u,st}$	HD force	Δ_{roof}	IDR	DI
$[\frac{m}{s^2}]$	[t]		[s]	[s]	[-]	[mm]	[kN]	[-]	[mm]	[kN]	[mm]	[-]	[-]
3- storey structure													
0.6	222.5	✓	1.48	1.70	1.255	48.3	309.5	1.0	154.8	212.2	22.72	0.55	0.15
1.0	222.5	✓	1.48	1.70				1.12		313.0	37.95	0.78	0.24
1.3	222.5	✓	1.48	1.70				1.45		366.6	52.39	1.02	0.28
160	222.5	✓	1.48	1.70				1.79		418.4	70.39	1.30	0.35
4- storey structure													
0.6	131.0	✓	1.55	1.70	1.303	66.92	309.5	1.0	193.5	201.2	22.53	0.42	0.11
1.0	131.0	✓	1.55	1.70				1.0		321.6	39.54	0.59	0.17
1.3	131.0	✓	1.55	1.70				1.09		383.8	54.24	0.80	0.20
1.6	131.0	✓	1.55	1.70				1.34		443.3	72.3	1.05	0.26
5- storey structure													
0.6	80.0	✓	1.59	1.70	1.34	94.17	308.3	1.0	240.2	212.0	25.51	0.34	0.08
1.0	80.0	✓	1.59	1.70				1.0		302.4	40.05	0.48	0.13
1.3	80.0	✓	1.59	1.70				1.0		378.7	54.62	0.62	0.15
1.6	80.0	✓	1.59	1.70				1.0		433.0	68.65	0.77	0.19
6- storey structure													
0.6	51.5	✓	1.62	1.70	1.37	128.8	308.2	1.0	294.2	212.5	28.68	0.29	0.07
1.0	51.5	✓	1.62	1.70				1.0		282.9	44.0	0.40	0.10
1.3	51.5	✓	1.62	1.70				1.0		345.7	53.55	0.48	0.11
1.6	51.5	✓	1.62	1.70				1.0		414.4	68.32	0.58	0.14
7- storey structure													
0.6	34.5	✓	1.64	1.70	1.395	173.1	308.2	1.0	367.1	208.7	31.47	0.25	0.05
1.0	34.5	✓	1.64	1.70				1.0		276.3	47.27	0.33	0.07
1.3	34.5	✓	1.64	1.70				1.0		316.5	53.99	0.40	0.08
1.6	34.5	✓	1.64	1.70				1.0		391.0	70.92	0.49	0.106

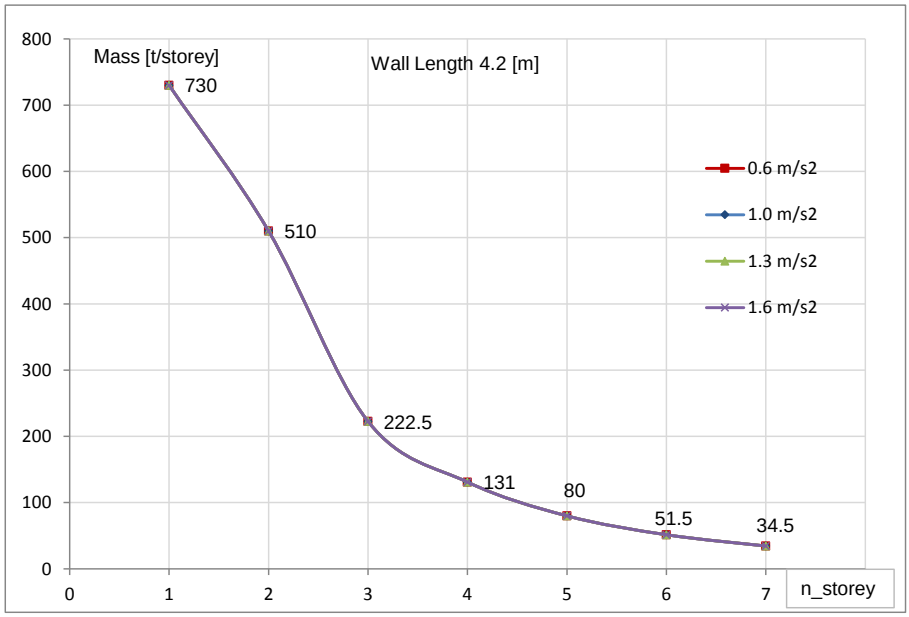

Fig. B.4: Outcome of the parameter study of the LFTW sheathed on both sides with OSB with a length of 4.2 [m], see also Table B.4

B.1.5 Tabular and graphical presentation for LFTW of a length $4.8[m]$ sheathed on both sides with OSB

The results of the parametric study for a 4.8 [m] long LFTW element sheathed with OSB on both sides are summarized in Table B.5. The typical, graphical presentation is given in Figure B.5

Tab. B.5: Results of the parameter study of a LFTW with a length of 4.8 [m] sheathed on both sides with OSB

Zone	Mass	IDA	Modal analysis			Pushover analysis				NLTH analysis			
a_g	m	check	T	T^*	Γ	Δ_y	F_y	μ	$\Delta_{u,st}$	HD force	Δ_{roof}	IDR	DI
$[\frac{m}{s^2}]$	[t]		[s]	[s]	[-]	[mm]	[kN]	[-]	[mm]	[kN]	[mm]	[-]	[-]
1- storey structure													
0.6	771.0	✓	1.09	1.70	1.0	34.42	362.6	1.0	107.1	144.1	22.14	0.76	0.20
1.0	771.0	✓	1.09	1.70				1.25		179.6	33.38	1.15	0.33
1.3	771.0	✓	1.09	1.70				1.63		197.6	43.5	1.50	0.41
160	771.0	✓	1.09	1.70				2.0		213.2	53.13	1.80	0.52
2- storey structure													
0.6	555.0	✓	1.55	1.70	1.18	29.52	352.4	1.05	100.5	217.1	23.18	0.81	0.25
1.0	555.0	✓	1.55	1.70				1.74		280.5	37.51	1.1	0.4
1.3	555.0	✓	1.55	1.70				2.27		307.9	53.75	1.53	0.47
163	555.0	✓	1.55	1.70				2.79		330.5	69.11	2.04	0.65

Zone	Mass	IDA	Modal analysis			Pushover analysis				NLTH analysis			
a_g	m	check	T	T^*	Γ	Δ_y	F_y	μ	$\Delta_{u,st}$	HD force	Δ_{roof}	IDR	DI
$[\frac{m}{s^2}]$	[t]		[s]	[s]	[-]	[mm]	[kN]	[-]	[mm]	[kN]	[mm]	[-]	[-]
3- storey structure													
0.6	232.5	✓	1.45	1.70	1.25	52.8	358.3	1.0	160.2	198.0	21.73	0.53	0.14
1.0	232.5	✓	1.45	1.70				1.02		285.6	36.27	0.74	0.22
1.3	232.5	✓	1.45	1.70				1.32		343.1	50.18	0.99	0.27
1.6	232.5	✓	1.45	1.70				1.63		404.6	68.0	1.30	0.35
4- storey structure													
0.6	142.0	✓	1.53	1.70	1.2953	70.26	356.8	1.0	199.3	187.0	21.15	0.43	0.11
1.0	142.0	✓	1.53	1.70				1.0		290.8	37.77	0.59	0.17
1.3	142.0	✓	1.53	1.70				1.03		364.2	54.25	0.80	0.20
1.6	142.0	✓	1.53	1.70				1.27		431.2	70.0	1.0	0.26
5- storey structure													
0.6	87.5.0	✓	1.56	1.70	1.33	97.67	356.9	1.0	247.5	197.9	24.14	0.35	0.09
1.0	87.5.0	✓	1.56	1.70				1.0		281.1	39.16	0.47	0.13
1.3	87.5.0	✓	1.56	1.70				1.0		365.9	52.32	0.62	0.15
1.6	87.5.0	✓	1.56	1.70				1.0		421.6	66.63	0.74	0.19
6- storey structure													
0.6	57.5	✓	1.59	1.70	1.36	130.2	355.3	1.0	301.1	198.1	26.29	0.30	0.07
1.0	57.5	✓	1.59	1.70				1.0		271.7	41.68	0.40	0.09
1.3	57.5	✓	1.59	1.70				1.0		335.8	51.4	0.48	0.11
1.6	57.5	✓	1.59	1.70				1.0		399.2	65.54	0.57	0.14
7- storey structure													
0.6	39.0	✓	1.62	1.70	1.39	172.5	356.7	1.0	370.8	206.2	29.6	0.26	0.06
1.0	39.0	✓	1.62	1.70				1.0		268.3	43.71	0.34	0.08
1.3	39.0	✓	1.62	1.70				1.0		314.0	51.61	0.40	0.09
1.6	39.0	✓	1.62	1.70				1.0		379.9	67.33	0.48	0.11
8- storey structure													
0.6	27.5	✓	1.64	1.70	1.406	223.7	356.7	1.0	453.4	202.0	34.26	0.22	0.05
1.0	27.5	✓	1.64	1.70				1.0		255.0	46.72	0.29	0.07
1.3	27.5	✓	1.64	1.70				1.0		290.0	53.64	0.34	0.07
1.6	27.5	✓	1.64	1.70				1.0		363.8	71.67	0.42	0.09

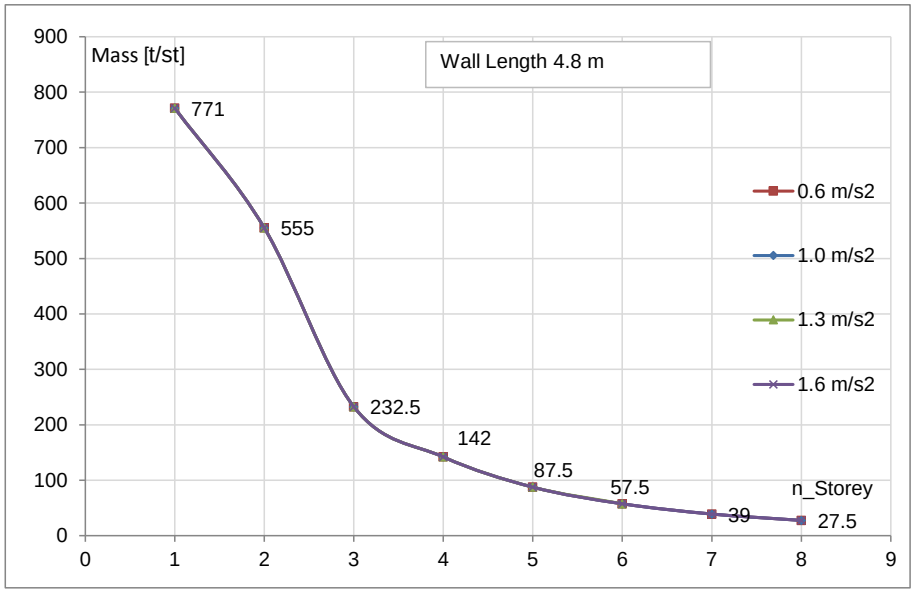

Fig. B.5: Outcome of the parameter study of the LFTW sheathed on both sides with OSB with a length of 4.8 [m], see also Table B.5

B.2 Soil conditions E

B.2.1 Tabular and graphical presentation for LFTW of a length $2.4[m]$ sheathed on both sides with OSB

The results of the parametric study for a 2.4 [m] long LFTW element sheathed with OSB on both sides are summarized in Table B.6. The typical, graphical presentation is given in Figure B.6

Tab. B.6: Results of the parameter study of a LFTW with a length of 2.4 [m] sheathed on both sides with OSB

Zone	Mass	IDA	Modal analysis			Pushover analysis				NLTH analysis			
a_g	m	check	T	T^*	Γ	Δ_y	F_y	μ	$\Delta_{u,st}$	HD force	Δ_{roof}	IDR	DI
$[\frac{m}{s^2}]$	[t]		[s]	[s]	[-]	[mm]	[kN]	[-]	[mm]	[kN]	[mm]	[-]	[-]
1- storey structure													
0.6	500.0	✓	1.27	1.70	1.0	24.22	163.7	1.88	105.1	170.9	52.13	1.80	0.56
1.0	446	✓	1.20	1.59				3.0		198.9	57.7	2.0	0.63
1.3	237.5	✓	0.87	1.1				3.0		208.5	61.22	2.0	0.65
1.6	147.0	✓	0.69	0.84				3.0		212.5	64.81	2.2	0.68
2- storey structure													
0.6	230.0	✓	1.47	1.70	1.188	33.48	162.4	1.62	125.9	252.1	44.48	1.17	0.36
1.0	230.0	✓	1.47	1.70				2.69		323.3	70.21	1.69	0.53
1.3	167.0	✓	1.25	1.44				3.0		344.8	80.15	1.92	0.60
1.6	112.0	✓	1.02	1.17				3.0		358.7	79.1	2.0	0.63

Zone	Mass	IDA	Modal analysis			Pushover analysis				NLTH analysis			
a_g	m	check	T	T^*	Γ	Δ_y	F_y	μ	$\Delta_{u,st}$	HD force	Δ_{roof}	IDR	DI
$\frac{m}{s^2}$	[t]		[s]	[s]	[-]	[mm]	[kN]	[-]	[mm]	[kN]	[mm]	[-]	[-]
3- storey structure													
0.6	110.0	✓	1.52	1.70	1.266	52.38	161.7	1.09	158.6	267.8	39.34	0.63	0.20
1.0	110.0	✓	1.52	1.70				1.82		380.9	69.12	1.09	0.33
1.3	110.0	✓	1.52	1.70				2.37		430.4	93.26	1.40	0.44
1.6	110.0	x	1.52	1.70				2.92		476.5	109.9	2.06	0.65
	97.0	✓	1.43	1.59				2.74		468.0	104.3	1.82	0.58
4- storey structure													
0.6	60.0	✓	1.58	1.70	1.318	79.85	162.4	1.0	217.4	256.1	41.57	0.48	0.14
1.0	60.0	✓	1.58	1.70				1.25		392.2	71.09	0.78	0.24
1.3	60.0	✓	1.58	1.70				1.62		454.6	95.6	1.11	0.35
1.6	60.0	✓	1.58	1.70				2.0		512.4	110.5	1.28	0.41
5- storey structure													
0.6	35.0	✓	1.61	1.70	1.357	117.5	162.3	1.0	283.7	241.0	43.18	0.38	0.11
1.0	35.0	✓	1.62	1.70				1.0		373.1	73.86	0.58	0.17
1.3	35.0	✓	1.62	1.70				1.0		465.9	102.7	0.81	0.25
1.6	35.0	✓	1.62	1.70				1.39		516.1	114.3	0.98	0.31
6- storey structure													
0.6	22.0	✓	1.66	1.71	1.386	168.6	163.0	1.0	368.3	216.3	45.27	0.30	0.09
1.0	22.0	✓	1.66	1.71				1.0		346.4	78.92	0.44	0.13
1.3	22.0	✓	1.66	1.71				1.0		436.5	104.9	0.64	0.19
1.6	22.0	✓	1.66	1.71				1.0		489.1	118.6	0.75	0.24

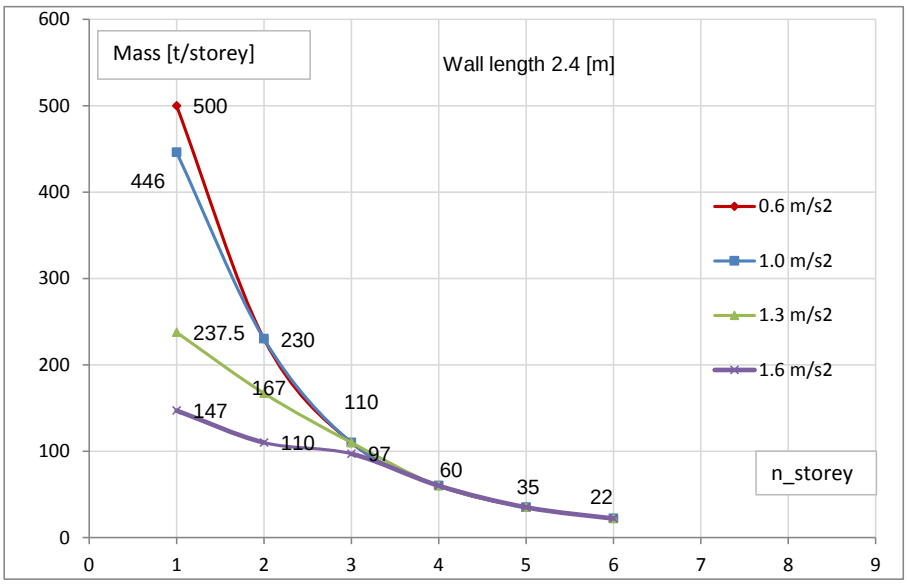

Fig. B.6: Outcome of the parameter study of the LFTW sheathed on both sides with OSB with a length of 2.4 [m], see also Table B.6

B.2.2 Tabular and graphical presentation for LFTW of a length $3.0[m]$ sheathed on both sides with OSB

The results of the parametric study for a 3.0 [m] long LFTW element sheathed with OSB on both sides are summarized in Table B.7. The typical, graphical presentation is given in Figure B.7

Tab. B.7: Results of the parameter study of a LFTW with a length of 3.0 [m] sheathed on both sides with OSB

Zone	Mass	IDA	Modal analysis			Pushover analysis				NLTH analysis			
a_g	m	check	T	T^*	Γ	Δ_y	F_y	μ	$\Delta_{u,st}$	HD force	Δ_{roof}	IDR	DI
$[\frac{m}{s^2}]$	[t]		[s]	[s]	[-]	[mm]	[kN]	[-]	[mm]	[kN]	[mm]	[-]	[-]
1- storey structure													
0.6	622.0	✓	1.13	1.70	1.0	25.8	220.8	1.75	103.9	190.5	47.56	1.6	0.574
1.0	591.5	✓	1.1	1.63				2.86		219.1		1.9	0.70
1.3	301.0	✓	0.79	1.05				2.93		231.9	60.43	2.08	0.70
1.6	189.0	✓	0.63	0.80				3.0		234.0	61.73	2.10	0.70
2- storey structure													
0.6	352.0	✓	1.46	1.71	1.188	29.69	219.9	1.82	120.5	290.9	48.66	1.4	0.50
1.0	352.0	x	1.46	1.71				3.03		359.7	70.8	1.76	0.65
	315.0	✓	1.38	1.61				2.87		359.6	67.97	1.65	0.60
1.3	204.0	x	1.11	1.29				3.03		375.6	74.65	1.82	0.66
1.3	195.0	✓	1.09	1.26				2.97		377.7	72.96	1.78	0.63
1.6	134.5	x	0.90	1.04				3.04		385.1	77.36	2.0	0.69

	117.5	✓	0.85	0.97				2.85		378.3	73.28	1.93	0.65
Zone	Mass	IDA	Modal analysis			Pushover analysis				NLTH analysis			
a_g	m	check	T	T^*	Γ	Δ_y	F_y	μ	$\Delta_{u,st}$	HD force	Δ_{roof}	IDR	DI
$[\frac{m}{s^2}]$	[t]		[s]	[s]	[-]	[mm]	[kN]	[-]	[mm]	[kN]	[mm]	[-]	[-]
3- storey structure													
0.6	167.0	✓	1.51	1.70	1.266	46.89	219.0	1.22	156.8	306.0	39.72	0.72	0.25
1.0	167.0	✓	1.51	1.70				2.04		434.5	71.1	1.19	0.41
1.3	167.0	✓	1.51	1.70				2.65		488.8	95.41	1.51	0.57
1.6	136.0	x	1.36	1.53				2.96		527.3	101.1	1.85	0.68
	107.5	✓	1.21	1.35				2.63		485.7	89.57	1.60	0.60
Continuation of Table B.7													
4- storey structure													
0.6	92.0	✓	1.57	1.70	1.318	70.21	219.1	1.0	200.1	306.1	40.97	0.55	0.18
1.0	92.0	✓	1.57	1.70				1.42		461.4	72.82	0.88	0.29
1.3	92.0	✓	1.57	1.70				1.84		535.0	97.01	1.20	0.41
1.6	92.0	✓	1.57	1.70				2.27		589.4	116.6	1.44	0.54
5- storey structure													
0.6	54.0	✓	1.61	1.70	1.357	102.5	218.2	1.0	252.5	289.6	43.95	0.42	0.14
1.0	54.0	✓	1.62	1.70				1.0		448.4	74.38	0.63	0.20
1.3	54.0	✓	1.62	1.70				1.3		532.4	97.26	0.87	0.28
1.6	54.0	✓	1.62	1.70				1.6		618.8	118.7	1.0	0.37
6- storey structure													
0.6	34.0	✓	1.65	1.70	1.386	145.9	218.1	1.0	316.8	275.7	47.56	0.33	0.10
1.0	34.0	✓	1.65	1.70				1.0		419.2	79.38	0.49	0.16
1.3	34.0	✓	1.65	1.70				1.0		521.7	105.5	0.69	0.23
1.6	34.0	✓	1.65	1.70				1.15		584.6	119.8	0.80	0.28
7- storey structure													
0.6	22.0	✓	1.67	1.70	1.409	202.4	218.1	1.0	316.8	247.1	49.45	0.25	0.08
1.0	22.0	✓	1.67	1.70				1.0		381.5	83.46	0.39	0.12
1.3	22.0	✓	1.67	1.70				1.0		483.9	108.4	0.52	0.17
1.6	22.0	✓	1.67	1.70				1.0		549.6	127.1	0.64	0.22

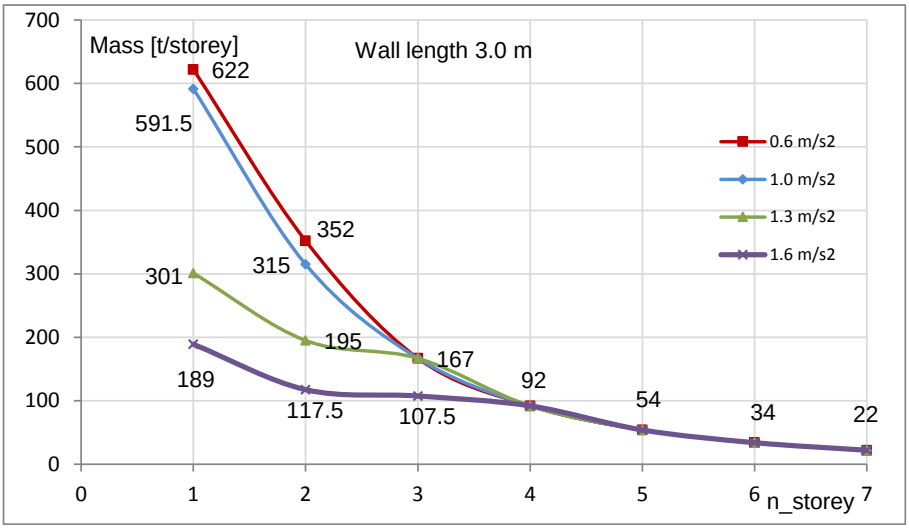

Fig. B.7: Outcome of the parameter study of the LFTW sheathed on both sides with OSB with a length of 3.0 [m], see also Table B.7

B.2.3 Tabular and graphical presentation for LFTW of a length $3.6[m]$ sheathed on both sides with OSB

The results of the parametric study for a 3.6 [m] long LFTW element sheathed with OSB on both sides are summarized in Table B.8. The typical, graphical presentation is given in Figure B.8

Tab. B.8: Results of the parameter study of a LFTW with a length of 3.6 [m] sheathed on both sides with OSB

Zone	Mass	IDA	Modal analysis			Pushover analysis				NLTH analysis			
a_g	m	check	T	T^*	Γ	Δ_y	F_y	μ	$\Delta_{u,st}$	HD force	Δ_{roof}	IDR	DI
$[\frac{m}{s^2}]$	[t]		[s]	[s]	[-]	[mm]	[kN]	[-]	[mm]	[kN]	[mm]	[-]	[-]
1- storey structure													
0.6	635.0	✓	1.15	1.70	1.0	30.36	260.8	1.0	98.83	180.9	40.27	1.39	0.44
1.0	635.0	✓	1.15	1.70				2.49		213.2	56.0	2.0	0.65
1.3	380.0	x	0.87	1.22				2.72		226.7	64.29	2.2	0.70
	352.5	✓	0.85	1.16				2.65		227.0	60.44	2.08	0.64
1.6	251.0	x	0.72	0.94				2.85		231.1	66.32	2.3	0.70
	200.0	✓	0.65	0.83				2.60		228.9	60.77	2.1	0.61
2- storey structure													
0.6	367.5	✓	1.47	1.70	1.183	32.73	258.7	1.64	117.0	271.3	44.35	1.27	0.42
1.0	367.5	✓	1.47	1.70				2.73		327.9	63.52	1.53	0.52
1.3	248.0	x	1.29	1.39				2.92		359.9	82.77	2.17	0.70
	210.0	✓	1.13	1.28				2.69		363.9	72.17	1.72	0.54
1.6	178.0	x	1.03	1.18				3.05		372.4	79.18	2.0	0.67

	130.0	✓	0.88	1.0				2.60		364.0	73.0	1.86	0.56
Zone	Mass	IDA	Modal analysis			Pushover analysis				NLTH analysis			
a_g	m	check	T	T^*	Γ	Δ_y	F_y	μ	$\Delta_{u,st}$	HD force	Δ_{roof}	IDR	DI
$[\frac{m}{s^2}]$	[t]		[s]	[s]	[-]	[mm]	[kN]	[-]	[mm]	[kN]	[mm]	[-]	[-]
3- storey structure													
0.6	175.0	✓	1.48	1.70	1.256	52.6	258.7	1.09	155.5	282.8	38.31	0.74	0.23
1.0	175.0	✓	1.48	1.70				1.83		377.6	59.59	1.0	0.30
1.3	175.0	✓	1.48	1.70				2.38		458.6	92.75	1.55	0.52
1.6	175.0	x	1.48	1.70				2.93		484.1	105.5	1.93	0.67
	120.0	✓	1.24	1.41				2.44		441.9	79.79	1.40	0.47
4- storey structure													
0.6	100.0	✓	1.54	1.70	1.305	73.95	257.7	1.0	198.2	274.4	39.03	0.55	0.16
1.0	100.0	✓	1.54	1.70				1.34		430.9	70.16	0.84	0.25
1.3	100.0	✓	1.54	1.70				1.74		489.3	94.38	1.21	0.38
1.6	100.0	✓	1.54	1.70				2.14		515.7	98.87	1.23	0.40
5- storey structure													
0.6	60.5	✓	1.58	1.70	1.343	104.3	257.7	1.0	249.0	266.2	41.48	0.44	0.13
1.0	60.5	✓	1.58	1.70				1.0		432.7	73.29	0.64	0.19
1.3	60.5	✓	1.58	1.70				1.30		504.2	67.69	0.89	0.27
1.6	60.5	✓	1.58	1.70				1.55		570.6	111.5	0.99	0.32
6- storey structure													
0.6	39.0	✓	1.61	1.70	1.373	143.5	257.5	1.0	315.8	251.8	43.27	0.36	0.10
1.0	39.0	✓	1.65	1.70				1.0		393.4	74.68	0.51	0.15
1.3	39.0	✓	1.65	1.70				1.0		493.9	100.3	0.68	0.20
1.6	39.0	✓	1.65	1.70				1.16		558.2	114.5	0.78	0.26
7- storey structure													
0.6	26.0	✓	1.67	1.70	1.397	194.2	258.6	1.0	397.2	232.2	45.37	0.30	0.08
1.0	26.0	✓	1.67	1.70				1.0		366.8	77.22	0.42	0.12
1.3	26.0	✓	1.67	1.70				1.0		461.5	102.2	0.54	0.16
1.6	26.0	✓	1.67	1.70				1.0		345.1	71.42	0.45	n

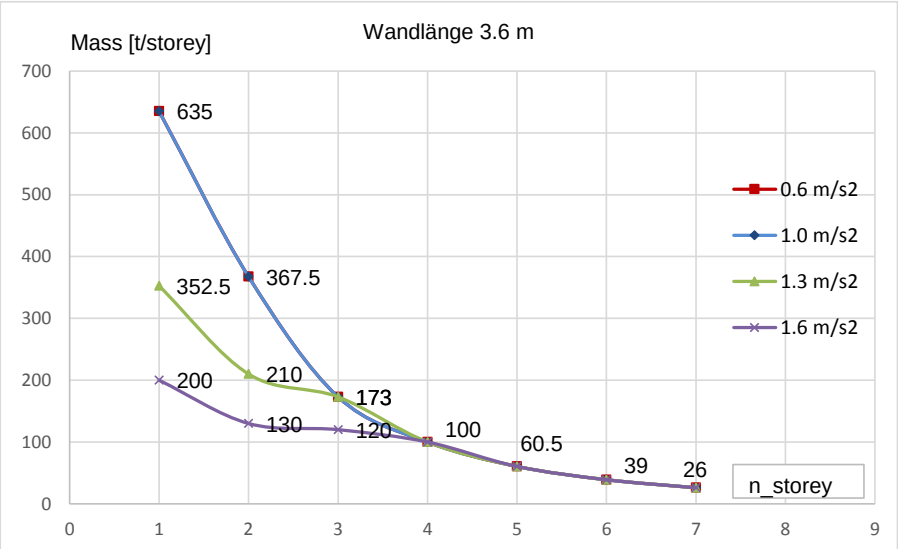

Fig. B.8: Outcome of the parameter study of the LFTW sheathed on both sides with OSB with a length of 3.6 [m], see also Table B.8

B.2.4 Tabular and graphical presentation for LFTW of a length $4.2[m]$ sheathed on both sides with OSB

The results of the parametric study for a 4.2 [m] long LFTW element sheathed with OSB on both sides are summarized in Table B.9. The typical, graphical presentation is given in Figure B.9

Tab. B.9: Results of the parameter study of a LFTW with a length of 4.2 [m] sheathed on both sides with OSB

Zone	Mass	IDA	Modal analysis			Pushover analysis				NLTH analysis			
a_g	m	check	T	T^*	Γ	Δ_y	F_y	μ	$\Delta_{u,st}$	HD force	Δ_{roof}	IDR	DI
$[\frac{m}{s^2}]$	[t]		[s]	[s]	[-]	[mm]	[kN]	[-]	[mm]	[kN]	[mm]	[-]	[-]
1- storey structure													
0.6	730.0	✓	1.1	1.70	1.0	31.34	314.4	1.43	107.3	190.8	37.85	1.30	0.36
1.0	730.0	✓	1.1	1.70				2.39		217.9	57.55	1.98	0.58
1.3	475.0	x	0.88	1.26				2.74		227.7	65.19	2.25	0.63
	460.0	✓	0.87	1.23				2.71		232.5	64.05	2.25	0.61
1.6	336.0	x	0.74	1.0				3.0		238.6	70.32	2.40	0.66
	265.0	✓	0.65	0.86				2.74		235.1	63.9	2.2	0.54
2- storey structure													
0.6	510.0	✓	1.53	1.70	1.183	28.48	310.7	1.90	119.9	290.0	55.51	1.70	0.50
1.0	464.0	✓	1.46	1.62				3.0		362.8	70.19	1.77	0.57
1.3	280.0	x	1.46	1.62				3.0		372.4	73.11	1.80	0.53
	265.0	✓	1.10	1.23				2.93		382.8	72.82	1.81	0.53
1.6	178.5	x	0.9	1.02				2.95		388.6	77.1	1.95	0.53

	162.0	✓	0.86	0.97				2.81		378.2	72.91	1.94	0.50
Zone	Mass	IDA	Modal analysis			Pushover analysis				NLTH analysis			
a_g	m	check	T	T^*	Γ	Δ_y	F_y	μ	$\Delta_{u,st}$	HD force	Δ_{roof}	IDR	DI
$[\frac{m}{s^2}]$	[t]		[s]	[s]	[-]	[mm]	[kN]	[-]	[mm]	[kN]	[mm]	[-]	[-]
3- storey structure													
0.6	222.5	✓	1.48	1.70	1.255	48.3	309.5	1.17	154.8	307.4	38.05	0.80	0.22
1.0	222.5	✓	1.48	1.70				1.96		418.8	60.54	1.06	0.28
1.3	222.5	✓	1.48	1.70				2.54		494.5	88.87	1.53	0.48
1.6	203.5	x	1.42	1.62				3.0		537.3	107.0	2.06	0.68
	150.0	✓	1.21	1.38				2.60		475.3	79.51	1.47	0.46
4- storey structure													
0.6	131.0	✓	1.55	1.70	1.303	66.92	309.5	1.0	193.5	306.1	39.25	0.60	0.16
1.0	131.0	✓	1.55	1.70				1.47		476.7	70.58	0.90	0.24
1.3	131.0	✓	1.55	1.70				1.90		544.8	95.95	1.3	0.36
1.6	131.0	x	1.55	1.70				2.35		564.2	105.2	1.5	0.47
	128.0	✓	1.53	1.68				2.32		554.6	109.7	1.46	0.45
5- storey structure													
0.6	80.0	✓	1.59	1.70	1.34	94.17	308.3	1.0	240.2	305.4	42.14	0.48	0.12
1.0	80.0	✓	1.59	1.70				1.08		479.7	73.56	0.67	0.16
1.3	80.0	✓	1.59	1.70				1.40		557.8	98.65	0.96	0.24
1.6	80.0	✓	1.59	1.70				1.72		628.0	109.1	1.07	0.31
6- storey structure													
0.6	51.5	✓	1.62	1.70	1.37	128.8	308.2	1.0	294.2	284.2	43.16	0.39	0.09
1.0	51.5	✓	1.62	1.70				1.0		445.0	75.68	0.55	0.13
1.3	51.5	✓	1.62	1.70				1.0		562.4	101.7	0.71	0.18
1.6	51.5	✓	1.62	1.70				1.0		614.0	114.3	0.83	0.25
7- storey structure													
0.6	34.5	✓	1.64	1.70	1.395	173.1	308.2	1.0	367.1	264.0	45.58	0.32	0.07
1.0	34.5	✓	1.64	1.70				1.0		415.3	77.85	0.45	0.10
1.3	34.5	✓	1.64	1.70				1.0		523.3	102.6	0.58	0.14
1.6	34.5	✓	1.64	1.70				1.29		584.8	114.7	0.66	0.18

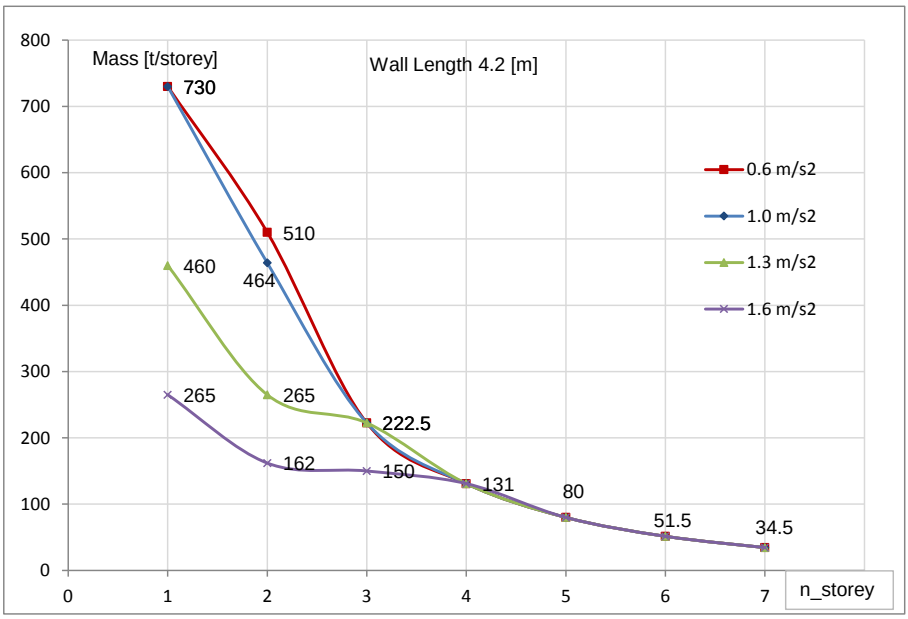

Fig. B.9: Outcome of the parameter study of the LFTW sheathed on both sides with OSB with a length of 4.2 [m], see also Table B.9

B.2.5 Tabular and graphical presentation for LFTW of a length $4.8[m]$ sheathed on both sides with OSB

The results of the parametric study for a 4.8 [m] long LFTW element sheathed with OSB on both sides are summarized in Table B.10. The typical, graphical presentation is given in Figure B.10

Tab. B.10: Results of the parameter study of a LFTW with a length of 4.8 [m] sheathed on both sides with OSB

Zone	Mass	IDA	Modal analysis			Pushover analysis				NLTH analysis			
a_g	m	check	T	T^*	Γ	Δ_y	F_y	μ	$\Delta_{u,st}$	HD force	Δ_{roof}	IDR	DI
$[\frac{m}{s^2}]$	[t]		[s]	[s]	[-]	[mm]	[kN]	[-]	[mm]	[kN]	[mm]	[-]	[-]
1- storey structure													
0.6	771.0	✓	1.09	1.70	1.0	34.42	362.6	1.31	107.1	184.9	36.8	01.27	0.34
1.0	771.0	✓	1.09	1.70				2.19		2.19	54.41	1.88	0.54
1.3	551.0	x	0.92	1.34				2.57		234.1	65.22	2.25	0.64
	490.0	✓	0.87	1.24				2.47		234.8	61.64	2.1	0.57
1.6	415.0	x	0.80	1.12				2.88		240.9	71.12	2.45	0.70
	290.0	✓	0.67	0.89				2.53		237.3	62.65	2.15	0.54
2- storey structure													
0.6	555.0	✓	1.55	1.70	1.18	29.52	352.4	1.83	100.5	280.8	47.55	1.43	0.45
1.0	535.0	✓	1.52	1.66				3.0		360.4	70.98	1.82	0.58
1.3	332.0	x	1.20	1.33				3.0		375.4	76.13	1.88	0.55
	291.0	✓	1.12	1.25				2.8		378.6	72.08	1.76	0.48

1.6	226.0	x	0.99	1.11				3.0		375.4	76.34	2.0	0.55
	175.0	✓	0.87	0.98				2.65		378.6	72.28	1.87	0.48
Zone	Mass	IDA	Modal analysis			Pushover analysis				NLTH analysis			
a_g	m	check	T	T^*	Γ	Δ_y	F_y	μ	$\Delta_{u,st}$	HD force	Δ_{roof}	IDR	DI
$[\frac{m}{s^2}]$	[t]		[s]	[s]	[-]	[mm]	[kN]	[-]	[mm]	[kN]	[mm]	[-]	[-]
3- storey structure													
0.6	232.5	✓	1.45	1.70	1.25	52.8	358.3	1.07	160.2	291.0	37.41	0.77	0.21
1.0	232.5	✓	1.45	1.70				1.78		408.8	61.07	1.07	0.29
1.3	232.5	✓	1.45	1.70				2.32		486.6	89.91	1.50	0.45
1.6	232.5	x	1.45	1.70				2.85		507.8	102.7	1.90	0.64
	167.5	✓	1.23	1.43				2.44		450.9	76.81	1.34	0.40
4- storey structure													
0.6	142.0	✓	1.53	1.70	1.2953	70.26	356.8	1.0	199.3	290.6	38.75	0.59	0.15
1.0	142.0	✓	1.53	1.70				1.39		455.0	68.64	0.88	0.23
1.3	142.0	✓	1.53	1.70				1.81		519.4	89.93	1.23	0.32
1.6	142.0	✓	1.53	1.70				2.23		587.0	105.4	1.41	0.41
5- storey structure													
0.6	87.5	✓	1.56	1.70	1.33	97.67	356.9	1.0	247.5	284.1	39.74	0.48	0.12
1.0	87.5	✓	1.56	1.70				1.03		457.4	71.03	0.69	0.17
1.3	87.5	✓	1.56	1.70				1.34		542.9	94.23	0.94	0.24
1.6	87.5	✓	1.56	1.70				1.65		606.2	109.2	1.05	0.30
6- storey structure													
0.6	57.5	✓	1.59	1.70	1.36	130.2	355.3	1.0	301.1	274.0	41.9	0.39	0.09
1.0	57.5	✓	1.59	1.70				1.0		433.6	73.17	0.55	0.14
1.3	57.5	✓	1.59	1.70				1.03		554.0	99.31	0.72	0.18
1.6	57.5	✓	1.59	1.70				1.26		600.4	111.9	0.80	0.23
7- storey structure													
0.6	39.0	✓	1.62	1.70	1.39	172.5	356.7	1.0	370.8	255.6	43.22	0.33	0.08
1.0	39.0	✓	1.62	1.70				1.0		408.3	74.91	0.44	0.10
1.3	39.0	✓	1.62	1.70				1.0		514.7	99.48	0.57	0.15
1.6	39.0	✓	1.62	1.70				1.0		568.4	110.3	0.66	0.18
8- storey structure													
0.6	27.5	✓	1.64	1.70	1.406	223.7	356.7	1.0	453.4	244.8	46.29	0.28	0.06
1.0	27.5	✓	1.64	1.70				1.0		379.8	76.85	0.39	0.09
1.3	27.5	✓	1.64	1.70				1.0		487.1	100.6	0.48	0.12
1.6	27.5	✓	1.64	1.70				1.0		550.8	115.8	0.56	0.16

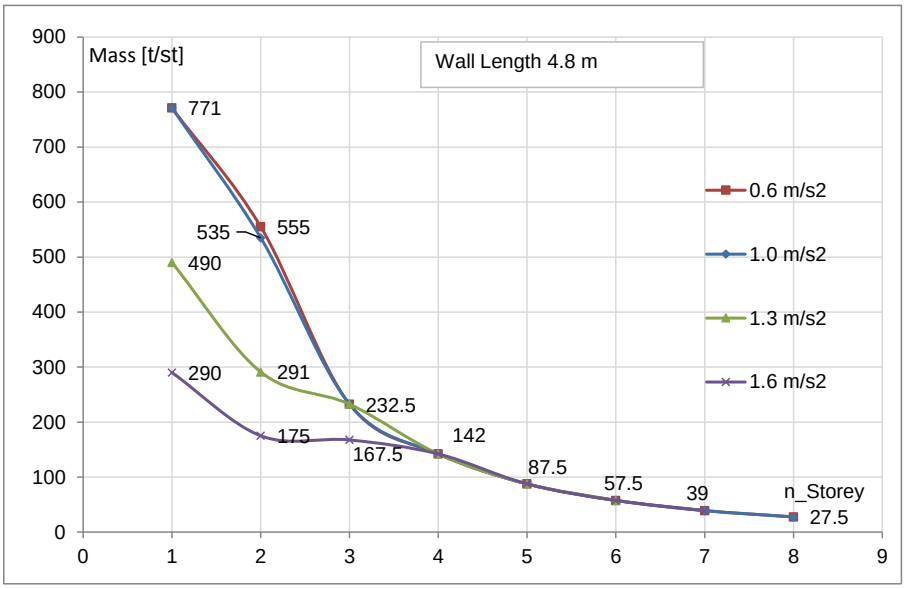

Fig. B.10: Outcome of the parameter study of the LFTW sheathed on both sides with OSB with a length of 4.8 [m], see also Table B.10

Appendix C

Comparison of the results for LFTWs Sheathed with OSB and GFB

In this section, all the results of the parameter study conducted in the previous chapters for LFTWs sheathed with OSB and GFB are graphically presented for the five different wall lengths, four considered hazard zones and corresponding soil conditions.

C.1 Soil Conditions A

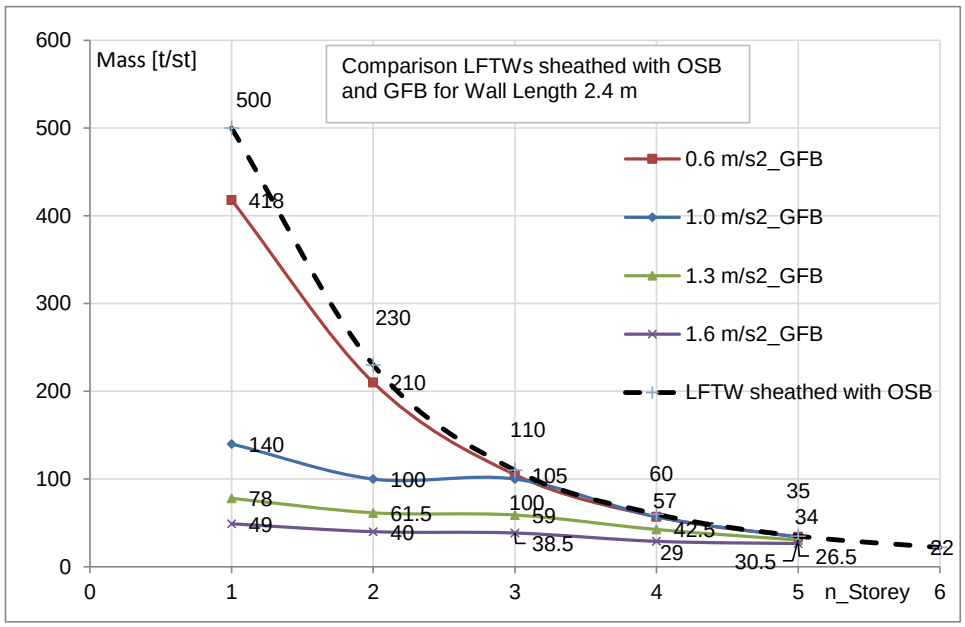

Fig. C.1: Comparison of the results for LFTWs sheathed with OSB and GFB for a wall length of 2.4 [m]

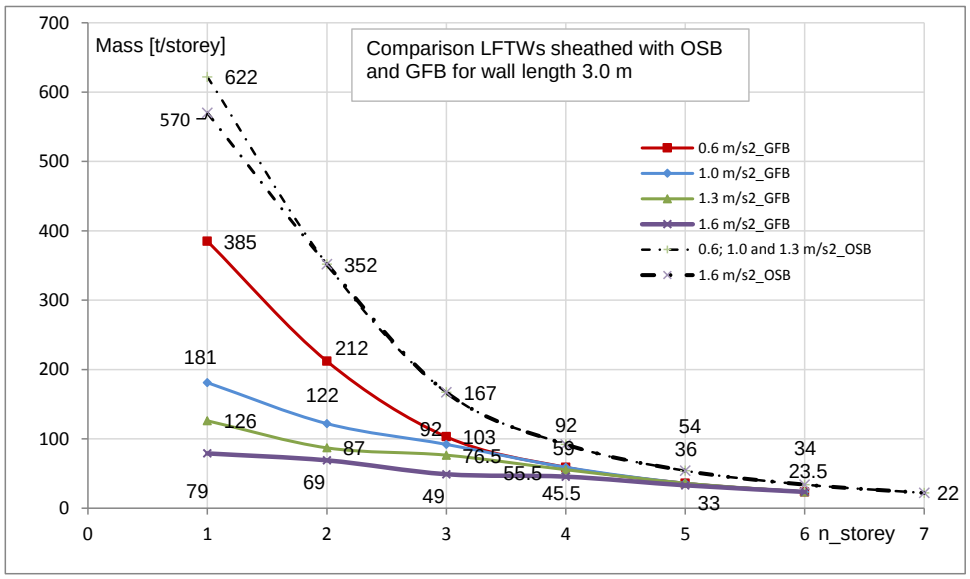

Fig. C.2: Comparison of the results for LFTWs sheathed with OSB and GFB for a wall length of 3.0 [m]

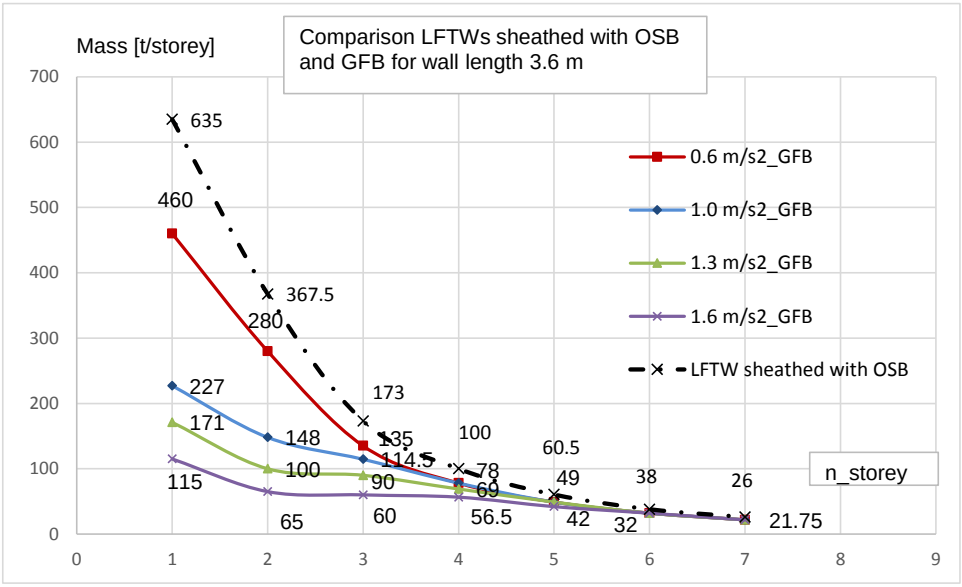

Fig. C.3: Comparison of the results for LFTWs sheathed with OSB and GFB for a wall length of 3.6 [m]

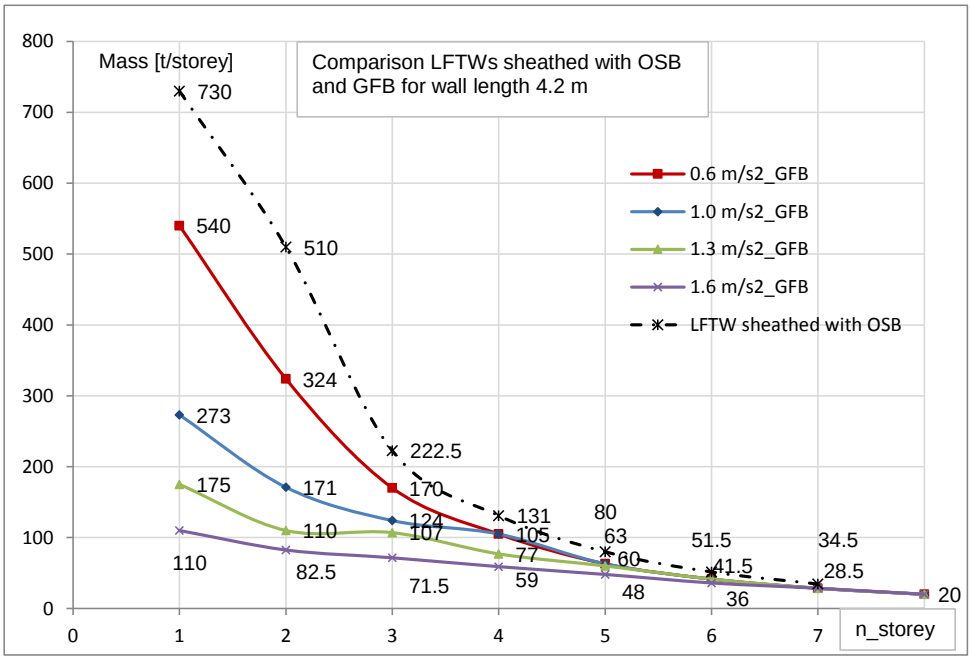

Fig. C.4: Comparison of the results for LFTWs sheathed with OSB and GFB for a wall length of 4.2 [m]

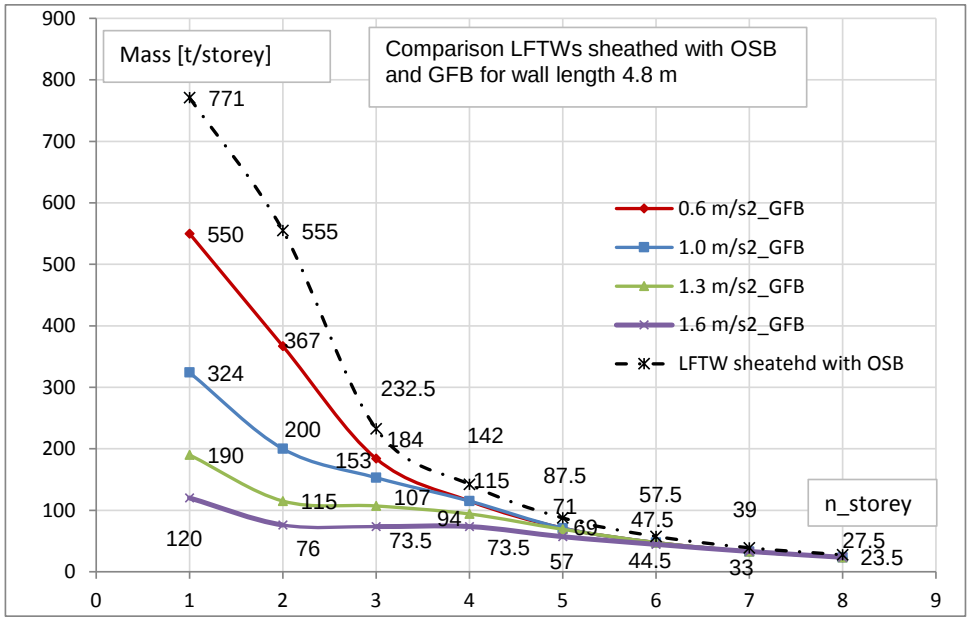

Fig. C.5: Comparison of the results for LFTWs sheathed with OSB and GFB for a wall length of 4.8 [m]

C.2 Soil Conditions C

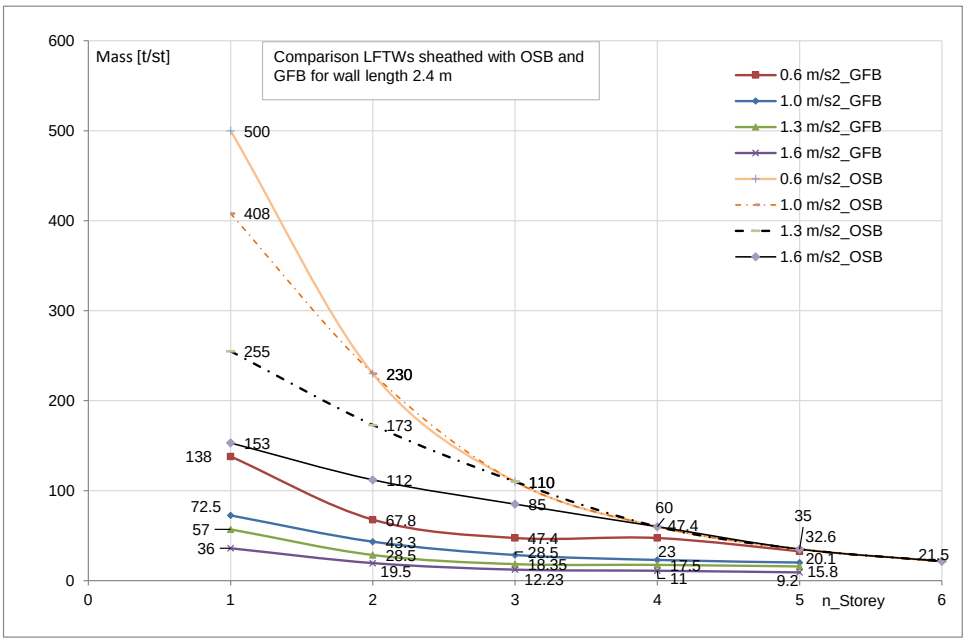

Fig. C.6: Comparison of the results for LFTWs sheathed with OSB and GFB for a wall length of 2.4 [m]

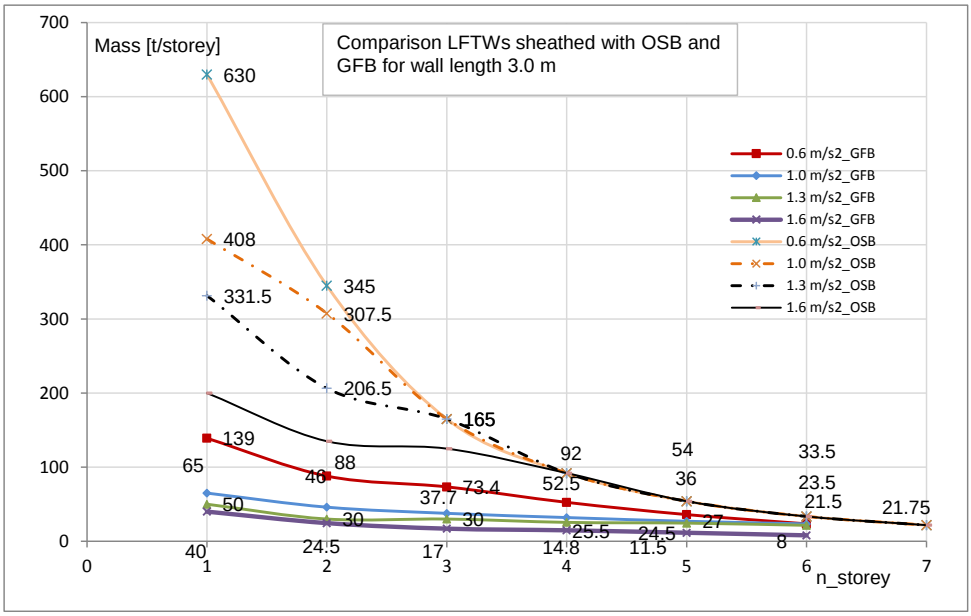

Fig. C.7: Comparison of the results for LFTWs sheathed with OSB and GFB for a wall length of 3.0 [m]

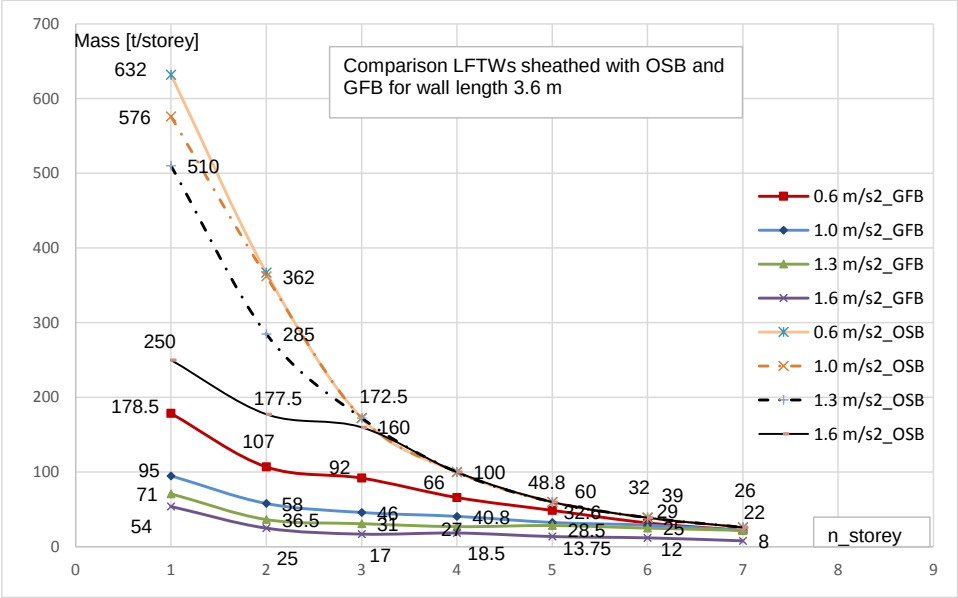

Fig. C.8: Comparison of the results for LFTWs sheathed with OSB and GFB for a wall length of 3.6 [m]

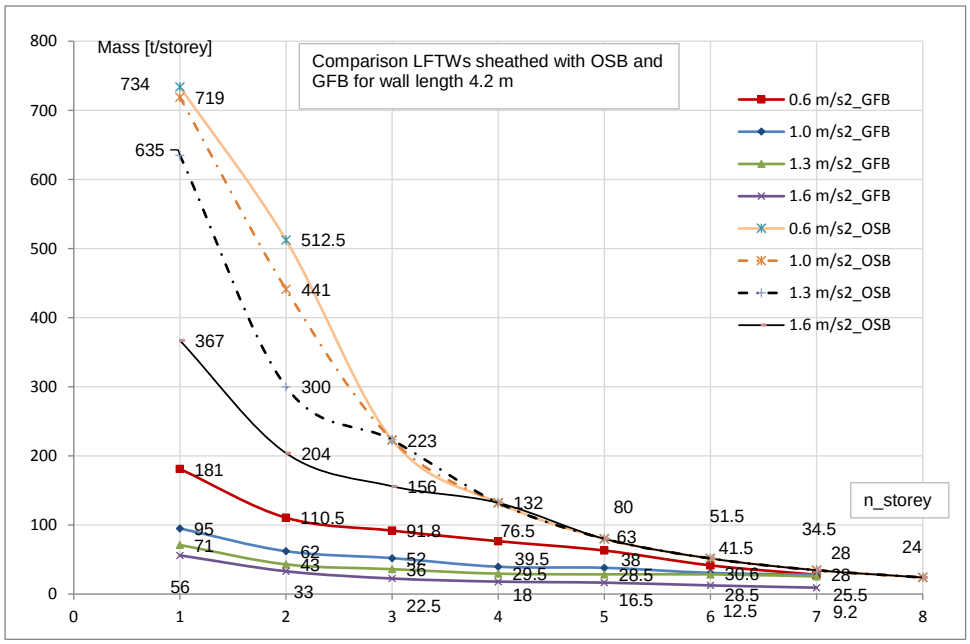

Fig. C.9: Comparison of the results for LFTWs sheathed with OSB and GFB for a wall length of 4.2 [m]

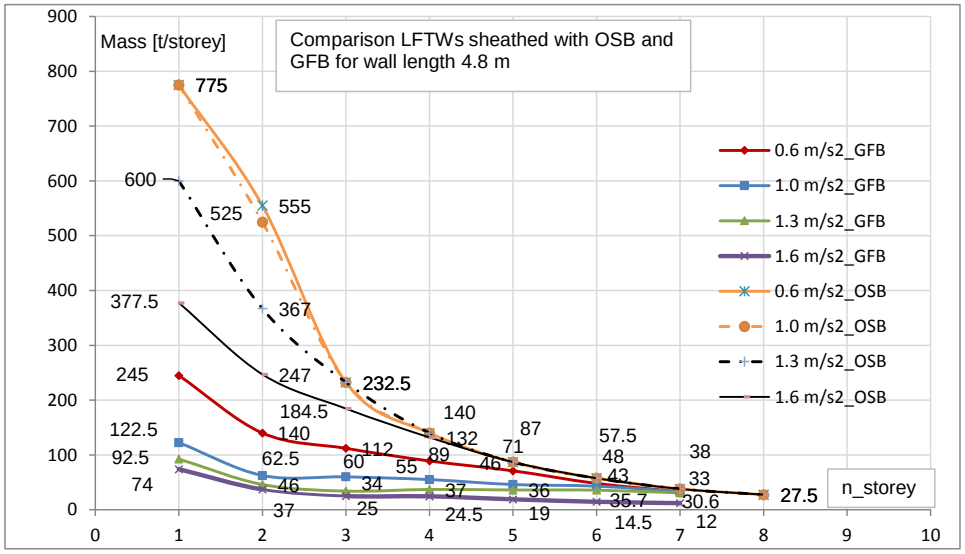

Fig. C.10: Comparison of the results for LFTWs sheathed with OSB and GFB for a wall length of 4.8 [m]

C.3 Soil Conditions E

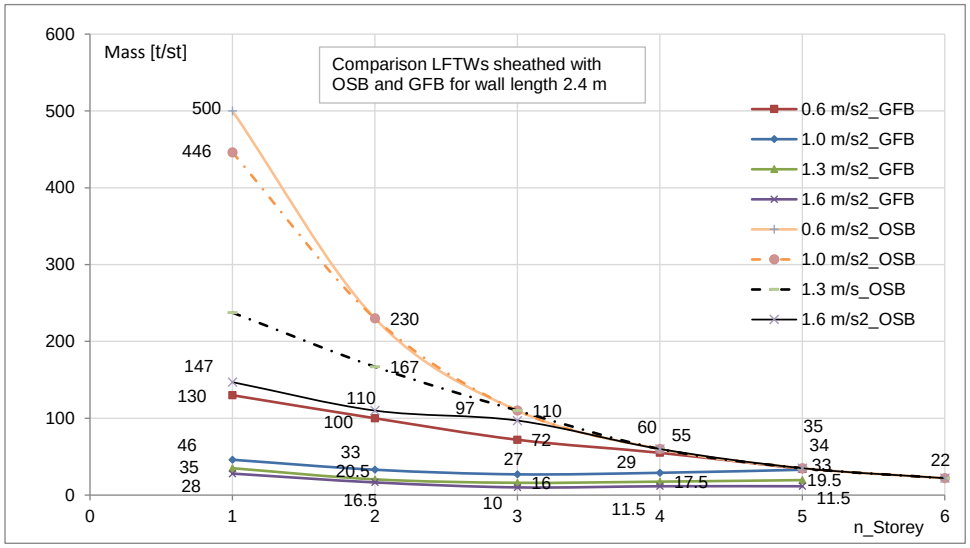

Fig. C.11: Comparison of the results for LFTWs sheathed with OSB and GFB for a wall length of 2.4 [m]

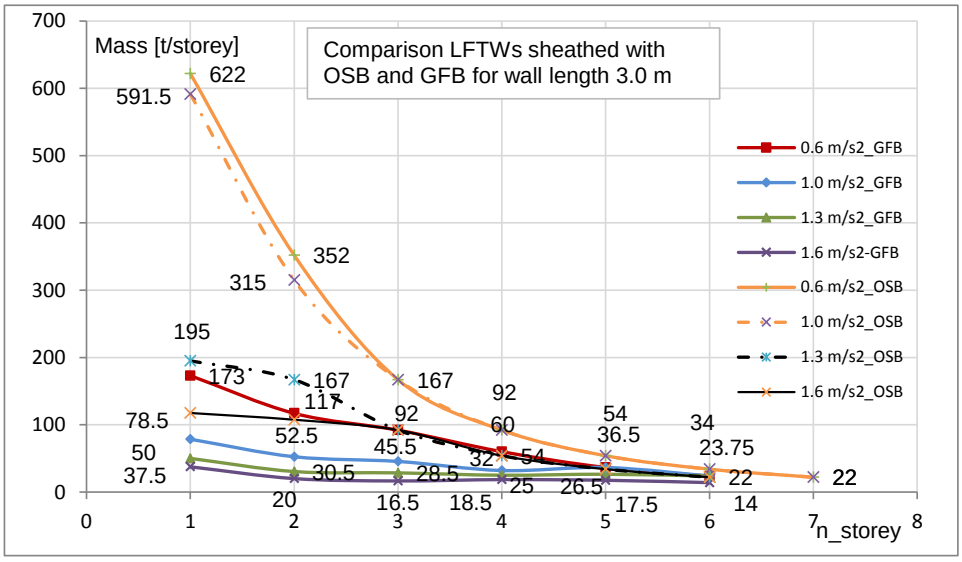

Fig. C.12: Comparison of the results for LFTWs sheathed with OSB and GFB for a wall length of 3.0 [m]

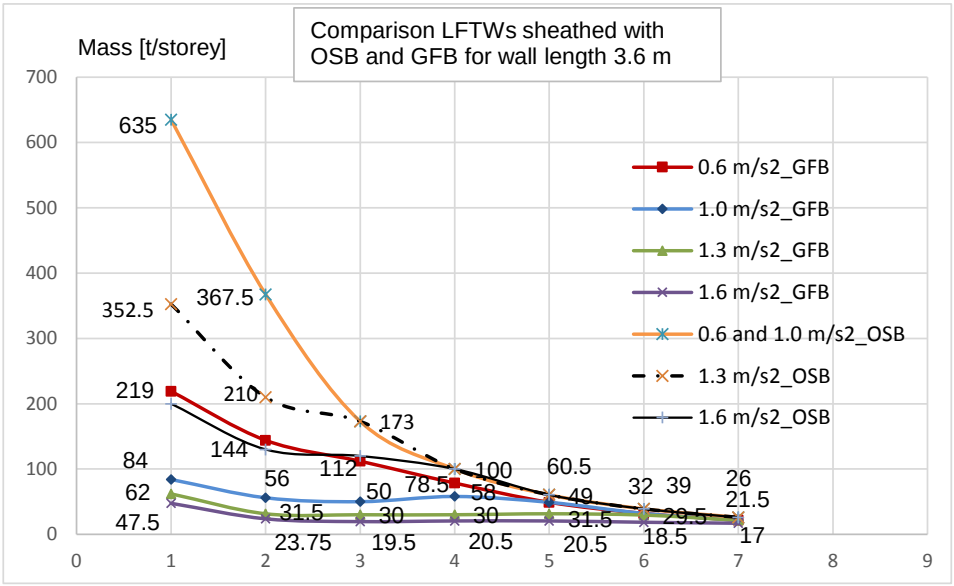

Fig. C.13: Comparison of the results for LFTWs sheathed with OSB and GFB for a wall length of 3.6 [m]

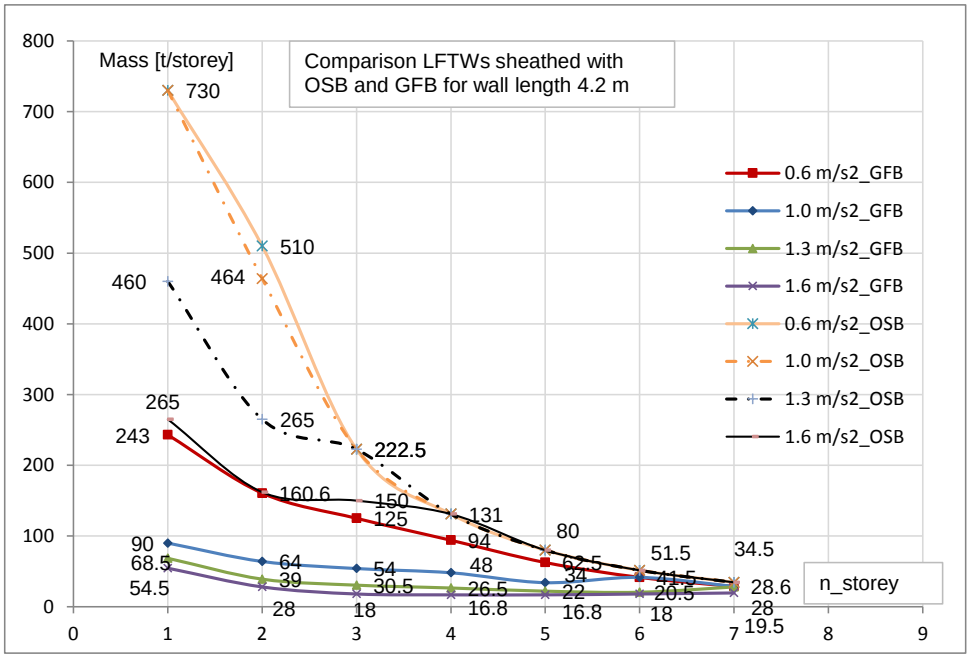

Fig. C.14: Comparison of the results for LFTWs sheathed with OSB and GFB for a wall length of 4.2 [m]

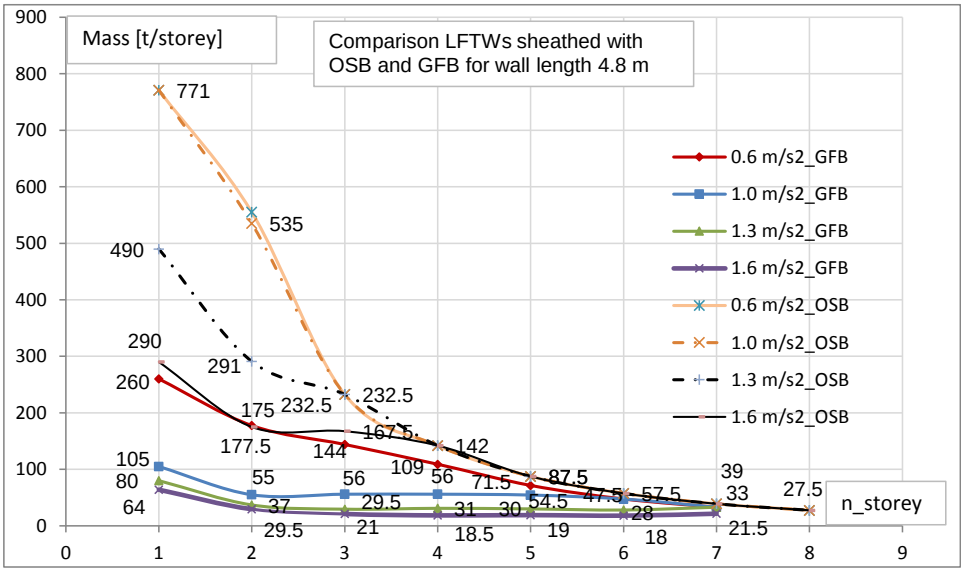

Fig. C.15: Comparison of the results for LFTWs sheathed with OSB and GFB for a wall length of 4.8 [m]